

An aerial photograph of a river delta, likely the Amazon, with a color-coded overlay. The land is shown in shades of orange, yellow, and brown, while the water bodies are highlighted in blue, green, and purple. The text is overlaid on the top portion of the image.

# **Earth Observation: Data, Processing and Applications**

Volume 1A: Data—Basics and Acquisition



The report is available in PDF format at <http://www.crcsi.com.au/earth-observation-series>  
We welcome your comments regarding the readability and usefulness of this report. To provide feedback, please contact us at [info@crcsi.com.au](mailto:info@crcsi.com.au).

**Publisher:**

Australia and New Zealand CRC for Spatial Information

**ISBN [ONLINE]:**

978-0-9943019-2-5

**Copyright:**

All material in this publication is licensed under a Creative Commons Attribution 4.0 Australia Licence, save for content supplied by third parties, and logos. Creative Commons Attribution 4.0 Australia Licence is a standard form licence agreement that allows you to copy, distribute, transmit and adapt this publication provided you attribute the work. The full licence terms are available from <https://creativecommons.org/licenses/by/4.0/legalcode>. A summary of the licence terms is available from <https://creativecommons.org/licenses/by/4.0/>.



**Disclaimer:**

While every effort has been made to ensure its accuracy, the CRCSI does not offer any express or implied warranties or representations as to the accuracy or completeness of the information contained herein. The CRCSI and its employees and agents accept no liability in negligence for the information (or the use of such information) provided in this report.

**Recommended Citation for Volume 1A:**

CRCSI (2016) *Earth Observation: Data, Processing and Applications. Volume 1A: Data—Basics and Acquisition*. (Eds. Harrison, B.A., Jupp, D.L.B., Lewis, M.M., Forster, B.C., Mueller, N., Smith, C., Phinn, S., Hudson, D., Grant, I., Coppa, I.) CRCSI, Melbourne.

**Latest Revision:**

April 2018

# Acknowledgements

Production of this series of texts would not have been possible without the financial support of CSIRO, CRCSI, GA, and BNHCRC, direction from members of the advisory panel (Peter Woodgate, Adam Lewis, Alex Held and Arnold Dekker) and input from reviewers and contributors.

Volumes 1 and 2 of this series are based on text originally published in Harrison and Jupp (1989, 1990, 1992 and 1993)<sup>1</sup>. Many illustrations and some text from these publications have been reproduced with permission from CSIRO. Selected tables and text have been reproduced (with amendments) from GA (2011), GA (2013a, 2013b)<sup>2</sup> and CSIRO (2012)<sup>3</sup>.

Other contributors are gratefully acknowledged:

- Chapter 15 authors: Glenn Newnham, John Armston, Bruce Forster and Catherine Ticehurst;
- reviewers: Clive Fraser (Sections 1, 2, 10, 11 and 12), John Richards (Section 13), Terry Cocks (Sections 13 and 14), Daniel Jaksa (Section 3, including Excursus), Alan Marks (Sections 6 to 9), Murray Richardson (Sections 6 to 8), Andrew Lewis (Section 7), Steve Tatham (Section 9), Zheng-Shu Zhou (Section 15), and Alfredo Huete and Laurie Chisholm (various sections);
- illustrations: Norman Mueller kindly supplied most of the lovely images; other contributors of graphical material include: Chris Roelfsema, Cheryl Brown, Christopher Griffin, Matthew Paget, Megan Lewis, Murray Richardson, Andrew Lewis, Darius Culvenor, Michael Schaefer, Thomas Schroeder, Arnold Dekker, David Lamb, Nina Putica, Arko Lucieer, Robert Norman, Ian Grant, James Prior, Graham Donald, Gary Shaw, John Le Marshall, Antoni Rogalski, Gail Kelly, Svetla Hristov-Veleva, Dave Winker, Kim Richardson;
- Paul Cockram and Matej Hrcek, who ‘translated’ the Harrison and Jupp (1989, 1990) files from Quark Express 2.0;
- Joost Kuckartz for meticulous formatting of references and equations, plus general editing;
- Daniel Rawson (Accessible Publication & Template Design) for layout and formatting;
- Carl Davies (CMDphotographics) for bespoke graphical illustrations; and
- last, but not least, Pete Harrison for last minute graphical updates.

We thank those owners of copyrighted illustrative material for permission to reproduce their work: Geoscience Australia, CHARIM, UNSW, CNES, Airbus D&S, Planet, ESA, IPCC, Lawrence Braille and MIT Lincoln Laboratory. Credits for individual illustrations are provided below the relevant graphic.

- 
1. Harrison, B.A., and Jupp, D.L.B. (1989) Introduction to Remotely Sensed Data: Part ONE of the microBRIAN Resource Manual. CSIRO, Melbourne. 156pp.  
Harrison, B.A., and Jupp, D.L.B. (1990) Introduction to Image Processing: Part TWO of the microBRIAN Resource Manual CSIRO, Melbourne. 256pp.  
Harrison, B.A., and Jupp, D.L.B. (1992) Image Rectification and Registration: Part FOUR of the microBRIAN Resource Manual. MPA, Melbourne.  
Harrison, B.A., and Jupp, D.L.B. (1993) Image Classification and Analysis: Part THREE of the microBRIAN Resource Manual. MPA, Melbourne.
  2. Geoscience Australia (2011) Continuity of Earth Observation Data for Australia: Operational Requirements to 2015 for Lands, Coasts and Oceans. Geoscience Australia, Canberra.  
Geoscience Australia (2013a) GA Earth Observation Product Description Framework and Templates. Unpublished report by Barbara Harrison, February 2013.  
Geoscience Australia (2013b) Draft Report on the National Dynamic Land Cover Dataset (Version 2). Unpublished report by Barbara Harrison, June 2013.
  3. CSIRO (2012) Continuity of Earth Observation Data for Australia: Research and Development Dependencies to 2020. CSIRO, Canberra.

# Table of Contents

Acknowledgements	i
------------------	---

<b>1 Introduction</b>	<b>1</b>
1.1 Why Observe the Earth?	1
1.2 What is Earth Observation?	1
1.2.1 Platforms and sensors	1
1.2.2 Indirect observations	3
1.2.3 A philosophical interlude	6
1.3 Observing the Earth	8
1.3.1 Historical background	8
1.3.2 EO data characteristics	10
1.4 Using Earth Observations	14
1.4.1 Detecting and mapping features	15
1.4.2 Monitoring changes	15
1.4.3 Modelling processes	17
1.5 The Global Picture	18
1.5.1 The Global Earth Observation System of Systems	18
1.5.2 Essential climate variables	18
1.6 Key Terms	21
1.7 Further Information	22
1.8 References	23

## Background 25

<b>2 Scientific Foundations</b>	<b>27</b>
2.1 Energy, Mass and Fundamental Forces	27
2.2 Matter	28
2.3 Measurement	28
2.3.1 Scales of measurement	29
2.3.2 International System of Units (SI)	29
2.3.3 SI metric prefixes	30
2.3.4 SI units for measuring waves	30
2.3.5 Angles	31
2.4 Force Fields	32
2.5 Waves	33
2.5.1 Wave types and characteristics	33
2.5.2 Reflection, refraction and diffraction	34
2.5.3 Polarisation	36
2.5.4 The Doppler effect	36
2.5.5 Coherence	36



<b>2.6</b>	Properties of EMR	36
2.6.1	Radiometric terms	36
2.6.2	Spectral terms	38
2.6.3	Photometric terms	38
<b>2.7</b>	Colour and Human Vision	38
2.7.1	Human visual system	38
2.7.2	Perception of colour and brightness	39
2.7.3	Colour models	40
<b>2.8</b>	Optics	41
2.8.1	Theories	41
2.8.2	Lenses	41
<b>2.9</b>	Radiation laws	43
2.9.1	Inverse-square law	43
2.9.2	Beer-Lambert law	45
<b>2.10</b>	Heat and Temperature	45
2.10.1	Thermal properties of matter	45
2.10.2	Latent heat	46
2.10.3	Thermodynamics	47
<b>2.11</b>	Blackbody Radiation	47
2.11.1	Stefan-Boltzmann's law	47
2.11.2	Kirchhoff's law	48
2.11.3	Wien's displacement law	48
2.11.4	Planck's law	48
2.11.5	Other bodies	48
<b>2.12</b>	Further Information	49
<b>2.13</b>	References	50
<b>3</b>	<b>Planet Earth</b>	<b>51</b>
3.1	The Earth in Space	51
3.2	Structure of the Earth	53
3.3	Shape of the Earth	56
3.4	Further Information	61
3.5	References	61
<b>4</b>	<b>Earth Systems and Processes</b>	<b>63</b>
4.1	Earth System Science	63
4.1.1	Atmosphere	64
4.1.2	Hydrosphere	66
4.1.3	Geosphere	66
4.1.4	Biosphere	67
4.2	Earth System Processes	67
4.2.1	Energy	67
4.2.2	Water	72
4.2.3	Earth	73
4.2.4	Carbon	75
4.3	Further Information	76
4.4	Reference	76

<b>5 Electromagnetic Radiation</b>	<b>79</b>
5.1 The EM Spectrum	79
5.2 Reflectance and Emission	81
5.2.1 Reflected energy	81
5.2.2 Emitted energy	83
5.3 Spectral Regions	84
5.4 Atmospheric Interactions	90
5.5 Further Information	93
5.6 References	93
<b>6 Radioactivity</b>	<b>95</b>
6.1 Introducing Radioactivity	95
6.2 Gamma Rays	96
6.3 Further Information	100
6.4 References	100
<b>7 Magnetism</b>	<b>101</b>
7.1 Introducing Magnetism	101
7.2 Magnetic Field	102
7.3 The Earth's Magnetic Field	103
7.4 Geomagnetism	106
7.5 Further Information	109
7.6 References	109
<b>8 Gravity</b>	<b>111</b>
8.1 The Earth's Gravitational Field	111
8.2 Measuring Gravity	113
8.3 Gravity Applications	115
8.4 Further Information	115
8.5 References	115
<b>9 Vibrations</b>	<b>117</b>
9.1 Sound Waves	117
9.2 Seismic Waves	119
9.2.1 What are earthquakes?	119
9.2.2 Types of seismic waves	121
9.2.3 Using seismic waves to determine the structure of Earth	122
9.2.4 Detecting seismic waves	123
9.3 Further Information	125
9.4 References	125



## Platforms for Earth Observation

127

<b>10 Ground-based Platforms</b>	<b>129</b>
10.1 In situ	129
10.2 Mobile Sensors	134
10.3 Citizen Science and Crowdsourcing	136
10.4 Further Information	137
10.5 References	137
<b>11 Airborne Platforms</b>	<b>139</b>
11.1 Manned Aircraft	140
11.2 Remotely Operated Aircraft	143
11.3 Further Information	144
11.4 References	144
<b>12 Spaceborne Platforms</b>	<b>145</b>
12.1 Manned Spacecraft	145
12.2 Satellites	146
12.2.1 Geostationary	148
12.2.2 Polar orbiting	156
12.3 Further Information	164
12.4 References	164

## EMR Sensors for Earth Observation

167

<b>13 Sensing Electromagnetic Radiation</b>	<b>169</b>
13.1 Measuring Electromagnetic Radiation	169
13.2 Earth Observation Sensors	170
13.2.1 Passive sensors	171
13.2.2 Active sensors	172
13.2.3 Sounders	172
13.3 Sensor Design Constraints	172
13.4 Sensor Performance Metrics	173
13.5 CEOS Sensor Categories	175
13.6 Further Information	178
13.7 References	178
<b>14 Passive Imaging Systems</b>	<b>179</b>
14.1 Optical and thermal sensor components	180
14.2 Image formation	183
14.2.1 Electromechanical	184
14.2.2 Linear array	185
14.2.3 Central perspective	186
14.3 Optical	186
14.3.1 Panchromatic	188
14.3.2 Multispectral	190
14.3.3 Hyperspectral	195

14.4	Thermal infrared	197
14.5	Passive microwave	201
14.6	Further Information	201
14.7	References	202
<b>15</b>	<b>Active Imaging Systems</b>	<b>203</b>
15.1	Lidar	203
15.2	Radar	207
15.2.1	Side-Looking Airborne Radar (SLAR) or Real Aperture Radar (RAR)	209
15.2.2	Synthetic Aperture Radar (SAR)	210
15.3	Further Information	213
15.4	References	213
<b>16</b>	<b>Non-imaging and Sounding Systems</b>	<b>215</b>
16.1	Non-imaging systems	217
16.1.1	Passive	217
16.1.2	Active	217
16.2	Sounding Systems	219
16.2.1	Passive	219
16.2.2	Active	220
16.3	Further Information	226
16.4	References	226



# List of Figures

<b>Figure 1.1</b> Earth from space	2
<b>Figure 1.2</b> Space photo of Berlin at night	3
<b>Figure 1.3</b> Median mosaic of Landsat-8 OLI	4
<b>Figure 1.4</b> From observation domain to attribute domain	5
<b>Figure 1.5</b> Data-Information-Knowledge-Wisdom triangle	7
<b>Figure 1.6</b> MODIS global composite image	8
<b>Figure 1.7</b> Historical development of remote sensing	9
<b>Figure 1.8</b> Nanosatellite imagery	10
<b>Figure 1.9</b> CubeSat	11
<b>Figure 1.10</b> Scales of EO	13
<b>Figure 1.11</b> Monthly composite	15
<b>Figure 1.12</b> Lake Disappointment	15
<b>Figure 1.13</b> Construction of Elizabeth Quay, Perth	16
<b>Figure 1.14</b> Modelling photosynthetically active radiation	17
<b>Figure 1.15</b> The global picture	19
<b>Figure 2.1</b> Planar and solid angles	32
<b>Figure 2.2</b> Force field example	32
<b>Figure 2.3</b> Longitudinal and transverse waves	33
<b>Figure 2.4</b> Components of waves	34
<b>Figure 2.5</b> Longitudinal or compression waves	34
<b>Figure 2.6</b> Law of reflection	35
<b>Figure 2.7</b> Specular and diffuse reflectors	35
<b>Figure 2.8</b> Refraction and diffraction	35
<b>Figure 2.9</b> Radiometric measurements	37
<b>Figure 2.10</b> Relative light absorption of human cones	39
<b>Figure 2.11</b> Perception of light intensity changes	39
<b>Figure 2.12</b> Additive and subtractive colour mixing	40
<b>Figure 2.13</b> Relationship between additive and subtractive primary colours	41
<b>Figure 2.14</b> Convex and concave lenses	42
<b>Figure 2.15</b> Field of view	42
<b>Figure 2.16</b> Object more than twice focal length from convex lens	42
<b>Figure 2.17</b> Inverse-square law	44

<b>Figure 2.18</b> Beer-Lambert law	45
<b>Figure 2.19</b> Blackbody radiation	48
<b>Figure 2.20</b> Spectral emissivity and spectral radiant exitance of various bodies	49
<b>Figure 3.1</b> Our solar system	51
<b>Figure 3.2</b> Earth's axis of rotation	52
<b>Figure 3.3</b> Variation in solar radiation due to Earth's elliptical orbit	53
<b>Figure 3.4</b> Cross-section of Earth	54
<b>Figure 3.5</b> Tectonic plates	55
<b>Figure 3.6</b> Tectonic plate boundaries	55
<b>Figure 3.7</b> Modelling the shape of the Earth	56
<b>Figure 3.8</b> Local versus geocentric datums	57
<b>Figure 3.9</b> Average number of visible satellites across all planned constellations	59
<b>Figure 3.10</b> Satellite Laser Ranging	60
<b>Figure 4.1</b> Earth System Science	63
<b>Figure 4.2</b> Processes and interactions within Earth System Science	64
<b>Figure 4.3</b> Interrelationship between atmosphere and ionosphere	65
<b>Figure 4.4</b> Impact of ionosphere on radio frequency waves	65
<b>Figure 4.5</b> Global ionospheric foF2 map	66
<b>Figure 4.6</b> Energy distribution and net radiation	68
<b>Figure 4.7</b> Earth's energy budget	68
<b>Figure 4.8</b> Solar illumination angle variation with latitude	70
<b>Figure 4.9</b> Variations in insolation with latitude and annual cycle	70
<b>Figure 4.10</b> Typical daily insolation cycle on equinox days	71
<b>Figure 4.11</b> Annual cycle of total daily solar irradiance	71
<b>Figure 4.12</b> Reflected solar radiation	72
<b>Figure 4.13</b> Outgoing radiation	72
<b>Figure 4.14</b> Net radiation	72
<b>Figure 4.15</b> Hydrological cycle	73
<b>Figure 4.16</b> Rock cycle	74
<b>Figure 4.17</b> Carbon cycle	75
<b>Figure 5.1</b> Electromagnetic wave	79
<b>Figure 5.2</b> Electromagnetic spectrum	80
<b>Figure 5.3</b> Common remote sensing systems	81
<b>Figure 5.4</b> Incident energy components	82
<b>Figure 5.5</b> Albedo of different materials	83



<b>Figure 5.6</b>	Solar radiation at top of atmosphere and at sea level	84
<b>Figure 5.7</b>	Refraction of polychromatic light through a prism	84
<b>Figure 5.8</b>	Reflectance characteristics of typical green leaf structure	85
<b>Figure 5.9</b>	Idealised spectral reflectance curves	86
<b>Figure 5.10</b>	Seeing water from space—Kerang, Victoria	87
<b>Figure 5.11</b>	Mapping permanent water	88
<b>Figure 5.12</b>	WOfS continental map	89
<b>Figure 5.13</b>	Atmospheric layers	90
<b>Figure 5.14</b>	Atmospheric opacity	92
<b>Figure 6.1</b>	Stable nuclei	95
<b>Figure 6.2</b>	Gamma ray ionisation	97
<b>Figure 6.3</b>	Gamma spectroradiometry	98
<b>Figure 6.4</b>	Radiometric map of Australia	99
<b>Figure 7.1</b>	Magnetic fields	101
<b>Figure 7.2</b>	Magnetic vector components	102
<b>Figure 7.3</b>	Magnetosphere	103
<b>Figure 7.4</b>	Southern Aurora	103
<b>Figure 7.5</b>	Geomagnetic observation network for Australia	104
<b>Figure 7.6</b>	Magnetic time series	104
<b>Figure 7.7</b>	Total intensity variability over Australia	105
<b>Figure 7.8</b>	AGRF 2010 model at epoch 2010.0	106
<b>Figure 7.9</b>	Aeromagnetic imagery	107
<b>Figure 7.10</b>	Australian Magnetic Anomaly Grid	108
<b>Figure 8.1</b>	Gravity, gravity variations, mass transport and distribution	112
<b>Figure 8.2</b>	Geoid surface	112
<b>Figure 8.3</b>	Global gravity field anomalies	113
<b>Figure 8.4</b>	Global gravity derived from GOCE	113
<b>Figure 8.5</b>	Isostatic Residual Gravity Anomaly Map of Australia	114
<b>Figure 9.1</b>	Speed of sound with varying water depth	118
<b>Figure 9.2</b>	Decibel range	118
<b>Figure 9.3</b>	Shock waves and sonic booms	119
<b>Figure 9.4</b>	Global earthquake occurrence	120
<b>Figure 9.5</b>	Earthquake focus and epicentre	120
<b>Figure 9.6</b>	Body waves	121
<b>Figure 9.7</b>	Surface waves	122

<b>Figure 9.8</b>	Shadow zones for seismic waves	123
<b>Figure 9.9</b>	Global earthquake frequency and energy	124
<b>Figure 10.1</b>	Dual wavelength Echidna™ LIDAR (DWEL)	130
<b>Figure 10.2</b>	VEGNET scanner	131
<b>Figure 10.3</b>	Marine in situ sensors	131
<b>Figure 10.4</b>	Flux Tower Function	132
<b>Figure 10.5</b>	NEON flux tower measurements	132
<b>Figure 10.6</b>	TERN OzFlux flux towers	133
<b>Figure 10.7</b>	Mobile sensors for Earth Observation	134
<b>Figure 10.8</b>	Hand-held sensors for Earth Observation	134
<b>Figure 10.9</b>	UNETracker	135
<b>Figure 10.10</b>	Livestock pasture usage compared with pasture productivity	135
<b>Figure 11.1</b>	Effect of wide scan angle	140
<b>Figure 11.2</b>	Nearmap imagery	141
<b>Figure 11.3</b>	Some manned airborne platforms	141
<b>Figure 11.4</b>	Urban development	142
<b>Figure 11.5</b>	Port operations	142
<b>Figure 11.6</b>	Monitoring construction projects	142
<b>Figure 11.7</b>	Mining operations	142
<b>Figure 11.8</b>	Remotely piloted aircraft systems	143
<b>Figure 12.1</b>	Comparison of satellite orbits	147
<b>Figure 12.2</b>	Some orbital inclinations	147
<b>Figure 12.3</b>	Satellite density around Earth	148
<b>Figure 12.4</b>	Geostationary orbit	149
<b>Figure 12.5</b>	Network of geostationary satellites	150
<b>Figure 12.6</b>	Himawari-8 disks	151
<b>Figure 12.7</b>	The launch of the first weather satellite, TIROS-1, in 1960	152
<b>Figure 12.8</b>	Early meteorological satellite imagery	152
<b>Figure 12.9</b>	A Himawari-8 colour image	154
<b>Figure 12.10</b>	Wind vectors over GMS-5 image of the Tasman Sea	155
<b>Figure 12.11</b>	Himawari-8 Atmospheric Motion Vectors (AMVs)	155
<b>Figure 12.12</b>	Orbit parameters	156
<b>Figure 12.13</b>	Daily acquisitions for MODIS/Aqua and MODIS/Terra	157
<b>Figure 12.14</b>	Landsat satellites	158
<b>Figure 12.15</b>	Polar orbiting satellites provide a variety of spatial scales	159

<b>Figure 13.1</b>	Information acquired by sensors	173
<b>Figure 13.2</b>	Sensor performance terms	174
<b>Figure 13.3</b>	Spectral response function of Hyperion SWIR band	174
<b>Figure 13.4</b>	Relative spectral variation across Hyperion image line	174
<b>Figure 14.1</b>	Simple example of monochromatic sensor	181
<b>Figure 14.2</b>	Spectral response functions	183
<b>Figure 14.3</b>	Scanning mechanisms	183
<b>Figure 14.4</b>	Operation of electromechanical aircraft scanner	184
<b>Figure 14.5</b>	MSS measurements along one scan line	184
<b>Figure 14.6</b>	Whiskbroom versus pushbroom scanners	185
<b>Figure 14.7</b>	Panchromatic imagery from Landsat-7 ETM+ and Landsat-8 OLI	188
<b>Figure 14.8</b>	Decommissioned Landsat-5 satellite visible from Landsat-8	189
<b>Figure 14.9</b>	Image sharpening	189
<b>Figure 14.10</b>	Comparison of bands acquired by Landsat-7, Landsat-8 and Sentinel-2	190
<b>Figure 14.11</b>	Differentiation within spectral regions	191
<b>Figure 14.12</b>	Colour composites	192
<b>Figure 14.13</b>	Landsat ETM+ optical channels	193
<b>Figure 14.14</b>	Gross Annual Pasture Production (GAPP) from 2007 to 2010 for southwestern WA	194
<b>Figure 14.15</b>	Compilation of hyperspectral data cube	195
<b>Figure 14.16</b>	Hyperspectral image interpretation	196
<b>Figure 14.17</b>	Simulated Landsat TM spectral signature	197
<b>Figure 14.18</b>	Detectivity of IR detectors	198
<b>Figure 14.19</b>	Spectral response of Landsat thermal bands	199
<b>Figure 14.20</b>	Thermography	200
<b>Figure 15.1</b>	Lidar operation	204
<b>Figure 15.2</b>	Perspective view of classified point cloud	205
<b>Figure 15.3</b>	Enlarged perspective view showing details of towers and power lines	205
<b>Figure 15.4</b>	Terrain model	206
<b>Figure 15.5</b>	The microwave and radio wave spectra	207
<b>Figure 15.6</b>	Radar wavelengths	208
<b>Figure 15.7</b>	Interaction of radar wavelengths with vegetation	208
<b>Figure 15.8</b>	Operation of side-looking airborne radar	209
<b>Figure 15.9</b>	Radar image distortions	210
<b>Figure 15.10</b>	Impact of radar distortions in imagery	210
<b>Figure 15.11</b>	Operation of synthetic aperture radar	211



<b>Figure 15.12</b>	Comparing SAR and Optical imagery	211
<b>Figure 16.1</b>	1 500 hPa height anomaly correlations	216
<b>Figure 16.2</b>	Laser altimeter	217
<b>Figure 16.3</b>	Radar altimetry	218
<b>Figure 16.4</b>	Cryosat radar altimeter	218
<b>Figure 16.5</b>	Wind estimates derived from SeaWinds observations	219
<b>Figure 16.6</b>	Profile of LITE observations over Sahara Desert	221
<b>Figure 16.7</b>	Profiles of CALIOP observations over Sahara Desert	221
<b>Figure 16.8</b>	TRMM Precipitation Radar	222
<b>Figure 16.9</b>	Cloudsat Cloud Profiling Radar	223
<b>Figure 16.10</b>	Spectral resolution of HIRS/2 compared with simulated AIRS spectra	225

# List of Tables

<b>Table 1.1</b>	Logical stages in EO data use	5
<b>Table 1.2</b>	Data-information-knowledge-wisdom hierarchy	6
<b>Table 1.3</b>	Observations, measurements and attributes	11
<b>Table 1.4</b>	GCOS essential climate variables	20
<b>Table 2.1</b>	Base Units in the International System of Units (SI)	29
<b>Table 2.2</b>	Derived Units in the International System of Units (SI)	29
<b>Table 2.3</b>	SI metric prefixes	30
<b>Table 2.4</b>	SI units of length	31
<b>Table 2.5</b>	SI units of frequency	31
<b>Table 2.6</b>	Radiometric terms	37
<b>Table 2.7</b>	SI units	37
<b>Table 2.8</b>	Spectral terms defined in terms of wavelength	38
<b>Table 2.9</b>	Equivalent photometric terms	38
<b>Table 2.10</b>	Energy required to convert 10 g ice to steam	46
<b>Table 3.1</b>	Comparison of planetary features	52
<b>Table 4.1</b>	Composition of planet Earth	66
<b>Table 5.1</b>	Sample albedo values	83
<b>Table 5.2</b>	Atmospheric layers	91
<b>Table 5.3</b>	Global cloud properties	91
<b>Table 5.4</b>	EMR spectral regions and atmospheric windows	92
<b>Table 6.1</b>	Isotope properties	97
<b>Table 7.1</b>	Magnetic components	102
<b>Table 12.1</b>	Satellite orbital characteristics	146
<b>Table 12.2</b>	Types of satellite orbits	147
<b>Table 12.3</b>	Geostationary meteorological satellites	150
<b>Table 12.4</b>	JMA Australasian coverage satellites	151
<b>Table 12.5</b>	Some Important Series of Weather Satellites	153
<b>Table 12.6</b>	Polar orbiting satellites	162
<b>Table 13.1</b>	Spectral regions observed by EO sensors	170
<b>Table 13.2</b>	Common sensor performance metrics	173
<b>Table 13.3</b>	CEOS sensor categories <sup>49</sup>	175
<b>Table 13.4</b>	EO sensors commonly used in Australia	177

<b>Table 14.1</b>	Potential components of generic passive sensor	181
<b>Table 14.2</b>	SWIR detector categories	182
<b>Table 14.3</b>	EMR sensitive materials	182
<b>Table 14.4</b>	Examples of satellite optical sensors	187
<b>Table 14.5</b>	Landsat TM/ETM+ channels	190
<b>Table 14.6</b>	Landsat OLI/TIRS channels	191
<b>Table 14.7</b>	Examples of hyperspectral imagers	197
<b>Table 14.8</b>	Commonly used thermal imaging sensors	200
<b>Table 14.9</b>	Examples of satellite passive microwave sensors	201
<b>Table 15.1</b>	Standard radar frequency and wavelength letter bands.	207
<b>Table 15.2</b>	Polarisation options for radar signals	209
<b>Table 15.3</b>	Examples of active and future satellite SAR sensors	212
<b>Table 16.1</b>	Characteristics of AIRS and HIRS sounding instruments	224

# List of Excurses

<b>Excursus 1.1</b> —Observing Australia	4
<b>Excursus 1.2</b> —How do EO sensors identify healthy vegetation?	5
<b>Excursus 1.3</b> —EO processing stages	12
<b>Excursus 3.1</b> —Datums and Geoids	57
<b>Excursus 3.2</b> —Space Geodesy and Reference Frames	59
<b>Excursus 4.1</b> —Insolation	70
<b>Excursus 5.1</b> —Water Observations from Space (WOfS)	86
<b>Excursus 6.1</b> — Australian Radiometric Map	99
<b>Excursus 7.1</b> —Australian Geomagnetic Reference Field Model	106
<b>Excursus 7.2</b> —Australian Magnetic Anomaly Grid	108
<b>Excursus 8.1</b> —Australian Gravity Anomaly Map	114
<b>Excursus 10.1</b> —GPS tracking in Precision Agriculture	135
<b>Excursus 11.1</b> —High resolution aerial imagery	142
<b>Excursus 12.1</b> —Meteorological Satellites	152
<b>Excursus 14.1</b> —Pastures from Space	194
<b>Excursus 15.1</b> —Airborne Lidar Applications	205
<b>Excursus 16.1</b> —Value of EO to Numerical Weather Prediction	215
<b>Excursus 16.2</b> —Meteorological Sensors and Applications	224







# 1 Introduction

## 1.1 Why Observe the Earth?

The Earth is our home. Our livelihood—past, present and future—is inextricably bound to the diversity and integrity of our planet. Our survival will inevitably depend on prudent management of its resources.

For several millennia, human civilisations have conducted a wide variety of inventories of Earth's resources. This information has allowed societies to understand their environment, and also to plan and monitor their opportunities for development and sustainability.

Mapping and monitoring the Earth's resources is a fundamental activity for governments, industries and communities at global, national, regional and now local scales. As the demands of growing populations emphasise the finite nature of our natural resources, their accurate and timely assessment has become

essential to land and water managers for both development and conservation purposes. Frequent, consistent and accurate information over large areas is needed to fully understand ecosystem processes and functions before we can reliably monitor and predict the composition and condition of the lands, coasts, oceans and atmosphere of planet Earth. Fortunately, the technology available to provide this information, as well as insight into the characteristics and impact of our celestial neighbours, has also become more sophisticated in the form of Earth Observation (EO; see Figure 1.1).

## 1.2 What is Earth Observation?

Gathering information about the Earth using remote sensing technologies is called Earth Observation (EO). Remote sensing refers to making observations of an object using a device that is physically remote from it. This term is most frequently used to describe imagery of the Earth and its atmosphere recorded by airborne and satellite-borne sensors (see Figure 1.2), but can also encompass observations from ground-based sensors.

### 1.2.1 Platforms and sensors

EO sensors basically detect energy from Earth, which may be either reflected from another source or intrinsic to our own planet. Remote sensing devices have been designed to detect various types of energy, including electromagnetic radiation (EMR), radioactivity, magnetism, gravity, and sound and seismic waves (see Sections 1 to 9 respectively). By definition, these sensors generally do not have direct contact with the Earth, so they need to be carried by an elevated platform. (An exception to this is ground-penetrating radar antennae, which achieve a stronger signal when in contact with the ground.) Three broad groups of platforms are used to carry EO sensors:

- spaceborne—satellites, shuttles, or space stations;
- airborne—manned aircraft, unmanned aerial vehicles, balloons or blimps; and
- ground-based—in situ, mobile devices, or animals (including humans).

**Background image:** Landsat-8 image of Rockhampton, Queensland, and nearby reefs acquired on 6 July 2016 (displayed using bands 6, 5, 3 as RGB).

**Source:** Norman Mueller, Geoscience Australia

Remote sensing devices are either passive, that is, the sensor detects energy from other sources such as the Sun, or active, in that the sensor emits pulses of energy then records a response. Some common examples of passive EO sensors include:

- eyes—detecting reflected light waves from ambient lighting;
- ears—detecting sound waves from ambient sounds; and
- digital cameras and sensors—measuring reflected or emitted visible and non-visible energy from ambient sources, e.g. mobile phone cameras, or satellite based imaging sensors.

Examples of active EO sensors include:

- digital camera with flashlight—measuring reflected light waves from both flashlight and ambient lighting;
- sonar—measuring echoes of sound waves generated by the sensor;
- lidar —measuring reflected light waves generated by the sensor; and
- radar—measuring reflected radio waves generated by the sensor.

Various sources of EO data are detailed in subsequent sections of this volume. One of the most commonly used sources of EO imagery is acquired by the Landsat series of satellites (see Excursus 1.1).

---

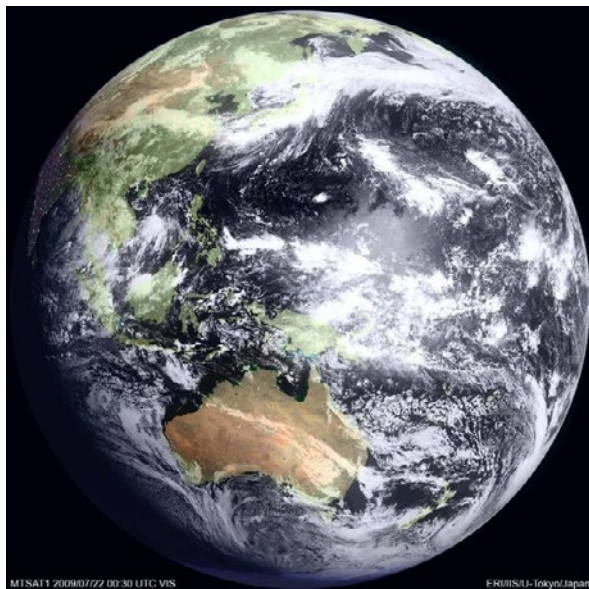
*In the fields of observation chance favours the prepared mind*  
(Louis Pasteur)

---

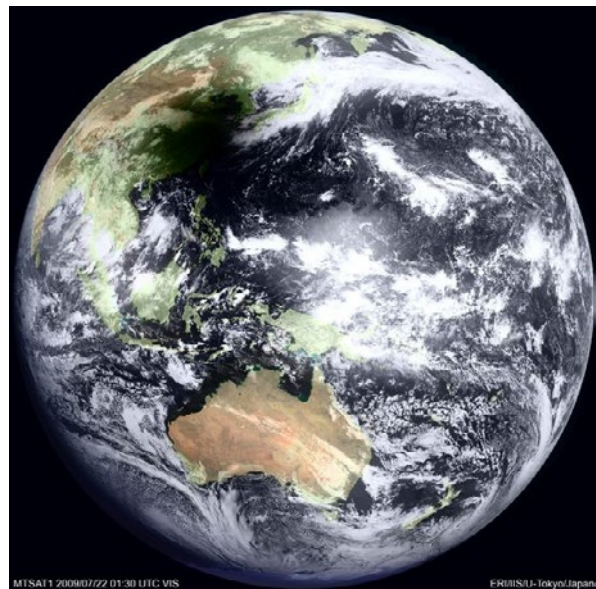
**Figure 1.1** Earth from space

The Japanese geostationary satellite (MTSAT) imaged the solar eclipse on 22 July 2009 over eastern China, when the Moon's shadow completely overlapped the Sun's disk and plunged Taiwan and southeast China into darkness.

a. MTSAT image taken at 8:30 am, combined with night lights background (from NASA Blue Marble Collection).



b. MTSAT image taken at 9:30 am showing locations in the centre of this shadow (the umbra) experiencing a total eclipse, while locations on the edge (penumbra) experienced a partial eclipse.

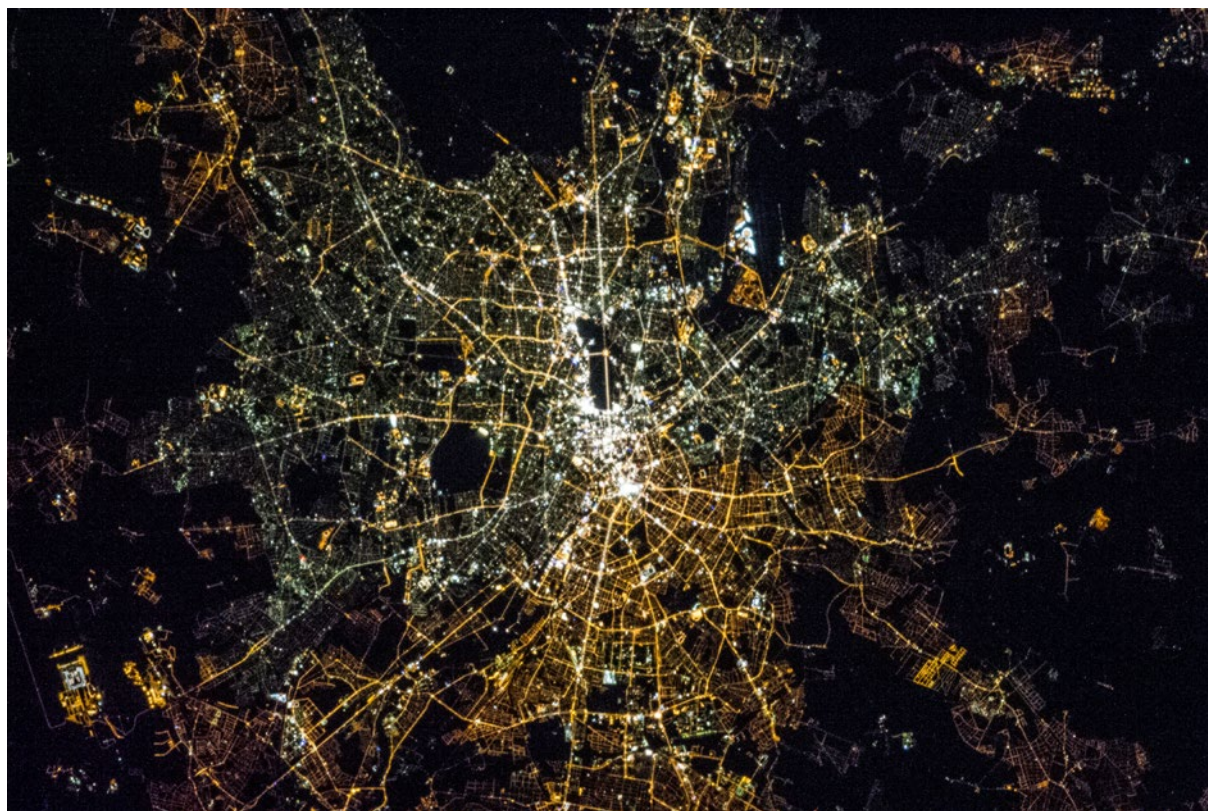


Source: NASA. Retrieved from <http://earthobservatory.nasa.gov/IOTD/view.php?id=39520>



**Figure 1.2** Space photo of Berlin at night

This photo, taken from the International Space Station (ISS) in April 2013, differentiates between East and West Berlin on the basis of night lighting. Lighting with sodium-vapour lamps in East Berlin is more yellow than the predominantly fluorescent (mercury arc and gas lamp) lighting in West Berlin.



Source: Chris Hadfield, NASA. Retrieved from <http://eo1.jsc.nasa.gov/Databaselmages/ESC/large/ISS035/ISS035-E-17210.JPG>

### 1.2.2 Indirect observations

The key characteristic that distinguishes remote sensors from other sensing devices is that their observations are indirect. Being remote, their sensing mechanism does not rely on contact with the object being observed, but rather detects some form of energy from the object. Use of remote sensing technologies assumes that the detected energy is indicative of properties of the object. Before observations from remote sensors can be used with confidence, their relationship with known properties of the Earth must be established using some form of reference data.

Interpretation of observations from EO sensors thus involves at least one level of inference (or indirection). The energy detected by an EO sensor is related to properties of the Earth's features and/or its physical, chemical or biological processes (see Excursus 1.2). The generalised process of using remotely sensed observations could be described in terms of three logical stages:

- acquisition—observations are made of the object or surface;
- processing—observed data is modified to represent a property of the object or surface; and
- interpretation—processed data is analysed with reference data for a specific end use or application.

These stages are implicitly linked by models that rely on prior knowledge of the:

- object (or surface) and its properties—observation domain;
- sensor and its properties—measurement domain; and
- intended end use of the remotely sensed data—attribute domain.

The relationships between stages, prior knowledge, and the underlying models are further developed in Table 1.1.



## Excursus 1.1—Observing Australia

**Source:** Norman Mueller, Geoscience Australia

**Further information:** Geoscience Australia: <http://www.ga.gov.au/>

The Landsat series of satellites has been observing Australia for several decades. The first Landsat satellite was launched in 1972 and quickly proved its value for global monitoring. Since then, a total of eight Landsat satellites have been launched (but Landsat-6 failed to reach orbit after launch). In some years, two Landsat satellites have been acquiring imagery.

The Landsat-1 to -5 satellites carried various sensors, with its multispectral scanner (MSS) being most commonly used for EO applications. Landsat-4 to Landsat-8 have carried a higher resolution MSS (originally called Thematic Mapper (TM), with successive improvements called ETM—enhanced TM— and ETM+). The MSS on board Landsat-8 is called the Operational Land Imager (OLI). A thermal sensor also acquires imagery on Landsat-5, -7, and -8, which is used to observe variations in surface temperature.

Australia established its own receiving station in

1979. In the current Landsat acquisition grid (WRS-2), 369 image scenes cover the Australian mainland and Tasmania. The current satellites, Landsat-7 and Landsat-8, fly over Australia every 16 days (8 days apart), creating 23 sets of scenes each year. Each satellite completes over 5,000 lapses around Earth each year, acquiring over 200,000 image scenes globally. Since the launch of Landsat-1, over half a million image scenes have been acquired over Australia, creating an unprecedented environmental record of our landscape and waterscape.

The mosaic shown in Figure 1.3 is a ‘synthetic image’, cleverly created by collecting all observations of Landsat-8 OLI over the less cloudy months (April to September) in 2014 and 2015, and calculating the median value of every pixel in those observations. This creates a ‘synthetic’ view of Australia, since each pixel is not a true observed value, but a statistical median value derived from a set of observations.

**Figure 1.3** Median mosaic of Landsat-8 OLI

All Landsat-8 OLI images acquired from April to September in 2014 and 2015 were selected, then the median value for each pixel was computed. This continental mosaic shows spatial variation in those median values.



**Source:** Norman Mueller, Geoscience Australia

**Table 1.1** Logical stages in EO data use

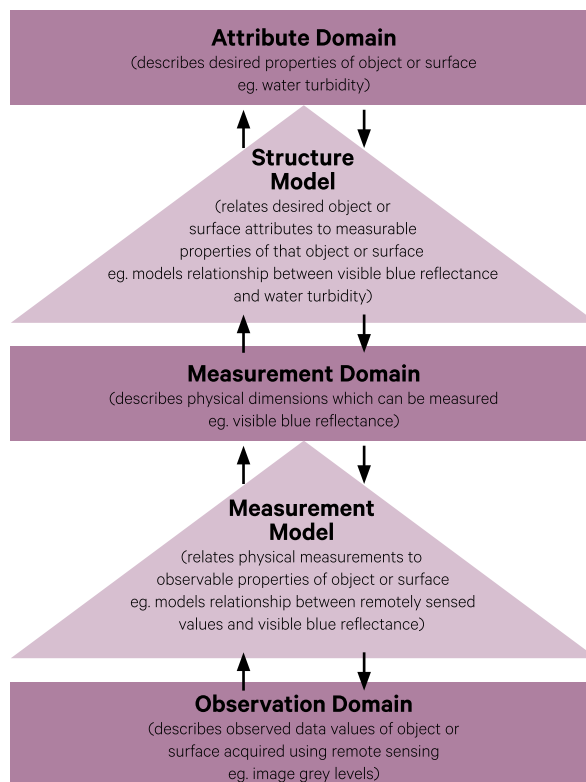
Stage	Description	Domain
Acquisition	Observe object or surface using remote sensing	Observation
Processing	Convert remote sensing observation to measurable property of object or surface using pre-defined measurement model	Measurement
Interpretation	Interpret measured properties of object or surface (that is, the converted remote sensing observation) in terms of a specific application using pre-defined structure model	Attribute

The indirect relationships between observation, measurement and variable domains are illustrated in Figure 1.4. An additional limitation, which must be considered, is that the observations we collect using a remote sensor only provide discrete samples of the potentially continuous range of measurements in any ‘measurement domain’. The measurement model also implicitly separates relevant information in the observations from ‘noise’, where the definitions of both relevant information and noise can differ for different applications. These concepts are further developed in Volume 1B—Sections 1 and 2.

While an individual image analysis exercise would progress from observations to attributes, the interconnections between these domains and models are invariably two-way. Improved understanding of attributes feeds back to improved tools and methods for acquisition and analysis. This ongoing cycle should form the basis of all scientific enquiry and is further considered in Volume 1B.

**Figure 1.4** From observation domain to attribute domain

Interpreting imagery from EO sensors is an indirect process, whereby a measurement model is used to transform remotely sensed observations to measurements of some measurable property, and a structure model is used to relate those measurements to application-specific attributes.



Adapted from: Harrison and Jupp (1989) Figure 33

## Excursus 1.2—How do EO sensors identify healthy vegetation?

Healthy vegetation appears green because green wavelengths of light are reflected, not absorbed, by photosynthesising foliage. Since the process of photosynthesis absorbs blue and red wavelengths, and the leaf structure reflects near infrared (NIR) wavelengths, green vegetation is characterised by high NIR reflectance and low visible red reflectance. Thus, identification of healthy vegetation using remote sensing relies on measuring NIR and visible red reflectance from the Earth's surface, then analysing the relative difference between these two measurements.

Before vegetation can be declared as healthy or otherwise on the basis of remotely sensed data, reference data is required to determine the threshold at which the relative difference between red and NIR reflectance measurements is significant. In this context, measurement necessarily implies that observations are calibrated to some defined standard, which enables them to be compared with other measurements that are calibrated to a comparable scale (see Section 2.3).

**Table 1.2** Data-information-knowledge-wisdom hierarchy

Zeleny (1987)		Ackoff (1989)				Bellinger et al. (2004)	
Concept	Definition	Concept	Definition	Timeframe	% Human Mind	Concept	Transition Process
Enlightenment	Sense of truth						
Wisdom	Know-why	Wisdom	Ability to see long-term consequences and evaluate them	Permanent	~0	Wisdom	
		Understanding	Ability to assess and correct for errors; Requires diagnosis and prescription	Aura of permanence	~10		Understanding Principles
Knowledge	Know-how	Knowledge	Refines information; Allows information to be transformed into instructions	Longer life span	~20	Knowledge	Understanding Patterns
Information	Know-what	Information	Data processed to be useful; Answers 'who', 'what', 'where', and 'when' questions	Ages rapidly	~30	Information	Understanding relations
Data	Know-nothing	Data	Product of observations; Symbols with no inherent structure or meaning	Transient	~40	Data	

### 1.2.3 A philosophical interlude

The three logical stages involved with using EO data directly correspond to the first three transitions outlined in the Data-Information-Knowledge-Wisdom (DIKW) hierarchy popularised by Ackoff (1989), and summarised in Table 1.2. The concepts of data, information, knowledge and wisdom are widely viewed as the building blocks of library and information science (Bernstein, 2009), and knowledge management (Zeleny, 1987).

While the following terms are sometimes used interchangeably in EO literature, the three equivalents below, and their definitions, are recommended for clarity:

- data ~ observations—raw representation(s) of a quantity;
- information ~ measurements—self-describing representation of a quantity, with defined scale and metadata; and
- knowledge ~ attributes—represents a quantity in terms of the application domain, and reflects the process that the interpreter is attempting to model.

We will not presume to suggest an equivalence for wisdom.

---

*Where is the wisdom we have lost in knowledge?  
Where is the knowledge we have lost in information?  
(Eliot, 1934)*

---

**Figure 1.5** Data-Information-Knowledge-Wisdom triangle

The Data-Information-Knowledge-Wisdom (DIKW) triangle represents the relative abundance of each type of ‘intelligence’ and the progression from data to wisdom. This sequence from data to wisdom is characterised by both decreasing volume and variety, and increasing control, understanding and connection. As a snapshot in time, It could also be argued that data is inherently relevant to the past, while derived wisdom should be relevant to the future. The antithesis of the DIKW hierarchy, the progression from folly to wisdom, reverses these relationships.



As illustrated in Figure 1.5a, the DIKW hierarchy is often represented as a triangle or pyramid in which the area or volume of each layer is indicative of the variety and volume of examples that exist for that layer. For example, the Data layer has the largest area, indicating the greatest number of data sources and the greatest number of data types. Conversely, in the smallest layer, Wisdom, there exist the fewest varieties and the smallest number of instances. Progression through this hierarchy has also been linked to increasing control, understanding and connectedness, as well as relevance to the passage of time.

Also of relevance to EO is the antithesis of the DIKW hierarchy discussed by Bernstein (2009) and illustrated in Figure 1.5b, where the extent of each antithesis layer is inversely proportional to its corresponding DIKW layer. For example, while there are few instances of wisdom, there are many of folly.

Science involves systematic enquiry into the structure and behaviour of the world using the tools of observation and experiment. This process should result in a base of knowledge and understanding about the world that is defensible. While the DIKW triangle implies that the process of moving from data to wisdom is one-directional, the resulting knowledge and wisdom also feed back to improved methods of data acquisition, processing and interpretation. The antithesis of the DIKW triangle could be attributed to a lack of enquiry.

Obviously, the goal of every EO project should be to increase our knowledge and understanding of the Earth. This task becomes more important and more difficult as both the volumes of available data sources and the expectations for instant answers increase at unprecedented rates. To maintain the integrity of EO it is imperative that its users remain focussed on attaining relevant and defensible knowledge outcomes—and understanding them.

---

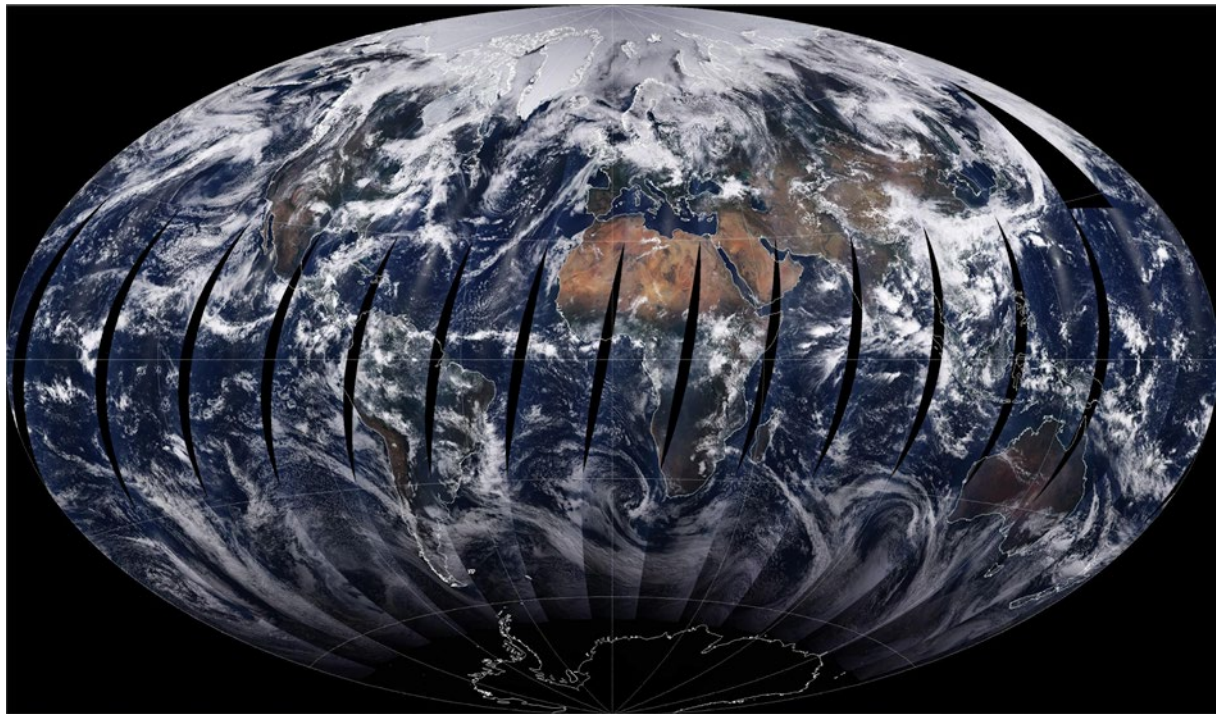
*One can survive without understanding, but not thrive. Without understanding one cannot control causes; only treat effect, suppress symptoms. With understanding one can design and create the future... people in an age of accelerating change, increasing uncertainty, and growing complexity often respond by acquiring more information and knowledge, but not understanding.*  
(Gharajedaghi and Ackoff, 1984)

---



**Figure 1.6** MODIS global composite image

This composite image demonstrates an example of the volume of data collected by one satellite sensor, MODIS, on 28 May 2001.



Source: Marc Imhoff, NASA

## 1.3 Observing the Earth

Remotely sensed data provide a synoptic or regional view of the Earth as well as the opportunity to observe and identify particular features and processes of interest. EO offers a unique perspective on our planet and delivers observations that are consistent and repeatable at a range of specific spatial and temporal scales. Sensing forms of energy that are outside the human visual range also allows early detection of many forms of environmental stress and degradation. These features combine to create a robust, flexible and cost-effective data source for mapping, monitoring and modelling Earth's resources (see Figure 1.6).

Relevant characteristics of the Earth are reviewed in Section 3. Many of these characteristics have been discovered or refined using remote sensing, including:

- precise measurements of distances to, and radiation from, other celestial bodies;
- more accurate models for the changing shape of the Earth;
- better models of the Earth's magnetic and gravitational fields;
- enhanced knowledge of the structural and chemical composition of the Earth's interior;

- global information concerning the extent and condition of land cover;
- detailed mapping of ocean colour, temperature and extent; and
- improved observations and models of the Earth's atmospheric processes.

### 1.3.1 Historical background

The origin of remote sensing of the Earth's surface (using sensors rather than eyes) can be traced back to the first photograph, which was taken in 1826 by Joseph Nicéphore Niépce looking onto the French countryside. The first aerial photograph was taken over Paris in 1858, by balloonist Gaspard-Félix Tourmachon Nadar, from an altitude of around 400 m. In 1908, the first photographs were taken from an aircraft being piloted by Wilbur Wright. Aerial photography was being used for civilian mapping, topography and cartography before World War 1, but its reconnaissance value was only realised and further developed during the two World Wars. Aerial photography and/or imagery can now be acquired using a range of platforms, including Remotely Piloted Aircraft Systems (RPAS) (which are also known as Unmanned Aerial Vehicles or UAV; see Section 11.2).

The first space photographs were taken from V-2 rockets in 1946. The first satellite, Sputnik, was launched in 1957 by the Soviet Union and was quickly followed by the US Corona Project in 1960, which demonstrated the vast potential of space photography. The first polar-orbiting meteorological satellite, TIROS-1, was also launched by the USA in 1960 and delivered operational weather imagery with global coverage from 1966 (see Excursus 12.1). The first of the Landsat series of satellites, originally called the Earth Resources Technology Satellite (ERTS), was launched in 1972 to map characteristics relating to land cover. This satellite has been followed by hundreds of spacecraft that routinely collect EO imagery at a range of scales for a wide variety of applications. Skylab, the first space station, was launched by the USA in 1973 as part of the Apollo program, and carried a range of remote sensing devices. The historical development of space-based EO is summarised in Figure 1.7.

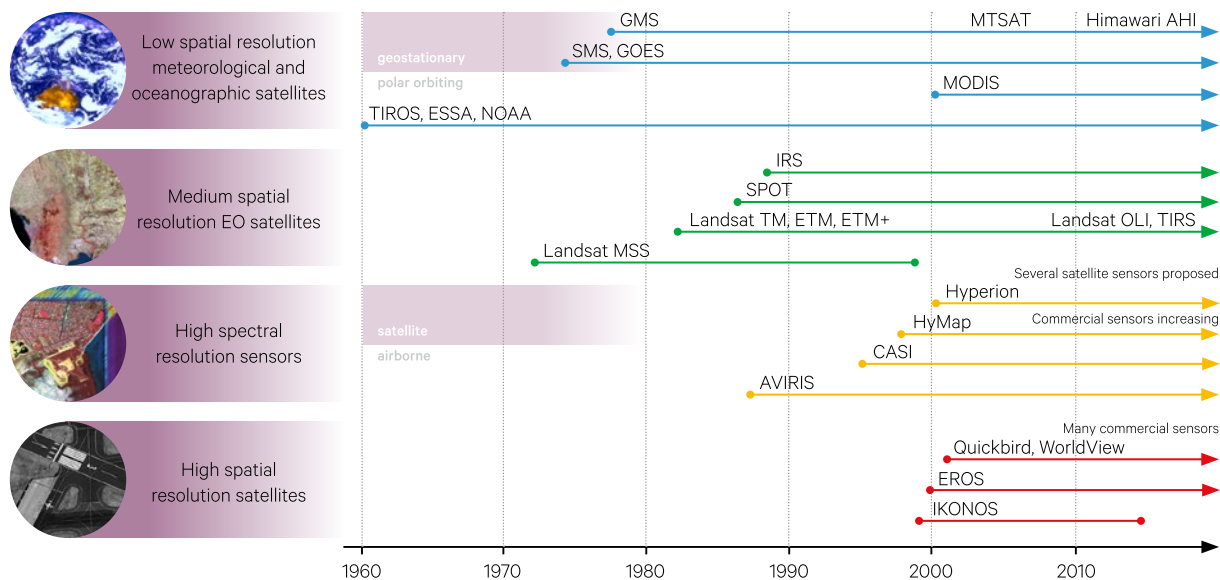
Both the quality and quantity of EO imagery has greatly increased since the initial EO satellites were launched, with an estimated 70 operational EO satellites currently providing public good (that is,

non-commercial) imagery and several hundred more satellites planned to become operational before 2025 (ATSE, 2009). The extent of operational usage of space-based EO data has enabled an increasing number of commercial companies to manage satellite platforms, with several dozen commercial satellites now supplying EO data internationally.

Recent advances in hardware and software, often borrowed from other industry sectors such as video games, mobile phones and medical technology, have enabled a new approach to satellite development. Various labels as microsatellites or nanosatellites (nanosats) these platforms are significantly smaller and cheaper than the traditional EO satellites, both to build and launch, making them affordable for a range of businesses and users. By early 2016<sup>4</sup>, hundreds of nanosats had been placed in orbit. These miniaturised satellites are often networked into larger constellations that enable multiple images of a selected location to be acquired each day (see Figure 1.8). Frequent imagery is particularly valuable for observing a range of disaster events, monitoring crop condition, and surveillance activities.

**Figure 1.7** Historical development of remote sensing

While the origins of remote sensing can be traced back to balloons, kites, pigeons and aeroplanes, this diagram illustrates the rapid advances in airborne and spaceborne remote sensors in recent decades.



Source: Megan Lewis, University of Adelaide

4. <http://www.nanosats.eu>



**Figure 1.8** Nanosatellite imagery

Image of Sydney acquired by Flock-1 satellites on 29 November 2015 showing the city centre, Port Jackson and Bondi Beach.



Source: Planet Labs, Inc. (CC BY SA 4.0). Retrieved from <https://www.planet.com/gallery/sydney-20151130/>

Another nanosatellite constellation is QB50, an international network of 36 CubeSats launched in 2017 to study Earth's largely unexplored thermosphere. Each Cubesat weighs about 1 kg and is expected to have a short lifespan (1 to 2 years).

Three of these satellites were developed in Australia—the first Australian satellites to be launched since 2002. The UNSW-ECO CubeSat, for example, was developed by the Australian Centre for Space Engineering Research at the University of NSW (UNSW) to observe the thermosphere's atomic composition (see Figure 1.9).

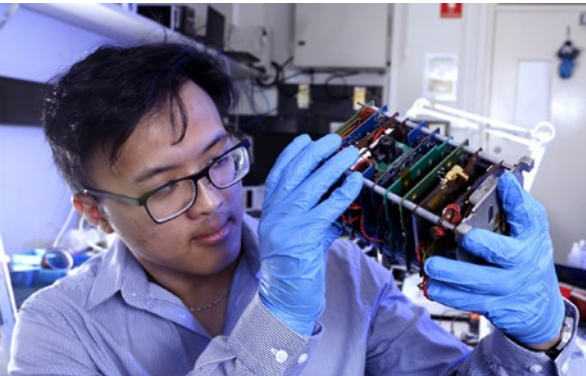
The volume and variety of EO data that is currently available, either as archives or ongoing acquisitions, is enormous. One of the major challenges for EO users is to select the most appropriate data for each specific application.

### 1.3.2 EO data characteristics

As introduced in Section 1.2.2, EO sensors acquire data in the form of observations. This data may be processed to become measurements then interpreted to become information. The initial observations of most remote sensing devices are quantitative, but only calibrated relative to a sensor-specific sensitivity range. The processing stage converts the initial observations so that they are comparable with a standard measurement scale and/or other data sources. This initial conversion is often undertaken by the data distributor, so may not be apparent to many data users. Nonetheless, when EO data is being used to underpin environmental monitoring and modelling activities, it is essential that its provenance can be verified and satisfies the expectations of end users. It should be noted that some forms of EO data, for which metadata and/or appropriate models do not exist, cannot be converted into measurements or variables so, in this context, can only be considered as observations.

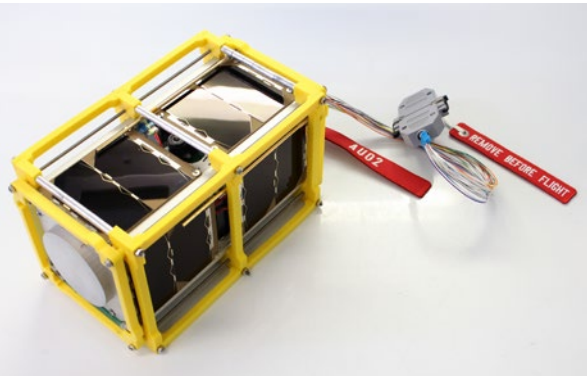
Figure 1.9 CubeSat

a. Dr Joon Wayn Cheong, Technical Lead, examining the UNSW-ECO QB50 CubeSat prior to the external solar panels and antennae being fitted. Photo Credit: Grant Hausler, UNSW



Source: Cheryl Brown, University of New South Wales

b. UNSW-ECO QB50 satellite in its protective 3D printed yellow frame, ready for shipment Photo Credit: John Lam, UNSW



The interrelationships between these terms and their relevance to remote sensing are summarised in Table 1.3. These stages and processes are most easily understood in the context of specific examples. The EO example traces the stages, or processes, involved with detecting potential fire hotspots using imagery from sensors that detect energy in visible, near infrared, middle infrared and thermal infrared wavelengths. The non-EO example relates the stages of acquisition, processing and interpretation, and their resulting observation, measurement and attribute,

to the operation of a traffic speed camera. As this example demonstrates, there are many uses of remote sensing technology that are not directly related to EO, however this book focuses on those that do.

Another example of the stages that can be involved with processing EO imagery is shown in Excursus 1.3 where features of interest are corrected, isolated then classified. In this example, Quickbird imagery is selected to classify benthic cover of coral reefs along the Queensland coast.

Table 1.3 Observations, measurements and attributes

Process	Result	Description	EO Example	Non-EO Example
Acquisition		Using sensors carried on platforms	Remote sensor records radiance of land area	Traffic speed camera photographs speeding vehicle
	Observation	Detect energy from an object or feature of interest	Images of visible and infrared radiation	Photograph vehicle number plate
Processing		Using pre-defined algorithms and prior knowledge about the sensor and/or platform	Land temperature computed from infrared images	Sharpen photograph to match standard clarity
	Measurement	Represent known properties of feature of interest	Brightness temperature image	Clear licence number of vehicle
Interpretation		Using reference information about feature of interest and measurements	Use visible and near infrared channels to exclude bright, non-fire pixels or cloud	Use registration records to link licence number to owner details
	Attribute	Relate directly to feature of interest	Hotspot imagery showing potential locations of active fires	Identification of vehicle owner



## Excursus 1.3—EO processing stages

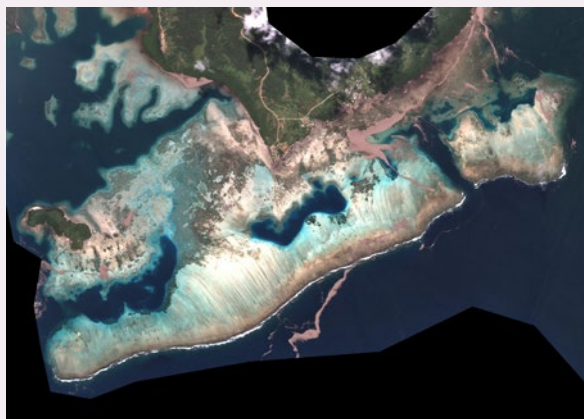
**Source:** Chris Roelfsema, University of Queensland

Processing of EO imagery involves a number of stages. The example below uses an image acquired by the Quickbird satellite on 17 October 2006 to map 21 benthic cover classes in Navakavu, Vanua Levu, Fiji (Phinn *et al.*, 2010).

a. Selected data with no corrections may not show the best contrast or geometry



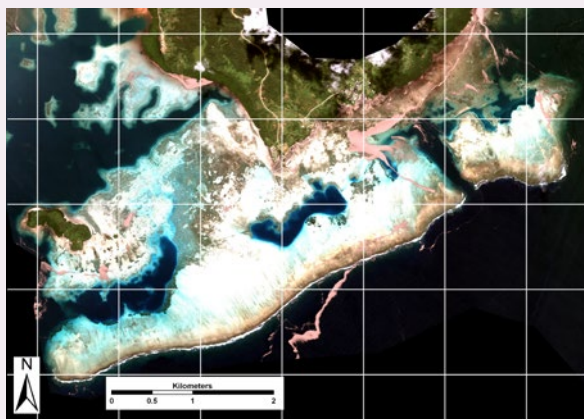
b. Correct distortions in image values due to atmospheric factors



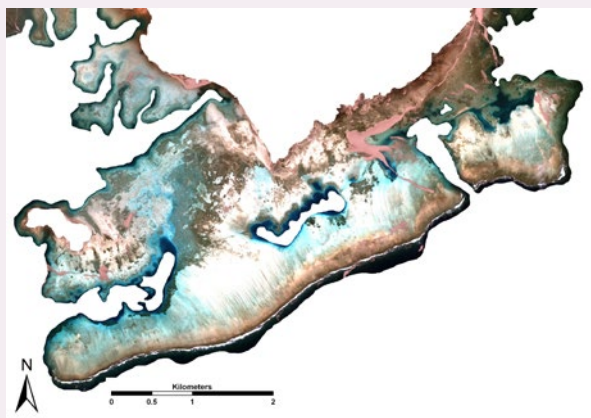
c. Correct distortions in image values due to water factors



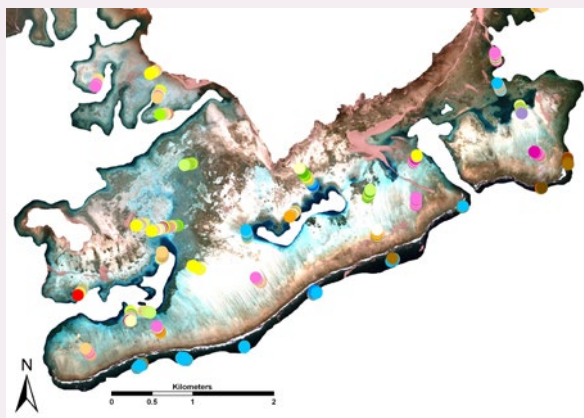
d. Correct geometric distortions



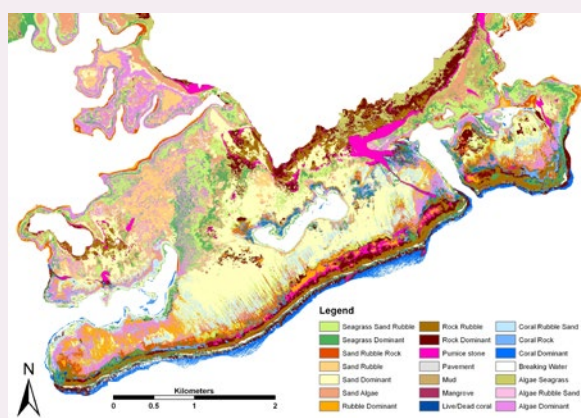
e. Remove features not related to the analysis, in this case land and deep water



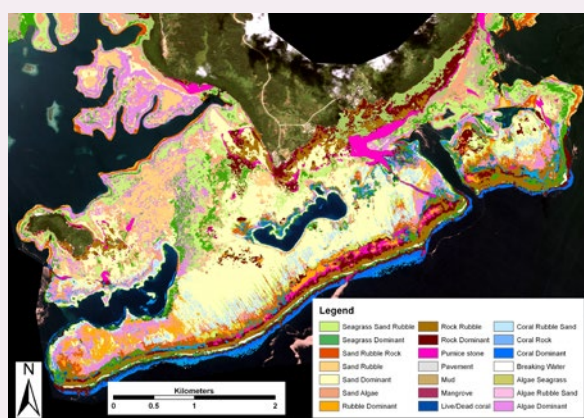
f. Compare image data with field information for this site



g. Classify image data to match field categories



h. Overlay final image classes on corrected image



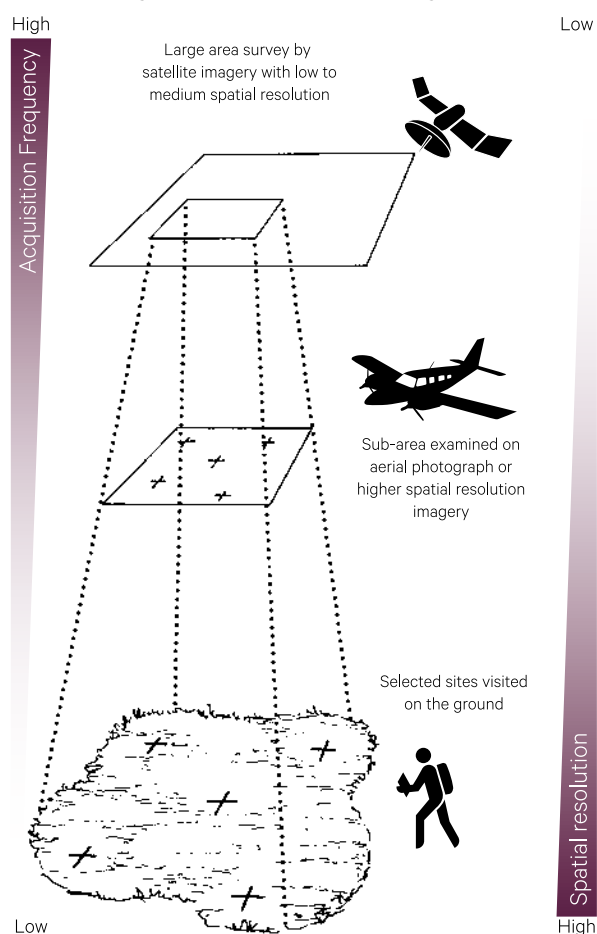
Thus, considering the logical stages involved with using remotely sensed data, the ability to relate objects, or features, and/or physical processes on the Earth's surface to data acquired by remote sensors rests on two underlying, but interrelated, considerations, namely the:

- intrinsic ability of the features to be resolved in the type of measurements being made—that is, the accuracy and precision of the sensing device; and the
- effectiveness of the models that relate features or physical processes to these measurements.

The issue of measurement is both fundamental and vital to planning EO data acquisition and its subsequent processing. The usual measurement space for EO data has a variety of measurement 'dimensions', such as intensity, wavelength and position. These can be considered as providing a coordinate framework in space and time. A data set is usually a sample in this coordinate framework. The objective of any data analysis exercise is to distinguish effects and/or events in the data. To achieve this objective, a data set must be sufficiently resolved, appropriately dense and cover an adequate extent.

**Figure 1.10** Scales of EO

Analysis of low and medium resolution imagery can be more easily related to ground data through high resolution imagery. Low resolution imagery tends to be acquired more quickly and cover a larger extent, so is most appropriate for large area surveys. Selected locations within the surveyed area would typically be checked using data with higher spatial resolution, such as aerial photography. Some of these locations would then be visited in the field to verify the image analysis. This scaled approach enables the results of expensive and time-consuming field work to be extended to a larger area.



Adapted from: Harrison and Jupp (1989) Figure 39



Resolution refers to level of detail, density refers to the intensity or rate of sampling, and extent refers to the overall coverage of a data set. Extent can be seen as relating to the largest object or feature, or range of features, which can be observed, while resolution relates to the smallest. Density indicates the continuity and frequency of sampling. For a feature to be distinguishable in the data, the resolution, density, and extent of the measurement dimensions of the data need to be appropriate to the measurable properties of the feature. For a feature to be separable from other features, these measurements must also be able to discriminate between the differences in reflectance from those features.

EO projects, however, do not need to be limited to a single source of imagery. Two or more sources of data, imaged at different scales, can be integrated, as discussed in Volume 1B—Section 9 and Volume 2D.

A further characteristic of EO data that impacts its value to particular applications is latency, or the time interval between acquisition of data and its dissemination to users. The EO data distribution process typically involves multiple data handling steps including reception, processing, quality assurance, and delivery. As EO data becomes increasingly important to a growing number of application areas, the demand for reduced latency is also growing, especially for disaster management. The inverse relationship between data acquisition (and dissemination) rates and spatial resolution are shown in Figure 1.10. Resolution, extent, and density of remotely sensed data are further discussed in Volume 1B—Section 1.

## 1.4 Using Earth Observations

As summarised in Section 1.3.1 above, EO data have been available from airborne platforms for over a century while imagery from spaceborne platforms have been available internationally for over five decades. Space-based imagery, in particular, offers a unique source of data about the Earth by recording:

- accurate geo-locations for contiguous target areas;
- objective, consistent measurements of physical properties of the Earth and its atmosphere that can be interpreted to define its features and condition; and
- repeated coverage to enable detection of changes in features and/or their condition.

No other source of data for the Earth provides comparable consistency, repeatability and coverage. Additionally, EO offers the least expensive form of environmental data acquisition. One example of the volume of data that is acquired in one day by a single sensor is illustrated in Figure 1.6. A monthly composite derived from such imagery is shown in Figure 1.11.

The results from EO analyses are now routinely used for a wide range of applications such as land use planning, agricultural management, land rehabilitation, transport planning, surveillance, disaster management, mineral exploration, geodesy, water resources management, and weather and climate forecasting (see Volume 3 for a detailed discussion of EO applications and case studies). Current usage of EO data can be considered in terms of three broad

functions, namely:

- detecting and mapping specific features of interest, such as determining the spatial distribution of crop health on a particular date (see 1.4.1);
- monitoring changes in specific features, such as quantifying the spatial variations in crop health over a season (see Section 1.4.2); and
- modelling environmental processes, such as identifying the relationship between crop health and management practices (see Section 1.4.3).

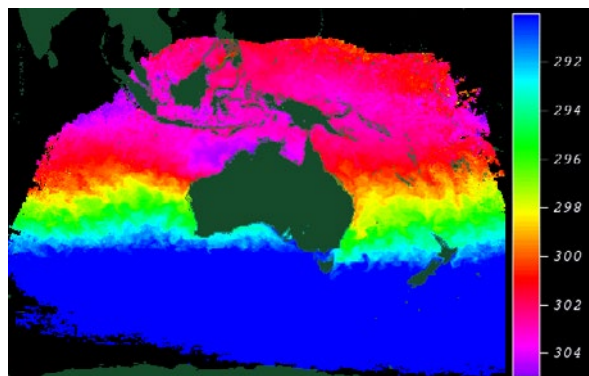
To ensure that the attributes derived from EO datasets are accurate, consistent and relevant, each of these three functions incorporates two fundamental processes:

- calibration—relates EO observations to standard measurement scales to ensure traceability both between sensors and through time. This process is a component of the measurement model introduced in Section 1.2 and is considered in greater detail in Volume 2A—Section 3; and
- validation—assesses the quality of derived attributes relative to independent datasets. This process is a component of the structure model introduced in Section 1.2 and is considered in greater detail in Volume 3.

Facilities and activities relevant to calibration and validation of satellite data in Australia are reviewed by Malthus and Li (2014).

**Figure 1.11** Monthly composite

Sea Surface Temperature (SST) from AVHRR mosaic of thermal images calibrated using measurements from ships and drifting buoys. This one-month composite was compiled from night-time data during April 2016. Scale units in K.



Source: Christopher Griffin, Bureau of Meteorology

### 1.4.1 Detecting and mapping features

For several decades, EO data has been used to map features associated with the Earth for a range of environmental and scientific applications. Relevant features being mapped include vegetation condition and extent, crop productivity and health, habitats, urban and rural land use, evapotranspiration, soil moisture, erosion, salinity, paleovalleys, archaeological sites, terrain and vegetation height, mineral deposits, surface deformation, potential fire locations, fire scars, snow cover and extent, ocean colour and temperature, water turbidity, flood events, and atmospheric composition, temperature and water vapour content (see Figure 1.12). EO data is also used for geodetic surveys, cartography, navigation and border surveillance.

As detailed in Volumes 2 and 3, procedures for mapping such features using specific EO data sources are now well established and yield reliable results on an operational basis. The resulting maps show the location and spatial distribution of the target feature at a particular point in time.

### 1.4.2 Monitoring changes

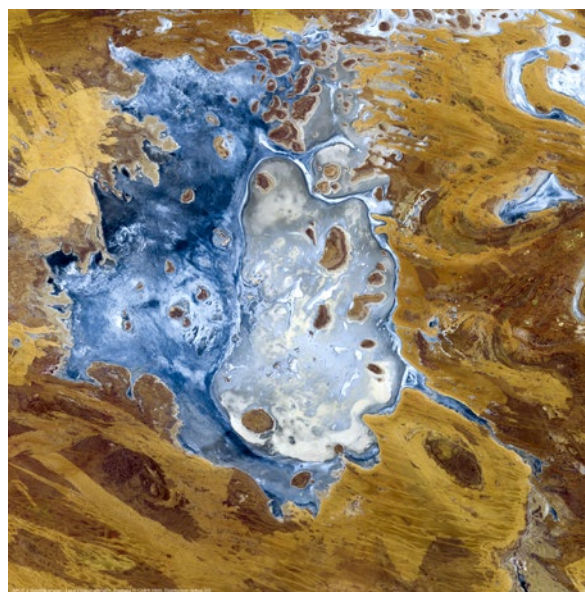
In many instances, Earth's features can be mapped from a single image and validated using appropriate reference data. To maximise the value of the recurrent imagery available from EO however, multiple images from one or more sources can be used to monitor changes in particular features and assess the extent of change within a selected time period. Given the dynamic nature of the Earth, EO offers an invaluable monitoring tool especially for early detection of various forms of environmental degradation.

EO data sources are used to quantify changes in a range of activities and resources including deforestation, agricultural production, city growth, land use change, wind erosion, waterlogging, remnant vegetation, rangelands, desertification, wetlands, sea floor topography, ocean currents, climatic indicators and pollution. For example, the construction of Elizabeth Quay, Perth, is monitored by a sequence of Nearmap aerial images in Figure 1.13.

Recent environmental legislation has further reinforced dependency on EO to monitor the ongoing status of various resources including inland water quality and carbon sequestration. The growing archive of EO data enables changes in environmental resources to be carefully tracked and correlated with potential drivers. This archive also offers the opportunity for time series analysis of relevant imagery and thus the separation of seasonal from longer-term trends.

**Figure 1.12** Lake Disappointment

Lake Disappointment is a salt lake in the Little Sandy Desert (Pilbara region, northern WA), mostly surrounded by sand dunes. This lake only contains water after heavy rain or floods and thus proved to be a disappointment when encountered by early explorers. The image below was acquired by SPOT-4 in March 2002 during a rare inundation event.



Source: © CNES (2016). Distribution Airbus DS.



**Figure 1.13** Construction of Elizabeth Quay, Perth

Elizabeth Quay, named after Queen Elizabeth II, is a major mixed-use development in Perth's CBD, spanning 10 ha on the northern shore of the Swan River. The development included construction of an artificial inlet, with 1.5 km of boardwalks and promenades, and will ultimately comprise office, retail and residential buildings, and recreational facilities. This sequence of Nearmap high-resolution aerial images monitors the development from the original Esplanade Reserve before the project commencement date of 26 April 2012, to after its official opening on 29 January 2016. Construction of buildings associated with the site is expected to be complete by 2018.

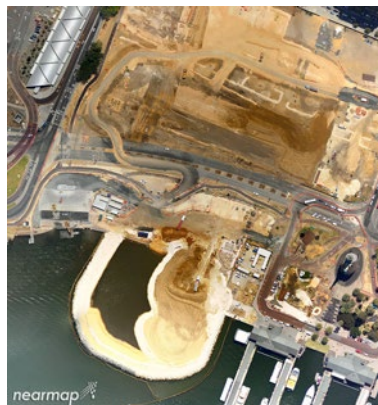
22 February 2012



30 June 2013



20 February 2014



8 August 2014



28 June 2015



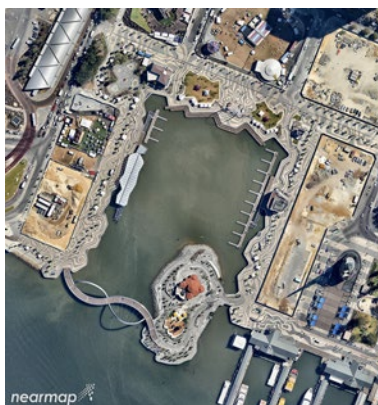
7 September 2015



22 November 2015



4 March 2016



10 May 2016



Source: © Nearmap

### 1.4.3 Modelling processes

The Earth is a dynamic planet. All aspects of Earth—its surface, water, air and interior—are continuously changing in terms of their biology, chemical composition, physical form, and energy. EO data have allowed these changes to be quantified and modelled. The elevated perspective of most EO sensors provides an ideal view of the Earth to observe its physical, chemical and biological processes. The fundamental goal of any EO analysis is to increase our understanding of Earth's dynamic processes and, in consequence, our management of the planet.

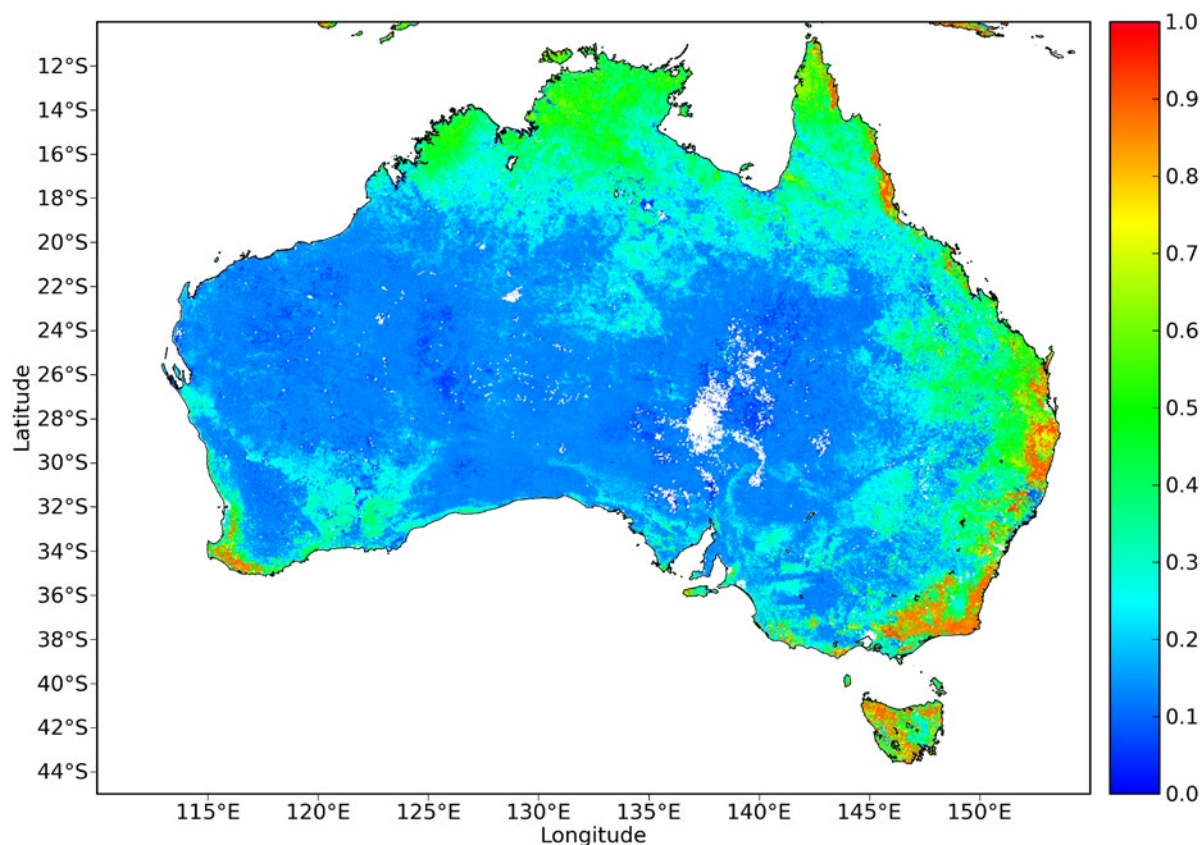
Monitoring changes using EO is a first step in quantifying these processes. However, we need to model the processes themselves in order to predict future states and/or determine their interdependence on other factors, such as management practices.

Reliable EO-based models already exist for weather forecasting and, in conjunction with other data sources, are being developed to better predict the dynamics of climate, vegetation, salinity, oceans, and natural disasters. Processes for modelling indicators of photosynthetic activity are well established and underpin a wide range of environmental and agricultural activities (see Figure 1.14).

By understanding the rate of change that is occurring in key environmental variables, land managers are better equipped to evaluate the impact of particular management strategies and modify management practices if appropriate. Improved efficiency in urban planning, agricultural production, freshwater management, natural resource utilisation and pollution control will undoubtedly benefit all inhabitants of planet Earth.

**Figure 1.14** Modelling photosynthetically active radiation

Fraction of Photosynthetically Active Radiation (fPAR) derived from MODIS/Terra imagery (LPDAAC MOD15A2 mosaic) acquired between 1 and 8 January 2016 (inclusive). This gridded 8-day composite shows fPAR on a scale from 0 to 1.



Source: TERN AusCover. Retrieved from <http://www.auscover.org.au/purl/lpdaac-mosaic-mod15a2-v5>

AusCover is the remote sensing data products facility of the Terrestrial Ecosystem Research Network (TERN; <http://www.tern.org.au>).



## 1.5 The Global Picture

EO is the only technology that offers the luxury of truly seeing the global picture (see Figure 1.15).

### 1.5.1 The Global Earth Observation System of Systems

The Group on Earth Observations (GEO) is an international body established in 2002 to encourage its member governments to coordinate projects, strategies and investments for EO. Since 2005, GEO has been implementing the Global Earth Observation System of Systems (GEOSS) ten year plan to advance and demonstrate the societal benefits of EO in nine Societal Benefit Areas (SBA):

- **Agriculture**—support local, national and regional activities for agriculture, rangelands, forestry and fisheries, including famine early warning, food security prediction, drought forecasting, agriculture production and forecasting, aquaculture production, timber, fuel and fibre management, forest perturbations and protection, and carbon and biomass estimation;
- **Biodiversity**—assess condition and extent of ecosystems, distribution and status of species, and genetic diversity in key populations, as well as tracking invasive species;
- **Climate**—model, mitigate, adapt and assess risks of climate change for atmosphere, lands and oceans;
- **Disasters**—predict and monitor earthquakes, floods, landslides, cyclones, volcanic eruptions, and wildfires;
- **Ecosystems**—monitor and evaluate ecosystem health, function and change in coastal and near-shore marine systems, forests, inland waters, oceanic islands and archipelagos, tundra, and watersheds;
- **Energy**—assess viability of renewable energy sources, including hydropower, wind power, bioenergy, solar power, geothermal power;
- **Health**—monitor aeroallergens, air quality, and infectious diseases, and provide early warning for public health risks such as heat waves and epidemic pre-conditions;
- **Water**—monitor terrestrial hydrology of surface waters, ground waters, forcings, water quality, and water usage; and
- **Weather**—improve weather information, forecasting and warning using numerical weather prediction (global and regional), synoptic, aeronautical and agricultural meteorology, and atmospheric chemistry.

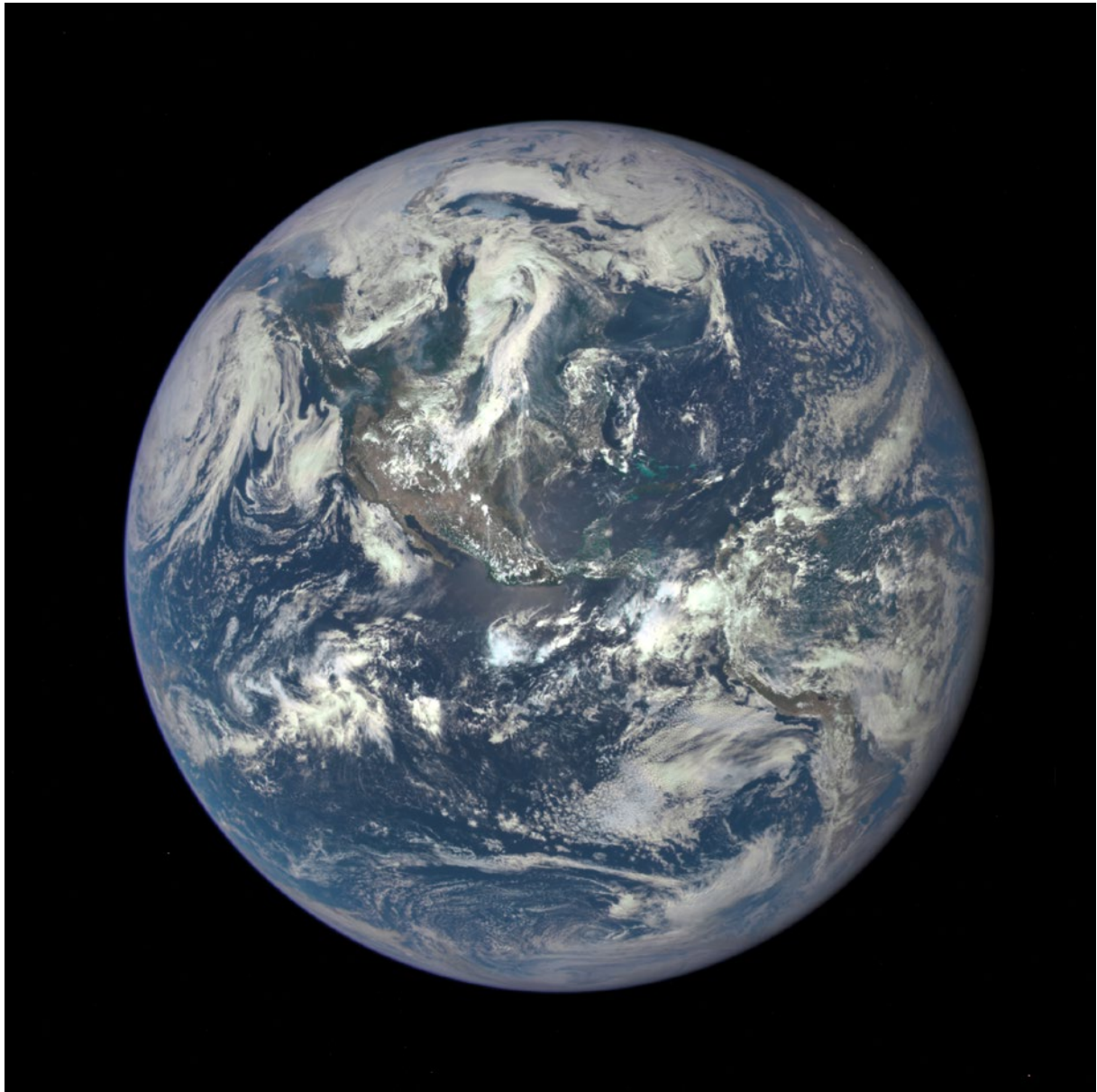
GEOSS aims to increase knowledge and understanding of Earth systems by continuous monitoring of its state and dynamics (van Zyl *et al.*, 2009). Realisation of this goal will require new, autonomous infrastructure, as envisioned by the Sensor Web Concept (Botts *et al.*, 2006; Botts *et al.*, 2007), to collate and disseminate relevant data. Such developments, and other global monitoring systems, are further discussed in Volume 3.

### 1.5.2 Essential climate variables

The Global Climate Observing System (GCOS) has defined a set of derived climate variables that are deemed essential for monitoring Earth's climate. These Essential Climate Variables (ECV) are listed in Table 1.4 (GCOS, 2010). Measurement of over half of the recognised ECVs is largely or exclusively dependent on EO data acquired from satellite platforms (see underlined entries). This list exemplifies the importance of EO data for a wide range of environmental monitoring and modelling applications.

**Figure 1.15** The global picture

This is the first view of the entire sunlit side of the globe from 'one million miles' (1.6 million km) away. It was taken by NASA's Earth Polychromatic Imaging Camera (EPIC) on 6 July 2015 from the Deep Space Climate Observatory (DSCOVR). This image uses the red, green and blue channels.



Source: NASA. Retrieved from <http://www.nasa.gov/press-release/nasa-satellite-camera-provides-epic-view-of-earth>

---

*As a former astronaut who's been privileged to view the Earth from orbit,  
I want everyone to be able to see and appreciate our planet as an integrated, interacting system.  
DSCOVR's observations of Earth, as well as its measurements and early warnings of space weather  
events caused by the sun, will help every person to monitor the ever-changing Earth,  
and to understand how our planet fits into its neighbourhood in the solar system.  
(Charlie Bolden, NASA)*

---



**Table 1.4** GCOS essential climate variables

Measurement of underlined ECVs can be derived from EO.

Domain	Type of Measurement	Essential Climate Variables
Atmospheric	<b>Surface</b> (includes measurements at standardized, but globally varying, heights in close proximity to the surface)	Air temperature <u>Wind speed and direction</u> <u>Water vapour</u> Pressure <u>Precipitation</u> Surface radiation budget
	<b>Upper-air</b> (up to the stratopause)	<u>Temperature</u> <u>Wind speed and direction</u> <u>Water vapour</u> <u>Cloud properties</u> <u>Earth radiation budget</u> (including solar irradiance)
	<b>Composition</b>	<u>Carbon dioxide</u> <u>Methane and other long-lived greenhouse gases</u> (including nitrous oxide (N <sub>2</sub> O), chlorofluorocarbons (CFCs), hydrochlorofluorocarbons (HCFCs), hydrofluorocarbons (HFCs), sulphur hexafluoride (SF <sub>6</sub> ), and perfluorocarbons (PFCs)) <u>Ozone and Aerosol properties</u> , supported by their precursors (in particular nitrogen dioxide (NO <sub>2</sub> ), sulphur dioxide (SO <sub>2</sub> ), formaldehyde (HCHO) and carbon monoxide (CO))
Oceanic	<b>Surface</b> (includes measurements within the surface mixed layer, usually within the upper 15m)	<u>Sea-surface temperature</u> <u>Sea-surface salinity</u> <u>Sea level</u> <u>Sea state</u> <u>Sea ice</u> Surface current <u>Ocean colour</u> Carbon dioxide partial pressure Ocean acidity Phytoplankton
	<b>Sub-surface</b>	Temperature Salinity Current Nutrients Carbon dioxide partial pressure Ocean acidity Oxygen Tracers
Terrestrial		River discharge Water use Groundwater <u>Lakes</u> <u>Snow cover</u> <u>Glaciers and ice caps</u> <u>Ice sheets</u> Permafrost <u>Albedo</u> <u>Land cover (including vegetation type)</u> <u>Fraction of absorbed photosynthetically active radiation (FAPAR)</u> <u>Leaf area index (LAI)</u> <u>Above-ground biomass</u> Soil carbon <u>Fire disturbance</u> <u>Soil moisture</u>

Adapted from: CEOS (2016) at <http://database.eohandbook.com/climate/gcosecvindex.aspx>

## 1.6 Key Terms

Terminology can be confusing in EO literature. To ensure consistency with terminology (and with reference to Ackoff, 1989; Rowley, 2007; OGC, 2012), this book assumes the meanings listed below for some basic terms. The reader is also referred to the glossary of photogrammetric terms compiled by Newby (2012).

**Accuracy**—degree to which information on a map or in a digital database [or remotely sensed image] matches true or accepted values. Accuracy pertains to the quality of data and the number of errors contained in a dataset or map.

**Acquisition**—process of observing an object or surface using a remote sensor.

**Application**—specific area of interest, or field of study, that will use the results from an EO analysis. Examples of applications include water quality, desertification, agriculture and climate studies.

**Attribute**—represents measured properties of object or surface in terms of a specific application using a pre-defined structure model. In the context of EO, end users are interested in attributes that directly relate to their application areas. Examples of attributes that might be derived from EO imagery include water turbidity, rate of erosion, crop yield, and rainfall variability.

**Attribute domain**—describes properties of an object or surface that are relevant to an end user (see Figure 1.4).

**Calibration**—process of defining the relationship between observations and physical measurement standards. In the context of EO, calibration relates remotely sensed observations to absolute references and standards to ensure consistency between sensors and through time<sup>5</sup>. Calibration is a component of the measurement model.

**Data**—symbols; discrete, unorganised and unprocessed objective facts or observations that represent properties of objects, events and environments. Data do not convey any specific meaning and are of no use until they are processed into a form relevant to a particular application.

**End user**—person or persons that will use the processed, interpreted EO data for a specific application.

**Feature**—starting point for modelling of geographic information; a digital representation of a real world entity or an abstraction of the real world. The terms feature and object are often used synonymously.

**Geographic Feature**—feature associated with a location relative to the Earth.

**Image**—collection of contiguous coverage data, usually from sampling at regular, discrete locations.

**Information**—data that are processed to be useful, contained in descriptions, and answers to questions that begin with such words as ‘who’, ‘what’, ‘when’ and ‘how many’. The difference between data and information relates to function rather than structure. Information is inferred from data and frequently includes metadata. Information contains tags to context. In the context of EO, information relates to application areas, implying interpretation via established models that link calibrated measurements to end user requirements.

**Interpretation**—process of understanding the measurable properties of an object or surface in terms of a specific application using a pre-defined structure model.

**Knowledge**—application of data and information; answers ‘how’ questions.

**Map**—two-dimensional visual portrayal of geospatial data as opposed to the data itself.

**Measurement**—a ‘self-describing’ observation associated with scale and metadata. A measurement usually refers to the measuring device and procedure used to determine the value, such as a sensor, analytical procedure, simulation or other numerical process. In the context of EO, this should imply calibrated observations.

**Measurement domain**—describes physical dimensions that can be measured, such as visible blue reflectance, relative to known scale and metadata as defined by associated measurement model (see Figure 1.4).

**Measurement model**—relates physical measurements to observable properties of an object or surface. For example, measurement models are used to relate remotely sensed observations to calibrated reflectance measurements (see Figure 1.4).

**Metadata**—appended information that describes other data, such as the coordinate framework in space and time for measurement dimensions. This involves documentation of data to enable managers or users to understand, compare and interchange the content of a dataset<sup>6</sup>.

**Noise**—part of observation considered irrelevant to the end-use of observations and, as a consequence, often removed in conversion to the measurement space.

5. See also: [http://calvalportal.ceos.org/cal/val-wiki/-/wiki/tag/terms+and+definition?p\\_auth=04F08ThF](http://calvalportal.ceos.org/cal/val-wiki/-/wiki/tag/terms+and+definition?p_auth=04F08ThF)

6. See also <https://www.e-education.psu.edu/geog486/node/1882>

**Object**—feature (on, or associated with, the Earth) that is being observed by a remote sensor.

**Observation**—an event that estimates an observed property of some feature of interest using a specified procedure and generates a result (Cox *et al.*, 2010; OGC, 2012). This can also be viewed as a raw representation of a quantity or attribute. In the context of EO, raw (that is, uncalibrated) image data can be viewed as observations.

**Observation domain**—describes observed data values of an object or surface acquired using remote sensing. For example, in the context of EO, uncalibrated image values can be viewed as observations (see Figure 1.4).

**Precision**—minimum level of differentiation in dataset, which is related to the limit of resolution in measurements and exactness of descriptions. Statistically, precision relates to the level of dispersion in observations (such as standard deviation), and thus to the repeatability of a measurement process. Measurements may be precise, but not accurate, due to errors in data acquisition or handling.

**Processing**—process of converting remote sensing observations to a measurable property of the observed object or surface using a pre-defined measurement model.

**Reference data**—reliable, independent data used to calibrate or validate primary data. In the context of EO, reference data may be derived from ground measurements and other EO sensors.

**Sensor Web**—networked collection of sensors that can be remotely read and/or controlled.

**Structure model**—relates desired object or surface attributes to measurable properties of that object or surface. In the context of EO, structure models link measurement domains to attribute domains. One example of a structure model allows visible blue reflectance measurements to be interpreted in terms of water turbidity (see Figure 1.4).

**Validation**—process of testing an application or system to ensure that it conforms to a specification. In the context of EO, validation compares attributes derived from calibrated EO measurements with reference data to determine the quality and limitations of those attributes. Validation is a component of the structure model.

**Variable**—attribute or physical characteristic of the object or surface being observed that is required by the end user. A variable is the result of moving from the measurement domain to the attribute domain and reflects the process an interpreter is attempting to model. In this context, the term ‘variable’ is used interchangeably with ‘attribute’.

**Wisdom**—evaluated understanding, up to the present time...

## 1.7 Further Information

---

### Earth Observation:

Geoscience Australia (GA): <http://www.ga.gov.au/scientific-topics/earth-obs>

European Space Agency (ESA): [http://www.eo-miners.eu/earth\\_observation/eo\\_introduction.htm](http://www.eo-miners.eu/earth_observation/eo_introduction.htm)

National Aeronautical and Space Agency (NASA): <http://neo.sci.gsfc.nasa.gov/>

Please also see Volume 1X—Appendices 1 to 3 for recommended reading and professional societies relevant to EO, plus sources of EO data and products.

### Image Galleries:

NASA Worldview: <https://worldview.earthdata.nasa.gov>

ESA Image pairs: <https://earth.esa.int/web/earth-watching/image-of-the-week/content>

(Note that some of these image pairs are from different seasons, which can accentuate the extent of change—see Volume 2D).

Astronaut photographs of Earth: <http://eol.jsc.nasa.gov/SearchPhotos/>

EOPortal Images: <https://eoportal.org/web/eoportal/images>

Airbus Defence and Space: <http://www.geo-airbusds.com/satellite-image-gallery/>

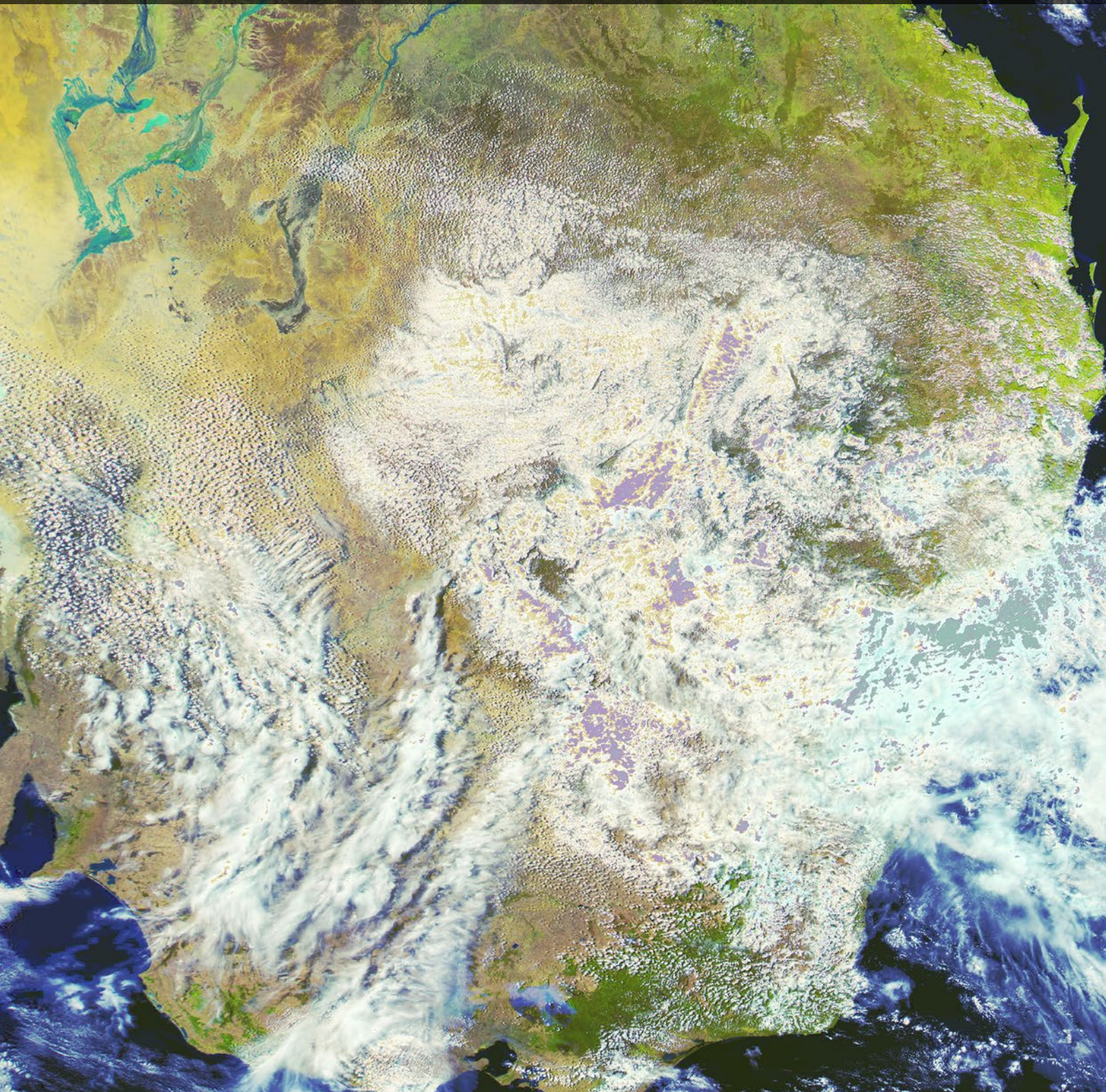
## 1.8 References

- Ackoff, R. L. (1989). From Data to Wisdom: Presidential Address to ISGSR, June 1988. *Journal of Applied Systems Analysis*, 16(1), pp. 3-9.
- ATSE (2009). An Australian Strategic Plan for Earth Observation from Space. Australian Academy of Technological Sciences and Engineering and Australian Academy of Science, Canberra.
- Bellinger, G., Castro, D., and Mills, A. (2004). Data, Information, Knowledge, and Wisdom. Retrieved from <http://www.systems-thinking.org/dikw/dikw.htm>.
- Bernstein, J. (2009). The Data-Information-Knowledge-Wisdom Hierarchy and its Antithesis. *Journal of Information Science*, 35(2), pp. 68-75.
- Botts, M., Percivall, G., Reed, C., and Davidson, J. (2007). OGC® Sensor Web enablement: Overview and high level architecture (OGC White Paper OGC 07-165, Version 3).
- Botts, M., Robin, A., Davidson, J., and Simonis, I. (2006). OpenGIS® Sensor Web Enablement Architecture Document (OGC 06-021r1, Version 1). OpenGIS® Discussion Paper.
- Cox, S., Botts, M., Robin, A., Atkinson, R., Falke, S., Woolf, A., and Portele, C. (2010). Geographic Information: Observations and Measurements OGC Abstract Specification Topic 20 (OGC 10-004r3 and ISO 19156, Version 2.0.0). Open Geospatial Consortium. Retrieved from [https://portal.opengeospatial.org/files/?artifact\\_id=41579](https://portal.opengeospatial.org/files/?artifact_id=41579).
- Eliot, T. S. (1934). *The Rock*. Faber and Faber, London, United Kingdom.
- Gharajedaghi, J., and Ackoff, R. L. (1984). Mechanisms, Organisms and Social-Systems. *Strategic Management Journal*, 5(3), pp. 289-300. doi:<http://dx.doi.org/10.1002/smj.4250050308>.
- Harrison, B. A., and Jupp, D. L. B. (1989). Introduction to Remotely Sensed Data. Part ONE of the microBRIAN Resource Manual (156 pages). CSIRO Australia, Melbourne.
- Malthus, T. J., and Li, F. (2015). Calibration of Optical Satellite and Airborne Sensors. Chapter 4 in 'AusCover Good Practice Guidelines: A technical handbook supporting calibration and validation activities of remotely sensed data products' (Eds: A. Held, S. Phinn, M. Soto-Berelov, and S. Jones). TERN AusCover, Australia. ISBN 978-0-646-94137-0.
- Newby, P. R. T. (2012). Photogrammetric Terminology: Second Edition. *The Photogrammetric Record*, 27(139), pp. 360-386. doi:<http://dx.doi.org/10.1111/j.1477-9730.2012.00693.x>.
- OGC (2012). Earth Observation Metadata profile of Observations and Measurements (OGC 10-157r3) (J. Gasperi, F. Houbie, A. Woolf, and S. Smolders Eds.). Open Geospatial Consortium.
- Phinn, S. R., Roelfsema, C. M., and Stumpf, R. (2010). Remote sensing: Discerning the promise from the reality. Chapter 15 in 'Integrating and applying science: A handbook for effective coastal ecosystem assessment' (Eds: B. J. Longstaff, T. J. B. Carruthers, W. C. Dennison, T. R. Lookingbill, J. M. Hawkey, J. E. Thomas, E. C. Wicks, and J. Woerner), pp. 201-222. IAN Press, Cambridge, Maryland, USA.
- Rowley, J. (2007). The wisdom hierarchy: representations of the DIKW hierarchy. *Journal of Information Science*, 33(2), pp. 163-180. doi:<http://dx.doi.org/10.1177/0165551506070706>.
- van Zyl, T. L., Simonis, I., and McFerren, G. (2009). The Sensor Web: systems of sensor systems. *International Journal of Digital Earth*, 2(1), pp. 16-30. doi:<http://dx.doi.org/10.1080/17538940802439549>.
- Zeleny, M. (1987). Management Support Systems - Towards Integrated Knowledge Management. *Human Systems Management*, 7(1), pp. 59-70.





# Background





The following three sections provide background information to review our current understanding of some basic principles that underlie remote sensing for Earth Observation (EO), including:

- scientific concepts and principles that are used to design remote sensing instruments and the algorithms that are used to transform these data into information about the Earth's environments (see Section 2);
- current knowledge about our planet—including its relative position in the universe and its structure, shape and life forms (see Section 3); and
- recycling pathways—thermal, hydrological, rock and carbon cycles (see Section 4).

These principles are referenced in subsequent sections and volumes. They are fundamental to understanding how remote sensing instruments operate, what they observe and how their observations are converted to measurements and information about the biological, chemical and physical properties and processes of the Earth.

## Contents

<b>2</b>	<b>Scientific Foundations</b>	<b>27</b>
<b>3</b>	<b>Planet Earth</b>	<b>51</b>
<b>4</b>	<b>Earth Systems and Processes</b>	<b>63</b>



## 2 Scientific Foundations

The scientific principles and concepts that enable and underpin remote sensing are summarised in this section, including:

- energy, mass and fundamental forces (see Section 2.1);
- matter (see Section 2.2);
- measurement (see Section 2.3)
- force fields (see Section 2.4);
- waves (see Section 2.5);
- properties of EMR (see Section 2.6);
- colour and human vision (see Section 2.7);
- optics (see Section 2.8);
- radiation laws (see Section 2.9);
- heat and temperature (see Section 2.10); and
- blackbody radiation (see Section 2.11).

All of these topics provide background information that is relevant to the acquisition and interpretation of Earth Observation (EO) data. Readers who are familiar with these concepts may prefer to simply refer to them as needed from subsequent sections. For those who do not have training in science, we have chosen to start with the basics and briefly include all topics that underpin the broad field of remote sensing.

---

*True science teaches, above all,  
to doubt and to be ignorant  
(Miguel de Unamuno)*

---

### 2.1 Energy, Mass and Fundamental Forces

Energy is traditionally defined as the capacity to do work. Note that this defines what energy can do, not what it is. Energy is one of those fundamental entities that we rely upon, but don't completely understand. We do know that it can take many forms—heat, light, sound, electrical, chemical, or nuclear—and that life wouldn't exist without it.

Mass is another fundamental property of objects. It measures the amount of matter in an object and thus its inertia, that is, its tendency to stay in its current state of motion, whether resting or moving. Weight, the force of gravity on an object, is used as a surrogate for mass in most practical applications on Earth.

Our understanding of energy and mass has developed over millennia, based on observations of how different types of matter move and interact. Modern physics recognises four fundamental interactions, or forces, listed in order of increasing strength and decreasing range of influence:

- gravitation—attraction between objects due to their mass;
- weak nuclear—responsible for radioactive decay of sub-atomic particles;
- electromagnetism—holds atoms and molecules together; and
- strong nuclear—holds together the nucleus of each atom.

---

**Background image:** Landsat-5 image of Gascoyne River in flood, acquired on 22 December 2010. The Gascoyne River is the longest river in WA (760km) but only flows above the surface for about one third of each year. The Gascoyne River stretches from the Robinson Ranges, west of the Gibson Desert to the Indian Ocean near Carnarvon. This image is displayed using bands 5, 4, 2 as RGB. **Source:** Norman Mueller, Geoscience Australia

External forces acting on an object can change the energy of that object. If the external forces acting on an object are balanced, it is in equilibrium, or a resting position. The laws of thermodynamics state that the mass-energy of the universe is constant, but is continually being changed from one form to another, or moved from one place to another. Energy and mass are related by the famous mass-energy equivalence equation:

$$E = mc^2$$

where

$E$  is energy;  
 $m$  is the mass of the object; and  
 $c$  is speed of light.

Potential demonstrations of mass changing into energy include radioactivity; the mass of the Sun, for example, is constantly decreasing as it radiates energy (see Section 6).

Energy is further differentiated as either kinetic, due to actual motion and being dependent on mass, or potential, due to possible motion and reliant on physical position and/or chemical composition.

## 2.2 Matter

Atoms are regarded as the basic building blocks of matter. According to current understanding, each atom can be visualised as a positively charged nucleus surrounded by small, negatively charged electrons. Each nucleus contains at least one positively charged proton. The nuclei of most atoms also contain uncharged neutrons, which stabilise the positive charges.

An element is distinguished by the number of protons in the nuclei of its atoms, which is also known as its unique atomic number. In a neutral state, the number of protons in an atom equals the number of electrons. Atoms combine in myriad different configurations to create molecules. These have distinct chemical properties and are characterised in terms of their atomic structure. Most matter exists as molecules rather than individual atoms.

The spatial distribution of electrons around a nucleus is described by atomic and molecular orbitals. Electrons are viewed to exist in probability shells or orbitals around the nucleus of an atom. Each orbital is associated with a discrete energy level, or quantum, such that the energy associated with an electron is that of its orbital. Electrons move between orbitals by absorbing or emitting a precise quantum of energy (such as a photon—see Section 2.11.4). The lowest energy level is referred to as the electron's ground state and higher energy levels are called excited states. This is the mechanism by which EM energy in the ultraviolet to visible wavelengths is absorbed by materials (see Section 5).

An atom with a different number of electrons than protons is referred to as an ion of that element. When atoms of an element have different numbers of neutrons, they are called isotopes. The nuclei of some isotopes are unstable, so release energy to achieve internal stability. This mechanism forms the basis of radioactivity and will be further discussed in Section 6.

Matter can exist in any one of four fundamental states:

- solid—molecules vibrate about fixed locations, often within crystal lattices, and cannot change position within a substance. Solids have defined shapes and volumes;
- liquid—molecules that can move but are bound loosely by intra-molecular forces. Liquids do not have a fixed shape, but can flow and maintain a near-constant volume with changes in pressure;
- gas—molecules in constant random motion without a fixed volume or shape; and
- plasma—ionised gas comprising charged particles, namely positive ions and negative electrons or ions.

The precise interaction between energy from an external energy source, such as the Sun, and matter depends on many factors, including the state and temperature of matter, its atomic composition and structure, and the intensity, frequency and proximity of the energy source.

## 2.3 Measurement

Measurement records numeric values to describe observations or events, where:

- an observation notes the state or condition of an object or relationship; and
- an event relates to a change in state or condition.

Recorded measurements allow the association(s) between multiple observations or events to be determined.

### 2.3.1 Scales of measurement

Four scales of measurement can be used to define numeric variables (Anderberg, 1973):

- nominal—assigns categories which define different states, in which case relationships between measurements are limited to their being the same or not, and no ordering can be inferred;
- ordinal—involves an implied ordering between different states, which allows relationships to imply rank, but the interval between different values does not imply distance;
- interval—measures the extent of difference between states, which allows measurements to be ordered and separation to be treated as distance; and
- ratio—uses a scaled measure with a meaningful zero. Like interval variables, ratio variables can be ordered and differenced, but given that they additionally have a true zero point, fractions can also be computed for ratio variables.

These distinctions are relevant when interpreting remotely sensed measurements to ensure that appropriate processes are selected for image enhancement and analysis (see Volume 2).

### 2.3.2 International System of Units (SI)

The International Bureau of Weights and Measures (Bureau International des Poids et Mesures: BIPM) is one of three international standards organisations that ensures the use of uniform weights and measures around the globe<sup>7</sup>. In particular, it maintains the International System of Measurement (Système International d'Unités: SI), which defines the seven base units of measurement summarised in Table 2.1.

Other quantities can be derived from these base units using standardised quantity equations. Some of the derived units that are relevant to EO are summarised in Table 2.2.

**Table 2.1** Base Units in the International System of Units (SI)

Measures	Unit	Abbreviation	Defined as
length	metre	m	length of the path travelled by light in vacuum during a time interval of $1/299,792,458$ of a second
mass	kilogram	kg	mass of the international prototype of the kilogram
time	second	s	duration of 9,192,631,770 periods of the radiation corresponding to the transition between the two hyperfine levels of the ground state of the cesium 133 atom
electric current	ampere	A	constant current which, if maintained in two straight parallel conductors of infinite length, of negligible circular cross-section, and placed 1 meter apart in a vacuum, would produce between these conductors a force equal to $2 \times 10^{-7}$ newton per metre of length
thermodynamic temperature	kelvin	K	$1/273.16$ of the thermodynamic temperature of the triple point of water
amount of substance	mole	mol	amount of substance of a system which contains as many elementary entities as there are atoms in 0.012 kilogram of carbon 12
luminous intensity	candela	cd	luminous intensity, in a given direction, of a source that emits monochromatic radiation of frequency $540 \times 10^{12}$ hertz and that has a radiant intensity in that direction of $1/683$ watts per steradian

Source: National Institute of Standards and Technology (NIST) at <http://physics.nist.gov/cuu/Units/current.html>

**Table 2.2** Derived Units in the International System of Units (SI)

Measures	Unit	Abbreviation	Expressed in terms of
angle	plane	radian	$\text{m} \cdot \text{m}^{-1} = 1$
	solid	steradian	$\text{m}^2 \cdot \text{m}^{-2} = 1$
frequency	hertz	Hz	$\text{s}^{-1}$
force	newton	N	$\text{m} \cdot \text{kg} \cdot \text{s}^{-2}$
energy	joule	J	$\text{m}^2 \cdot \text{kg} \cdot \text{s}^{-2}$ (or $\text{N} \cdot \text{m}$ )
power, radiant flux	watt	W	$\text{m}^2 \cdot \text{kg} \cdot \text{s}^{-3}$ (or $\text{J} / \text{s}$ )
Celsius temperature	degrees Celsius	°C	K ( $0^\circ\text{C} = 273.15\text{K}$ )
luminous flux	lumen	lm	$\text{m}^2 \cdot \text{m}^{-2} \text{cd} = \text{cd}$
luminance	lux	lx	$\text{m}^2 \cdot \text{m}^{-4} \text{cd} = \text{m}^{-2} \cdot \text{cd}$

Source: National Institute of Standards and Technology (NIST) at <http://physics.nist.gov/cuu/Units/units.html>

7. For further information, visit <http://www.bipm.org/en/publications/si-brochure/>



In the context of EO, relevant units based on these derived units include:

- Heat flux density, irradiance (W/m<sup>2</sup>);
- Specific heat capacity (J/(kg·K));
- Specific energy (J/kg);
- Radiant intensity (W/sr); and
- Radiance (W/(sr·m<sup>2</sup>)).

2.3.3 SI metric prefixes

Standard prefixes are used to define multiples and submultiples of SI units. Prefixes adjoin the SI base units names and abbreviations to modify the size of the base unit. There are currently 20 prefixes used to represent powers of 10, as listed in Table 2.3.

As shown in Tables 2.3 and 2.4, it is convenient to use scientific notation for particularly large and small numbers. For example, a quantity with the value 1,900,000, can be written in terms of its factors:

$1.9 \times 1,000,000$

or

$1.9 \times 10^6$

Similarly, a microscopic quantity of 0.0000019 can be expressed as:

$1.9 \times 0.000001$

or

$1.9 \times 10^{-6}$

This notation both simplifies arithmetic operations and emphasises the order of magnitude associated with a measurement.

2.3.4 SI units for measuring waves

Commonly used measurement units in EO relate to measuring the wavelengths or frequencies of different forms of radiation. SI units of length are based on the metre as summarised in Table 2.4. SI units for frequency are based on the hertz as listed in Table 2.5. In this text, units of length are generally used to distinguish different forms of EMR.

Table 2.3 SI metric prefixes

Prefix	Abbreviation	Decimal value	Scientific Notation	Colloquial Name
yocto	y	0.000 000 000 000 000 000 000 001	10 <sup>-24</sup>	septillionth
zepto	z	0.000 000 000 000 000 000 000 001	10 <sup>-21</sup>	sexillionth
atto	a	0.000 000 000 000 000 000 001	10 <sup>-18</sup>	quntillionth
femto	f	0.000 000 000 000 001	10 <sup>-15</sup>	quadrillionth
pico	p	0.000 000 000 001	10 <sup>-12</sup>	trillionth
nano	n	0.000 000 001	10 <sup>-9</sup>	billionth
micro	m	0.000 001	10 <sup>-6</sup>	millionth
milli	m	0.001	10 <sup>-3</sup>	thousandth
centi	c	0.01	10 <sup>-2</sup>	hundredth
deci	d	0.1	10 <sup>-1</sup>	tenth
---	---	1	10 <sup>0</sup>	one
deka	da	10	10 <sup>1</sup>	ten
hecto	h	100	10 <sup>2</sup>	hundred
kilo	k	1,000	10 <sup>3</sup>	thousand
mega	M	1,000,000	10 <sup>6</sup>	million
giga	G	1,000,000,000	10 <sup>9</sup>	billion
tera	T	1,000,000,000,000	10 <sup>12</sup>	trillion
peta	P	1,000,000,000,000,000	10 <sup>15</sup>	quadrillion
exa	E	1,000,000,000,000,000,000	10 <sup>18</sup>	quintillion
zetta	Z	1,000,000,000,000,000,000,000	10 <sup>21</sup>	sextrillion
yotta	Y	1,000,000,000,000,000,000,000,000	10 <sup>24</sup>	septillion

Source: Astronomy Education at the University of Nebraska-Lincoln at [http://astro.unl.edu/classaction/tables/intro/si\\_prefixes.html](http://astro.unl.edu/classaction/tables/intro/si_prefixes.html)

**Table 2.4** SI units of length

Unit		Distance	
Name	Abbreviation	In metres (decimal value)	In metres (scientific notation)
Kilometre	km	1,000	$10^3$
Metre	m	1	$10^0$
Centimetre	cm	0.01	$10^{-2}$
Millimetre	mm	0.001	$10^{-3}$
Micrometre <sup>10</sup>	$\mu\text{m}$	0.000 001	$10^{-6}$
Nanometre	nm	0.000 000 001	$10^{-9}$
Angstrom	Å	0.000 000 000 1	$10^{-10}$

**Table 2.5** SI units of frequency

Unit		Frequency	
Name	Abbreviation	In cycles per second (decimal value)	In cycles per second (scientific notation)
Hertz	Hz	1	$10^0$
Kilohertz	kHz	1,000	$10^3$
Megahertz	MHz	1,000,000	$10^6$
Gigahertz	GHz	1,000,000,000	$10^9$

### 2.3.5 Angles

On a (two-dimensional) plane, the angle between two intersecting lines can be readily conceived and illustrated. The SI unit for planar angles is the radian (see Section 2.3.2), such that a full circle equates to  $2\pi$  radians (or  $360^\circ$ ). A reference circle can be used to define any angle ( $\theta$ ) formed by two lines radiating from its centre (see Figure 2.1a):<sup>8</sup>

$$\theta = \frac{s}{R}$$

where

- s is the length of the arc formed by angle  $\theta$  along the circumference of the circle; and
- R is the radius of the circle.

In geometrical terms, the angle  $\theta$  is said to be subtended by the arc of length s. By definition the perimeter of a circle equals  $2\pi R$ , so for a unit circle (radius = 1), the perimeter subtends an angle of  $360^\circ$  or  $2\pi$  radians.

Solid angles occur in three-dimensional structures, such as cones, and are quantified in terms of reference spheres. The SI unit for solid angles is the steradian (see Section 2.3.2). A solid angle ( $\Omega$ ) represented by the apex of a cone originating at (or radiating from) the centre of a sphere can be computed from the radius of the sphere ( $R$ ) and the area on the sphere's surface that it intersects ( $A$ ; see Figure 2.1b), such that (in steradians):

$$\Omega = \frac{A}{R^2}$$

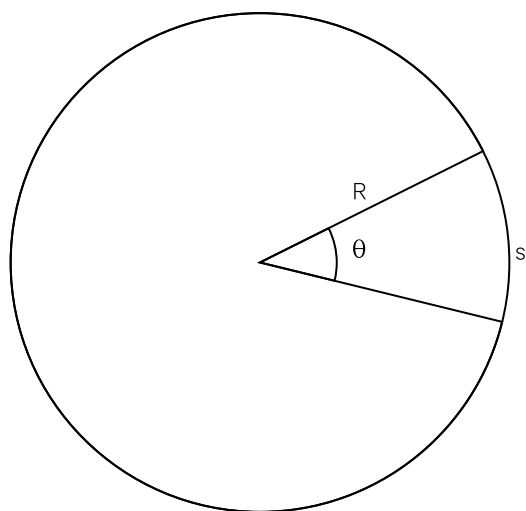
As with planar angles,  $\Omega$  is described as the angle subtended by the area A. Since the surface area of a sphere equals  $4\pi R^2$  radians, the solid angle subtended by a whole unit sphere (radius = 1) is  $4\pi$  radians.

8. Formerly micron.

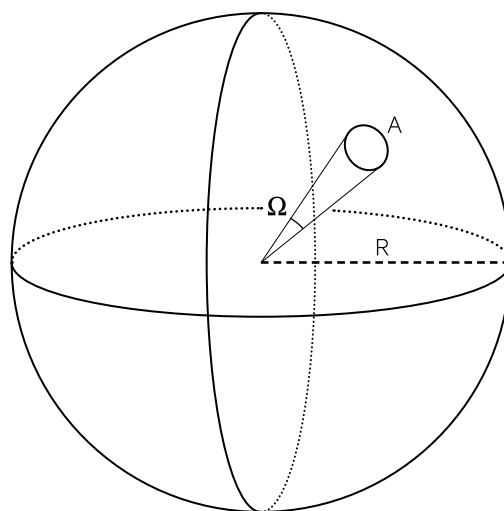
**Figure 2.1** Planar and solid angles

Planar angles define the angular separation between two intersecting lines (vectors) in two dimensions, while solid angles define the three-dimensional equivalent, and are often represented as cones.

a. Plane angle  $\theta = \frac{s}{R}$  radians, where  $s$  is the length of an arc on a circle of radius  $R$ .



b. Solid angle  $\Omega = \frac{A}{R^2}$  steradians, where  $A$  is the area on the surface a sphere of radius  $R$  that is intersected by a cone originating from the centre of the sphere.



A solid angle effectively quantifies how large an object appears to an observer. An understanding of solid angles is essential for many aspects of remote

sensing, including measurement of radiation (see Sections 2.6 and 13) and mapping projections (see Volume 2B).

## 2.4 Force Fields

Work involves force and motion, such as pushing or pulling an object some distance. Since energy is neither created nor destroyed, work can be viewed as an energy transfer mechanism:

$$\text{work} = \text{force} \times \text{distance}$$

where

*work* is measured in newton-metres;

*force* is measured in newtons; and

*distance* is measured in metres.

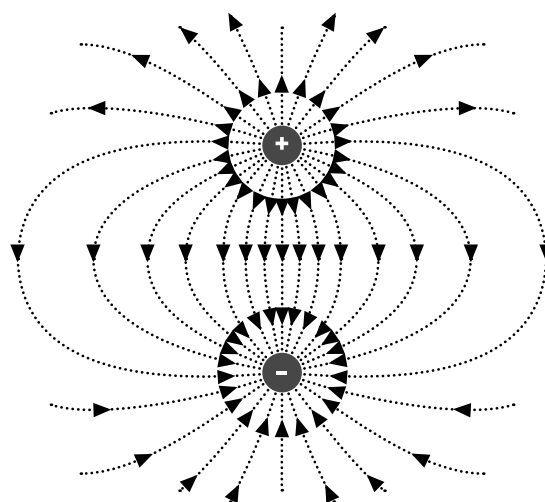
A force field defines the region in space within which an object would experience that force. Examples of force fields include:

- gravitational field—region where an object would feel a gravitational pull;
- electric field—region where an object would feel an electric force;
- magnetic field—region where an object would feel a magnetic force; or
- electromagnetic field—region where an object would feel an electromagnetic force.

All force fields are associated with a source, such as an electric charge. A force field is generally depicted by a set of imaginary field lines that indicate the direction of the force (see Figure 2.2).

**Figure 2.2** Force field example

Direction of force in a dipole electric field is shown by a set of imaginary field lines away from a positive charge to a negative charge.



An electric charge is a fundamental property of certain sub-atomic particles. Electric charges are generated by a flow of electrons between atoms, such as occurs in static electricity. The electric charge associated with an object is the sum of its component charged particles.

Every charged object is surrounded by an electric field. Charged objects also experience the electric field created by other charged objects. Charges may be positive or negative. Objects with different charges are attracted to each other while those with the same charge (both positive or both negative) repel each other.

Charged particles that are moving create and experience an additional force, called a magnetic force. Every moving charged object is surrounded by a magnetic field. Moving charged objects also experience the magnetic fields created by other moving charged objects.

An oscillating electric field will induce an oscillating magnetic field and, conversely, an oscillating magnetic field will induce an oscillating electric field. Together these oscillating fields form electromagnetic (EM) waves, which travel at 300,000 km/s (or  $3 \times 10^8$  m/s). Since visible light is a form of EMR, this velocity is better known as the speed of light.

Maxwell's equations integrate studies of electricity, magnetism and optics into a unified theory (Maxwell, 1873; Signell, 2001). This set of four partial differential equations combine the work of Coulomb, Oersted, Ampere and Faraday to describe the propagation of electric and magnetic fields, their interaction, and their impact on objects. EMR is further discussed in Sections 1 and 13.

## 2.5 Waves

Many forms of energy are transported by waves. A wave can be viewed as a disturbance that allows energy to travel through a medium without transporting matter. Wave propagation may result in temporary displacement of particles of the medium, but these particles then (theoretically) return to their original position.

Mechanical waves, such as sound waves, carry energy through a medium—solid, liquid, gas or plasma—without transporting any of the matter of the medium (see Section 9.1). EM waves are produced by the vibration of charged particles, such as electrons and protons, and can be transmitted without a medium so can travel through a vacuum. Since EM waves exhibit behaviours characteristic of both particles and waves, they are considered to have a dual nature (see Section 5).

### 2.5.1 Wave types and characteristics

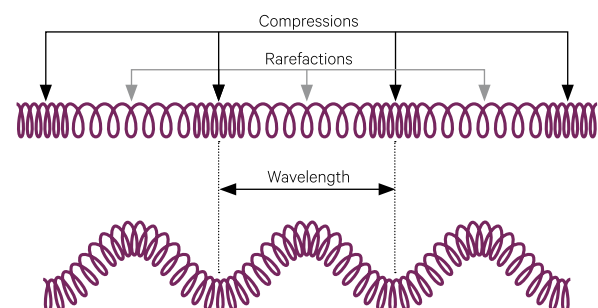
Waves are further characterised by the orientation of oscillations relative to their direction of travel (see Figure 2.3):

- transverse waves, such as EM waves and secondary seismic waves, oscillate in a plane that is perpendicular to the direction the waves are travelling; these are often pictured as a sinusoidal waveform and, when travelling through a medium, move particles of matter up and down;

- particles associated with compression or longitudinal waves, such as sound waves in air or seismic waves through the Earth, move in the same plane as the wave; these are most simply viewed as the back and forth movement that occurs through the length of 'slinky' toys; and
- surface or circular waves, such as occur in water bodies, carry particles of the medium in a circular motion and diminish with depth.

**Figure 2.3** Longitudinal and transverse waves

a. Longitudinal or compression wave—energy moves particles of medium in the direction of wave propagation. This is comparable to pushing a slinky toy at one end, which causes the coils to compress and dilate as the energy moves to the other end.  
b. Transverse wave—energy moves particles of medium in a direction that is orthogonal to wave propagation. This is comparable to shaking a slinky toy at one end, which move the coils up and down or side to side as the energy is transferred to the other end.





The energy of a transverse wave is determined by its repeat cycle, that is the distance it travels from one crest to the next trough and back to the next crest. The wavelength ( $\lambda$ ) is the length of one complete wave cycle from crest to crest. The period of a wave ( $T$ ) is the time taken to travel one wavelength. The frequency ( $\nu$ ) is the inverse of the period, that is the number of complete wave cycles in a given time unit, such as per second. For energy forms with constant velocity, such as light, as wavelength increases, frequency decreases and vice versa (see Figure 2.4). These components are related by the wave equation:

$$\text{velocity} = \nu\lambda$$

where

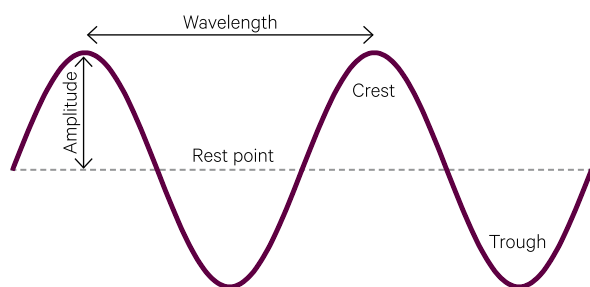
$\nu$  is frequency of the wave; and  
 $\lambda$  is the wavelength.

The amplitude of a longitudinal wave increases as the pressure difference between compressions and dilations (or rarefactions) increases. Figure 2.5 compares longitudinal wave representations with the more common sine wave representations of waves with different amplitudes. As the amplitude increases, the compressions of longitudinal waves become more dense (darker in Figure 2.5) and the rarefactions less dense (lighter in Figure 2.5).

While the power and the intensity of a wave are related, they are not the same. Power is the term used to define the energy at the source of a disturbance, while intensity is the energy at any particular point on the wave front. The two are related by the equation:

$$\text{intensity} = \frac{\text{power}}{\text{area}}$$

**Figure 2.4** Components of waves



Source: Langlopress (2016)

**Figure 2.5** Longitudinal or compression waves

Three waves are represented as both compressions and sine waves:

a. No signal



b. Low amplitude wave



c. High amplitude wave



Source: Langlopress (2016)

## 2.5.2 Reflection, refraction and diffraction

It is of relevance to remote sensing that all waves obey physical laws involved with reflection, refraction and diffraction. Waves are reflected when they encounter a surface. Regardless of the angle at which a wavefront approaches a barrier, the law of reflection (see Figure 2.6) applies:

$$\text{angle of incidence} = \text{angle of reflection}$$

The extent to which a surface obeys the law of reflection depends on its physical structure relative to the wavelength of the wave (see Volume 1B—Section 3). A totally smooth surface, or specular reflector, will reflect all incoming energy without any scattering (see Figure 2.7a). Diffuse or ‘Lambertian’ reflectance occurs when the surface is rough relative to the wavelength(s) of the incoming radiation and causes the energy to be reflected in many directions (see Figure 2.7b).

Waves also change direction when they pass from one medium to another, such as from air to water. This type of change is called refraction and varies with the 'refractive index' of the medium as described by Snell's law (see Figure 2.8a):

$$n_1 \sin \theta_1 = n_2 \sin \theta_2$$

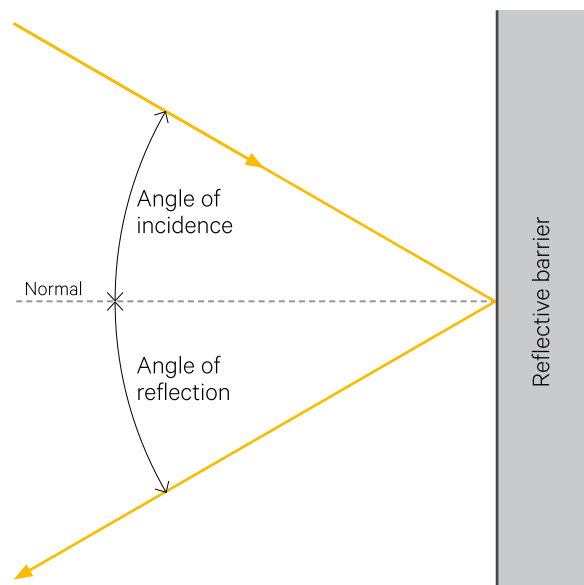
where

$n$  is the refractive index; and  
 $\theta$  is the angle of incidence.

Waves can also change direction, or are diffracted, as they pass through an opening or around a barrier (see Figure 2.8b). This effect is most obvious when the size of the barrier is comparable to the wavelength. Transverse waves, such as EM and gravitational waves, can oscillate with multiple orientations whereas longitudinal waves, such as sound waves, only oscillate in the direction of travel.

**Figure 2.6** Law of reflection

When a light wave encounters a reflectance barrier it is reflected such that the angle of incidence equals the angle of reflection

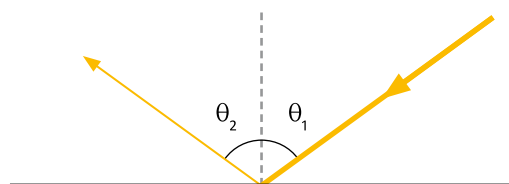


Source: Langlopress (2016)

**Figure 2.7** Specular and diffuse reflectors

The extent to which a surface obeys the law of reflection depends on its surface texture relative to the wavelength of incident radiation.

a. Specular reflection from a smooth surface—angle of incidence  $\theta_1$  equals angle of reflection  $\theta_2$ .



Source: Harrison and Jupp (1989) Figure 7

b. Diffuse reflection from a rough surface—light is scattered in many directions

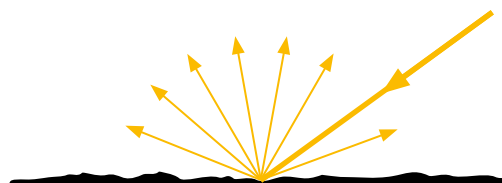
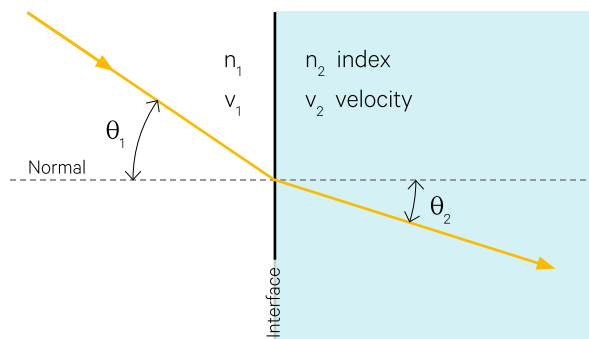


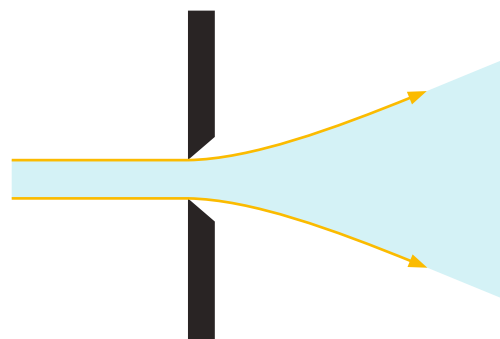
**Figure 2.8** Refraction and diffraction

a. Refraction through an interface between two media



Source: Langlopress (2016)

b. Diffraction through a narrow opening



### 2.5.3 Polarisation

Each EM wave comprises an electric force field and a magnetic force field, which are perpendicular to each other, and transverse to the direction of travel. Maxwell's equations (see Section 2.4) allow the direction and magnitude of one of these fields to be derived from knowledge of the direction and magnitude of the other (Suits, 1983).

Polarisation describes the orientation of the electric field (or its electric vector) relative to a reference plane. Horizontal (or plane) polarisation applies when the wave's plane of incidence and vertical polarisation is perpendicular to the horizontal polarisation, that is, the electric vector is aligned with the plane of incidence and also the direction of travel. Other types of polarisation include circular, when the electric field spirals to the right or left, and elliptical, when plane and circular polarisations combine to form an electric field with an elliptical cross-section (Elachi and van Zyl, 2006).

Transverse waves can be polarised to restrict their vibrations to a single plane. By contrast, randomly polarised energy vibrates in all potential orientations that are perpendicular to the direction of energy propagation. Light waves can be polarised using specially aligned filters, while microwaves and radio waves are polarised by orienting the antenna to transmit and receive specific wave planes (see Volume 1B—Section 8).

## 2.6 Properties of EMR

The energy properties of EMR that are most commonly detected and quantified can be described in terms of:

- radiometric terms—describe the energy radiated per unit time (see Section 2.6.1);
- spectral terms—focus on the energy of specific wavelength(s) (see Section 2.6.2); and
- photometric terms—consider those wavelengths detected by the human visual system (see Section 2.6.3).

For a more detailed treatment of these topics, readers are referred to the *Manual of Remote Sensing* (Colwell, 1983), *The Light Measurement Handbook* (Ryer, 1997), *ASPRS Manual of Remote Sensing* (Morain and Budge, 1998), or Elachi and van Zyl (2006).

### 2.5.4 The Doppler effect

The Doppler Effect is observed whenever the wave source is moving relative to the observer such that a change in frequency is perceived. For example, when an observer is approaching an energy source, the wave frequency will be observed to be higher than when the observer is moving away. This perception is in fact due to the relative motion of the observer rather than an actual change in frequency of the wave. This effect can be observed with sound and light waves and is particularly of interest to astronomy for determining the radial velocity of stars and galaxies relative to Earth. Several forms of remote sensing using radar sensors are based on the Doppler Effect (see Sections 14 and 15).

### 2.5.5 Coherence

Two waves with a systematic relationship between their amplitudes are called coherent, that is, they oscillate in phase. In terms of EMR, which comprises two three-dimensional vectors, definition of the underlying physics of coherence is complex, but this characteristic can be simply viewed as their relationship in time. Lasers, for example, generate coherent radiation. Conversely, waves are 'incoherent' when their amplitudes are randomly related, that is, their waves oscillate out of phase. Sunlight, candles, and incandescent light globes generate incoherent radiation.

### 2.6.1 Radiometric terms

In physics, the term 'power' describes the rate of energy flow, that is, energy per unit time. Radiometry is concerned with measuring power and radiometric terms define specific quantities related to power. In SI units, power is measured in Watts (W; see Section 2.3.2). CIE regulations denote radiometric quantities with the subscript *e* (for energy). The most commonly encountered radiometric terms in EO are defined in Table 2.6 and ground measurement of these quantities is detailed in Volume 1X—Appendix 5. Definitions of relevant standard SI units (see Section 2.3.2) are provided in Table 2.7.

**Table 2.6** Radiometric terms

Term	Symbol	Definition	Unit
Radiant Energy	$Q_e$	Energy carried by EMR	J
Radiant Energy Density	$W_e$	Energy per unit volume	J/m <sup>3</sup>
Radiant Flux (or Radiant Power)	$\Phi_e$	Radiant energy per unit time	W
Irradiance	$E_e$	Density of radiant flux incident upon a unit area of a plane surface	W/m <sup>2</sup>
Radiant exitance (or Radiant emittance)	$M_e$	Density of radiant flux radiated from a unit area of a plane surface	W/m <sup>2</sup>
Radiant Intensity	$I_e$	Radiant flux radiated from a point source per unit solid angle in a specified direction	W/sr
Radiance	$L_e$	Radiant flux radiated from a unit projected area per unit solid angle in a specified direction	W/(sr·m <sup>2</sup> )

Adapted from: Suits (1983)

**Table 2.7** SI units

Unit	Symbol	Measures	Definition
Candela	Cd	luminous intensity	One candela is the luminous intensity, in a given direction, of a source that emits monochromatic radiation of frequency $540 \times 10^{12}$ Hz and has a radiant intensity in that direction of $1/683$ watts per steradian.
Joule	J	work or energy	Work done by a force of one newton when its point of application moves one meter in the direction of action of the force, equivalent to one 3600 <sup>th</sup> of a watt-hour
Lumen	lm	luminous flux	Amount of light emitted per second in a unit solid angle of one steradian from a uniform source of one candela
Radian	rad	planar angle	Angle at the centre of a circle whose arc is equal in length to the radius
Steradian	sr	solid angle	Angle at the centre of a sphere subtended by a part of the surface equal in area to the square of the radius
Watt	W	power	One joule per second, corresponding to the power in an electric circuit in which the potential difference is one volt and the current one ampere

Source: BIPM (2016)

For a constant flow of energy in time  $t$ ,

$$Q = \Phi t$$

where

$Q$  is radiant energy; and  
 $\Phi$  is radiant flux.

For a point source, the radiant intensity ( $I$ ) in a given direction can be computed as:

$$I = \frac{\Phi}{\Omega}$$

where the solid angle  $\Omega = \frac{A}{R^2}$ , for surface area  $A$  at distance  $R$  (see Figure 2.1).

Remote sensors measure radiance ( $L$ ) from a source area in a particular direction within a defined solid angle (see Figure 2.9). Radiance can be defined as:

$$L = \frac{\Phi / \Omega}{A \cos \theta}$$

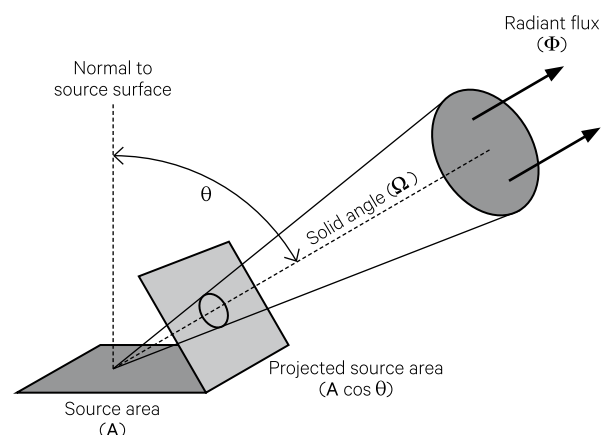
$$= \frac{I}{A \cos \theta}$$

where  $\theta$  indicates the direction from the source.

**Figure 2.9** Radiometric measurements

The radiance  $L$  from a source surface area  $A$  is measured in terms of the radiant flux  $\Phi$  within a specified solid angle  $\Omega$  in a

given direction  $\theta$  and computed as  $L = \frac{\Phi / \Omega}{A \cos \theta}$



Adapted from: Elachi and van Zyl (2006) Figure 2-10



## 2.6.2 Spectral terms

Spectral terms describe radiometric quantities as a function of wavelength. These terms are generally prefixed by the word ‘spectral’. Their symbols either use the subscript  $\lambda$  to indicate relevant wavelengths or the subscript  $\nu$  to indicate relevant frequencies.

For example, spectral intensity may be defined as the radiant intensity per unit wavelength or the radiant intensity per unit frequency. Relevant spectral terms are summarised in Table 2.8. For simplicity, the ‘e’ subscript is often omitted, and the specific range of wavelengths or frequencies may be appended in parentheses.

**Table 2.8** Spectral terms defined in terms of wavelength

Term	Symbol	Definition	Unit
Spectral Flux	$\Phi_{e\lambda}$	Radiant flux per unit wavelength	W/m
	$\Phi_{e\nu}$	Radiant flux per unit frequency	W/Hz
Spectral irradiance	$E_{e\lambda}$	Irradiance of a surface per unit wavelength	W/m <sup>2</sup>
	$E_{e\nu}$	Irradiance of a surface per unit frequency	W/(m <sup>2</sup> ·Hz)
Spectral exitance (or Spectral emittance)	$M_{e\lambda}$	Radiant exitance per unit wavelength	W/m <sup>2</sup>
	$M_{e\nu}$	Radiant exitance per unit frequency	W/(m <sup>2</sup> ·Hz)
Spectral Intensity	$I_{e\lambda}$	Radiant intensity per unit wavelength	W/(sr·m)
	$I_{e\nu}$	Radiant intensity per unit frequency	W/(sr·Hz)
Spectral radiance	$L_{e\lambda}$	Radiance of a surface per unit wavelength	W/(sr·m <sup>2</sup> )
	$L_{e\nu}$	Radiance of a surface per unit frequency	W/(sr·m <sup>2</sup> ·Hz)

## 2.6.3 Photometric terms

For visible wavelengths, EMR can be measured both in terms of electrical and optical properties (see Section 5). Various quantities are used to represent the amount of light associated with EMR<sup>9</sup>. As introduced in Section 2.6.1, flux measures the amount of radiation, or number of photons, incident on an area in a given time. While EO scientists working with

visible wavelength data generally describe EMR in radiometric or spectral quantities, colour scientists use photometric (light) units (see Table 2.9). The term ‘luminous’ implies that the wavelengths being referenced are within the human visual range (400 to 700 nm), and the subscript  $v$  is sometimes used in conjunction with relevant radiometric symbols to denote this qualification (WMO, 2008).

**Table 2.9** Equivalent photometric terms

Quantity	Radiometric		Photometric	
	Attribute	Unit	Attribute	Unit
Flux	Power	W	Luminous Flux	lm
Flux/Area	Irradiance	W/m <sup>2</sup>	Illuminance	lm/m <sup>2</sup>
Flux/Solid Angle	Radiant Intensity	W/sr	Luminous Intensity	lm/sr
Flux/Area/Solid Angle	Radiance	W/(sr·m <sup>2</sup> )	Luminance	lm/(sr·m <sup>2</sup> )

## 2.7 Colour and Human Vision

### 2.7.1 Human visual system

Human vision relies on the detection of light by two types of photochemical receptors in the retina of the eye: rods and cones. It has been estimated that each human eye contains approximately:

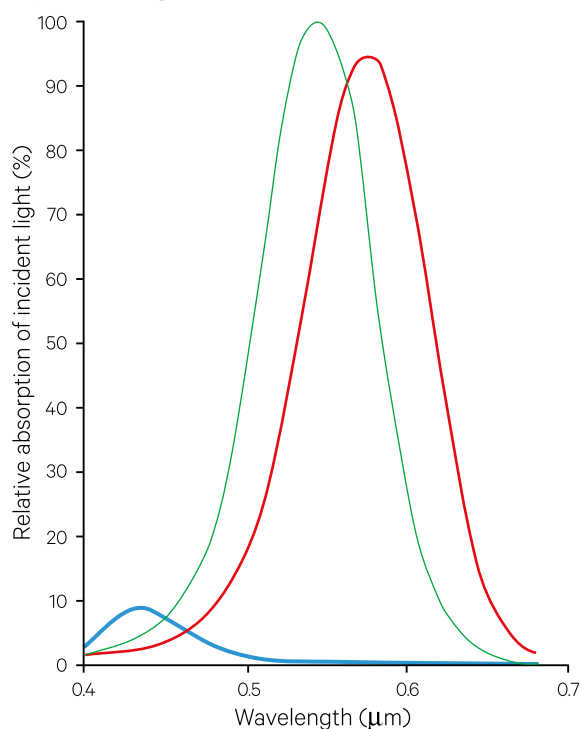
- seven million cones—which differentiate colours; and
- 120 million rods—which essentially respond to luminance (the amount of intercepted light) and are particularly important for night vision (Padgham and Saunders, 1975).

9. See also tutorials on light measurements: <http://light-measurement.com/tutorials-on-light-measurement/>

The human sensation of colour is considered to be due to the sensitivities of three types of neurochemical sensors to different wavelengths in the visible region of the EM spectrum. Each sensor is associated with one type of cone and responds with varying sensitivity to a range of wavelengths as shown in Figure 2.10. One type of sensor is maximally sensitive to short wavelengths with a peak response at approximately  $0.44\ \mu\text{m}$ . This is often referred to as the blue sensor and is insensitive to wavelengths longer than  $0.52\ \mu\text{m}$ . The second sensor has peak sensitivity at  $0.53\ \mu\text{m}$ , or green light. The third is referred to as the red sensor although peak sensitivity actually occurs at  $0.57\ \mu\text{m}$ , which is the wavelength of yellow light. However, of the three, this third sensor still has the highest absorption of red light and its sensitivity avoids responding to near infrared wavelengths (which would be rather undesirable in vegetated landscapes).

**Figure 2.10** Relative light absorption of human cones

In the human eye, the relative absorption of light differs for different cones, with blue cones (a) being significantly less responsive than green or red cones.



Source: Harrison and Jupp (1989) Figure 9 [Adapted from Cornsweet (1970)]

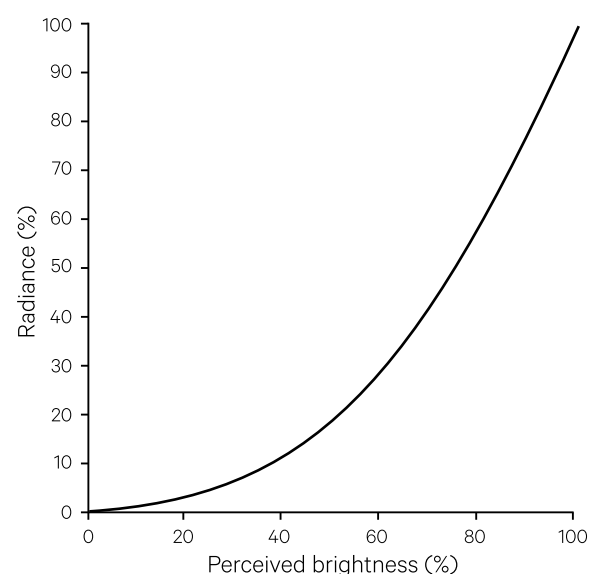
The human colour response is determined by the relative ratios of neural activities in these three sensors, which change with the wavelength of perceived light. For example, a single wavelength light at  $0.45\ \mu\text{m}$  produces a strong response from the blue sensor, a weaker response from the green sensor and a still weaker response from the red sensor. Similarly, red radiation produces strongest response from the red sensor and much weaker responses from the other two sensors. Yellow light will also invoke a strong response from the red sensor but the green and blue responses will be stronger than for red light, hence allowing the two colours to be differentiated.

## 2.7.2 Perception of colour and brightness

However, our final perception of the colour of an object is influenced by the ambient light intensity, its size and proximity to other objects, and the peculiar sensitivities of each human eye. As illustrated in Figure 2.11, small differences in dark colours (lower radiance) are better discriminated than comparable differences in brighter colours (with higher radiance). Because of the variable relationship between visual sensitivity and wavelength, it is difficult to classify colours in terms of brightness. Accordingly, while luminance measures physical brightness in photopic terms (see Section 2.6.3), luminosity, a scale on which the energy of light is corrected for the human eye's sensitivities, is used as a rough approximation for perceived brightness (Padgham and Saunders, 1975).

**Figure 2.11** Perception of light intensity changes

The human eye does not differentiate between high intensities (brighter shades or colours) as well as between low intensities (darker colours).



Source: Harrison and Jupp (1990) Figure 39 [Adapted from Land (1977)]

Although the eye has a remarkable capacity for detecting light, it is not a good discriminator in terms of perceived brightness (see Figure 2.11). Drury (1987) reports that for objects with visual angles which are similar to those typically found in remotely sensed imagery, only 20–30 different brightness steps are discernible. Perception of colour is a different matter, however, with hundreds of thousands, or even millions, of colours being distinguishable to the human eye. These human factors have considerable relevance to visual interpretation of remotely sensed imagery. While photointerpretation of EO image products yields valuable information about Earth surface features, it should be remembered that human colour perception is not implicitly related to the physical measurement of spectral colour. Notwithstanding the complexities of human colour perception, however, a trained interpreter can derive significant detail from both colour and panchromatic imagery.

### 2.7.3 Colour models

Colour spaces, or models, attempt to describe the colours perceived by human beings. The three peak sensitivity wavelengths described above (blue, green and red) form a natural basis or coordinate system for describing colour measurement. In colour science, these peak-sensitivity wavelengths are referred to as the additive primaries, since they add together to give white light, or the RGB (red-green-blue) system (see Figures 2.12 and 2.13). As shown in Figure 2.12, the brighter, secondary colours may be formed by combining different pairs of primary colours. In the additive system:

- red and green combine to produce yellow;
- blue and red combine to produce magenta; and
- green and blue combine to produce cyan.

Various colour representation devices such as projectors and display screens utilise this additive property of radiation. Colour display screens use various technologies based on red, green and blue ‘sub-pixels’, each of which can be activated separately, to achieve a mixture of coloured light at the screen’s surface (see Volume 2A—Section 7).

Colour mixing for film dyes and print media uses the subtractive primaries of yellow, magenta and cyan (YMC). These coloured pigments are mixed to produce a range of colours by being ‘subtracted’ from a white background. In the subtractive colour system:

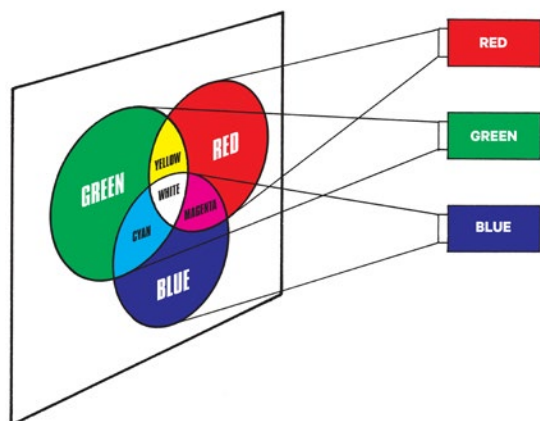
- magenta and cyan combine to produce blue;
- yellow and cyan combine to produce green; and
- yellow and magenta combine to produce red.

As illustrated in Figure 2.12, these subtractive primaries produce secondary colours by removing their complementary colours from white. The relationship between additive and subtractive primaries is illustrated in Figure 2.13.

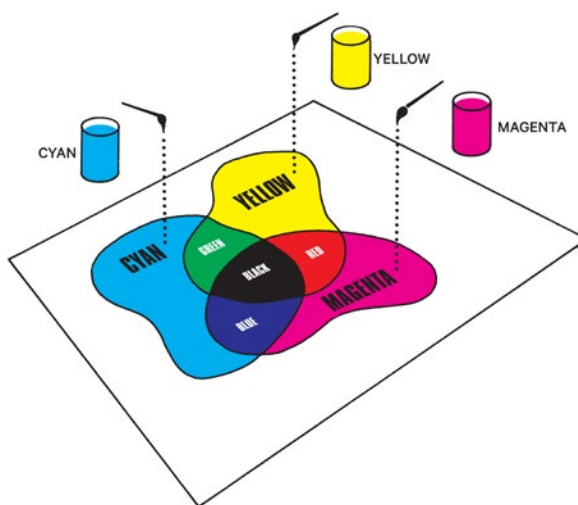
Other models order colours in terms of their hue (apparent colour), saturation (purity or chroma) and intensity (brightness), or on the basis of chromaticity. The use of colour in image processing, interpretation and presentation is further discussed in Volume 2A—Sections 5 and 6 and Volume 2X—Appendix 3.

**Figure 2.12** Additive and subtractive colour mixing

a. Red, green and blue primaries are added to a black background to give other colours



b. Yellow, magenta and cyan primaries subtract from a white background to produce other colours

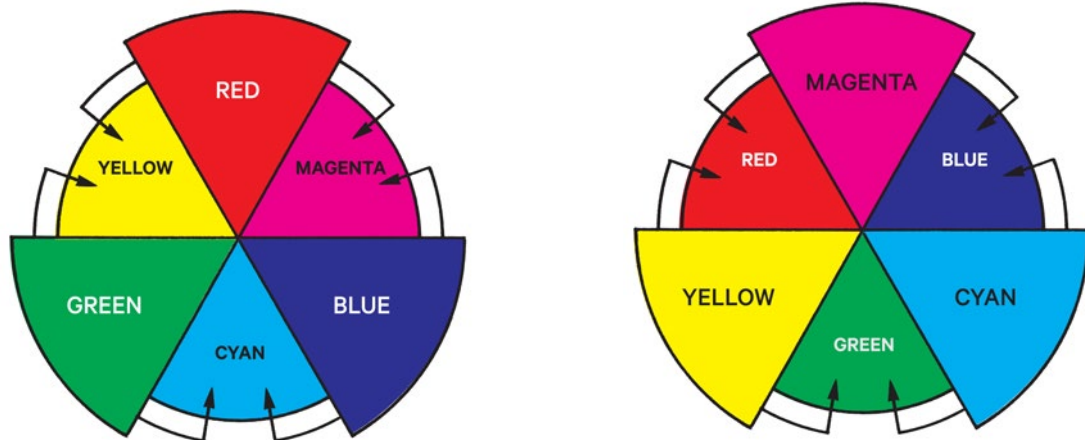


Source: Harrison and Jupp (1989) Figures 10 and 11

**Figure 2.13** Relationship between additive and subtractive primary colours

a. Additive primaries—can be combined to form brighter, secondary colours; added all together they give white light

b. Subtractive primaries—produce secondary colours by removing their complementary colours from white; added all together they produce black



Source: Harrison and Jupp (1989) Figure 12

## 2.8 Optics

As a branch of physics, optics is concerned with the way light is generated, propagated and detected.

### 2.8.1 Theories

Three major theories have been proposed to describe the behaviour of light:

- geometric or ray optics, based on the Newtonian view of an EM wave comprising a stream of particles (now called photons), simply considers light in terms of ‘rays’ that reflect and refract as described in Section 2.5.2;
- physical or wave optics, based on “Huygens’ Principle” (which visualised light as a wave vibrating vertically and perpendicular to the direction of propagation), which was also able to model non-geometric wave behaviours such as diffraction and interference; and
- quantum optics, based on the work of Planck and Einstein, which applies quantum mechanics to optical systems and accounts for the dual wave-particle nature of light (Ditchburn, 1952).

While the term ‘optical’ implies the wavelengths of visible light, in this context it is generally applied to those wavelengths whose behaviour is best described by ray optics. This includes wavelengths that are small relative to the lenses and sensors that interact with them and applies to those EMR wavelengths that are shorter than visible (ultraviolet—UV) and longer (near infrared (NIR), short wave infrared (SWIR) and thermal infrared (TIR)).

### 2.8.2 Lenses

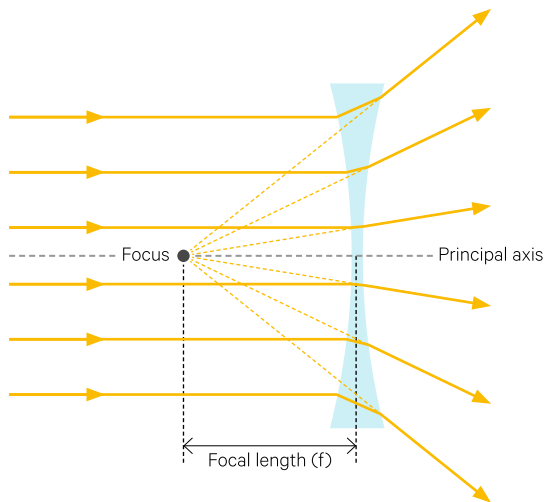
The surface of a lens is designed to make the rays of incident light converge or diverge. A beam of light travelling parallel to the optical (principal) axis of a convex lens will be focused to a single point on the axis beyond the lens (see Figure 2.14a). This point is known as the focus of the lens. The distance from the centre of the lens to the focus is known as the focal length of the lens. The same beam of light will diverge when passing through a concave lens (see Figure 2.14b). The divergent beam will appear to be emanating from a particular point on the axis on the other side of the lens. This point is also known as the focus, and the distance from the centre of the lens is called the focal length, although in this case the focal length is usually negative.

*We must be mindful of the fact that our sense of vision is limited to only a narrow band of vibration within the spectrum, and the colours as we perceive them are not necessarily real, in a definitive and absolute sense.*  
(Ark Redwood, *The Art of Mindful Gardening*)

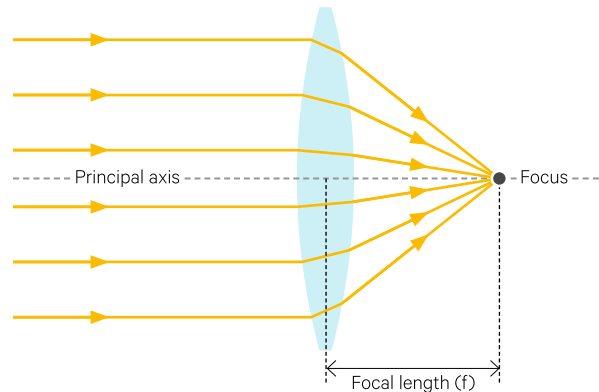


**Figure 2.14** Convex and concave lenses

a. Convex lens—a beam of light travelling parallel to the optical (principal) axis will be focused to a single point (or focus) on the axis beyond the lens



b. Concave lens—a beam of light will diverge when passing through a concave lens, with the divergent beam appearing to be emanate from a particular point (the focus) on the axis on the other side of the lens



Source: Langlopress (2016)

The field of view (FOV) for any optical system is the extent of the world it can observe (see Figure 2.15). An increase in focal length would result in a decrease in field of view. The field of view can be computed as:

$$FOV = 2 \cdot \arctan\left(\frac{1}{2} \frac{\text{image dimension}}{\text{focal length}}\right)$$

When the object is further than twice the focal length from a convex lens, as occurs in EO, the image optics can be represented as in Figure 2.16.

**Figure 2.15** Field of view

The field of view (FOV) for an optical system is inversely proportional to the focal length. The FOV defines how much of the world can be observed by the optical system.

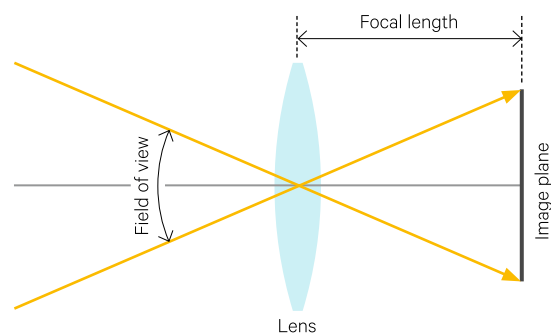
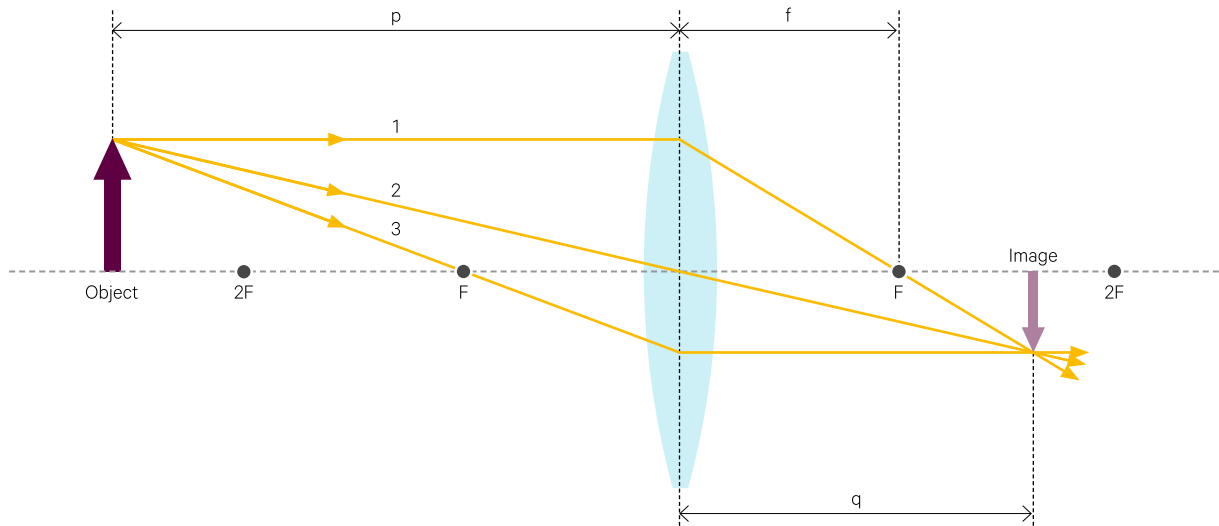


**Figure 2.16** Object more than twice focal length from convex lens



Source: Langlopress (2016)

A thin lens is defined as one whose thickness is much less than its focal length. Given the altitude of most EO systems, this lens model is an appropriate one to use when calculating scaling parameters. The thin lens approximation relates the object distance ( $p$ ), image distance ( $q$ ) and focal length ( $f$ ) by the equation:

$$\frac{1}{p} = \frac{1}{q} + \frac{1}{f}$$

A compound lens comprises an array of simple convex and concave lenses sharing a common axis. While simple convex lenses are used in some photographic cameras, compound lenses are used in high quality photographic cameras, telescopes, microscopes and other optical instruments.

## 2.9 Radiation laws

A number of physical laws apply to EMR. Two laws that are particularly relevant to EO are the:

- inverse-square law, which quantifies the radiant intensity of EMR emanating from a point source as a function of distance from the source (see Section 2.9.1); and
- Beer-Lambert law, which quantifies attenuation of energy through an absorbing medium (see Section 2.9.2).

### 2.9.1 Inverse-square law

The inverse-square law in physics describes how an omnidirectional point source spreads its 'influence' into three-dimensional space. This physical law applies to many natural phenomena, including EMR, gravity, and sound. Using simple geometric relationships, the intensity of an influence at a given distance from the source is inversely proportional to the square of the distance from the source (see Figure 2.17a). When applied to EMR, radiant intensity from a point source of radiation can be seen to decrease as a function of the square of the distance from the source (see Figure 2.17c). Thus, for a target area,  $A$ , if the radiant intensity at distance  $r$  from the source is  $x$ , then the radiant intensity at distance  $2r$  is  $x/4$ . As a target of constant area moves further from the source, the solid angle it subtends at the source reduces in proportion to  $1/r^2$  (see Figure 2.17b). Likewise, the radiant intensity reaching the target at increasing distances is reduced in the same proportion (see Figure 2.17c).

---

*Science operates according to a law of conservation of difficulty.  
The simplest questions have the hardest answers;  
to get an easier answer, you need to ask a more complicated question.  
(George Musser)*

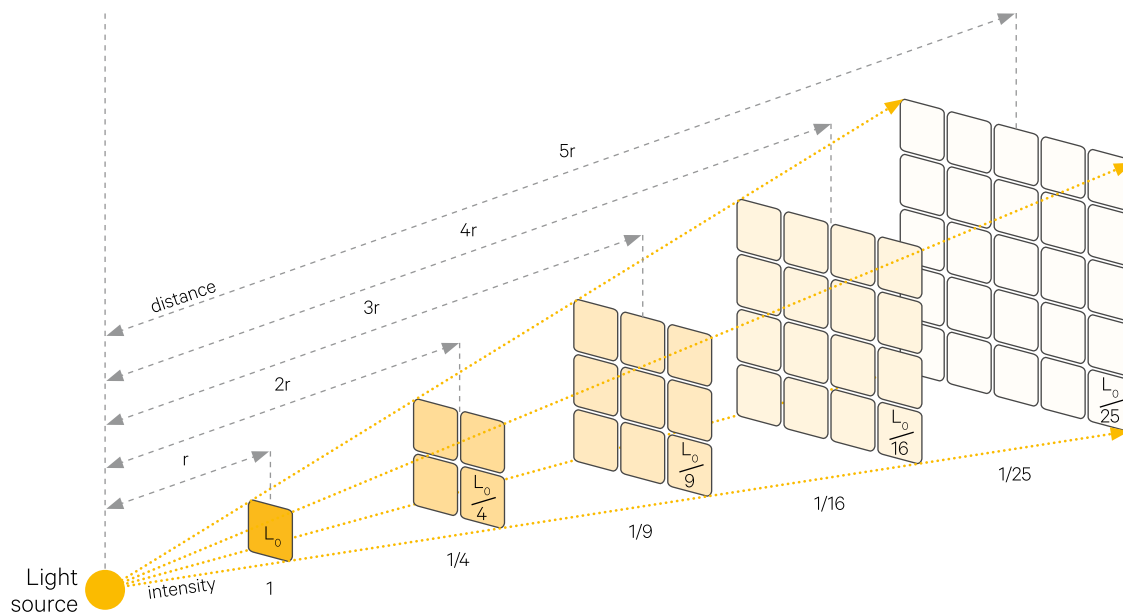
---

**Figure 2.17** Inverse-square law

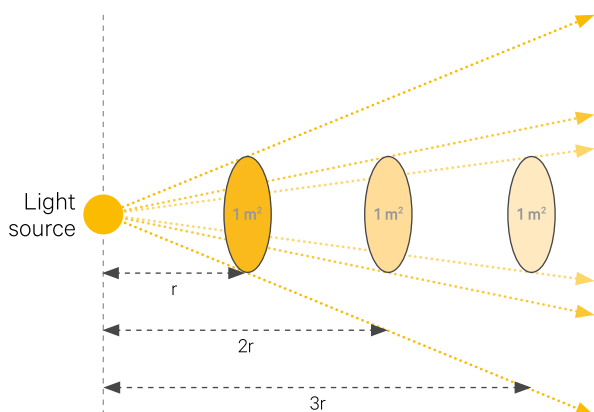
The intensity of a constant point source can be seen to decrease with increasing distance from the source by the relationship:

$$\text{intensity} = \frac{1}{\text{distance}^2}$$

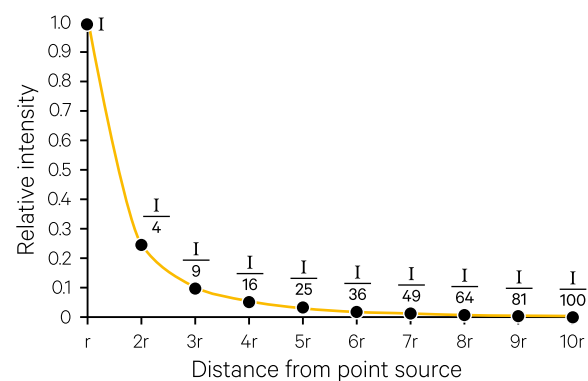
a. At a distance  $r$  from the source, the energy is spread over area  $A$ , but at distance  $2r$  the same energy is spread over four times the area ( $4A$ ). Accordingly, the resulting intensity of the energy at distance  $2r$  is only  $\frac{1}{4}$  of its intensity at distance  $r$ .



b. As a target of constant area moves further from the source, the solid angle it subtends at the source reduces in proportion to the square of the distance such that at twice a given distance, the target detects a quarter of the energy.



c. The radiant intensity from a point source decreases in proportion to the square of distance from the source.



### 2.9.2 Beer-Lambert law

It has been observed that the radiant intensity of light is reduced, or attenuated, as it passes through a medium. This is due to some light being absorbed by the medium. The rate of attenuation is described by the Beer-Lambert law:

$$A = a(\lambda)bc$$

where

- $A$  is the measured absorbance;
- $a(\lambda)$  is a wavelength-dependent absorptivity coefficient (rate of attenuation per unit distance);
- $b$  is the length travelled by the light through the medium (or path length); and
- $c$  is the concentration of the homogeneous medium.

This is commonly expressed in terms of radiant intensities of incident and transmitted light, that is, the intensity of light before and after travelling through the medium:

$$A = \log_{10} \frac{\Phi_o}{\Phi_t}$$

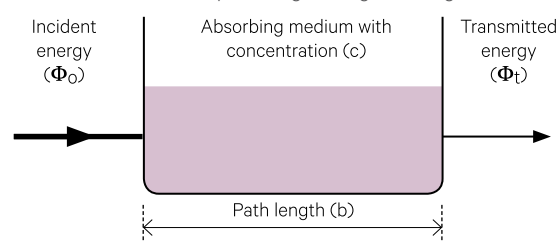
where

- $\Phi_o$  is the radiant intensity of the incident light; and
- $\Phi_t$  is the radiant intensity of the transmitted light (see Figure 2.18).

Non-linear attenuation can also occur due to chemical and instrumental factors.

**Figure 2.18** Beer-Lambert law

This law quantifies how much light is absorbed as it passes through a medium. Absorption is dependent on both the concentration of the medium (assumed to be homogeneous) and its thickness (or the path length of light through it).



## 2.10 Heat and Temperature

The energy of particles in random motion is called kinetic energy or kinetic heat. The temperature of an object is indicative of its internal energy, that is, the average kinetic energy of its particles. The particles of all matter with a temperature above 0K exhibit the random motion of kinetic heat. The temperature of an object can be expressed in terms of:

- internal temperature—kinetic motion of particles; and
- external temperature—emitted EMR resulting from internal kinetic energy (see Section 2.11).

Heat can be described as the thermal energy that is transferred from matter with a higher temperature to matter with a lower temperature. Heat is transferred between materials via one of three fundamental processes:

- conduction—adjacent molecules of a solid material are agitated without visible motion of the solid, resulting in the transfer of heat along the material. Conduction of heat from one material to another requires materials to be in physical contact. Metals are good conducting materials due to the presence of free electrons.
- convection—circulating currents within fluids resulting from a temperature gradient. Heat is transferred by convection due to movement of the heated material.

- radiation—EM energy that is transferred through a medium or vacuum. On Earth, emission of EM energy generally only occurs after shorter wave EMR from the Sun has been absorbed (see Section 5.1). Radiation is the only mechanism by which energy can be transmitted through a vacuum.

### 2.10.1 Thermal properties of matter

The heat of a material that can be sensed or measured is called its *Sensible Heat*. *Heat (or thermal) capacity (c)* defines the amount of heat required to increase the temperature of matter by 1°C (or 1K):

$$c = \frac{Q}{\Delta T}$$

where

$T$  is temperature.

Heat is measured in joules (J) or calories (cal), where 1 calorie represent the amount of heat needed to increase the temperature of 1 gm of water by 1°C and 1 cal = 4.184 J (see Section 2.3).

*Specific Heat (c<sub>p</sub>)* is the ratio of the heat capacity of an object to its mass and represents the energy required to increase the temperature of 1 gm of matter by 1°C (or 1K) in an environment of constant pressure. For example, the specific heat of water is 4.184 kJ/(kg·K), while the specific heat of carbon



is 0.71 kJ/(kg·K). This implies that over 4 times the energy is required to increase the temperature of water compared to the energy required to heat carbon. Water has a higher heat capacity than any other substance on Earth, which is the reason that waterbodies heat and cool more slowly than nearby land surfaces. By comparison, gold, which heats up and cools down rapidly, has a specific heat capacity of 0.13 kJ/(kg·K).

*Thermal conductance and thermal conductivity* describe the rate at which heat can pass through matter. Thermal conductance measures the energy that flows through a unit area in unit time, where opposite faces of the area maintain a constant difference in unit temperature, with units of J/(m<sup>2</sup>·s·K). Thermal conductivity (*k*) measures the energy that flows through a unit length in unit time, where opposite faces of the area or length maintain a constant difference in unit temperature. The SI unit for measuring thermal conductivity is W/(m·K). Thermal conductivity varies with moisture content and particle size. For example, the thermal conductivity of fresh water, with slow heat transfer, is 0.6 W/(m·K), whereas the thermal conductivity of gold, with rapid heat transfer, is 300 W/(m·K).

*Thermal inertia (P)* measures the thermal response of matter to changes in ambient temperature in the units of J m<sup>-2</sup> K<sup>-1</sup> s<sup>-1/2</sup>:

$$P = \sqrt{k\rho c}$$

where

*k* is thermal conductivity (W m<sup>-1</sup> K<sup>-1</sup>);

*ρ* is the density (g cm<sup>-3</sup>); and

*c* is specific heat capacity (J kg<sup>-1</sup> K<sup>-1</sup>).

Thermal inertia of a material generally increases proportionally with increasing density. Apparent thermal inertia can be derived from EO by comparing registered images of a particular location that were acquired at different times during the diurnal cycle (see Sections 14.1.3 and Volume 1B—Section 7).

## 2.10.2 Latent heat

When a substance changes state, such as from solid to liquid, additional energy is required to overcome cohesion between molecules. The heat required for this process is called *Latent Heat*. Thus, heat can either increase the kinetic energy of molecular vibrations in a substance or break the bonds between its molecules. Latent heat effectively changes the potential energy of the molecules. The Latent Heat of Fusion converts a solid to a liquid without a temperature change. In the case of ice, most of the energy involved in this melting process rearranges the molecules from crystal lattice to the weaker bonds between liquid water molecules. The Latent Heat of Vaporisation refers to the energy required to convert a liquid to a gas without a change in temperature. Again using the example of water, this energy completely separates the water molecules so that they can move freely as a gas. The energy requirements corresponding to changing the states of water are summarised in Table 2.10.

**Table 2.10** Energy required to convert 10 g ice to steam

Temperature (°C)	State	Temperature	Energy Transfer (J)	Heat Function
-25 – 0	Ice	increasing	522	Increase kinetic energy of molecules
0	melting	same	3,330	Latent heat of fusion
0 – 100	water	increasing	4,190	Increase kinetic energy of molecules
100	boiling	same	22,600	Latent heat of vaporisation
100–125	steam	increasing	502	Increase kinetic energy of molecules

Adapted from: Holt Physics, Table 10-5

### 2.10.3 Thermodynamics

Thermodynamics is a field of physics that examines the impact of heat and work energy on the temperature, volume and pressure of ‘systems’. In this context, a system refers to a specific area of study with a defined boundary and a finite volume. Transfers of energy across a system boundary (between the system and its surroundings) are the focus of thermodynamics. Open systems permit exchanges of energy and matter, closed systems only allow exchanges of energy but not matter, and isolated systems exchange neither. The planet Earth most nearly approximates a closed system in which matter cycles between the lithosphere, hydrosphere, atmosphere and biosphere, and solar energy enters the system through the atmosphere.

The first law of thermodynamics relates to conservation of energy within a system:

$$\Delta E = Q + W$$

where

$E$  is internal energy of a system;  
 $Q$  is heat added to the system; and  
 $W$  is work done to the system.

This is equivalent to the statement that the energy in the universe is constant—it cannot be created or destroyed but changes from one form to another. A cyclic process is one that enables a system to return to its initial state so that its internal energy does not change. When heat flows into a system ( $Q$  is positive in the equation above), the process is endothermic; when heat flows out of the system ( $Q$  is negative), the process is exothermic.

The second law of thermodynamics states that the disorder, or entropy, of the universe is always increasing. This law allows for the reality of converting heat energy into work. Since it is not possible to attain complete efficiency in any energy transfer, some amount of heat is also transferred outside of the system. Thermodynamic efficiency indicates the proportion of heat that is transferred out of a system during the process of energy conversion.

## 2.11 Blackbody Radiation

Radiation transfers EM energy by emission from a source through a medium or a vacuum. EMR emitted by an object is called the radiant flux ( $\Phi$ ; measured in watts—see Section 2.6.1). EM energy is continuously being emitted at all wavelengths by every material with a temperature above absolute zero ( $-273.15^\circ\text{C}$  or  $0\text{K}$ ). With no other objects in the universe, a material would gradually cool to  $0\text{K}$  by radiating all of its energy. Absorption of energy increases both the temperature and rate of emission of a material.

A blackbody is a theoretical object or system that absorbs all incident EMR, hence has an apparent colour of black. The wavelengths of energy emitted by a blackbody are determined by the temperature of the blackbody, rather than either its chemical composition or the incident radiation. While no blackbodies actually exist, this concept is valuable for describing the radiative properties of matter.

Four physical laws have been derived to characterise blackbody behaviour:

- Stefan-Boltzmann’s law (see Section 2.11.1);
- Kirchof’s law (see Section 2.11.2);
- Wien’s displacement law (see Section 2.11.3); and
- Planck’s law (see Section 2.11.4).

These laws are used to derive apparent temperature estimates from measurements of thermal IR emission (see Volume 1B—Section 7).

### 2.11.1 Stefan-Boltzmann’s law

The total radiation (across the full EM spectrum) emitted from a blackbody is proportional to the fourth power of its absolute temperature:

$$W_b = \sigma T^4$$

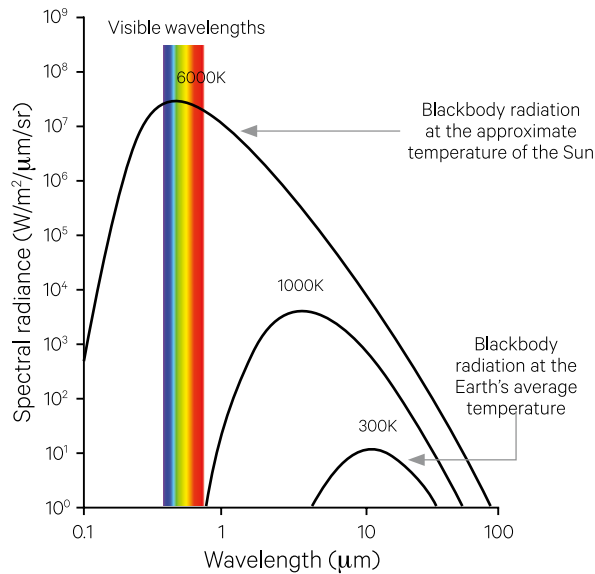
where

$W_b$  is total emitted radiation, or emitted radiance, from the blackbody;  
 $T$  is the absolute temperature of the blackbody; and  
 $\sigma$  is the Stefan-Boltzmann constant =  $5.670373 \times 10^{-8} \text{ W}/(\text{m}^2\cdot\text{K}^4)$ .

Thus, per unit area, more energy is emitted from hot objects than from cool ones.

**Figure 2.19** Blackbody radiation

The wavelength of peak radiant exitance for a blackbody decreases as its temperature increases (Note: Scales are logarithmic)



Adapted from: NASA/USGS Astrogeology Science Center Radiance Calculator at <http://astrogeology.usgs.gov/tools/thermal-radiance-calculator/>

### 2.11.2 Kirchhoff's law

The *emissivity* of a target object ( $\epsilon$ ) is quantified relative to the behaviour of a blackbody at a given wavelength by comparing their emitted radiances at a selected wavelength,  $\lambda$ :

$$\epsilon = \frac{\text{emitted radiance at } \lambda}{\text{blackbody radiance at } \lambda}$$

This law is more commonly written as:

$$W = \epsilon W_b$$

where

- $\epsilon$  is emissivity of target object (scaled 0–1);
- $W_b$  is total emitted radiation, or emitted radiance, from the blackbody; and
- $W$  is the total emitted radiation from the target object.

The emissivity index can be viewed as a measure of radiating efficiency across the whole spectrum.

### 2.11.3 Wien's displacement law

The wavelength of peak radiant exitance of a blackbody is inversely proportional to its absolute temperature:

$$\lambda_{\max} T = \text{constant} = 2897.756 \mu\text{m K}$$

where

$\lambda_{\max}$  is the wavelength of peak radiant exitance;  
and

$T$  is the absolute temperature of the target object.

This law quantifies the observation that the wavelength corresponding to the peak radiance of a target object decreases as its temperature increases (see Figure 2.19).

### 2.11.4 Planck's law

The frequency distribution of energy emitted by a blackbody is explained by the Planck Hypothesis (see Figure 2.19). This states that energy exists in discrete quanta, called photons, in proportion to the energy's frequency:

$$L_{\lambda}(T) = \frac{2hc^2}{\lambda^5} \times \frac{1}{e^{\frac{hc}{\lambda k_B T}} - 1}$$

where

$L_{\lambda}$  is the spectral radiance at wavelength  $\lambda$   
and temperature  $T$  (energy per unit time  
per unit surface area per solid angle per unit  
wavelength);

$h$  is the Planck constant =  $6.6206896 \times 10^{-34}$  J s  
(Joule seconds);

$c$  is the speed of light; and

$k_B$  is the Boltzmann constant =  $1.38065156 \times 10^{-23}$   
J/K.

Planck's law allows the proportion of radiation within specific wavelength intervals to be determined.

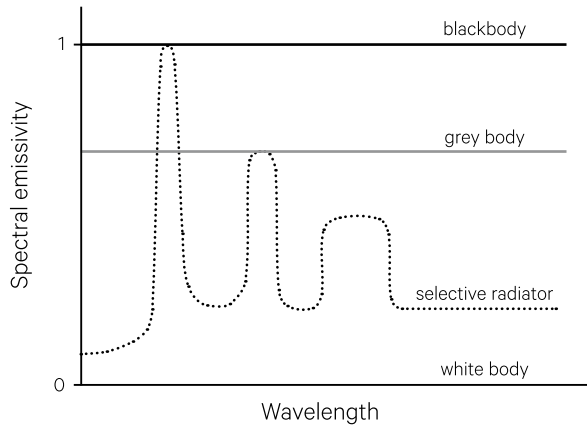
### 2.11.5 Other bodies

In contrast with blackbodies, a white body has zero emissivity across all wavelengths. A greybody is a theoretical energy source that reflects some incident radiation equally across all wavelengths, thus has an apparent colour of grey and emissivity less than one. This property is also expressed as constant emissivity over all wavelengths. Greybodies are used to approximate the emission properties of real world materials.

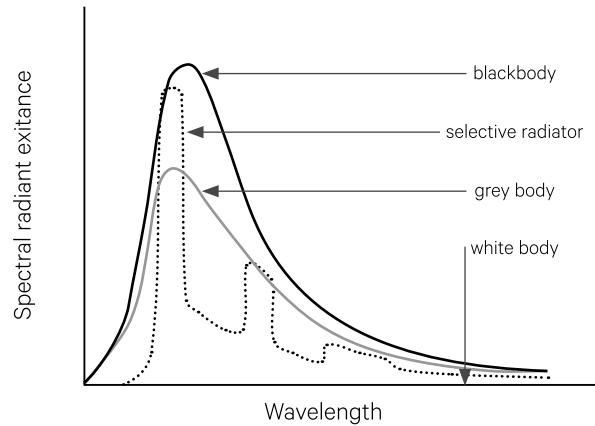
The term selective radiator describes an object whose emissivity varies with wavelength. A selective radiator with higher emissivity but the same temperature as another selective radiator will have a higher radiance, that is, it will radiate more strongly. The emissivity differences between blackbodies, greybodies, white bodies and selective radiators are illustrated in Figure 2.20.

**Figure 2.20** Spectral emissivity and spectral radiant exitance of various bodies

a. By definition, the emissivity ( $\epsilon$ ) for a blackbody equals 1 and for a white body equals zero. A greybody both reflects and emits energy equally over all wavelengths, so has a constant emissivity value which is less than 1. Emissivity from a selective radiator, however, varies with wavelength.



b. Spectral radiant exitance for blackbody, greybody, selective radiator and white body.



Adapted from: Remote Sensing lectures by Wataru Takeuchi, University of Tokyo at <http://wtlab.iis.u-tokyo.ac.jp/~wataru/lecture/rsgis/rsnote/cp1/1-7-2.gif>

## 2.12 Further Information

### Basic Physics Topics:

<http://hyperphysics.phy-astr.gsu.edu/hbase/hph.html>

<http://www.physnet.de/PhysNet/education.html>

<http://www.olympusmicro.com/primer/lightandcolor/index.html>

<http://langlopress.net/homeeducation/resources/science/index.php?op=scienceoutline>

### Basic Chemistry Topics:

<http://www.chem.ucla.edu/~gchemlab/>

<http://teaching.shu.ac.uk/hwb/chemistry/tutorials/>

<http://langlopress.net/homeeducation/resources/science/index.php?op=scienceoutline>

### Thermal Remote Sensing lectures:

<http://topex.ucsd.edu/rs/Lec06.pdf>

<http://wgbis.ces.iisc.ernet.in/envisrs/?q=node/40>

### Measurement:

<http://physics.nist.gov/cuu/Units/index.html>

<http://www.cleavebooks.co.uk/dictunit/>

<http://www.bipm.org/en/publications/si-brochure/>

### Wave Motion:

<http://www.acs.psu.edu/drussell/Demos/waves/wavemotion.html>

### Blackbody Radiation:

[https://www.e-education.psu.edu/astro801/content/l3\\_p5.html](https://www.e-education.psu.edu/astro801/content/l3_p5.html)

<http://astrogeology.usgs.gov/tools/thermal-radiance-calculator/>

### Light:

Ryer (1997)

<http://www.livescience.com/50678-visible-light.html>

<https://optics.synopsys.com/lighttools/pdfs/illuminationfund.pdf>

### Solid angles:

<http://marine.rutgers.edu/dmcs/ms552/2009/solidangle.pdf>



## 2.13 References

- Anderberg, M. A. (1973). *Cluster Analysis for Applications*. Academic Press, New York.
- BIPM (2016). Bureau International de Poids et Mesures. Retrieved from <http://www.bipm.org/en/about-us/>.
- Colwell, R. N. (1983). *Manual of Remote Sensing*, Second Edn. American Society of Photogrammetry, Falls Church, Virginia.
- Cornsweet, T. N. (1970). *Visual Perception*. Academic Press, New York.
- Drury, S. A. (1987). *Image Interpretation in Geology*. Allen and Unwin, London.
- Elachi, C., and van Zyl, J. (2006). *Introduction to the Physics and Techniques of Remote Sensing*, Second Edn. Wiley Interscience, New Jersey.
- Harrison, B. A., and Jupp, D. L. B. (1989). *Introduction to Remotely Sensed Data. Part ONE of the microBRIAN Resource Manual (156 pages)*. CSIRO Australia, Melbourne.
- Harrison, B. A., and Jupp, D. L. B. (1990). *Introduction to Image Processing. Part TWO of the microBRIAN Resource Manual (256 pages)*. CSIRO Australia, Melbourne.
- Land, E. (1977). The retinex theory of colour vision. *Scientific American*, 237(6), pp. 108-128.
- Langlopress (2016). *Scientific Illustrations*. Retrieved from <http://langlopress.net/homeeducation/resources/science/index.php?op=sciencethumbs>.
- Maxwell, J. C. (1873). *A Treatise on Electricity and Magnetism*, Vol. 1 and 2, Clarendon Press Series. Macmillan and Co, London.
- Morain, S. A., and Budge, A. M. (1998). *Earth Observing Platforms and Sensors*, Vol. 1, Third Edn., Ed: R. A. Ryerson, *Manual of Remote Sensing*. American Society for Photogrammetry and Remote Sensing (ASPRS); John Wiley & Sons, Inc., New York.
- Padgham, C. A., and Saunders, J. E. (1975). *The Perception of Light and Colour*. Academic Press, New York.
- Ryer, A. (1997). *Light Measurement Handbook*. Retrieved from <http://www.intl-lighttech.com/services/ilt-light-measurement-handbook>.
- Signell, P. (2001). *Electromagnetic Waves from Maxwell's Equations*. Retrieved from [http://www.physnet.org/modules/pdf\\_modules/m210.pdf](http://www.physnet.org/modules/pdf_modules/m210.pdf).
- Suits, G. H. (1983). The Nature of Electromagnetic Radiation. Chapter 2 in 'Manual of Remote Sensing' (Ed: R. N. Colwell), pp. 27-60. ASPRS, Falls Church, Virginia.
- WMO (2008). *Nomenclature of Radiometric and Photometric Quantities*. Chapter 7A in 'Guide to Meteorological Instruments and Methods of Observation', Vol. 8. 7th Edn. World Meteorological Organisation, Geneva.

# 3 Planet Earth

As the name implies, Earth Observation (EO) is about observing the Earth. An understanding of the target is invaluable for any investigative exercise and this is especially true for one that is as large, varied and unique as our own planet.

Before discussing EO in more detail, this section will review our current understanding of planet Earth in terms of:

- its place in space (see Section 3.1);
- its structure (see Section 3.2);
- its shape (see Section 3.3); and
- its life forms (see Section 3.4).

It should be emphasised that much of our current knowledge of each of these aspects of the Earth has been derived and/or refined using EO, especially at global and regional scales. Indeed, EO offers a unique perspective for observing changes in features and processes on the Earth, integrating multiple observations with ground-based validation measurements, and testing models that attempt to describe the observed changes.

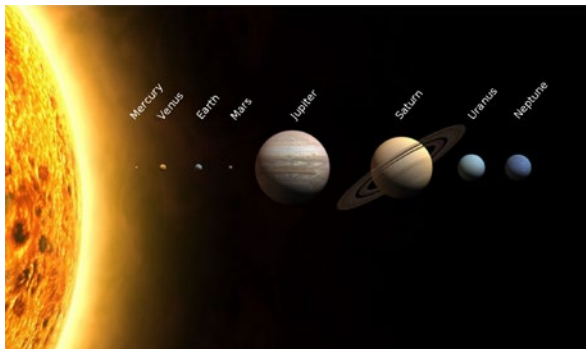
51

## 3.1 The Earth in Space

The Earth is the third of eight planets that revolve around the Sun<sup>10</sup> (see Figure 3.1).

**Figure 3.1** Our solar system

The Earth is the third of eight planets in our solar system. Note: that distances are not to scale.



Source: NASA. Retrieved from <https://commons.wikimedia.org/wiki/File:Planets2013.svg>

Planets move according to Kepler's three laws:

- Law of ellipses—planets move in ellipses with the Sun at one focus, that is, the elliptical orbit is anchored on one side by the Sun;
- Law of Equal Areas—the radius vector describes equal areas in equal times, that is, a line between the planet and the Sun would sweep the same area in equivalent time intervals; and
- Law of Harmonies—the square of the periodic times are to each other as the cubes of the mean distance, that is, the orbit period squared is proportional to the cube of the semi-major axis of the orbit (NASA, 2015).

*What's the use of a fine house if you haven't got a tolerable planet to put it on?*  
(Henry David Thoreau)

**Background image:** This Landsat-5 image was acquired on 18 February 2009 and shows the rivers flowing into the Gulf of Carpentaria in flood conditions (displayed using bands 2, 4, 5 as RGB). **Source:** Norman Mueller, Geoscience Australia

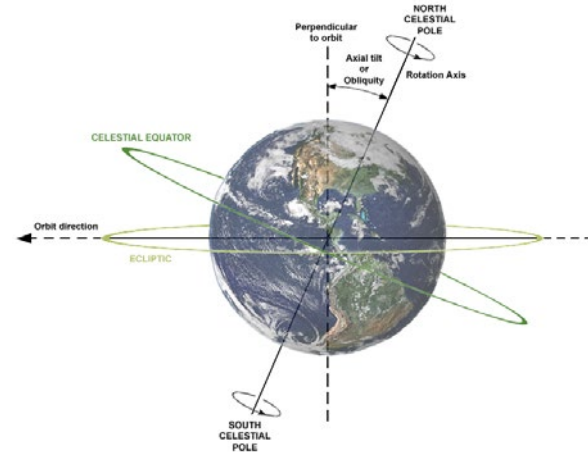
<sup>10</sup> Pluto was demoted from full planetary status in 2006, and is now considered a dwarf planet.

All planets do not share a common axial tilt, or obliquity (the angle between the rotational axis and the orbital axis; see Table 3.1). This is equivalent to the angle between the equatorial and orbital planes of the planet (see Figure 3.2), or solar declination, and equals 23.4° for planet Earth. The plane of Earth's orbit around the Sun is called the elliptic plane (Iqbal, 1983). The plane that is orthogonal to Earth's rotational axis is the plane of the celestial equator, which can be used to track the position of the Sun relative to Earth. On two days each year, these planes coincide so that the Sun is positioned directly over Earth's equator. On these equinox days<sup>11</sup> all locations on Earth experience 12 hours of daylight and 12 hours of night (20/21 March and 22/23 September). The solstices<sup>12</sup> occur on days of maximum solar declination (21/22 June and 21/22 December, when there is maximum difference between the length of day and night (Iqbal, 1983).

Based on spherical geometry principles, irradiance decreases with the square of the distance from a radiation source (see Section 2.9.1). Accordingly, the total solar irradiance reaching Earth is about half that reaching Venus and more than twice that reaching Mars. Features of Earth are compared with other planets in Table 3.1.

**Figure 3.2** Earth's axis of rotation

Relationship between axial tilt (or obliquity), rotation axis, plane of orbit, celestial equator and ecliptic (plane of Earth's orbit). Earth is shown as viewed from the Sun, with the orbit direction counter-clockwise (to the left).



Source: Dennis Nilsson (CC BY 3.0). Retrieved from [https://en.wikipedia.org/wiki/Earth%27s\\_rotation#/media/File:AxialTiltObliquity.png](https://en.wikipedia.org/wiki/Earth%27s_rotation#/media/File:AxialTiltObliquity.png)

**Table 3.1** Comparison of planetary features

Planet Characteristic	Mercury	Venus	Earth	Mars	Jupiter	Saturn	Uranus	Neptune
Mass (10 <sup>24</sup> kg)	0.33	4.87	5.97	0.642	1898	568	86.8	102
Equatorial diameter (km)	4879	12,104	12,756	6792	142,984	120,536	51,118	49,528
Average density (kg/m <sup>3</sup> )	5427	5243	5514	3933	1326	687	1271	1638
Equatorial gravity (m/s <sup>2</sup> )	3.7	8.9	9.8	3.7	23.1	9	8.7	11
Rotation period (hours)	1407.6	-5832.5	23.9	24.6	9.9	10.7	-17.2	16.1
Length of day (hours)	4222.6	2802	24	24.7	9.9	10.7	17.2	16.1
Distance from Sun (10 <sup>6</sup> km)	57.9	108.2	149.6	227.9	778.6	1433.5	2872.5	4495.1
Astronomical Units (AU) <sup>15</sup>	0.387	0.723	1	1.52	5.20	9.58	19.20	30.05
Solar irradiance (W/m <sup>2</sup> )	9,000	2,640	1,370	590	50	15	3.7	1.5
Perihelion (10 <sup>6</sup> km)	46	107.5	147.1	206.6	740.5	1352.6	2741.3	4444.5
Aphelion (10 <sup>6</sup> km)	69.8	108.9	152.1	249.2	816.6	1514.5	3003.6	4545.7
Orbital Period (days)	88	224.7	365.2	687	4331	10,747	30,589	59,800
Average orbital velocity (km/s)	47.4	35	29.8	24.1	13.1	9.7	6.8	5.4
Orbital inclination (degrees)	7	3.4	0	1.9	1.3	2.5	0.8	1.8
Orbital Eccentricity	0.205	0.007	0.017	0.094	0.049	0.057	0.046	0.011
Obliquity to orbit (degrees)	0.01	177.4	23.4	25.2	3.1	26.7	97.8	28.3
Mean temperature (°C)	167	464	15	-65	-110	-140	-195	-200
Number of moons	0	0	1	2	67	62	27	14

Source: NASA (2015)<sup>13</sup>

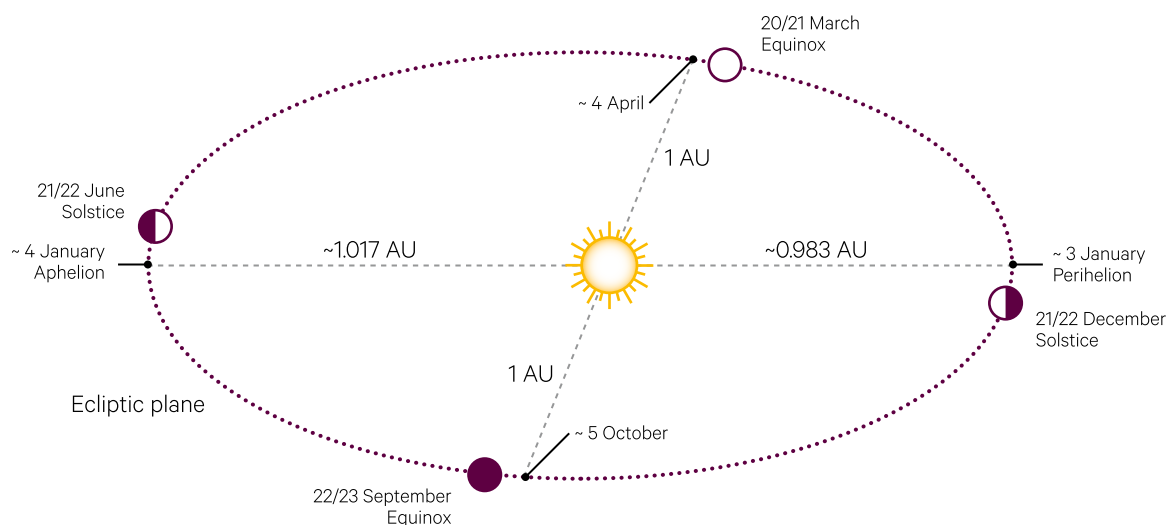
11. From Latin/Old French: equi = equal, nox = night

12. From Latin/Old French: sol = Sun, stit = stationary or stopped

13. Measurement unit equaling 149,597,870.7 km (mean distance from the Earth to the Sun). (Source: <http://neo.jpl.nasa.gov/glossary/au.html>)

**Figure 3.3** Variation in solar radiation due to Earth's elliptical orbit

Seasonal characteristics of Earth's orbit. Note: Distances are not to scale.



Adapted from: Iqbal (1983) Figure 1.2.1

The Earth rotates once around its own axis each day and completes one revolution around the Sun each year. Its solar orbit is elliptical, which results in variations in the distance from the Sun to Earth within each annual orbit. The combination of an elliptical orbit and a tilted axis of rotation change the amount of solar radiation reaching each part of the Earth's surface during each year, and this differential heating cycle produces our seasons.

The approximate distance from Earth to our moon is 384,000 km and its mean diameter is around one quarter the diameter of Earth (NASA, 2015). The synchronous rotation of the moon around Earth exerts enough gravitational force on the waters of the Earth to create tides. While the surface area on Earth is over 510 million km<sup>2</sup>, the surface area of the Moon spans 37.9 million km<sup>2</sup>—less than the Asian continent—and 7.4% of the surface area of Earth (Cain, 2016).

The Earth's elliptical orbit around the Sun brings it closest to the Sun in early January. This point is called the periapsis (smallest radial distance of an ellipse) or the perihelion (smallest radial distance in an elliptical orbit around the Sun). The point of greatest distance is called the apoapsis (greatest radial distance of an ellipse) or aphelion (furthest distance from the Sun in an elliptical orbit; see Figure 3.3). The Earth is furthest from the Sun in early July and closest in January, with the actual dates varying from year to year. This configuration varies the amount of solar radiation reaching the top of Earth's atmosphere throughout the year, such that around 6.7% more radiation is received at periapsis than at apoapsis (see also Section 5).

## 3.2 Structure of the Earth

Current knowledge of Earth's internal structure is heavily reliant on remote sensing techniques. Our understanding of the internal structure of Earth is based on investigations relating to:

- earthquake waves and how they travel through the Earth;
- geology of surface rocks;
- Earth's movement in the Solar System;
- Earth's gravity and magnetic fields; and
- heat transfer from inside the Earth.

On the basis of these observations, geophysicists have inferred the structure of the Earth in terms of both compositional and mechanical layers as illustrated in Figure 3.4. Traditionally the Earth has been viewed as being composed of three layers: the innermost and densest core, an intermediate mantle layer, and a surface crust, on which we live. Our knowledge of these compositional layers has recently been expanded by new data relating to their mechanical properties. The density transitions between layers are stepped, rather than continuous, with a marked change occurring at the boundary between the mantle and the outer core (Dziewonski and Anderson, 1981).



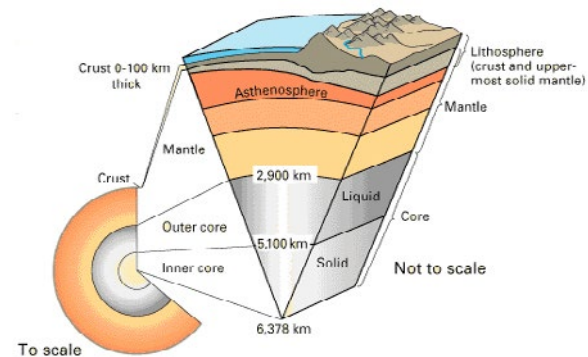
According to Dynamo Theory, the Earth's magnetic field derives from properties of fluid in the outer core, spurred into motion by the Coriolis Effect, which results from Earth's rotation. While the inner solid core appears to be too hot to retain a magnetic field, the average magnetic field strength in the outer core is believed to be 50 times stronger than at the surface (Buffett, 2010).

The theory of Plate Tectonics views the crust and the upper mantle as forming a rocky mosaic called the lithosphere (Kious and Tilling, 1996). Averaging at least 80 km in thickness over much of the Earth, the lithosphere has been broken up into large, slowly moving, plates that contain the world's continents and oceans. Pangaea is believed to be the most recent supercontinent, which started to fragment some 175 million years ago to ever so slowly form the current land masses on Earth (see Figure 3.6). The boundaries between tectonic plates have been classified into four groups, according to the relative movement of their plates (see Figure 3.6):

- divergent boundaries—plates pull apart allowing magma to be pushed up from the mantle to form new lithosphere; these boundaries are characterised by chains of volcanoes, which form oceanic ridges, or rift valleys;
- convergent boundaries—plates push together so that one plate slides under another, causing some lithosphere to be consumed into the mantle. This process is called subduction and occurs under oceans (to form deep ocean trenches) or along coastlines. Volcanoes, earthquakes and orogenesis occur in these zones;
- transform boundaries—adjacent plates slide in opposite directions, resulting in fault lines; these zones are characterised by earthquakes; and
- plate boundary zones—boundaries and their interaction are not clearly defined (Kious and Tilling, 1996).

**Figure 3.4** Cross-section of Earth

The structure of layers comprising Earth can be viewed in terms of composition or mechanics. This cutaway diagram shows the Earth's internal structure (to scale), with an inset showing the breakdown in terms of mechanical layers (not to scale)



Source: USGS (CC BY). Retrieved from [https://commons.wikimedia.org/wiki/File:Earth\\_internal\\_structure.png](https://commons.wikimedia.org/wiki/File:Earth_internal_structure.png)

Below the lithosphere is a narrow zone called the asthenosphere, which appears to be composed of hot, mobile material. Movement of the rigid lithospheric plates appears to be driven by convection within the asthenosphere. Most of the movement of tectonic plates occurs along boundaries, where plates can separate, collide, or slide. Most earthquakes and active volcanoes can be observed to occur along these boundaries and records of such geodynamic events were used to locate them.

For further information on the interior of the Earth, please refer to Rencz (1999) and Robertson (2001). Specific EO applications to geology are discussed in Volume 3.

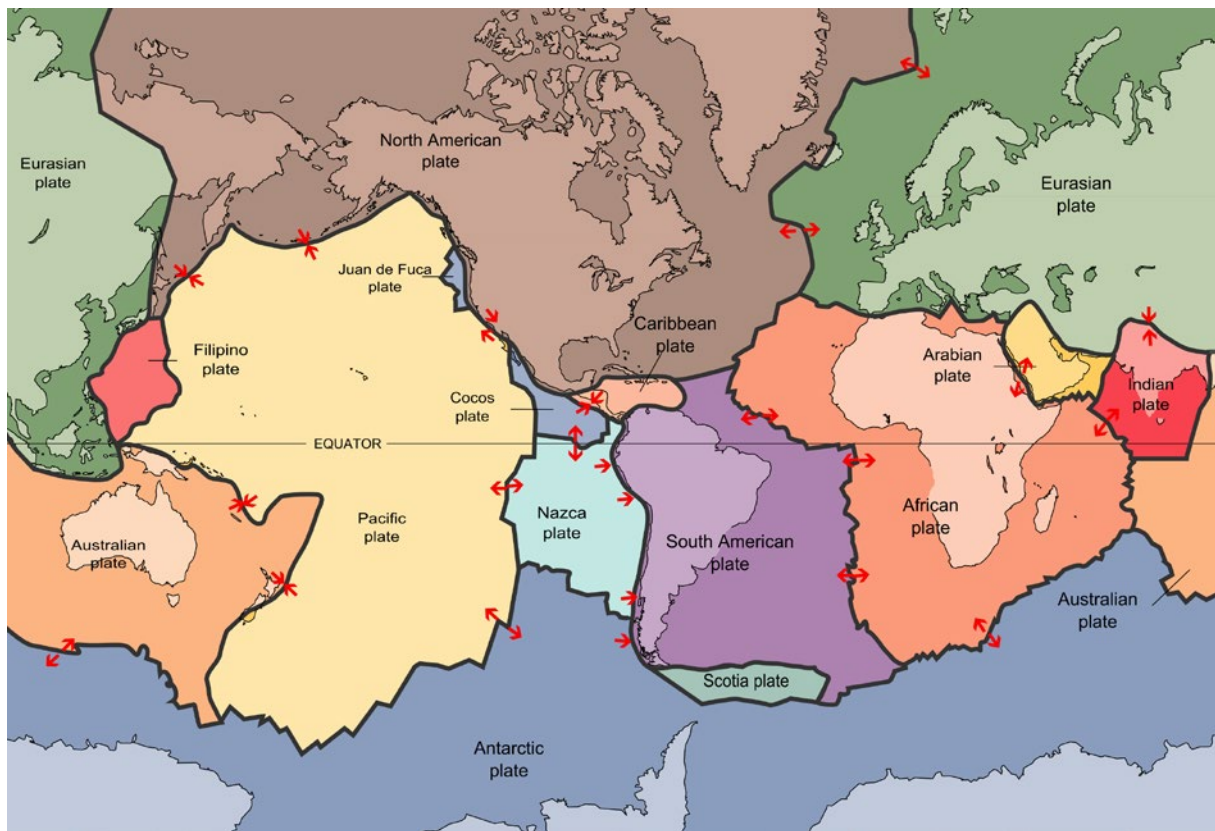
---

*It suddenly struck me that that tiny pea, pretty and blue, was the Earth.  
I put up my thumb and shut one eye, and my thumb blotted out the planet Earth.  
I didn't feel like a giant. I felt very, very small.  
(Neil Armstrong)*

---

**Figure 3.5** Tectonic plates

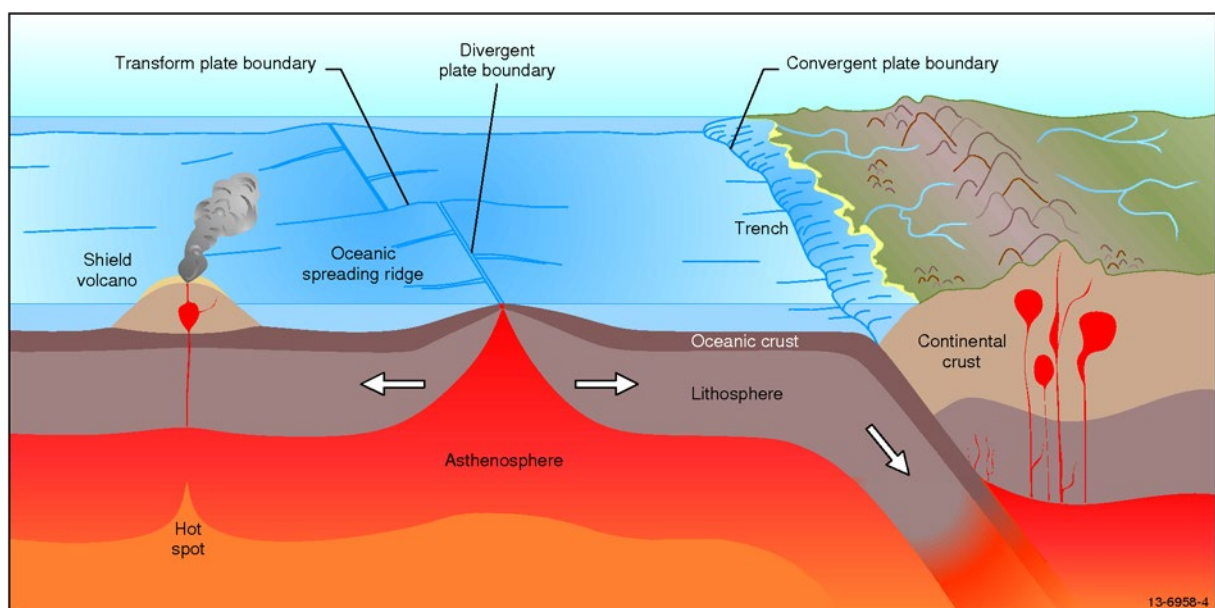
The layer of the Earth we inhabit comprises several rigid plates. These tectonic plates are moving in relatively different directions as indicated by the red arrows.



Source: Wikimedia Commons (CC BY) from USGS original. Retrieved from [https://commons.wikimedia.org/wiki/File:Plates\\_tect2\\_en.svg](https://commons.wikimedia.org/wiki/File:Plates_tect2_en.svg)

**Figure 3.6** Tectonic plate boundaries

The tectonic plates comprising the lithosphere 'float' and move on the slowly flowing asthenosphere. Tectonic plates are constantly moving towards, away from or past each other resulting in three major types of boundaries—divergent, convergent and transform—as illustrated below.



Source: Geoscience Australia

Source: Lewis and Collins (2014), Geoscience Australia

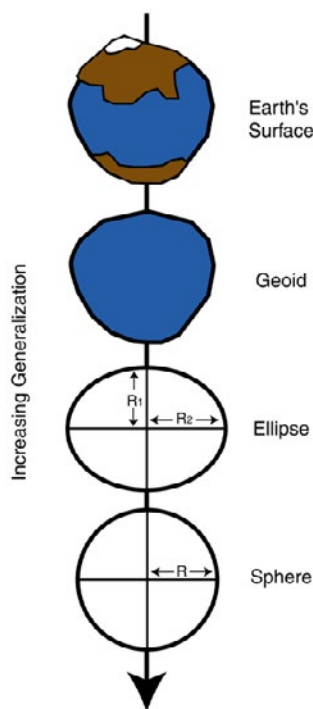
### 3.3 Shape of the Earth

Geodesy allows locations and elevations on the Earth's surface to be defined precisely. This branch of applied mathematics measures the size and shape of the Earth, and its gravity field, and quantifies changes in these attributes. It also defines frames of reference to locate the Earth in space and monitor its movements relative to other celestial bodies.

Earth is not a sphere (see Figure 3.7). It approximates the shape of an ellipsoid, being slightly flattened at the poles and widest at the equator. A reference ellipsoid is a mathematical model of the Earth's size and shape, which is used to derive coordinate systems that precisely define unique locations on the Earth's surface. This underpins all cartographic and positioning activities.

**Figure 3.7** Modelling the shape of the Earth

The shape of Earth is irregular. With increasing accuracy, it can be modelled by a sphere, an ellipse or a geoid.



Source: ©The Pennsylvania State University (CC BY-NC-SA 3.0). Retrieved from <https://www.e-education.psu.edu/geog486/node/1883>

Multiple ellipsoids have been derived to best fit the curvature of particular regions of the Earth, but in recent years satellite positioning measurements have allowed development of global ellipsoids for large area mapping. Sets of permanent reference locations, or horizontal datums, have been established around the globe to define coordinates on an ellipsoid. Similarly, networks of precise elevation measurements define vertical datums for mapping topography.

However, the Earth is not an ellipsoid either but has a highly irregular surface that is continuously changing. Surface elevation on Earth varies from a maximum at Mt Everest (8,850 m above mean sea level) to a minimum in the Mariana Trench (10,924 m below mean sea level).

A geoid attempts to model the topographic shape of the Earth more accurately than an ellipsoid (see Excursus 3.1). This interpolated model can be viewed as a surface on which every point is perpendicular to gravity and experiences the force of gravity at mean sea level. This shape has been likened to that which would result if the globe were covered by water, unaffected by tides, and only impacted by gravity. The geoid is the most logical reference surface for measuring and mapping heights.

Detailed geodetic models have been made possible using accurate distance measurements from satellites (see Excursus 3.2). The use of geodetic models to improve the geometry of EO imagery is discussed in Volume 2B.

---

*We live at the bottom of a deep gravity well, on the surface of a gas-covered planet going around a nuclear fireball 90 million miles away*  
(Douglas Adams)

---

## Excursus 3.1—Datums and Geoids

**Source:** Geoscience Australia: GA: <http://www.ga.gov.au/>

**Further information:** Intergovernmental Committee on Surveying and Mapping (ICSM): <http://www.icsm.gov.au/mapping/index.html>

A map represents features on Earth and shows the spatial relationship between different features. Global maps require:

- a reference system to describe the locations of points on Earth's surface, eg. latitude/longitude or local grids;
- a datum to mathematically define how the reference system is placed on the Earth's surface,
- a measurement system to calculate coordinates of locations on Earth;
- a projection to convert three-dimensional coordinates onto a two-dimensional map;
- additional information such as metadata, legends, scale, and annotation.

### Datums

There are many datums and projections to best suit particular regions on the Earth's surface and/or specific mapping purposes. Horizontal datums define spatial locations and vertical datums define the surface height above a fixed reference point.

While a datum is intended to map to the surface of the Earth, this is very difficult given the variations in shape that occur. Also, we now know that the surface of Earth is moving on a system of tectonic plates. Accordingly, datums map to a three-dimensional surface that models the shape of the Earth, such as a spheroid, an ellipsoid or a geoid.

Datums can be either:

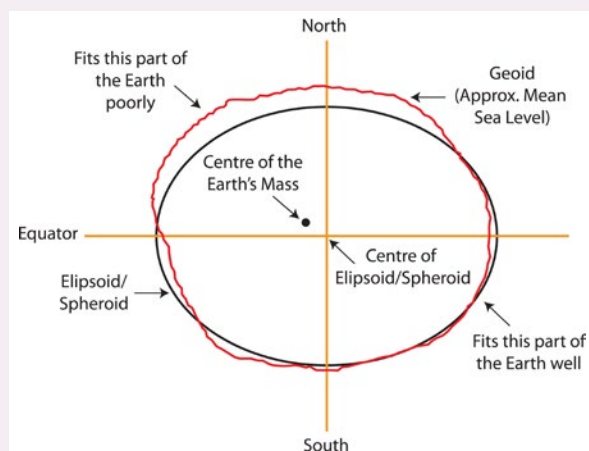
- plate-fixed—relative to a tectonic plate so that coordinates are unchanged by plate movement. Traditional mapping datums have been plate-fixed; or
- Earth-fixed—move over time with tectonic plate movement. GNSS coordinates are Earth-fixed.

Datums can also be:

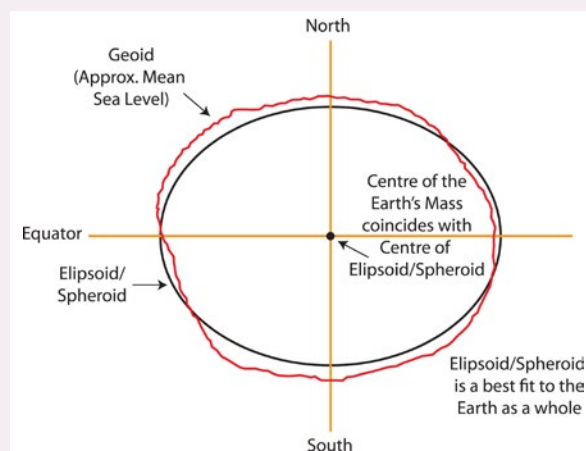
- local or regional—defined to fit a specific region of the Earth but may be a poor fit for other regions (see Figure 3.8a); or
- geocentric—defined to achieve best fit over the whole globe (see Figure 3.8b).

**Figure 3.8** Local versus geocentric datums

a. Local or regional datum suits a specific region only



b. Geocentric datum is best suits the whole globe



**Source:** © Commonwealth of Australia 2014—on behalf of the Intergovernmental Committee on Surveying & Mapping (ICSM). Retrieved from <http://www.icsm.gov.au/mapping/datums1.html#difference>



## Australian Horizontal Datums

Australia has used three plate-fixed datums:

- Australian Geodetic Datum of 1966 (AGD66), which used the Australian National Spheroid for geodetic computations, relative to the Johnston Geodetic Station in central Australia. Coordinates in this regional datum were derived from classical triangulation, traversing and astrogeodetic and aero observations.
- Australian Geodetic Datum of 1984 (AGD84), which added refinements to AGD66 that were derived from space-based geodetic techniques, such as Doppler satellite measurements, Very Long Baseline Interferometry and Satellite Laser Ranging (see Section 8).
- Geocentric Datum of Australia (GDA94), which was based on the internationally recognised Geodetic Reference System 1980 (GRS80).

While these datums work well for a single continent, they are not compatible with global positioning satellite technology. Our tectonic plate is moving north-north-east at around 7 cm per year, resulting in more than 1.5 m difference between GDA94 coordinates and GNSS devices in 2016.

The National Positioning Infrastructure (NPI) Plan is working towards a precise, Earth-fixed system to ensure Australian spatial information is totally compatible with GNSS (see Volume 1B—Section 10: Excursus 10.1).

## Australian Vertical Datum

The Australian Height Datum (AHD) was adopted in 1971 as the national reference for vertical control of elevation mapping. This datum surface passes through mean sea level at 32 defined tide gauges around the coastline of Australia.

## Our Dynamic Earth

The structure and shape of Earth changes constantly both in terms of horizontal and vertical motion. While we are aware of some rapid crustal shape changes, such as earthquakes and subsidence, the tectonic plates are also slowly moving. Australia, for example, is moving in a north-north-easterly direction at a rate of around 7 cm per year, and this slow movement becomes highly significant for locational accuracy over time.

The horizontal and vertical motion of the Australian landmass is monitored by Geoscience Australia (GA) as part of an international effort to monitor the changing shape and motion of Earth. This work integrates continuous measurements from a system of ground stations with various EO data sets to provide a uniform and accurate foundation for all spatial data in Australia (see Section 8).

## Geoids

A geoid is a three-dimensional level surface representing equal gravitational potential. By definition, this surface is perpendicular to the direction of the gravity vector at all points. However, as the mass and density distribution of the Earth are not uniform or constant, the direction of gravity varies (see Section 8). As a result, the shape of the geoid is both irregular and dynamic.

While there are an infinite number of possible equipotential surfaces for the Earth, the term ‘geoid’ is most commonly used to describe the equipotential surface that most closely approximates mean sea level.

Across Australia, mean sea level and its onshore model, the Australian Height Datum (AHD), correspond to within approximately  $\pm 0.5$  m of the geoid. This discrepancy is due to differences in temperature and density of coastal waters in northern and southern Australia, with the warmer water being about one metre higher off the northern coast.

## Global Navigation Satellite System (GNSS)

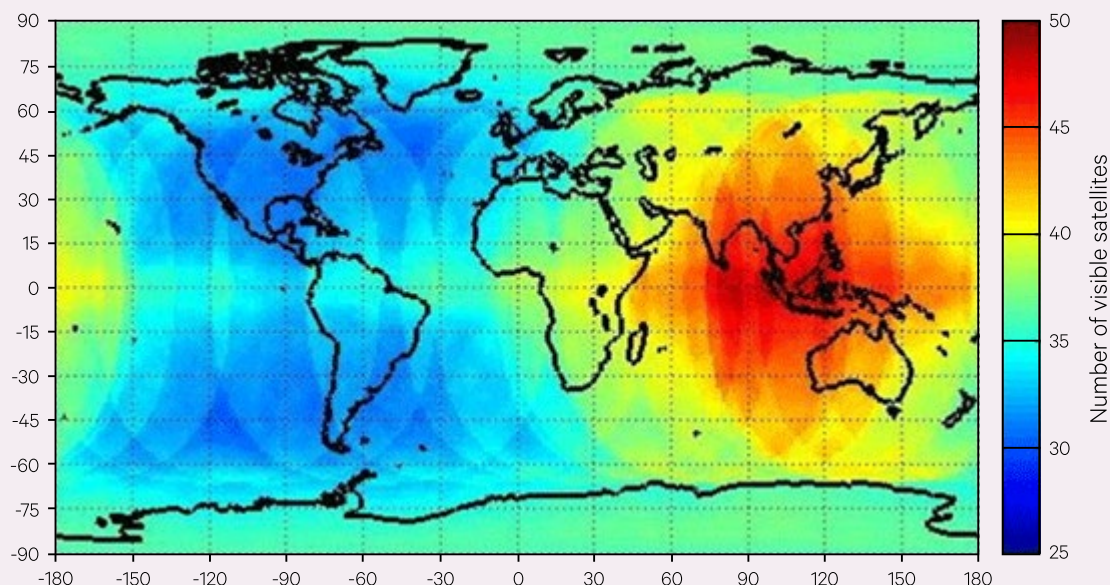
Satellite systems that provide geospatial positioning on Earth are collectively called the Global Navigation Satellite System (GNSS). This system currently comprises over 100 operational satellites, owned and managed by six national and regional jurisdictions, namely:

- USA (GPS),
- Russia (GLONASS),
- China (BeiDou),
- EU (Galileo),
- India (Navic) and
- Japan (QZSS).

The average number of satellites that will be visible from the planned constellations is mapped in Figure 3.9. As well as providing precise location and time, these satellites enable the movement of tectonic plates to be measured accurately (see Volume 1B—Section 10).

**Figure 3.9** Average number of visible satellites across all planned constellations

The average number of current and planned GNSS satellites visible from different locations over a 24 hour period is shown as a colour scale from blue (25 satellites) to red (50 satellites). Australia and Southeast Asia are well situated for good GNSS coverage.



Source: Dempster and Rizos (2009) Adapted from: Dempster and Hewitson (2007). Used with permission.

## Excursus 3.2—Space Geodesy and Reference Frames

**Source:** Geoscience Australia (GA): <http://www.ga.gov.au>

**Further information:** International Earth Rotation and Reference Systems Service (IERS) : <http://www.iers.org>

International Astronomical Union (IAU) <http://www.iau.org>

International GNSS Service (IGS): <https://www.iers.org/IGS/EN/Organization/TechniqueCentres/IGS/igs.html>

International DORIS Service: <http://ids-doris.org>

NASA Space Geodesy Project: <http://space-geodesy.nasa.gov/techniques/VLBI.html>

International Laser Ranging Service (ILRS): <http://ilrs.gsfc.nasa.gov>

Global Geodetic Observing System (GGOS) <http://www.ggos.org>

Just as the shape and structure of Earth are dynamic, so are its placement, orientation and motion in space. Earth's rotational vector does not have a fixed axis and the rate of rotation is not uniform. Its surface shape and energy fields are also affected by the gravitational influence of other celestial bodies.

While datums are required to measure positions on Earth relative to a standard referencing system, accurate reference frames are required to monitor the changes in Earth's position, orientation and movement in space. These are defined as the Geocentric Celestial Reference Frame (GCRF) and the International Terrestrial Reference Frame (ITRF).

The International Earth Rotation and Reference Systems Service (IERS) maintains procedures and models to transform between the GCRF and the ITRF. These transformations require continuous monitoring

of several fundamental parameters that quantify irregularities in Earth's rotation (known as Earth Orientation Parameters: EOP):

- Universal time difference (UT1)—based on Earth's rotation—variations indicate changes in Earth's rotational speed;
- Pole Coordinates—show the movement of Earth's rotational axis relative to its crust; and
- Celestial Pole Offsets—show changes in the orientation of the Earth's rotational axis (such as precession, nutation, obliquity).

Reference system—specifies how a celestial coordinate system is defined, including origin and axes, plus models, constants and algorithms to convert between conformal observations and reference data

Reference frame—set of identifiable fiducial points, and their coordinates, that realise the reference system.

## Celestial Reference Frame

The International Celestial Reference Frame (ICRF) realizes an ideal reference system, the International Celestial Reference System (ICRS), by precise equatorial coordinates of extragalactic radio sources observed in Very Long Baseline Interferometry (VLBI) programs. (IERS, 2013)<sup>14</sup>

The GCRF is the geocentric equivalent of the ICRS.

## Terrestrial Reference Frame

A Terrestrial Reference System (TRS) is a spatial reference system co-rotating with the Earth in its diurnal motion in space. In such a system, positions of points attached to the solid surface of the Earth have coordinates which undergo only small variations with time, due to geophysical effects (tectonic or tidal deformations). (Ch. 4 in Petit and Luzum, 2010)

## ITRF

The International Terrestrial Reference System (ITRS) constitutes a set of prescriptions and conventions, together with the modeling required to define origin, scale, orientation and time evolution of a Conventional Terrestrial Reference System (CTRS). The ITRS is an ideal reference system, ... realised by the International Terrestrial Reference Frame (ITRF). ...The ITRS can be connected to the International Celestial Reference System ICRS by use of the IERS EOP (IERS, 2013)<sup>15</sup>

The ITRF2014 (released in early 2016) is viewed as the most accurate terrestrial reference frame available for geodesy, in both global and regional applications. The ITRF2014 is based on data from 1,499 ground stations at 975 sites, often co-located with space geodetic instruments:

- Global Navigation Satellite Systems (GNSS; see Volume 1B—Section 10);
- Satellite Laser Ranging (SLR; see Volume 1A—Sections 8 and 16.1.2.1);
- Lunar Laser Ranging (LLR);
- Very Long Baseline Interferometry (VLBI); and
- Doppler Orbitography Radio Positioning Integrated by Satellite (DORIS; see Section 16.1.2.2).

## Laser Ranging

The International Laser Ranging Service (ILRS) provides global satellite and lunar laser ranging data and products. SLR (see Figure 3.10) and LLR actually measure the distance (based on two-way time interval) between ground stations and retroreflector arrays on orbiting satellites and the Moon using

short-pulse lasers. Such measurements highlight variations in Earth's centre of mass, which is the origin of geocentric reference systems.

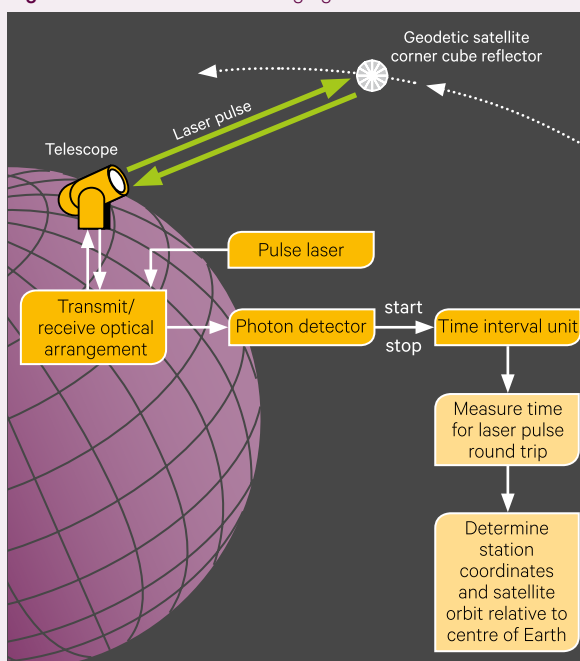
## DORIS

The DORIS (Doppler Orbitography Radio Positioning Integrated by Satellite) system relies the Doppler shift between transmitted and received signals between a ground station and a member satellite to determine orbital information. A radio signal is transmitted from a ground beacon to a passing satellite then, based on the observed frequency shift of the signal, the relevant positions of the satellite and ground beacon can be computed. Two Australian ground stations (managed by Geoscience Australia) are part of an international network. These measurements have also been valuable for highlighting changes in the Earth's crust.

## VLBI

VLBI is a geometric technique that collects signals from distant astronomical radio sources, such as quasars, at multiple radio antennae on Earth. Since these measurements are precise to picoseconds (with hydrogen maser clock accuracy of one second in one million years), the positions of the antennae relative to the quasars can be determined accurately. These measurements have been invaluable for defining the inertial reference frame for our planet and tracking crustal and surface water changes. Australia operates three VLBI observatories, located near Hobart, Perth and Darwin.

Figure 3.10 Satellite Laser Ranging



Adapted from: Geoscience Australia

14. International Earth Rotation and Reference Systems Service: <https://www.iers.org/IERS/EN/DataProducts/ICRF/icrf.html>

15. International Earth Rotation and Reference Systems Service: <https://www.iers.org/IERS/EN/DataProducts/ITRS/itrs.html>

### 3.4 Further Information

#### International Earth Rotation and Reference Systems Service (IERS):

[https://www.iers.org/ IERS/EN/Home/home\\_node.html](https://www.iers.org/ IERS/EN/Home/home_node.html)

#### Geodesy:

Geoscience Australia: <http://www.ga.gov.au/scientific-topics/positioning-navigation/geodesy>

International Committee on Surveying and Mapping (ICSM): <http://www.icsm.gov.au/index.html>

#### Earth Structure:

Robertson (2001)

Windows to the Universe (NESTA): [http://www.windows2universe.org/earth/Interior\\_Structure/interior.html](http://www.windows2universe.org/earth/Interior_Structure/interior.html)

### 3.5 References

- Buffett, B. A. (2010). Tidal dissipation and the strength of the Earth's internal magnetic field. *Nature*, 468(7326), pp. 952-954. doi:<http://dx.doi.org/10.1038/nature09643>.
- Cain, F. (2016). The Moon compared to Earth. *Universe Today*. Retrieved from <http://www.universetoday.com/20489/moon-compared-to-earth/>.
- Dempster, A. G., and Hewitson, S. (2007). The 'System of Systems' Receiver: an Australian Opportunity? Paper presented at the International Global Navigation Satellite System Society IGNSS Symposium 2007, Sydney, Australia.
- Dempster, A. G., and Rizos, C. (2009). Implications of a "system of systems" receiver. Paper presented at the Surveying & Spatial Sciences Institute Biennial International Conference, Adelaide, Australia.
- Dziewonski, A. M., and Anderson, D. L. (1981). Preliminary reference Earth model. *Physics of the Earth and Planetary Interiors*, 25(4), pp. 297-356. doi:[http://dx.doi.org/10.1016/0031-9201\(81\)90046-7](http://dx.doi.org/10.1016/0031-9201(81)90046-7).
- Iqbal, M. (1983). *An Introduction to Solar Radiation*. Academic Press, Toronto.
- Kious, W. J., and Tilling, R. I. (1996). *This Dynamic Earth: The Story of Plate Tectonics*. USGS, Washington, DC. Retrieved from <http://pubs.usgs.gov/gip/dynamic/dynamic.html>.
- Lewis, G., and Collins, C. (2014). Earthquakes - Teacher notes and student activities (2014/06). Geoscience Australia, Canberra. Retrieved from [https://d28rz98at9flks.cloudfront.net/76611/Rec2014\\_006.pdf](https://d28rz98at9flks.cloudfront.net/76611/Rec2014_006.pdf). doi:<http://dx.doi.org/10.11636/Record.2014.006>.
- NASA (2015). Lunar and Planetary Science. Retrieved from <http://nssdc.gsfc.nasa.gov/planetary/>.
- Petit, G., and Luzum, B. (2010). Verlag des Bundesamts für Kartographie und Geodäsie. IERS Conventions, Frankfurt am Main.
- Rencz, A. N. (1999). *Remote Sensing for the Earth Sciences*, Vol. 3, Third Edn., Ed: R. A. Ryerson, Manual of Remote Sensing. American Society for Photogrammetry and Remote Sensing (ASPRS); John Wiley & Sons, Inc., New York.
- Robertson, E. C. (2001). *The Interior of the Earth*. Retrieved from <http://pubs.usgs.gov/gip/interior/>.





# 4 Earth Systems and Processes

This section introduces the integrated systems (see Section 4.1) and processes (see Section 4.2) that keep our planet alive. Much of this information has been derived using Earth Observation (EO) technologies. Volume 3 describes some of the specific applications of EO that have been used to monitor Earth System processes.

## 4.1 Earth System Science

The Earth can be viewed as an integrated system comprising four spheres (Lindsey, 2009):

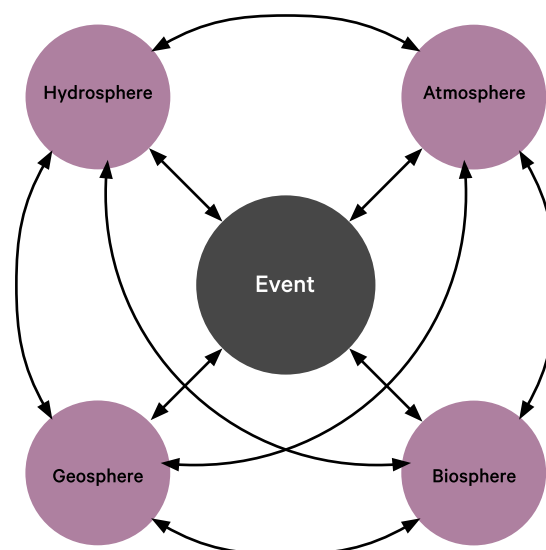
- atmosphere—gaseous, protective layer around the Earth (see Section 4.1.1).
- hydrosphere—all surface waters, groundwater and atmospheric water in any state (see Section 4.1.2);
- geosphere—solid components of Earth on land and under water (see Section 4.1.3); and
- biosphere—all forms of life on Earth (see Section 4.1.4).

This multi-disciplinary approach assumes a holistic perspective, such that individual events on Earth can be related to all four spheres (see Figure 4.1).

Earth System Science analyses the dynamic geochemical processes and interactions occurring between these spheres to better understand the Earth—its past, present and future—at global to local scales (see Figure 4.1). Some of these processes and interactions are illustrated in Figure 4.2.

**Figure 4.1** Earth System Science

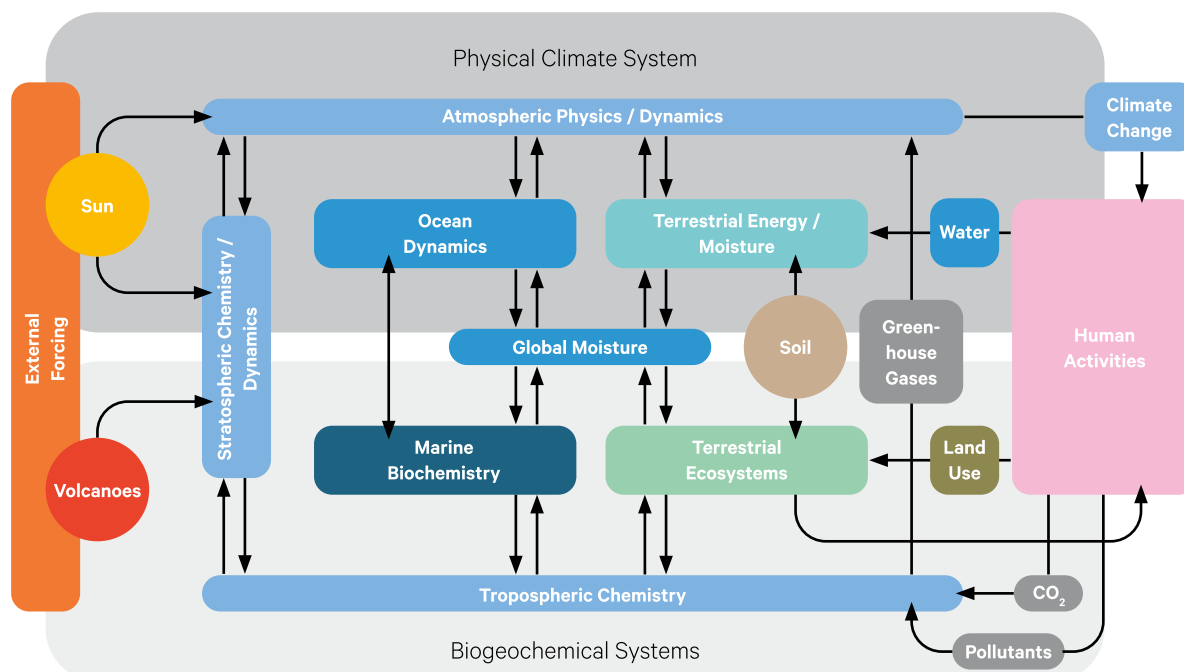
Events on Earth can be interpreted in the context of four, integrated spheres: Biosphere, geosphere, hydrosphere and atmosphere.



*The history of life on Earth has been a history of interaction between living things and their surroundings. To a large extent, the physical form and habits of the Earth's vegetation and its animal life have been moulded by the environment. Considering the whole span of earthly time, the opposite effect, in which life actually modifies its surroundings, has been relatively slight. Only within the moment of time represented by the [last] century has one species – man – acquired significant power to alter the nature of his world.*  
(Rachel Carson, *Silent Spring*)

**Figure 4.2** Processes and interactions within Earth System Science

All processes on Earth are interrelated and impacted by human activities. This conceptual framework was proposed by Francis Bretheton (NASA Bretheton) to link major components with the processes that impact them.



Adapted from: NASA at <http://education.gsfc.nasa.gov/experimental/all98invproject.site/pages/trl/inv4-3.abstract.html>

## 4.1.1 Atmosphere

*Atmosphere (from) Greek, atmos meaning 'vapour' and sphaira meaning 'sphere'*

The atmosphere is a gaseous layer surrounding the Earth that protects the planet from the solar wind and high-energy solar radiation (cosmic rays, X-rays and some UV rays) as well as most meteors. It has been divided vertically into four layers, defined by the way air temperature changes with increasing altitude: the troposphere, stratosphere, mesosphere, and thermosphere (see Section 5.4). Most major weather and climate activity occurs in the troposphere. These layers vary in terms of temperature, barometric pressure and chemical composition. A fifth layer, the exosphere, forms the boundary with space.

The ionosphere, where solar radiation ionises the upper atmosphere, lies approximately 80–600 km above the Earth (NOAA, 2016). During the daytime, three distinct layers of the ionosphere layers are ionized by solar radiation (see Figure 4.3):

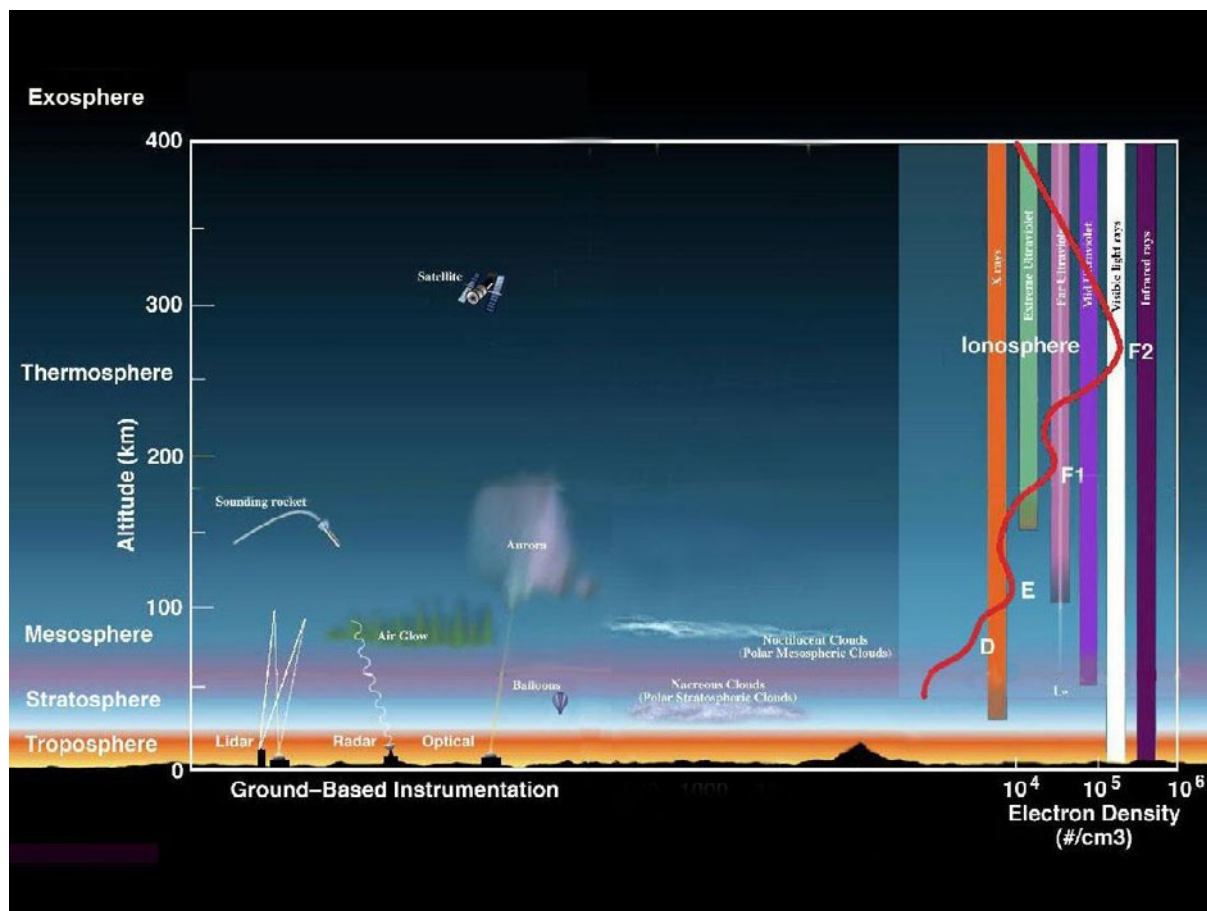
- D layer—highest frequency ionisation of NO and hard X-ray ionisation of  $N_2$  and  $O_2$ ;
- E layer—soft X-ray and UV ionisation of  $O_2$ ; and
- F layer—extreme UV ionisation of atomic O. This layer deforms to a second layer during the day. The lower of these layers,  $F_2$ , facilitates long distance HF communication.

At night, the weaker cosmic rays only ionize the E and F layers (see Figure 4.4). The ionosphere is particularly significant for telecommunications and remote sensing since it influences the propagation of radio waves away from Earth. The Space Weather Network (SWN) updates global ionospheric maps on a regular basis as shown in Figure 4.5.

*The saddest aspect of life right now is that science gathers knowledge faster than society gathers wisdom.*  
(Isaac Asimov)

**Figure 4.3** Interrelationship between atmosphere and ionosphere

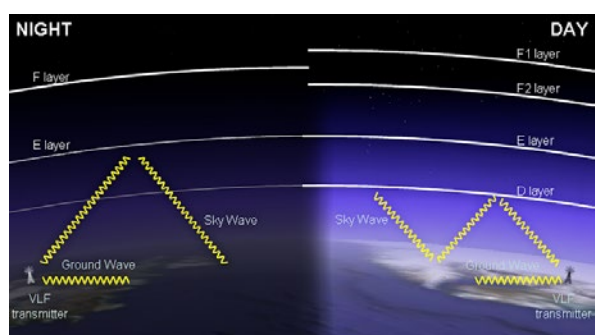
Approximate altitudes of atmospheric and ionospheric layers. The structure of ionospheric layers changes with the diurnal cycle (see Excursus 4.1).



Source: NASA. Retrieved from [http://www.nasa.gov/sites/default/files/images/463940main\\_atmosphere-layers2\\_full.jpg](http://www.nasa.gov/sites/default/files/images/463940main_atmosphere-layers2_full.jpg)

**Figure 4.4** Impact of ionosphere on radio frequency waves

Very low frequency (VLF) waves bounce off the ionosphere. During the daytime, all three layers of the ionosphere are ionized by solar radiation, enabling 'over the horizon' communication.

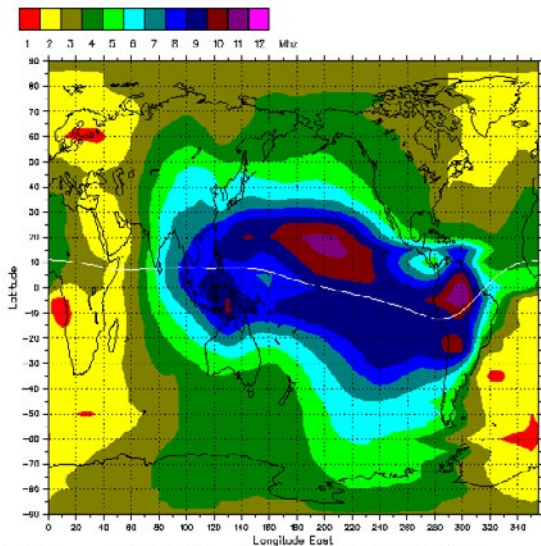


Source: SID Monitoring Station (CC-BY-NC-SA 3.0). Retrieved from <http://sidstation.loudet.org/ionosphere-en.xhtml>



**Figure 4.5** Global ionospheric foF2 map

As part of the Space Weather Network (SWN), global ionospheric foF2 maps are updated hourly based on the previous two hours of data (acquired at half hour intervals). This map was created at 01:00 UT on 29 September 2016. The geomagnetic equator (where magnetic dip equals zero) is shown as a white line (see Section 7).



Source: © Bureau of Meteorology. Retrieved from [http://www.sws.bom.gov.au/HF\\_Systems/6/5](http://www.sws.bom.gov.au/HF_Systems/6/5)

### 4.1.2 Hydrosphere

*Hydrosphere (from) Greek, hydro meaning ‘water’ and sphaira meaning ‘sphere’*

The hydrosphere includes all surface waters, both liquid and frozen, as well as groundwater stored in soil and rocks, and water vapour in the atmosphere. The oceans cover over 70% of the Earth’s surface and provide most of the water vapour in the atmosphere. Oceans also act as a heat source and sink, or storage medium. The hydrologic cycle, or water cycle, involves vertical and horizontal movement of water (in vapour, liquid or solid form) between the Earth’s surface, atmosphere and oceans (see Section 4.2.2).

The total volume of water of Earth has been estimated as 1,386 million km<sup>3</sup>, 97.5% are saline (Shiklomanov, 1998). Of the 2.5% freshwater, nearly 69% is frozen in permanent ice and glaciers and around 30% exists as groundwater, leaving only 0.26% for use in lakes, reservoirs and rivers. These routinely available freshwater sources total around 93,000 km<sup>3</sup> or 0.023% of the Earth’s mass. Components of the hydrosphere are described in greater detail in Volume 3.

*The fact that a cloud from a minor volcanic eruption in Iceland— a small disturbance in the complex mechanism of life on the Earth— can bring to a standstill the aerial traffic over an entire continent is a reminder of how, with all its power to transform nature, humankind remains just another species on the planet Earth. (Slavoj Žižek)*

### 4.1.3 Geosphere

*Geosphere (from) Greek, geo meaning ‘earth’ and sphaira meaning ‘sphere’*

Solid Earth, both on land and under water, is called the geosphere. The structure of the geosphere is illustrated in Figure 3.4 in terms of mechanical and compositional layers. The compositional layers are summarised in Table 4.1.

As introduced in Section 3.2, the upper part of the geosphere is the lithosphere, which rests on the asthenosphere and comprises moving tectonic plates. The topography of the geosphere is shaped by the various dynamic processes associated with the rock cycle (see Section 4.2.3), often occurring over very long time periods. Soil, the focus of many studies using remote sensing, is one of the outputs from the rock cycle.

**Table 4.1** Composition of planet Earth

Layer	Thickness (km)	Density (g/cm <sup>3</sup> )	Composition
Crust	30 (5-50) Thinner under ocean basins and rift valleys and thicker under mountain ranges	2.2–2.9	Predominately silicates at surface, basalt at base
Upper mantle	720	3.4–4.4	Molten (500–900°C)
Lower mantle	2,171	4.4–5.6	More dense (~4,000°C)
Outer core	2,259	9.9–12.2	Molten
Inner core	1,221	12.8–13.1	Solid

Source: Robertson (2001), <http://pubs.usgs.gov/gip/interior/> from Anderson (1989)

#### 4.1.4 Biosphere

*Biosphere (from) Greek, bios meaning 'life' and sphaira meaning 'sphere'*

Biosphere was first defined as 'the place on Earth's surface where life dwells' (Suess, 1875). This has been expanded to include all parts of the planet that can support life, including land, sea and air. The biosphere comprises all living organisms and has been subdivided into biomes on the basis of climate and geography. Since all organic compounds contain the element carbon, it is considered to be the foundation for all forms of life on Earth.

While all spheres are involved in the carbon cycle, carbon is primarily recycled within the biosphere. The transfer of energy within the biosphere

generally involves the exchange of carbon, water and air—principally via photosynthesis, which is part of the carbon cycle (see Section 4.2.4). All plants photosynthesise, that is, produce oxygen and sugar from carbon dioxide, water and sunlight. This photochemical reaction occurs in chloroplasts, specialised organelles that contain the pigment chlorophyll. Pores on the leaf surface open and close, as required, to exchange carbon dioxide and oxygen with the atmosphere. The sugar product stores energy and provides raw materials for synthesising other compounds. Photosynthesis is the ultimate primary energy production mechanism on Earth, enabling plant growth and providing food and shelter for other life forms. More details on photosynthesis in leaves are provided in Volume 3A.

## 4.2 Earth System Processes

Almost all energy on Earth ultimately derives from the Sun (with a relatively minor component originating from the Earth's interior). The solar radiation that reaches the Earth's surface is called solar irradiance, or insolation (and measured in  $\text{W}/\text{m}^2$ , or accumulated over time as solar exposure in  $\text{MJ}/\text{m}^2$  or  $\text{Wh}/\text{m}^2$ —see Section 2.3). At any single point on the globe, variations in insolation can result from solar output fluctuations, atmospheric transmission, and seasonal and diurnal cycles. Around the globe, insolation also varies with latitude, altitude, and aspect.

Energy and matter are transferred between the geosphere, hydrosphere, atmosphere and biosphere via a number of ongoing pathways. These can be considered in terms of four broad areas, namely:

- energy—heat transfer and storage (see Section 4.2.1);
- water—cycling of matter and some energy with the movement of water (see Section 4.2.2);
- earth—transfer of matter and energy in the rock cycle (see Section 4.2.3); and
- carbon—slow and fast cycling of carbon between the spheres (see Section 4.2.4).

An understanding of these transfers provides insight into the broader concerns of efficient energy consumption and storage, and conservation of fundamental ecological resources.

### 4.2.1 Energy

The Earth is commonly viewed as a closed system, that is, a unit with defined boundaries that permit the exchange of energy but not matter (see Section 2.10.3). Exceptions to this definition include the entry of meteorites and journeys of spacecraft, but most of Earth's processes do not exchange matter with the rest of the universe.

Solid matter on Earth absorbs solar energy as:

- sensible heat, leading to a change in temperature, or
- latent energy, leading to a change in state (see Section 2.10.2).

The flow, or flux, of thermal energy on Earth is driven by two major factors:

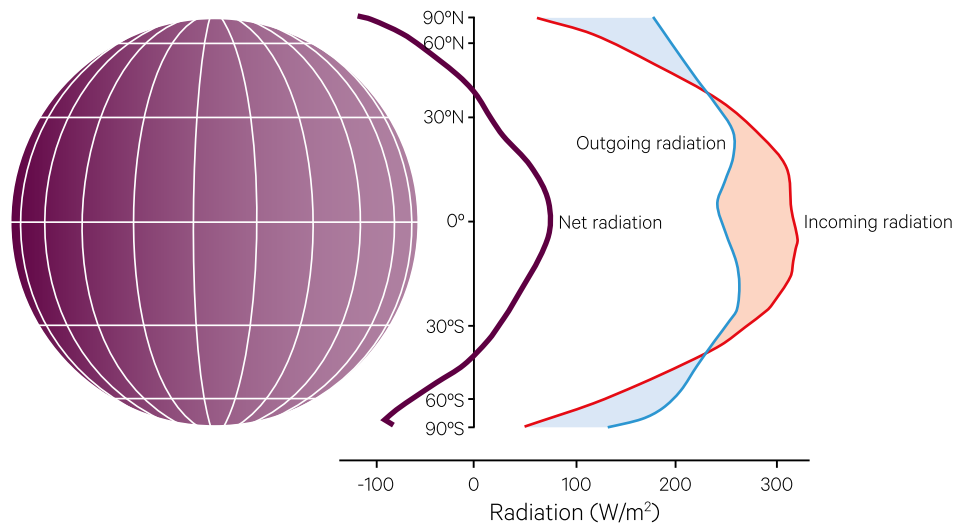
- amount of solar energy that reaches the surface; and
- how Earth surface materials interact with that energy (see Sections 2.10 and 2.11).

Minor sources of heat also originate within Earth due to its material composition, friction resulting from internal changes, and radioactivity.

As a consequence of the inclination, revolution and rotation of the Earth relative to the Sun, insolation around the globe varies markedly with latitude, season and time of day (see Excursus 4.1). These variations result in differential heating around the globe. To balance global energy, heat is moved from the tropics to the poles via large-scale circulation of air and water, our two most mobile and ubiquitous fluids (see Figure 4.6, plus Volume 3). Overall, this 'meridional' circulation allows the 'surplus' solar energy received between  $40^\circ\text{N}$  and  $38^\circ\text{S}$  to balance the 'deficit' of energy nearer the poles. Heat is also transferred out of Earth's system into space (see Figure 4.7 and Volume 3).

**Figure 4.6** Energy distribution and net radiation

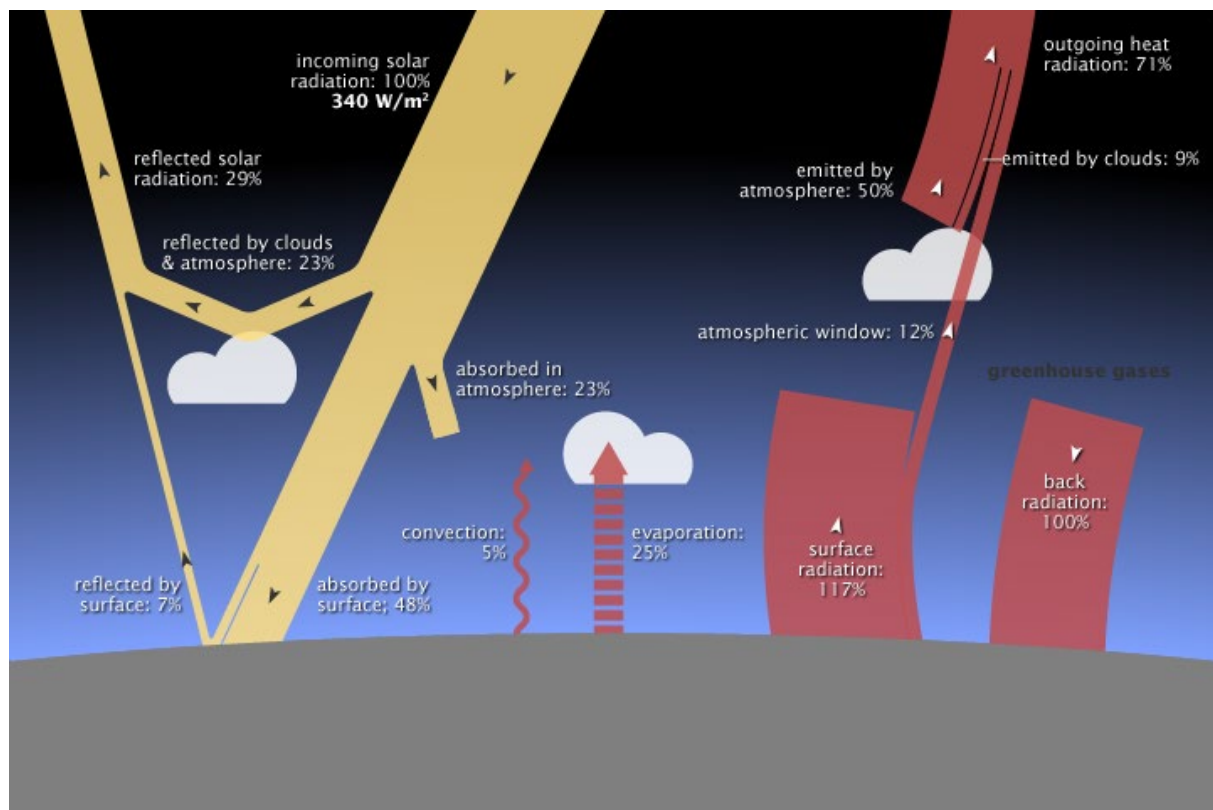
Between around 40°N and 38°S, there is more incoming than outgoing energy, resulting in a net energy gain (pink). At higher latitudes this relationship is reversed, causing a net energy loss (blue). Overall, the surplus energy moves from the warmer equatorial latitudes to the poles via atmospheric and ocean circulation patterns.



Adapted from: Adapted from: RAPID/NOC at SEOS Ocean Currents (CC-BY-SA). Retrieved from <http://www.seos-project.eu/modules/oceancurrents/oceancurrents-c03-p02.html>

**Figure 4.7** Earth's energy budget

Of the 340 W/m² of solar energy that reaches the top of Earth's atmosphere, an equal amount of energy is returned to space as either reflected or emitted energy. This balance is essential to maintain a stable temperature on Earth.



Source: Lindsey (2009). Retrieved from <http://earthobservatory.nasa.gov/Features/EnergyBalance/page6.php>

Three processes facilitate this circulation:

- sensible heat flux—conduction and convection of energy from the surface to the atmosphere, which then moves warm equatorial air to the poles by advection, then colder air returns to the equator (see Section 2.10);
- latent heat flux—vertical and horizontal energy transfer due to evaporation of solid and liquid water (see Section 2.10.2);
- surface heat flux:
  - ◆ into oceans—warm surface water is circulated vertically within the water column by conduction and convection and horizontally by ocean currents; or
  - ◆ into soil and solid surfaces.

Water surfaces have a high specific heat capacity so heat and cool slowly, can readily cool by evaporation, and can transfer heat to a greater depth than land. Land surfaces thus experience a greater seasonal temperature range, especially on larger continents. Land is cooled more slowly by evapotranspiration. Air temperatures above land and water surfaces vary in a similar way to those of their underlying surface.

The flow of energy into and out of the Earth's system is referred to as the Earth's energy or radiation budget (see Figure 4.7 and Excursus 4.1). This considers both the solar energy reaching Earth and the energy being radiated from Earth back to space, that is:

$$\text{net radiation} = \text{incoming radiation} - \text{outgoing radiation}$$

where

*incoming radiation* is short wave direct and indirect solar radiation plus long wave radiation from the atmosphere; and

*outgoing radiation* is short wave reflection and long wave emission from Earth.

Indirect radiation includes radiation that has been scattered by atmospheric particles and other surfaces.

It is estimated that around:

- 29% of the solar energy that reaches the top of Earth's atmosphere is returned to space by reflection primarily from the atmosphere and water vapour (clouds), or highly reflective surface features such as ice or snow;
- 23% of solar radiation is absorbed in transit through the atmosphere;
- 48% is absorbed by the Earth's surface.
- Thus, the Earth's surface and atmosphere together absorb approximately 71% of the incoming radiation (Lindsey, 2009).

For any system to stay in equilibrium there needs to be a long-term balance between energy inputs and outputs. The Earth's energy budget can be compartmentalised into three sub-budgets:

- at the surface;
- within the atmosphere; and
- at the top of the atmosphere.

To maintain equilibrium, each of these sub-budgets also needs to balance incoming and outgoing energy levels. At the surface, of the 48% of net solar radiation absorbed, approximately:

- 25% is transferred into the atmosphere by evaporation (latent heat);
- 5% is transferred via convection of air in direct contact with warmed surfaces; and
- 17% is emitted as thermal infrared energy (Lindsey, 2009); see Volume 1B—Section 7 and Volume 3).

---

*Seldom if ever does nature operate in closed and separate compartments, and she has not done so in distributing the earth's water supply. Rain, falling on the land, settles down through pores and cracks in soil and rock, penetrating deeper and deeper until eventually it reaches a zone where all pores of the rock are filled with water, a dark, subsurface sea, rising under hills, sinking beneath valleys. This ground water is always on the move, sometimes at a pace so slow that it travels no more than 50 feet [17 m] a year, sometimes rapidly, by comparison, so that it moves nearly a tenth of mile [160 m] a day. It travels by unseen waterways until here and there it comes to the surface as a spring, or perhaps it is tapped to feed a well. But mostly it contributes to streams and so to rivers. Except for what enters streams directly as rain or surface run-off, all the running water of the earth's surface was at one time ground water.*

*(Rachel Carson, Silent Spring)*

---



## Excursus 4.1—Insolation

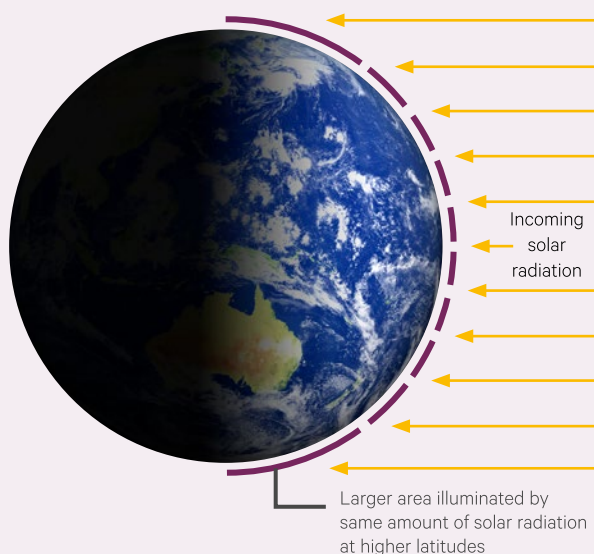
**Further information:** Lindsey (2009)

The total solar irradiance is defined as the average intensity of solar energy at the top of Earth's atmosphere (TOA). This is based on the average distance between the Earth and the Sun (around 150 million km) and was previously believed to be constant, but is now known to vary with solar activity (see Section 3).

The Total Irradiance Monitor (TIM) on the Solar Radiation and Climate Experiment (SORCE) determined total solar irradiance as  $1360.8 \pm 0.5 \text{ W/m}^2$  during the 2008 solar minimum (NASA, 2016)<sup>16</sup>. This estimate only applies to surfaces that are perpendicular to incoming radiation (namely midday at the equator) and decreases towards the poles (see Figure 4.8). The average solar irradiance at TOA over the whole globe reduces to  $340 \text{ W/m}^2$ .

**Figure 4.8** Solar illumination angle variation with latitude

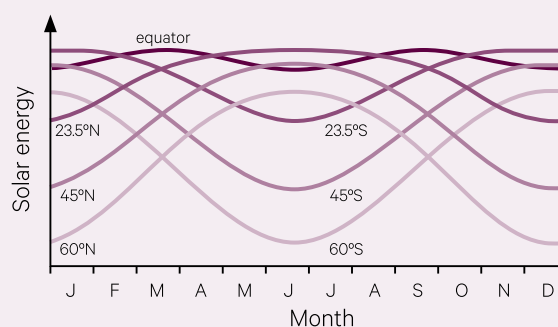
At higher latitudes, the Sun angle (measured as elevation) decreases. Accordingly the average solar irradiance reaching the surface of Earth decreases, and the area being irradiated increases.



Adapted from: Lindsey (2009)

**Figure 4.9** Variations in insolation with latitude and annual cycle

Insolation at solar noon for different latitudes through the year. Peak energy shows little annual variation at the equator, but significant seasonal variations nearer the poles.



Adapted from: Lindsey (2009)

The actual solar irradiance intercepted by the Earth's surface varies significantly with latitude, season and time of day (see Figure 4.9). This variation results from the inclination, revolution and rotation of Earth relative to the Sun (see Section 3).

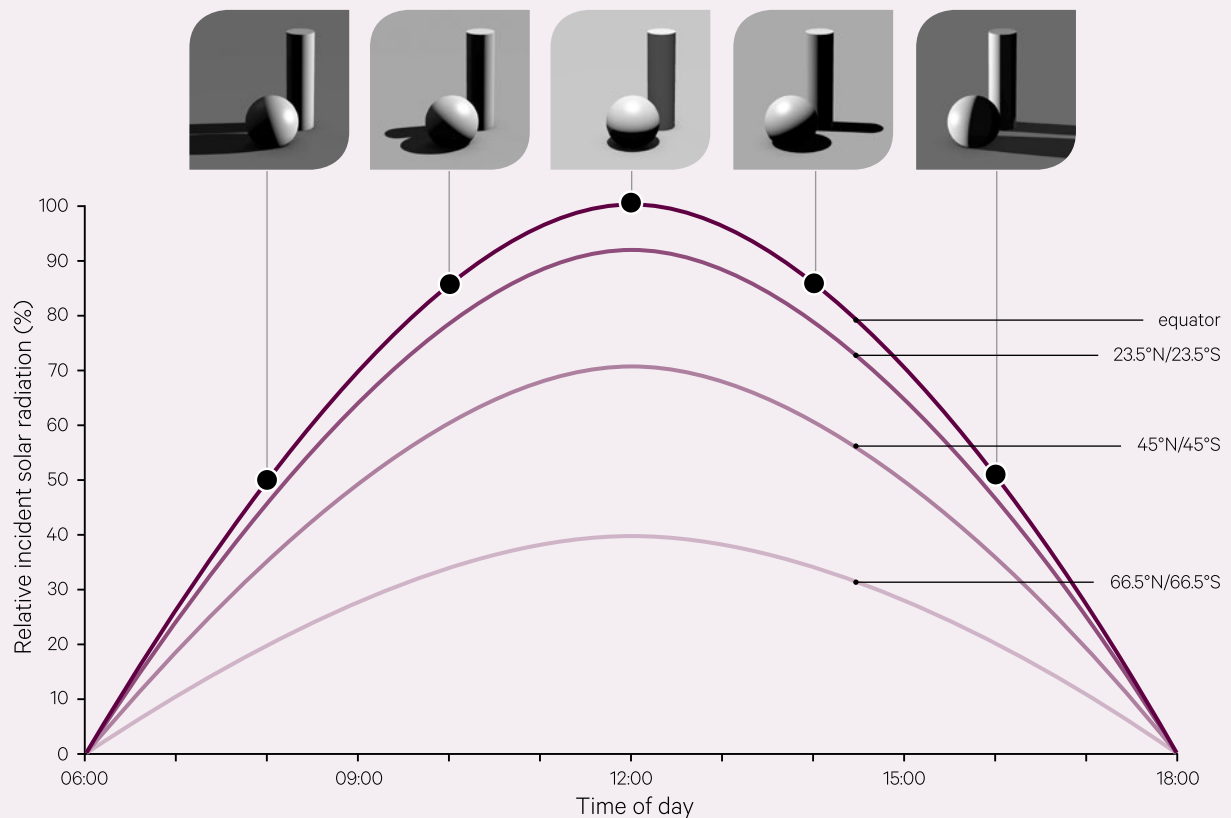
Moving away from the equator, the angle of solar illumination (relative to the horizon) decreases, which both decreases the average solar irradiance reaching the surface through the atmosphere and increases the area of its effective footprint (see Figures 4.8 and 4.10). At each latitude, both the length and intensity of insolation varies each day of the year (see Figure 4.10), with the number of sunlight hours per day ranging from 0 in winter to 24 in summer for polar regions, compared with 12 hours throughout the year at the equator.

Asymmetry in the Earth's orbit also introduces differences in peak solar radiation between hemispheres. Since the Earth is closer to Sun during summer in the southern hemisphere, that hemisphere receives more summer energy overall (see Figure 4.11).

<sup>16</sup> For more details, please see: <http://atmospheres.gsfc.nasa.gov/climate/?section=136>

**Figure 4.10** Typical daily insolation cycle on equinox days

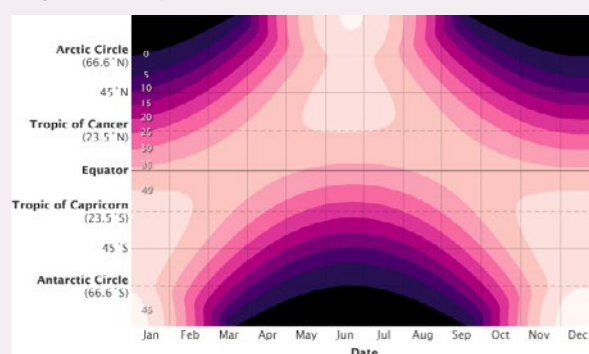
Typical solar radiation reduces with increasing latitude



Adapted from: Lindsey (2009)

**Figure 4.11** Annual cycle of total daily solar irradiance

Shown on a colour scale from dark (low) to pale (high), the total solar irradiance at TOA varies with latitude and season. High latitudes receive the highest levels of incoming energy during long summer days.



Source: Lindsey (2009)

## CERES

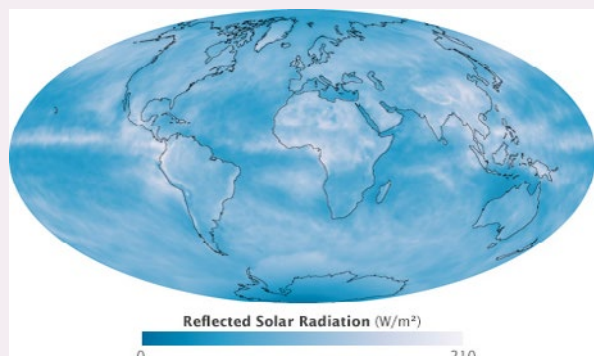
The Clouds and the Earth's Radiant Energy System (CERES) includes instruments on several NASA satellite missions. This mission measures two types of outgoing energy from Earth:

- reflected solar radiation (short wave EMR; see Figure 4.12); and
- emitted radiation (long wave EMR; see Figure 4.13).

The difference between the incoming solar radiation and total outgoing radiation is called the net radiation (see Figure 4.14). These global imbalances in energy drive circulation of the atmosphere and oceans to create our weather and climate.

**Figure 4.12** Reflected solar radiation

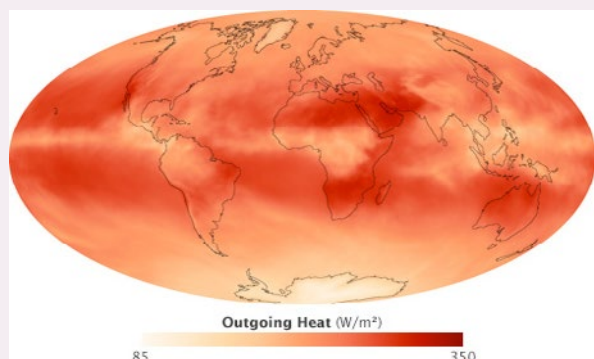
Clouds and bright surfaces reflect more solar radiation. Derived from CERES data for September 2008, averaged over one month.



Source: Robert Simmon, NASA. Retrieved from <http://earthobservatory.nasa.gov/Features/EnergyBalance/page3.php>

**Figure 4.13** Outgoing radiation

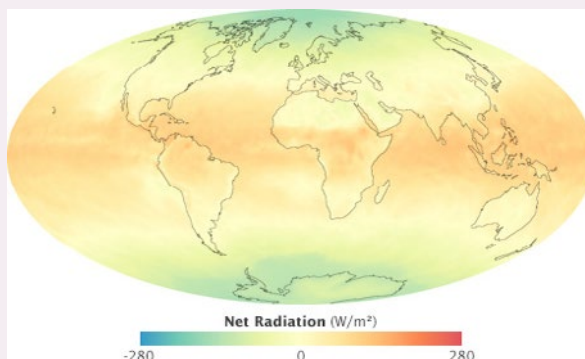
Distribution of thermal infrared emission derived from CERES data during the month of September 2008. Clouds around the equator reduce heat loss, with maximum loss occurring in the warm, relatively cloud-free middle latitudes.



Source: Robert Simmon, NASA. Retrieved from <http://earthobservatory.nasa.gov/Features/EnergyBalance/page4.php>

**Figure 4.14** Net radiation

This global image shows the difference between incoming solar radiation and outgoing radiation during September 2008, an equinox month. In areas with positive net radiation (orange and red—such as near the equator) there was more incoming than outgoing radiation, that is, they absorbed more energy. In areas with negative net radiation (green and blue—such as the poles) more radiation was outgoing than incoming.



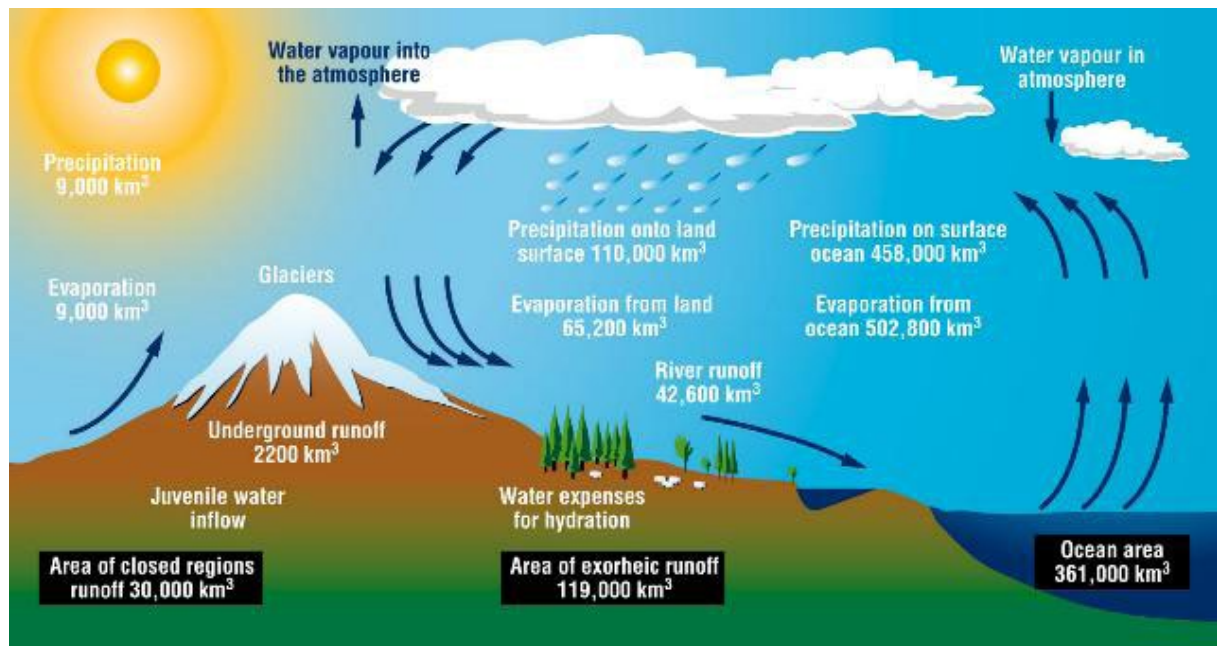
Source: Robert Simmon, NASA. Retrieved from <http://earthobservatory.nasa.gov/Features/EnergyBalance/page3.php>

## 4.2.2 Water

Each year, more than half a million cubic kilometres of water moves between locations on the Earth's surface, between the surface and sub-surface storage, and between the surface and the atmosphere (Shiklomanov, 1998). This constant movement can occur in the form of liquid water, steam, ice or snow and may be close to pure or contain dissolved and/or suspended substances see Figure 4.15.

**Figure 4.15** Hydrological cycle

More than half a million cubic kilometres of water is moved around the Earth's surface, between the surface and sub-surface storage, and between the surface and the atmosphere each year.



Source: Shiklomanov (1998) © UNESCO. Retrieved from <http://webworld.unesco.org/water/ihp/publications/waterway/webpc/pag5.html>

As surface water is heated by the Sun, it evaporates to become water vapour in the atmosphere. Plants also release water to the atmosphere by evapotranspiration. As water vapour rises in the atmosphere, it cools and condenses, forming clouds. Global air currents move clouds until they release their water as precipitation, in the form of rain, hail or snow.

Water on the surface of the Earth is stored in the natural depressions of oceans and lakes, or the man-made storage facilities of reservoirs and dams. Some surface water is frozen, as occurs in polar ice caps and glaciers, and may remain in that form for millennia. Other frozen surface water regularly melts with seasonal changes.

Water running on the Earth's surface, or runoff, can come directly from precipitation or melting sources. Before flowing towards a drainage channel, precipitation can be intercepted by vegetation, buildings or small surface depressions within a catchment. Interception of rainfall allows some precipitation to soak into the ground rather than flow away. Water can infiltrate into the soil layer and be stored as soil moisture or percolate through the soil until it reaches the water table.

Beneath the Earth's surface, soil and/or rock are layered in two distinct zones. The upper zone is aerated, that is, it contains some air. Water in this zone is available to plants. In the lower, rocky zone, air pockets are saturated with water. The boundary between these zones is called the water table. The depth of the water table varies with the volume of water that is added (recharge) and/or removed (discharge). Globally, extraction of groundwater is increasing by 1% to 2% per year (WWAP, 2012).

### 4.2.3 Earth

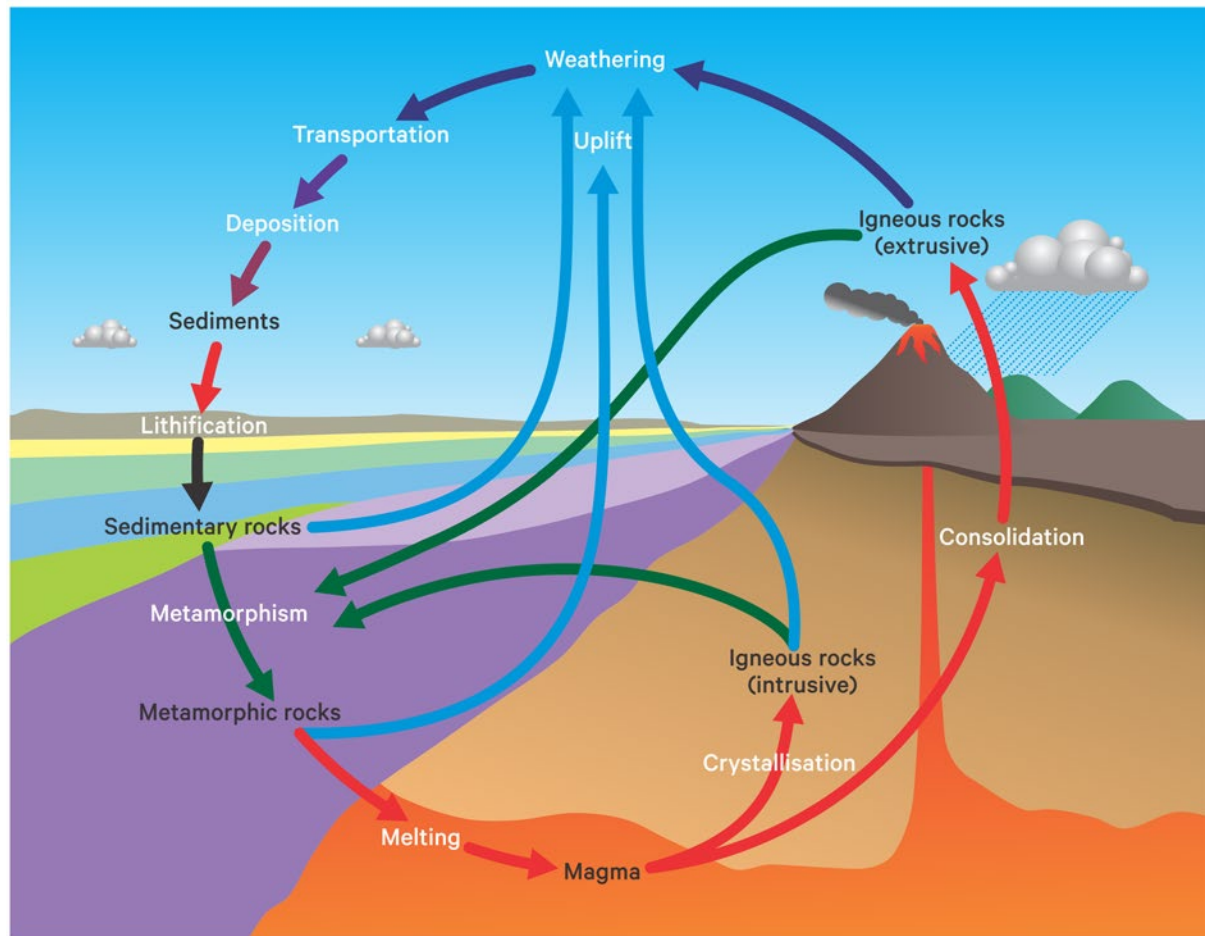
Just as water is transformed and moved around the planet by the hydrological cycle, so inorganic solids are recycled by the rock cycle (see Figure 4.16). This cycle explains the origins and interrelationships between the three basic rock types:

- igneous—formed by cooling and solidification of magma below or on the surface;
- sedimentary—formed by compaction of accumulated sediments that have been loosened by erosive agents of water, wind and ice; and
- metamorphic—formed from parent rock by heat and pressure deep within the Earth, and/or contact with chemically active fluids.



**Figure 4.16** Rock cycle

Sedimentary, igneous and metamorphic rocks are manufactured and reconstituted in cycles.



Adapted from: Monroe and Wicander (1992) Figure 1-15

Rocks are manufactured and reconstituted in cycles. They comprise minerals, naturally occurring inorganic solids with a defined chemical composition and characteristic crystalline structure. Rocks are formed as different combinations of minerals become fused and aggregated in different ways. Although 4,000 minerals are known to exist, only a few dozen commonly occur and 98% of the Earth's crust is formed from just eight elements (O, Si, Al, Fe, Ca, Na, K, Mg). Silicates are the most commonly occurring group of minerals (Tarbuck and Lutgens, 2005).

All igneous rocks are formed from magma, molten material from the asthenosphere. When extruded onto the surface of Earth by volcanoes, magma becomes lava, which cools quickly to form rocks with fine crystals. Igneous rocks also form when magma intrudes into 'plutons' below the Earth's surface, where slower cooling produces larger crystals.

Sedimentary rocks are the result of weathering. Fragments of rocks are gradually eroded by wind, water or ice. These grains, or sediments, are

transported by wind, water or gravity until they settle and solidify. Over time, sediments are compacted and/or chemically cemented together.

Metamorphic, igneous and sedimentary rocks can be transformed by heat and pressure, and/or contact with chemically active fluids to become new metamorphic rocks. Heat typically comes from contact with magma. Extremely high temperatures and pressures can re-form minerals.

The extremely slow movement of plate tectonics explains many geological processes and most changes in geology occur at the boundaries of tectonic plates (see Section 3.2). At a landscape level, the rock processes combine with tectonic activity to shape the surface of Earth:

- Surface rocks are gradually worn down by weathering and erosion, with the loosened sediments being deposited to form sedimentary rocks;
- Sediments can become buried and compressed or may be uplifted by tectonic movement. With heat and pressure they can become metamorphic rocks;

- Metamorphic rocks can be either uplifted to form new mountain ranges or can sink into the mantle to form magma;
- By internal pressure or convection, magma is forced from the mantle to the Earth's surface or into the lithosphere where it cools and solidifies to form igneous rock; and
- Movement of the mantle or crust push rocks to the surface, where they are subject to weathering.

This ongoing cycle, which has continued for millenia, creates the topography of our planet (Lutgens and Tarbuck, 1998).

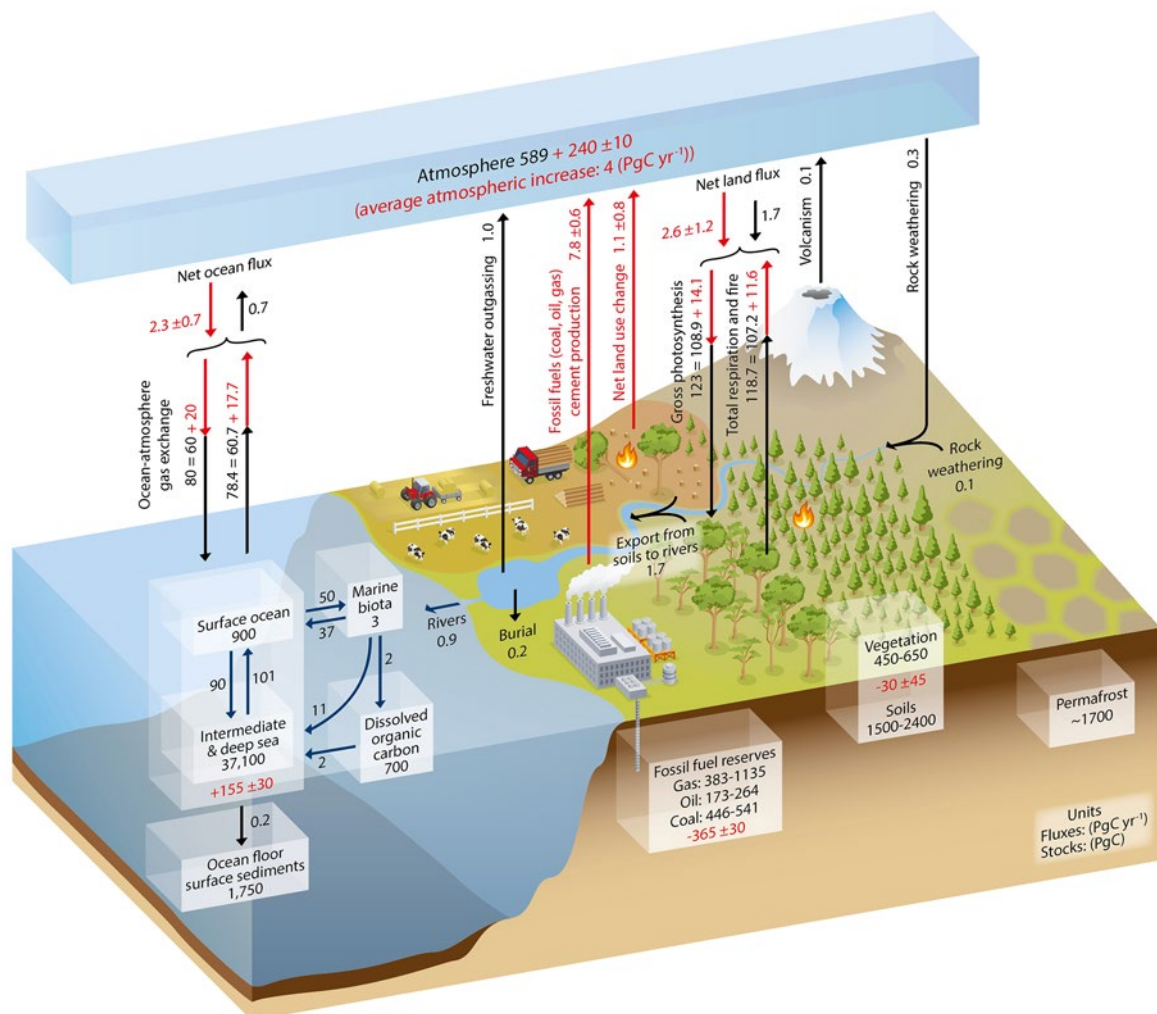
#### 4.2.4 Carbon

An integral part of the biosphere involves the way carbon is cycled through ecosystems. The element carbon characterises all living organisms and ranks as the fourth most abundant element in the universe on the basis of mass, after hydrogen, helium and oxygen. On Earth, it exists in many forms including carbon dioxide, limestone, dolomite, graphite, diamonds, and fossil fuels, and organic compounds.

While the largest proportion of Earth's carbon is stored in rocks, it also exists in the ocean, atmosphere, vegetation, humans, animals, soil and fossil fuels. The carbon cycle describes the process of carbon flowing from one type of storage, or reservoir, to another via natural processes (see Figure 4.17).

**Figure 4.17** Carbon cycle

Carbon reservoirs on Earth exchange stores in the global carbon cycle. These exchanges are called fluxes. Estimates of reservoir stores are shown in PgC ( $10^{15}$  g of elemental carbon). Pre-industrial reservoirs and fluxes are shown in black. Additional fluxes resulting from anthropogenic activity between 2000 and 2009 are shown in red. Red numbers in reservoirs indicate the cumulative change in anthropogenic carbon from 1750 to 2011, with positive numbers indicating a gain and negative numbers indicating a loss.



Source: Figure 6.1 from Ciais et al. (2014) © IPCC. Retrieved from [https://www.ipcc.ch/pdf/assessment-report/ar5/wg1/WG1AR5\\_Chapter06\\_FINAL.pdf](https://www.ipcc.ch/pdf/assessment-report/ar5/wg1/WG1AR5_Chapter06_FINAL.pdf)

The slow carbon cycle, occurring over hundreds of million years, is defined as a series of processes involving chemical reactions and tectonic activity, which transfer carbon between the lithosphere, hydrosphere and atmosphere. Rain moves carbon from the atmosphere into the lithosphere in the form of carbonic acid. The process of surface weathering is aided by this weak acid to release calcium ions from rocks. These ions gradually flow into surface waters where they combine with bicarbonate ions to form calcium carbonate. Carbon is returned to the atmosphere through volcanoes as carbon dioxide.

It is estimated that around 80% of carbon in the Earth's lithosphere derives from inorganic sources. Under certain circumstances, layers of organic carbon from dead vegetation accumulate at a faster rate than they decay, forming subterranean seams of oil, coal or natural gas which together comprise the remaining 20% of carbon stores involved in the slow cycle.

The fast carbon cycle occurs much more quickly as a much smaller amount of carbon moves through various forms of life in the biosphere, particularly

vegetation. Terrestrial plants and phytoplankton absorb atmospheric carbon dioxide in the process of photosynthesis. This reaction allows carbon to be stored in vegetation as carbohydrates (sugars), which provide energy. That energy can be released by:

- plants using energy to grow;
- animals eating plants for energy;
- microorganisms eating plants in the decay process; or
- fire consuming the plant as fuel.

All four mechanisms effectively reverse the photosynthetic process to release carbon dioxide back into the atmosphere. Thus, the fast carbon cycle is an important energy transfer process in all ecosystems.

The global carbon budget attempts to account for the exchange (or flux) of carbon between reservoirs (or sinks) and helps to monitor the balance of carbon in different forms (see Figure 4.17). Research has indicated that the global carbon cycle has been modified in recent centuries, particularly in terms of elevated atmospheric carbon, which is correlated with changes in climate (see Volume 3).

### 4.3 Further Information

Photosynthesis: <http://www.photobiology.info/Brennan.htm>

Earth Energy Balance: <http://earthobservatory.nasa.gov/Features/EnergyBalance/page1.php>

Ionosphere: [http://www.sws.bom.gov.au/HF\\_Systems/6/5](http://www.sws.bom.gov.au/HF_Systems/6/5)

Geology: <http://www.geolsoc.org.uk/heresources>

Tectonic Plates: Kious and Tilling (1996)

### 4.4 Reference

Anderson, D. L. (1989). *Theory of the Earth* (366 pages). Blackwell Publications, Boston.

Ciais, P., Sabine, C., Bala, G., Bopp, L., Brovkin, V., Canadell, J., Chhabra, A., DeFries, R., Galloway, J., Heimann, M., Jones, C., Le Quéré, C., Myneni, R. B., Piao, S., and Thornton, P. (2014). Carbon and Other Biogeochemical Cycles. Chapter 6 in 'Climate Change 2013 - The Physical Science Basis Working Group I Contribution to the Fifth Assessment Report of the Intergovernmental Panel on Climate Change' (Eds: T. F. Stocker, D. Qin, G.-K. Plattner, M. Tignor, S. K. Allen, J. Boschung, A. Nauels, Y. Xia, V. Bex, and P. M. Midgley), pp. 465-570. Cambridge University Press, Cambridge, United Kingdom.

Kious, W. J., and Tilling, R. I. (1996). *This Dynamic Earth: The Story of Plate Tectonics*. USGS, Washington, DC. Retrieved from <http://pubs.usgs.gov/gip/dynamic/dynamic.html>.

Lindsey, R. (2009). *Climate and Earth's Energy Budget*. Retrieved from <http://earthobservatory.nasa.gov/Features/EnergyBalance/>.

Lutgens, F. K., and Tarbuck, E. J. (1998). *Essentials of Geology*, 6th Edn. Prentice Hall, New Jersey, USA.

Monroe, J. S., and Wicander, R. (1992). *Physical Geology: Exploring the Earth*. West Publishing Company, St. Paul.

NOAA (2016). *Space Weather Prediction Centre*. Retrieved from <http://www.swpc.noaa.gov/phenomena/ionosphere>.

Robertson, E. C. (2001). *The Interior of the Earth*. Retrieved from <http://pubs.usgs.gov/gip/interior/>.

Shiklomanov, I. A. (1998). *World Water Resources: A new appraisal and assessment for the 21st Century*. United Nations Educational, Scientific and Cultural Organization (UNESCO), Paris, France. Retrieved from [http://webworld.unesco.org/water/ihp/publications/waterway/webpc/world\\_water\\_resources.html](http://webworld.unesco.org/water/ihp/publications/waterway/webpc/world_water_resources.html).

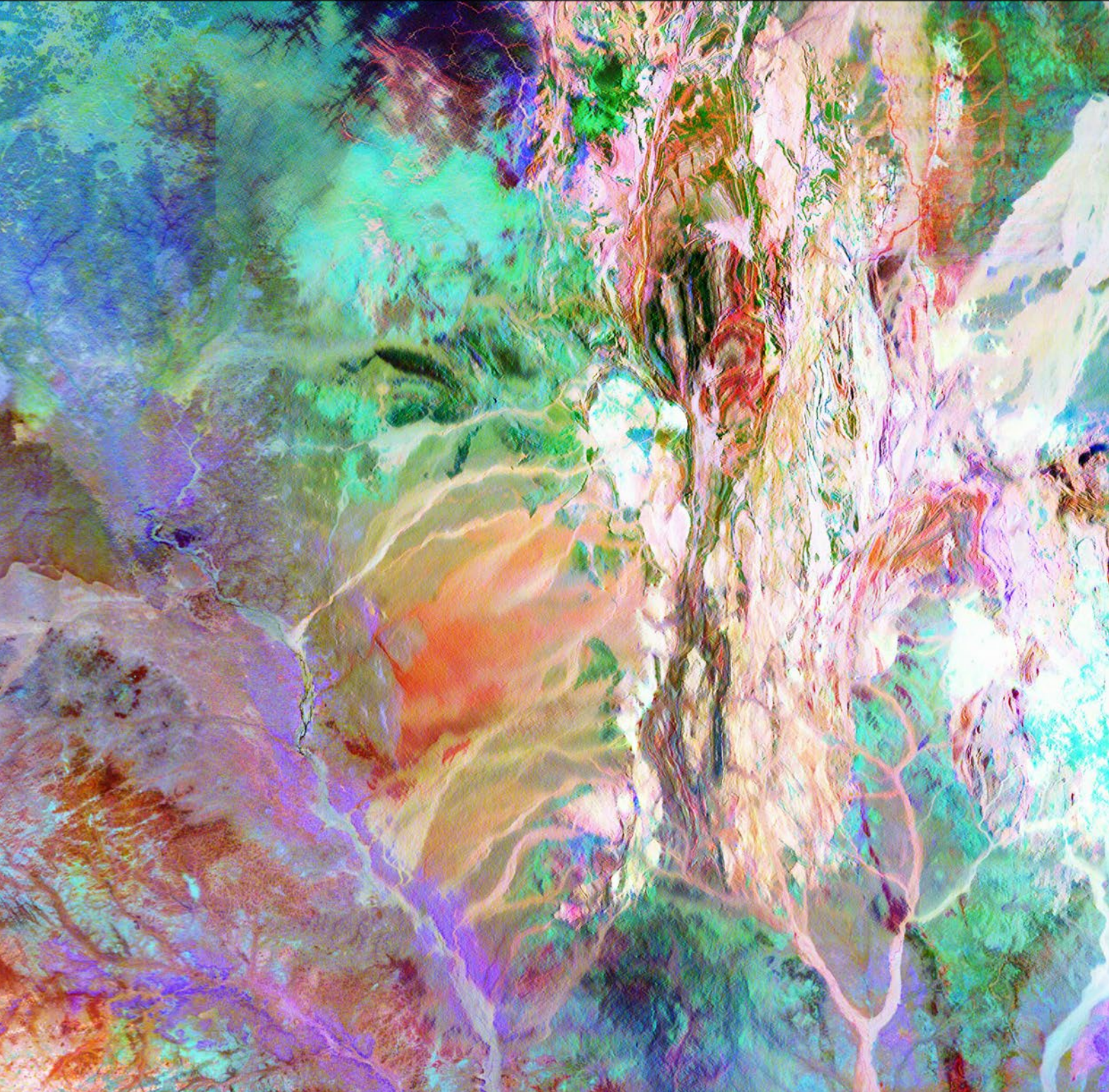
Suess, E. (1875). *Die Entstehung der Alpen (The Origin of the Alps)*. W. Braunmuller, Vienna.

Tarbuck, E. J., and Lutgens, F. K. (2005). *Earth*, 8th Edn. Prentice Hall, New Jersey, USA.

WWAP (2012). *The United Nations World Water Development Report 4: Managing Water under Uncertainty and Risk*. United Nations Educational, Scientific and Cultural Organization (UNESCO), Paris, France.



# **Energy Sources for Earth Observation**





All sources of energy sensed by Earth Observation (EO) relate to the mass, composition, internal processes and/or movements of the various celestial bodies that compose our universe and the interactions that occur between them. Indeed, our understanding of the masses, compositions, movements and interactions of these bodies has been significantly extended since the advent of spaceborne remote sensing technologies.

Energy exists in many different forms, many of which can be detected remotely, that is, using sensors that are not in direct contact with the energy source. Understanding the different types of energy—how they are transmitted and how they interact with the Earth’s environments—is essential for designing appropriate remote sensing instruments, and for designing algorithms to transform the resulting images into measurements of relevant environmental properties.

The following sections introduce the major energy sources detected by EO sensors:

- electromagnetic energy (see Section 5);
- radioactivity (see Section 6);
- magnetism (see Section 7);
- gravity (see Section 8); and
- vibrations (see Section 9).

## Contents

<b>5</b>	<b>Electromagnetic Radiation</b>	<b>79</b>
<b>6</b>	<b>Radioactivity</b>	<b>95</b>
<b>7</b>	<b>Magnetism</b>	<b>101</b>
<b>8</b>	<b>Gravity</b>	<b>111</b>
<b>9</b>	<b>Vibrations</b>	<b>117</b>

# 5 Electromagnetic Radiation

Electromagnetic (EM) radiation (EMR) is the energy form most commonly sensed by Earth remote sensing devices. EM energy is measured in defined regions of the EM spectrum, as outlined in the Section 5.1. This energy is either reflected from the Earth's surface or emitted by Earth (see Section 5.2). Known interactions between EMR and specific targets determine the most relevant spectral regions to measure. For example, the molecular structures of different minerals absorb light energy in specific and characteristic wavelengths. Similarly, the chemical chlorophyll, which drives photosynthesis in foliage, can be identified and quantified by the way EMR is reflected by vegetation. EMR spectral regions are defined in Section 5.3 and atmospheric interactions with EMR are described in Section 5.4.

## 5.1 The EM Spectrum

The Sun provides most of the energy that we sense as light. This energy consists of EM waves, which travel in harmonic, sinusoidal motion as shown in Figure 5.1. The electric and magnetic fields are perpendicular to each other and to the direction of travel, making EM waves a type of transverse wave (see Section 2.5), which can be characterised by wavelength ( $\lambda$ ) and frequency ( $\nu$ ):

$$c = \nu \lambda$$

where

$c$  is the speed of light in a vacuum.

The energy of these waves is not strictly continuous, but is also considered to be packaged into discrete units called photons, with the number of photons being related to the intensity of the EMR. The Planck-Einstein relation states that:

$$E = h\nu = h\frac{c}{\lambda}$$

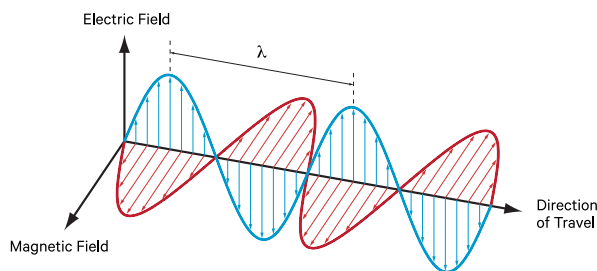
where

$E$  is energy of photon; and

$h$  is Planck's constant =  $6.626 \times 10^{-34}$  Joule seconds.

**Figure 5.1** Electromagnetic wave

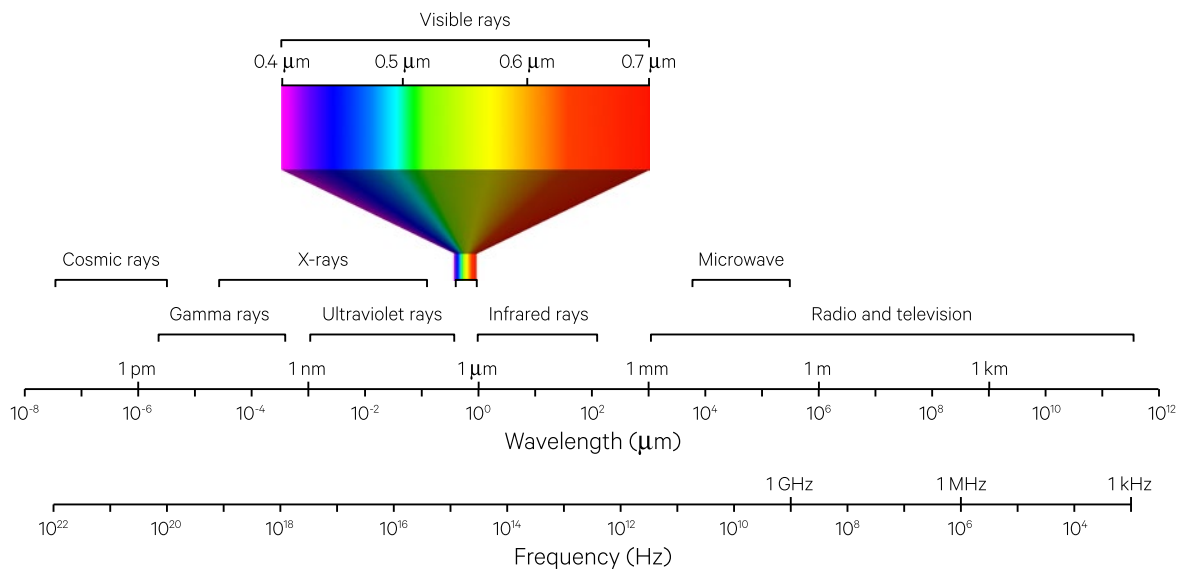
An EM wave comprises two sinusoidal waves: an electric wave (E) and a magnetic wave (H). Each component wave is perpendicular to the other and also to the direction of travel. Wavelength ( $\lambda$ ) is measured as the distance between successive wave peaks or troughs. Frequency ( $\nu$ ) is measured as the number of cycles per second passing a fixed point.



Source: Pete Harrison, Langlopress

**Figure 5.2** Electromagnetic spectrum

Names are assigned to regions of the spectrum for convenience – there are no clearly defined divisions. Cosmic rays are high energy, charged particles that travel at close to the speed of light. They are not EMR but included for comparison. Note: scales are logarithmic



Adapted from: Harrison and Jupp (1989) Figure 2

Although all EMR travels at the same speed ( $3 \times 10^8$  m/s—the speed of light in a vacuum), the wavelengths (that is, the distance between consecutive troughs or crests) of the waves can and do vary. The resulting range of wavelengths gives rise to the Electromagnetic Spectrum (EM Spectrum), illustrated in Figure 5.2. The higher energy forms of EMR, such as X-rays, have short wavelengths and high frequency (since the shorter the distance per cycle, the greater the number of cycles required to achieve the same speed), while low energy forms, such as radio waves, have long wavelengths and low frequency.

The small part of the continuous EM spectrum to which the human eye is sensitive is known as ‘light’. This visible portion of the spectrum approximately spans the wavelengths from 0.4–0.7  $\mu\text{m}$  ( $10^{-6}$  m). For convenience, names are assigned to the various regions of the spectrum, but there are no precise division between them. The regions are generally defined by the sensing method by which they are detected. Commonly accepted ranges for EMR spectral regions are:

- visible: 0.38–0.7  $\mu\text{m}$
- infrared (IR): 0.7–1,000  $\mu\text{m}$
- microwave: > 1 mm–1 m

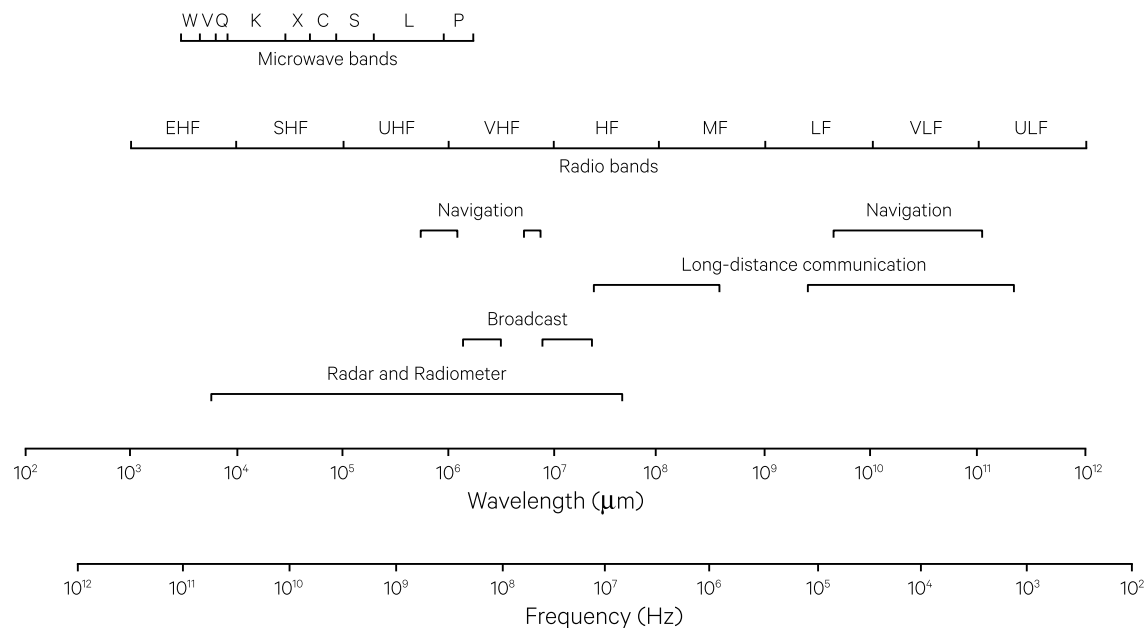
Infrared wavelengths are often sub-divided into the regions:

- near infrared (NIR): 0.7–1.3  $\mu\text{m}$
- short wave infrared (SWIR): 1.3–3  $\mu\text{m}$
- middle infrared (MIR) or mid-wavelength (or medium wave) infrared (MWIR): 3–8  $\mu\text{m}$
- thermal infrared (TIR) or long wavelength infrared (LWIR): 8–15  $\mu\text{m}$
- far infrared (FIR): 15–1,000  $\mu\text{m}$

In Earth Observation (EO), the shorter wavelengths regions denoted visible, NIR and SWIR are often collectively referenced as ‘optical’ (or reflective) wavelengths, and the term TIR may be used to include the wavelengths from 3–5  $\mu\text{m}$ . Much of the longer wavelength energy cannot be seen or photographed but can be sensed with radiometers and scanners. The range of wavelengths in which various sensors can operate is shown in Figure 5.3. Specific remote sensors are designed to measure EMR for a defined range of wavelengths (see Sections 13 to 15).

**Figure 5.3** Common remote sensing systems

Scanners and radiometers can operate outside the visible and photographic wavelength regions. Note: scale is logarithmic.



Adapted from: Harrison and Jupp (1989) Figure 4

## 5.2 Reflectance and Emission

All materials both reflect EMR that comes from external sources and emit EMR as a function of their temperature (see Section 2.11). Reflectance and emission from a material depend on chemical and physical characteristics of that material, and can thus be used to determine those characteristics. Remote sensors have been designed to detect both reflected and emitted EM energy from objects.

### 5.2.1 Reflected energy

Reflected energy originates from an external energy source and is determined by the interaction of the incident energy from that energy source with the illuminated object. Matter either absorbs or transmits incoming, or incident, energy, depending on whether or not that energy excites physical processes in the matter's atoms and molecules (see Section 2.2). Excitation varies with the wavelength or frequency of the energy and the molecular composition of the matter being radiated. For example, the human body absorbs EMR in the visible, infrared and microwave wavelengths, but transmits—is transparent to—X-rays and radio waves. However, both absorption and transmission may be partial, such that some of the incident energy may also be reflected.

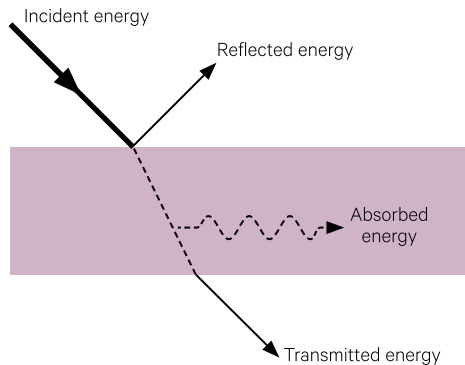
Thus, EM energy is selectively absorbed by materials depending on how different frequencies of EMR interact with the molecules, atoms and nuclei of the material (see Section 2.2). These fundamental components of matter are generally characterised by discrete, quantized energy levels, and transition between these levels is typically characterised by the absorption or emission of photons. Visible and ultraviolet wavelengths are primarily absorbed by a material when its electron transitions (that is the change in energy required to move from the initial state to an excited state) precisely match the quantum energy of the photon. Infrared wavelengths correspond to the range of energies that occur in molecular vibrations or chemical bonds, so tend to heat the materials that absorb them. The quantum energy of microwave photons is in the range of energies that separate the quantum states of molecular rotation and torsion<sup>17</sup> (see Volume 1B—Section 3 for more detail).

17. Other interactions can lower the energy of excited electrons in atoms and molecules: fluorescence happens when matter instantaneously emits a photon with lower energy and longer wavelength, while phosphorescence occurs when matter can retain the energy of excitation for a period of time then emit that energy gradually.



**Figure 5.4** Incident energy components

The energy incident on a surface is reflected, transmitted or absorbed.



When the frequency of the incident EM energy does not match the energy levels required for absorption, that energy is transmitted through or reflected by the object. The transparency of an object (allowing transmission of incident radiation through the object) and its opacity (resulting in reflectance of incident radiation) are determined by the physical and chemical structure of the object, relative to the wavelength of the radiation.

Thus the relationship between an external energy source and an illuminated target can be summarised by the equation (see Figure 5.4):

$$\text{incident energy} = \text{reflected energy} + \text{transmitted energy} + \text{absorbed energy}$$

where

*incident energy* is the EM energy striking the surface of a target;

*reflected energy* is the energy being bounced back from the target;

*transmitted energy* is the energy passing through the target; and

*absorbed energy* is the energy penetrating into and remaining in the target.

Firstly, the proportions of reflected, transmitted and absorbed energy vary for different objects, depending on their material type and condition. Secondly, for a particular material, these proportions also vary for different wavelengths. These relationships allow remote sensors detecting radiation in the visible and near infrared regions to derive information relating to the type and condition of materials on the Earth's surface. The same principles are used to characterise chemical compounds by atomic absorption spectroscopy.

The reflectance of an object is defined as the ratio of reflected energy relative to the incident energy:

$$\text{reflectance} = \frac{\text{reflected energy}}{\text{incident energy}}$$

Similarly, absorptance and transmittance are defined as:

$$\text{transmittance} = \frac{\text{transmitted energy}}{\text{incident energy}}$$

$$\text{absorptance} = \frac{\text{absorbed energy}}{\text{incident energy}}$$

Thus, these components of incident radiation sum to one:

$$\text{reflectance} + \text{transmittance} + \text{absorptance} = 1$$

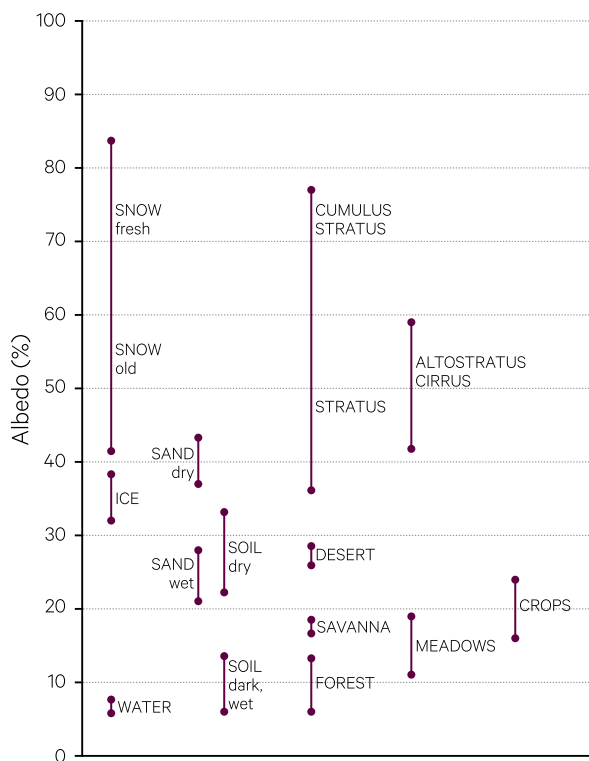
(Note that reflectance, transmittance and absorptance are sometimes computed as percentages—using the above ratios multiplied by 100—in which case they sum to 100.)

In terms of EO, the interaction of incoming radiation with surface features depends on both the spectral reflectance properties of the surface materials and the surface smoothness relative to the radiation wavelength (see Section 2.5). A relatively 'smooth' surface, which reflects energy without any scattering (that is, where the angle of incidence equals the angle of reflection), is called a 'specular' or 'mirror' reflector. 'Diffuse' or 'Lambertian' reflectance occurs when the surface is rough relative to the wavelength(s) of the incoming radiation and causes the energy to be reflected equally in all directions (see Figure 2.7). Calm water can act like a specular reflector. Most of the Earth's other surface materials are diffuse reflectors in the visible wavelengths but may display specular reflectance properties in the microwave wavelengths. Surface orientation relative to both the energy source and sensing device also affects the amount of radiation detected by the sensor. Other aspects of the interaction of EMR with the Earth's surface are discussed in Volume 1B—Sections 4 to 6.

A less precise measure of the proportion of radiation that is reflected by a surface is albedo. This is computed as the ratio of all reflected radiation (both specular and diffuse—see Section 2.5.2) to the incident radiation over a given area (see Volume 1B—Sections 6.5 and 7). This property varies with different types of material, different wavelengths of EM energy, latitudes on Earth and seasons (see Figure 5.5). Albedo measurements are used in studies related to Environmental Physics, for broad topics such as energy balance and evapotranspiration. Typical albedo values for some common materials are listed in Table 5.1.

**Figure 5.5** Albedo of different materials

Albedo is the proportion of incident energy that is reflected by a material. Some materials, such as snow, reflect radiation more strongly than others.



Adapted from: Hannes Grobe (CC BY-SA 2.5) at [http://en.wikipedia.org/wiki/Albedo#/media/File:Albedo-e\\_hg.svg](http://en.wikipedia.org/wiki/Albedo#/media/File:Albedo-e_hg.svg)

**Table 5.1** Sample albedo values

Surface Material	Sample Albedo Values
Perfect absorber (blackbody)	0
Ocean	0.03–0.10
Forest	0.05–0.20
Bare Soil	0.05–0.40
Grass and Crops	0.1–0.25
Granite	0.30–0.35
Sand	0.15–0.45
Ice	0.20–0.50
Clouds	0.30–0.90
Snow	0.40–0.90
Perfect reflector (absolutely white surface)	1

Source: Dobos (2003); Budikova (2013)

## 5.2.2 Emitted energy

Emitted energy is determined by the physical properties of matter (see Section 2.10). The quantity of radiant flux emitted from an object is called its radiant temperature ( $T_{rad}$ ). Generally, the kinetic temperature ( $T_{kin}$ ) of an object is highly correlated with its radiant temperature (see Section 2.10).

Remote thermal infrared radiometers can be used to measure radiant temperature (see Sections 14.4, 16.1.1.1 and Volume 1B—Section 7). The physical laws introduced in Section 2.11 allow radiant temperature measurements to be converted to kinetic temperature. The variation between radiant flux from a real object compared with the radiation from a blackbody is described by a thermal property called emissivity ( $\epsilon$ —see Section 2.11.2). Emissivity varies with EMR wavelength for all types of matter. Factors such as colour, surface texture, moisture content, and density can also change the emissivity of an object. Emissivity variations between substances at a given wavelength can be used to differentiate between them using thermal remote sensing (see Volume 1B—Section 7).

Kirchhoff's Radiation Law (see Section 2.11.2) applies to targets in 'thermodynamic equilibrium' and can be summarised as:

*Good absorbers are good emitters and good reflectors are poor emitters.*

Thus, for a given wavelength ( $\lambda$ ), absorptance ( $\alpha$ ) can be used to approximate emissivity ( $\epsilon$ ):

$$\alpha_{\lambda} \sim \epsilon_{\lambda}$$

Using Kirchhoff's radiation law, and assuming minimal transmittance, absorbed energy can be replaced with emissivity to reduce the incident energy relationship to:

$$\text{reflectance} + \text{emissivity} = 1$$

so that:

$$\text{emissivity} = 1 - \text{reflectance}$$

Combining the Stefan-Boltzmann law (see Section 2.11.1) with Kirchhoff's radiation law allows us to derive a relationship between the apparent radiant temperature ( $T_{rad}$ ) of an object and its true kinetic temperature ( $T_{kin}$ ):

$$\sigma T_{rad}^4 = \epsilon \sigma T_{kin}^4$$

or

$$T_{rad} = \epsilon^{0.25} T_{kin}$$

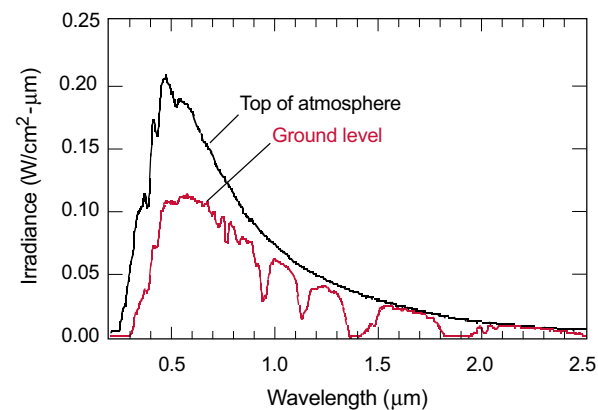
The Sun is not a blackbody but its radiation is similar to that of a blackbody at approximately 5800K with peak intensity being in the spectral region we detect as visible light (see Figure 2.19). Solar radiation is EMR emitted by the Sun's surface. At the top of Earth's atmosphere, the total irradiance from the Sun is approximately 1,360 W/m<sup>2</sup> (see Excursus 3.1). 99% of this energy is within the wavelength range 0.15–4.0  $\mu\text{m}$ , with the maximum emission having the approximate wavelength 0.5  $\mu\text{m}$ , which we perceive as visible green. Solar radiation is dispersed as it travels from the Sun to the Earth so that reduced energy levels are detected at the Earth compared with the theoretical curve shown in Figure 5.6. Due to the Earth's elliptical orbit around the Sun, the amount of solar radiation received at the top of the atmosphere varies throughout the year by  $\pm 3.37\%$  (see Figure 3.3).

The Earth is not a blackbody either, but it does emit radiation in a similar way to a blackbody at 300K (or  $\sim 27^\circ\text{C}$ ). This temperature is the result of various interactions between the Earth's surface and the atmosphere and is determined by all the Earth's processes that produce heat. This radiation is the Earth's thermal radiation and may provide information about soil moisture status, geological properties and hot surface features such as fires (see Volume 1B—Section 7). The EMR emissions associated with Earth's

temperature are in the spectral wavelength range of thermal infrared. By comparison, adult humans, with a skin temperature of approximately  $33^\circ\text{C}$ , emit energy in the infrared region ( $\sim 100$  Watts).

**Figure 5.6** Solar radiation at top of atmosphere and at sea level

While the spectrum of solar radiation that reaches the top of Earth's atmosphere resembles the spectrum of a blackbody at around 5800K (Sun's temperature; see Figure 2.19), some of that radiation is absorbed by the atmosphere before it reaches sea level. As shown in the graph below, the atmosphere absorbs selected wavelengths more strongly than others.



Source: Shaw and Burke (2003). Reprinted with permission courtesy of MIT Lincoln Laboratory, Lexington, Massachusetts.

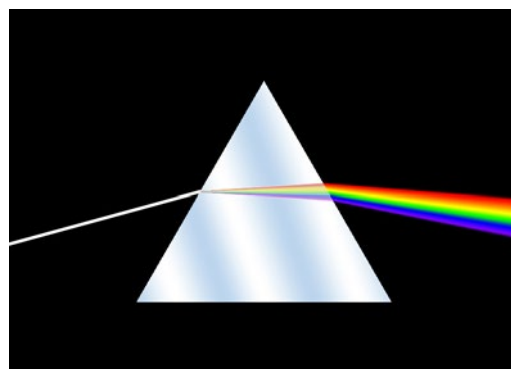
### 5.3 Spectral Regions

The EM spectrum describes the full range of wavelengths that have been detected for EMR. Most of the radiant energy from the Sun is within the wavelength range 0.28 to 2.8  $\mu\text{m}$ , that is, those regions of the EMR spectrum described as UV, visible and NIR. This wavelength range is commonly referred to as short wave radiation. Only 15% of the Sun's energy involves wavelengths in the range 2.8 to 100  $\mu\text{m}$  (SWIR and TIR), which is referred to as long wave radiation. The balance between incoming solar radiation (predominantly short wave) and outgoing radiation from the Earth (predominantly long wave) is discussed in Section 4.2.1 above.

The visible region can be sub-divided into component colours ranging from the higher energy, shorter wavelengths of violet, indigo and blue, through those of green and yellow, to the lower energy wavelengths of orange and red. What is known as 'white' light, such as sunlight, is actually a mixture of all these wavelengths and is also correctly called polychromatic light. When polychromatic light is refracted through a prism, different wavelengths are refracted by different amounts, resulting in the characteristic rainbow spectrum shown in Figure 5.7.

**Figure 5.7** Refraction of polychromatic light through a prism

Transmission of light waves slows as they pass through glass. Different wavelengths of light travel at different speeds and disperse along different paths, with shorter wavelengths 'bending' more than longer ones. This mechanism is used to separate different spectral components of light into the visible light spectrum.



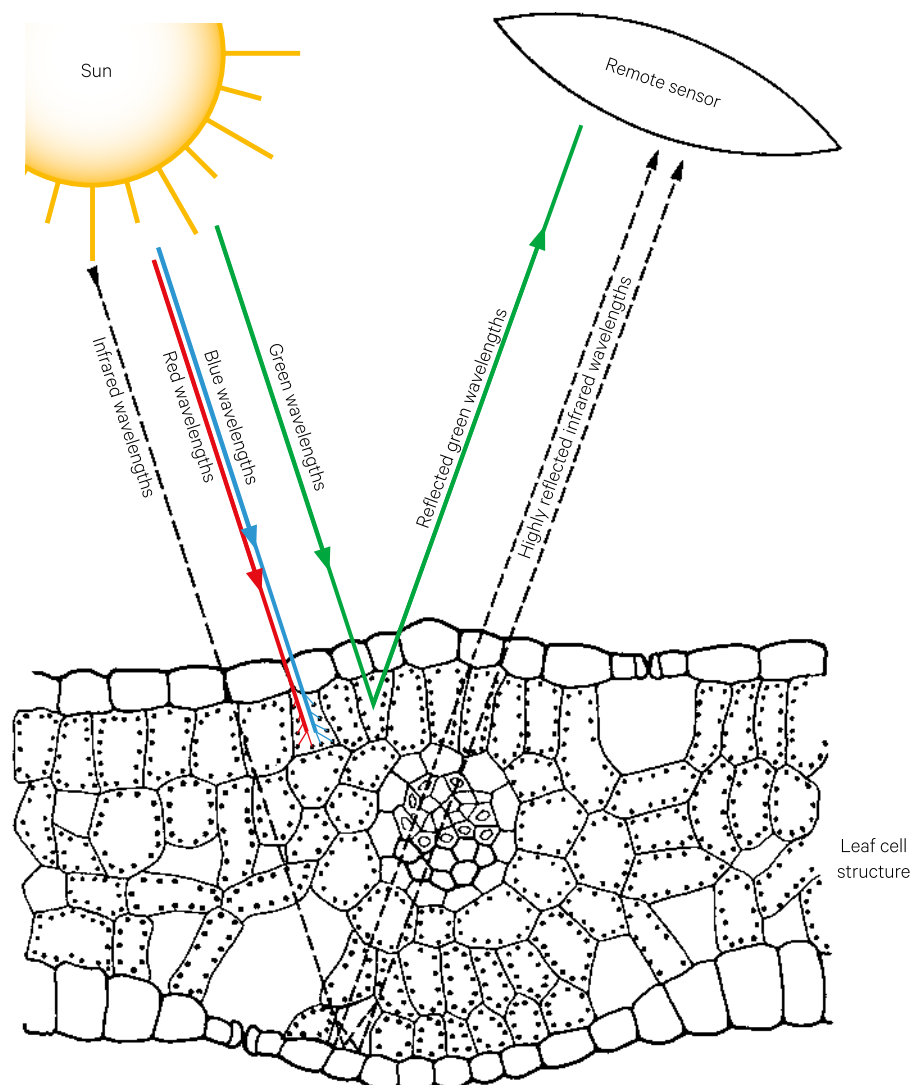
Source: Wikimedia Commons (CC BY-SA 1.0). Retrieved from [https://en.wikipedia.org/wiki/History\\_of\\_spectroscopy#/media/File:Dispersion\\_prism.jpg](https://en.wikipedia.org/wiki/History_of_spectroscopy#/media/File:Dispersion_prism.jpg)

The feature we describe as the colour of an object is the energy not absorbed by that object. In the case of a green leaf, for example, the blue and red wavelengths of light are absorbed by the chloroplasts and used as an energy source for photosynthesis, but a greater proportion of the green wavelengths is reflected (see Figure 5.8). In this case our eyes detect this reflectance as the colour green. By a learned association of the colour green with living foliage, combined with other features such as size and shape, we identify the object and its state (living and dead). The same principle forms the basis of identifying features in remote sensing.

Different land cover features have varying, and often characteristic, reflectance in the non-visible wavelengths (such as infrared or thermal infrared). Consequently, engineered sensors, which are capable of detecting and quantifying these waves, give us more information than what we perceive as colour with which to identify an object. Figure 5.9 illustrates this for three major land cover features (vegetation, water and bare soil). Examples of using EO to identify land cover features are provided in Excursus 1.2, 1.3 and 5.1.

**Figure 5.8** Reflectance characteristics of typical green leaf structure

Chloroplasts reflect green wavelengths but absorb blue and red wavelengths for use in photosynthesis. Spongy mesophyll cells strongly reflect infrared wavelengths.

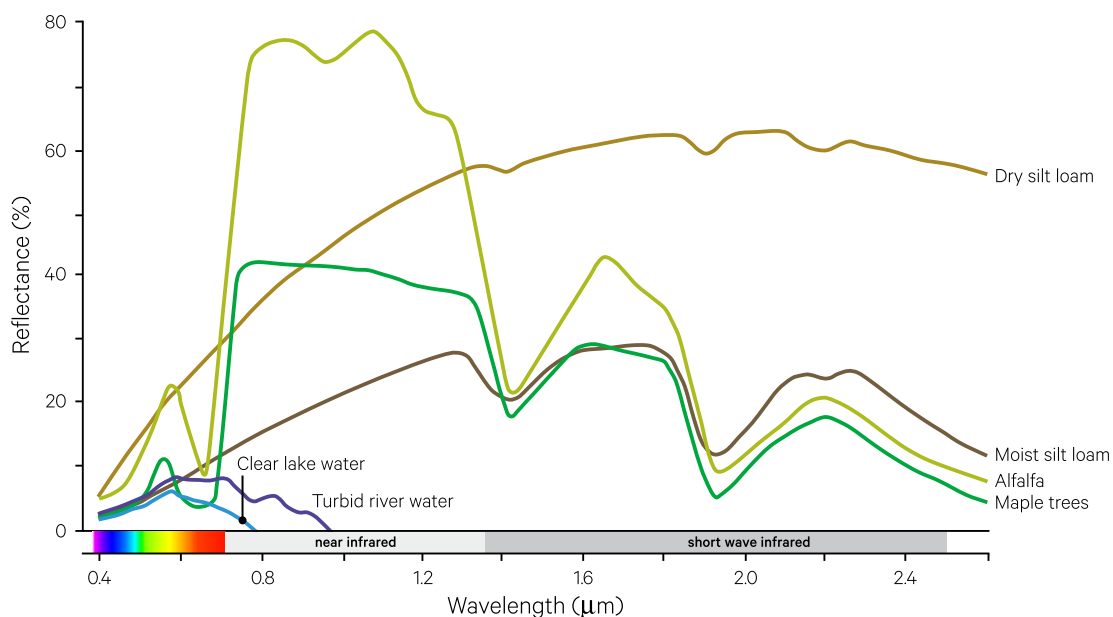


Source: Harrison and Jupp (1989) Figure 5



**Figure 5.9** Idealised spectral reflectance curves

Reflectance from different Earth surface features varies for different wavelengths. Characteristic spectral reflectance curves can be created for different features to indicate a 'typical' shape over a particular range of wavelengths. This information can be used to differentiate between different surface features on the basis of their observed reflectance characteristics.



Source: Harrison and Jupp (1989) Figure 6

## Excursus 5.1—Water Observations from Space (WOfS)

**Source:** Norman Mueller, Geoscience Australia

**Further information:** <http://www.ga.gov.au/scientific-topics/hazards/flood/wofs>, <http://www.datacube.org.au>

Following from the Natural Disaster Insurance Review in 2011, Geoscience Australia (GA) developed an access point for flood models and satellite observations in Australia—National Flood Risk Information Program (NFRIP). One of the components of NFRIP is Water Observations from Space (WOfS) which shows where water has been observed in Australia by the Landsat satellites since 1987 (see Excursus 1.1). This service provides improved understanding of water in the Australian landscape—where it is usually present, where it is seldom observed and where it occasionally floods the surface.

In conjunction with updated national guidelines for flood risk information from Engineers Australia, NFRIP aims to provide a single authoritative source of information related to floods for Australia.

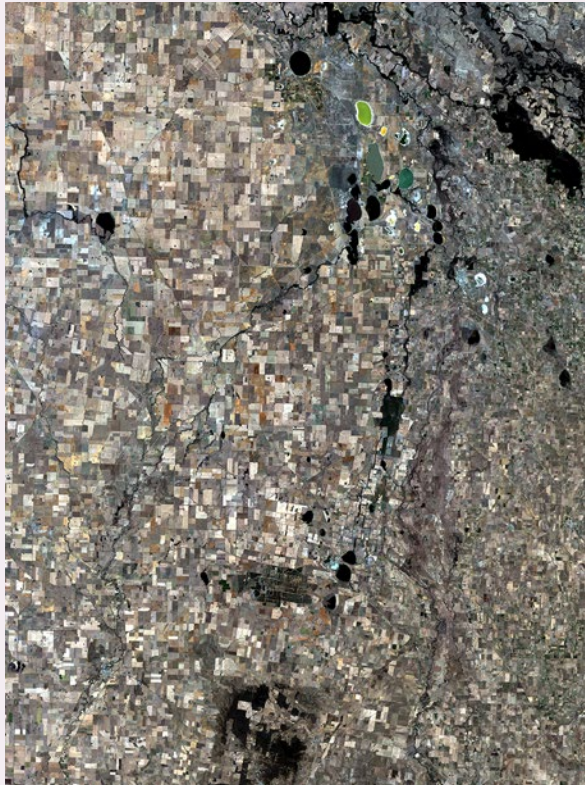
### How do satellites 'see' water?

EO satellites that observe optical wavelengths measure the amount of sunlight reflected from Earth. Different materials on the Earth's surface reflect light differently. Water absorbs the infrared portion of the EMR spectrum that is not visible to human eyes. These characteristic absorption features allow us to differentiate water from other surface materials (see Figure 5.10).

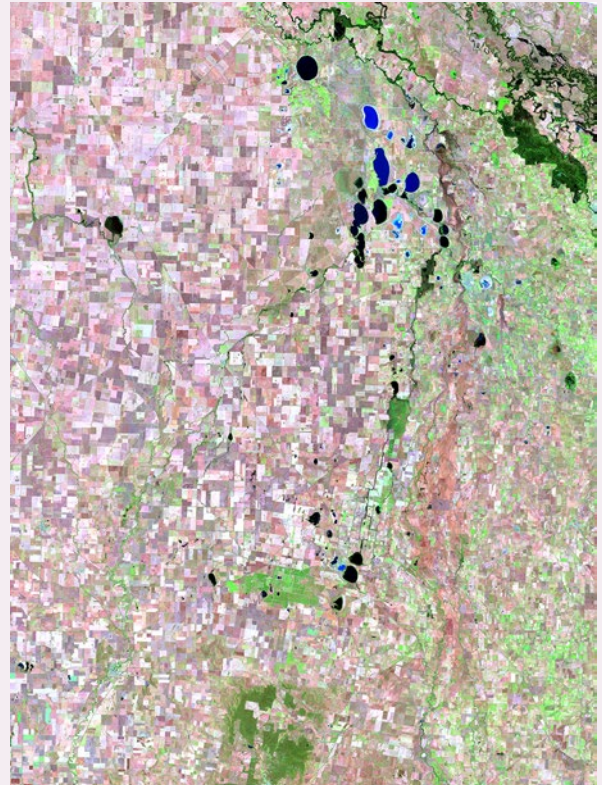


**Figure 5.10** Seeing water from space—Kerang, Victoria

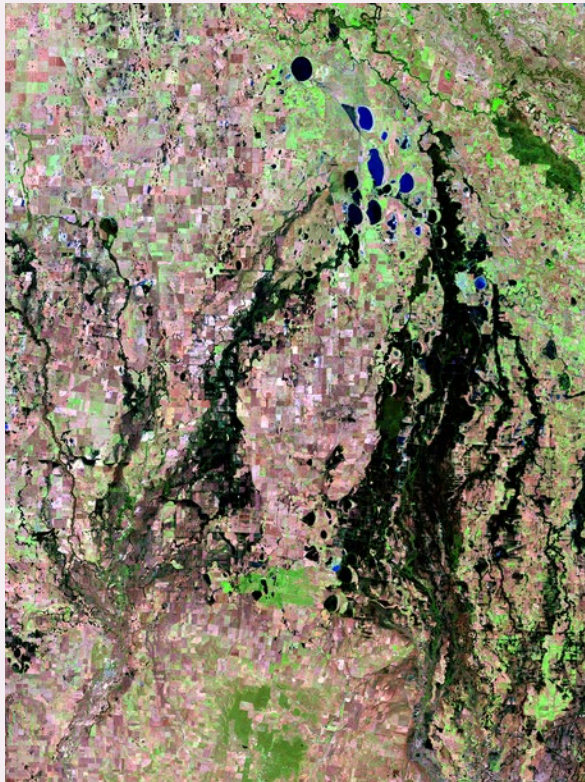
a. 4 January 2011—true colour image approximates what a human would see from space before the flood



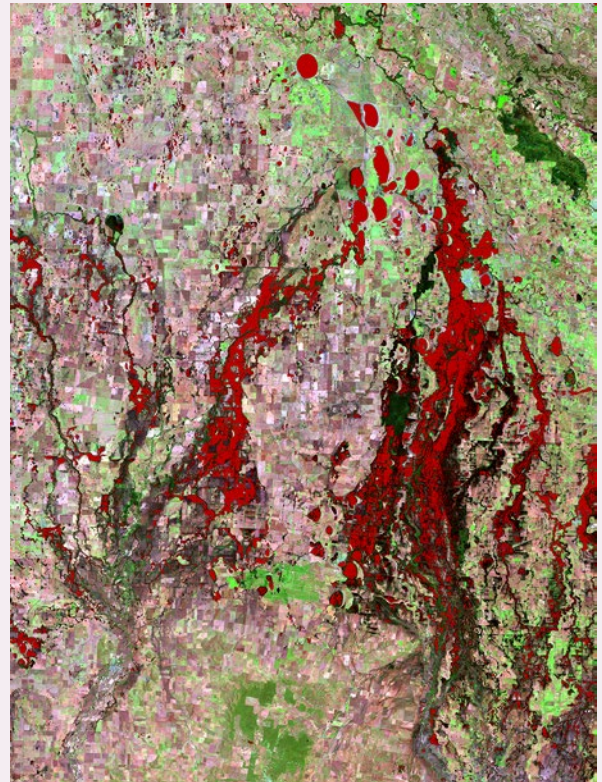
b. 4 January 2011—False colour image highlights differences between water and vegetation before the flood (TM bands 5, 4, 2)



c. 20 January 2011—during floods the area covered by water is defined by low infrared reflectance in this false colour image (TM bands 5, 4, 2) so area of inundation appears as black



d. 20 January 2011—extent of flood is mapped from the satellite images as red overlay



Source: Norman Mueller, Geoscience Australia



## Mapping permanent water

When water is mapped in every image over a given location, we can see where water occurs regularly, as in lakes and rivers, and where it only occurs occasionally, as in floods. This process was applied to Landsat imagery of the Menindee Lakes, NSW, between 1987 and 2016 (see Figure 5.11). In this image, regularly observed water is shown in shades of blue to purple, and occasional water is shown as red. Sequences of such images can be used to effectively map the process of the lakes drying out.

This analysis can be applied to every Landsat-5, -7 and -8 scene acquired over Australia since 1987 (standardised in the Australian Geoscience Data Cube: AGDC) to understand surface water over the whole continent. WOfS analyses have provided insight into:

- water cycles in braided stream networks in inland Australia;
- likely extent of flooding from permanent water bodies; and
- coastline changes such as isthmus breaches.

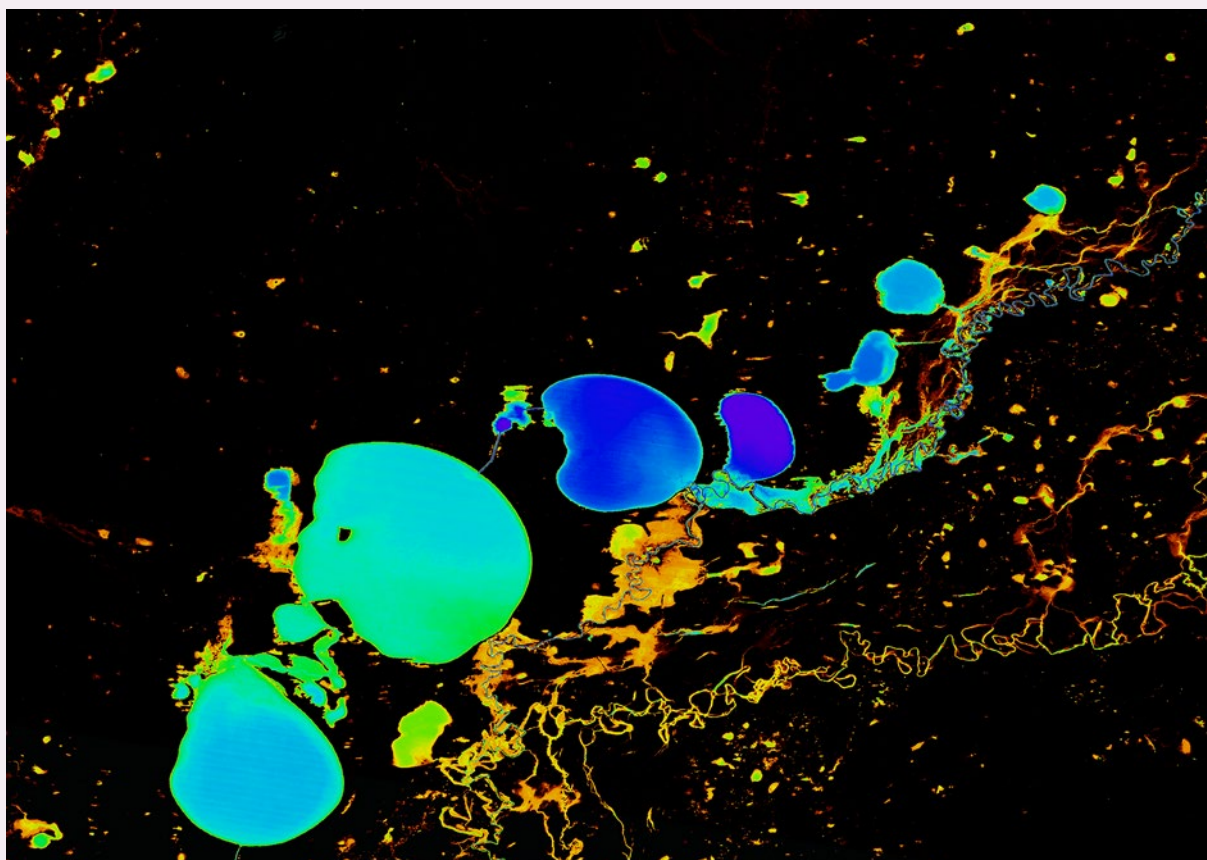
## WOfS service

Results from these analyses can be viewed on the WOfS viewer: <http://www.ga.gov.au/interactive-maps/#/theme/water/map/wofs>. This service enables users to view higher resolution maps for specified locations of interest within the Australian continent and Tasmania (see Figure 5.12). From 1987 to the present, for each 25 m × 25 m grid cell WOfS displays:

- number of clear satellite observations;
- number of times water was detected;
- percentage of clear observations with water; and
- probability that water observation is correct.

**Figure 5.11** Mapping permanent water

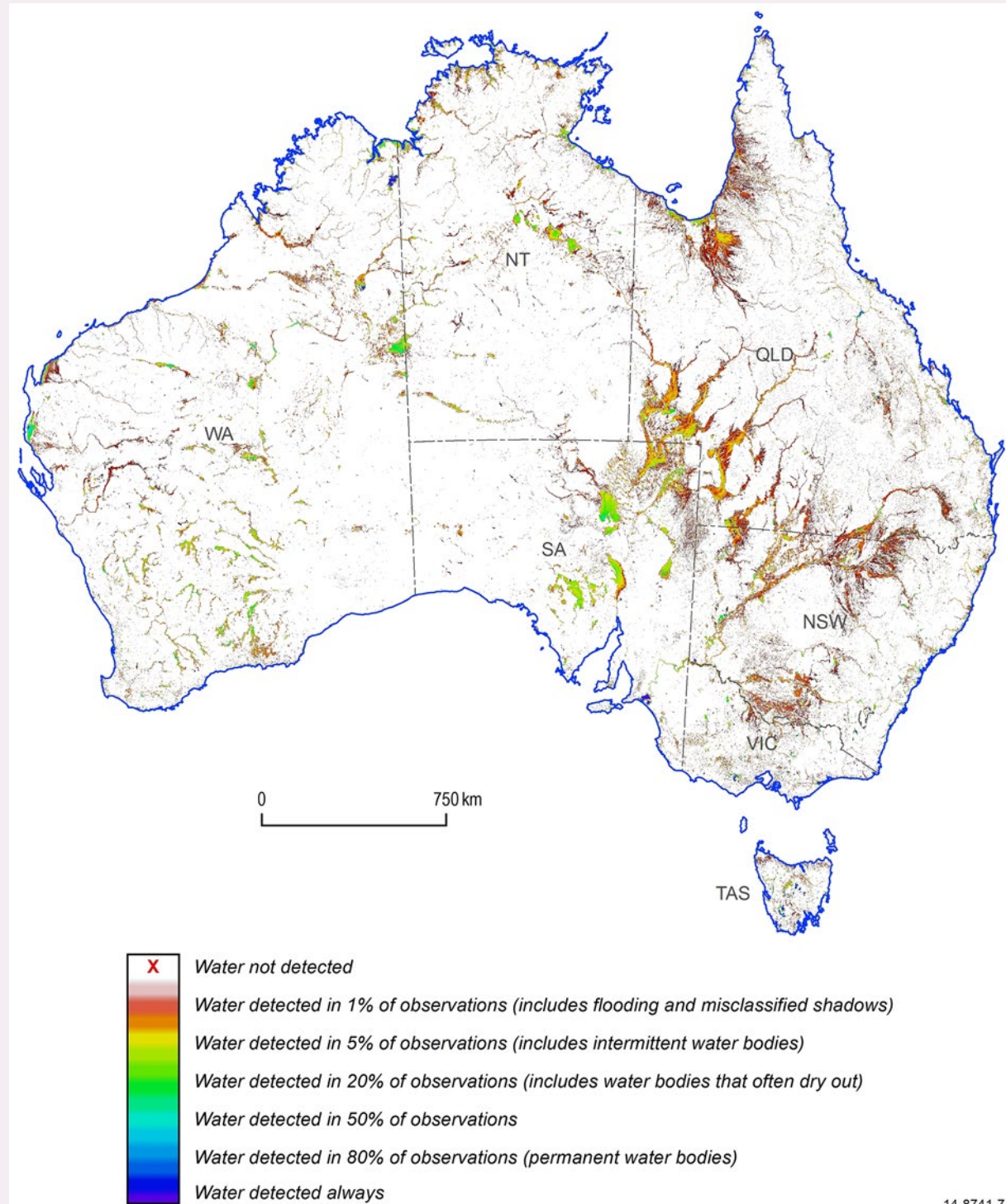
Landsat imagery of the Menindee lakes system, NSW, acquired between 1987 and 2016, was processed using WOfS to show where water was observed regularly (blue to purple) versus occasionally (orange to red).



Source: Norman Mueller, Geoscience Australia

**Figure 5.12** WofS continental map

This continental map, produced by WofS processing of Landsat imagery, highlights the permanence of water in the Australian landscape.



Source: Norman Mueller, Geoscience Australia



## 5.4 Atmospheric Interactions

The atmosphere extends away from the Earth's surface for over 100 km. The atmosphere is 'heaviest' or most dense close to Earth, with half its mass below 5.5 km in altitude, and only 1% above 30 km altitude. While largely comprising gases, the atmosphere also contains varying concentrations of aerosols and water. Table 5.2 summarises the relevant characteristics of atmospheric layering. Each layer is bounded by abrupt changes in temperature (see Figure 5.13). These boundaries are known as pauses and inhibit vertical mixing between atmospheric layers. Most of Earth's weather and water vapour occurs in the troposphere.

Atmospheric aerosols or particulate matter comprise solid and/or liquid particles with diameters in the range 0.002–100  $\mu\text{m}$  that are suspended in the air. They derive from both natural and anthropogenic sources. Natural sources include water vapour, sea spray, wind-blown dust, volcanic ash, and smoke from bushfires, while anthropogenic sources include biomass burning, various agricultural activities and industrial and domestic emissions.

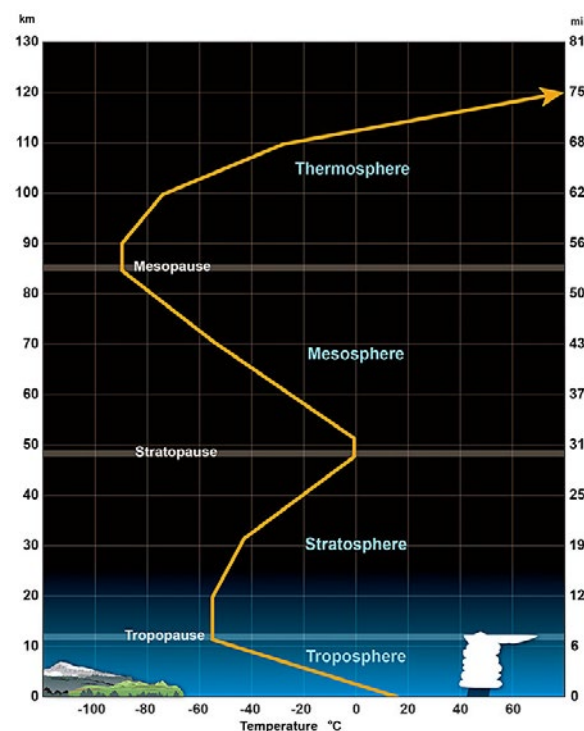
Clouds cover around 60% of the Earth's surface. As such, the presence of clouds and cloud shadows are very relevant to the interpretation of EO imagery. Thin cloud presents a particular challenge to the processing and interpretation of EO imagery since it allows the sensor to detect Earth surface radiance, but attenuates that radiance. Higher cloud cover tends to occur over oceans than over land. While some variation occurs with latitude, global averages for base heights and coverage of different types of cloud over land and ocean are summarised in Table 5.3. For detailed global information on clouds refer to Warren *et al.* (2013).

Certain regions of the EM spectrum are completely absorbed by the various gases that make up the atmosphere (particularly  $\text{O}_3$ ,  $\text{CO}_2$ ,  $\text{H}_2\text{O}$ ), so that wavelengths in these regions cannot be used for remote sensing of the Earth's surface. The regions of the EM spectrum where radiation is not affected by the Earth's atmosphere are called 'atmospheric windows' (see Figure 5.14). Remote sensing data of the Earth's surface can only be obtained from systems operating within these regions of the EM spectrum. These windows allow detection of reflected solar energy from the Earth's surface in the visible and infrared wavelengths, Earth's emitted energy in the thermal infrared and passive microwave wavelengths, plus microwaves emitted by active sensors (see Table 5.4). Middle infrared wavelengths can originate from both reflected solar radiation and emitted EMR from the Earth's surface (Chuvieco and Huete, 2010).

**Figure 5.13** Atmospheric layers

The atmospheric layers are distinguished by the way temperature changes with altitude:

- Troposphere: temperature decreases with increasing altitude;
- Stratosphere: temperature increases with increasing altitude;
- Mesosphere: temperature decreases with increasing altitude; and
- Thermosphere: temperature increases with increasing altitude.



Source: NOAA (2016). Retrieved from [http://www.srh.noaa.gov/jetstream/atmos/atmos\\_intro.html](http://www.srh.noaa.gov/jetstream/atmos/atmos_intro.html)

*I happen to have discovered a direct relation between magnetism and light,  
also electricity and light, and the field it opens is so large and I think rich.  
(Michael Faraday, 1845)*

**Table 5.2** Atmospheric layers

Layer	Max Altitude <sup>20</sup> (km)	Depth (km)	Mass (%)	Temperature (°C)	Composition	Description
Troposphere	20	~6 at poles 9 at mid-latitudes 18–20 at equator	~80	17 to -51 (air temperature decreases with height by 6.5°C per km to altitude of 11 km unless temperature inversion exists)	Water vapour mostly < 6km Nitrogen (78%) Oxygen (21%) Aerosols	80% of atmosphere's mass
Stratosphere	50	Lower boundary is higher near equator and lower over poles	19	-60 to -15 (air temperature increases with height above 20 km altitude)	Aerosols, ozone, chlorofluorocarbons (CFCs). Very little water vapour or air movement	Contains ozone layer
Mesosphere	85	35 (average)	0.1	0 to -90 (air temperature decreases with height)	Noctilucent clouds. Sodium layer (5–10 km depth between altitudes 80–105 km)	Most meteors burn up in this layer
Thermosphere	600	~500	-	-90 to 2,000+ (air temperature increases with height above 90 km altitude)	Extremely low densities of hydrogen and helium; Contains ionosphere where sparse gases absorb high energy incoming radiation	International Space Station orbits in this layer
Exosphere	10,000	-	-	-	Atoms and molecules escape into space; satellites orbit	Fades into space

Source: NOAA (2016) at [http://www.srh.noaa.gov/jetstream/atmos/atmos\\_intro.html](http://www.srh.noaa.gov/jetstream/atmos/atmos_intro.html)<sup>18</sup>

**Table 5.3** Global cloud properties

Average amount of cloud and average cloud base heights over land and ocean based on surface observations.

Data observations used for coverage estimates: land values—1971–2009; ocean values—1954–2008.

Data observations used for base heights estimates: land values—1971–1996; ocean values—1954–1997.

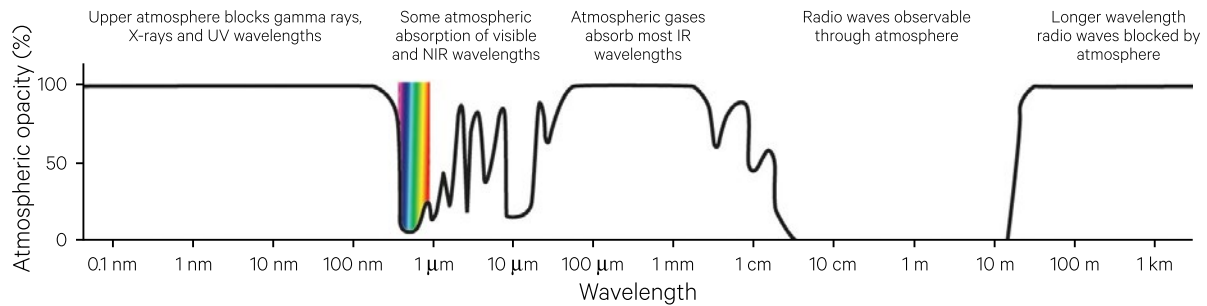
Category		Base Height (m above surface)		Average Coverage (%)	
Height Level	Type	Land	Oceans	Land	Oceans
Low	Stratus	500	400	5	13
	Stratocumulus	1000	600	12	22
	Nimbostratus	-	-	4	5
Mid	Altostratus	-	-	4	6
	Altostratus	-	-	17	18
High	Cirriform	-	-	22	12
Vertical Development	Cumulonimbus	1000	500	5	6
	Cumulus	1100	600	5	13
Total		-	-	54	68

Source: Eastman and Warren (2013)

<sup>18</sup> Varies with latitude and weather.

**Figure 5.14** Atmospheric opacity

Some wavelength regions of the EM spectrum are absorbed by atmospheric gases so cannot be used for remote sensing of the Earth's surface features. Note: Scale is logarithmic.



Adapted from: Wikimedia Commons at [https://commons.wikimedia.org/wiki/File:Atmospheric\\_electromagnetic\\_opacity.svg](https://commons.wikimedia.org/wiki/File:Atmospheric_electromagnetic_opacity.svg) (original source: NASA)

**Table 5.4** EMR spectral regions and atmospheric windows

Energy Source	Spectral Region		Wavelengths of spectral region	Wavelengths of atmospheric window
Reflected solar radiation (plus radiation from active optical sensors, such as lidar)	Optical	Visible	0.38–0.7 $\mu\text{m}$	0.38–0.7 $\mu\text{m}$
		Near infrared	0.7–1.1 $\mu\text{m}$	0.77–0.91 $\mu\text{m}$
		Short wave infrared	1.1–3.0 $\mu\text{m}$	1.55–1.75 $\mu\text{m}$ 2.05–2.40 $\mu\text{m}$
Both reflected solar radiation and emitted by Earth's surface	Middle infrared		3.0–8.0 $\mu\text{m}$	3.0–5.0 $\mu\text{m}$
Emitted by Earth's surface	Thermal infrared		> 8.0–15 $\mu\text{m}$	8.0–9.2 $\mu\text{m}$
				10.2–12.4 $\mu\text{m}$
Emitted by Earth's surface or radar sensor	Microwave		>1 mm–1 m	7.5–11.5 mm
				> 20 mm

Within these atmospheric windows, atmospheric conditions such as haze, fog and clouds can still affect remote sensing of features on the Earth's surface through scattering of the EM waves by particles in the atmosphere. These interactions can be described in terms of three types of scattering:

- Rayleigh scattering—by gas molecules that are much smaller than the radiation wavelength;
- Mie scattering—by smoke, dust, salt and water particles which are similar size to the radiation wavelength; and
- non-selective scattering—by water droplets, ice fragments or large dust particles that are much larger than the radiation wavelength.

These various forms of scattering increase the haze level or reduce the contrast in an image and are further considered in Volume 1B—Section 4.2. Image processing methods can be applied to data obtained under such conditions to remove or reduce the effect of atmospheric 'noise' as discussed in Volume 1B—Section 5 and Volume 2A. Consideration of various sources of atmospheric 'effects' is particularly important when comparing multiple image sources. Remote sensing studies of the atmosphere itself, however, use absorption and scattering characteristics to measure atmospheric state and composition. In such studies the absorption bands, rather than atmospheric windows, are preferred and scattering effects are indicative of atmospheric condition. These are further discussed in Volume 3.

## 5.5 Further Information

### Introduction to Electromagnetic Radiation:

EO Miners: [http://www.eo-miners.eu/earth\\_observation/eo\\_eof\\_rst\\_electrmag\\_remote\\_sensing.htm](http://www.eo-miners.eu/earth_observation/eo_eof_rst_electrmag_remote_sensing.htm)

Natural Resources Canada: <http://www.nrcan.gc.ca/earth-sciences/geomatics/satellite-imagery-air-photos/satellite-imagery-products/educational-resources/14621>

### The Atmosphere:

NOAA (2016)

### Solar radiation characteristics and programs for calculating spectral irradiance:

National Renewable Energy Laboratory (NREL): [http://www.nrel.gov/rredc/solar\\_resource.html](http://www.nrel.gov/rredc/solar_resource.html)

## 5.6 References

- Budikova, D. (2013). Albedo. The Encyclopedia of Earth. Retrieved from <http://www.eoearth.org/view/article/149954>.
- Chuvieco, E., and Huete, A. (2010). Fundamentals of Satellite Remote Sensing. CRC Press, Boca Raton.
- Dobos, E. (2003). Albedo. 'Encyclopedia of Soil Science' (Ed: R. Lal), Vol. 1. Second Edn., pp. 64-66. Taylor & Francis Group, New York.
- Eastman, R., and Warren, S. G. (2013). A 39-Yr Survey of Cloud Changes from Land Stations Worldwide 1971–2009: Long-Term Trends, Relation to Aerosols, and Expansion of the Tropical Belt. *Journal of Climate*, 26(4), pp. 1286-1303. doi:<http://dx.doi.org/doi:10.1175/JCLI-D-12-00280.1>.
- Harrison, B. A., and Jupp, D. L. B. (1989). Introduction to Remotely Sensed Data. Part ONE of the microBRIAN Resource Manual (156 pages). CSIRO Australia, Melbourne.
- NOAA (2016). National Weather Service Atmosphere Topics. Retrieved from [http://www.srh.noaa.gov/jetstream/atmos/atmos\\_intro.html](http://www.srh.noaa.gov/jetstream/atmos/atmos_intro.html).
- Shaw, G. A., and Burke, H. K. (2003). Spectral Imaging for Remote Sensing. *Lincoln Laboratory Journal*, 14(1), pp. 3-27.
- Warren, S. G., Hahn, C. J., and Eastman, R. (2013). Climatic Atlas of Clouds Over Lands and Oceans. Retrieved from <http://www.atmos.washington.edu/CloudMap/>





# 6 Radioactivity

Radiometrics, also known as Gamma-Ray Spectrometry, measures the natural radioactivity from the Earth's surface to infer the presence of particular minerals. Radiometric surveys detect gamma-rays resulting from the natural radioactive decay of three elements (Potassium (K), Thorium (Th) and Uranium (U)) located in the upper 30–45 cm of the Earth's crust, or associated with artificial sources such as nuclear power plants. This is the most energetic form of EM energy, with very high frequencies (above  $10^{19}$  Hz) and very short wavelengths (less than  $10^{-12}$  m—equivalent to the nucleus of an atom).

For Earth Observation (EO) applications, radioactivity is typically measured using gamma-ray spectrometers carried by aircraft. The resultant images can be

subsequently processed to indicate the relative proportions of U, Th and K in each pixel.

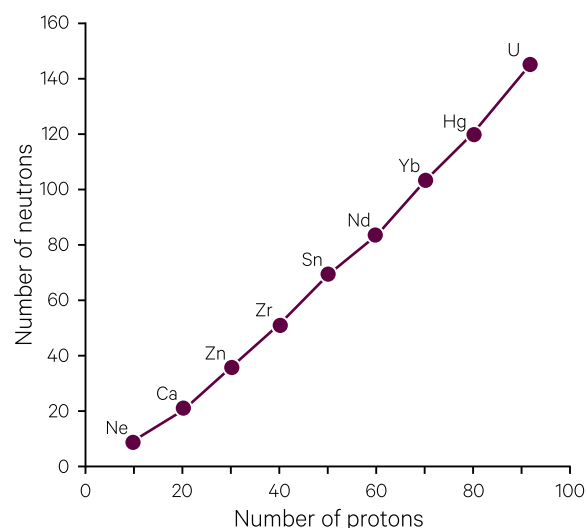
## 6.1 Introducing Radioactivity

Each element has a unique atomic number that indicates the number of protons contained in its nucleus. For the nucleus of an atom to be stable, the positive charge of protons needs to be balanced by an equal or greater number of neutrons. Elements with larger atomic numbers (that is, larger numbers of protons) appear to require a greater number of neutrons. Nuclei with more than 82 protons are not stable and tend to decay to regain stability (see Figure 6.1).

*Radioactivity is shown to be accompanied by chemical changes in which new types of matter are being continually produced... The conclusion is drawn that these chemical changes must be sub-atomic in character.*  
(Ernest Rutherford)

**Figure 6.1** Stable nuclei

Those elements that are not on the stability line are unstable and tend to decay.



Adapted from: Andy Darvill at <http://www.darvill.clara.net/nucrad/moretypes.htm>

**Background image:** Airborne radiometric image of the Gulf of Carpentaria in northwest Queensland. The area shown is 450 km wide. Potassium is displayed as red, equivalent thorium as green and uranium as blue (derived from Ternary Radiometric image of Australia, Version 3, 2015; see Excursus 6.1 for details).

**Source:** Geoscience Australia

A nuclide is a species of atom with a specific number of protons, neutrons and energy state in its nucleus. An element can have multiple nuclides (that is, the same number of protons but different numbers of neutrons), which are called isotopes of that element. Nuclides and isotopes are referenced as:

Ename-A

or



where

Ename is the element name;

A is the number of protons plus neutrons (or the atomic mass) of the atom;

Z is the number of protons (or the atomic number) of the atom; and

X is the element symbol (determined by the atomic number).

Since the atomic number is implied by the element name, the subscript can be, and often is, omitted. For example, the most commonly occurring form of elemental carbon has six protons and six neutrons, thus an atomic number of 12. This isotope is referenced as  ${}^{12}_6\text{C}$  or  ${}^{12}\text{C}$ . Radioactive carbon has an extra proton, so is referenced as  ${}^{13}_6\text{C}$  or  ${}^{13}\text{C}$ .

Unstable isotopes, called radioisotopes, emit ionising radiation to stabilise their nuclei. This process seeks to rebalance the ratio of protons to neutrons and often involves decreasing the number of protons in the nucleus, in which case the resulting atom becomes a different element. The process is called radioactive decay and frequently comprises a chain of decays that results in multiple intermediate (or daughter) nuclides of many elements (USEPA, 2012). These intermediate nuclides can exist for microseconds or millennia, and can be used to identify the parent isotopes.

Radioactive decay is spontaneous such that it is not possible to predict if or when an individual atom will decay. Over time, however, the frequency of decay has been observed to follow the Poisson distribution. Each radioisotope is characterised by its decay rate, such that:

$$N = N_0 e^{-\lambda t}$$

where

$N_0$  is the number of radionuclides at time  $t=0$ ;

$N$  is the number of radionuclides after time  $t$ ; and

$\lambda$  is the decay constant for the radioisotope.

The half-life of a radioisotope indicates the time required for half the nuclei to decay:

$$T_{1/2} = \frac{0.693}{\lambda}$$

The most common methods of radioactive decay produce:

- positively charged alpha particles—ejected from an unstable nucleus to reduce the number of protons; since the number of protons changes, the decaying atom becomes a new element;
- negatively charged beta particles—created when an excess neutron changes into a proton and an electron, and the new electron is expelled from the nucleus; this process also changes the original atom into a new element; or
- uncharged gamma rays—mass-less energy that is emitted by a new nucleus with an energy surplus, often following emission of an alpha or beta particle.

Alpha particles comprise two protons and two neutrons, so have mass and a discrete energy that can be used to identify the emitting isotope. They have low penetration range and are generally stopped by a few centimetres of air, whereas beta particles can travel several metres in air but are stopped by solid materials. Gamma rays are EM waves with high energy and can travel kilometres through air, 50 cm through rock and a few centimetres through lead (Minty, 1997; IAEA, 2003).

## 6.2 Gamma Rays

The only form of radioactivity that can be sensed remotely for EO is gamma radiation. In the Earth's crust, gamma rays result from naturally occurring radioisotopes and their intermediate decay products. They can also originate from isotopes created by the interaction of cosmic rays with our atmosphere and are occasionally generated during thunderstorms. Artificial sources of gamma rays include radioactive isotopes resulting from nuclear fission in nuclear reactors.

During radioactive decay, the radioisotopes of only three elements in the Earth's crust emit gamma radiation that can be detected remotely, namely Potassium (K), Uranium (U), and Thorium (Th). Detection of gamma rays depends on the relative abundance of the isotopes, which, in turn, is related to their half-life. While other elements have naturally occurring radioisotopes that emit gamma radiation, their levels of radiation are too low to be measured using airborne remote sensors (Minty, 1997).

**Table 6.1** Isotope properties

Element			Naturally Occurring Isotopes			
Name	Symbol	Crustal Abundance (ppm) <sup>21</sup>	Symbol	% of Element	Half-life (years)	Gamma ray Emission
Potassium	K	$2.09 \times 10^4$	$^{40}\text{K}$	0.012	$1.3 \times 10^9$	Yes
Uranium	U	2.7	$^{238}\text{U}$	99.28	$4.46 \times 10^9$	Only from radioactive daughter products
			$^{235}\text{U}$	0.72	$7.13 \times 10^8$	Energy too low for remote sensing
Thorium	Th	9.6	$^{232}\text{Th}$	100	$1.39 \times 10^{10}$	Only from radioactive daughter products

Adapted from: IAEA (2003)<sup>19</sup>

The occurrence of K, U and Th isotopes is summarised in Table 6.1.  $^{40}\text{K}$  occurs as a constant proportion of K so can be used to estimate the abundance of this element. The  $^{235}\text{U}$  isotope occurs infrequently and emits low levels of gamma radiation so is not detected by remote sensing. The total amount of U and Th can only be inferred from the gamma radiation emitted by daughter products in their radioactive decay chains, as neither  $^{238}\text{U}$  nor  $^{232}\text{Th}$  emit gamma rays.

Since each intermediate nuclide in a radioactive decay chain decays at its own rate, it is possible that the 'residence' time, and hence relative abundance, of each intermediate nuclide can vary and create a situation of 'disequilibrium'. When an element's abundance is being estimated from the concentration of intermediate nuclides it is essential that the radioactive decay chain is in a state of equilibrium. This situation is most relevant to estimates of U which are derived from the detected concentrations of its distant descendants after several 'generations' of radioactive decay and whose decay chain is often in disequilibrium. In this case, the estimate of Uranium is generally reported as 'equivalent Uranium' (eU) and can be erroneous. Similarly, estimates of Thorium are referenced as 'equivalent Thorium' (eTh), although its decay chain is usually in equilibrium.

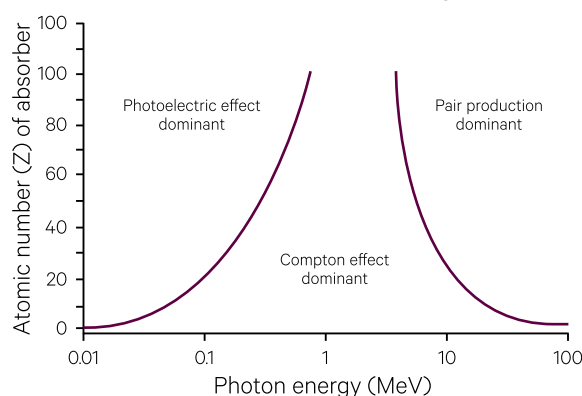
The impact of gamma rays on a material depends on its thickness, density and absorption cross-section. The energy of gamma rays determines how they ionise atoms (see Figure 6.2):

- at low energy levels, a gamma photon transfers its energy to an electron bound to an atom, resulting in emission of the electron and heating. This mechanism is called the photoelectric effect;
- at medium energy levels, a gamma photon transfers some of its energy to a bound electron as occurs in the photoelectric effect, with its remaining energy being scattered as a lower energy gamma photon. This process is referred to as Compton scattering;
- and
- at high energy levels, a gamma photon is absorbed by the nucleus of an atom, which quickly decays and emits as two medium energy gamma photons. This sequence is called Pair Production.

The energy of a gamma photon is characteristic of its source isotope and can be used to identify that source. Gamma radiation is usually characterised by its energy level, expressed in eV (electron volts), rather than by wavelength. Sensors which record total energy counts and/or spectra for terrestrial gamma radiation are discussed in Volume 3. Gamma spectroradiometry images are typically displayed as a colour composite using red for potassium, green for thorium and blue for uranium as illustrated in Figure 6.3 and Excursus 6.1.

**Figure 6.2** Gamma ray ionisation

A photon at gamma ray energies interacts with matter in terms three principal mechanisms: the photoelectric effect, the Compton effect or via pair production. This graph shows the relative importance of these three interactions for different photon energy levels and attenuating materials (represented in terms of atomic number). Note: X-axis scale is logarithmic.



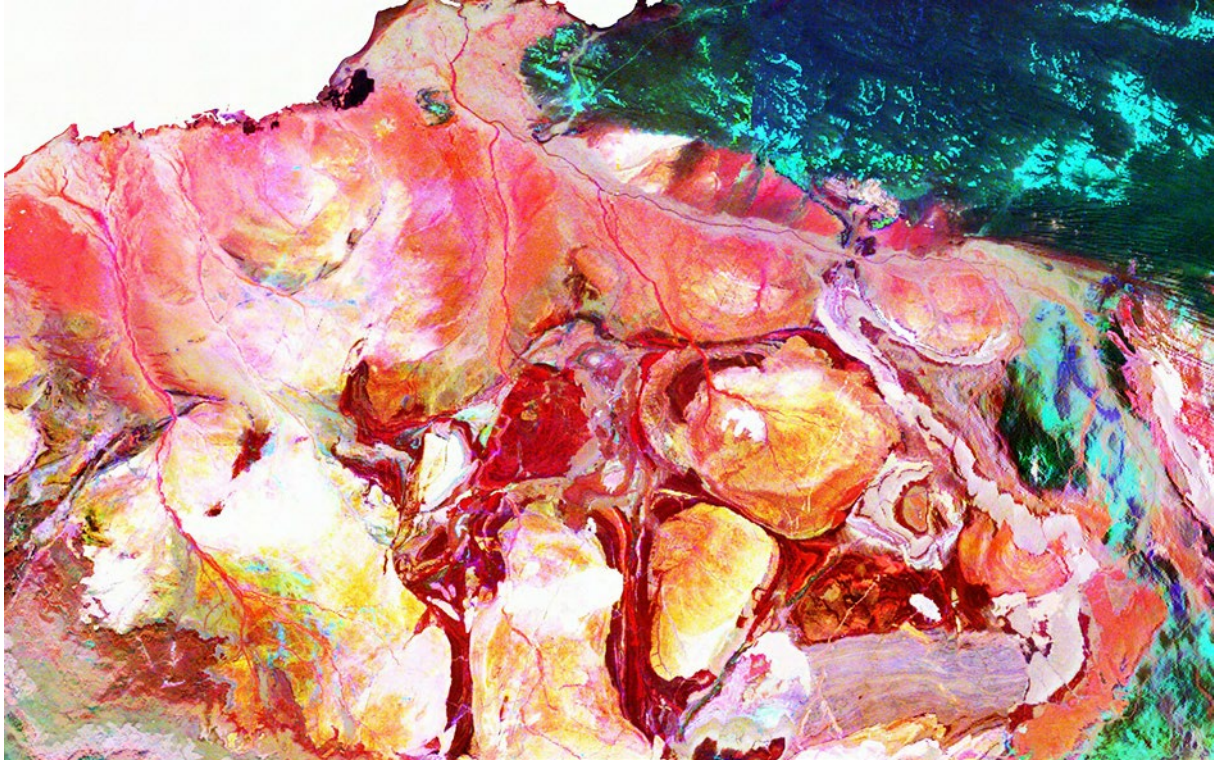
19. Lide (2008) cited in [http://www.knowledgedoor.com/2/elements\\_handbook/element\\_abundances\\_in\\_the\\_earth\\_s\\_crust.html](http://www.knowledgedoor.com/2/elements_handbook/element_abundances_in_the_earth_s_crust.html)



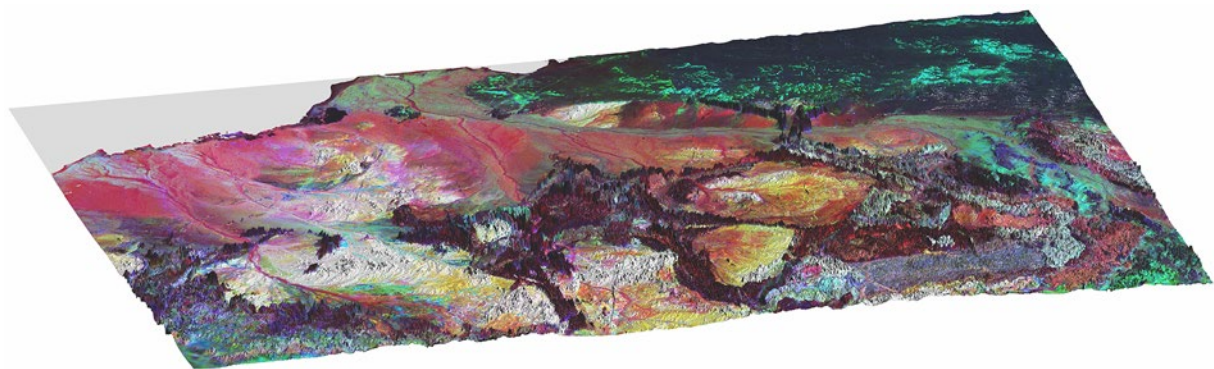
### Figure 6.3 Gamma spectroradiometry

The Archaean Pilbara Craton of northwestern Western Australia consists of granitoid-greenstone terrain (3.6-2.8 Ga). Rocks include granite (white and red hues), basalts and ultra-mafics lithologies (black hues). Overlying sediments associated with the Canning Basin consist of aeolian sands, sandstone and conglomerate (east of image in black and green hues). Extensive alluvial and colluvial plains in reddish hues occur between the granitoid-greenstone terrain and the coast. This relatively well exposed province is an excellent example of how airborne gamma-ray spectrometry can be used to map bedrock types (including zonation within the granites) and structures. The image extends 210 km N-S (North to the top of the page) and 340 km E-W (East to the right of the page).

a. Two-dimensional image



b. Three-dimensional overlay of image on regional topography



Source: Geoscience Australia

---

*Thus the radio elements formed strange and cruel families in which each member was created by spontaneous transformation of the mother substance: radium was a 'descendant' of uranium, polonium a descendant of radium.*  
(Eve Curie)

---



## Excursus 6.1— Australian Radiometric Map

**Source:** Murray Richardson, Geoscience Australia

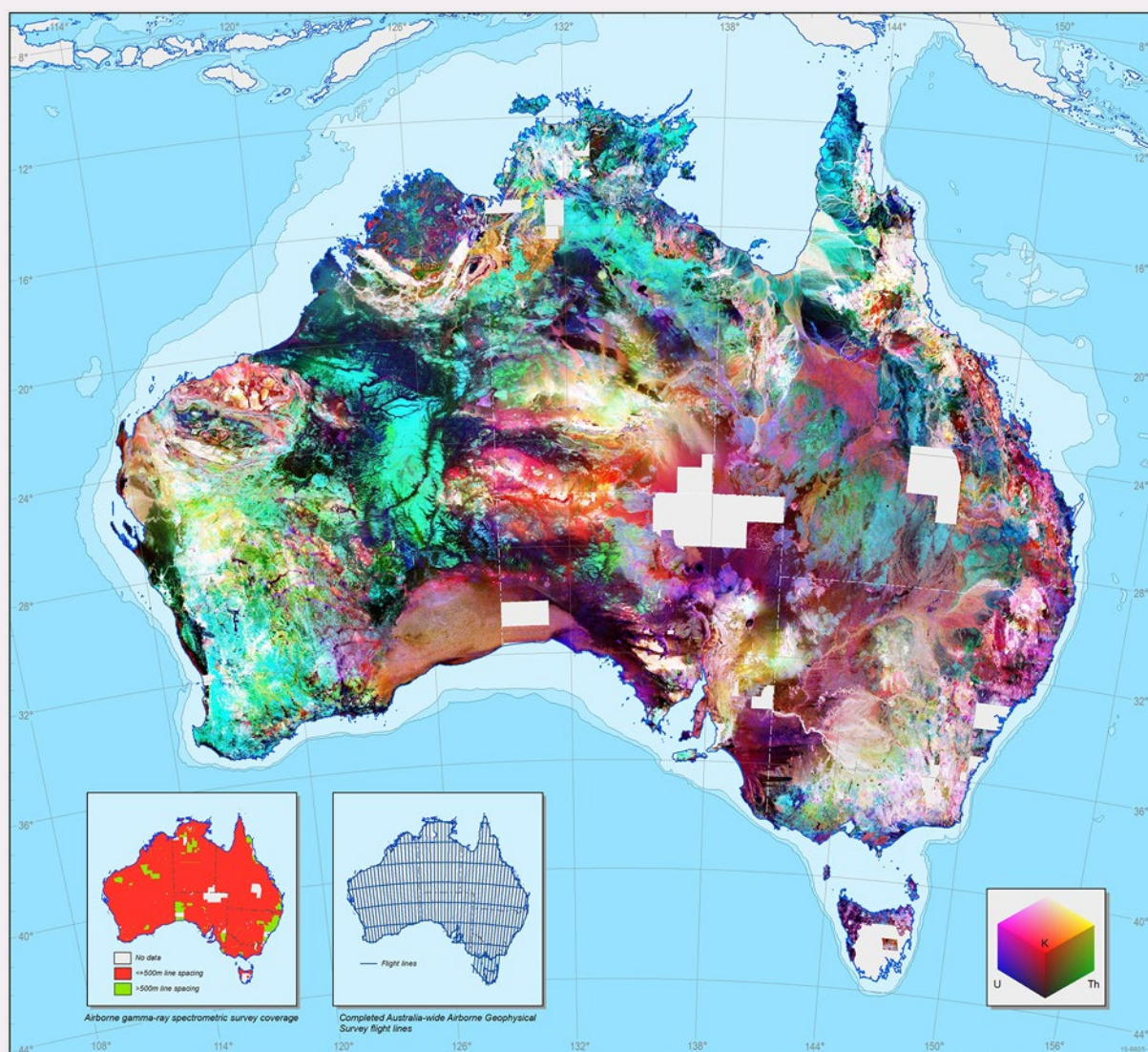
**Further Information:** Minty *et al.* (2008); Geoscience Australia (2016)

Geoscience Australia and the State and Northern Territory geological surveys have systematically surveyed the Australian continent for over 50 years using airborne radiometric surveys to map potassium, uranium and thorium elemental concentrations at the Earth's surface. Since the data had been collected and processed using a range of specifications,

technologies and procedures over this period, the radiometric data in the national database were not all registered to the same datum. This made it difficult to combine surveys into regional compilations or to make accurate comparisons between radiometric responses over different parts of the continent, which limited the value of the database.

**Figure 6.4** Radiometric map of Australia

Ternary image of Australia from the updated National Radioelement database showing equivalent uranium as blue, equivalent thorium as green and potassium as red.



Source: Geoscience Australia

In 2007 Geoscience Australia conducted an Australia-wide airborne geophysical survey (AWAGS) that covered the entire continent with north-south flight lines spaced 75 kilometres apart, and east-west tie lines spaced 400 kilometres apart (Johnson, 2006). Gamma-ray spectrometric data, acquired at an 80 m height along the flight lines during AWAGS, were processed according to international specifications, and the final estimates of the concentrations of the radioelements (potassium, uranium and thorium) comprise the new Australian radioelement datum. The national radiometric database was levelled by minimising both the differences in radioelement estimates between surveys (where these surveys overlap) and the differences between the surveys and the AWAGS traverses (where these overlap). This effectively levels the surveys to the new national datum.

A ternary image derived from the levelled national radioelement database is shown in Figure 6.4. This updated database, on a 100 m grid, will directly assist:

- uranium and thorium exploration through the ability to make quantitative comparisons between the radiometric signatures in different survey areas;
- heat flow studies and assessment of geothermal energy resources;
- geological mapping, mineral and petroleum exploration;
- geomorphological studies and environmental mapping; and
- derivation of a radiation risk map of Australia.

The improved datasets will lead to an increased understanding of the geology, structure, geochemistry and geomorphology of the continent. For example, palaeozoic granites in eastern Australia can now be quantitatively compared and assessed for areas of potential mineralisation and geothermal prospectively. These datasets are freely available from the Australian Geoscience Information Network (AUSGIN: <http://www.geoscience.gov.au>) and by accessing the Geophysical Archive Data Delivery System (GADDS).

### 6.3 Further Information

Radiometrics: <http://www.ga.gov.au/scientific-topics/disciplines/geophysics/radiometrics>

Gamma spectroscopy: Minty (1997)  
IAEA (2003)

Gamma ray interactions: <http://www.hep.wisc.edu/~prepost/407/gamma/gamma.html.html>

Radiometric Map of Australia: <http://www.ga.gov.au/ausgeonews/ausgeonews200812/radiometrics.jsp>

### 6.4 References

Geoscience Australia (2016). Geoscience Australia. Retrieved from <http://www.ga.gov.au>.

IAEA (2003). Guidelines for radioelement mapping using gamma ray spectrometry data (IAEA-TECDOC-1363). International Atomic Energy Agency, Vienna. Retrieved from [http://www-pub.iaea.org/mtcd/publications/pdf/te\\_1363\\_web.pdf](http://www-pub.iaea.org/mtcd/publications/pdf/te_1363_web.pdf).

Johnson, J. (2006). Onshore Energy Security Program underway. AusGeo News, 84. Geoscience Australia, Canberra, Australia. Retrieved from <http://www.ga.gov.au/ausgeonews/ausgeonews200612/onshore.jsp>.

Lide, D. R. (2008). CRC Handbook of Chemistry and Physics, 88th Edn. Taylor & Francis Group, Boca Raton, Florida.

Minty, B. R. S. (1997). Fundamentals of airborne gamma-ray spectrometry. AGSO Journal of Australian Geology and Geophysics, 17(2), pp. 39-50.

Minty, B. R. S., Richardson, M., and Wilford, J. (2008). New Radiometric Map of Australia. AusGeo News, 92. Geoscience Australia, Canberra, Australia. Retrieved from <http://www.ga.gov.au/ausgeonews/ausgeonews200812/radiometrics.jsp>.

USEPA (2012). United States Environmental Protection Agency. Retrieved from <http://www.epa.gov/radiation/understand/index.html>.



# 7 Magnetism

Magnetism is a physical phenomenon that allows materials to attract or repel other materials. Certain materials called ferromagnets produce a persistent magnetic field (rather than a temporary magnetic field in response to contact with one). At an atomic level, this is due to the 'spin' of both the electrons around the nucleus and the elementary particles within the nucleus (see Section 2.2).

Magnetometers are instruments that remotely sense the magnitude and/or direction of a magnetic field. For Earth Observation (EO) studies, magnetometers can be ground-based or carried aboard aircraft or

ships. The resulting measurements can be converted into maps showing the distribution and abundance of magnetic minerals, which are used for geological and mining applications.

## 7.1 Introducing Magnetism

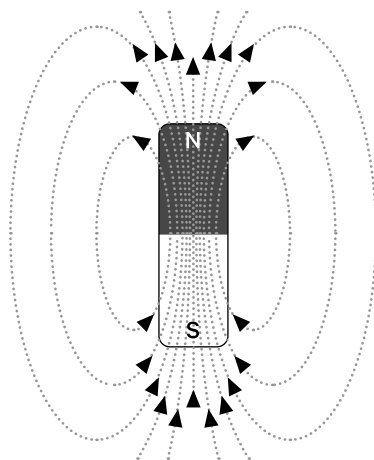
As introduced in Section 2.4, magnetism is fundamentally a force between two electric currents, such that two currents in the same direction attract each other and two currents in opposite directions

repel each other. This principle applies whether the currents are parallel, as in bar magnets, or circular, as in an electromagnet. The region influenced by a magnet is called its magnetic field (see Figure 7.1).

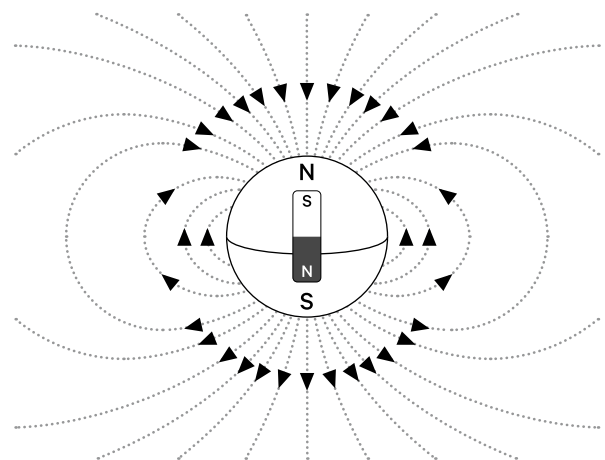
**Figure 7.1** Magnetic fields

By convention, magnetic field lines are drawn in the direction of attraction from the north pole to the south pole. The magnetic field is strongest inside the magnetic material, with the strongest external magnetic fields occurring near the poles. A magnetic compass is attracted to the south pole of a bar magnet, or the North Pole of our planet.

a. Magnetic field of a bar magnet is usually drawn with the north pole at the top, and parallel magnetic field lines moving up, around and down the magnet to the south pole.



b. Earth's magnetic field resembles an electromagnet, with the equivalent of the south pole of the magnet near the North pole of the planet. Since a magnetic compass is attracted to the south pole of a bar magnet, the magnetic field lines on Earth point north.



**Background image:** Airborne total magnetic intensity image of the Gulf of Carpentaria, northwest, Queensland. The area shown is 450 km wide. This pseudo-colour image displays Total Magnetic Intensity as a spectrum from high values as red to low values as blue (derived from Magnetic Map of Australia, Version 6, 2015, with variable reduction to the pole; see Excursus 7.2 for details). **Source:** Geoscience Australia



While the ‘spin’ of any electron can produce a magnetic field, in the atoms of most materials this energy is countered by the opposite movement of other electrons, resulting in no net magnetic moment. In ferromagnetic materials, the magnetic moments of most atoms in the material are aligned. The magnetic state, or ‘phase’ of a material varies with temperature,

pressure and external magnetic fields. Ferromagnetic materials such as nickel, iron, cobalt, gadolinium and their alloys display magnetic properties up to a particular temperature. The temperature at which a material loses its permanent magnetism is called its Curie temperature.

## 7.2 Magnetic Field

A magnetic field is commonly characterised by seven parameters, or magnetic elements, as summarised in

Table 7.1. The relationship between these elements is illustrated in Figure 7.2.

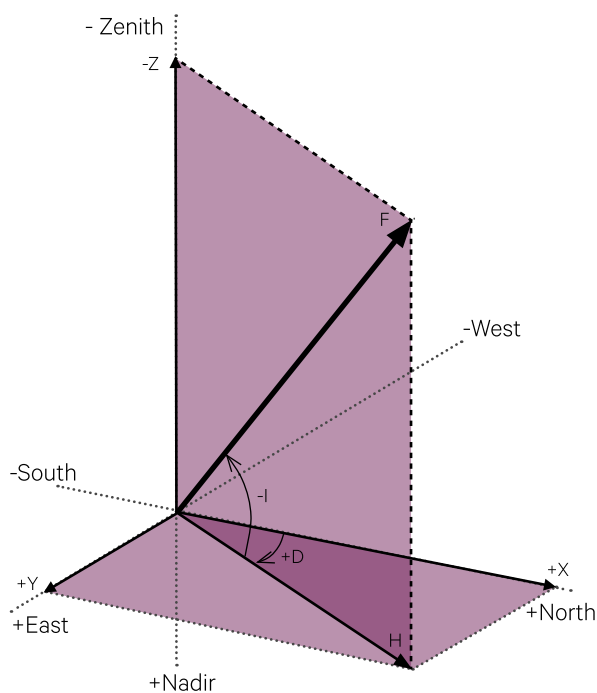
**Table 7.1** Magnetic components

Element	Abbreviation	Unit	Description
Declination (or variation)	D	degrees	Difference between true and magnetic north
Inclination (or dip)	I	degrees	Angle of magnetic field above or below horizon (90° at magnetic pole) <sup>20</sup>
Total Intensity	F	Gauss or nanotesla (nT)	Strength of magnetic field varies between 25,000 and 65,000 nT
Horizontal Component	H	Gauss or nanotesla (nT)	Horizontal component of total intensity (direction of horizontal component is magnetic north)
North Component	X	Gauss or nanotesla (nT)	Component of total intensity in northerly direction
East Component	Y	Gauss or nanotesla (nT)	Component of total intensity in easterly direction
Vertical Component	Z	Gauss or nanotesla (nT)	Vertical component of total Intensity

Source: Geoscience Australia (2016) <sup>20</sup>

**Figure 7.2** Magnetic vector components

In the Southern Hemisphere, Z is upwards and negative. Declination (D) is positive in most of continental Australia, except in southwest WA where it is negative.



Source: Geoscience Australia

*Magnetism, you recall from Physics class, is a powerful force that causes certain items to be attracted to refrigerators.*  
(Dave Barry)

20. The magnetic field is vertical at the poles and horizontal at the equator.

### 7.3 The Earth's Magnetic Field

The Earth essentially acts like a giant magnet surrounded by a magnetic field. Being a vector quantity, the Earth's magnetic field, which is also known as the geomagnetic field (see Figure 7.1b), has both magnitude and direction. Both the direction and intensity of Earth's magnetic field vary with time and location on the Earth, so the direction of magnetic north also varies. The Magnetic North Pole is currently offset by  $11^\circ$  from Earth's axis of rotation, which means that magnetic north differs from geographic (or true) north.

The configuration of the Earth's magnetic field resembles the field that would be produced if a bar magnet were buried deep within the Earth. It appears that the Earth's magnetic field is produced by the 'dynamo effect' resulting from movement of fluids within its outer core. The solid inner core can be likened to a hot iron ball (at around  $6000^\circ\text{C}$ ) that spins inside the molten outer core. The inner core spins at a different rate to the rotation of Earth. These movements cause circulation of fluids in the outer core resulting in electric currents, which in turn create a magnetic field (Stern, 2004). The geomagnetic field is also affected by processes in the upper atmosphere and in the Earth-Sun space environment.

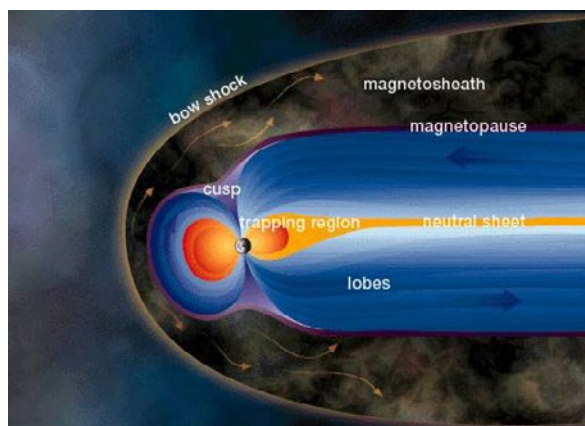
The extent of the geomagnetic field is called its magnetosphere. While the geomagnetic field is depicted with symmetrical force lines in Figure 7.1b, the actual shape is distorted by the influence of the supersonic solar wind, a stream of ionised particles released by the Sun. The speed of the solar wind effectively compresses the geomagnetic field on the Sun side of Earth, creating the magnetopause, and induces a long tail in the magnetosphere on the opposite side of Earth, which extends over 150,000 km (see Figure 7.3).

Like the Sun, the solar wind is not constant and abrupt release of plasma streams can create magnetic storms, or significant variations in the geomagnetic field, which can last for hours or days (Love, 2008; Love and Finn, 2011). Magnetic storms can result in major changes in currents, plasmas and fields in the magnetosphere, which have been known to impact satellite orbits and communication systems, disrupt radio broadcasts and power grids on Earth, and cause inaccuracies in compass readings (NOAA, 2016).

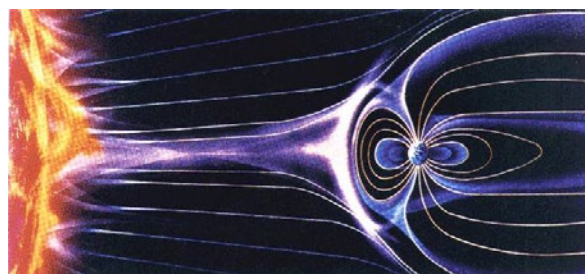
Within the magnetosphere, zones of trapped radiation were detected by the Explorer-1 satellite. These zones are called the Van Allen Belts and appear to protect the Earth from the solar wind and cosmic rays. These belts are weaker nearer the poles, which allows more particles from space to interact with the upper atmosphere and create the spectacular phenomena of aurora (see Figure 7.4).

**Figure 7.3** Magnetosphere

a. Components of magnetosphere



b. Solar wind colliding with Earth's magnetosphere



Source: NASA. Retrieved from <http://ccmc.gsfc.nasa.gov/educational/MagnetosphereWebPage.php>

**Figure 7.4** Southern Aurora

Photo taken by magnetic observer at Casey Station in 2010



Source: Tim Bolton, Geoscience Australia

The numerous satellites that have been launched to observe the magnetosphere have enabled mapping and modelling of the global distribution of Earth's magnetic field over time. These measurements have been supported by those made with magnetometers at approximately 200 magnetic observatories around the world. As part of this global network, in Australia GA maintains a national network of geomagnetic observatories which measure four components of the geomagnetic field (true north (X), true east (Y), vertical (Z) and the total intensity (F) every second (Hopgood (2007); see Figure 7.5). These real-time measurements (available online) show how the Earth's magnetic field continuously changes in the Australian region (see Figures 7.6 and 7.7). A range of indices have been developed to summarise the variability of Earth's magnetic field (Geoscience Australia, 2016), coordinated by the International Services of Geomagnetic Indices (ISGI).

**Figure 7.5** Geomagnetic observation network for Australia

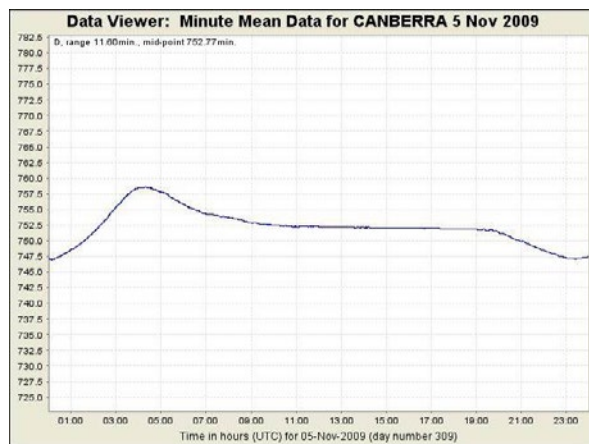


Source: Geoscience Australia

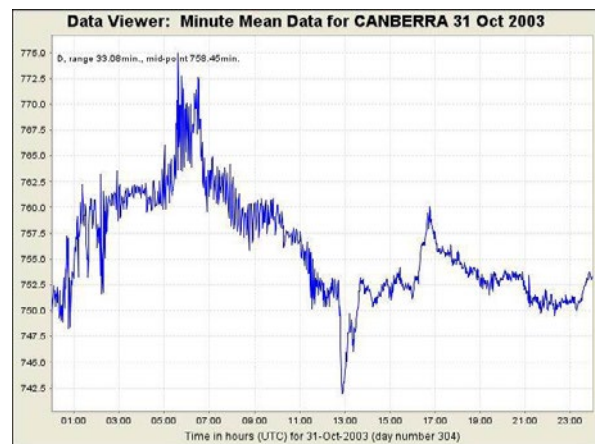
**Figure 7.6** Magnetic time series

Two images of magnetic time series from the Canberra magnetic observatory show 24 hours of declination data (x-axis: time; y-axis: magnetic declination in minutes-of-arc).

a. 5 November 2009 – a quiet day in terms of magnetic variation



b. 31 October 2003 — a day with magnetic disturbance



Source: Geoscience Australia

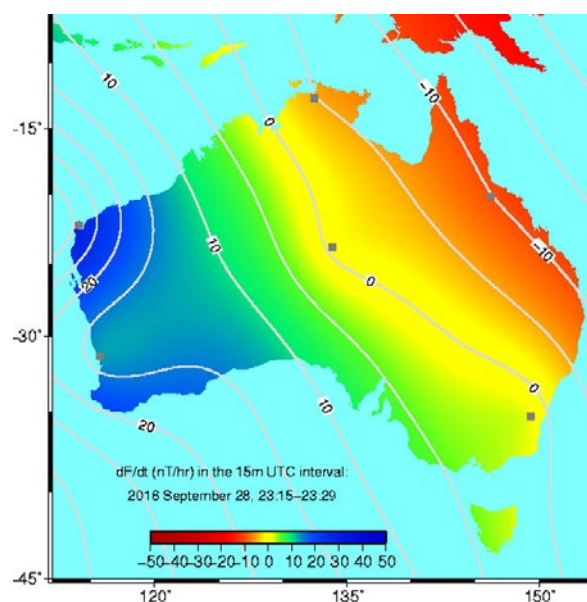
Models of the direction and intensity of Earth's magnetic field have been developed to understand how the field is changing, and these models can be used to predict future changes (see Excursus 7.1). The standard mathematical models, the International Geomagnetic Reference Field (IGRF) and the World Magnetic Model (WMM), are updated every five years and, given the variable nature of the geomagnetic field, are only valid for a five-year period. Relevant calculators, data and software are available from NOAA (2013).

The geomagnetic field is relevant to a range of applications, including navigation, mineral and resource exploration, space weather analysis, and geomagnetic hazard mitigation. A range of related products and services are provided by Geoscience Australia (2016), such as:

- compass-based navigation,
- finding magnetic direction;
- mitigating the potential hazards generated by magnetic storms; and
- calibration of compasses and magnetometers

**Figure 7.7** Total intensity variability over Australia

Data recorded within a 15 minute time interval from six magnetic observatories in continental Australia are used to generate a contour display showing the rate of change in magnetic total intensity ( $F$ ; in units of nanotesla per hour). This display is updated every 15 minutes. This image was generated from data recorded on 28 September 2016, 23:15–23:29. Locations of magnetic observatories are shown as grey squares.



Source: Geoscience Australia

*MAGNET, n. Something acted upon by magnetism.*

*MAGNETISM, n. Something acting upon a magnet.*

*The two definitions immediately foregoing are condensed from the works of one thousand eminent scientists, who have illuminated the subject with a great white light, to the inexpressible advancement of human knowledge.*

*(Ambrose Bierce)*



## Excursus 7.1—Australian Geomagnetic Reference Field Model

**Source:** Andrew Lewis, Geoscience Australia

**Further Information:** <http://www.ga.gov.au/ausgeonews/ausgeonews201006/geomagnetic.jsp>

The Australian Geomagnetic Reference Field (AGRF) is a mathematical model of the geomagnetic field and its predicted annual changes over the Australian region, including continental Australia and nearby offshore areas, most of Papua New Guinea and parts of eastern Indonesia. The 2010 revision is a mathematical representation of the undisturbed geomagnetic main field at epoch 2010.0 and its predicted annual changes during the period 2010 to 2015 (see Figure 7.8).

The model is the sixth in the series of AGRF models and describes the field originating from internal sources using spherical cap harmonics. The main field is modelled to a nominal minimum spatial wavelength of 1500 km and the annual change to 2000 km. Extensive vector geomagnetic survey datasets were used to derive the main field model, including magnetic data from the German CHAMP satellite, high elevation airborne data, and ground based vector survey data across Australia.

Based on knowledge of the past behaviour of the magnetic field, the secular variation model should be appropriate out to epoch 2015. The extensive regional data sets used in developing the AGRF model make it the most accurate available model for the Australian regional magnetic field for the interval 2010 to 2015.

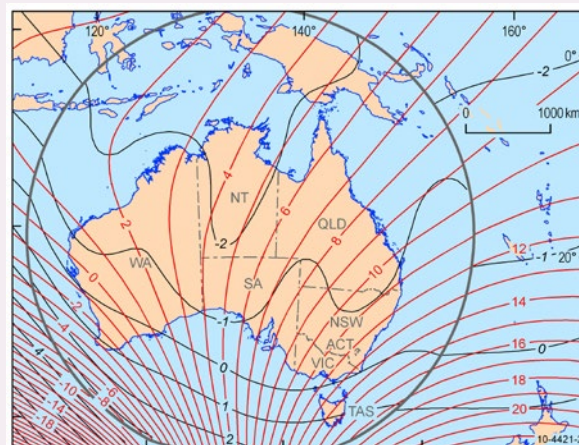
The 2010 AGRF model is based on the recently released eleventh revision of the International Geomagnetic Reference Field (IGRF), which is a global spherical harmonic model of the geomagnetic field. The eleventh generation of the International Geomagnetic Reference

Field (IGRF-11) was released by the International Association of Geomagnetism and Aeronomy (IAGA) in late December 2009. This release adds a definitive main field model for 2005.0, a new model for 2010.0 and a secular variation model for the period between 2010 and 2015.

The development of the IGRF is the result of international collaboration between magnetic field modellers and the scientific institutions and government agencies that undertake satellite magnetic surveys and operate geomagnetic observatories.

**Figure 7.8** AGRF 2010 model at epoch 2010.0

Contours of magnetic declination (in degrees) are shown as red lines and annual change of declination (in minutes-of-arc per year) are shown as black lines. The limit of the AGRF model is marked as a black circle. Contours outside this circle are derived from the IGRF-11 at 2010.0.



Source: Geoscience Australia

## 7.4 Geomagnetism

The geomagnetic field associated with planet Earth is the sum of magnetic fields from three major sources:

- the main field derived from internal processes within the Earth's core, which accounts for more than 90% of the total intensity;
- the external field derived from electrical processes in the ionosphere and magnetosphere driven by solar activity; and
- the crustal field derived from magnetism generated in iron minerals in the Earth's crust.

While rocks comprise various minerals, their magnetic properties depend mainly on the amount of iron-rich

minerals. Magnetite, for example, is a magnetic iron mineral, which occurs in small quantities in rocks. By measuring and mapping the crustal magnetic field, the general distribution of magnetic rocks and the associated subsurface geology can be mapped.

Local variations, or anomalies, in the Earth's magnetic field are generally due to variations in the chemical and magnetic properties of rocks and, thus, are valuable indicators of potentially commercial minerals, principally magnetite. Magnetic surveys use airborne, ship-borne or ground-based magnetometers to measure small changes in the intensity of the Earth's magnetic field (see Figure 7.9). These measurements

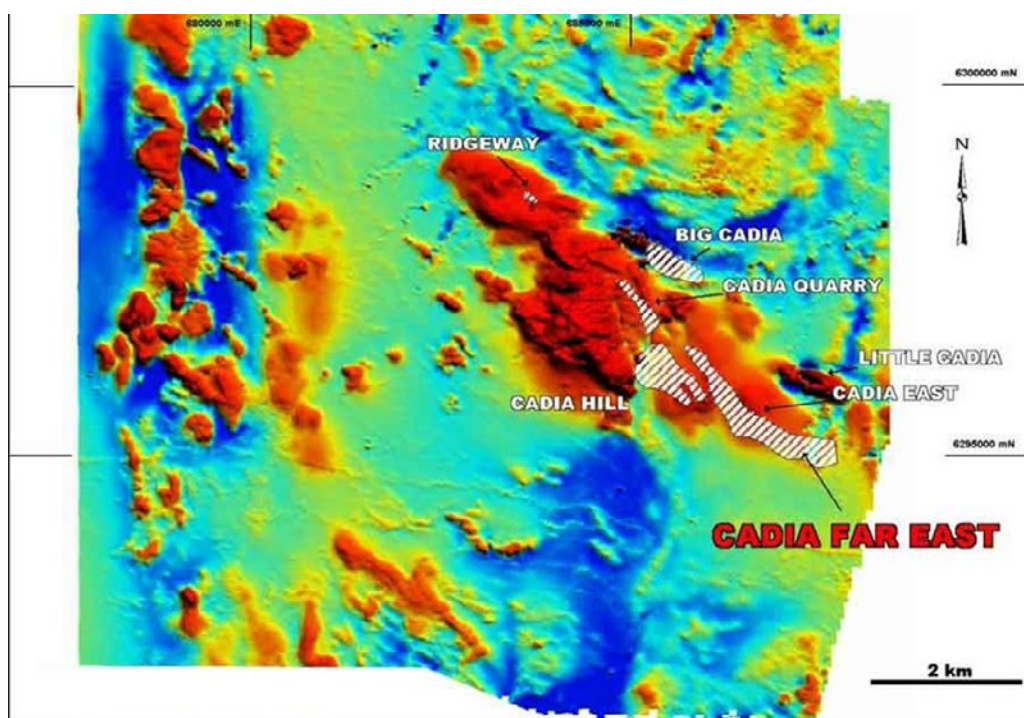
are adjusted for known variations due to global and regional magnetic variation. The resulting maps indicate the distribution and abundance of magnetic minerals and are commonly used for geological mapping, mineral exploration, archaeological surveys

and locating buried ferrous objects. For example, the most recent Magnetic Anomaly Grid for Australia is shown in Excursus 7.2. Acquisition and applications of this source of EO data is further discussed in Volume 3.

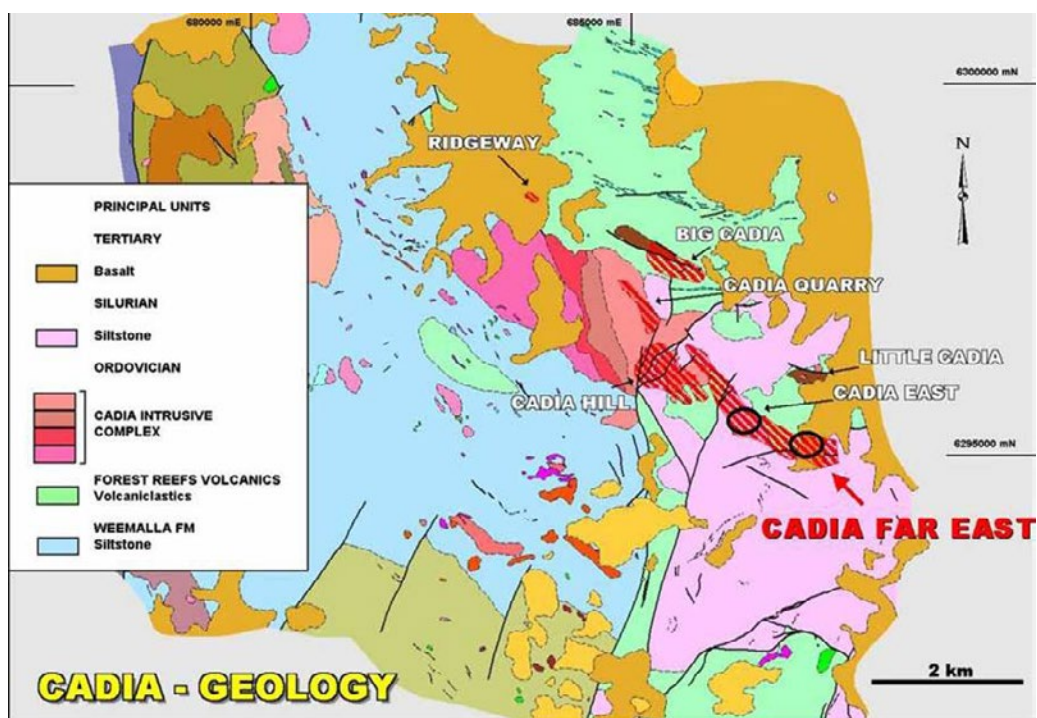
**Figure 7.9** Aeromagnetic imagery

Total Magnetic Intensity (TMI or F) for Cadia-Ridgeway Mine (about 20 km south of Orange, NSW).

a. This pseudo-colour image shows TMI values as a spectrum from high values as red to low values as blue.



b. Geologic map of Cadia region. The known extent of significant ore bodies are hatched.



Source: Geoscience Australia



## Excursus 7.2—Australian Magnetic Anomaly Grid

**Source:** Milligan *et al.* (2010)

**Further information:** <http://www.ga.gov.au/news-events/news/latest-news/latest-editions-of-magnetic-anomaly-grid-and-radiometric-map-released>; [http://www.ga.gov.au/webtemp/image\\_cache/GA18012.pdf](http://www.ga.gov.au/webtemp/image_cache/GA18012.pdf)

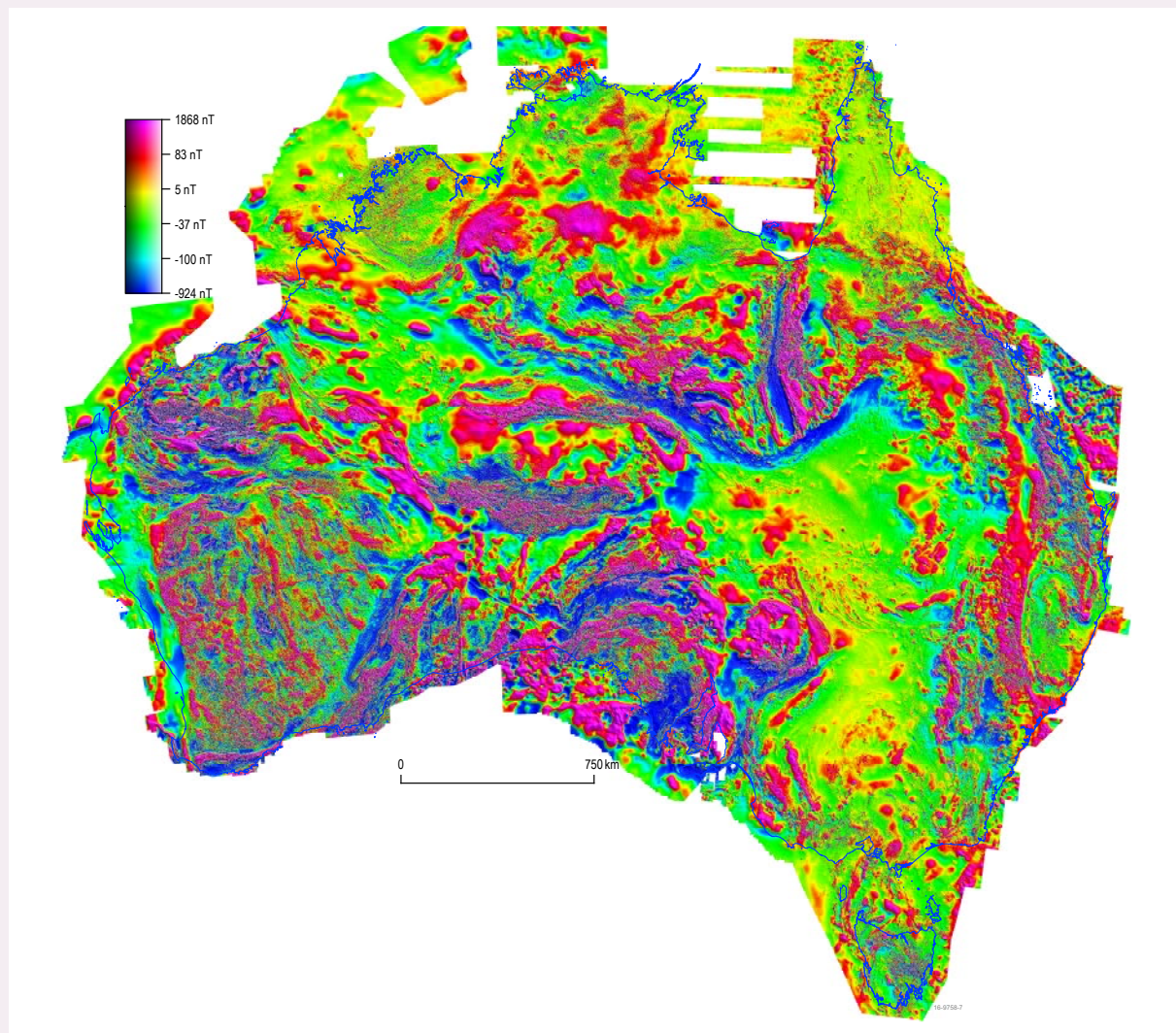
After more than 60 years of airborne surveys by state, territory and Australian Government geoscience agencies, and private companies, the Australian continent is impressively covered by a calibrated grid of magnetic data. The sixth Total Magnetic Intensity (TMI) grid of Australia is based on a cell resolution of approximately 80m (3 seconds of arc; see Figure 7.10). This grid comprises around 31.5 million line-kilometres of acquired magnetic survey data, which is 4.5 million more line-kilometres than the fifth edition released in 2010.

This grid was processed using a technique called Variable Reduction to Pole (VRTP), which makes adjustments to the location and shape of magnetic anomalies due to the variation in the inclination of the Earth's magnetic field with latitude. The VRTP process adjusts the magnetic anomalies so that simple features are mapped directly over the magnetic bodies. Without VRTP magnetic anomalies appear shifted relative to their true position.

The datasets are available for free download from the Geophysical Archive Data Delivery System (GADDS).

**Figure 7.10** Australian Magnetic Anomaly Grid

Sixth edition of TMI anomaly grid for Australia was derived from more than six decades of airborne survey data with VRTP adjustments.



Source: Geoscience Australia

## Australia-wide Airborne Geophysical Survey (AWAGS)

The Australia-wide Airborne Geophysical Survey (AWAGS), completed in 2008, flew the entire continent in a standardised grid at an altitude of 80 m. This grid, based on north-south flight lines

75 km apart and east-west flight lines 400 km apart, collected both magnetic and radiometric data. The consistent AWAGS dataset has allowed disparate sources of magnetic and radiometric data to be levelled and merged to a common datum (see Excursus 6.1).

## 7.5 Further Information

### Magnetism:

Geoscience Australia: <http://www.ga.gov.au/scientific-topics/disciplines/geophysics/magnetics>

### Geomagnetism:

Geoscience Australia: <http://www.ga.gov.au/oracle/geomag/agrfform.jsp>

NASA: <http://image.gsfc.nasa.gov/poetry/magnetism/magnetism.html>  
[http://www.nasa.gov/vision/earth/lookingatearth/29dec\\_magneticfield.html](http://www.nasa.gov/vision/earth/lookingatearth/29dec_magneticfield.html)

### Magnetosphere:

NOAA: <http://www.swpc.noaa.gov/phenomena/earths-magnetosphere>  
<http://www.swpc.noaa.gov/phenomena/geomagnetic-storms>

Southwest Research Institute: <http://pluto.space.swri.edu/image/glossary/magnetosphere.html>

Space Weather impacts: [http://www.wmo.int/pages/prog/sat/spaceweather-intro\\_en.php](http://www.wmo.int/pages/prog/sat/spaceweather-intro_en.php)

Atmospheric Optics: <http://www.atoptics.co.uk/highsky/auror2.htm>

## 7.6 References

Geoscience Australia (2016). Geoscience Australia. Retrieved from <http://www.ga.gov.au>.

Hopgood, P. (2007). Activity of magnetic total intensity across continental Australia. *Australian Society of Exploration Geophysicists*, 130, pp. 18-24.

Love, J. J. (2008). Magnetic monitoring of Earth and space. *Physics Today*, 61(2), pp. 31-37. doi:<http://dx.doi.org/10.1063/1.2883907>.

Love, J. J., and Finn, C. A. (2011). The USGS Geomagnetism Program and Its Role in Space Weather Monitoring. *Space Weather-the International Journal of Research and Applications*, 9. doi:<http://dx.doi.org/10.1029/2011sw000684>.

Milligan, P. R., Franklin, R., Minty, B. R. S., Richardson, L. M., and Percival, P. J. (2010). *Magnetic Anomaly Map of Australia (Fifth Edition)*, 1:15 000 000 scale. Geoscience Australia, Canberra, Australia.

NOAA (2013). National Geophysical Data Centre. Retrieved from <http://www.ngdc.noaa.gov/geomag/>.

NOAA (2016). Space Weather Prediction Centre. Retrieved from <http://www.swpc.noaa.gov/phenomena/ionosphere>.

Stern, D. P. (2004). The Great Magnet, the Earth. <http://www.phy6.org/earthmag/dmglist.htm>.





# 8 Gravity

Gravitational forces exist between any two bodies in the Universe. The gravitational influence exerted by one body on another is relative to both their respective masses and the distance between the two bodies. Since changes in Earth's gravity field strength at a particular location are related to its mass at that location, Earth's gravitational field can be measured indirectly by its impact on the orbital attitude of spaceborne sensors.

The most obvious illustration of gravitational force is that objects remain on the surface of the Earth. Since the gravitational force acting on an object is directly proportional to the mass of the object, those objects with greater mass are more difficult to move away from the Earth. The gravitational force between two objects is inversely proportional to the distance between them. Objects can remain in orbit around the Earth because the Earth is still exerting some gravitational influence on them.

Newton proposed the fundamental law of gravity, which relates the masses of two bodies and the Universal Gravitational Constant ( $G$ ):

$$F = G \left( \frac{m_1 m_2}{r^2} \right)$$

where

$F$  is the gravitational force (in N);  
 $G = 6.673 \times 10^{-11}$  (in  $\text{N} \cdot \text{m}^2 / \text{kg}^2$ );  
 $m_1$  is the mass of body 1 (in kg);  
 $m_2$  is the mass of body 2 (in kg); and  
 $r$  is the distance between the centres of mass of the bodies  $m_1$  and  $m_2$  (in m).

Gravitational forces are not limited to forces imposed by a larger body on a smaller body as the smaller body also has an impact on the larger body. For example, the gravitational influence of the Moon on the Earth causes the movement of water in the oceans that gives rise to tides.

## 8.1 The Earth's Gravitational Field

Were the Earth a perfect sphere with uniform density, its gravity would be constant at all locations. However, as introduced in Section 3, neither the shape nor composition of the Earth is uniform in any sense. The structure of Earth varies both in terms of internal layering and surface topography, as well as in material type and density so that the strength of gravity varies in different locations. The interactions between the major factors shaping the Earth are illustrated in Figure 8.1.

The standard gravity for Earth is accepted to be  $9.81275 \text{ m/s}^2$ . Section 3.3 introduced the geoid, a mathematical surface representing sea level equipotential, that is, where gravity would be equal to its mean sea level strength for all points on Earth. As illustrated in Figure 8.2, the shape of the geoid varies with the underlying masses so undulates relative to an ellipsoidal surface.

---

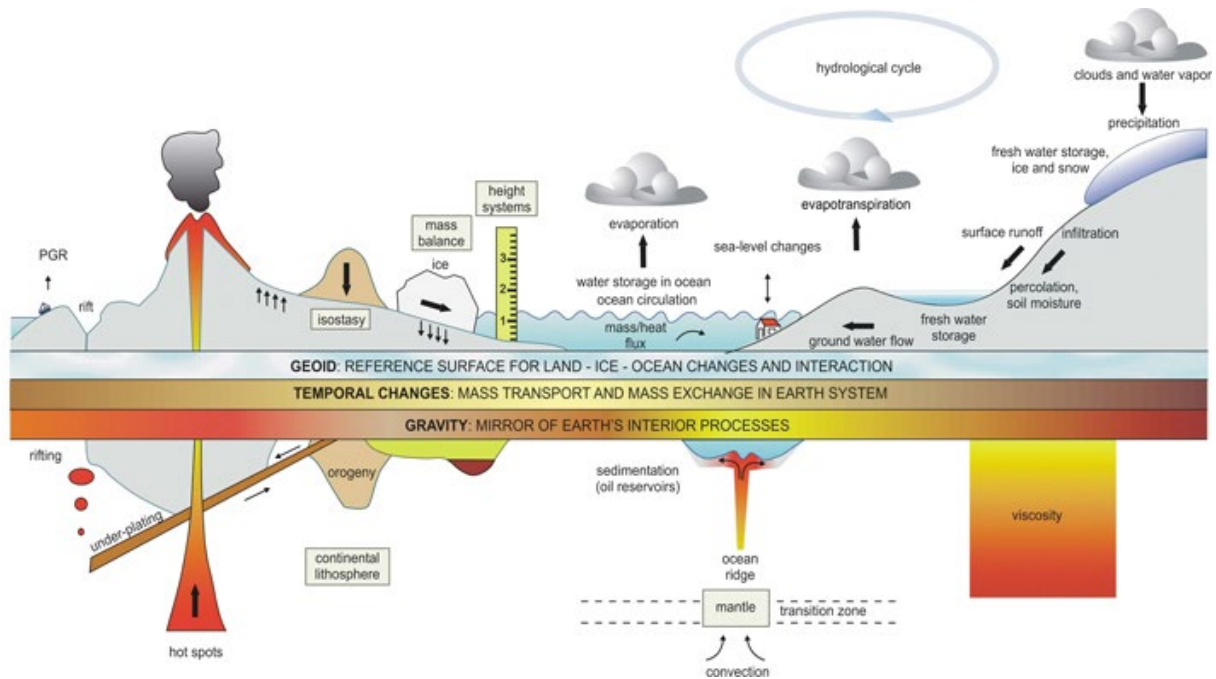
*Our two greatest problems are gravity and paperwork.  
We can lick gravity, but sometimes the paperwork is overwhelming.*  
(Wernher von Braun)

---

**Background image:** Isostatic residual gravity anomaly image of the Gulf of Carpentaria, northwest, Queensland. The area shown is 450 km wide. Variations in the strength of the gravity field are shown in pseudo-colour, from high values as red to low values as blue (derived from Isostatic residual gravity anomaly map for Australia, Version 2, 2016; see Excursus 8.1 for details). **Source:** Geoscience Australia

**Figure 8.1** Gravity, gravity variations, mass transport and distribution

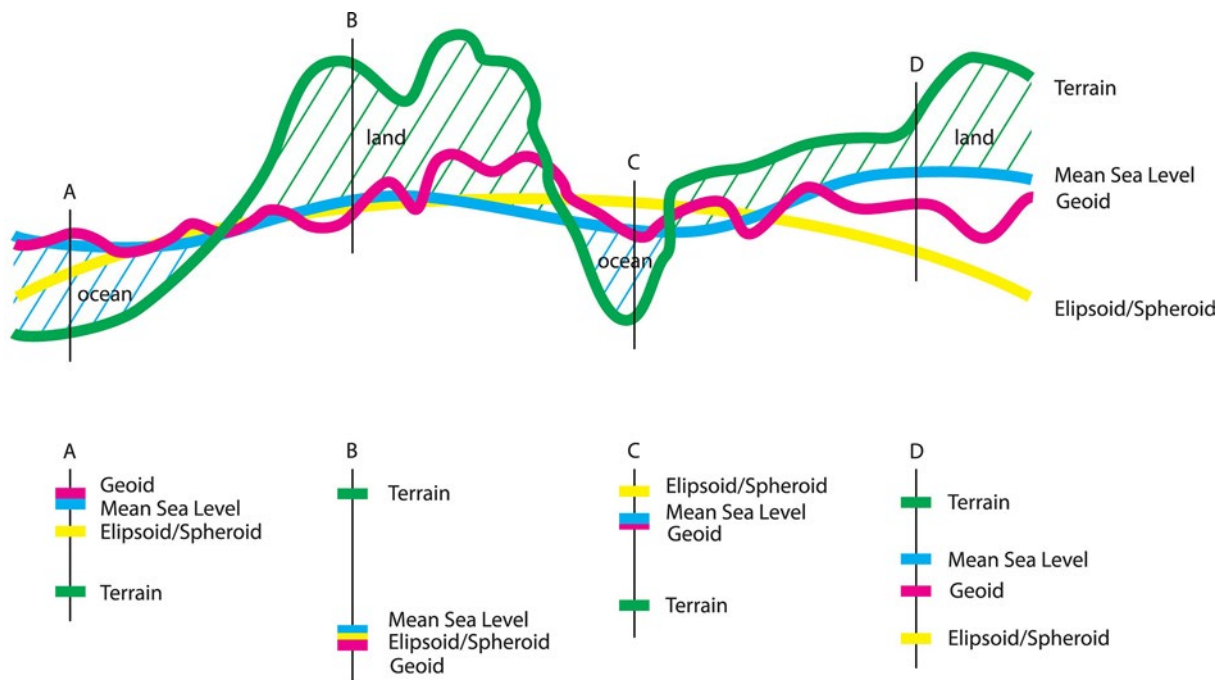
Gravity and its variations interact with the transport and distribution of masses above, on and within Earth to shape our planet.



Source: Ilk et al. (2005) p.4

**Figure 8.2** Geoid surface

This illustration exaggerates the relationship between Earth's terrain, mean sea level, an ellipsoid/spheroid model and a geoid model. At locations A and C, Earth's terrain is below mean sea level with the geoid being close to mean sea level, so these sites would be typical of an area of surface water. At locations B and D, the terrain is higher than mean sea level, which implies land.



Source: © Commonwealth of Australia 2014 on behalf of the Intergovernmental Committee on Surveying & Mapping (ICSM). Retrieved from <http://www.icsm.gov.au/mapping/datums1.html>

## 8.2 Measuring Gravity

Gravimeters or pendulums are used to measure gravity on the ground. Gravimeters can be:

- relative—measure the relative difference in gravity between two locations using a calibrated spring; and
- absolute—precisely measure the acceleration of an object falling in a vacuum at a fixed location.

Relative gravimeters are portable and can be used in various vehicles.

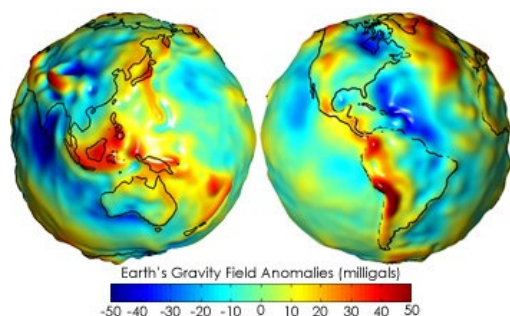
Airborne accelerometers and gradiometers have traditionally been used for continental gravity surveys, with the Global Positioning System (GPS) significantly improving the accuracy of flight line locations. These measurements can be presented as a map of gravitational ‘anomalies’, areas where measurements are higher or lower than the geoidal model. By convention, positive anomalies, where gravity is higher than the geoid, are coloured red, and negative anomalies, where gravity is lower than the geoid, are coloured blue (see Excursus 8.1).

Gravity anomalies often result from unusual concentrations of mass, such as a mountain range, which typically strengthen the gravitational force. Ocean trenches and land depressions can cause negative gravity anomalies (NASA, 2016). The most recent gravity anomaly map for Australia (Nakamura *et al.*, 2011) is described in Excursus 8.1.

Since their orbital altitudes are influenced by Earth’s gravitational field, spaceborne instruments offer another opportunity to measure gravity. Measurements of satellite orbital variations have enabled the development of regional and global geoidal models for land and seafloor surfaces (see Figure 8.3). Some of the sensors that underpin Space Geodetic Techniques are introduced in Excursus 3.2.

**Figure 8.3** Global gravity field anomalies

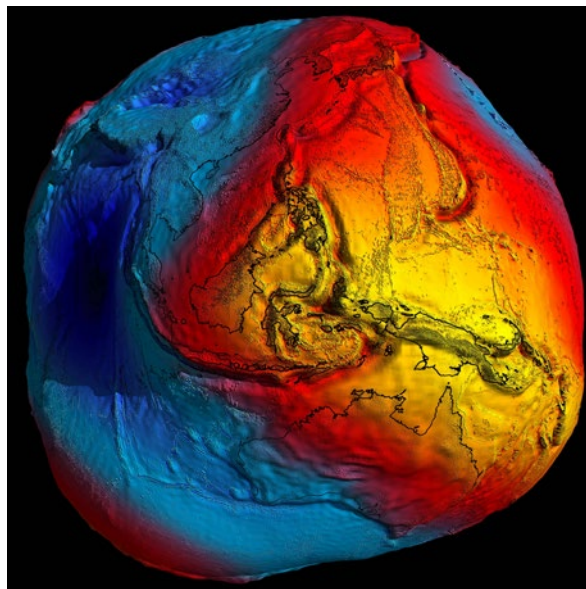
Gravity anomaly images highlight regions where gravitational force is higher or lower than the geoid. Mountainous regions typically have stronger gravitational forces than the geoid (hence have positive gravity anomalies), while ocean trenches and low-lying landmasses typically have weaker gravitational forces (or negative gravity anomalies).



Source: NASA (2016). Retrieved from <http://earthobservatory.nasa.gov/Features/GRACE/page3.php>

**Figure 8.4** Global gravity derived from GOCE

This model, released on 28 March 2011, is derived from one year’s data from the GOCE mission (ESA/HPF/DLR). Colours represent deviations from an ideal geoid, with blue being low values (down to -100 m) and red being high values (up to 100 m).



Source: ©ESA/HPF/DLR. Retrieved from [http://www.esa.int/spaceimages/Images/2011/03/Best\\_view\\_yet\\_of\\_global\\_gravity](http://www.esa.int/spaceimages/Images/2011/03/Best_view_yet_of_global_gravity)

Recent satellite missions have provided new means for measuring and mapping the Earth’s gravity field. The Gravity Recovery and Climate Experiment (GRACE) developed a pair of satellites to precisely measure distances from Earth and each other, while the low-orbit Gravity field and steady-state Ocean Circulation Explorer (GOCE) used three pairs of accelerometers within a single satellite to measure the gravity field. Such detailed gravity measurements enable accurate mapping of the geoid (at centimetre level), and highlight geophysical features such as subduction zones at tectonic plate boundaries (see Figure 8.4).

Earth’s gravity changes with rotation, surface composition and topography, water storage and movement, and interior structure. These factors necessitate ongoing monitoring of our gravity field. Continuous monitoring of the geoid has also quantified seasonal variations in gravity due to isostasy, that is, changes in the Earth’s surface due to pressures such as ice cover.

Gravity measurement systems are further discussed in Volume 3.



## Excursus 8.1—Australian Gravity Anomaly Map

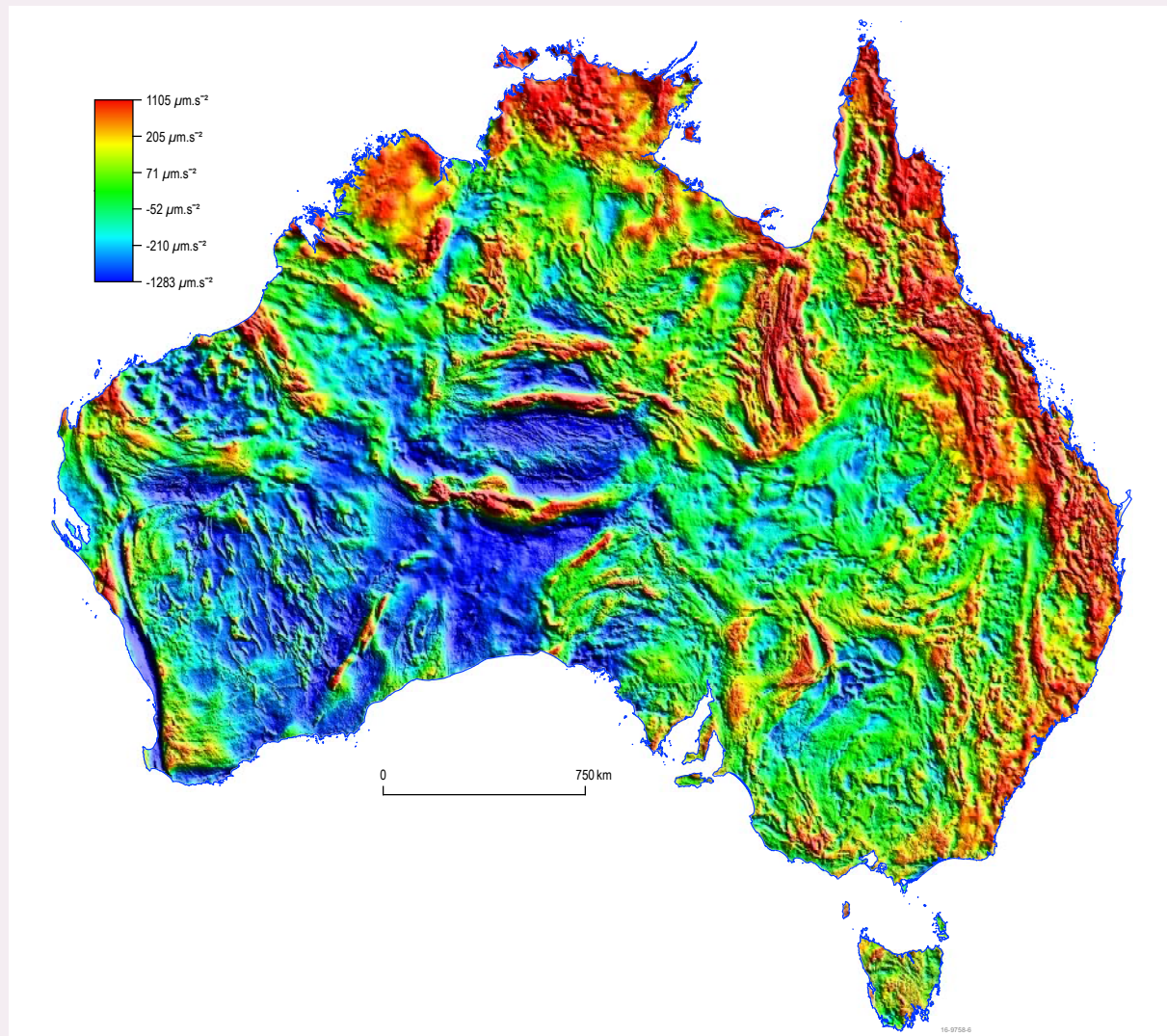
**Source:** Geoscience Australia AusGeo News 103, September 2011: <http://www.ga.gov.au/ausgeonews/ausgeonews201109/productnews.jsp>

**Further Information:** Tracey *et al.* (2008); Tracey and Nakamura (2010); Nakamura *et al.* (2011)

The most recent Isostatic Residual Gravity Anomaly Map of Australia at 1:5 million scale was released by Geoscience Australia in 2011 (see Figure 8.5). The map shows isostatic residual gravity anomalies across onshore Australia. Analysis of gravity anomaly values shows a relationship between terrain-corrected Bouguer anomaly values and the terrain height. This relationship is less evident after the isostatic correction, which improves the resolution of anomalies.

The dataset is derived from observations recorded at approximately 1,500,000 gravity stations (or reference points) held in the Australian National Gravity Database (ANGD) by Geoscience Australia. The onshore data were acquired by the federal, state and territory governments, the mining and exploration industry, universities and research organisations over the six decades since the 1950s.

**Figure 8.5** Isostatic Residual Gravity Anomaly Map of Australia



Source: Geoscience Australia

---

*And make us as Newton was, who in his garden watching  
The apple falling towards England, became aware  
Between himself and her of an eternal tie.  
(Wystan Hugh Auden)*

---

### 8.3 Gravity Applications

Given that the density of rocks in the Earth's crust affect the measured gravity at a particular location, gravity surveys can also be interpreted to remotely map the:

- distribution of rock types and rock structure;
- three-dimensional structure of sub-surface rocks to highlight potential energy or mineral resources;
- sub-surface structure for archaeological studies, urban engineering and military applications.

The Australian National Gravity Database (ANGD) is maintained by Geoscience Australia (GA). This database compiles gravity surveys in Australia undertaken by Federal, State and Territory governments, private companies and academic institutions. This data set is freely available online. The Australian Fundamental Gravity Network (AFGN), a network of permanent gravity base stations, serves as the datum for these gravity surveys (Geoscience Australia, 2016).

### 8.4 Further Information

**Gravity:** <http://www.ga.gov.au/scientific-topics/disciplines/geophysics/gravity>  
<http://www.ga.gov.au/about/what-we-do/projects/minerals/current/continental-geophysics/gravity>

**Gravity Field and Steady-State Ocean Circulation Explorer (GOCE):** [http://www.esa.int/Our\\_Activities/Observing\\_the\\_Earth/The\\_Living\\_Planet\\_Programme/Earth\\_Explorers/GOCE/Satellite](http://www.esa.int/Our_Activities/Observing_the_Earth/The_Living_Planet_Programme/Earth_Explorers/GOCE/Satellite)

<http://esamultimedia.esa.int/multimedia/publications/BR-285/pageflip.html>

**Gravity Recovery and Climate Experiment (GRACE):**  
**ESA (2016)**  
**NASA (2016)**<http://earthobservatory.nasa.gov/Features/GRACE/>

### 8.5 References

ESA (2016). European Space Agency. Retrieved from <http://www.esa.int/ESA>.

Geoscience Australia (2016). Geoscience Australia. Retrieved from <http://www.ga.gov.au>.

Ilk, K. H., Flury, J., Rummel, R., Schwintzer, P., Bosch, W., Haas, C., Schröter, J., Stammer, D., Zahel, W., Miller, H., Dietrich, R., Huybrechts, P., Schmelig, H., Wolf, D., Götze, H. J., Riegger, J., Bardossy, A., Güntner, A., and Gruber, T. (2005). Mass Transport and Mass Distribution in the Earth System: Contribution of the New Generation of Satellite Gravity and Altimetry Missions to Geosciences. GOCE-Projektbüro Deutschland, Technische Universität München, GeoForschungsZentrum Potsdam, Munich, Germany. Retrieved from [http://mt.dgfi.tum.de/typo3\\_mt/fileadmin/Dokumente/programmschrift-Ed2.pdf](http://mt.dgfi.tum.de/typo3_mt/fileadmin/Dokumente/programmschrift-Ed2.pdf).

Nakamura, A., Bacchin, M., Milligan, P. R., Wynne, P., and Tracey, R. (2011). Isostatic Residual Gravity Anomaly Map of Onshore Australia, scale 1:5,000,000 (GEOCAT 69878). Geoscience Australia, Canberra, Australia.

NASA (2016). Gravity Recovery and Climate Experiment (GRACE). Retrieved from <http://earthobservatory.nasa.gov/Features/GRACE/page3.php>.

Tracey, R., Bacchin, M., and Wynne, P. (2008). A new absolute gravity datum for Australian gravity and new standards for the Australian National Gravity Database. Paper presented at the 19th International Geophysical Conference and Exhibition.

Tracey, R., and Nakamura, A. (2010). Complete Bouguer Anomalies for the Australian National Gravity Paper presented at the 21st International Geophysical Conference and Exhibition.



# 9 Vibrations

Vibrational waves are disturbances that transfer energy through different media. Sound waves (see Section 9.1) and seismic waves (see Section 9.2) are vibrations that can be sensed remotely to obtain information about the Earth.

Vibrational energy is measured using both active sensors (which emit energy and then record the echo from a target) and passive systems (which detect energy from another source). Vibrations are detected

most commonly within water or solid earth. The measurements are formed into images to derive maps of surface properties, including the distance between the target and the sensor.

## 9.1 Sound Waves

Sound is a form of energy that is propagated as longitudinal or compression waves (see Figure 2.3a). Unlike EMR, which travels at a constant speed through a medium, and for which frequency and wavelength definitions can be used interchangeably, the speed of sound waves varies considerably with the elastic properties of the medium through which the waves are travelling. For example, in seawater, the speed of sound is a function of water density and compressibility, both of which are dependent on temperature, pressure, and salinity (see Figure 9.1):

- in deep ocean below 1500 m, the speed of sound is governed by pressure, so increases with depth;
- in upper ocean at equatorial and temperate latitudes, greater variation in temperature and some variation in salinity occurs, so the speed of sound is more variable, but tends to decrease with temperature; and
- minimum velocity occurs at the thermocline (Wells, 1986).

As a result, in ocean water the speed of sound is minimised at depths in the range 750–1,000 m. This zone of minimum speed is known as the Deep Sound Channel (DSC; formerly Sound Fixing and Ranging channel: SOFAR), and enables the guided propagation of undistorted sound for distances up to thousands of kilometres. This channel is commonly used for ocean acoustic tomography (Munk *et al.*, 1995) and submarine surveillance.

The human ear detects changes in the frequency of sound waves as changes in pitch. The range of human hearing is about 20–20,000 Hz. Sound above the human hearing range is generally known as ultrasound and that below the hearing range as infrasound. High frequency waves are heard as high pitch sounds and low frequency waves are heard as low pitch sounds.

In a spherical wave, such as a sound wave, energy propagates equally in all directions. As such, the power ( $P$ ) emitted by the source is distributed evenly over a spherical surface (area =  $4\pi r^2$ ), and assuming that there is no absorption in the medium, the intensity of the wave is given by the formulae:

$$\text{intensity} = \frac{P}{4\pi r^2}$$

Thus the intensity of a sound wave decreases with the square of the distance from the source, since the same amount of energy is spread over an increasingly larger area. The intensity of sound waves is measured in watts per square metre ( $\text{W/m}^2$ ). Since the human ear is capable of detecting sound levels across a very large range, however, sound intensity is usually measured using a logarithmic scale, in units of decibels (see Figure 9.2).

**Background image:** This seismogram shows one day's worth of aftershocks of three large earthquakes near Tennant Creek, Northern Territory in January 1988.  
**Source:** Geoscience Australia



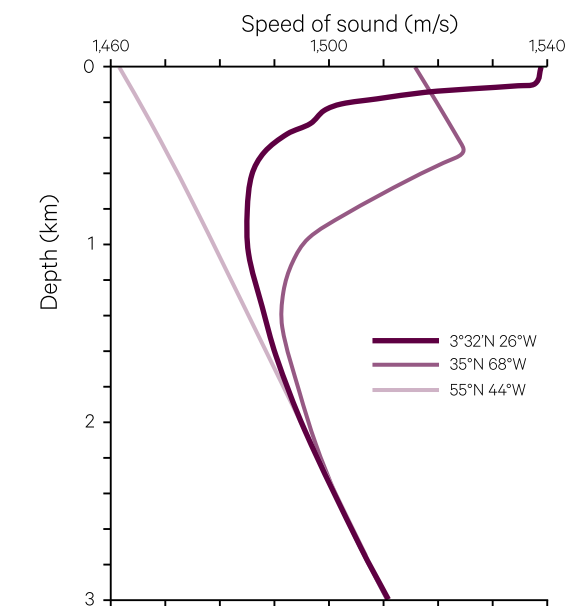
*There is something very basic to the sense of listening.  
The sense of hearing is the only one that operates totally from vibrations,  
without other physical or chemical reactions to receive the sensations.  
(Henry Reed)*

Like other waves, sound waves undergo reflection, refraction and diffraction (see Section 2.5.2). The reflection of sound waves off surfaces can produce reverberations and echoes. Diffraction occurs when the wavelength of a sound wave is larger than an object it encounters, but if the wavelength is smaller than the object it tends to reflect off the object rather than diffract around it.

**Figure 9.1** Speed of sound with varying water depth

In seawater, the speed of sound is mostly governed by temperature and pressure. From the surface to 1000 m depth, the effect of temperature dominates. At depths greater than 1000 m, the effect of pressure is more dominant.

- At equatorial latitude (3°32'N, 26°W)
- At sub-tropical latitude (35°N, 68°W)
- At sub-polar latitude (55°N, 44°W)



Adapted from: Wells (1986) Figure 2.4

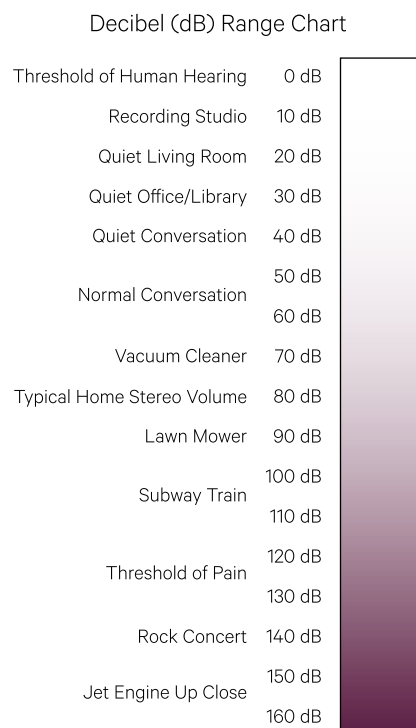
The Doppler effect (introduced in Section 2.5.4) is an observed rather than actual change in vibrational frequency. This effect is due to the relative movement of the sound source and the observer, such that when the observer and source are approaching each other the wave frequency seems higher than when they are moving apart.

When a sound source is moving at the same speed as the sound waves it is producing, a shock wave is created as the compression waves ahead of the source become 'bunched up' (see Figure 9.3a and 9.3b). Since waves are a disturbance to a medium, the shock wave can be considered to be the result of the medium not having time to compensate for the disturbance. An observer hears a shock wave as a sonic boom (see Figure 9.3c).

Sound waves may be detected by remote sensors, using both active and passive devices. Sonar (Sound Navigation and Ranging) is an active remote sensing technique for navigation, communication and detection under water. Techniques for sensing sound remotely are detailed in Volume 3.

**Figure 9.2** Decibel range

Sound intensity is measured in units of decibels. Note: scale is logarithmic.



Source: Langlopress (2016)

**Figure 9.3** Shock waves and sonic booms

a. Air becomes compressed ahead of a moving object, such as an aircraft. At subsonic speeds, sound is radiated in all directions. The perceived drop in pitch that occurs as an aircraft passes an observer is due to the Doppler Effect.

b. Compression of pressure waves increases with speed up to the speed of sound (Mach 1), forming a pressure cone starting at the nose of the aircraft.

c. Shock Waves are created when an object moves at, or faster than, the speed of sound. A Sonic Boom is heard when an observer's ear intersects the pressure cone from a supersonic aircraft. A vapour cloud can also occur around the aircraft as it breaks the sound barrier.



Source: Langlopress (2016)

## 9.2 Seismic Waves

*Seismic (from) Greek, seismos meaning 'earthquake'*

Seismology is the study of earthquakes and the associated propagation of seismic energy waves through the Earth. Earthquakes produce different types of seismic waves that display different characteristics in different materials. As a result, they can be used to map structures deep within the Earth.

### 9.2.1 What are earthquakes?

Earthquakes are the Earth's natural means of releasing stress. When the Earth's tectonic plates push against each other, the lithosphere becomes stressed and ultimately fractures or shifts, creating what is known as a fault (see Section 3). When such fractures occur, stress is released as vast quantities of energy that move through the Earth as vibrations. Tectonic plate boundaries coincide with the locations of most major earthquakes (see Figure 9.4). Intraplate earthquakes, which occur in the interior of tectonic plates, tend to be less significant and less common. Earthquakes occur rarely in Australia (mainland and Tasmania) and all are intraplate (Lewis and Collins, 2014).

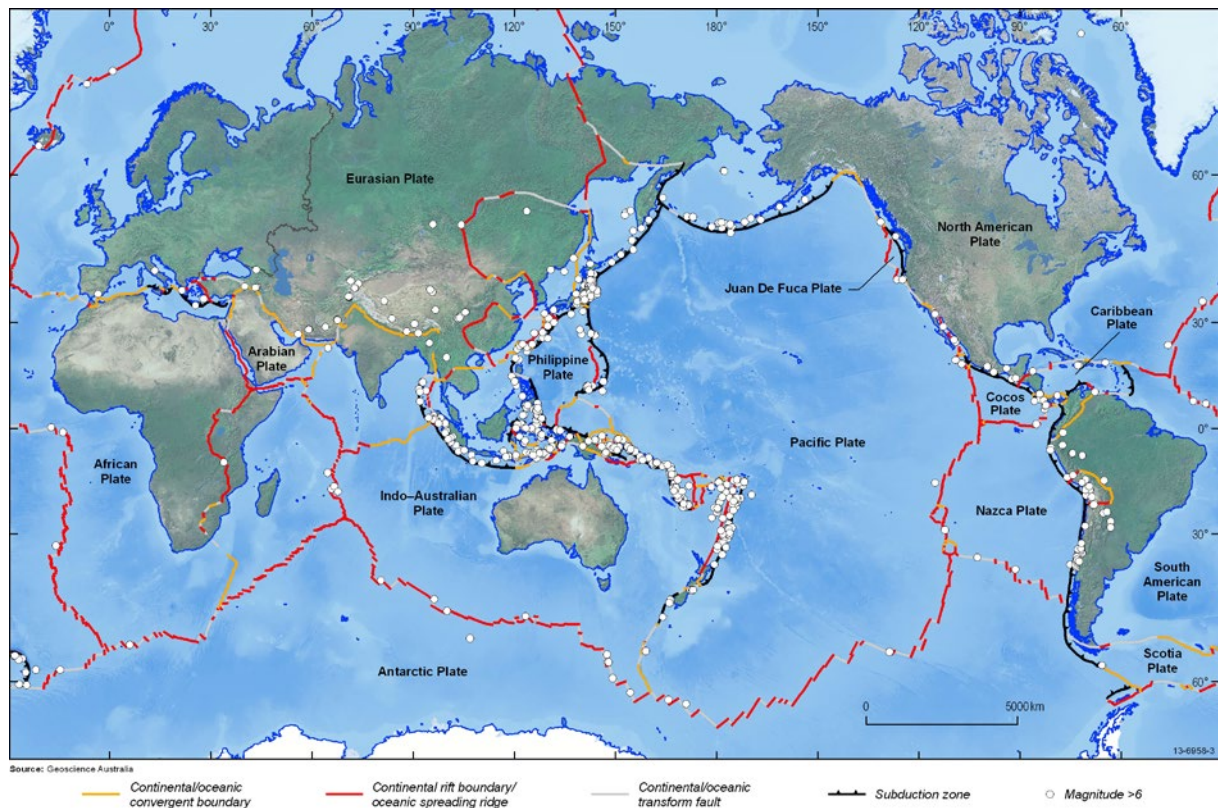
As the initial fracture in the lithosphere propagates, it releases energy along the fault, which may be up to 1,000 km long. The point of origin of an earthquake is called the focus and this may be close to the surface or many hundreds of kilometres below it. The point on the Earth's surface directly above the focus is called the epicentre (See Figure 9.5).

Earthquakes can result from both natural and human activities. Tectonic earthquakes occur when rocks in the Earth's crust break due to movement of tectonic plates (see Section 3.2). Earthquakes may also occur due to movement of magma in volcanoes, and serve as early warning of volcanic eruptions. Collapse earthquakes are associated with breakage of underground caverns and mines. Earthquakes can also result from detonation of nuclear and chemical devices, but these explosion earthquakes are characterised by different wave patterns and can thus be readily distinguished from natural events.

*As seismologists gained more experience from earthquake records,  
it became obvious that the problem could not be reduced to a single peak acceleration.  
In fact, a full frequency of vibrations occurs.  
(Charles Frances Richter)*

**Figure 9.4** Global earthquake occurrence

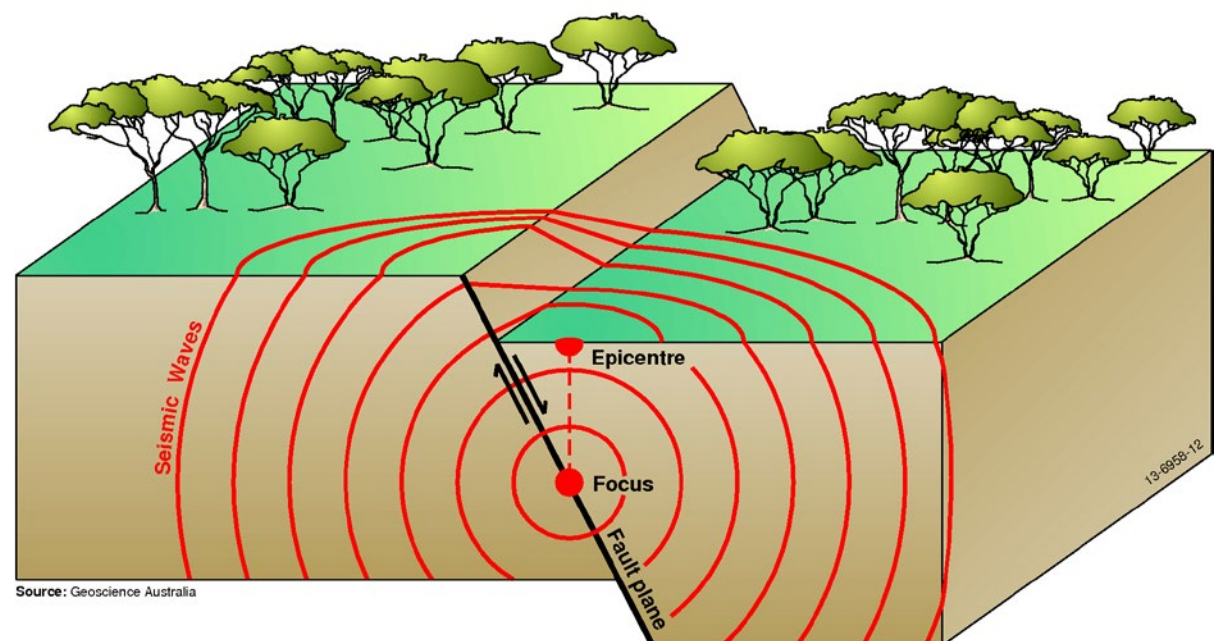
Most major earthquakes occur at tectonic plate boundaries, as a consequence of adjacent plates moving at different speeds in different directions. In Australia, most earthquakes are intraplate



Source: Lewis and Collins (2014) Figure 3

**Figure 9.5** Earthquake focus and epicentre

An earthquake originates from a location known as the focus. The point on the Earth's surface that is directly above the focus is called the epicentre. This illustration shows an earthquake resulting from displacement of the Earth's crust along a fault plane. Seismic waves carry energy generated by the earthquake away from the focus in all directions.



Source Lewis and Collins (2014) Figure 12



*If you want to find the secrets of the universe, think in terms of energy, frequency and vibration.*  
(Nikola Tesla)

## 9.2.2 Types of seismic waves

Two major types of seismic waves are generated by earthquakes:

- body waves—which rapidly travel through the interior of Earth (see Section 9.2.2.1); and
- surface waves—which destructively travel along the surface of Earth (see Section 9.2.2.2).

### 9.2.2.1 Body waves

Body waves travel more quickly than the destructive surface waves. Two forms of body waves travel through the interior of the Earth:

- P-waves—Primary waves are compression or longitudinal waves that propagate using a ‘push-pull’ motion, by alternating from compression to expansion in the direction of wave movement (see Figures 2.3a and 9.6a). P-waves travel through all types of media (solid, liquid and gas) and temporarily change its volume (Lutgens and

Tarbuck, 1998). They typically travel at speeds of 8–14 km/s in the crust and mantle, generally increasing with depth to the core-mantle boundary. Being the fastest seismic waves, they are the first to be detected when an earthquake occurs; and

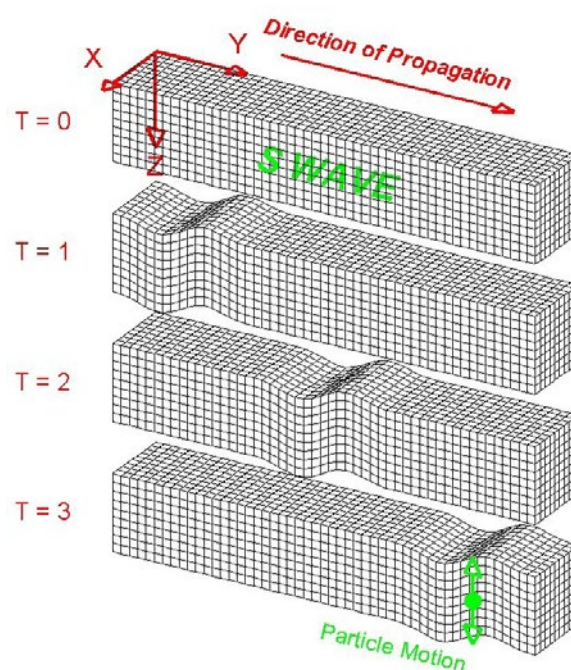
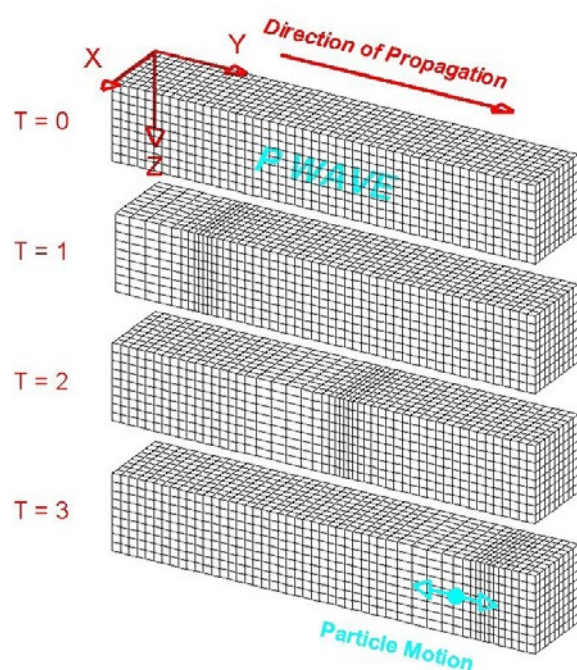
- S-waves—Secondary (or shear) waves are transverse waves, which only travel through solid media, and effectively ‘shake’ the particles of the media (see Figures 2.3b and 9.6b). These waves travel more slowly than P-waves, in the range of 4–7 km/s in the crust and mantle, generally increasing with depth to the core-mantle boundary. The lower speeds correspond to the waves in loose, unconsolidated sediment, the higher to those near the base of Earth’s mantle. S-waves move rock particles in a direction that is perpendicular to the wave direction, that is, up and down or side-to-side. They are also called Shear waves because they don’t change the volume of the material through which they propagate but rather shear, or fracture, it (Lutgens and Tarbuck, 1998).

**Figure 9.6** Body waves

Body waves travel through Earth’s interior as primary (P) or secondary (S) waves. In these diagrams, particles are represented by cubes.

a. P-waves are compression or longitudinal waves that alternate between compression and expansion in the direction of wave propagation.

b. S-waves are transverse waves that shake rock particles in direction perpendicular to wave propagation.



Source: Braille (2006) Figures 1 and 2. © L. Braille with permission granted to reproduce for non-commercial purposes



### 9.2.2.2 Surface waves

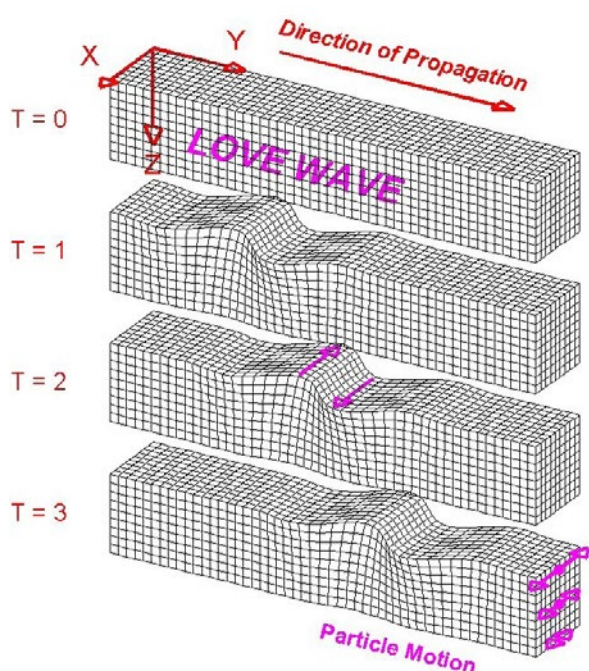
Surface waves, generated by the interaction of P-waves and S-waves with the surface of the Earth and with each other, only travel through the surface of Earth's crust, albeit at varying depths. They have a lower frequency than body waves, but are responsible for most of the damage associated with earthquakes.

Two different types of surface waves have been observed: Love waves and Rayleigh waves. Love waves result from S waves that are trapped near the surface of the Earth while Rayleigh waves form when P and S waves interact with each other near the surface of the Earth. Love waves are the faster surface waves, travelling at over 4 km/s (~15,000 km/hour) and move in a horizontal plane (see Figure 9.7a), while the slower Rayleigh waves roll along the surface creating vertical movement of the Earth's crust (see Figure 9.7b).

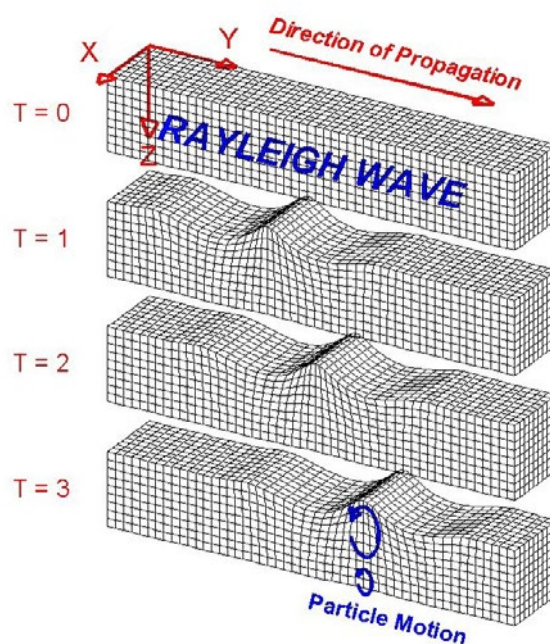
**Figure 9.7** Surface waves

Surface waves travel through the Earth's crust at different depths. In these diagrams, particles are represented by cubes.

a. Love waves travel most quickly in a horizontal plane.



b. Rayleigh waves roll along the surface, creating vertical movement of the Earth's crust.



Source: Braille (2006) Figures 3 and 4. © L. Braille with permission granted to reproduce for non-commercial purposes.

### 9.2.3 Using seismic waves to determine the structure of Earth

If the interior of the Earth had uniform composition and density, seismic waves would emanate from an earthquake and travel in straight paths, showing a proportional increase in time to travel greater distances and with uniform reduction in strength. However, body waves travel faster in the mantle than in the crust, which suggests that the mantle is denser. P-waves die out about 105° from the epicentre, then reappear about 140° away, and arrive much later than expected (see Figure 9.8). The region without P-waves is called the P-wave shadow zone. S-waves

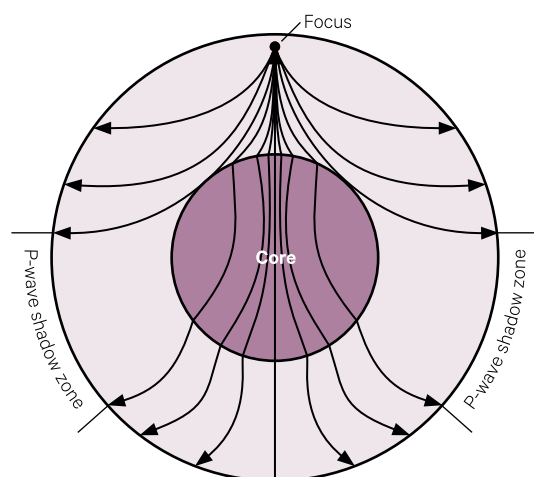
die out completely around 105° from the epicentre. This discrepancy implies that part of the Earth's core comprises liquid, not solid material. More recently, using improved seismographs, a solid inner core has also been distinguished.

The relatively new imaging technique of seismic tomography uses seismic waves to detect very slight seismic velocity differences, which indicate variations in temperature throughout the mantle (see Section 3.2). Since waves move faster through cold material and slower through hot material, these images contribute to our understanding of the process of convection in the mantle.

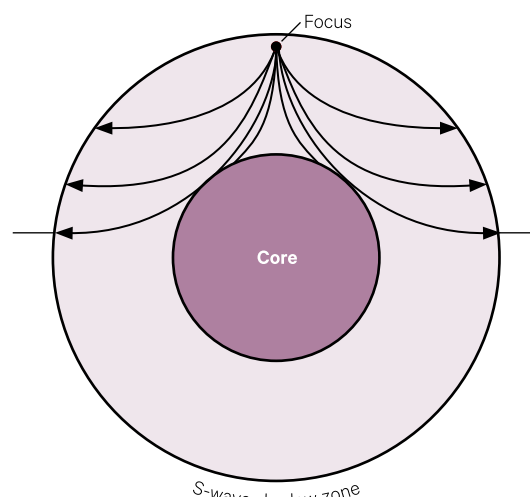
**Figure 9.8** Shadow zones for seismic waves

Seismic shadows are areas of the Earth, relative to the epicentre of an earthquake, where seismic waves are not detected. These are usually defined as angular distances from the epicentre on a plane through the centre of the Earth.

a. P-waves are refracted by the liquid outer core of Earth, so are not detected in two P-wave shadow zones between angular distances  $105^\circ$  to  $140^\circ$  from the epicentre.



b. S-waves do not propagate through the liquid outer core, which results in a S-wave shadow zone comprising all angular distances greater than  $105^\circ$  from the epicentre.



Adapted from: Earth Science Australia (CC BY NC SA 3.0) at <http://earthsci.org/index.html>

### 9.2.4 Detecting seismic waves

Seismographs are used to record the energy generated by earthquakes. When seismic waves are detected by a seismograph, their size and duration are recorded as a seismogram. By combining the information from several seismographic recordings, the epicentre and focus of the earthquake can be located using triangulation. More modern approaches use Earth models of seismic velocity to compare predicted and measured seismic wave arrivals. By adjusting the earthquake parameters like origin time and focal point the differences or residuals can be minimised to produce the most accurate location solution. Traditional instruments employed a pen on a pendulum-like arm that recorded ground movements on a revolving drum. Current instruments use electronic sensors connected directly to computers that can provide instant access to seismic information from locations all around the globe.

Because P-waves are the fastest seismic waves, they will typically be the first ones recorded, followed by S-waves, which, while slower, are generally larger. Surface waves travel a little slower than S-waves so they are generally recorded just after the S-waves. For shallow earthquakes, the surface waves may be the largest waves recorded by the seismograph and they are often the only ones recorded a long distance from medium-sized earthquakes.

A number of standard scales have been used to compare earthquakes. These use logarithmic scales to describe:

- magnitude—the extent of shaking caused by the earthquake; or
- intensity—the destructive power of released energy from the earthquake.

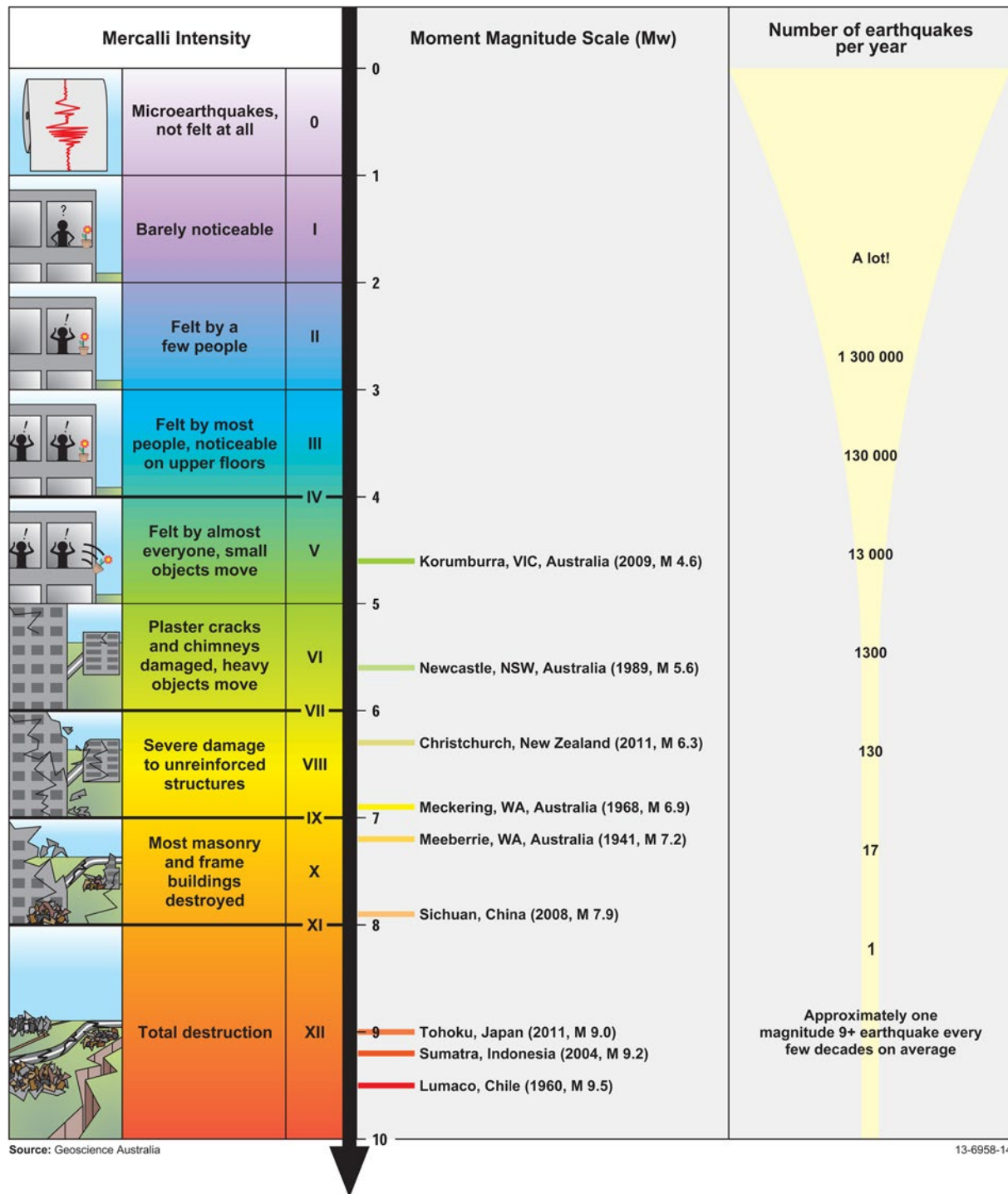
Common examples of earthquake comparison scales include:

- Richter scale (Richter, 1935), which measures magnitude in logarithmic increments;
- Modified Mercalli scale (Wood and Neumann, 1931) which describes intensity in 12 qualitative increments, expressed in roman numerals; and
- Moment magnitude scale ( $M_w$ ; Hanks and Kanamori, 1979) which considers the total energy release of the earthquake, that is the distance the relevant fault or fracture actually moved during the earthquake and the force that was required to move it. The  $M_w$  generates more precise magnitudes than the Richter scale over a wider range of earthquakes, and has been the official scale used by USGS since 2002 (see Figure 9.9).

The number of seismic stations has increased from about 350 in 1931 to many thousands, which means that many more earthquakes are now being detected. The USGS estimates that, since 1900, there have been an average of 18 major earthquakes (magnitude 7.0–7.9) and one great earthquake (magnitude 8.0 or greater) per year, and that this average has been relatively stable (USGS, 2016).

**Figure 9.9** Global earthquake frequency and energy

The Modified Mercalli Intensity scale is compared with the Moment Magnitude Scale for some recent earthquakes. The average global frequency of global earthquakes is shown relative to their magnitude.



Source: Lewis and Collins (2014) Figure 14

## 9.3 Further Information

### Sonar:

<http://www.nauticalcharts.noaa.gov/hsd/SSS.html>

### Seismology:

#### Australia

Geoscience Australia: <http://www.ga.gov.au/scientific-topics/hazards/earthquake>

Lewis and Collins (2014)

South Australia, Primary Industries and Resources  
South Australia: <http://www.pir.sa.gov.au/minerals/earthquakes/>

The University of Western Australia: <http://www.seismicity.see.uwa.edu.au>

The University of Queensland: <http://www.quakes.uq.edu.au>

Earth Science Australia: <http://earthsci.org/index.html>

Bureau of Meteorology, Australian Tsunami Warning  
Centre: <http://www.bom.gov.au/tsunami/about/jatwc.shtml>

#### USA

US Geological Survey Earthquake Hazards Program:  
<http://earthquake.usgs.gov/>

UPSeis: <http://www.geo.mtu.edu/UPSeis/waves.html>

Incorporated Research Institutions for Seismology  
(IRIS): Comprehensive site with animations of  
earthquakes and a live world map showing locations  
and magnitudes of earthquakes in real time: <http://www.iris.edu/hq>

## 9.4 References

Braille, L. W. (2006). Seismic Waves and the Slinky. The IRIS Consortium, Purdue University. Retrieved from <http://web.ics.purdue.edu/~braile/edumod/slinky/slinky4.htm>.

Hanks, T. C., and Kanamori, H. (1979). A moment magnitude scale. *Journal of Geophysical Research: Solid Earth*, 84(B5), pp. 2348-2350. doi:<http://dx.doi.org/10.1029/JB084iB05p02348>.

Langlopress (2016). Scientific Illustrations. Retrieved from <http://langlopress.net/homeeducation/resources/science/index.php?op=sciencethumbs>.

Lewis, G., and Collins, C. (2014). Earthquakes - Teacher notes and student activities (2014/06). Geoscience Australia, Canberra. Retrieved from [https://d28rz98at9flks.cloudfront.net/76611/Rec2014\\_006.pdf](https://d28rz98at9flks.cloudfront.net/76611/Rec2014_006.pdf). doi:<http://dx.doi.org/10.11636/Record.2014.006>.

Lutgens, F. K., and Tarbuck, E. J. (1998). *Essentials of Geology*, 6th Edn. Prentice Hall, New Jersey, USA.

Munk, W., Worcester, P., and Wunsch, C. (1995). *Ocean Acoustic Tomography*. Cambridge University Press.

Richter, C. F. (1935). An instrumental earthquake magnitude scale. *Bulletin of the Seismological Society of America*, 25(1), pp. 1-32.

USGS (2016). US Geological Survey Earthquake Hazard Program. Retrieved from <http://earthquake.usgs.gov>.

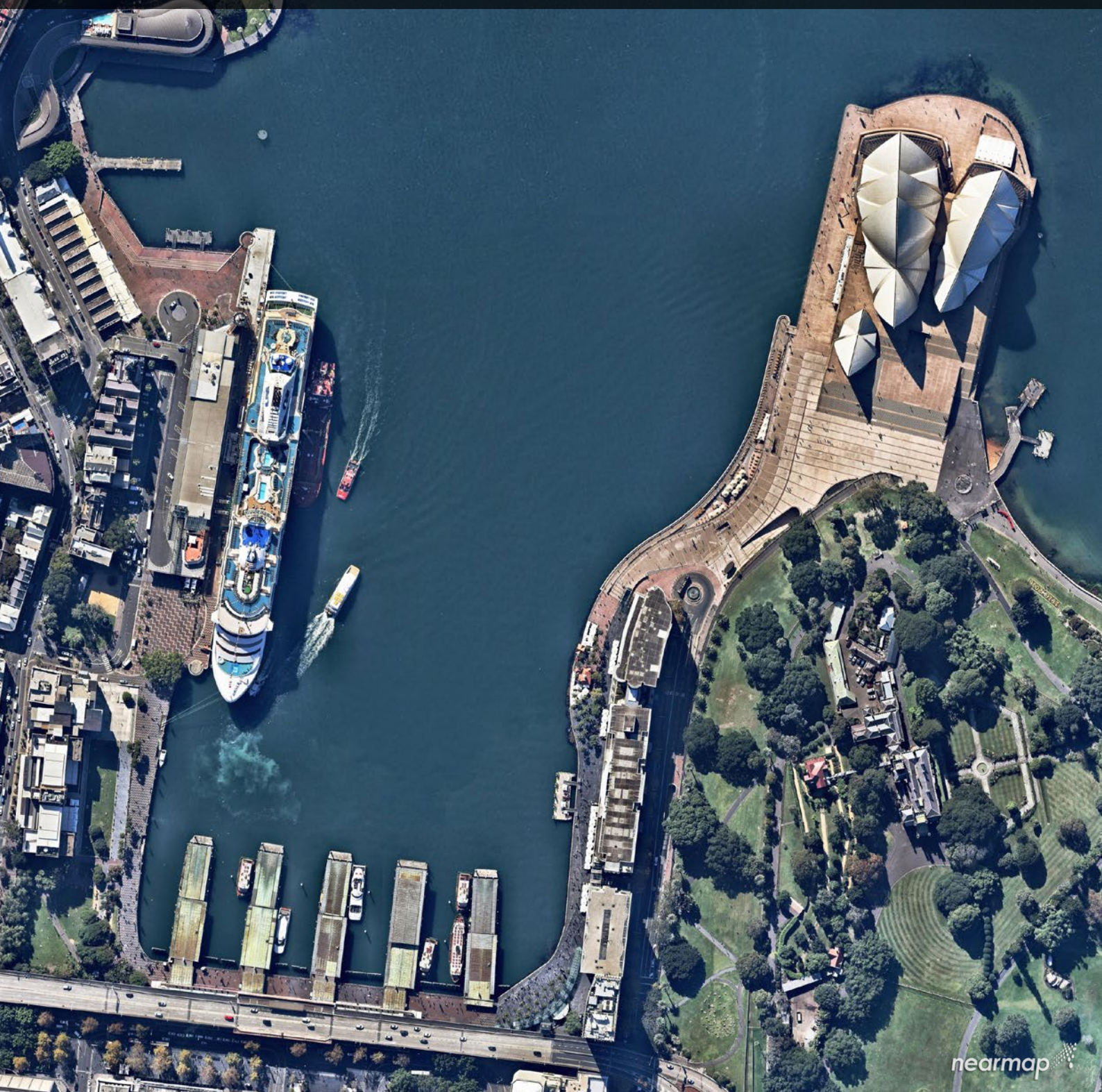
Wells, N. (1986). *The Atmosphere and Ocean: A Physical Introduction* (347 pages). Taylor & Francis, London.

Wood, H. O., and Neumann, F. (1931). Modified Mercalli intensity scale of 1931. *Bulletin of the Seismological Society of America*, 21(4), pp. 277-283.





# Platforms for Earth Observation





Remote sensing devices—both analogue and digital—may be operated from a variety of platforms. These can range from elevated, but ground-based, platforms such as tripods and cherry pickers, through balloons and aircraft (both manned and unmanned) at various altitudes within the Earth's atmosphere (up to about 100 km), to spacecraft, which operate outside the atmosphere. These different types of platforms provide variable performance in terms of image quality and repetitive coverage. The most commonly used platforms for remote sensing have been piloted aircraft and spacecraft, but deployment of remotely piloted or tower-mounted remote sensors is rapidly increasing.

Non spaceborne platforms such as aircraft, balloons, flux towers, hand-held instruments and ground sensors provide essential calibration and validation information for spaceborne sensor data and also offer valuable information in their own right. In addition to the use of specific sensors near the Earth, remotely sensed data has traditionally been compared with measurements and observations of ground features obtained from field surveys. This data is used to characterise specific sample locations, as points, lines or areas. Such locations or sites may be temporary or permanent, depending on the purpose of the survey, and its associated funding. There are now numerous national and international programs consistently and systematically collecting ground reference data for calibration and validation of remotely sensed data. The use of field data is further discussed in Section 10 below, Volume 1B—Section 9, and Volume 2E—Section 10.

The following sections describe the three broad types of platform used for Earth Observation (EO):

- ground-based (see Section 10);
- airborne (see Section 11); and
- spaceborne (see Section 12).

## Contents

<b>10</b>	Ground-based Platforms	129
<b>11</b>	Airborne Platforms	139
<b>12</b>	Spaceborne Platforms	145



# 10 Ground-based Platforms

Ground-based observations are collected to calibrate, validate and supplement airborne and spaceborne data. These can involve the use of *in situ* or ‘proximal’ sensors, mobile sensors or people, including hand-held sensors, vehicle-mounted sensors, temporary ground-based sensors and measurement of atmospheric properties. Such observations require accurate knowledge of location and typically provide a direct measure of some biophysical property for a specific target. ‘Close’ measurements enable the spectral properties of materials to be characterised directly, without interference from the atmosphere.

Ground-based measurements allow field sites to be monitored more frequently to identify variations related to diurnal and seasonal cycles, and more flexibly to respond to specific climatic events or emergencies. The spatial density of measurements can be designed to match the distribution and density of specific features, such as individual plants, and changed and repeated as required. As less expensive and more reliable hardware has become available, the use of ground-based remote sensors has increased rapidly, and this trend is expected to continue (Wark *et al.*, 2011).

Calibration data are also necessary to accurately locate observations on the ground. These data take many forms including Global Positioning System (GPS) locations, reflective targets, satellite laser ranging (to improve knowledge of the location of the satellite; see Volume 1B—Section 9), reference images and digital elevation models (see Volume 2A—Section 3 for details of image calibration approaches).

## 10.1 *In situ*

The calibration and validation (CalVal) of Earth Observation (EO) observations, and validation of information derived from the data, are increasingly reliant on records from *in situ* or proximal sensors installed at strategically located field sites. *In situ* sensors are generally installed in a network to measure specific physical properties of landscape attributes (such as water, leaves, or soil).

Instrumentation at CalVal sites record measurements continuously, or at regular intervals, for relevant physical parameters of the Earth surface and the atmosphere. *In situ* sensors are being used to record a wide range of measurements related to vegetation and carbon dynamics, soil moisture, gravity fields, topography, bathymetry, ocean colour, water quality, sea ice, and meteorology. Examples of *in situ* sensors include:

- lidar—used to determine Leaf Area Index (LAI) and vegetation profiles (e.g. VEGNET<sup>21</sup>, Culvenor *et al.* (2014); Portillo-Quintero *et al.* (2014); see also Volume 3A);
- IR thermometer or thermal camera—used to measure soil, water or vegetation temperature. (In vegetation, temperature variations are related to plant vigour since increased photosynthesis means increased transpiration resulting in a cooler plant.);
- solar radiometers—used to measure insolation;
- spectrometers—used to characterise vegetation, water and soil reflectance;
- video—used to identify species and/or monitor movement of plants, animals and clouds;
- audio—used to characterise sound spectrum, which has been linked to a ‘naturalness index’;

**Background image:** Intensity image created from the 1556 nm laser output of DWEL. This scan was taken in the Himalayan Cedar forest at the National Arboretum, Canberra. **Source:** Michael Schaefer, TERN AusCover/University of New England

21. <http://www.sensingsystems.com.au/public/VEGNET.pdf>



- carbon dioxide sensors—used to measure ecosystem-atmosphere exchanges in order to estimate primary productivity and carbon balances;
- soil water sensors—used to monitor the moisture available for plant growth;
- weather sensors—used to measure air temperature and pressure, precipitation, relative humidity, wind speed and direction; and
- cameras—including:
  - ♦ high spatial resolution digital images—used to characterise sample sites in detail; and
  - ♦ time-lapse photography—used to monitor phenology and temporal changes.

**Figure 10.1** Dual wavelength Echidna™ LIDAR (DWEL)

DWEL is a dual wavelength, ground-based lidar which can generate three-dimensional images of ground scenes.

a. DWEL instrument in operation.



b. False colour scan of Tumbarumba Forest using the Dual Wavelength Echidna LiDAR (DWEL), acquired August 2014. Dark colours shown the woody fraction and green colours show the vegetation fraction. Shading is scaled by distance such that lighter shades are further away from the scanner.



Source: Michael Schaefer, TERN Auscover/University of New England.

- In particular, gigapixel imagery (one billion ( $10^9$ ) pixels) capture very high spatial resolution in visible and NIR wavelengths for a broad range of applications (Brown *et al.*, 2012).

An example of one *in situ* sensor is the Dual Wavelength Echidna LIDAR (DWEL) illustrated in Figure 10.1, which comprises two lasers with different wavelengths that can generate precise three-dimensional images of forests and other objects, such as buildings. Such information provides a detailed record of structure at a particular time, and can be updated at selected time intervals to quantify change. VEGNET is a vegetation monitoring instrument that automatically scans the canopy on a daily basis using an upward-looking LIDAR sensor (see Figure 10.2). Operated as stand-alone instruments or as part of a distributed sensor network, this system complements the detailed three-dimensional structure measurements from Echidna by capturing the temporal variability in canopy structure (Culvenor *et al.*, 2014; Portillo-Quintero *et al.*, 2014; Griebel *et al.*, 2015).

---

*Calibration and validation ... can be considered a process that encompasses the entire system, from remote sensing instrument to data product. The objective is to develop a quantitative understanding and characterization of the measurement system and its biases in time and space.*  
(National Research Council, 2007)

---

**Figure 10.2** VEGNET scanner

VEGNET is a vegetation monitoring instrument that automatically scans the canopy on a daily basis using an in situ, upward-looking LIDAR sensor. This time lapse photo of VEGNET shows a few minutes of the laser scan.



Source: Amory Culvenor and Darius Culvenor, Environmental Sensing Systems

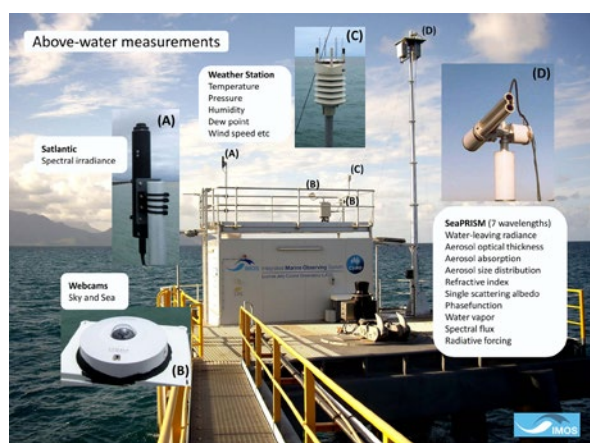
In Australia, CalVal sites are often designed to satisfy international scientific standards. Field sites enable collaboration with international EO researchers and are an important mechanism for interaction with satellite operators. Calibration sites at stable target locations ensure that the accuracy of airborne and EO data is known for specific conditions. Most developed countries now operate public data collection and sharing portals for ecosystem data, including CalVal data for remote sensing. In Australia, this capability is provided by the Terrestrial Ecosystem Research

Network (TERN<sup>22</sup>) and the Integrated Marine Observing System (IMOS<sup>23</sup>), along with key agencies such as Geoscience Australia, CSIRO and the Bureau of Meteorology. For example, an observation jetty for in-water measurements that is managed by CSIRO under IMOS is illustrated in Figure 10.3.

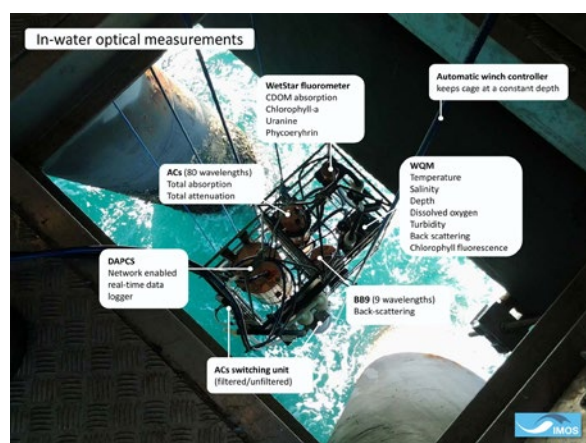
Towers that reach above vegetation canopies are being increasingly used for proximal sensing in terrestrial landscapes (see Figure 10.4). These instrumented towers or ‘flux’ towers house a range of sensors to remotely sense physical and chemical characteristics of key atmospheric and ecosystem processes. An international network of over 500 flux towers has been established to provide continuous, long-term micrometeorological measurements for global ecosystem monitoring, with a focus on understanding energy, carbon and water exchange between the atmosphere and major ecosystems. Flux towers use a suite of instruments and eddy covariance methods to measure exchanges of carbon dioxide, water vapour and energy between terrestrial ecosystems and the atmosphere (see also Volume 3). In the USA, the National Ecological Observatory Network (NEON)<sup>24</sup> will comprise 106 terrestrial and aquatic sites, which represent a diversity of vegetation, landforms, climate and ecosystem performance. Flux towers located at NEON terrestrial sites routinely measure the physical, chemical and biological parameters listed in Figure 10.5. The TERN OzFlux<sup>25</sup> network performs a similar function in Australia and New Zealand, comprising over 30 sites in a variety of locations and landscapes (see Figure 10.6).

**Figure 10.3** Marine in situ sensors

a. Lucinda Jetty Coastal Observatory (IMOS/CSIRO) showing instruments used for above-water measurements



b. Lucinda Jetty Coastal Observatory (IMOS/CSIRO) showing instruments used for in-water optical measurements



Source: Thomas Schroeder, CSIRO. IMOS (2016). Data was sourced from the Integrated Marine Observing System (IMOS), a national collaborative research infrastructure, supported by the Australian Government.

22. TERN: <http://www.tern.org.au>

23. IMOS: <http://www.imos.org.au>

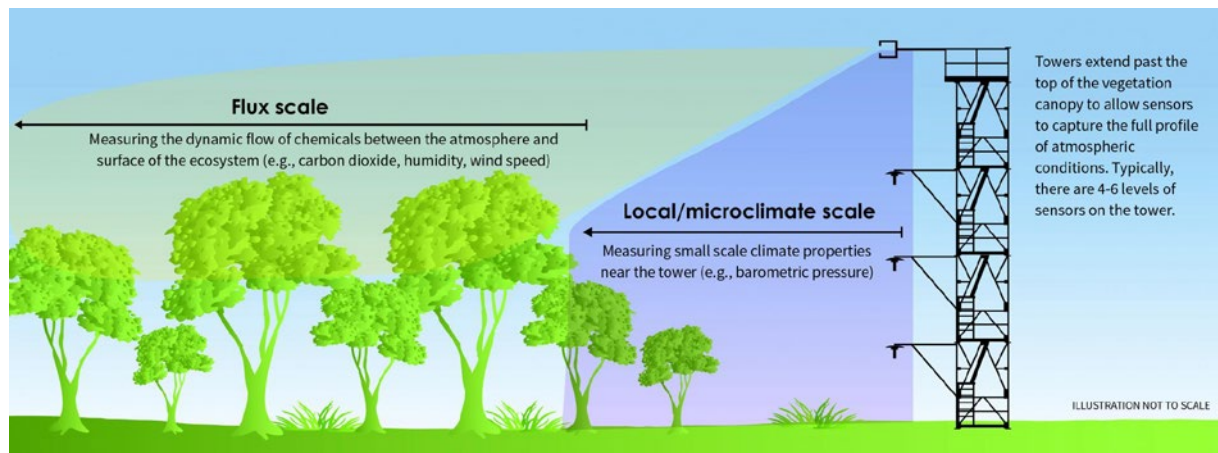
24. NEON: <http://www.neonscience.org>

25. TERN OzFlux: <http://www.ozflux.org.au>



**Figure 10.4** Flux Tower Function

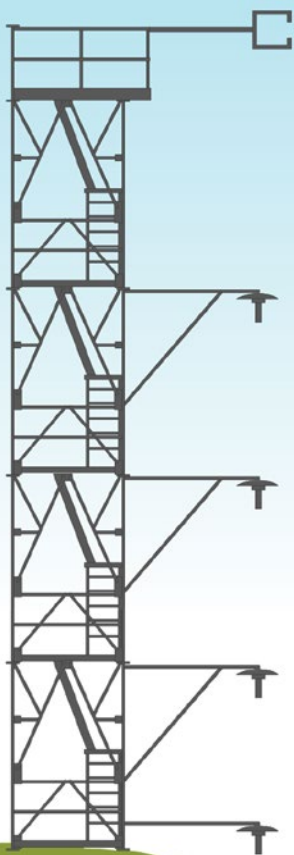
Flux towers use a suite of instruments and eddy covariance methods to measure exchanges of carbon dioxide, water vapour and energy between terrestrial ecosystems and the atmosphere.



Source: National Ecological Observatory Network, Inc (NEON). Retrieved from <http://www.neoninc.org/science-design/collection-methods/flux-tower-measurements>. The information provided may not have been reviewed or prepared by the NEON. It is provided AS IS without any warranty of any kind, express or implied, and may not reflect NEON's views or opinions.

**Figure 10.5** NEON flux tower measurements

Flux towers located at terrestrial sites in the National Ecological Observatory Network (NEON) routinely measure the parameters listed below.



Measurements	Frequency	Tower top	Mid-levels	Near ground surface
CO <sub>2</sub> /H <sub>2</sub> O concentration & flux	20 Hz	✓		
3D wind speed & direction	20 Hz	✓		
Dust (particulate mass)	2 wks	✓		
Dust (particulate size)	1 Hz	✓		
Aerosol optical depth	30 min	✓		
Secondary precipitation (absence/presence)	when event occurs	✓		
Direct & diffused radiation	1 Hz	✓		
Incident short-wave radiation	1 Hz	✓		
Net short-wave & net long-wave radiation	1 Hz	✓		
Wet deposition chemistry & precipitation isotope	2 wks	✓		
Phenological image & snow depth	15 min	At the tower top & 3 m above ground		
Isotopes in CO <sub>2</sub> , <sup>13</sup> C concentrations	.5 Hz	✓	✓	✓
Isotopes in H <sub>2</sub> O ( <sup>18</sup> O, <sup>2</sup> H concentrations)	.5 Hz	✓	✓	✓
CO <sub>2</sub> concentration	1 Hz	✓	✓	✓
H <sub>2</sub> O concentration	1 Hz	✓	✓	✓
PAR (Photosynthetically Active Radiation)	1 Hz	✓	✓	✓
Air temperature	1 Hz	✓	✓	✓
Biological temperature	1 Hz		✓	✓
2D wind speed & direction	1 Hz		✓	✓
Barometric pressure	1 Hz	4.95 m above ground		

Source: National Ecological Observatory Network, Inc (NEON). Retrieved from <http://www.neoninc.org/science-design/collection-methods/flux-tower-measurements>. The information provided may not have been reviewed or prepared by the NEON. It is provided AS IS without any warranty of any kind, express or implied, and may not reflect NEON's views or opinions.

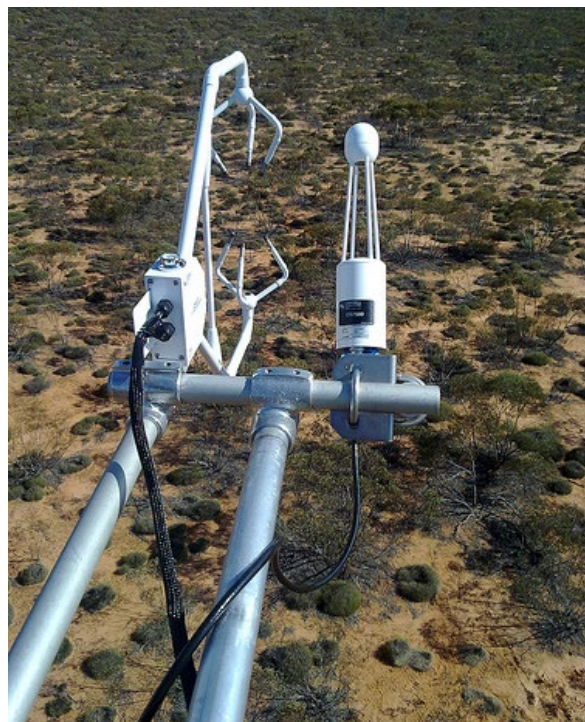
**Figure 10.6** TERN OzFlux flux towers

The TERN OzFlux network in Australia and New Zealand comprises flux towers at over 30 sites in a variety of locations and landscapes.

a. 80m tower at Warra Tall Eucalypt SuperSite, Tasmania



b. Example of flux instruments on tower at Calperum Mallee Supersite, SA



Source: TERN SuperSites and TERN OzFlux (Australian and New Zealand Flux Research and Monitoring) (2016). Retrieved from a. <http://www.supersites.net.au/supersites/wrra>; b. [http://www.ozflux.org.au/monitoringsites/calperum/calperum\\_pictures.html](http://www.ozflux.org.au/monitoringsites/calperum/calperum_pictures.html)

Some of the advantages of well-designed, wireless sensor networks over traditional field surveys include:

- reduced human effort with increased data output;
- increased spatial coverage in heterogeneous environments;
- synchronous sampling across sensors;
- real-time data retrieval; and
- reduced impact on ground area.

Use of *in situ* sensors involves multiple complexities and challenges, including power requirements, battery risks, network design, data storage and communications. The maintenance of field sensors also requires consideration of the adverse impact of wildlife (of all scales—insects, birds and mammals), water penetration, temperature extremes, UV damage, natural disasters, and vandals. When observing the natural environment, it is imperative that the operation of each sensor does not change the target in any way, nor interfere with natural processes.

The time series data produced by frequent *in situ* measurements is enabling a fresh look at the dynamics of ecosystems—from plant to biome scales.

Maximisation of the value of this unprecedented volume of data also demands new tools for data access and analysis. While the potential of *in situ* sensors for EO is still being realised, examples of their use are documented in Pastorello *et al.* (2011).

A number of countries are adopting standardised procedures for collecting field data using both proximal sensing instruments and quantitative sampling (such as Held *et al.*, 2015). Monitoring sites are typically instrumented, but can also require manual sampling due to the nature of the measurements and sampling schemes involved. To encourage consistency between monitoring sites, various international coordinating groups specify standards for common field measurements required for EO (such as the International Ocean Colour Coordinating Group (IOCCG)<sup>26</sup> for biological oceanography products, and the Group on Earth Observations (GEO)<sup>27</sup> and Committee on EO Satellites (CEOS)<sup>28</sup> Cal/Val working groups for validation of land products). For more information regarding *in situ* sensors and field surveys for EO the reader is referred to Held *et al.* (2015).

26. International Ocean Colour Coordinating Group (IOCCG): <http://www.ioccg.org>

27. Group on Earth Observation (GEO): <http://www.earthobservations.org>

28. Committee on Earth Observation Satellites (CEOS): <http://www.ceos.org>



## 10.2 Mobile Sensors

Mobile mapping embraces a broad range of instrumentation. Recent advances in technology have enabled the collection of high quality, geo-referenced remotely sensed data using a wide variety of devices. The availability of high definition digital cameras and other environmental sensors (such as spectrometers and laser ranging systems, and accurate, precise location (GPS) and attitudinal—inertial measurement—instruments) has extended significantly in parallel with open access software for combining environmental measurements with positional information. Many forms of mobile mapping are now employed by the general public, research institutions, governments and private industry in a range of application areas.

Mobile sensors effectively bridge the gap between terrestrial and airborne or satellite data. In most cases a measurement sensor is combined with a GPS on a mobile platform, which could be worn by an individual who is walking, diving or flying. Examples include:

- collections of digital photographs or terrestrial laser scanner data acquired from moving vehicles (such as Google Streetview, as illustrated in Figure 10.7a)—a technique that is commonly used for asset and infrastructure assessment along roads, railway lines and other utility supply corridors;
- detailed measurement of crop condition, moisture levels and/or soil properties for precision agriculture applications (Lamb *et al.*, 2008);
- tracking collars worn by livestock to monitor pasture usage and circulation patterns within paddocks (Falzon *et al.* (2013)—Figure 10.7b and Excursus 10.1); and
- hand-held sensors used in field work (see Figure 10.8).

In all cases, these measurements can be acquired at centimetre-scale pixels and tied to accurate and precise three-dimensional positioning data. Good examples of mobile sensing technologies include the Google photospheres, used to construct three-dimensional rendering of digital photographs for viewing in Google Earth, or Google Maps.

**Figure 10.7** Mobile sensors for Earth Observation

a. Google street view car



b. Tracking collar on cattle



Source: a. Google, [http://en.wikipedia.org/wiki/Mobile\\_mapping#/media/File:Google\\_Street\\_View\\_Car\\_in\\_Honolulu.jpg](http://en.wikipedia.org/wiki/Mobile_mapping#/media/File:Google_Street_View_Car_in_Honolulu.jpg); b. David Lamb, University of New England

**Figure 10.8** Hand-held sensors for Earth Observation

a. Measuring underwater spectra of coral



b. Measuring vegetated canopy in arid region of South Australia



Source: a. Arnold Dekker, CSIRO; b. Megan Lewis, University of Adelaide (Photo credit: Erika Lawley)

## Excursus 10.1—GPS tracking in Precision Agriculture

**Source:** David Lamb, UNE

**Further information:** <http://www.une.edu.au/parg>

Research Partners: Precision Livestock Research Alliance, UNE Precision Agriculture Research Group, CRCSI

- What is the role of different landscape systems in overall livestock production?
- Can stocking rates be better managed to optimize grazing pressure on different land systems?
- How could paddocks be better fenced to balance grazing variability?
- Space-based technologies are now being used to answer these questions.

### GPS tracking

GPS tracking is being increasingly used as a research tool for monitoring livestock activity. UNETracker is a low-cost, accurate and robust GPS collar that can be deployed in large numbers for monitoring the movement of stock and other animals (see Figure 10.9). This technology is being used on grazing properties to:

- map the movement of livestock in paddocks;
- correlate paddock grazing preferences with pasture type and productivity, elevation, aspect, slope, and soil characteristics; and
- monitor diurnal activity of livestock to distinguish between preferred grazing and camping locations (see Figure 10.10).

GPS collars are also being used to track:

- guard dogs and their interactions with wild dogs;
- movements of domestic and wild horses;
- sheep and their behavioural changes under parasite burden; and
- livestock in wetland environments.

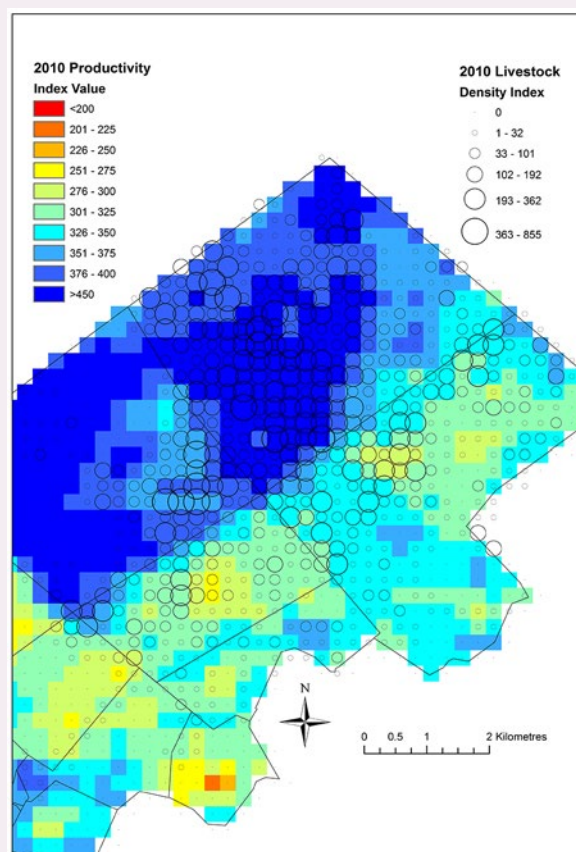
At Willoh Station, a mixed farming property near Brewarrina, NSW, cattle movement and pasture production were monitored from 2009 to 2010. *Pastures from Space* data (see Excursus 14.1) were used to map relative pasture productivity, and selected animals were tracked using GPS collars. The results from this study highlight the spatial variability in pasture utilisation, with significant under-utilisation of some areas. Farm productivity and profitability can be improved by identifying the underlying factors that determine such grazing patterns.

**Figure 10.9** UNETracker



**Figure 10.10** Livestock pasture usage compared with pasture productivity

In this image of Willoh Station for the period 2009 to 2010, the most productive pasture is shown as blue and least productive as red. Cattle show strong preference for some areas of pasture. Understanding the underlying reasons for this preference can help managers improve farm productivity.



## 10.3 Citizen Science and Crowdsourcing

An increasing number of individuals and groups are making observations and measurements of environmental conditions or events around the world. These include observing natural disasters, such as fires, floods, and earthquakes, but also more gradual environmental changes, such as pollution, vegetation extent and faunal abundance. In recent decades, the advent of portable technologies (such as cameras and GPS) in mobile phones has enabled non-scientists to make quantitative observations more frequently and more easily.

Citizen Science is defined as ‘the systematic collection and analysis of data; development of technology; testing of natural phenomena; and the dissemination of these activities by researchers on a primarily avocational basis’ (<http://www.openscientist.org/2011/09/finalizing-definition-of-citizen.html>). In short, this includes all people who contribute to traditional, organised science, whether officially employed to do so or not. Some Australian projects that are encouraging input from Citizen Scientists include the Atlas of Living Australia (<http://www.ala.org.au>), TeachWild (<http://www.teachwild.org.au>) and the Australian Seismometers in Schools network (<http://www.ausis.edu.au>). Each of these endeavours involves citizen input into an organised and regulated system of observations that can be cross-checked against existing knowledge.

A new category of observations about the Earth, namely crowdsourcing, is also emerging from the proliferation of mobile phones and associated devices. Crowdsourcing, ‘obtaining needed services, ideas, or content by soliciting contributions from a large group of people, and especially from an online community, rather than from traditional employees or

suppliers’ (<http://www.merriam-webster.com/dictionary/crowdsourcing>), is similar, but not necessarily synonymous with Citizen Science. This input may provide useful information, but its unregulated nature requires that it be used with caution in scientific analyses. However, now that collection and checking standards can be applied to very large data sets, these data are used increasingly. For example, photos collected at field sites by members of the public can be uploaded and used to check various maps derived from remotely sensed imagery (see <http://www.geo-wiki.org>; in Australia: <http://www.geo-wiki.org/branches/auscover/>; see also the Atlas of Living Australia). Similarly, implementations of Volunteered Geographic Information (VGI) allow citizens to contribute local and current knowledge and images to global web-based repositories (Goodchild, 2007). Examples include the Wikimapia gazetteer (<http://www.wikimapia.org>) and OpenStreetMap (<http://www.openstreetmap.org>). These systems enable timely updates to be disseminated rapidly, which are particularly valuable during natural disaster events.

While data from Citizen Science and Crowdsourcing may be used to supplement existing data about environmental conditions and events, these sources cannot be relied upon to the same extent as other forms of ground-based remote sensing, so are not recommended to validate EO analyses. It is important that all data sources can be calibrated and verified before being used as reference data. Multiple subjective observations may provide useful contextual information, but cannot be substituted for objective measurements. Quite simply, in science, consensus is not the same as truth. The issue of ‘Trust in Data’ is further explored in Hudson (2015).

---

*Anti-intellectualism has been a constant threat winding its way through our political and cultural life, nurtured by the false notion that democracy means that my ignorance is just as good as your knowledge.*  
(Isaac Asimov)

---



## 10.4 Further Information

### Research Networks:

Terrestrial Ecosystem Research Network (TERN): <http://www.tern.org.au>

Integrated Marine Observing System (IMOS): <http://www.imos.org.au>

TERN OzFlux: <http://www.ozflux.org.au>

TERN SuperSites: <http://www.supersites.net.au/>

NEON: <http://www.neoninc.org>

### Ground-based Measurements:

AusCover Good Practice Guidelines (Held *et al.*, 2015)

Flux towers Measurements: <http://www.neoninc.org/science-design/collection-methods/flux-tower-measurements>

International Ocean Colour Coordinating Group (IOCCG): <http://www.ioccg.org>

Dual Wavelength Echidna LIDAR (DWEL): <http://www.auscover.org.au/DWEL>

### International Committees:

Group on Earth Observation (GEO): <http://www.earthobservations.org>

Committee on Earth Observation Satellites (CEOS): <http://ceos.org>

## 10.5 References

- Brown, T., Zimmermann, C., Panneton, W., Noah, N., and Borevitz, J. (2012). High-resolution, time-lapse imaging for ecosystem-scale phenotyping in the field. *Methods in molecular biology*, 918, pp. 71-96. doi:[http://dx.doi.org/10.1007/978-1-61779-995-2\\_7](http://dx.doi.org/10.1007/978-1-61779-995-2_7).
- Culvenor, D. S., Newnham, G. J., Mellor, A., Sims, N. C., and Haywood, A. (2014). Automated In-Situ Laser Scanner for Monitoring Forest Leaf Area Index. *Sensors*, 14(8), pp. 14994-15008. doi:<http://dx.doi.org/10.3390/s140814994>.
- Falzon, G., Trotter, M. G., Schneider, D., and Lamb, D. W. (2013). Correlating movement patterns of merino sheep to faecal egg counts using global positioning system tracking collars and functional data analysis. *Small Ruminant Research*, 111(1-3), pp. 171-174. doi:<http://dx.doi.org/10.1016/j.smallrumres.2012.09.001>.
- Goodchild, M. F. (2007). Citizens as Sensors: The World of Volunteered Geography. *GeoJournal*, 69(4), pp. 221-221.
- Griebel, A., Bennett, L., Culvenor, D., Newnham, G., and Arndt, S. (2015) Reliability and limitations of a novel terrestrial laser scanner for daily monitoring of forest canopy dynamics. *Remote Sensing of Environment*, 166(1): 205-213.
- Held, A., Phinn, S. R., Soto-Berelov, M., and Jones, S. (2015). AusCover Good Practice Guidelines: A technical handbook supporting calibration and validation activities of remotely sensed data products. TERN AusCover. Retrieved from <http://www.auscover.org.au/xwiki/bin/view/Good+Practice+Handbook/WebHome>.
- Hudson, D. (2015). Uptake of sensor data in emergency management. (Ph.D thesis), Fenner School, Australian National University.
- IMOS (2016). Integrated Marine Observing System. Retrieved from <http://www.imos.org.au/>.
- Lamb, D. W., Frazier, P., and Adams, P. (2008). Improving pathways to adoption: Putting the right P's in precision agriculture. *Computers and Electronics in Agriculture*, 61(1), pp. 4-9. doi:<http://dx.doi.org/10.1016/j.compag.2007.04.009>.
- National Research Council (2007). *Earth Science and Applications from Space: National Imperatives for the Next Decade and Beyond* (454 pages). The National Academies Press, Washington, DC. doi:<http://dx.doi.org/doi:10.17226/11820>.
- Pastorello, G. Z., Sanchez-Azofeifa, G. A., and Nascimento, M. A. (2011). Enviro-Net: From Networks of Ground-Based Sensor Systems to a Web Platform for Sensor Data Management. *Sensors*, 11(6), pp. 6454-6479. doi:<http://dx.doi.org/10.3390/s110606454>.
- Portillo-Quintero, C., Sanchez-Azofeifa, A., and Culvenor, D. (2014). Using VEGNET In-Situ Monitoring LiDAR (IML) to Capture Dynamics of Plant Area Index, Structure and Phenology in Aspen Parkland Forests in Alberta, Canada. *Forests*, 5(5), pp. 1053-1068. doi:<http://dx.doi.org/10.3390/f5051053>.
- Wark, T., O'Rourke, D., Kottege, N., Hu, W., and Moore, D. (2011). Opportunities for multimedia environmental sensor networks. *IEEE COMSOC MMTC E-letter*, 6(12), pp. 5-8.





# 11 Airborne Platforms

Various forms of Earth Observation (EO) sensors have been carried on a wide variety of airborne platforms for over a century, including balloons, blimps, unmanned aerial vehicles (UAV) and manned aircraft. Various aerial platforms are now widely used to acquire detailed imagery of Earth surface features. In this context, aerial platforms range from expensive, large, fixed wing aircraft to low-cost, remotely operated systems, which are commercially available. Airborne platforms are also used to simulate and validate satellite-borne sensors and can acquire data at times when weather may limit the utility of satellite image acquisition.

Acquiring EO data from airborne sensors has the advantage of flexibility—in timing, instrumentation and coverage. This flexibility ensures that the acquired data coincide with favourable atmospheric conditions and optimal target discrimination over the region of interest. This is particularly advantageous for natural disasters, such as bushfires or floods, where timely information is required to both direct the response effort and record the severity of the event. Timely information is also valuable for monitoring agricultural production and national security.

For remote sensing, aircraft have traditionally used photographic devices, however, these have almost been completely replaced in the past decade by metric, multispectral digital cameras. As detailed in Section 13, these sensors can record radiation over a wider spectral range than photographic devices and provide data in (multispectral) digital format.

To obtain an image swath of sufficient width, aircraft scanners generally use wider scan angles than satellite scanners. This angle is referred to as the Field of View (FOV) and may be between 70° and 90°. However, image pixel size is determined by a constant angle of view (known as the Instantaneous Field of View: IFOV). As shown in Figure 11.1, the effects of panoramic distortion become quite significant toward the edges of the FOV with the ground pixel size increasing many times across each scan line.

For image sensors that acquire data using a scanning mechanism (see Section 14.2), aircraft provide a less stable platform than spacecraft and result in imagery with significant geometric distortions (which requires subsequent correction by specific rectification processing—see Volume 2B). Frame-based digital imagery, however, which dominates the aerial sector of EO image acquisition, is captured from a central perspective (see Section 14.2) and is thus not impacted by platform instability. While the instability inherent to aerial platforms has complicated image mosaicking between adjacent flight lines acquired by scanning sensors, recent advances in camera and image processing technologies now enable production of high resolution, orthorectified image products with large area coverage (such as Nearmap imagery<sup>29</sup>).

Airborne platforms for EO are discussed below in terms of manned aircraft (see Section 11.1) and remotely piloted (or unmanned) aircraft (see Section 11.2).

---

*Heavier-than-air flying machines are impossible.*  
(Lord Kelvin, President, Royal Society, 1895)

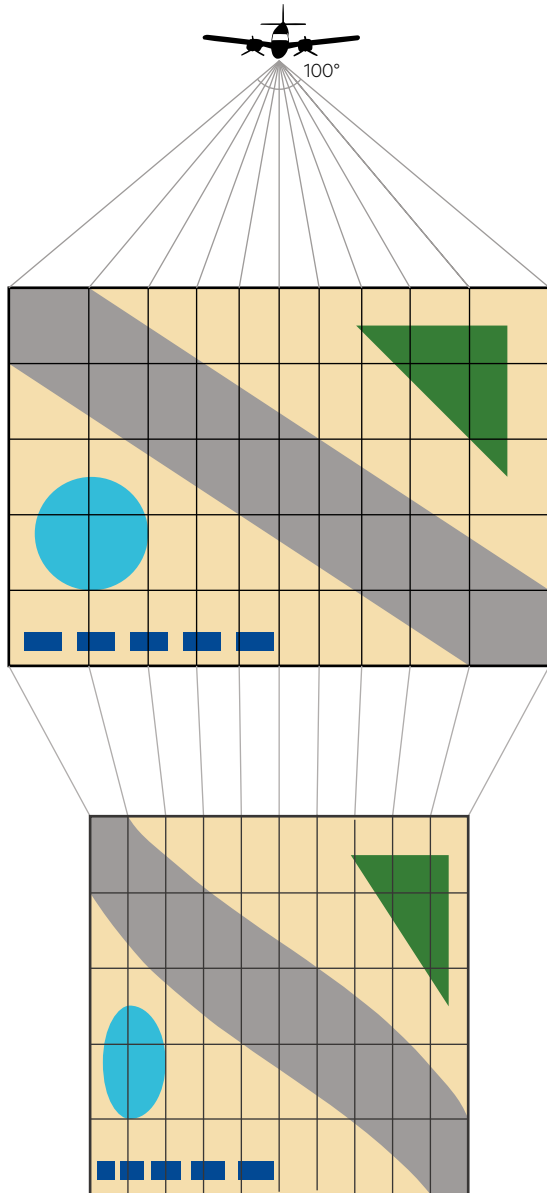
---

Background image: Nearmap high resolution airborne image acquired on 5 May 2016 over the Sydney Opera House and Circular Quay. Source: © Nearmap

29. nearmap: <http://au.nearmap.com>

**Figure 11.1** Effect of wide scan angle

- a. Panoramic distortion: ground pixel width increases significantly away from a vertical view.
- b. Resulting image distortions: image features have lateral distortion when displayed with a constant pixel width.



Adapted from: Harrison and Jupp (1992) Figure 18

---

*The example of the bird  
does not prove that man can fly.  
Imagine the proud possessor of the aeroplane  
darting through the air at a speed of  
several hundred feet per second.  
It is the speed alone that sustains him.  
How is he ever going to stop?  
(Simon Newcomb, 1903)*

---

## 11.1 Manned Aircraft

Aircraft offer maximum flexibility for acquiring remotely sensed imagery in terms of mission timing, altitude and selection of spectral regions and gains. A flight may be scheduled to coincide with the best daily or seasonal conditions and avoid poor weather or cloud cover. The image spatial resolution is determined by a combination of flight altitude and sensor characteristics so flying height can be selected to best suit each application. Aircraft imagery also potentially offers much finer spatial resolution than

can currently be obtained from non-military remote sensing satellites (see Figure 11.2). Airborne scanners frequently provide more spectral bands with narrower spectral bandwidth, which can be selected to detect specific targets. Similarly, the preferred view angle and direction may be specified for each flight, allowing the acquisition of stereo pairs of imagery if required. However, aircraft imaging missions are generally more expensive and more restricted in spatial coverage than satellite-derived imagery for the same area.



**Figure 11.2** Nearmap imagery

This bird's eye view of Sydney's Wet'n'wild shows the water park in great detail



Source: © Nearmap

Aerial imaging can be acquired from both low and high altitude aircraft, including ultralights (Alexander, 2008) and helicopters (see Figure 11.3). Low-altitude platforms (<10 km) tend to fly more slowly, have moderate stability, can be operated from remote sites and offer limited coverage (< 1,000 km<sup>2</sup>), whereas high-altitude platforms travel at faster speeds, with more stability and greater coverage (> 10,000 km<sup>2</sup>), but are restricted to excursions from large airports.

While airborne EO data may be more expensive than data acquired from satellite borne sensors for some applications, recent improvements mean significant areas can be covered and processed rapidly and automatically, thereby enabling the delivery of accurate and cost-effective solutions for regional areas (for example, Nearmap<sup>30</sup>—see Excursus 11.1). Licensing arrangements for most airborne EO data, however, are generally more relaxed and favourable to 'creative commons' licensing than those applying to some high resolution sources of spaceborne imagery.

In some circumstances airborne sensors can replace the service provided by satellite EO capabilities, for example in high spatial resolution images of major cities. However, there are also substantial disadvantages to airborne sensors including mobilisation costs, inconsistent timing of observations, limited coverage, difficulties obtaining repeat observations, and calibration of observations.

These problems are lessening as digital camera systems are used more consistently over larger area projects. As the industry matures, these problems will be reduced but not altogether removed.

**Figure 11.3** Some manned airborne platforms

a. Cessna 414—used for low to mid-altitude flights



b. Beechcraft Kingair 200T—used for mid to high altitude flights



c. Learjet—used for high altitude flights



Source: Robert Norman, Air Affairs Australia Pty Ltd

30. Nearmap: <http://au.nearmap.com>



## Excursus 11.1—High resolution aerial imagery

**Source:** Nearmap

**Further information:** <http://nearmap.com.au>

High resolution aerial imagery acquired and processed by Nearmap helps organisations inspect locations remotely by seeing what is on the ground, in great detail, and how it has changed over time. This unique technology enables aerial imagery and digital elevation data to be processed and published online within days of capture. Both current and historical imagery is available for tracking change over time. (see Figure 11.3).

This imagery is being used by organisations across all industries for:

- business development—identifying sites with business potential or newly developed areas;
- estimating & quoting—solar panel positioning, estimate property values, estimate material needed for a job/project, measuring objects for instant quoting;
- planning and inspecting—site planning, site assessment, site measurement;
- monitoring and validating—validating data and measurements, monitor project progress, observing vegetation and seasonal changes;
- risk assessment—assessing road conditions, vegetation risk, on-site hazards, determining site accessibility; and
- communicating—including imagery in presenting, OH&S reports, emergency maps (see Figures 11.4 to 11.7).

**Figure 11.4** Urban development

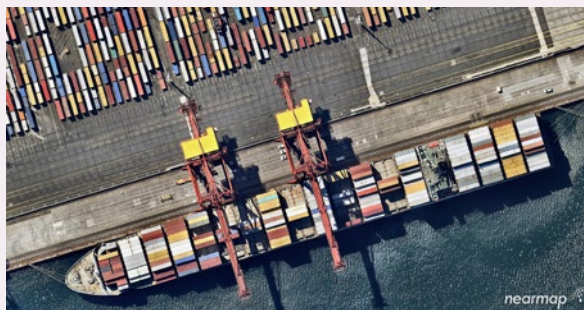
High resolution, aerial image of the man-made James Cook Island in Sylvania Waters, approximately 25km south of Sydney CBD.



Source: © Nearmap

**Figure 11.5** Port operations

Aerial image of port operations in one of Port Botany's container terminals in Botany, NSW



Source: © Nearmap

**Figure 11.6** Monitoring construction projects

This high resolution Perth Stadium in Perth, WA is a 60,000 seat capacity facility due to be completed for the 2018 AFL season.



Source: © Nearmap

**Figure 11.7** Mining operations

The Super Pit, largest open pit gold mine in Australia, located in Kalgoorlie, WA.



Source: © Nearmap

## 11.2 Remotely Operated Aircraft

Remotely piloted aircraft (RPA; or remotely piloted aircraft systems: RPAS) are also known as drones or unmanned aerial vehicles (UAV)<sup>31</sup>. As the name implies, these systems allow an airborne platform to be controlled remotely, without a pilot, and comprise an increasing range of capabilities, including:

- simple, cheap individually operated airborne systems (see Figure 11.8a);
- larger commercial grade systems with metric digital cameras or multi/hyperspectral and lidar systems, precise positioning and attitudinal measurement capabilities (see Figure 11.8b); and
- military-grade surveillance aircraft with size similar to small light aircraft (see Figure 11.8c).

In each case, both platforms and/or sensors can be pre-programmed to capture data over a certain area or be operated manually. This provides maximum flexibility in terms of user control on data acquisition, however the area being covered by these systems is limited, with smaller model aircraft, glider, and heli/octo/quad-copters covering up to 1km<sup>2</sup>, while larger commercial systems, with bigger platforms, covering tens of square kilometres in a day. Surveillance systems operated for military purposes can cover thousands of square kilometres in a day.

The payload and on-board power that can be carried by each platform also determines its data acquisition capabilities, with the smallest systems being limited to carrying digital cameras and GPS, and commercial systems capable of carrying multi/hyperspectral or lidar sensors with a GPS and IMU. The surveillance systems can have larger and higher quality sensors and positional measurements as well as larger data storage and real-time data transmission capabilities. Currently, this is an emerging area with government agencies and private industry investing heavily in commercial grade systems to assist with fieldwork, collect highly detailed spatial data and provide detailed data for calibration/validation of satellite image data sets. For example, the Terraluma project<sup>32</sup> integrates unmanned aircraft systems and specialised sensors for a range of EO applications (Lucieer *et al.*, 2014b; Turner *et al.*, 2014; Wallace *et al.*, 2014). Such systems allow multispectral (optical and thermal), hyperspectral and lidar imagery to be recorded simultaneously at high spatial resolution (Lucieer *et al.*, 2014a). One of the unmanned aircraft platforms currently employed in the Terraluma project is illustrated in Figure 11.8b.

**Figure 11.8** Remotely piloted aircraft systems

a. Maja UAV (1 kg payload; 20–30 minute flight)



b. Mikrokoopter Oktokopter (1kg payload; 5 minute flight)



c. Military operations—Reaper, part of 39 Squadron Royal Air Force, is used for intelligence, surveillance and reconnaissance in Afghanistan. This is a medium-to-high altitude, long endurance RPAS.



Source: a: Arko Lucieer, University of Tasmania (Terraluma). Retrieved from <http://terraluma.net/platforms/fixed-wing-uavs/>  
 b: Arko Lucieer, University of Tasmania (Terraluma). Retrieved from <http://terraluma.net/platforms/multi-rotor-uavs/>  
 c: Cpl Mark Webster/MOD (OGL 1.0). Retrieved from [https://commons.wikimedia.org/wiki/File:Reaper\\_Remotely\\_Piloted\\_Air\\_System\\_\(RPAS\)\\_MOD\\_45152482.jpg](https://commons.wikimedia.org/wiki/File:Reaper_Remotely_Piloted_Air_System_(RPAS)_MOD_45152482.jpg)

31. Civil Aviation Safety Authority: <http://casa.gov.au>

32. Terraluma: <http://www.terraluma.net/index.html>



## 11.3 Further Information

---

Airborne Research Australia (ARA): <http://aras.flinders.edu.au>

AAM Group: <http://www.aamgroup.com>

Nearmap: <http://www.nearmap.com>

Spookfish: <https://www.spookfish.com>

Terraluma: <http://www.terraluma.net>

## 11.4 References

---

Alexander, D. (2008). Remote sensing and the coast: Development of advanced techniques to map nuisance macro-algae in estuaries. *New Zealand Geographer*, 64(2), pp. 157-161. doi:<http://dx.doi.org/10.1111/j.1745-7939.2008.00140.x>.

Harrison, B. A., and Jupp, D. L. B. (1992). Image Rectification and Registration. Part FOUR of the microBRIAN Resource Manual (draft only). MPA, Melbourne.

Lucieer, A., Malenovsky, Z., Veness, T., and Wallace, L. (2014a). HyperUAS—Imaging Spectroscopy from a Multirotor Unmanned Aircraft System. *Journal of Field Robotics*, 31(4), pp. 571-590. doi:<http://dx.doi.org/10.1002/rob.21508>.

Lucieer, A., Turner, D., King, D. H., and Robinson, S. A. (2014b). Using an Unmanned Aerial Vehicle (UAV) to capture micro-topography of Antarctic moss beds. *International Journal of Applied Earth Observation and Geoinformation*, 27, pp. 53-62. doi:<http://dx.doi.org/10.1016/j.jag.2013.05.011>.

Turner, D., Lucieer, A., Malenovsky, Z., King, D. H., and Robinson, S. A. (2014). Spatial Co-Registration of Ultra-High Resolution Visible, Multispectral and Thermal Images Acquired with a Micro-UAV over Antarctic Moss Beds. *Remote Sensing*, 6(5), pp. 4003-4024. doi:<http://dx.doi.org/10.3390/rs6054003>.

Wallace, L., Lucieer, A., and Watson, C. S. (2014). Evaluating Tree Detection and Segmentation Routines on Very High Resolution UAV LiDAR Data. *IEEE Transactions on Geoscience and Remote Sensing*, 52(12), pp. 7619-7628. doi:<http://dx.doi.org/10.1109/tgrs.2014.2315649>.



# 12 Spaceborne Platforms

Spacecraft, both manned and unmanned, have provided platforms for a wide range of remote sensing devices since the early days of space exploration. The majority of Earth Observation (EO) data comes from satellites with imaging sensors in either polar (north-south circle around earth) or geostationary (above a fixed location) orbits. These systems are operated by national space and weather agencies, private companies, and military organisations.

Spaceborne platforms offer several advantages over lower altitude platforms, particularly:

- a synoptic viewing position for regional and global coverage of the Earth's surface;
- frequent and predictable overpasses (by most spaceborne platforms); and
- standardised imaging characteristics.

## 12.1 Manned Spacecraft

Various manned spacecraft have acquired large series of space photography and a number have operated scanning systems<sup>33</sup>. These spacecraft operate between about 60° north and south of the equator at altitudes between approximately 200–500 km to enable safe re-entry and recovery of vehicle, instrumentation, and, most importantly, crew.

The spatial resolution of space photography varies considerably, with reported image pixel size being between 5 m and 150 m. The operator-controlled nature of image collection allows selection of solar illumination angle and viewing direction. As the mode of acquisition does not yet provide for regular, repetitive coverage, the utility of the imagery is generally limited to inventory-type surveys rather than monitoring studies.

The US Mercury, Gemini and Apollo series of satellites, launched during the 1960s, provided over 1,000 normal colour photographs and some false colour infrared photographs taken from hand-held 70 mm cameras. While these images have been the subjects of considerable research, their age, oblique view and restricted coverage limit their current utility for environmental applications. The Apollo mission also tested the usefulness of multispectral imagery taken from a simultaneously triggered array of four 70 mm cameras, which were fitted with filters

simulating Landsat MSS spectral bands. The positive results of this test contributed to the development of the Landsat series of unmanned satellites.

Other manned spacecraft include Skylab, in the 1970s, and the Space Shuttle series, in the 1980s. Skylab was launched in May 1973 and decommissioned in February 1975. It carried several instrument packages including the EREP (Earth Resources Experiment Package), which contained a 13-channel scanner called the S192 MSS. This scanner sampled visible, near infrared, middle infrared and thermal infrared wavelengths and produced imagery of comparable spatial resolution to the Landsat MSS.

The Space Shuttle series were reusable spacecraft, designed to commute between the Earth and space. The shuttles have carried a range of remote sensing equipment, including the Metric Camera, Large Format Camera, the first test of the Modular Optical-Electronic MSS (MOMS) and the Shuttle Imaging Radar (SIR) experiments. The latter have provided unique microwave imagery of selected regions of the Earth's surface. These have been used for research into radar applications and the development of operational, satellite-borne radar imagers. The Space Shuttle was the base platform for the most comprehensive global digital elevation mapping project completed to date, the Shuttle Radar Topography Mapping Mission (SRTM). SRTM data are publicly available as a digital elevation surface at a range of pixel sizes<sup>34</sup>.

**Background image:** Southern portion of the full disk image captured by Himawari-8 geostationary satellite on 1 January 2016, displayed as natural colour composite. **Source:** © Bureau of Meteorology/JMA

33. NASA Astronaut photography: <http://eol.jsc.nasa.gov>

34. Shuttle Radar Topography Mapping Mission: <http://srtm.usgs.gov/index.php>



In the USSR, the major remote sensing space platforms have been manned satellites with a manned space station having been established in 1986. These platforms carried a variety of photographic equipment at an altitude of 250 km. The equivalent pixel resolution of available Russian space photography varies between 5 m and 60 m and is acquired in both multi-band and panchromatic format.

With the decommissioning of the Space Shuttle, the International Space Station (ISS) has now become a similar research and development site<sup>35</sup>. At present the ISS has several windows established specifically for imaging sensor payloads, the most recent example being the Hyperspectral Coastal Imager (HICO)<sup>36</sup>.

## 12.2 Satellites

Data acquired by EO satellites provide numerous benefits for studying the Earth's surface and atmosphere, including:

- continuous acquisition of data over time periods suited to monitoring a range of processes;
- regular revisit capabilities, resulting in frequent and up-to-date information, from two minutes (Geostationary) to daily and weekly;
- multiple spatial scales of collection, from site specific (0.5 m pixels over 10's km<sup>2</sup>) to continental and global (1000 m pixels over 10<sup>6</sup>'s km<sup>2</sup>) coverage;
- range of spectral resolutions sampling several parts of the EM spectrum;
- ability to enhance or manipulate digital data with a wide range of software;
- ability to combine satellite digital data with other digital data;
- cost effective data source, much of which is freely available;
- good geo-locational accuracy;
- possibility of stereo viewing; and
- large archive of historical data.

Particular advantages offered by satellites over airborne platforms include:

- regular, repeated acquisition at predictable times;

- consistency of data in terms of spatial, spectral, radiometric and temporal characteristics;
- breadth of coverage; and
- extent and availability of archival data (Geoscience Australia, 2016).

Satellites can be differentiated in terms of several orbital characteristics as summarised in Table 12.1.

Satellite orbits are commonly classified into three groups in terms of altitude:

- low Earth orbit (LEO: 180–2,000 km)—used for polar orbiting EO satellites, the International Space Station (ISS) and the Hubble Telescope;
- medium Earth orbit (MEO: 2,000–35,780 km)—used for navigation and speciality satellites; and
- high Earth orbit (HEO: 35,780 km)—used for meteorological satellites (NASA, 2009).

A range of different orbital inclinations and shapes (or eccentricities) are used for satellites, some of which are summarised in Table 12.2 and illustrated in Figures 12.1 and 12.2. The most commonly used satellite orbits for EO are:

- geostationary—used for meteorological and communications satellites (see Section 12.2.1); and
- sun-synchronous or (near) polar—used for most other EO satellites (see Section 12.2.2).

**Table 12.1** Satellite orbital characteristics

Characteristic	Description
Altitude	Height above mean sea level (km)
Inclination	Angular distance between the satellite orbital plane and Earth's equator (decimal degrees)
Eccentricity	Deviation of the orbit shape from a perfect circle
Period	Time taken to complete one overpass of Earth (minutes or orbits/day)
Repeat Cycle	Interval between overpasses at a given point (days or orbits/year)
Equatorial Crossing Time	Time satellite passes over the equator (24 hour clock in local time)

35. International Space Station sensors: [http://www.nasa.gov/mission\\_pages/station/research/benefits/remote\\_sensing.html](http://www.nasa.gov/mission_pages/station/research/benefits/remote_sensing.html)

36. Hyperspectral Coastal Imager: <http://hico.coas.oregonstate.edu/>

**Table 12.2** Types of satellite orbits

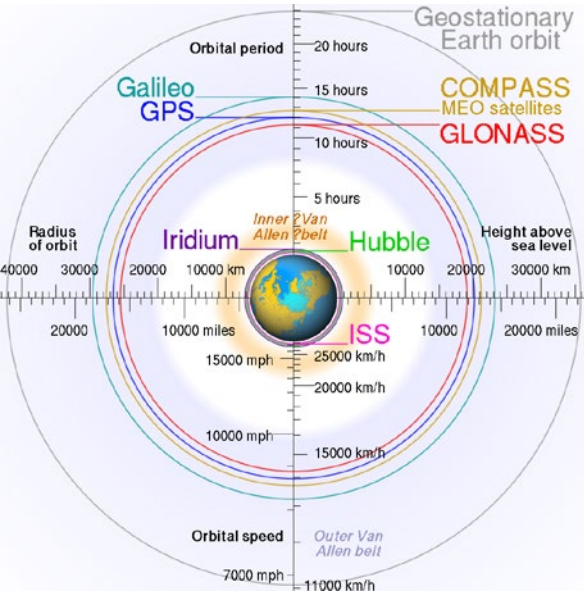
LEO: low Earth orbit; MEO: Medium Earth orbit; HEO: High Earth orbit

Characteristic	Description	Typical altitude	Advantages
Polar	Satellite that (nearly) passes from pole to pole as Earth rotates beneath it (inclination ~ 90°)	LEO	Polar coverage
Sun-synchronous, near polar	Satellite follows a near polar and near circular orbit and passes over a given point on the Earth's surface at the same local time on each overpass	LEO	Minimises surface illumination and shadowing differences, so commonly used for Earth Observation
Semi-synchronous	Satellite orbital period equals 12 hours (half the rotational period of Earth) and is near circular	MEO	Frequent coverage
Molniya	Highly elliptical orbit inclined at 63.4° (and 111.6°) with 2 revolutions of Earth per day	MEO	Optimum coverage of high northern latitudes, so used by Russian satellites
Equatorial	Satellite follows a near equatorial orbit, usually circular (inclination ± 9°)	HEO	Equatorial coverage; observing tropical weather patterns
Geostationary	Circular orbit at an average altitude of 35,786 km above the equator (inclination 0°) at a specific longitude moving with Earth's rotation such that the satellite appears to remain stationary when viewed by an observer at a particular location on Earth <sup>39</sup>	HEO	One hemisphere of Earth is viewed continuously, so used for communications, weather and global coverage

Source: NASA (2009)<sup>37</sup>

**Figure 12.1** Comparison of satellite orbits

Stylised view of satellite orbits around Earth, from a perspective above the North pole.. The outer ring (~36,000 km altitude) shows the geostationary orbit, commonly used for meteorological satellites. Middle rings are medium Earth orbits (20,000–25,000 km altitude), which are primarily used for navigation satellites. The inner rings depict the low Earth orbits (180–2,000 km) of the Hubble Space Telescope, the International Space Station (ISS) and Iridium constellation. In this graphic, all orbits have been shown on common, equatorial plane for comparison, but only the geostationary orbit is equatorial—all others are significantly inclined (see Figure 12.2). The Moon orbits at a distance around nine times further from Earth than the geostationary orbit.

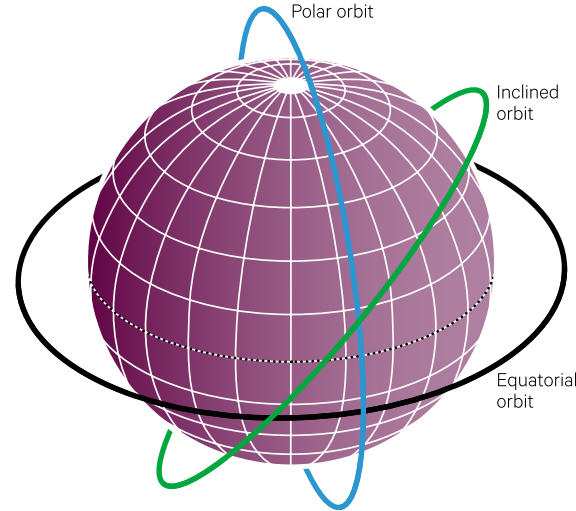


Source: Geo Swan (CC-BY-SA 3.0). Retrieved from: [https://en.wikipedia.org/wiki/Geostationary\\_orbit#/media/File:Comparison\\_satellite\\_navigation\\_orbits.svg](https://en.wikipedia.org/wiki/Geostationary_orbit#/media/File:Comparison_satellite_navigation_orbits.svg)

It is worth noting that the number of ‘objects’ orbiting Earth is increasing each year, with nearly 300 launches in 2014 alone (see Volume 1B—Section 10.1.2). 70% of catalogued objects are in LEO where satellites travel at the fastest speeds, with a greater density at higher latitudes (see Figure 12.3).

**Figure 12.2** Some orbital inclinations

The inclination of a satellite orbit indicates the relationship between the orbital plane and Earth’s equator. The orbital inclination of many EO satellites is near polar, typically covering the latitudes 82° N and 82° S.



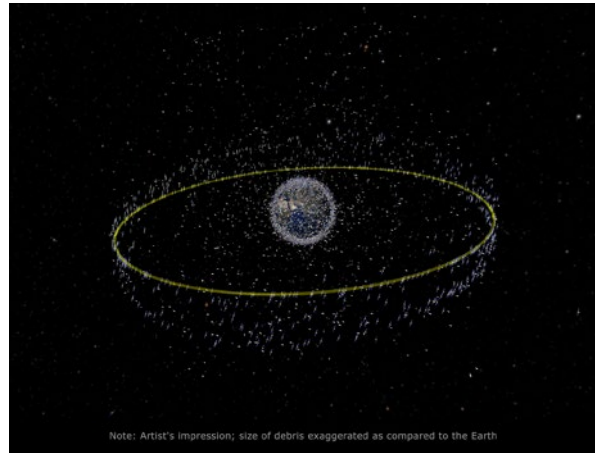
37. For example, to receive signals from geostationary communications satellites, antennae on Earth are pointed at a zenith angle equivalent to the latitude from the equator (that is, towards south for northern hemisphere locations and towards north for southern hemisphere locations) and at a fixed azimuth depending on the longitude of the satellite position.

**Figure 12.3** Satellite density around Earth

a. Low Earth Orbit (LEO < 2,000 km altitude) satellites are used for most EO studies. 70% of catalogued objects are in LEO, with the spatial density of objects increasing at higher latitudes.



b. Geostationary Orbit (~36,000 km altitude) satellites are used for meteorology and telecommunications.



Source: © ESA (2016). Retrieved from a. [http://www.esa.int/spaceinimages/Images/2008/03/Debris\\_objects\\_-\\_mostly\\_debris\\_-\\_in\\_low\\_Earth\\_orbit\\_LEO\\_-\\_view\\_over\\_the\\_equator](http://www.esa.int/spaceinimages/Images/2008/03/Debris_objects_-_mostly_debris_-_in_low_Earth_orbit_LEO_-_view_over_the_equator); b. [http://www.esa.int/spaceinimages/Images/2008/03/The\\_geostationary\\_ring](http://www.esa.int/spaceinimages/Images/2008/03/The_geostationary_ring)

### 12.2.1 Geostationary

Geostationary, or geosynchronous, satellites are positioned in an orbit at an altitude of approximately 36,000 km above the equator. In this equatorial orbit they move with the same angular velocity as the Earth rotates and so remain over the same point on the Earth's surface. From this viewpoint the same region of the Earth's surface can be imaged at frequent, regular intervals by the satellite (see Figure 12.4).

The history of meteorological satellites is summarised in Excursus 12.1. More recently, a network of geostationary and LEO satellites has been established by the Coordination Group for Meteorological Satellites (CGMS), which provide global coverage for atmospheric monitoring as shown in Figure 12.5 and listed in Table 12.3.

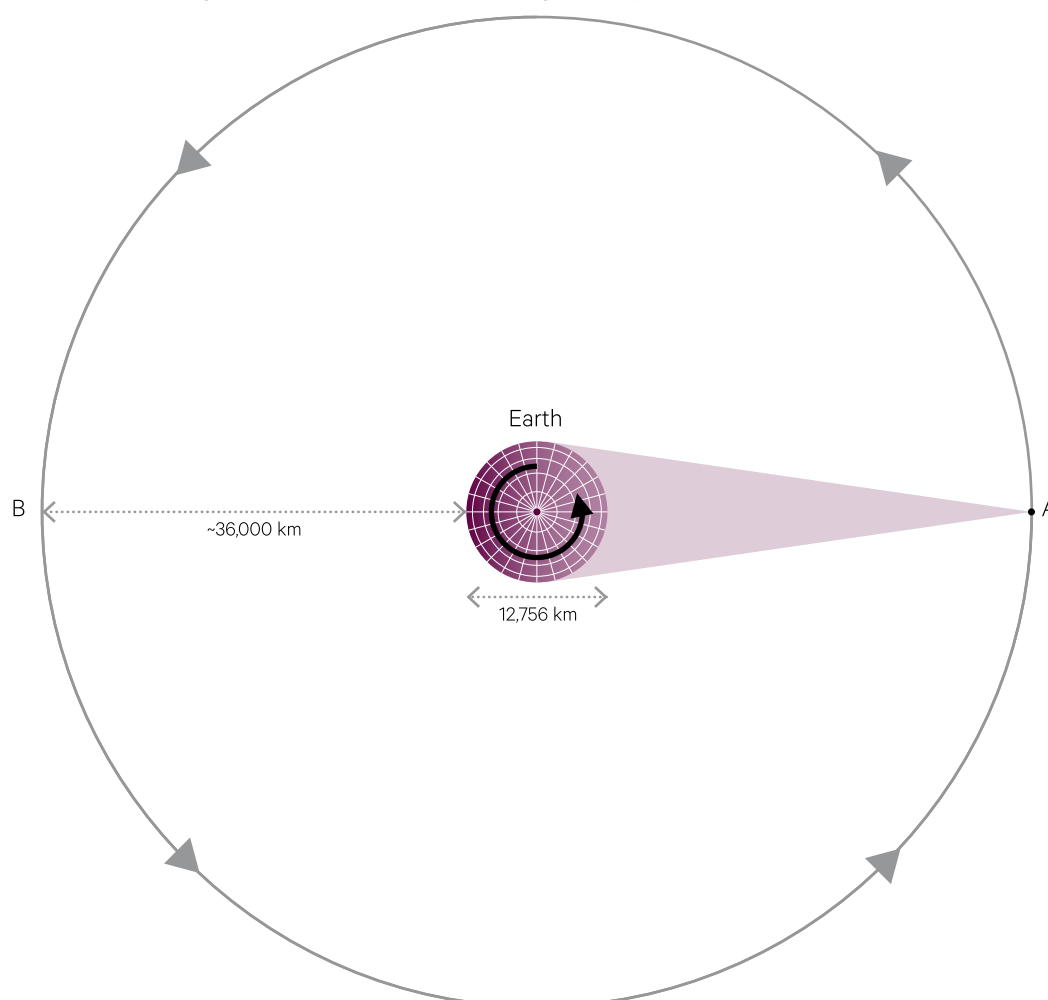
---

*When I arrived in Gombe 50-plus years ago, looking up at the stars, it never occurred to me that one day, we'd be relying on remote sensing—satellites circling the globe high above—to help unite communities of people and save Gombe's chimpanzees. NASA—through its resources and data and funding—is helping us to apply the kinds of innovative solutions needed to address the complex problems people and chimpanzees face today.*  
(Jane Goodall)

---

**Figure 12.4** Geostationary orbit

The geostationary orbit, at an average altitude of 35,786 km above the equator<sup>38</sup>, allows satellites to move with the same angular velocity as the Earth's rotation. By rotating synchronously with Earth, geostationary satellites remain at their allocated longitude and continuously view the same hemisphere of Earth. Himawari-8, for example, stays at longitude 140.7°E to acquire the full disk images shown in Figures 12.6 and 12.7. In this illustration, 12 hours after the geostationary satellite is at position A, it will be at position B, but still located over the same longitude on Earth. 12 hours later it will again be at position A.



Since 1977, the Geostationary Meteorological Satellites (GMS) and Multifunctional Transport Satellites (MTSAT, renamed Himawari after launch) operated by Japan Meteorological Agency (JMA) have provided imagery for Australasia from its position around 145° E (see Figure 12.5). The principal sensor carried by MTSAT-2 (Himawari-7) is Japanese Advanced Meteorological Imager (JAMI), with five spectral channels (see Table 12.4). The replacement satellite (Himawari-8) was launched in late 2014 observes from a slightly different longitude (140.7° E).

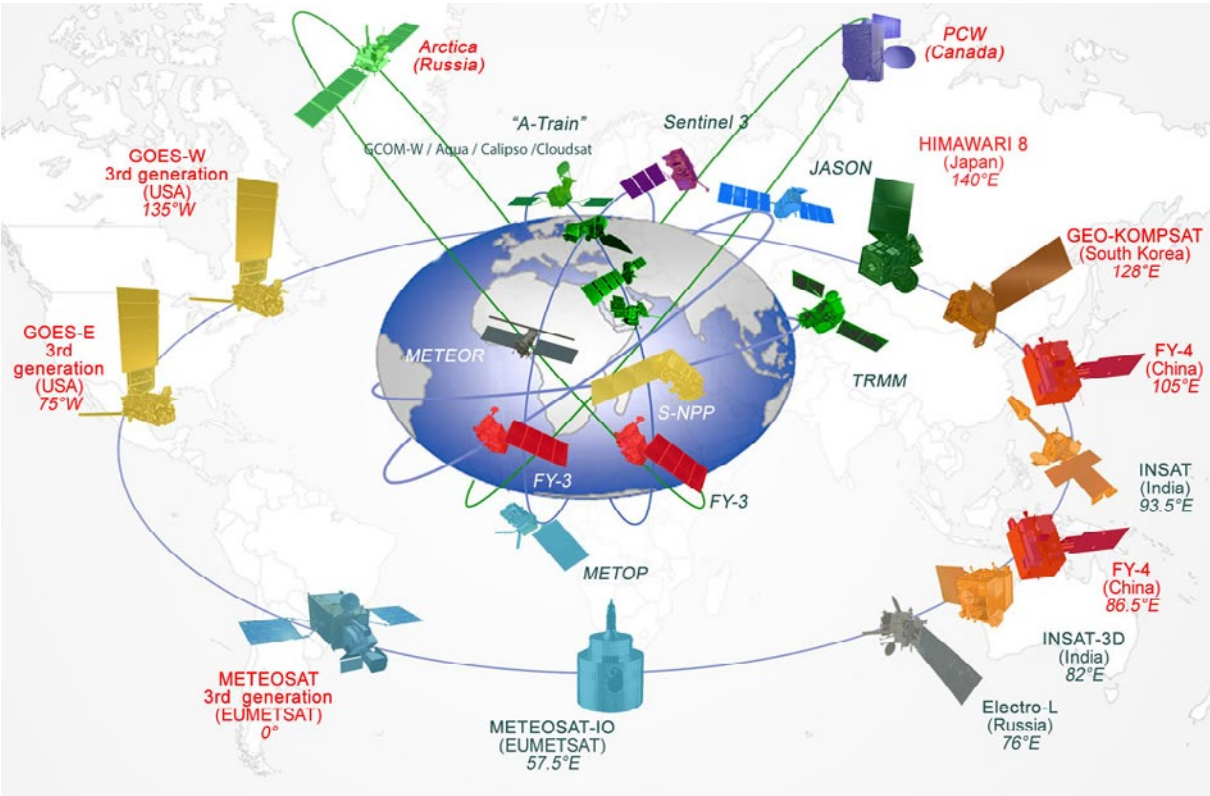
It carries the dedicated meteorological payload, Advanced Himawari Imager (AHI), to provide more frequent coverage with higher spatial and spectral resolution (see Table 12.4 for details). This sensor will enable a full disk image of Earth (as visible from 140.7° E) to be acquired every ten minutes (see Figure 12.6). Himawari-9 is scheduled for launch in late 2016, initially as a backup system, and ultimately to provide a replacement for Himawari-8.

38. EUMETSAT: <http://www.eumetsat.int/website/home/Satellites/LaunchesandOrbits/SatelliteOrbits/index.html>



Figure 12.5 Network of geostationary satellites

19 geostationary meteorological satellites are currently listed as operational or on stand-by, with an ongoing plan for replacements into the future (CGMS, 2016).



Source: © WMO (2016). Retrieved from [http://www.wmo.int/pages/prog/sat/globalplanning\\_en.php](http://www.wmo.int/pages/prog/sat/globalplanning_en.php)

Table 12.3 Geostationary meteorological satellites

The nominal constellation includes six operational geostationary satellites to ensure full coverage between the latitudes 50° N and 50° S, with a zenith angle below 70°.

Region	Nominal location	Nominal operator	Example Satellite
America (North, Central and South)	135° W	USA (NOAA)	GOES-15
East Pacific	75° W	USA (NOAA)	GOES-13
Europe and Africa	0°	EUMETSAT	Meteosat-10
Indian Ocean	76° E	Russian Federation (Roshydromet)	GOMS-2/Elektro-L
Asia	105° E	China (CMA)	Feng Yun-2G
West Pacific	140° E	Japan (JMA)	Himawari-8

Source: CGMS (2016); WMO (2016)

The viewpoint of a geostationary satellite is similar to that of a photographic camera, with the scanner viewing the whole image from a central perspective (see Section 14.2.3). The GMS satellites were spin-stabilised on a north-south axis so unlike the orbiting satellites, which can utilise the relative motion of

the platform to separate successive scan lines in an image, these satellites used a stepping-motor to adjust the angle of view on each spin. The recent Himawari satellites are three-axis stabilised, with the view scanned relative to the platform in two directions (JMA, 2016).

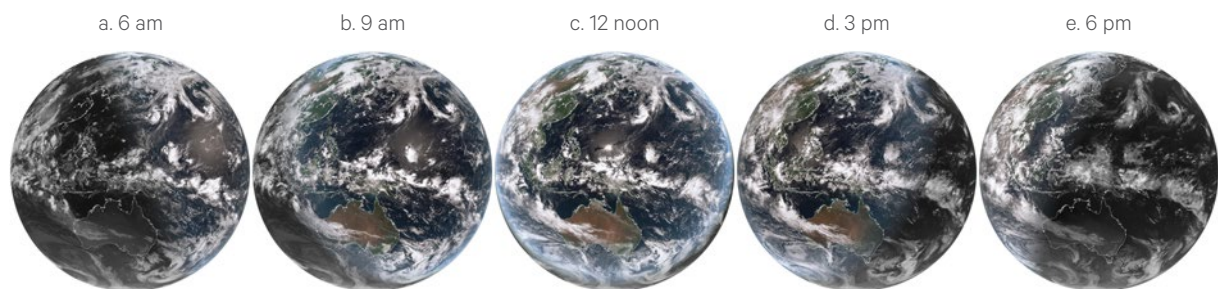
**Table 12.4** JMA Australasian coverage satellites

Himawari-7			Himawari-8/-9		
Channel	Spectral Range (nm)	Spatial Resolution (km) <sup>39</sup>	Channel	Central Wavelength (μm)	Spatial Resolution (km) <sup>40</sup>
1	0.55–0.80	1	1	0.47	1
			2	0.51	1
			3	0.64	0.5
5	3.5–4.0	4	4	0.86	1
			5	1.6	2
			6	2.3	2
4	6.5–7.0	4	7	3.9	2
			8	6.2	2
			9	6.9	2
2	10.3–11.3	4	10	7.3	2
			11	8.6	2
			12	9.6	2
3	11.5–12.5	4	13	10.4	2
			14	11.2	2
			15	12.4	2
			16	13.3	2

Source: JMA (2016) at <http://www.data.jma.go.jp/mscweb/en/himawari89/index.html> <sup>39,40</sup>

**Figure 12.6** Himawari-8 disks

The Himawari-8 satellite, operated by JMA, is positioned over the equator at longitude 140.7° E. From this vantage point, full disk images covering the Asian and Australian continents are acquired every ten minutes. Five image samples from the daily sequence on 23 July 2016 are shown below using true colour channels (merged with thermal on the night side of the planet and overlaid with coastlines in white). These images were acquired at the following local times for longitude 135° E (central to Australia):



Source: © Bureau of Meteorology/JMA

*I suppose that we shall soon travel by air-vessels; make air instead of sea voyages;  
and at length find our way to the Moon, in spite of the want of atmosphere.  
(Lord Byron, 1822)*

39. horizontal resolution in image centre

40. horizontal resolution in image centre

## Excursus 12.1—Meteorological Satellites

**Source:** John Le Marshall, Bureau of Meteorology

**Further Information:** [johnlemarshall@hotmail.com](mailto:johnlemarshall@hotmail.com), [j.lemarshall@bom.gov.au](mailto:j.lemarshall@bom.gov.au)

### The First Weather Satellites

The first weather satellite, TIROS 1, launched on 1 April 1960 (Figure 12.7), enabled the use of Earth Observations from Space (EOS) to help determine atmospheric state. Visible and infrared imagery became increasingly available from the early TIROS, ESSA and NIMBUS series of satellites with TIROS-8 introducing Automatic Picture Transmission (APT) capability (see Figure 12.8). APT facilitated the use of direct readout imagery around the globe for analysis, forecasting, warning and research. Before the use of satellite sounding data, these image data were used to construct mean sea level pressure charts and upper atmospheric geopotential charts over the southern hemisphere as part of operational meteorological analysis.

Here, we summarize the development and the past, current and future use of weather satellites, particularly in the southern hemisphere. Table 12.5 provides a time-referenced list indicating the development of meteorological satellite series over the last half-century.

**Figure 12.7** The launch of the first weather satellite, TIROS-1, in 1960

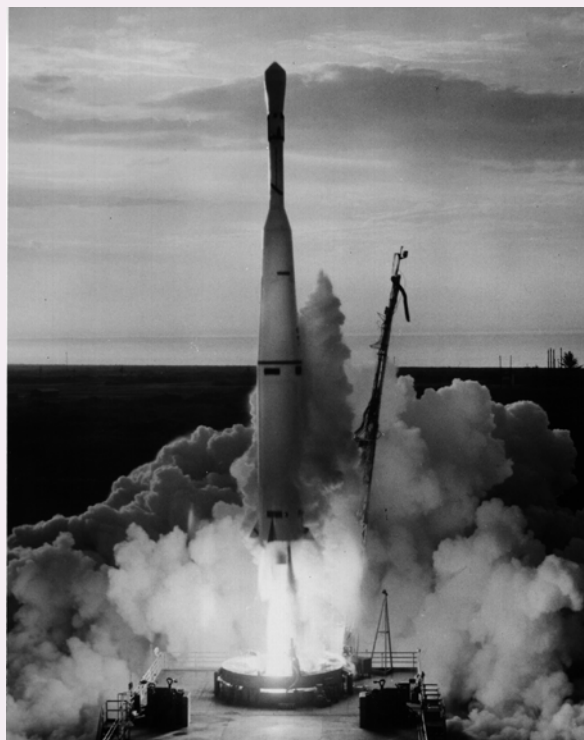
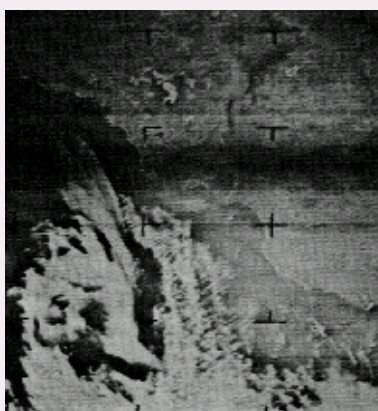


**Figure 12.8** Early meteorological satellite imagery

a. First TIROS-8 image received at the Bureau of Meteorology, Melbourne, Christmas day 1963



b. NIMBUS II image Christmas day 1964, showing a cold front and low pressure system approaching south-eastern Australia, and also bushfires over southeast Australia.



c. NOAA-5 Mosaic covering much of the Pacific Ocean, received from NOAA via geostationary satellite on 8 November 1976

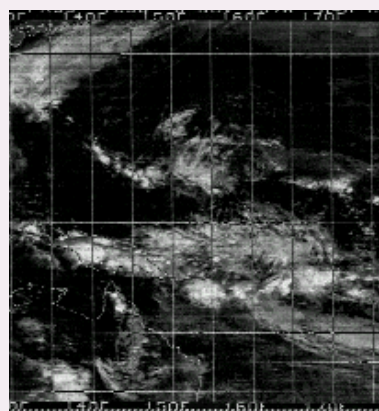


**Table 12.5** Some Important Series of Weather Satellites

Satellite Series	Duration	Number of Satellites	Origin
TIROS 1 – 10	1960–1965	9	USA
DMSP (OPS)	1962–	68	USA
NIMBUS 1 – 7	1964–1978	7	USA
COSMOS 44 – 2292	1964–1994	5	USSR
OPS 8068 – 5390	1965–1979	4	USA
ESSA 1 – 9	1966–1969	9	USA
METEOR 1	1969–1977	25	USSR
ITOS-1 (TIROS-M) – ITOS-H (NOAA5)	1970–1976	8	USA
GOES 1 – 15	1975–2010	15	USA
HIMAWARI 1 – 8	1977–	8	JAPAN
METEOSAT 1 – 11	1977–2015	10	EUROPE
TIROS-N, NOAA-6 – NOAA19 (POES)	1978–2009	16	USA
INSAT	1983–2011	24	INDIA
FENGYUN 1A – 1D	1988–2002	4	CHINA
GOMS	1994–	3	USSR
FENGYUN 2A– 2G,	1997–2014	7	CHINA
EOS	1997–	9	USA, GER, FR, JAP, EU
METOP A – B	2006–	2	EUROPE
FENGYUN 3A – 3C	2008–2013	3	CHINA
COMS-1	2010–	1	S.KOREA
NPP	2011–	1	USA

## The First Geostationary Satellites

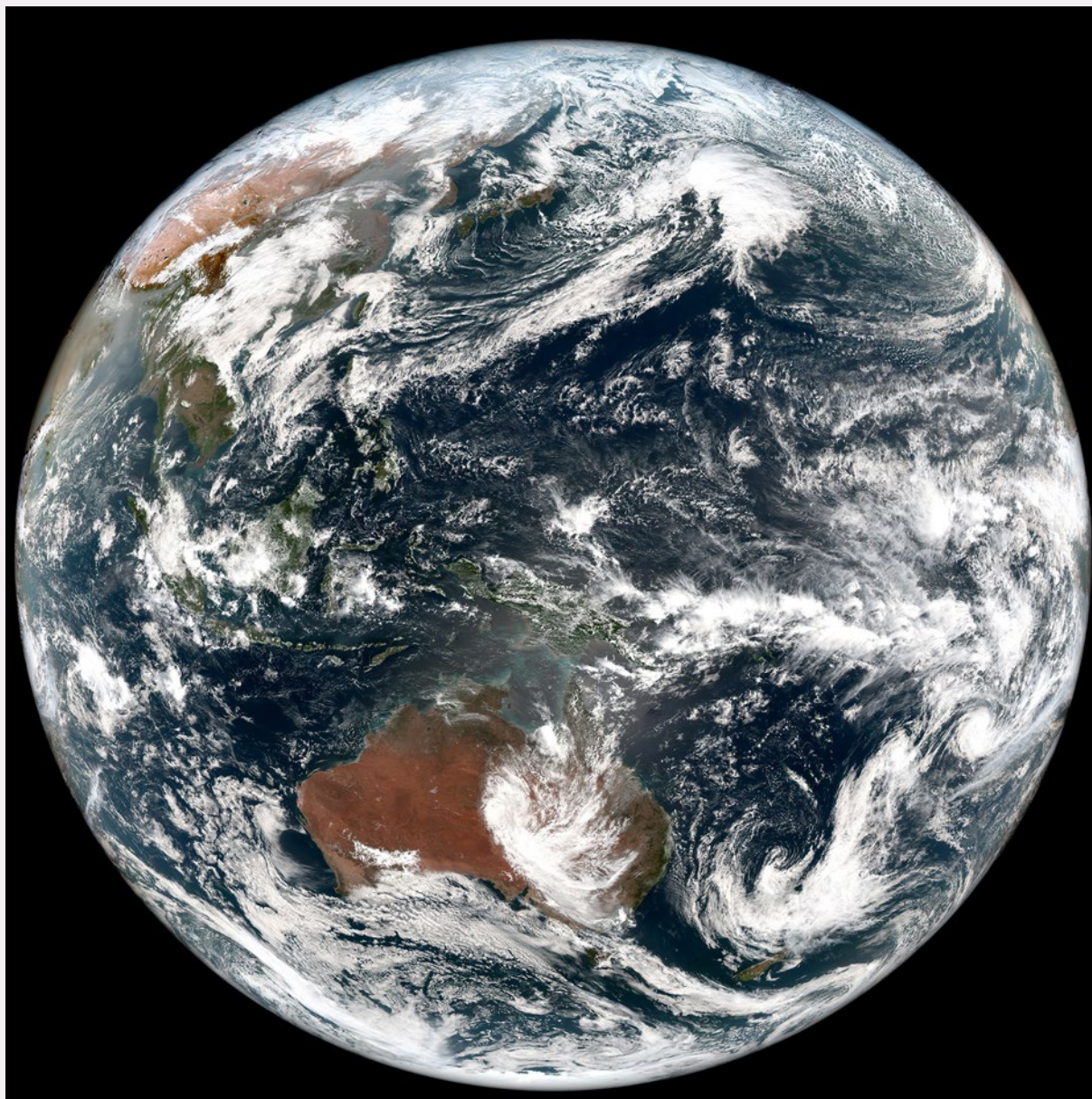
The geostationary satellite, ATS-1 was launched in 1968 and, by the 1970s, the use of sequential geostationary observations in the visible and infrared bands was well established for a number of meteorological applications, including nowcasting, forecasting, severe weather monitoring and the estimation of winds or atmospheric motion vectors (Fujita *et al.*, 1968; Young *et al.*, 1972).

The first geostationary satellite in the Australian region was GMS-1, which was provided by JMA in 1976. The most recent satellite, Himawari-8, was launched in late 2014 and was placed into geostationary orbit over the equator at 140.7° E. A colour image from Himawari-8 is seen in Figure 12.9.



**Figure 12.9** A Himawari-8 colour image

This image was taken from geostationary orbit over the equator at 140.7°E on 1 January 2016.



Source: © Bureau of Meteorology/JMA

## Second Generation Satellites

With the launch of TIROS-N in 1978 and the subsequent Polar Orbiting Environmental Satellites (POES) series satellites with second generation sounders (HIRS, MSU; Smith *et al.*, 1979) and, later, AMSU, real time infrared and microwave radiances and derived temperature and moisture profiles were available to the global community. The derived products (temperature and moisture profiles) were used globally for hemispheric and regional forecasting. Direct readout of the satellite data from ground stations in a number of countries was able to provide radiances which were used, first with simple

statistical inversion models (Kelly *et al.*, 1983) and, later, with full physical inversion models to improve regional forecasting (such as Le Marshall *et al.*, 1989).

In many places, use of these data was facilitated by community software, such as the International TOVS Processing Package (Smith *et al.*, 1983). The resulting improvements to regional and global forecast systems from the sounding data are well documented (Kelly *et al.*, 1978; Le Marshall *et al.*, 1994; Zapotocny *et al.*, 2007, 2008) and these data have assumed an ever-increasing role in numerical analysis and prognosis.



## Blowing in the wind

By the mid 1980s, water vapour imagery was used routinely to detect atmospheric movement and generate Atmospheric Motion Vectors (AMVs), which have been particularly useful for Numerical Weather Prediction (NWP; Le Marshall *et al.*, 1985). During the 1980s, the ability to process digitised, sequential Global Meteorological Satellite (GMS) Special Observation imagery and generate winds was also developed in Australia. With the introduction of digital GMS Stretched-VISSR data in 1989, sequential digitised images available every hour or half-hour were processed and used to provide cloud drift winds.

The world's first, fully automatic, operational system to derive IR image-based cloud motion vectors every six hours was developed for the Australian region (Le Marshall *et al.*, 1992; Le Marshall *et al.*, 1993; Le Marshall *et al.*, 1994). The improved spectral coverage of GMS-4 and -5 provided observations in the visible, infrared and water vapour absorption bands and these were used to provide high spatial and temporal resolution AMVs.

With the availability of hourly image data and the expansion of the number of channels, AMVs could be generated on an hourly basis, in real time, at high spatial resolution, using both visible and infrared imagery. This enabled the first operational, fully automatic generation of hourly cloud drift winds (Le Marshall *et al.*, 1996a; Le Marshall *et al.*, 1999) with documented benefits to operational NWP (see Excursus 16.1). Winds generated by the operational

system at the Bureau of Meteorology are seen in Figure 12.10 displayed over a GMS-5 and MTSAT-2 image. In addition, in a series of studies examining tropical cyclone track and intensity predictions, significant gains were found in forecasting track accuracy, including a beneficial influence on intensity prediction, from use of these high resolution wind data (Le Marshall *et al.*, 1996b; Leslie *et al.*, 1998). AMVs derived from Himawari-8 imagery are shown in Figure 12.11.

In a series of studies examining tropical cyclone track and intensity predictions, significant gains were also found in forecasting track accuracy, including a beneficial influence on intensity prediction, from use of these high resolution wind data (Le Marshall *et al.*, 1996b; Leslie *et al.*, 1998; Le Marshall *et al.*, 1999).

**Figure 12.10** Wind vectors over GMS-5 image of the Tasman Sea

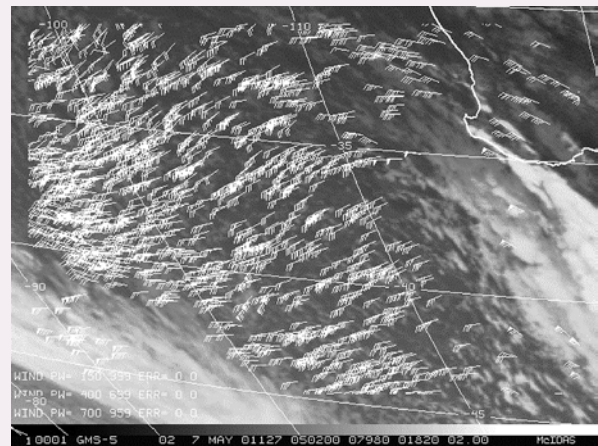
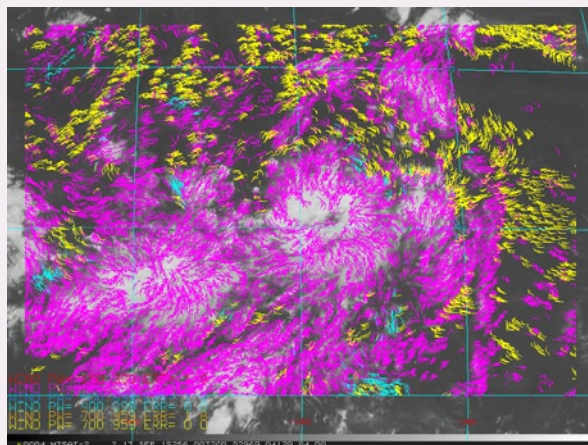


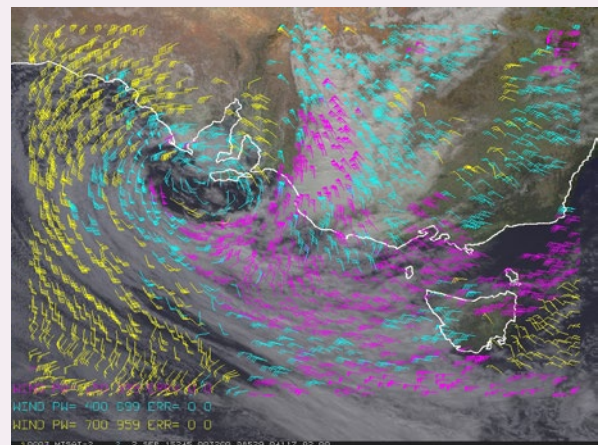
**Figure 12.11** Himawari-8 Atmospheric Motion Vectors (AMVs)

Yellow vectors—low level AMV; magenta vectors—upper level AMV.

a. Over tropical storms in the equatorial Pacific north of Australia on 12 September 2015



b. Over southeast Australia



## 12.2.2 Polar orbiting

Polar-orbiting satellites provide imagery with a range of resolutions—spectral, spatial, radiometric and temporal (see Volume 1B—Section 1). These satellites operate in sun-synchronous orbits, that is, they always pass over given latitude at the same local solar time (see Figure 12.12). Their orbits are near polar, covering the latitudes 82° N to 82° S, with altitudes varying between 700 km and 1500 km.

A strip, or swath, of the Earth's surface is imaged with each satellite pass such that consecutive satellite paths follow a set pattern to image different ground areas. The orbital characteristics of these satellites provide near global coverage of the Earth's surface on a regular and predictable basis. The orbital track of these satellites relies on the rotation of Earth beneath the satellite. To maintain an orbit that is synchronous with the sun, the satellite orbital plane deviates slightly from a true north-south direction (see Figure 12.13).

Polar orbiting satellites are designed to collect data in either their ascending (when moving from south to north—see Figure 12.13a) or descending (moving north to south—see Figure 12.13b) mode. Local solar time necessarily varies during each orbit, but the equatorial crossing time, in terms of local solar time, is constant. Most current satellite sensors have recording facilities to allow collection of imagery in regions that are outside the range of ground stations.

Such recorded data are subsequently transmitted to Earth when the satellite is within range of an appropriate receiving station.

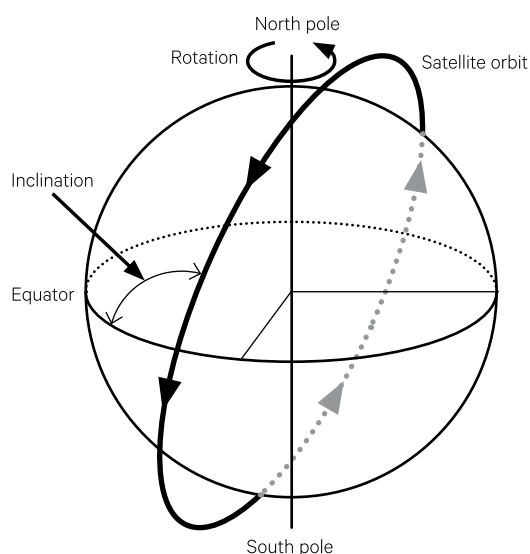
The Worldwide Reference System (WRS) is a global standard for cataloguing Landsat Imagery. Landsat-1, -2 and -3 followed WRS-1, while Landsat-4, -5, -7 and -8 follow WRS-2. This notation systematically subdivides continuous swaths of imagery acquired along each orbital path into discrete scenes (NASA, 2016).

The various sensing and communications components of the venerable Landsat-5 satellite, which acquired over 2.5 million images during its 22 years of operation, are labelled in Figure 12.14a, and the Landsat-7 satellite is shown in Figure 12.14b. It is interesting to note that the body of each of these satellites could fit into the average car parking space<sup>41</sup>.

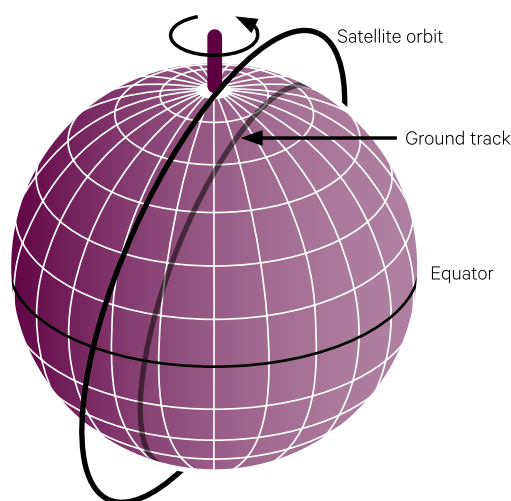
While the Landsat series of satellites have been the best-known polar-orbiting satellites for EO, and have provided the most commonly used data, imagery is now available from a very wide range of satellite sensors. Some of these systems are illustrated in Figure 12.15 and listed in Table 12.6. (Please refer to the Glossary for full details of acronyms used in this table). A more comprehensive list of operational, non-commercial, EO satellite missions is provided in the *Earth Observation Handbook* (CEOS, 2015).

**Figure 12.12** Orbit parameters

a. Spherical representation of Earth's globe showing satellite orbit relative to equator and poles. Descending node describes satellite movement from north to south and ascending node describes satellite movement from south to north.



b. Inclined view of spherical globe showing near polar orbit relative to northern latitudes



Adapted from: (Campbell, 2006)

41. The bodies of Landsat-1, -2, and -3 measured 3 m in length with diameter 1.5 m; and the bodies of Landsat-7 and -8 measured 4.3 m in length with diameter 2.8 m (see Figure 12.14). Landsat-4 and -5 were of similar size to Landsat-7 (<https://directory.eoportal.org/web/eoportal/satellite-missions>).



---

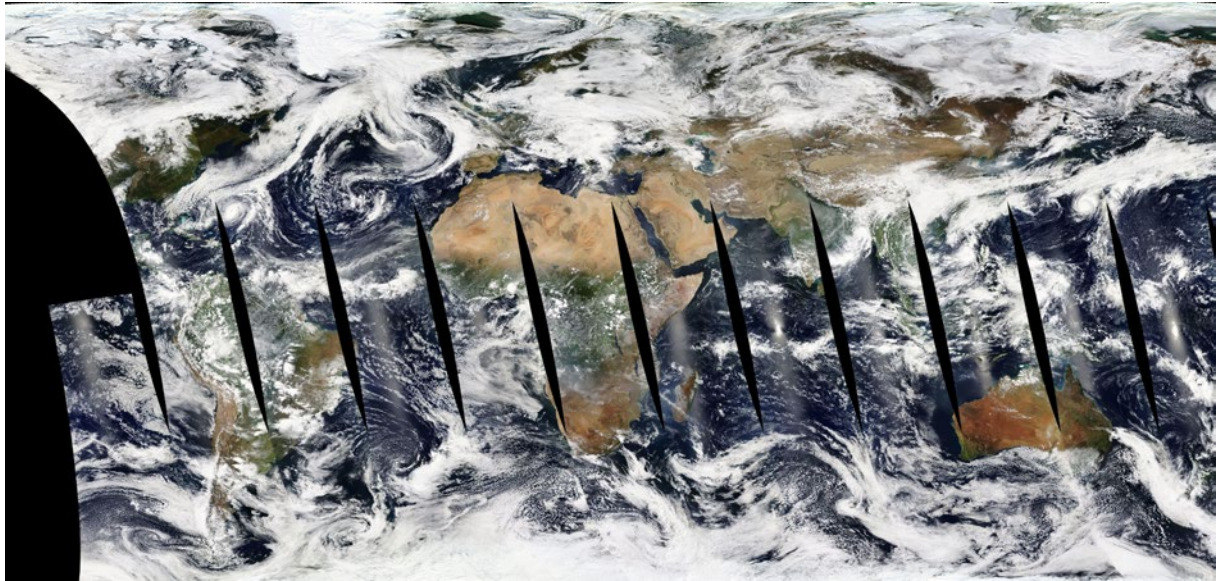
*Science has reached such a stage that...  
the creation of an artificial satellite  
of the Earth is a real possibility.  
(A.N. Nesmeyanov, 1953)*

---

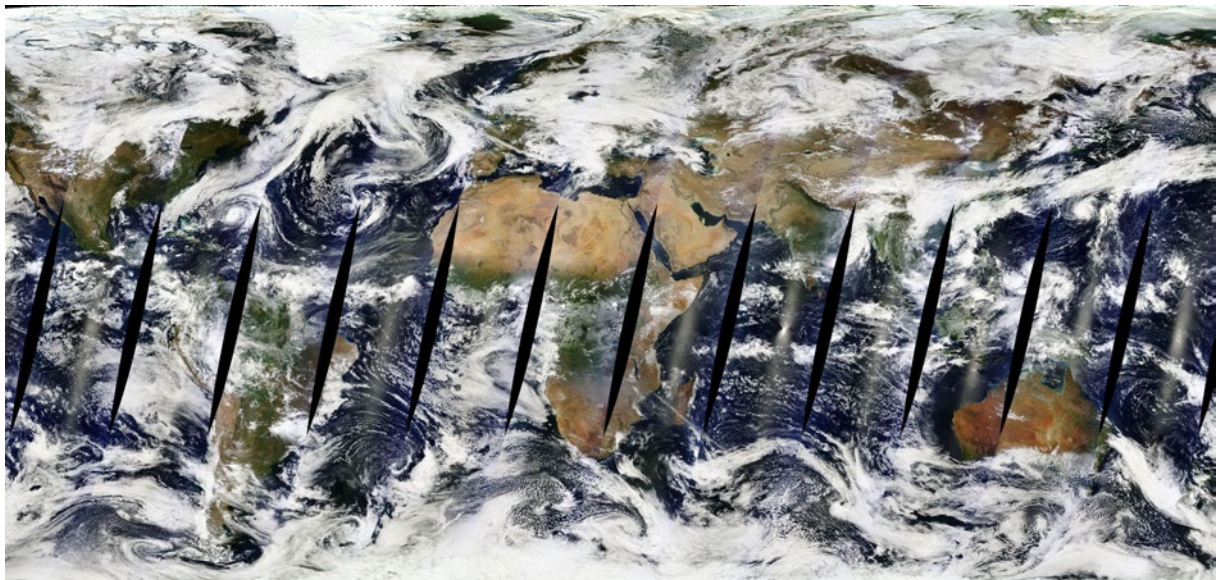
**Figure 12.13** Daily acquisitions for MODIS/Aqua and MODIS/Terra

These illustrations generated by NASA Worldview show the image paths acquired on 11 October 2016 by the MODIS sensor carried by the Aqua and Terra satellites (shown at 5 km resolution).

a. MODIS/Aqua collects imagery during its ascending mode so image strips are skewed in northwest/southeast direction.



b. MODIS/Terra collects imagery during its descending mode, so image strips are skewed in northeast/southwest direction.



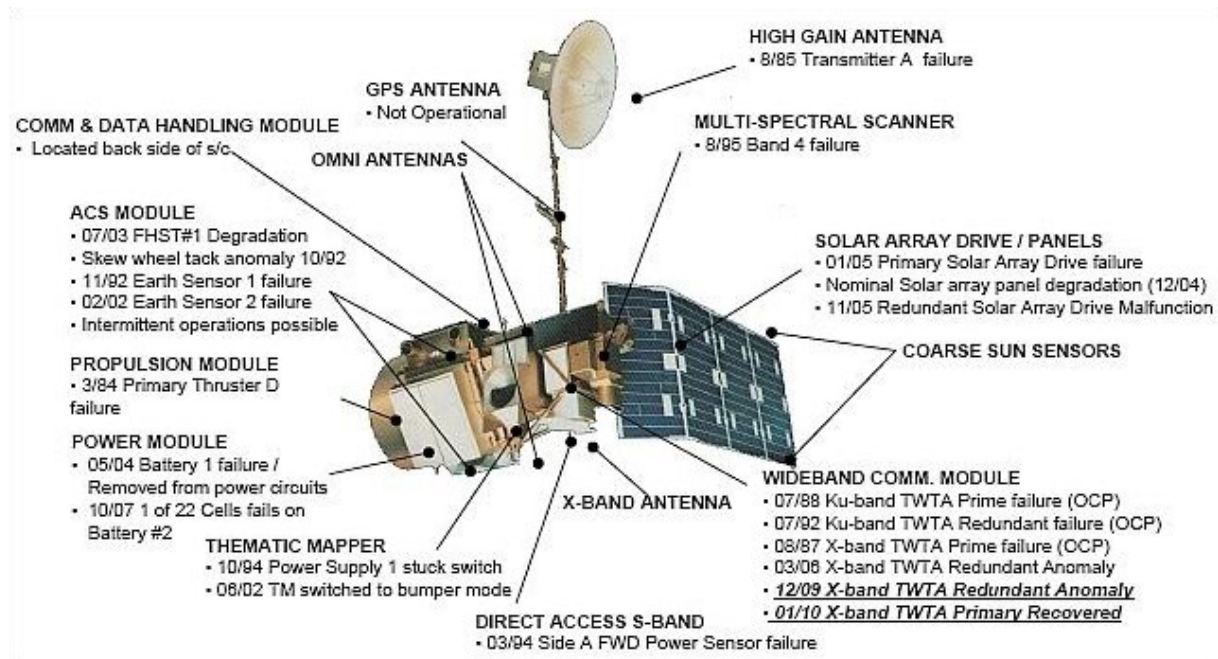
Source: NASA Worldview. Retrieved from <https://worldview.earthdata.nasa.gov>



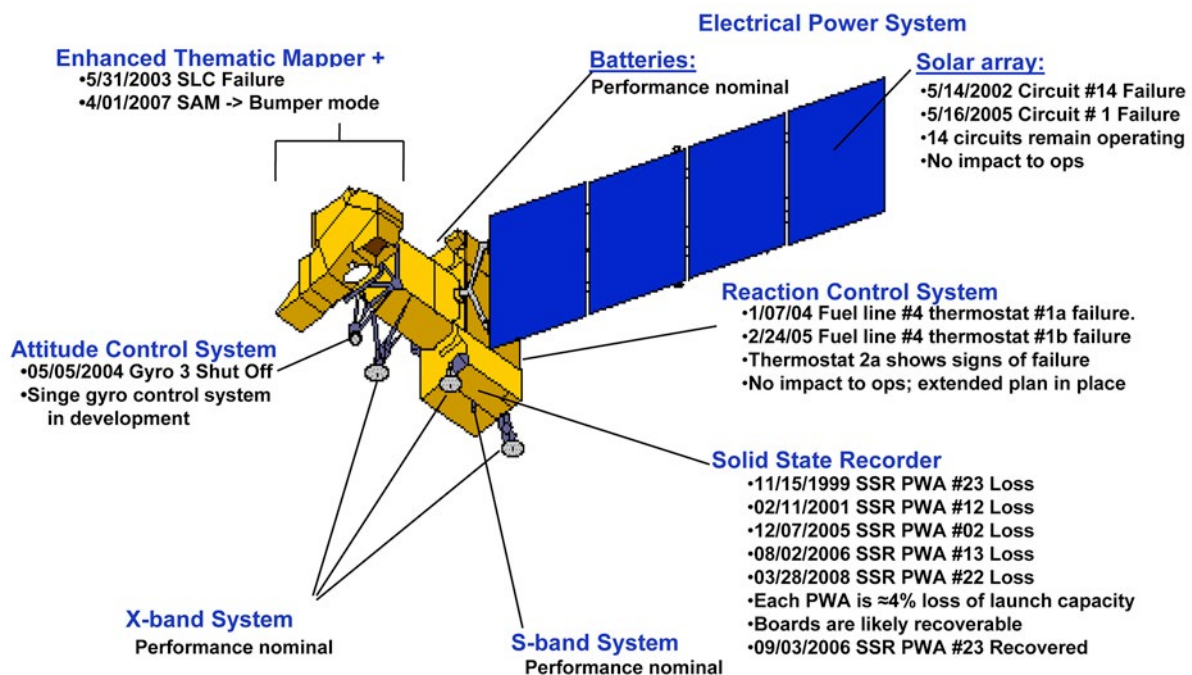
**Figure 12.14** Landsat satellites

Components of Landsat satellites including malfunctions and recoveries before February 2010

a. Landsat-5 (similar body dimensions to Landsat-7)<sup>42</sup>



b. Landsat-7 (body length: 4.3m and diameter 2.8 m; each solar panel: 1.88 m × 2.26 m)

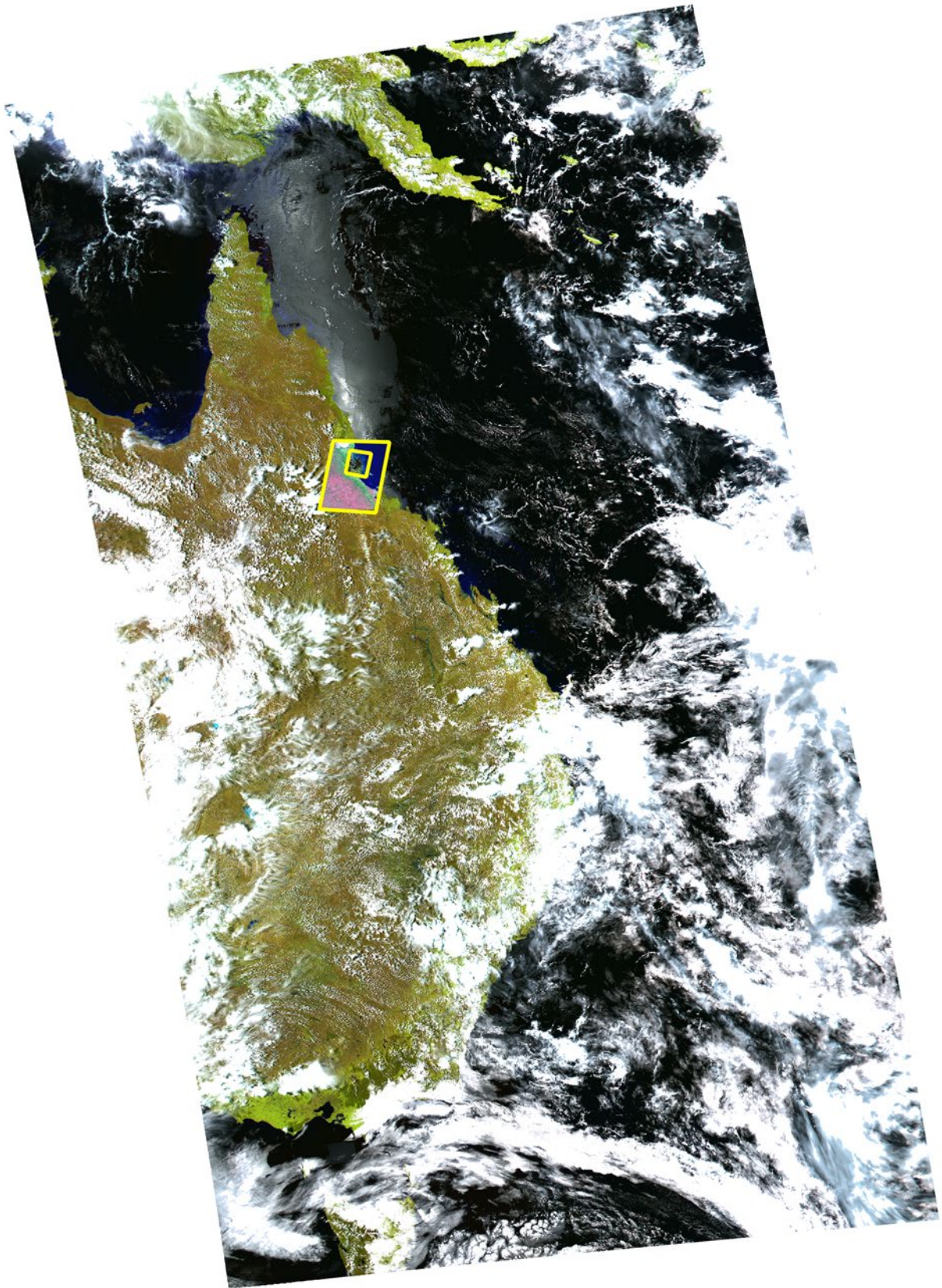


Source: Kalvelage (2010). Retrieved from <https://directory.eoportal.org/web/eoportal/satellite-missions/l/landsat-4-5>

42. Pers. Comm. Dennis Helder (USGS) and Leo Lyburner (GA)

**Figure 12.15** Polar orbiting satellites provide a variety of spatial scales

a. Full scene MODIS image showing the eastern half of Australia. Scene is 2250 km wide, acquired on 5 December 2010, and processed to 250 m spatial resolution

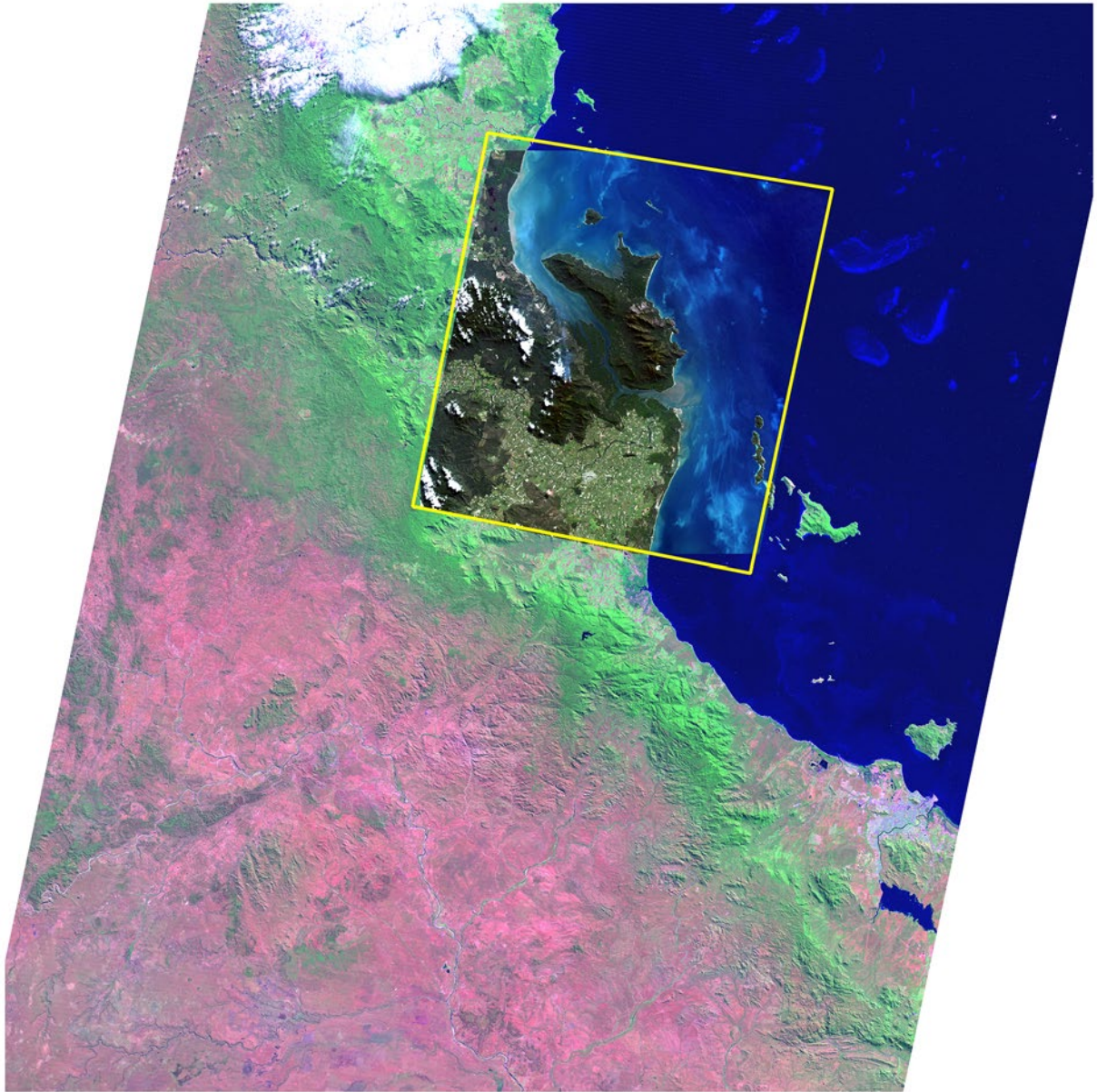




b. Full scene Landsat-5 TM image, showing the area around Hinchinbrook Island in Queensland. Scene is 185 km wide, acquired on the 1 June 2010, and processed to 25 m spatial resolution



c. ALOS AVNIR2 scene over the southern portion of Hinchinbrook island. Scene is 70km wide, acquired on the 12<sup>th</sup> June 2010, and processed to 10 m spatial resolution



Source: Norman Mueller, Geoscience Australia



**Table 12.6** Polar orbiting satellites

For a comprehensive listing of non-commercial EO satellites and sensors visit CEOS (2016).<sup>4344</sup>

Satellite (Agency)	Sensor	Number of Channels (in latest sensor)	Spectral range (in latest sensor)	Spatial Resolution (m, at nadir, in latest sensor)	Swath Width (km, at nadir, in latest sensor)	Image Archive	Radiometric Quantisation (bits)
ALOS (JAXA, Japan)	AVNIR-2	4	Optical	10	70	2006–2011	8
	PALSAR	1	L-band SAR in 3 modes with selectable polarisation	7–100	40–350	2006–2011	5
	PRISM	1	Panchromatic/ Stereo	2.5	70 (35 in triplet mode)	2006–2011	8
TIROS/ AVHRR (NOAA, USA)	AVHRR	6	Optical /thermal	1,100	~2700 <sup>45</sup>	1978–present	10
Landsat (NASA/USGS, USA)	MSS	5	Optical /thermal	68 × 83	185	1972–1997	8
	TM/ETM+	7	Optical /thermal	30/120	185	1987–2011	8
	OLI/TIRS	11	Panchromatic/ optical /thermal	15/30/100	185	2014–present	12
Terra and Aqua (NASA, USA)	MODIS	36	Optical /thermal	250/500/ 1,000	2330	2000–present	12
Quickbird (Digital Globe, USA)	Quickbird	5	Panchromatic/ optical	0.55/2.16 (at 400 km altitude)	14.9 (at 400 km altitude)	2001–2015	11
SPOT (Airbus DS, France <sup>46</sup> )	SPOT PAN SPOT MS	5	Panchromatic/ optical /stereo	1.5/6	60	1986–present	8–12
Geoeye	Geoimage	5	Panchromatic/ optical	0.41/1.65	15.2	2008–present	11

In Australia, the receiving station for Landsat imagery is located near Alice Springs, where Geoscience Australia (GA—and its predecessors) has been routinely receiving Landsat series data since 1979. At this central location, the station maintains contact with the satellite over the largest possible land area. The current Landsat 7 and 8 satellites take 16 days and 232 orbits to cover the measurable surface of the Earth, with each full orbit taking about 100 minutes and spanning 185 km in width. Landsat satellites 4 and 5 also followed this orbital pattern. The imaged paths are later subdivided into rows using the Worldwide Reference System (WRS-2) to form 185 km square scenes (representing 25 seconds of satellite time)<sup>45</sup>.

Each scene can then be referenced by a path number to indicate east-west location, and a row number to define north-south position. The precise north-south location of a scene may be varied by defining a non-standard row, but obviously the east-west location is

fixed by the orbital pattern. A similar system is used for other satellite imagery to define individual image scenes.

Continental scale imagery is provided by several sensors including AVHRR and MODIS. The AVHRR (Advanced Very High Resolution Radiometer) is currently carried on the NOAA 15, 16, 18 and 19 satellites. These spacecraft are part of the longest established series of low-altitude environmental satellites (TIROS/ESSA/ITOS/NOAA), TIROS-1 having been launched by the USA in April 1960. AVHRR imagery is used in two modes:

- Large Area Coverage (LAC) records spectral channels in 1.1 km pixels; while
- Global Area Coverage (GAC) sub-samples the LAC data to pixels sized 5.5 × 3.3 km.

43. Edward King (pers. comm.); see also Frulla et al. (1995)

44. Formerly Astrium/CNES

45. Image scenes for Landsat 1, 2 and 3 satellites were based on WRS-1; scenes for Landsat 4, 5, 7 and 8 are based on WRS-2. [http://landsat.usgs.gov/worldwide\\_reference\\_system\\_WRS.php](http://landsat.usgs.gov/worldwide_reference_system_WRS.php)

While the AVHRR was designed for meteorological, hydrologic and oceanographic studies, its imagery is also useful for land-based studies. Since April 1982, NOAA has been using GAC data to compute global vegetation index (GVI) imagery, which reduces the effects of cloud cover. This imagery is produced by compositing geographically registered data sets over weekly imaging periods and has obvious application for monitoring global vegetation resources (Justice *et al.*, 1985). The orbital patterns of the two NOAA satellites provide two daytime and two night-time overpasses each day for any region, with the wide swath overlap at temperate latitudes actually providing more frequent coverage. This repeat cycle offers valuable coverage of dynamic events such as flood and fire. Day/night image pairs also provide data for studies of thermal inertia. A number of organisations in Australia now receive AVHRR imagery, with large national repositories being available through GA, BoM and research stores such as IMOS and TERN<sup>46</sup>.

A number of satellite sensors have been designed to observe ocean colour, starting with the Coastal Zone Colour Scanner (CZCS), launched in 1978. Subsequent missions include MOS, OCTS, POLDER, and SeaWiFS. As detailed in Volume 3B (Surface Waters), imagery from these sensors have been used to map chlorophyll concentration, sediment distribution and general ocean dynamics, including sea surface temperature. Details of these sensors and their calibration/validation for a range of applications are provided by IOCCG (2015).

Imagery from the Moderate Resolution Imaging Spectroradiometer (MODIS) (Justice and Townshend, 2002) has also proved valuable for mapping ocean colour. MODIS data are acquired by two NASA satellites—Terra (launched 1999) and Aqua (launched 2002)—which provide global coverage every one to two days. The frequency of MODIS imagery not only ensures up-to-date coverage of environmental change, but also allows the seasonal progression and longer-term dynamics of land cover change to be monitored and modelled (see Figure 12.13). The MODIS time series now comprises regular snapshots of Earth for over a decade, and is being increasingly exploited to understand and quantify various states and processes of the Earth's surface. Since 2000, up to four MODIS images have been acquired daily over most of Australia (see CEOS (2016) satellite and sensor details).

MODIS measures a total of 36 spectral bands, ranging from 400 nm to 14.4  $\mu\text{m}$ . Two of these bands (band 1: visible red (620–670 nm) and band 2: near infrared (841–876 nm)) are imaged at 250 m spatial resolution. These bands were specifically included to detect land cover changes resulting from human activity (Townshend and Justice, 1988), and have been successfully used to map change associated with natural and anthropogenic causes (Hansen *et al.*, 2000; Wessels *et al.*, 2004). In addition to the MODIS spectral band data, NASA offers a range of MODIS image products, which allow improved characterisation of biophysical and biochemical characteristics of vegetation. Two of these products are 16-day composites of the standard vegetation indices, the Normalised Difference Vegetation Index (NDVI) and the Enhanced Vegetation Index (EVI; see Volumes 2 and 3A).

To avoid the problems associated with cloud cover in visible and infrared data, several northern hemisphere space agencies have developed and operate a number of microwave sensors on satellite platforms. The Canadian Radarsat series carry a C-band SAR with movable incidence angle and can acquire imagery with a range of spatial resolutions. Radarsat-2 SAR has multiple polarisation modes including a fully polarimetric mode. The ESA operated ERS-1 from 1991 to 2000, ERS-2 from 1995–2011 and launched Envisat in 2001. Each of these satellites carried an array of imaging and non-imaging devices, including C-band radar and optical/thermal radiometers and spectrometers. The JERS-1 satellite (Japan, 1992–1998), which carried an L-band SAR and optical camera, was replaced by the ALOS platform and its optical/SAR sensors (see Table 12.6). Data from these sensors have been used for numerous global applications (see Volumes 2 and 3).

46. TERN AusCover Remote Sensing Data Facility: <http://www.auscover.org.au/data/product-list>

## 12.3 Further Information

EO Handbook (CEOS, 2016): <http://www.eohandbook.com>

Geoscience Australia (GA): <http://www.ga.gov.au/earth-observation.html>

National Aeronautical and Space Agency (NASA): <http://www.nasa.gov>

NASA World Wind: <http://worldwind.arc.nasa.gov>

NASA Worldview: <https://worldview.earthdata.nasa.gov>

Landsat: <http://landsat.gsfc.nasa.gov>  
<http://landsat.usgs.gov>

MODIS: <http://modis.gsfc.nasa.gov>

NOAA Geostationary Satellite Server: <http://www.goes.noaa.gov/index.html>

World Meteorological Organisation (WMO): [http://www.wmo.int/pages/index\\_en.html](http://www.wmo.int/pages/index_en.html)

Coordinating Group of Meteorological Satellites (CGMS): <http://www.cgms-info.org>

ASPRS Guide to Land Imaging Satellites (Stoney, 2008)

European Space Agency (ESA): <http://www.esa.int/ESA>

Japanese Aerospace Exploration Agency (JAXA): <http://global.jaxa.jp>

Interactive Satellite Map: <http://richiecar michael.github.io/sat/index.html>

## 12.4 References

- Campbell, J. B. (2006). Introduction to Remote Sensing, Fourth Edn. Guilford Press.
- CEOS (2015). The Earth Observation Handbook. Committee on Earth Observation Satellites, ESA Communications, The Netherlands. Retrieved from <http://www.eohandbook.com>.
- CEOS (2016). The CEOS Database. Retrieved from <http://database.eohandbook.com>.
- CGMS (2016). Coordinating Group of Meteorological Satellites. Retrieved from <http://www.cgms-info.org>.
- ESA (2016). European Space Agency. Retrieved from <http://www.esa.int/ESA>.
- Frulla, L. A., Milovich, J. A., and Gagliardini, D. A. (1995). Illumination and Observation Geometry for NOAA-AVHRR Images. International Journal of Remote Sensing, 16(12), pp. 2233-2253.
- Fujita, T. G., Bradbury, D. L., Murino, C., and Mull, L. (1968). A study of mesoscale cloud motions computed from ATS-1 and terrestrial photographs from satellite (Research Paper 71). Mesometeorological research project. Department of Geophysical Sciences, University of Chicago.
- Geoscience Australia (2016). Geoscience Australia. Retrieved from <http://www.ga.gov.au>.
- Hansen, M. C., Defries, R. S., Townshend, J. R. G., and Sohlberg, R. (2000). Global land cover classification at 1km spatial resolution using a classification tree approach. International Journal of Remote Sensing, 21(6-7), pp. 1331-1364. doi:<http://dx.doi.org/10.1080/014311600210209>.
- JMA (2016). Japan Meteorological Agency. Retrieved from <http://www.jma.go.jp/jma/jma-eng/satellite/introduction/history.html>.
- Justice, C. O., and Townshend, J. R. G. (2002). Special issue on the moderate resolution imaging spectroradiometer (MODIS): a new generation of land surface monitoring. Remote Sensing of Environment, 83(1-2), pp. 1-2. doi:[http://dx.doi.org/10.1016/S0034-4257\(02\)00083-4](http://dx.doi.org/10.1016/S0034-4257(02)00083-4).
- Justice, C. O., Townshend, J. R. G., Holben, B. N., and Tucker, C. J. (1985). Analysis of the phenology of global vegetation using meteorological satellite data. International Journal of Remote Sensing, 6(8), pp. 1271-1318. doi:<http://dx.doi.org/10.1080/01431168508948281>.
- Kalvelage, T. (2010). Landsat Project Status—Landsat Science Team Meeting 2010. United States Geological Survey. Retrieved from [http://landsat.usgs.gov/documents/Jan\\_2010\\_ScienceTeamMeeting\\_LandsatOverview\\_TomK\\_final\\_Jan19.pdf](http://landsat.usgs.gov/documents/Jan_2010_ScienceTeamMeeting_LandsatOverview_TomK_final_Jan19.pdf).
- Kelly, G. A., Forgan, B. W., Powers, P. E., Le Marshall, J. F., Hassett, M., and O'Connor, B. (1983). A satellite-based operational system for upper air analysis in the Australian region. Remote Sensing of Environment, 13(5), pp. 369-390. doi:[http://dx.doi.org/10.1016/0034-4257\(83\)90007-X](http://dx.doi.org/10.1016/0034-4257(83)90007-X).
- Kelly, G. A., Mills, G. A., and Smith, W. L. (1978). Impact of Nimbus-6 Temperature Soundings on Australian Region Forecasts. Bulletin of the American Meteorological Society, 59, pp. 393-405.
- Le Marshall, J. F., C., S., and Pescod, N. (1996a). Estimation and assimilation of hourly high spatial resolution wind vectors based on GMS 5 observations. Australian Meteorological Magazine, 45, pp. 279-284.

- Le Marshall, J. F., Davidson, R. E., Willmott, M. E., and Powers, P. E. (1989). A physically based operational atmospheric sounding system for TOVS data in the Australian region. *Australian Meteorological Magazine*, 37, pp. 193-199.
- Le Marshall, J. F., Leslie, L. M., and Bennett, A. F. (1996b). Tropical Cyclone Beti - an example of the benefits of assimilating hourly satellite wind data. *Australian Meteorological Magazine*, 45, pp. 275-279.
- Le Marshall, J. F., Pescod, N., Seaman, B., Mills, G., and Stewart, P. (1994). An Operational System for Generating Cloud Drift Winds in the Australian Region and Their Impact on Numerical Weather Prediction. *Weather and Forecasting*, 9(3), pp. 361-370. doi:[http://dx.doi.org/10.1175/1520-0434\(1994\)009%3C0361:AOSFGC%3E2.0.CO;2](http://dx.doi.org/10.1175/1520-0434(1994)009%3C0361:AOSFGC%3E2.0.CO;2).
- Le Marshall, J. F., Pescod, N. R., Khaw, A., and Allen, G. (1993). The real time generation and application of cloud drift winds in the Australian region. *Australian Meteorological Magazine*, 42, pp. 89-103.
- Le Marshall, J. F., Pescod, N. R., Mills, G. A., and Stewart, P. K. (1992). Cloud drift winds in the Australian Bureau of Meteorology. *Australian Meteorological Magazine*, 40, pp. 247-250.
- Le Marshall, J. F., Pescod, N. R., Mills, G. A., and Stewart, P. K. (1999). Local estimation of GMS-5 water vapour motion vectors and their application to Australian region numerical weather prediction. *Australian Meteorological Magazine*, 48, pp. 73-77.
- Le Marshall, J. F., Smith, W. L., and Callan, G. M. (1985). Hurricane Debby—An Illustration of the Complementary Nature of VAS Soundings and Cloud and Water Vapor Motion Winds. *Bulletin of the American Meteorological Society*, 66(3), pp. 258-263. doi:[http://dx.doi.org/doi:10.1175/1520-0477\(1985\)066%3C0258:HDIOTC%3E2.0.CO;2](http://dx.doi.org/doi:10.1175/1520-0477(1985)066%3C0258:HDIOTC%3E2.0.CO;2).
- Leslie, L. M., Le Marshall, J. F., Morison, R. P., Spinoso, C., Purser, R. J., Pescod, N., and Seecamp, R. (1998). Improved Hurricane Track Forecasting from the Continuous Assimilation of High Quality Satellite Wind Data. *Monthly Weather Review*, 126(5), pp. 1248-1258. doi:[http://dx.doi.org/10.1175/1520-0493\(1998\)126%3C1248:IHTFFT%3E2.0.CO;2](http://dx.doi.org/10.1175/1520-0493(1998)126%3C1248:IHTFFT%3E2.0.CO;2).
- NASA (2009). Catalog of Earth Satellite Orbits. Retrieved from <http://earthobservatory.nasa.gov/Features/OrbitsCatalog/>.
- NASA (2016). WRS-2 map. Retrieved from <http://landsat.gsfc.nasa.gov/wp-content/uploads/2013/01/wrs2.gif>
- Smith, W. L., Woolf, H. M., Hayden, C. M., Schreiner, A. J., and Le Marshall, J. F. (1983). The Physical Retrieval TOVS Export Package. Paper presented at the First International TOVS Study Conference, Igls, Austria.
- Smith, W. L., Woolf, H. M., Hayden, C. M., Wark, D., and McMillin, L. (1979). The TIROS-N operational vertical sounder. *Bulletin of the American Meteorological Society*, 60, pp. 1177-1187.
- Stoney, W. E. (2008). ASPRS Guide to Land Imaging Satellites. Noblic Inc. Retrieved from [http://www.asprs.org/a/news/satellites/ASPRS\\_DATABASE\\_021208.pdf](http://www.asprs.org/a/news/satellites/ASPRS_DATABASE_021208.pdf).
- Townshend, J. R. G., and Justice, C. O. (1988). Selecting the Spatial-Resolution of Satellite Sensors Required for Global Monitoring of Land Transformations. *International Journal of Remote Sensing*, 9(2), pp. 187-236.
- Wessels, K. J., De Fries, R. S., Dempewolf, J., Anderson, L. O., Hansen, A. J., Powell, S. L., and Moran, E. F. (2004). Mapping regional land cover with MODIS data for biological conservation: Examples from the Greater Yellowstone Ecosystem, USA and Para State, Brazil. *Remote Sensing of Environment*, 92(1), pp. 67-83. doi:<http://dx.doi.org/10.1016/j.rse.2004.05.002>.
- WMO (2016). World Meteorological Organisation. Retrieved from <http://wmo.int>.
- Young, M. T., Doolittle, R. C., and Mace, M. (1972). Operational procedures for estimating wind vectors and geostationary satellite data (NESS 39). NOAA Technical Memorandum. National Environmental Satellite Service, National Oceanographic and Atmospheric Administration, U.S. Department of Commerce.
- Zapotocny, T. H., Jung, J. A., Le Marshall, J. F., and Treadon, R. E. (2007). A Two-Season Impact Study of Satellite and In Situ Data in the NCEP Global Data Assimilation System. *Weather and Forecasting*, 22(4), pp. 887-909. doi:<http://dx.doi.org/10.1175/WAF1025.1>.
- Zapotocny, T. H., Jung, J. A., Le Marshall, J. F., and Treadon, R. E. (2008). A Two-Season Impact Study of Four Satellite Data Types and Rawinsonde Data in the NCEP Global Data Assimilation System. *Weather and Forecasting*, 23(1), pp. 80-100. doi:<http://dx.doi.org/10.1175/2007WAF2007010.1>.







# **EMR Sensors for Earth Observation**





The next three sections consider aspects of sensors that detect electromagnetic radiation (EMR) for Earth Observation (EO). Section 13 introduces the basic principles of sensing EMR, including sensor design and sensor categories. Detection systems that are used to remotely acquire EO data can be considered in terms of three broad groups:

- imaging—active and passive sensors that record radiation for a contiguous grid of locations on the Earth’s surface (see Sections 14 and 15);
- non-imaging—active and passive sensors that record radiation for discrete locations on the Earth’s surface (see Section 16.1); and
- sounding—active and passive sensors that record the vertical distribution of radiation within Earth’s atmosphere and oceans, often at defined altitudes/depths (see Section 16.2).

## Contents

<b>13</b>	<b>Sensing Electromagnetic Radiation</b>	<b>169</b>
<b>14</b>	<b>Passive Imaging Systems</b>	<b>179</b>
<b>15</b>	<b>Active Imaging Systems</b>	<b>203</b>
<b>16</b>	<b>Non-imaging and Sounding Systems</b>	<b>215</b>



# 13 Sensing Electromagnetic Radiation

An overview of measuring EMR is provided in Section 13.1 below and the major types of Earth Observation (EO) sensors are introduced in Section 13.2. Aspects of EM sensor design and performance are discussed in Sections 13.3 and 13.4 respectively. CEOS categories for EO sensors are reviewed in Section 13.5.

## 13.1 Measuring Electromagnetic Radiation

As introduced in Section 5 above, EMR is a form of energy that can be transmitted through empty space and between objects. The EMR spectrum spans from very short wavelengths (such as gamma rays and X-rays), through the visible spectrum, to very long waves (such as microwaves and radio frequency waves). While all EMR waves travel at the speed of light ( $3 \times 10^8 \text{ m sec}^{-1}$ ), the energy they carry varies with both the wavelength/frequency of radiation and its intensity. Being a wave, EMR has properties described in terms of intensity and phase as a function of wavelength. These properties are both used in various forms of remote sensing. As introduced in Section 2.5, EMR can be observed in terms of several characteristics, including:

- amplitude—maximum oscillation of wave from midpoint and proportional to the energy carried;
- wavelength or frequency—distance travelled in one full wave cycle or number of cycles per unit time, with shorter wavelength at higher frequency EMR carrying more energy;
- polarisation—orientation of electric field of EMR relative to reference vector; and
- coherence—extent to which two waves oscillate in phase; for EM waves, this characteristic describes a relationship in time (see Section 2.5.5).

EMR that is emitted by a source can be reflected, transmitted, absorbed or re-emitted by objects or surfaces (see Section 5). Most passive EO sensors detect the intensity of incoming solar energy that is reflected, transmitted (that is, scattered) or re-emitted by terrestrial materials into the field of view of the

sensor. Active sensors generate their own energy source, which is radiated towards a target, and can detect range to the target using phase information of the energy backscattered from the target.

The specific geometric relationships between the sensor and target directly impact on the energy being detected by a remote sensing device. In simple terms, the energy that is observed by a sensor can be considered as falling within a viewing ‘cone’. Accordingly, measured radiation needs to be quantified in terms of solid (three-dimensional) angles, which are represented units of steradians (see Figure 2.1). Specific aspects of illumination and viewing geometries are further discussed in Volume 1B—Section 3 and Volume 1X—Appendix 5.

The terminology used to quantify electromagnetic radiation (EMR) is introduced in Section 2.6. It is recommended that readers review this material in conjunction with the following sub-sections. For a more detailed treatment of these topics, readers are referred to the *Manual of Remote Sensing* (Colwell, 1983), *The Light Measurement Handbook* (Ryer, 1997), *ASPRS Manual of Remote Sensing* (Morain and Budge, 1998), or Elachi and van Zyl (2006).

Similarly, the mechanism of human colour vision and the representation of colour are introduced in Section 2.7. As detailed in Volumes 2 and 3, in order to detect and identify features in EO imagery, most image-based thematic mapping techniques attempt to mimic the processes of human vision, often using wavelengths undetected by the human visual system.

**Background image:** Hymap airborne hyperspectral image mosaic of Hawker Springs Complex, 80 km west of Lake Eyre, SA. It is displayed using the  $2.22 \mu\text{m}$  band as red, the  $0.833 \mu\text{m}$  band as green and the  $0.444 \mu\text{m}$  band as blue. This region features wetlands in an arid environment, fed by Great Artesian Basin springs. This imagery was acquired by HyVista Corporation for the Allocating Water and Maintaining Springs of the Western Great Artesian Basin project in 2009.  
**Source:** Megan Lewis, University of Adelaide



## 13.2 Earth Observation Sensors

By definition, a remote sensing device acquires information about a target, such as an object or surface, by detecting energy from it. Since there is no physical contact between the sensor and the target, the sensor must rely on measuring some form of energy that is being radiated by the target. In this text, we use the ‘sensor’ to refer to the remote sensing device or instrument and ‘detector’ to describe the component of a sensor which actually detects EMR.

The source of the radiation detected by a remote sensor may or may not be independent of the sensing device. Active remote sensing devices, such as radar (microwave) and lidar (optical), radiate a particular form of energy towards a target object or surface and then detect the amount of that energy which is scattered or reflected by it. Passive sensors, however, detect energy that originates from an independent source and is scattered or reflected by a target. The major source of EMR detected by passive remote sensors is the Sun, but some radiation also comes

from other celestial bodies and cosmic background radiation. While the Sun is commonly assumed to be a point source of constant illumination, its energy does not emanate from a point and is not constant. The intensity of solar radiation has been shown to vary with time, and remote sensing measurements have contributed to the growing body of knowledge on the precise extent of this variation.

One category of remote sensors, polarimeters, measures polarisation, rather than radiation, characteristics of targets (see Section 2.5.3). These characteristics indicate the shape, shading and roughness of surface and atmospheric features, which are generally uncorrelated with spectral and intensity data acquired by sensors that are designed to observe the radiation reflected or emitted by surface materials (Tyo *et al.*, 2006; Snik *et al.*, 2014).

The major categories of EO sensors are grouped in terms of EMR spectral region in Table 13.1.

**Table 13.1** Spectral regions observed by EO sensors

Note that, in practice, atmospheric windows restrict these ranges for observing Earth’s features (see Table 5.4).

Spectral region	Wavelength	EO sensor	
		Passive	Active
Visible	0.38 to 0.7 $\mu\text{m}$	Passive radiometers	Lidar
Near Infrared (NIR)	0.7 to 1.1 $\mu\text{m}$	Passive spectroradiometers	
Short wave Infrared (SWIR)	1.1 to 3.0 $\mu\text{m}$	Passive imaging spectrometers	
		Polarimeters	
Middle Infrared (MIR)	3.0 to 8.0 $\mu\text{m}$	Passive radiometers	
Thermal Infrared (TIR)	8.0 to 15.0 $\mu\text{m}$	Polarimeters	
Microwave	1 mm to 1 m	Microwave radiometers Microwave spectrometers	Radar Polarimeters Scatterometers
Radio	>10 cm	Passive radiometers Sounders	Imaging radar Altimeters Sounders

*We have all kinds of limitations as human beings.  
I mean we can’t see the whole electromagnetic spectrum;  
we can’t see the very small; we can’t see the very far.  
So we compensate for these short comings with technological scaffoldings.  
(Jason Silva)*

EO sensors for terrestrial, coastal and ocean monitoring (as opposed to atmospheric monitoring) primarily measure EMR that is reflected or emitted from the Earth's surface. These sensors, however, can vary considerably in terms of the resolution and extent of the data they acquire (see Volume 1B—Section 1). Since the characteristics of each sensor are designed to optimise discrimination of specific target features, EO sensors differ in terms of:

- spectral characteristics—such as the wavelength region(s) detected;
- spatial characteristics—such as the ground area 'viewed' for each observation (or pixel size in imagery);
- radiometric characteristics—such as the 'threshold' of energy required to differentiate target radiance levels; and
- temporal characteristics—such as the repeat cycle for subsequent measurements.

Sections 14, 15 and 16 provide a detailed introduction to a range of EO sensors in terms of their spectral sensitivity, operation and application areas. Here we briefly introduce three broad types of sensors in terms of instrument type and function:

- passive sensors—radiometers, spectroradiometers and spectrometers that detect reflected EMR in optical wavelengths and emitted EMR in thermal wavelengths (see Section 13.2.1);
- active sensors—lidar and radar sensors that generate their own energy source then detect its 'echo' (see Section 13.2.2); and
- sounders—active and passive sensors that acquire observations at specific water depths or atmospheric altitudes (see Section 13.2.3).

### 13.2.1 Passive sensors

Reflected solar energy is detected by passive remote sensing devices in the visible, near infrared and middle infrared regions, while the Earth's emitted energy may be detected in the middle infrared, thermal infrared and microwave wavelengths (see Section 5.2.2). A passive sensor actually records the 'radiance', that is the radiation within a solid angle of view, of its target (see Section 2.6.1). To account for variations in the level of incident radiation, 'reflectance' is defined as the ratio of reflected to incident radiation, that is, the proportion of energy reflected by an object. In well-designed passive remote sensing systems, material properties, which are encapsulated in reflectance, dominate (or can be extracted from) the recorded signal.

A wide range of sensors has been designed to cater for the different priorities that can be placed on potential target information. These requirements have produced three fundamental types of passive EMR remote sensing instruments:

- radiometers—measure target radiation in broad wavelength intervals (see Section 13.2.1.1);
- spectroradiometers—measure target radiation in narrow wavelength bands (see Section 13.2.1.2);
- spectrometers—measure target radiation in discrete wavelengths over a wide range to generate a spectrum for the target (see Section 13.2.1.3); and
- polarimeters—measure polarisation characteristics of targets (see Section 13.2.1.4).

#### 13.2.1.1 Radiometers

Radiometers measure EMR from a target in defined wavelength bands. These instruments are used for sensing relatively weak signals, such as thermal infrared or passive microwave, and/or when few spectral measurements per target are required, as in panchromatic or multispectral imagery. Radiometers are often named to indicate the spectral range that they detect, such as 'microwave radiometer'. Imaging radiometers combine a scanning mechanism with one or more radiometer(s) to measure target radiance over an extended area (see Section 14.2). When measuring strong radiance signals, such as in optical wavelengths, radiometers can deliver high spatial resolution imagery (see Section 14.3.1), whereas measurement of weaker emitted radiation delivers imagery with lower spatial resolution (see Sections 14.4 and 14.5).

#### 13.2.1.2 Spectroradiometers

Spectroradiometers are advanced radiometers that measure target radiance for multiple, narrowly-defined, wavelength channels. They are principally designed to capture detailed optical information about the Earth's surface. As further discussed in Section 14.3.2, most current, satellite-borne, multispectral sensors for EO are spectroradiometers.

#### 13.2.1.3 Spectrometers

Spectrometers are precise instruments designed to measure spectra. Imaging spectroscopy (or hyperspectral imaging) acquires imagery in numerous, narrow contiguous spectral channels such that a spectrum for imaged targets can be derived (see Section 14.3.3). Within a finite spectral range, spectrometers separate EMR from a target into a frequency spectrum that shows the constituent wavelengths.

#### 13.2.1.4 Polarimeters

Both imaging and non-imaging passive polarimeters have been designed to measure a range of polarisation information in optical and thermal wavelengths, including specific wavelength regions (spectropolarimeters). In EO, passive polarimeters are primarily used to observe aerosols in the Earth's atmosphere, but can also provide valuable information for surveillance and military applications. Operation of passive polarimeters is beyond the scope of this volume, but interested readers are referred to Tyo *et al.* (2006).

#### 13.2.2 Active sensors

Active remote sensing systems operate in the visible and microwave parts of the EM spectrum. The major categories of active, satellite-borne EO sensors include:

- lidar—measure the vertical distribution of features in the atmosphere, on the Earth's surface, or in shallow water, potentially using multiple polarisations in optical wavelengths (see Section 15.1);
- Synthetic Aperture Radar (SAR)—measure microwave response from surface features, potentially using multiple polarisations (see Sections 15.2);

- altimeters—based on radar or lidar to measure radiation at specific altitudes (see Sections 16.1.2.1 and 16.1.2.2);
- scatterometers—based on radar to measure surface texture (see Section 16.1.2.3); and
- polarimeters—radar instruments for observing polarisation characteristics of a target.

The operation of radar and lidar sensors is further detailed in Sections 15 and 16.

#### 13.2.3 Sounders

A final category of EO instruments includes sounders, which can be designed as both active and passive sensors. Sounders are used to observe properties of:

- the atmosphere at particular altitudes, to derive information about air composition, temperature and movement; or
- water bodies at specified depths, to determine profiles of water depth, colour and temperature.

The types of measurements derived from sounding sensors are further discussed in Section 16.2.

### 13.3 Sensor Design Constraints

Remote sensing devices may record EMR directly onto photographic film or electronically code the radiation in numeric form to produce a digital image. Photographic recording of data simply requires standard film processing to obtain an image for human interpretation, but such data need to be digitised before being processed by a computer (see Volume 1X—Appendix 4.3).

A digital remote sensor observes energy that is radiated by a target then quantifies the observed energy levels as a digitised electronic signal. Since the nature of interaction between EMR and matter changes across the EMR spectrum, different techniques are required to observe energy in different wavelength regions. For example, sensors that detect optical wavelengths use lenses and optical components to observe radiation, whereas sensors detecting longer EMR wavelengths (such as microwave and radio frequencies) commonly use antennae for this purpose.

The simplest sensors incorporate components to detect and record radiation, but most also include components for focussing and separating radiation into sub-categories, such as specific wavelength or frequency ranges (known as spectral channels or bands) or polarisations, and standardising the detected and digitised levels of radiation to a reference measurement scale. Components of specific sensors are discussed in greater detail in Sections 14, 15 and 16.

While we have introduced EO sensors in generic terms, each sensor is designed for a specific purpose and only produces reliable observations when operated within defined conditions, such as the specified ranges for:

- platform speed and stability;
- target radiation levels; and
- ambient temperature and humidity.

The engineering embodied in all sensors is the result of design decisions, which have been dictated by technical and management constraints. Each sensor has a finite time to measure the radiance from a target object or surface. The time interval required for a sensor to register a valid observation is known as the dwell time. Thus, the sensor platform must travel at an appropriate speed to provide sufficient dwell time for each observation. For a given dwell time, trade-offs are necessary between both:

- the number of measurements of a target and the strength of the measured signal(s); and
- the number of targets measured and the strength of the measured signal(s).

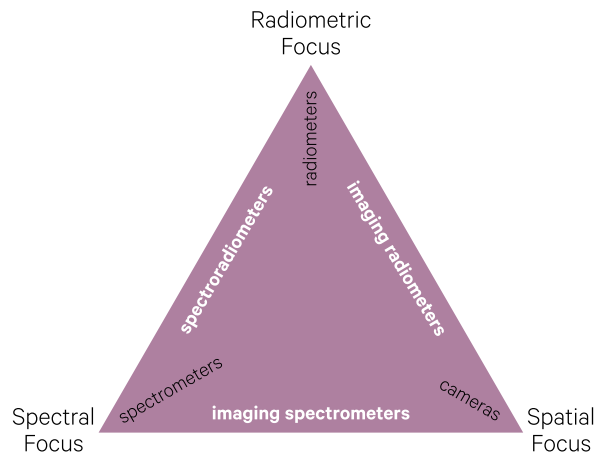
As illustrated in Figure 13.1a, these relationships can be viewed as a triad in which the apexes represent focus on:

- spatial information about the target;
- spectral information about the target; and
- radiometric information about the target (Elachi and van Zyl, 2006).



**Figure 13.1** Information acquired by sensors

Sensor design involves trade-offs between focussing on radiometric, spectral and spatial detail.



Adapted from: Elachi and van Zyl (2006) Figure 1-1

The design of any sensor implicitly involves assigning priorities to each type of potential information about the target object or surface. For example, in a passive imaging sensor:

- spatial focus could equate to the spatial resolution of the image (pixel size);
- spectral focus could equate to the spectral density of the image (number of spectral channels); and
- radiometric focus could equate to the radiometric resolution of the image (number of bits per pixel).

In essence, for the reasons discussed above, any given sensor cannot simultaneously acquire detailed spatial, spectral *and* radiometric information. The implications of design constraints for particular types of sensors are further considered in Volume 1B—Sections 1 and 2.

## 13.4 Sensor Performance Metrics

One of the primary goals in sensor design is to minimise ‘noise’. In this context, noise means the acquisition of false readings that result from the sensor components rather than the target object or surface. It is also important that, for a given spectral band, the sensor response is uniform both over the detected wavelengths and over time, and linear with respect to the incident radiation (Norwood and Lansing, 1983).

The most commonly encountered metric to indicate noise levels registered by a sensor is the Signal-to-Noise Ratio (SNR or S/N). Ideally sensors register much higher levels of signal than noise, so higher SNR values are more desirable (see also Volume 1B—Section 2.1.3). Some of the other performance metrics commonly used to compare sensors are summarised in Table 13.2. These metrics are referenced in subsequent sections.

**Table 13.2** Common sensor performance metrics

$V_n$  = RMS noise voltage;  $A$  = detector area;  $q$  = electron charge;  $R$  = responsivity  
 $f$  = frequency of optical signal;  $\Delta f$  = bandwidth;  $h$  = Planck’s constant (see Section 2.11)

Performance Measure	Abbreviation	Definition	Units	Indicates
Signal-to-noise ratio	SNR	$\frac{P_{\text{signal}}}{P_{\text{noise}}}$	–	Strength of sensor signal relative to background noise
Quantum Efficiency	$\eta$	$\frac{\text{signal electrons}}{\text{incident photons}}$	%	Conversion efficiency of incident photons to signal electrons (wavelength-dependent)
Spectral responsivity	$R_\lambda$	$\eta \frac{q}{hf}$	A/W	Electrical output per optical input (wavelength-dependent)
Noise Equivalent Power	NEP	$\frac{V_n}{R}$	W	Signal power to result in SNR ratio of 1 in 1 Hz output bandwidth
Spectral Noise Equivalent Power	$NEP_\lambda$	$\frac{V_n}{R_\lambda}$	W	Wavelength-dependent NEP
Detectivity	$D$	$\frac{1}{NEP}$	$W^{-1}$	Smallest detectable signal (reciprocal of NEP)
Specific detectivity	$D^*$	$\frac{\sqrt{A \Delta f}}{NEP}$	$W^{-1} \text{ cm} \cdot \text{sec}^{-1/2}$	Normalised measure of smallest detectable signal

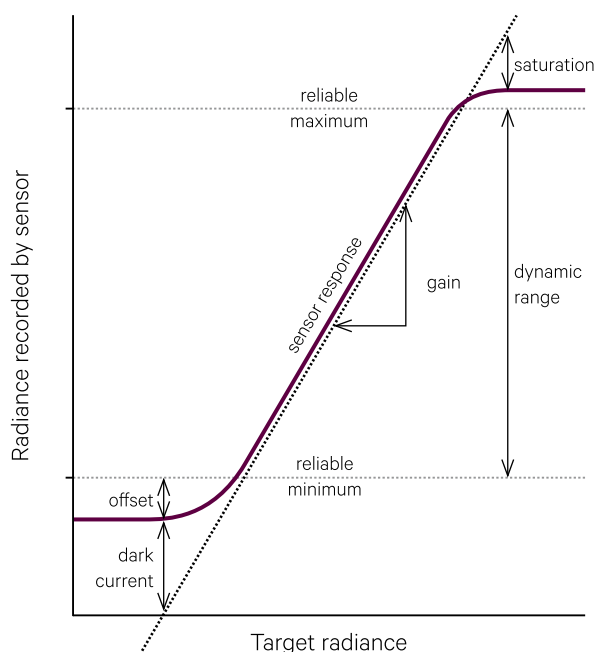
Source: Colwell (1983); Accetta and Schumaker (1993)

Each sensor band is designed to detect target radiance within a defined energy range, known as its dynamic range. As illustrated in Figure 13.2, this range conservatively lies within the actual minimum and maximum sensitivity of the sensor, with the difference between the actual minimum and the dynamic range minimum being known as the offset. Below the actual minimum sensitivity, observations are known as ‘dark current’, which is likely to result from the electronic components rather than target radiance. Similarly, above the actual maximum sensitivity, the sensor reaches saturation, that is, it cannot detect any additional target radiance. In image sensors, the characteristics of individual detector components can permit a saturated pixel to impact the values observed for adjacent pixels, potentially resulting in an imaging artefact that is more extensive than a single pixel (see Volume 1B—Section 2).

Within the dynamic range, sensor design aims to result in sensor readings that are confidently related to the radiance of the target object or surface. Ideally, the relationship between the target radiance and the observed radiance, or the *gain*, is linear (see Figure 13.2), in which case this relationship can be summarised as the slope of the line. For a given target object or surface, a high gain sensor would record a larger range of radiance values than one with low gain. In some sensors, the gain can be selected from pre-defined ranges to be most appropriate to the target being observed.

**Figure 13.2** Sensor performance terms

Each sensor band detects radiance within a defined energy range—the dynamic range—between its actual minimum and maximum sensitivities. The relationship between input and output radiance values is known as the gain.

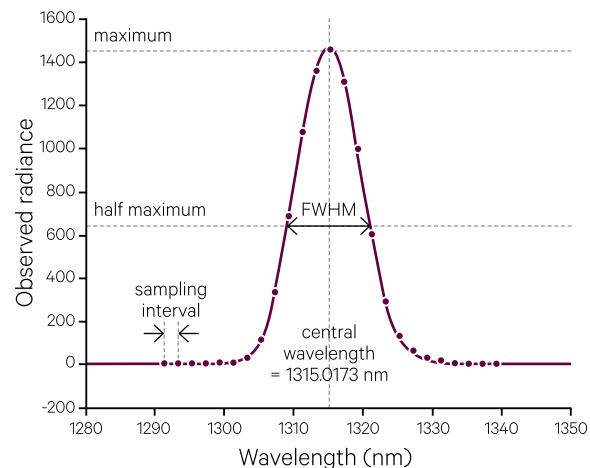


Adapted from: Campbell and Wynne (2011) Figure 4.5

**Figure 13.3** Spectral response function of Hyperion SWIR band

The spectral response function of a sensor band shows the magnitude of sensor sensitivity over a range of wavelengths. This function can be characterised by the central wavelength and the Full Width Half Maximum (FWHM), where FWHM defines the wavelength range detected at half the maximum signal.

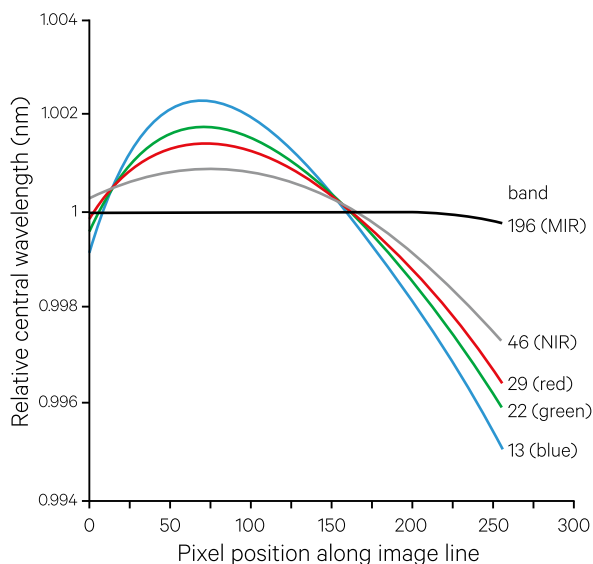
This graph shows the spectral response function of a Hyperion SWIR pixel with FWHM = 10.8335 nm.



Source: Jupp et al. (2004) Figure 2

**Figure 13.4** Relative spectral variation across Hyperion image line

When sensor optics are not in perfect alignment, different wavelengths may be detected for different pixels across an image line. Note: Scale of y-axis is exaggerated.



Source: Jupp et al. (2004) Figure 3

Gains vary between different sensors and also between different bands in a single sensor. Each sensor band measures radiant energy over a range of wavelengths, with instrument sensitivity to different wavelengths varying slightly within this range. The magnitude of sensor response as a function of wavelength is called the ‘spectral response function’ (or ‘bandpass response function’). In many cases, the response can be modelled by an analytic function, as illustrated in Figure 13.3. In this example, the response function can be conveniently characterised by the central wavelength ( $\lambda_c$ ) and the Full Width Half Maximum (FWHM) of the spectral response function, where FWHM defines those wavelengths with half the energy of the maximum signal (Jupp *et al.*, 2004).

In some sensors, both the central wavelength and FWHM can vary across a line of pixels. For example, the Hyperion sensors formed lines of image pixels by dispersing an imaged slit across the detectors of two primary arrays of the pushbroom (Barry, 2001), which can lead to a minor, non-uniform spectral response across the elements of the arrays, or the ‘spectral smile’ (or frown). As illustrated in Figure 13.4, this effect also varies with wavelength, in this case being most active in visible and NIR wavelengths, and virtually non-existent in SWIR.

### 13.5 CEOS Sensor Categories

The comprehensive publication, *The Earth Observation Handbook* (CEOS, 2015) compiles recent, current and future satellite missions and instrument sensors managed by member organisations of the Committee on Earth Observation Satellites (CEOS). The 2015 edition includes 260 satellites and 400 different instruments. This compendium does not include commercially-operated systems. In the 2015

edition, sensors are grouped into 16 categories on the basis of instrument design and function (see Table 13.3). This list demonstrates the diversity of EO sensors that currently provide information about our planet. Examples of sensors in those categories that are most commonly used for EO research and development in Australia are summarised in Table 13.4.

**Table 13.3** CEOS sensor categories<sup>47</sup>

Instrument Type	Design Purpose	EM Wavelengths	Radiation Source	Detection System	Applications
Atmospheric chemistry instruments	Various techniques and different parts of the EM spectrum to measure atmospheric composition	UV, optical, thermal infrared, microwave	Passive	Non-imaging, Sounding	Atmospheric studies
Atmospheric temperature and humidity sounders	Measure distribution of IR or microwave radiation emitted by the atmosphere, to deliver vertical profiles of temperature and humidity through the atmosphere	Thermal Infrared, microwave	Passive (and Active)	Sounding	Atmospheric studies
Cloud profile and rain radars	Radars at cm wavelengths for rainfall, as well as very short wavelength (mm) radar (typically 94 GHz), and lidar to detect scattering from non-precipitating cloud droplets or ice particles, to deliver data on cloud characteristics such as moisture content and base height	Microwave	Active	Sounding	Weather prediction, climate studies
Earth radiation budget radiometers	Measure the radiation balance between the incoming radiation from the Sun and the outgoing reflected and scattered solar radiation, plus the thermal infrared emission to space	Optical, thermal infrared, microwave	Passive	Imaging Sounding	Climate studies
<i>Gravity, magnetic field and geodynamic instruments<sup>49</sup></i>	<i>Instruments and supporting systems used to derive information on the Earth's gravity field, magnetic field or geodynamic activity</i>	<i>Non-EM</i>	<i>Passive</i>	<i>Imaging (non-EM)</i>	<i>Geoid monitoring, ice studies, hydrology</i>
High Resolution Optical Imagers	Measure detailed optical radiance from the Earth's surface; generally nadir-viewing panchromatic and multispectral instruments with a horizontal spatial resolution up to 100 m and swath widths around 100 kilometres	Optical	Passive	Imaging	Land cover mapping and monitoring, geological mapping and cartography

47. Note: instruments sensing energy sources other than EMR are italicised.



Instrument Type	Design Purpose	EM Wavelengths	Radiation Source	Detection System	Applications
Hyperspectral Imagers (or imaging spectroscopy)	Measure optical reflectance from Earth's surface in many (usually 100 or more), narrow, contiguous, spectral bands	Optical	Passive	Imaging	Characterising spectral properties, especially for minerals, vegetation and coastal studies
Imaging multispectral radiometers (visible/infrared)	Measure optical and thermal infrared reflectance from the Earth's surface and atmosphere, generally with spatial resolution from 100 m to several kilometres, for broad ground swaths (thousands of km)	Optical, Thermal Infrared	Passive	Imaging, Sounding	Global and regional studies of vegetation, snow, ice and surface temperature, especially to identify and monitor biosphere and ocean processes
Imaging multispectral radiometers (passive microwave)	Measure microwave emittance (1-40 GHz and 80-100 GHz) from the Earth's surface at low spatial resolutions	Microwave	Passive	Imaging	Snow and ice mapping and monitoring soil moisture, vegetation health and ocean salinity
Imaging microwave radars (X-Band, C-Band, and L-Band)	Measure backscattered signals from transmissions in the range 1-10 GHz at spatial resolutions between 10 m and 100 m, with a swath width of 100-500 km. Includes both synthetic aperture radars (SARs) and real aperture side-looking imaging radar systems	Microwave	Active	Imaging (after processing)	Ocean waves and pollution, vegetation structure especially in tropical areas, snow and ice sheet measurements, flood monitoring, subsidence studies
Lidars	Measure radiation reflected from the Earth's surface or atmosphere when illuminated by a laser source	Optical	Active	Imaging (after processing)	Surface topography, vegetation height, atmospheric studies
Lightning Instruments	Optical sensors (~777nm) with high-speed cameras, focussed on cloud tops, detect lightning	Optical	Passive	Imaging	Weather prediction, climate studies
Multiple direction/polarisation SAR instruments (or polarimeters)	Custom-built radar instruments for observing the direction/polarisation characteristics of the target's signature to derive geophysical information	Microwave	Active	Imaging (after processing), sounding	Surface temperature, aerosol modelling for improved Radiative transfer models and biomass estimates, soil moisture and ocean salinity estimates
Ocean colour instruments	Measure radiance from marine waters in visible and near infrared wavelengths (400-800 nm), typically with high spectral resolution and low spatial resolution	Optical	Passive	Imaging	Shallow water mapping, chlorophyll content, suspended sediment, water dynamics, marine pollution
Radar altimeters	Use the ranging capability of radar to measure the topographic profile of the Earth's surface (land and ocean) along the satellite track	Microwave	Active	Non-imaging	Topography of water surface and substratum (seafloor), sea ice, ocean wind speeds, wave height
Scatterometers	Transmit radar pulses and receives backscattered energy, the intensity of which depends on the roughness and dielectric properties of a particular target	Microwave	Active	Non-imaging	Sea surface wind speed and direction, weather and wave prediction, soil moisture, snow levels

Adapted from: Geoscience Australia (2011); CEOS (2016)

**Table 13.4** EO sensors commonly used in Australia

EO Data Type	Recent, current and planned key providers (and missions)	Predominant Latency Requirement
Optical: Low Resolution	NASA (MODIS) NOAA/EUMETSAT (AVHRR/ NPP/JPSS series) JMA (Himawari series) ESA/EC (Sentinel-3 series) JAXA (GCOM-C series) CMA (FY-2 series)	Hours/Weeks
Optical: Medium Resolution	USGS (Landsat-5/7/8) ESA/EC (Sentinel-2 series)	Days/Weeks
Optical: High Resolution	USA & European commercial providers (Worldview, GeoEye, Pleiades) Airborne operators	Days/Weeks
SAR: C-band	ESA/EC (Envisat/Sentinel-1 series) CSA (Radarsat/RCM)	Weeks
SAR: L-band	CONAE-ASI (SAOCOM-1A) JAXA (ALOS-2)	Weeks
SAR: X-band	ASI (COSMO-Skymed series) DLR (TerraSAR-X series)	Weeks
Passive Microwave Radiometry	NASA (Aqua/ GPM, Aquarius, SMAP) NOAA/DOD (DMSP series) JAXA/NASA (TRMM/ GCOM-W series) ESA (SMOS) ISRO (Megha-Tropiques, RISAT-3)	Hours
Radar Altimetry	EUMETSAT-NOAA (Jason series) ESA/EC (Envisat/Sentinel-3 series)	Hours
Hyperspectral Imagery	NASA (EO-1) DLR (EnMAP) ASI (PRISMA) METI/JAXA (ALOS-3)	Weeks
Lidar	NASA (CALIPSO) ESA/JAXA (EarthCARE)	Weeks
Ocean Colour	NASA (MODIS) ISRO (OCEANSAT) ESA/EC (MERIS/Sentinel-3 series) JAXA (GCOM-C series) NOAA (NPP/JPSS series)	Hours

Adapted from: CSIRO (2012) Table 6-1

## 13.6 Further Information

---

### Measurement of Light:

Ryer (1997)

Gigahertz-Optik: <http://www.light-measurement.com/tutorials-on-light-measurement/>

### EO Sensors:

Colwell (1983)—see chapters 7 and 8.

EMR Basics for Remote Sensing: [http://www.usna.edu/Users/oceano/raylee/SP212/EMR/RLee\\_EMR\\_fundamentals.pdf](http://www.usna.edu/Users/oceano/raylee/SP212/EMR/RLee_EMR_fundamentals.pdf)

NASA Earth System Science Remote Sensors: <https://earthdata.nasa.gov/data/standards-and-references/nasa-earth-system-science-remote-sensors>

CEOS (2016)

## 13.7 References

---

Accetta, J. S., and Schumaker, D. L. (1993). Electro-Optical Systems Design, Analysis, and Testing. Chapter 4 in 'The Infrared and ElectroOptical Systems Handbook' (Ed: M. C. Dudzik). Environmental Research Institute of Michigan, Ann Arbor, Michigan.

Barry, P. (2001). EO-1/Hyperion Science Data User's Guide, Level 1B (CAGE Number 11892). TRW Space, Defense and Information Systems, Redondo Beach, CA.

Campbell, J. B., and Wynne, R. H. (2011). Introduction to Remote Sensing, Fifth Edn. The Guilford Press, New York.

CEOS (2015). The Earth Observation Handbook. Committee on Earth Observation Satellites, ESA Communications, The Netherlands. Retrieved from <http://www.eohandbook.com>.

CEOS (2016). The CEOS Database. Retrieved from <http://database.eohandbook.com>.

Colwell, R. N. (1983). Manual of Remote Sensing, Second Edn. American Society of Photogrammetry, Falls Church, Virginia.

CSIRO (2012). Continuity of Earth Observation Data for Australia: Research and Development Dependencies to 2020. CSIRO, Canberra.

Elachi, C., and van Zyl, J. (2006). Introduction to the Physics and Techniques of Remote Sensing, Second Edn. Wiley Interscience, New Jersey.

Geoscience Australia (2011). Continuity of Earth Observation Data for Australia: Operational Requirements to 2015 for Lands, Coasts and Oceans. Geoscience Australia, Canberra.

Jupp, D. L. B., Datt, B., Lovell, J., Campbell, S., King, E., and others (2004). Discussions around Hyperion Data: Background Notes for the Hyperion Data Users Workshop. CSIRO Office of Space Science and Applications Earth Observation Centre, Canberra.

Morain, S. A., and Budge, A. M. (1998). Earth Observing Platforms and Sensors, Vol. 1, Third Edn., Ed: R. A. Ryerson, Manual of Remote Sensing. American Society for Photogrammetry and Remote Sensing (ASPRS); John Wiley & Sons, Inc., New York.

Norwood, V. T., and Lansing, J. C. (1983). Electro-optical Imaging Sensors. Chapter 8 in 'Manual of Remote Sensing' (Ed: R. N. Colwell). 2nd Edn. American Society of Photogrammetry, Falls Church, Virginia.

Ryer, A. (1997). Light Measurement Handbook. Retrieved from <http://www.intl-lighttech.com/services/ilt-light-measurement-handbook>.

Snik, F., Craven-Jones, J., Escuti, M., Fineschi, S., Harrington, D., de Martino, A., Mawet, D., Riedi, J., and Tyo, J. S. (2014). An Overview of Polarimetric Sensing Techniques and Technology with Applications to Different Research Fields. 'Polarization: Measurement, Analysis, and Remote Sensing XI' (Eds: D. B. Chenault, and D. H. Goldstein), Vol. 9099.

Tyo, J. S., Goldstein, D. L., Chenault, D. B., and Shaw, J. A. (2006). Review of passive imaging polarimetry for remote sensing applications. *Applied Optics*, 45(22), pp. 5453-5469. doi:<http://dx.doi.org/10.1364/ao.45.005453>.



# 14 Passive Imaging Systems

Passive Earth Observation (EO) sensors either detect solar energy reflected by the Earth's surface in the visible to middle infrared region of the EM spectrum, or measure the thermal IR or microwave radiation emitted from the Earth. While traditional, film-based cameras have recorded countless images for EO and other purposes, the focus in this section is on current digital camera technology, which directly converts detected radiation into a digital value for each cell (pixel) in some pre-defined image grid. Relevant aspects of aerial photography acquisition and usage, and the process of digitising an image, are described in Volume 1X—Appendix 4.

In a digital image, colours are represented by numbers (see Volume 2A). A grid (or some other systematic tessellation) pattern is used to record the colours in the image, each cell being assigned one or more colour numbers. Each cell in the image grid is called a 'picture element' or pixel.

Imaging systems record a two-dimensional array of pixel values for each image channel. When an image is acquired digitally, radiance (in a specific range of wavelengths) is quantified for each pixel. This set of measurements comprises one image 'channel' or 'band'. For example, in a panchromatic image, which records a single channel, each pixel has only one value, which is commonly represented pictorially as a shade of grey (see Section 14.3.1). In a multispectral image, which records multiple channels, each pixel has multiple values, which can be viewed separately or in combination (see Section 14.3.2).

The following sub-sections will introduce passive sensors that are commonly used in EO, in the categories of:

- sensor components for optical and thermal imagery, including an overview of detector technology (see Section 14.1);
- image formation methods—electromechanical, linear array, and central perspective (see Section 14.2);
- optical—radiometers, spectroradiometers and imaging spectrometers that record visible and infrared radiance (see Section 14.3):
  - ◆ panchromatic—radiometers that record a single, very broad, channel in optical wavelengths (see Section 14.3.1);
  - ◆ multispectral—radiometers and spectroradiometers that record several broad channels in optical wavelengths (see Section 14.3.2); and
  - ◆ hyperspectral—imaging spectrometers that record numerous, narrow channels in optical wavelengths (see Section 14.3.3);
- thermal infrared—radiometers that record few broad channels in middle and thermal infrared wavelengths (see Section 14.4); and
- passive microwave—radiometers that record few broad channels in microwave wavelengths (see Section 14.5).

**Background image:** Landsat-8 image, acquired on 8 October 2014, of Coopers Creek, Australia's second longest inland river system (displayed using bands 5, 4, 2 as RGB). Primarily located in western Queensland, this inland river feeds into the Lake Eyre Basin. **Source:** Norman Mueller, Geoscience Australia



The implications of image sampling methods on the geometry and fidelity of the resultant imagery are further discussed in Volume 1B—Sections 1 and 2 and Volume 2A—Sections 3 and 6 respectively. It should also be noted that a given sensor may be carried on two or more concurrent platforms. A sensor being carried on multiple satellites, that follow identical orbits within a single mission series (such as the Landsat TM sensor on the Landsat 5 and Landsat 7 satellites), is specifically designed and calibrated to produce comparable image values from each satellite<sup>48</sup>. Some sensors are also carried by multiple satellite missions. This is the case for MODIS (Moderate Resolution Imaging Spectroradiometer), which operates on both the Terra and Aqua

satellites<sup>49</sup>. These satellites follow different orbits to allow acquisition of MODIS data up to four times per day. Image acquisition at different times in the diurnal cycle, however, can result in image value differences that are directly attributable to changes in sun position and view angle, rather than changes in the properties of the imaged surface. Advanced correction procedures are applied to such data sets to ensure their final image values are comparable for digital analyses (see Volume 2D).

Before discussing specific passive imaging sensors, we will describe components of optical and thermal sensors and the major mechanisms that can be used to form an image.

## 14.1 Optical and thermal sensor components

Most optical and thermal sensors comprise some or all of a number of generic components that capture, quantify and record radiation, including:

- a collector—intercepts and directs radiation for a finite period of time known as the dwell time (see Section 13.4); in an optical sensor, the aperture size of a collector determines the maximum level of radiation that the sensor can detect;
- a focussing device—focuses intercepted radiation towards the detector, which may involve shaping and correction;
- a beam splitter—separates the focussed radiation into different wavelength bands;
- a detector—transforms EMR into another form of energy, such as chemical (for photographic film), electrical (for electronic components) or magnetic (for digital media);
- a reference—provides a standard to which the measured radiation can be precisely quantified; and
- a recording device—retains the final result for further analyses.

Specific components used by passive sensors to sense optical and thermal wavelengths are summarised in Table 14.1. Thermal infrared radiometers generally require a temperature reference, which is checked regularly to calibrate sensed observations. They also incorporate a cryocooling mechanism to maintain the detectors at an extremely low temperature to minimise dark current, which ensures that the detected temperatures are relevant to the target rather than the sensing device (see Section 13.4).

Some of the methods used by passive sensors to detect specific spectral ranges include:

- dispersing light through a prism (see Figure 5.7) or diffraction grating (see Figure 14.1);
- using thin film interference filters (such as splitting or superimposing multiple waveforms) to define a narrow range of wavelengths;
- incorporating a reference sample of gas to be identified and only detecting wavelengths that correspond to the gas absorption lines; or
- enhancing the incoming signal by mixing with a monochromatic local oscillator to produce a higher frequency signal that can be analysed more easily.

One example of a monochromatic sensor, which uses a diffraction grating to separate collected radiation, is shown in Figure 14.1. Various correction components may also be added to specific sensors to compensate for known image distortion resulting from sensor and/or platform operation. For example, to correct for platform movement, the scan line corrector component of Landsat TM ‘straightens’ imaged scan lines relative to the satellite path (see Volume 2B).

48. See <http://landsat.gsfc.nasa.gov>

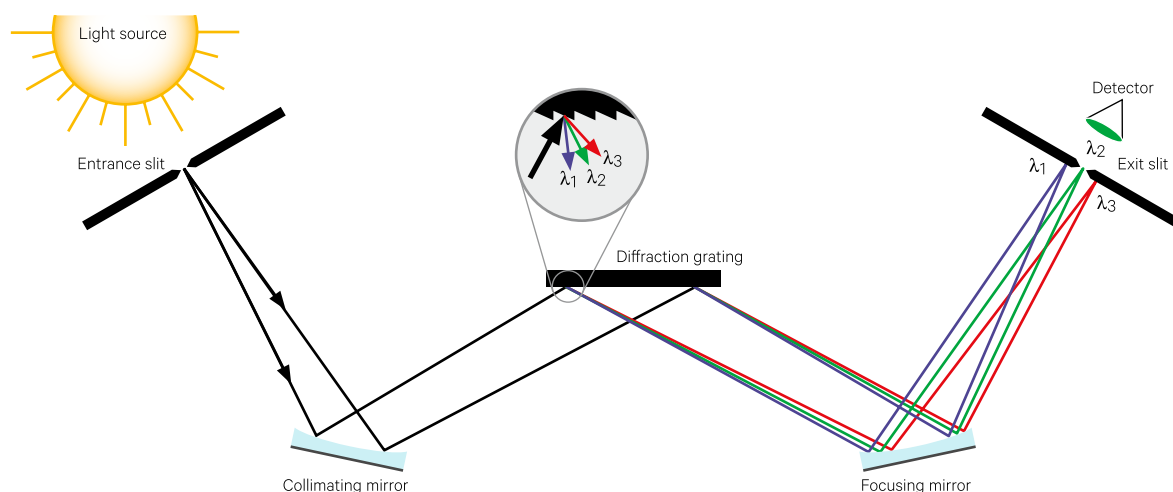
49. See <http://modis.gsfc.nasa.gov>

**Table 14.1** Potential components of generic passive sensor

Component	Function	EM Wavelength Region	
		Optical	Thermal
Collector	Collect incoming radiation for a finite time	aperture, telescope, scanning mirror	aperture, telescope, scanning mirror
Focussing Device	Direct collected radiation towards detector	lens, focussing mirrors, filter	lens, focussing mirrors, filter
Beam Splitter	Divide focussed radiation into sub-regions	prism, filters (interference/dichroic), diffraction grating, Spectroscope	prism, filters (interference/dichroic), diffraction grating, Spectroscope
Detector	Transform split radiation to different form of energy	photographic film, photoemissive device, photodiode, solid-state semiconductor (such as CCD array), CMOS	thermal infrared detectors, solid-state semiconductor (such as CCD array)
Reference	Correct detected signal against a standardised reference	reference detector solar-illuminated panel	blackbody source reference
Recording Device	Retain result for future analyses	amplifier recording device	amplifier recording device

**Figure 14.1** Simple example of monochromatic sensor

Sensor components: entrance slit, collimating mirror, diffraction grating, focussing mirror, exit slit and detector. A diffraction grating uses a surface textured with parallel and equidistant grooves to separate incident polychromatic (white) light into different optical frequencies/wavelengths by the relationship  $d(\sin a \pm \sin b) = m\lambda$ , where  $a$  is the angle of incidence,  $b$  is the angle of diffraction,  $d$  is the distance between striations,  $m$  is the order and  $\lambda$  is the wavelength of incident light beam.



Adapted from: David Harvey (CC BY-NC-SA) Figure 10.12 at <http://www.saylor.org/site/wp-content/uploads/2012/07/Chapter1011.pdf>

Two types of detectors, thermal and quantum, have been most commonly used to detect short wave EMR (Kinch (2000); see Table 14.2). Thermal detectors contain heat sensitive material, which is heated by incident radiation, to cause a measurable change in resistance or voltage. Thermal detectors are slower and less sensitive than quantum sensors, thus generally not used in current optical sensors. Quantum (or photon) detectors utilise photoemissive, photoconductive, or photovoltaic components, which allow the incident radiation to directly interact with the detector material to generate free-charge carriers. Quantum detectors can be designed as one-dimensional (linear) or two-dimensional (area) arrays to reduce the need for moving components to scan across the image target (see Section 14.2), and hence allow a longer dwell time to collect each signal.

Charge-Coupled Device (CCD) and Complementary Metal Oxide Semiconductor (CMOS) detectors utilise the photoelectric effect, by which photons are ‘converted’ to electrons after contact with a doped silicon lattice. Since CCD and CMOS devices simply

respond to the number of electrons accumulated in their photodiodes, they cannot actually detect specific wavelengths, but require filters to limit the incoming radiation to the required wavelength bands. The *Quantum Efficiency* of a photoelectric detector indicates its photon-to-electron conversion efficiency, which is related to specific design aspects of sensor components, such as the illumination period, the threshold of each photodiode, and the efficiency of storing charges before measurement (see Table 13.2 in Section 13.4).

Different materials can be used to fabricate detectors, with each having unique sensitivity to different wavelengths. Some of the materials commonly used for photodiodes are summarised in Table 14.3. It should be noted that the spectral sensitivity of specific detectors often varies from these figures, depending on design requirements. The quantum efficiency of specific photodetectors also varies within and between different detector materials, depending on design criteria, ambient temperature and other components.

**Table 14.2** SWIR detector categories

Characteristic	Detector Category	
	Thermal	Quantum
Operation	Radiation absorbed by thermally isolated detector material to change its temperature, which is sensed by resistivity, dielectric current, etc.	Radiation absorbed by interaction with detector material; generate free carriers which are sensed; electronic readout circuit
Spectral response	Response dependent on radiant power so independent of wavelength	Response varies with wavelength
Features	Traditionally slow, insensitive, bulky, costly, but recent advances have introduced options for mass production	High SNR; fast; generally require cooling outside the visible range
Examples	Bolometers (e.g. thermistor—measures change in electrical resistance; metal; semiconductor) Pyroelectric (measures change in internal electrical polarisation) Thermoelectric (e.g. thermopile—series of thermocouples)	Intrinsic semiconductors (absorption by detector material) Extrinsic semiconductors (absorption by impurities) Photoemissive (e.g. CCD, CMOS) Quantum Well (e.g. QWIP)

Source for data: Kinch (2000); Rogalski (2012)

**Table 14.3** EMR sensitive materials

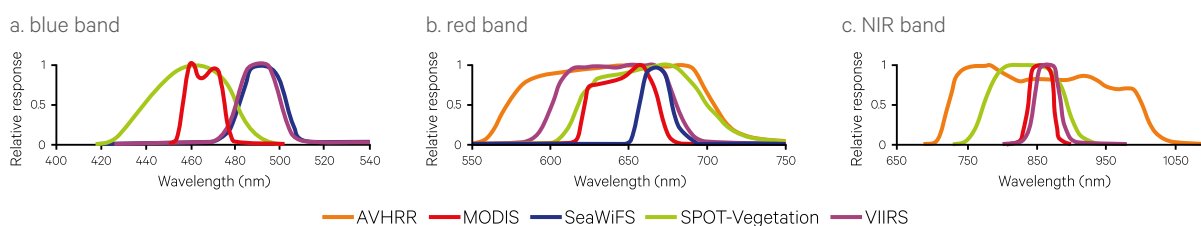
These materials are commonly used to make photodiodes to detect EMR in particular wavelength regions. The sensitivity and performance of specific photodiode products may vary from these figures.

Material	Typical EMR Sensitivity Range (μm)	Peak Sensitivity (μm)	Used for sensing
Silicon (Si)	0.2–1.1	0.9–1.0	visible and NIR
Germanium (Ge)	0.4–1.8	1.35–1.45	NIR
Indium gallium arsenide (InGaAs)	0.4–2.6	1.4–1.55	NIR
Lead sulfide (PbS)	1.0–3.5	2–3	SWIR
Indium antimonide (InSb)	1–7.5	3–4	MIR
Mercury-doped Germanium (GeHg)	2–14 μm	~10	TIR
Mercury-Cadmium-Telluride (HgCdTe)	0.6–16 μm	8–15	SWIR, MIR, TIR

Source for data: Sharma (2005), Rogalski (2012)

**Figure 14.2** Spectral response functions

Normalised spectral response functions for selected EO sensors: AVHRR (orange), MODIS (red), SeaWiFS (blue), SPOT-Vegetation (green) and VIIRS (purple) for:



Adapted from: Kim *et al.* (2010) Figure 1

By virtue of detector sensitivities and other design criteria, each spectral band in optical and thermal sensors can be characterised by its sensitivities to different wavelengths, which is also known as its spectral response function or band pass function. For example, the spectral response functions for selected bands in five different EO sensors are illustrated in Figure 14.2.

*The economic value of just one year of Landsat data far exceeds the multi-year total cost of building, launching, and managing Landsat satellites and sensors.*  
(USGS, 2015)

## 14.2 Image formation

EO image scanning systems can be grouped into three basic categories depending on the mechanism used by the sensors to view each pixel, namely:

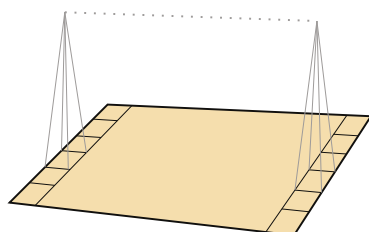
- electromechanical—the sensor oscillates from side-to-side to form the image;
- linear array—an array of detectors is used to simultaneously sense the pixel values along a line; and
- central perspective or framing—the sensing device does not actually move, relative to the object being sensed, during image formation so views all pixels from the same central position in a similar way to a photographic camera (see Volume 1X—Appendix 4).

These mechanisms are illustrated in Figure 14.3.

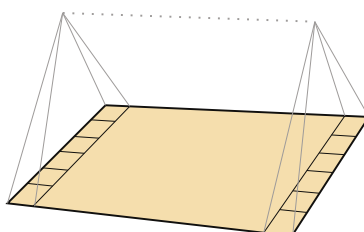
These generic mechanisms assume that the sensor is viewing the Earth's surface from a nadir position at the scene centre, that is, looking vertically downwards. Some sensors, however, can extend their area of coverage from a particular platform location by pointing the sensor to an off-nadir or side-looking position. The impact of off-nadir viewing on image geometry is discussed in Volume 2B.

**Figure 14.3** Scanning mechanisms

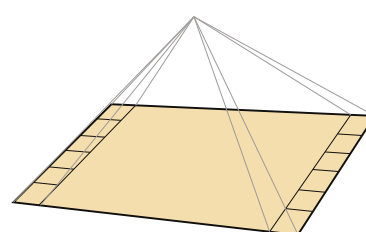
a. Electromechanical: sensor records pixels sequentially along each line from line centre



b. Linear array: pixels recorded simultaneously along each line using an array of detectors at line centre



c. Central perspective: sensor is positioned at image centre and records lines sequentially



Source: Harrison and Jupp (1989) Figure 18

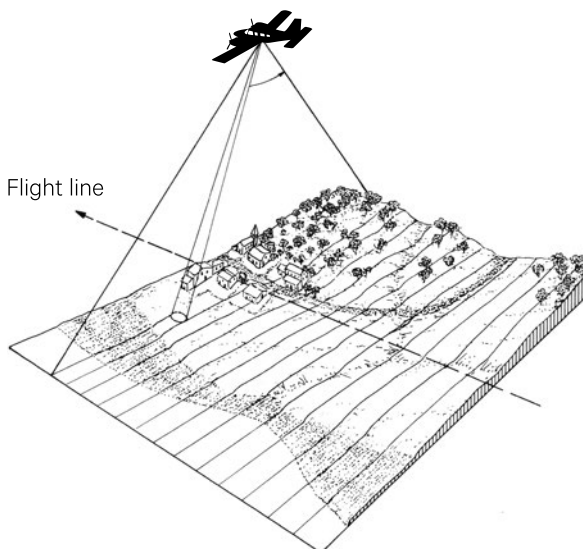


## 14.2.1 Electromechanical

As the name suggests, an electromechanical scanner comprises electronic and mechanical components. The operation of an electromechanical sensor being carried on an aircraft is illustrated in Figure 14.4, although the same principle applies to satellite-borne scanners. In this example, the image is formed by a side-to-side scanning movement as the plane travels along its path. Each line is automatically divided into pixels in the scanning process. This process is illustrated in Figure 14.5 for a multispectral scanner (MSS), with the land cover(s) within each individual pixel determining the radiation levels detected by the scanner. It should be noted that this simplistic description tends to imply that remotely sensed image pixels neatly correspond to discrete ground areas (or ground resolution elements), which is not the case. The relationship between ground resolution elements and image pixels is discussed in Volume 1B—Section 1.2 and Volume 2B.

**Figure 14.4** Operation of electromechanical aircraft scanner

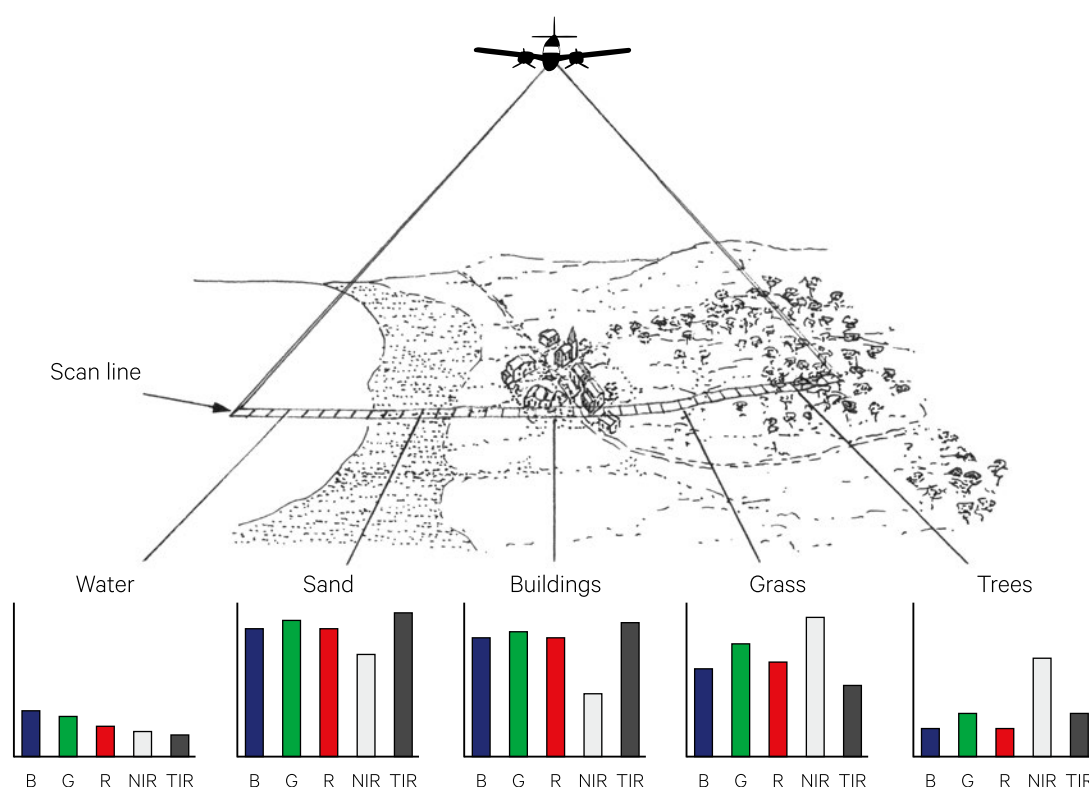
Image lines are formed sequentially by scanning side-to-side across the flight path



Source: Harrison and Jupp (1989) Figure 19

**Figure 14.5** MSS measurements along one scan line

Each set of radiance readings along the line represents a pixel in the image



Source: Harrison and Jupp (1989) Figure 20

An electromechanical scanner uses an oscillating mirror to reflect incident radiation onto a relatively small number of detectors, with different types of detectors being used for different wavelengths and sensitivities (see Section 14.1). These detectors are located behind grating (or less commonly optical) filters that separate EMR into broad spectral bandwidths, which are simultaneously registered by the detector array then sequentially read as data. The detected radiation is converted into a continuous electronic signal that is then sampled at regular time intervals to give discrete measurements, or pixels, along each scan line. Sensors using this scanning mechanism are also referred to as across-track or ‘whiskbroom’ scanners. Examples of such sensors include Landsat MSS, TM and ETM+, and AVHRR.

The main limitation of this scanning mechanism is the restricted time available to read each detector. This generally requires that such scanners have rather broad spectral bands to achieve an adequate Signal-to-Noise Ratio (SNR; see Section 13.4 and Volume 1B—Section 2.1.4). The oscillating movement of the mirror may also result in some inconsistencies in the scanning rate, leading to geometric problems in the imagery (see Volume 2B). Moving components are also subject to wear and tear over time.

Landsat MSS and TM sensors used oscillating electromechanical scanners and the satellite’s forward velocity to form imagery. Unlike the MSS, Landsat TM

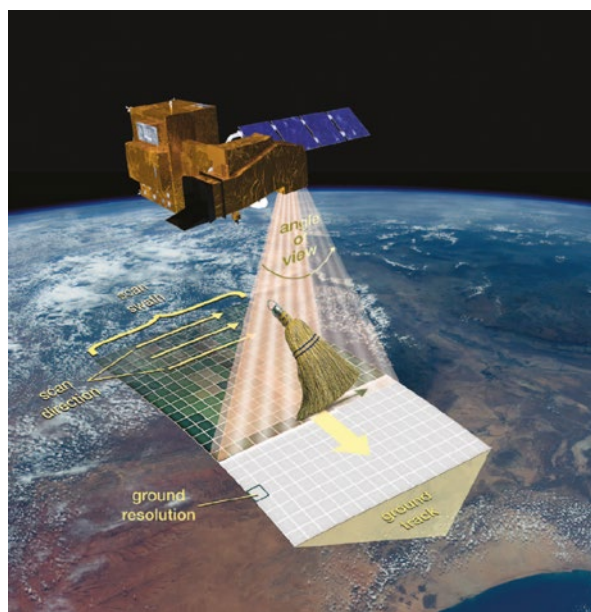
and ETM used a scanning mirror that collected data on both the forward and reverse scans. Landsat MSS comprised six sensors for each spectral band, so that six lines of image data were received each time the scanner moved from side-to-side. For Landsat TM/ETM+, sixteen lines of image data were collected on each scan using a ‘whiskbroom’ scanner. The satellite travelled from north to south as the sensing system scanned west to east. These combined movements produce the characteristic westerly skew in Landsat imagery (see Figure 12.15 and Volume 2B). Also, since each of the six (or sixteen) lines was imaged by a separate detector, slight miscalibration between the detectors led to a horizontal striping pattern in the imagery. This problem is further discussed in Volume 2.

### 14.2.2 Linear array

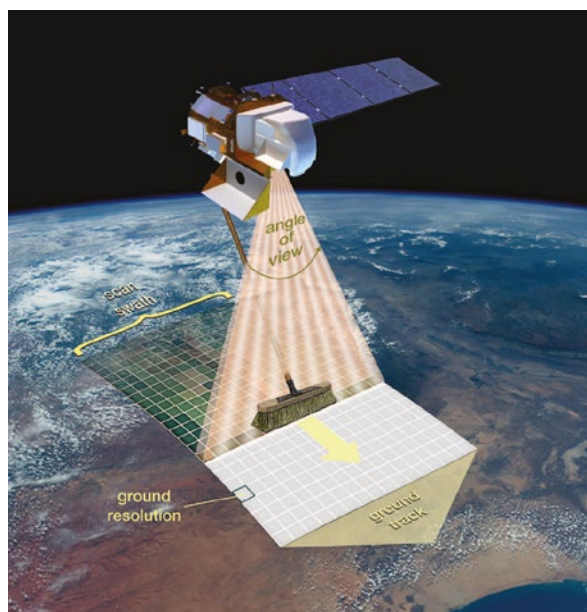
A second scanner design uses a linear array of detectors (commonly CCD) to form an image line, with each detector recording the value for an individual pixel along the line (see Figure 14.3b). This design is also referred to as a ‘push-broom’ scanner, since the image is formed as the sensor is swept forward by the velocity of the platform. Examples of such sensors include SPOT HRV, SPOT NRVI, SPOT-VGT, MISR, ASTER, IKONOS, IRS, OrbView, QuickBird, MOMS, MESSR, and Landsat OLI. The operation of a ‘push-broom’ scanner is compared with a ‘whiskbroom’ scanner in Figure 14.6.

**Figure 14.6** Whiskbroom versus pushbroom scanners

a. A ‘whiskbroom’ scanner (such as Landsat-7 ETM+) relies on an oscillating mirror to scan each pixel across an image line.



b. A ‘pushbroom’ scanner (such as Landsat-8 OLI) utilises linear arrays of detectors to record each image line.



Source: NASA. Retrieved from [http://landsat.gsfc.nasa.gov/wp-content/uploads/2012/12/LDCM\\_Brochure\\_Dec20121.pdf](http://landsat.gsfc.nasa.gov/wp-content/uploads/2012/12/LDCM_Brochure_Dec20121.pdf)

The advantages of this design are that the scanner does not have any moving parts to cause timing inconsistencies and can allow a longer dwell time, and hence narrower spectral channels, per detector (see Section 13.4). This results in a cheaper, lighter and smaller device with lower power requirements and greater reliability as well as higher spatial and radiometric resolutions. A disadvantage however is that the larger number of detectors requires very accurate calibration to avoid vertical striping in the imagery. A further limitation is that CCD technology is not readily available for wavelengths longer than near infrared. In certain cases, due to finite detector read-out times, the number of spectral bands also needs to be limited in linear array scanners to ensure that the same ground locations are being imaged in each band.

### 14.2.3 Central perspective

The third category of sensors utilises an area array of CCD detectors to form an image from a central perspective (see Figure 14.3c). This sensor is used in

a wide range of instruments, from mobile phones to satellite imaging scanners. The central perspective results in similar geometric distortions in an image to those that occur in photographic data, that is, distortion increases with radial distance from the focal point. In satellite-derived imagery however, radial displacement effects are barely noticeable because the field of view is so small relative to orbital altitude.

Laboratory-based scanners commonly use the central viewing perspective for image formation. The extent of distortion in the resulting image depends on the optics of the scan configuration used, including the size of the original being scanned. The early frame sensors used in vidicon cameras (such as the Return Beam Vidicon in the Landsat 1, 2 and 3 satellites) operated from a central perspective by exposing a two-dimensional array of detectors (or photosensitive tubes in the early models) for a shutter-controlled time period. Although operating with a different mechanism, imagery from the geostationary satellites (described in Section 12.2.1) is essentially formed from this perspective.

## 14.3 Optical

Optical sensors detect and record radiance in visible, near infrared and short wave infrared wavelengths (see Section 5.3) for either:

- one channel (panchromatic—see Section 14.3.1);
- several channels (multispectral—see Section 14.3.2); or
- numerous channels (hyperspectral—see Section 14.3.3).

As wavelengths in these regions of the spectrum are strongly affected by atmospheric scattering, the usefulness of these devices for Earth surface studies may be limited by atmospheric conditions (see Section 5.4). Optical scanners are often divided into sub-categories on the basis of their spatial resolution:

- low resolution: > 80 m;
- medium resolution: 10–80 m;
- high resolution: < 10 m; and
- very high resolution: < 1 m.

The most commonly used satellite sensors acquiring low, medium and high resolution imagery are listed in Table 14.4.

---

*Satellite imagery can be used retrospectively, meaning that the data collected by satellites today will probably help solve issues we are not currently even aware of—an advantage which is invaluable.*  
(Nathalie Pettorelli)

---

**Table 14.4** Examples of satellite optical sensors

Note: Hyperion (italicised in this table) is a hyperspectral imaging system

Spatial Resolution	Instrument	Mission(s)	Agency
Low	MERIS	Envisat	ESA
	IMAGER	MTSAT-2	JMA
	GOCI	COMS	KARI
	MODIS	Aqua	NASA
	MODIS	Terra	NASA
	AVHRR/3	NOAA-15, 16, 17, 18, 19	NOAA
	VIRR	FY-3A, 3B, 3C	NRSCC (CAST)
	VIIRS	NPP	NASA
	SeaWiFS	ORBITVIEW 2	Orbimage
Medium	HRVIR	SPOT-4	CNES/Astrium
	MSS	Beijing-1	DMCii
	SSTL MSS – 3 band	DMC Deimos-1	DMCii
	CHRIS	PROBA-1	ESA (BNSC)
	AwIFS	RESOURCESAT-2	ISRO
	LISS-III	RESOURCESAT-2	ISRO
	ALI	NMP EO-1	NASA
	<i>Hyperion</i>	<i>NMP EO-1</i>	<i>NASA</i>
	OLI	LDCM	NASA (USGS)
	NigeriaSat Med Res	NigeriaSat-1, X	NASRDA
	TM	Landsat-5	USGS (NASA)
	ETM+	Landsat-7	USGS (NASA)
High	MSS/Pan	SPOT 6, 7	Astrium
	HiRI	Pleiades-HR 1, HR 2	CNES/Astrium
	HRG/HRS	SPOT-5	CNES/Astrium
	Quickbird 2	QUICKBIRD 2	Digital Globe
	WV60	WORLDVIEW-1	Digital Globe
	WY110	WORLDVIEW-2	Digital Globe
	Multispectral	WORLDVIEW-3	Digital Globe
	MSI	RapidEye	DLR
	PAN	Beijing-1	DMCii
	GIS	GeoEye-1	GeoEye
	GeoEye-2	GeoEye-2	GeoEye
	IKONOS 2	IKONOS 2	GeoEye
	LISS-IV	RESOURCESAT-2	ISRO
	TES PAN	TES	ISRO
	NigeriaSat	NigeriaSat-2	NASRDA
	PAN	BJ-1	NRSCC (CAST)
	RSI	FORMOSAT 5, 2	NSPO/Astrium
	MSI	Sentinel-2	ESA

Adapted from: Geoscience Australia (2011) Tables F-1 to F-3



### 14.3.1 Panchromatic

Panchromatic scanners are imaging radiometers that record EMR in a single band, typically including all wavelengths spanning from the visible to infrared region (see Section 13.2.1.1). A single channel captures the broad contrast between features, and allows delineation of land cover transitions and boundaries. For a given volume of image data, if each pixel only has a single band value, the image can contain a greater number of pixels. Accordingly, panchromatic sensors generally deliver higher spatial resolution imagery than multispectral scanners. The design trade-offs between spectral and spatial detail in scanning systems is introduced in Section 13 and further discussed in Volume 1B—Sections 1 and 2. It should be realised that the engineering implications of increasing data volume impact not only image acquisition and recording, but also the download capacity required for remote sensors (see Volume 1B—Section 9).

Panchromatic data is typically displayed as a grey-scale image, in which pixels with lower image values appear dark and those with higher values appear bright (see Figure 14.7). For optical imagery, panchromatic channels typically record low values for water and dense vegetation and high values for urban and bare areas. As such, engineering works such as roads, mines and urban infrastructure clearly contrast with vegetation, and boundaries of waterbodies can be delineated.

Successive generations of panchromatic scanners have rendered significant advances in both spatial resolution and image quality. For example, images

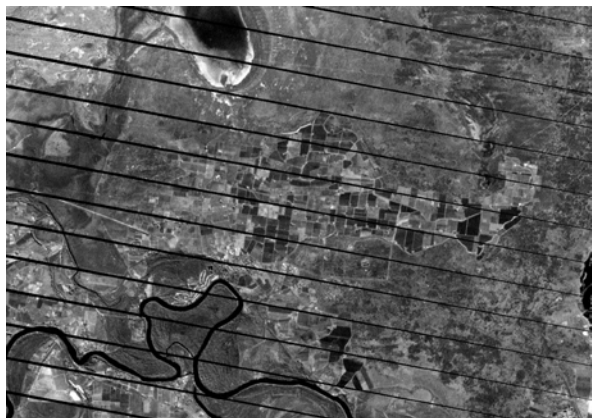
acquired by Landsat-7 ETM+ and Landsat-8 OLI are contrasted in Figure 14.7. While both scanners record 15 m pixels, Figure 14.7a was acquired years before Figure 14.7b, so some land surface features have changed. However, the unchanged features in these two images are cleaner and crisper in Figure 14.7b due to the higher imaging fidelity of Landsat-8 OLI, which offers greater radiometric resolution and utilises linear arrays of detectors per image scan line ('pushbroom' scanner) rather than oscillating mirrors ('whiskbroom' scanner)<sup>50</sup>. A more nostalgic example of the spatial 'acuity' of the Landsat-8 panchromatic channel is shown in Figure 14.8, where the decommissioned Landsat-5 satellite is visible in an image over Brazil (see Figure 12.14).

Interpretation of panchromatic imagery relies on spatial rather than spectral analysis of features. Various image processing techniques, such as rescaling, can be used to change image contrast to enhance specific features (see Volumes 2A and 2C). Transitions between adjacent pixels can be highlighted using algorithms that enhance edges or texture (see Volume 2C). Pseudo-colouring can also be applied to panchromatic images, which maps image values to selected colours (see Volumes 2A and 2E).

Panchromatic scanners often accompany multispectral scanners on satellite missions. Panchromatic imagery is not only valuable for providing crisp images of Earth features, which are invaluable for various cartographic purposes, but can also be used to visually sharpen edges in multispectral imagery (see Figure 14.9). Such techniques are detailed in Volume 2C.

**Figure 14.7** Panchromatic imagery from Landsat-7 ETM+ and Landsat-8 OLI

a. Landsat-7 ETM+ 15 m pixels acquired on 25 June 2016



b. Landsat-8 OLI 15 m pixels acquired on 3 July 2016



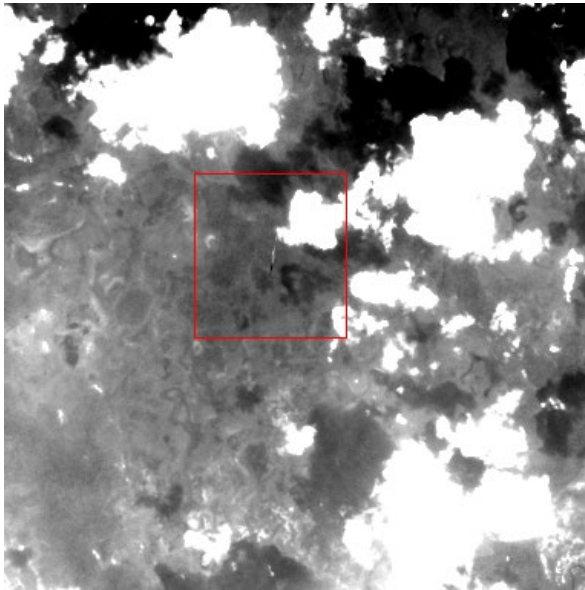
Source: Norman Mueller, Geoscience Australia

50. Please note that the spectral response functions for the Landsat 7 ETM+ and Landsat 8 OLI sensors are also different. For more details on the Landsat 8 mission and instruments visit <http://landsat.usgs.gov/documents/Landsat8DataUsersHandbook.pdf> or <https://directory.eoportal.org/web/eoportal/satellite-missions/l/landsat-8-lc1cm>

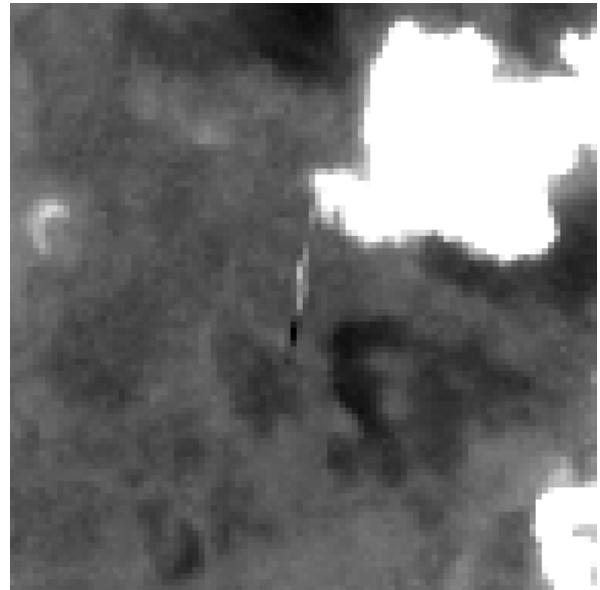
**Figure 14.8** Decommissioned Landsat-5 satellite visible from Landsat-8

Landsat-8 panchromatic image over northwestern Brazil on 22 November 2013 detects the decommissioned Landsat-5 satellite below its overpass (see Figure 12.14 for satellite dimensions).

a. Landsat-5 satellite appears as a streak of pixels within the red box



b. Enlarged view of red box shown in image a



Source: RIT/USGS/NASA. Retrieved from <http://landsat.gsfc.nasa.gov/?p=7849>

**Figure 14.9** Image sharpening

Panchromatic imagery with high spatial resolution can be merged with multispectral imagery to create high resolution colour images.

a. Pleiades panchromatic image acquired on 15 May 2016 over Parliament House, Canberra



b. Pleiades multispectral image acquired on 15 May 2016 over Parliament House, Canberra



c. Pleiades images in a. and b. merged into sharper colour image



Source: © CNES (2016). Distribution: Airbus DS.

### 14.3.2 Multispectral

Multispectral scanners (MSS), as the name implies, are a particular class of remote sensing device that senses and digitally records radiation in multiple, defined wavelength regions of the visible and infrared parts of the EM spectrum using imaging radiometers or imaging spectroradiometers (see Section 13.2.1). The principle of this mode of operation is comparable to using filters on a camera to photograph limited parts of the visible spectrum. For example, when using an appropriate filter to photograph only blue light, a purely red object would appear black since only blue radiation will pass through the filter to expose the film. Thus, different information is obtained by recording the reflectance in different wavelength regions.

While the prolific MSS instrument carried by the Landsat 1 to 5 satellites (see Section 12.2.2) sensed four 'bands' of the EM spectrum for each image pixel (green: 0.5–0.6  $\mu\text{m}$ ; red: 0.6–0.7  $\mu\text{m}$ ; near infrared: 0.7–0.8  $\mu\text{m}$ ; and near infrared: 0.8–1.1  $\mu\text{m}$ ), the more recent Landsat sensors, TM, ETM+ and OLI, were designed to record additional image channels (see Table 14.5). It should be noted that the spectral sensitivities (or response) of these wavelength bands do not precisely correspond to their stated wavelength ranges, as illustrated in Figure 14.2. The spectral bands of most terrestrial EO sensors are selected primarily to detect differences in land cover, and also to avoid atmospheric absorption bands (see Figure 14.10 and Section 5).

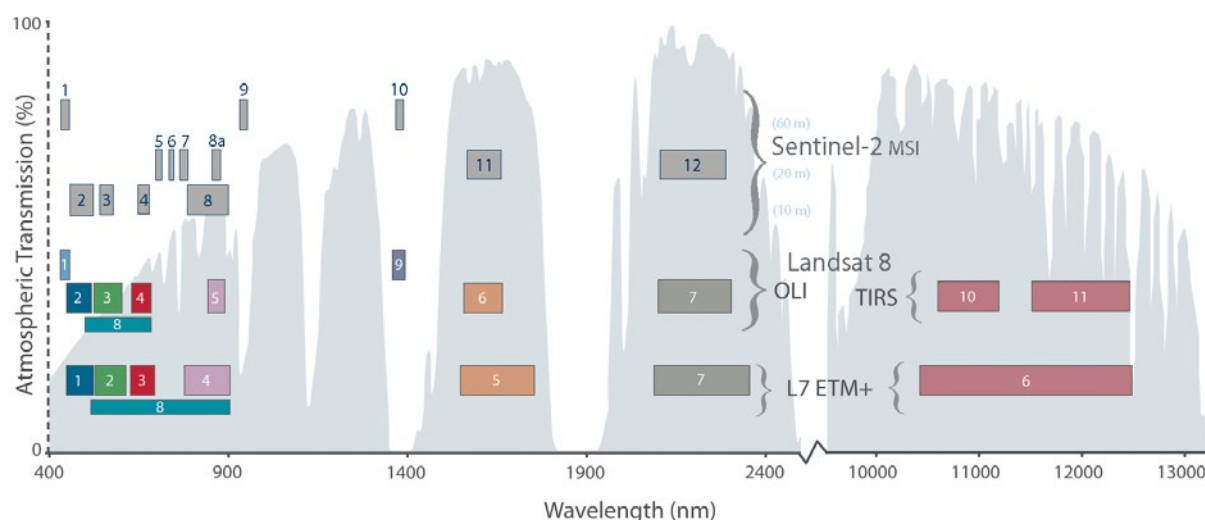
**Table 14.5** Landsat TM/ETM+ channels

Landsat TM recorded the multispectral channels 1 to 7 only. Note: Band 8 is only measured by Landsat ETM+.

Band	Spectral Range ( $\mu\text{m}$ )	EM Region	Application	Nominal Pixel Size
1	0.45 – 0.52	Visible Blue	Coastal water mapping, vegetation versus soils	30
2	0.52 – 0.60	Visible Green	Vegetation vigour assessment	30
3	0.63 – 0.69	Visible Red	Chlorophyll absorption for vegetation differentiation	30
4	0.76 – 0.90	Near Infrared	Biomass surveys and delineation of water bodies	30
5	1.55 – 1.75	Middle Infrared	Vegetation and soil moisture; snow versus cloud	30
6	10.40– 12.50	Thermal Infrared	Thermal mapping, soil moisture, plant heat stress	120
7	2.08 – 2.35	Middle Infrared	Hydrothermal mapping	30
8 (ETM+ only)	0.52 – 0.90 (panchromatic)	Green, Visible Red, Near Infrared	Large area mapping, urban change studies	15

**Figure 14.10** Comparison of bands acquired by Landsat-7, Landsat-8 and Sentinel-2

This graphic compares the bands acquired by Landsat-7 and Landsat-8 with those acquired by Sentinel-2. The wavelength regions where EMR transmission is not permanently affected by Earth's atmosphere are shaded in the background (see Section 5).



Source: NASA. Retrieved from <http://landsat.gsfc.nasa.gov/wp-content/uploads/2015/06/Landsat.v.Sentinel-2.png>

**Table 14.6** Landsat OLI/TIRS channels

OLI records channels 1 to 9; TIRS records channels 10 and 11

Band	Spectral Range (μm)	EM Region	Application	Nominal Pixel Size
1	0.427–0.459	Visible blue	Ocean colour in coastal zones and aerosols	30
2	0.436–0.528	Visible blue	Pigments, atmospheric scattering, coastal monitoring	30
3	0.513–0.611	Visible green	Pigments, coastal monitoring	30
4	0.626–0.692	Visible red	Pigments, coastal monitoring	30
5	0.830–0.901	Near Infrared	Foliage, coastal monitoring	30
6	1.516–1.699	Middle Infrared	Foliage	30
7	2.038–2.356	Middle Infrared	Minerals, litter, no scattering	30
8	0.488–0.693	Panchromatic	Image sharpening	15
9	1.341–1.410	Middle Infrared	Cirrus cloud detection	30
10	10.6–11.2	Thermal Infrared	Land and ocean temperature plus atmospheric studies	100
11	11.5–12.5	Thermal Infrared	Land and ocean temperature plus atmospheric studies	100

As detailed in Table 14.5, Landsat TM recorded the multispectral bands 1 to 7 only, while Landsat ETM+ also recorded a panchromatic channel at higher spatial frequency. The channels recorded by Landsat OLI/TIRS are detailed in Table 14.6. Landsat OLI/TIRS delivers imagery with 12 bit radiometric resolution whereas Landsat 7 ETM+ provided radiometric resolution of 8 bits (selected from the best of 9 bits).

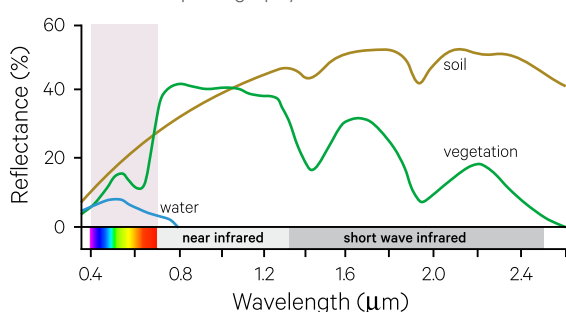
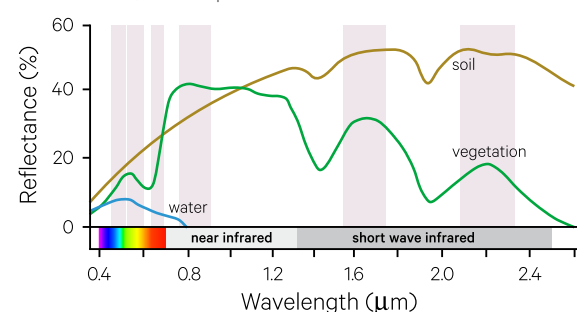
The advantage of sensing radiation in multiple spectral regions is illustrated in Figure 14.11, which shows ‘typical’ spectral reflectance curves (or ‘signatures’) for soil, dry grass and green plant material. Figure 14.11a highlights the wavelengths recorded by standard colour photography, while Figure 14.11b superimposes the optical regions detected by the Landsat TM/ETM+ sensors. Although the recorded reflectance levels in an image depend upon a wide range of factors relating to the structure and condition of a particular land cover type (see

Volume 1B—Sections 3 and 6), the Landsat imagery clearly provides more spectral information than aerial photography to differentiate between different types of land cover. Note that ‘signature diagrams’, such as those shown in Figure 14.11, have typically been drawn from spectral reflectance data with much finer spectral resolution than those provided by the multispectral scanner bands.

The (spatially registered) channels recorded by a MSS, such as Landsat TM, can be recombined into a single colour image using the colour additive technique described in Section 2.7. Channels representing reflected blue, green and red light can be combined to form a natural colour composite, which should resemble the colours of the imaged object (see Figure 14.12a). Different sets of channels can also be combined using the colour additive process to render false colour composites (see Figures 14.12b and 14.12c).

**Figure 14.11** Differentiation within spectral regions

Wavelengths recorded by EO sensor are shaded grey against typical spectral ‘signatures’ for soil (brown), water (blue) and green vegetation (green).

**a.** Standard colour photography**b.** Landsat TM/ETM+ optical bands

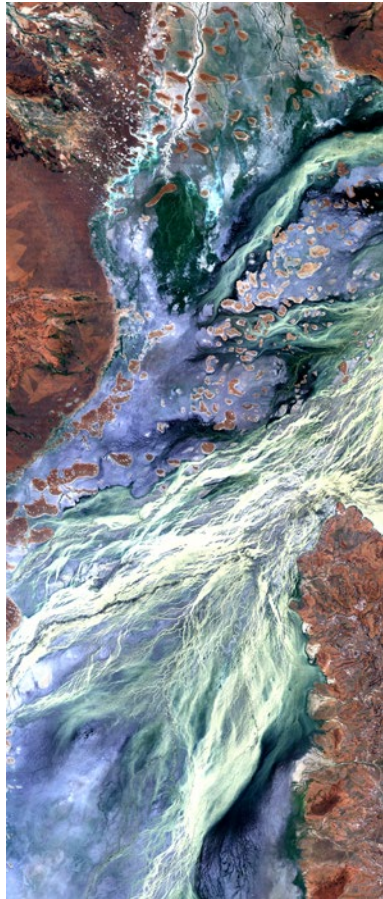
Adapted from: Harrison and Jupp (1989) Figure 28



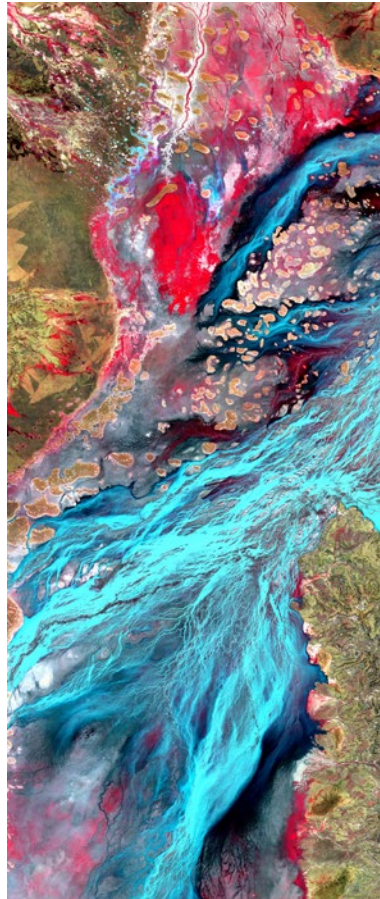
**Figure 14.12** Colour composites

Landsat TM imagery acquired over Coopers Creek, near Windorah, Queensland, on 1 December 2010.

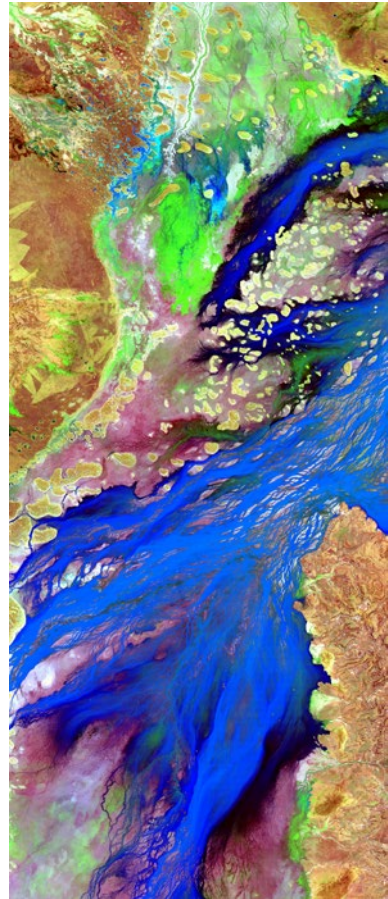
a. True colour composite—band 1 displayed blue, band 2 displayed green, band 3 displayed red



b. Standard false colour composite—band 2 displayed blue, band 3 displayed green, band 4 displayed red



c. Different false colour composite—band 2 displayed blue, band 4 displayed green, band 5 displayed red



Source: Norman Mueller, Geoscience Australia

The grey scale images corresponding to the six optical Landsat ETM+ bands are shown in Figure 14.13. The reflectance level in each of the spectral bands illustrated in Figure 14.12 tells us something about the ‘object’ being sensed:

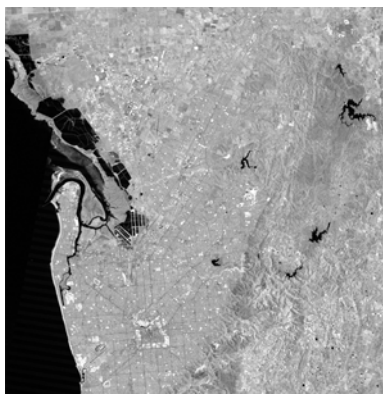
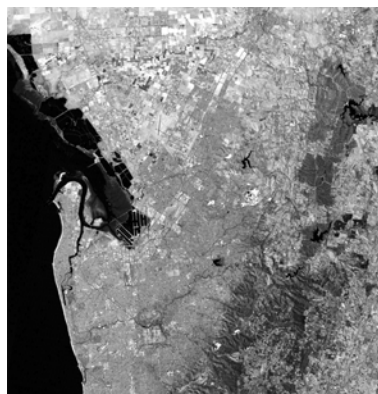
- water is brightest, and more variable, in the visible blue channel (ETM band 1) and darkest in the near infrared and middle infrared channels (ETM bands 4, 5, and 7);
- urban and bare areas are brightest in the visible blue channel (ETM band 1) and darkest in the middle infrared channels (ETM bands 5 and 7); and
- vegetation is brightest in the near infrared channel (ETM band 4) and darkest in visible blue.

As introduced in Section 5, vegetation features are frequently identified by their characteristically high NIR reflectance and low red reflectance. For an image pixel containing both vegetation and background soil, the colour and visibility of the soil will modify the detected radiation levels. A light coloured soil will show a larger decrease in red radiation for increasing vegetative cover while a dark soil will cause a larger increase in the near infrared radiation. Image processing techniques of ratioing or differencing these data channels enhances the differences between them and reduces the influence of background soil colour. For example, such processes are used to monitor daily variations in pasture (see Excursus 14.1). Details of these techniques are provided in Volumes 2C and 3A. Interpretation of optical MSS imagery is further considered in Volume 1B—Sections 6.



**Figure 14.13** Landsat ETM+ optical channels

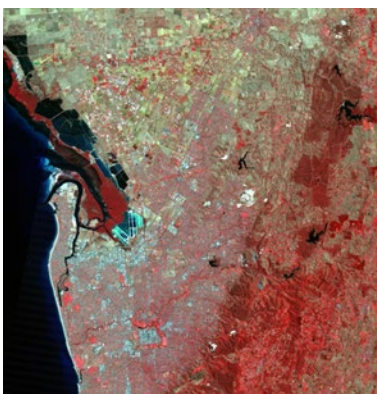
Landsat ETM+ image over Adelaide, South Australia January 2000. The scene includes shallow coastal water, urban areas, forested reserves to the east and agricultural lands in the north.

a. Band 1—visible blue (0.45–0.52  $\mu\text{m}$ )b. Band 2—visible green (0.52–0.60  $\mu\text{m}$ )c. Band 3—visible red (0.63–0.69  $\mu\text{m}$ )d. Band 4—near infrared (0.76–0.90  $\mu\text{m}$ )e. Band 5—middle infrared (1.55–1.75  $\mu\text{m}$ )f. Band 7—middle Infrared (2.08–2.35  $\mu\text{m}$ )

g. True colour composite (bands 1, 2 and 3 as blue, green and red)



h. False colour composite (bands 2, 3 and 4, as blue, green and red)



i. Location map with broad land covers and scale bar



Source: Megan Lewis, University of Adelaide using imagery supplied by Geoscience Australia

## Excursus 14.1—Pastures from Space

**Source:** Graham Donald, CSIRO

**Further information:** [www.pasturesfromspace.csiro.au](http://www.pasturesfromspace.csiro.au)

[https://www.landgate.wa.gov.au/foundationr2/channel\\_content.jsp?channel=farm&contentId=farmchannel-start-pasturesfromspace&source=cms&title=Pastures%20from%20Space](https://www.landgate.wa.gov.au/foundationr2/channel_content.jsp?channel=farm&contentId=farmchannel-start-pasturesfromspace&source=cms&title=Pastures%20from%20Space)

Australia is the largest exporter of beef, mutton, goat meat and wool in the world, and a major exporter of lamb, pork and dairy products. In 2009, Australia's livestock exports totalled nearly \$1 billion.

Farm profitability is heavily dependent on the efficient use of pasture by livestock. Given the seasonal patterns of pasture growth in southern Australia, accurate and timely information is required to match total pasture production to consumption by livestock. This information has been routinely provided by satellite image analyses for over a decade.

*Pastures from Space* uses daily satellite imagery to monitor variations in pastures, both within individual paddocks and across growing regions in southern Australia (see Figure 14.14). This information is

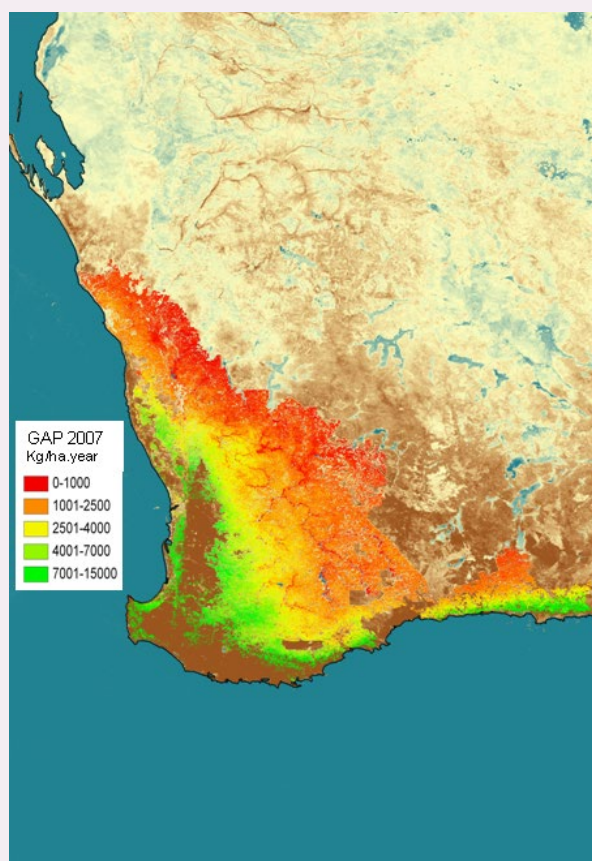
combined with meteorological data to model plant growth. Weekly estimates of Pasture Growth Rate (PGR) are supplied to farmers via an on-line service. Current research is extending this product to Australia's eastern agricultural regions and northern rangelands.

This pasture growth information enables farmers to improve pasture utilisation and optimise the use of fertilisers. It also allows timely management of erosion, weeds, and pasture health. Over the longer term, at paddock, farm and regional scales, changes in Gross Annual Pasture Production (GAPP) can be used to assess the impact of local and regional management practices, as well as the ramifications of climatic variations.

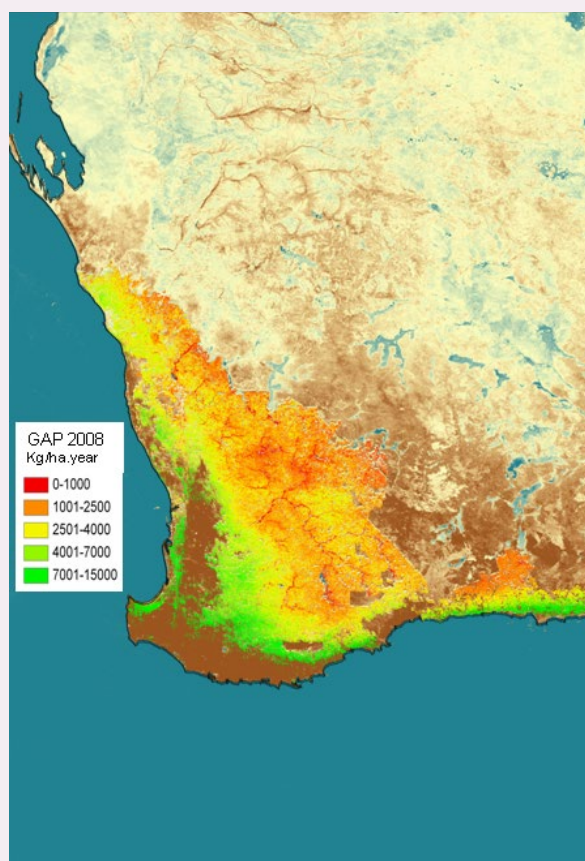
**Figure 14.14** Gross Annual Pasture Production (GAPP) from 2007 to 2010 for southwestern WA

The total above ground pasture production for individual paddocks, farms and regions can be monitored over time to determine optimal management regimes and the impact of environmental changes. GAPP is derived from the Pasture Growth Rate (PGR) model and quantified as kilograms of dry matter per hectare.

a. GAP 2007

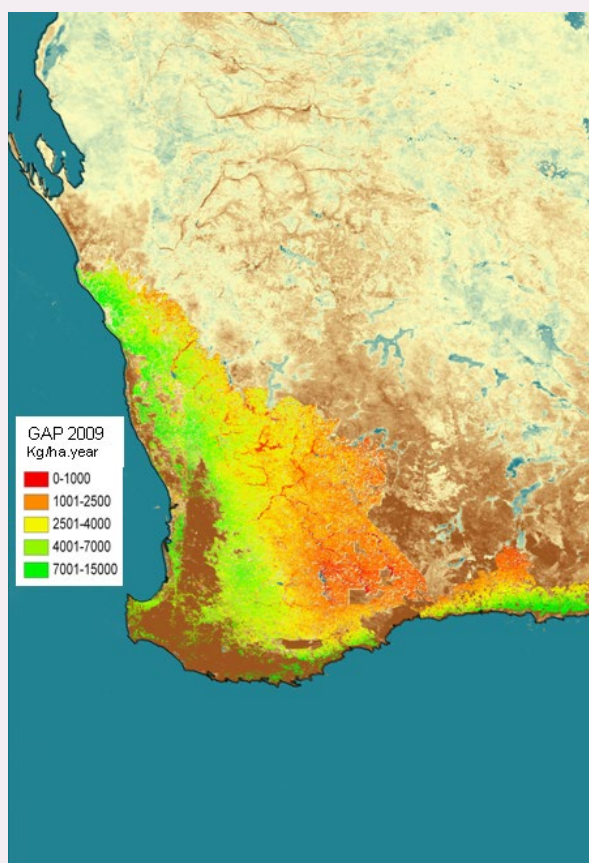


b. GAP 2008

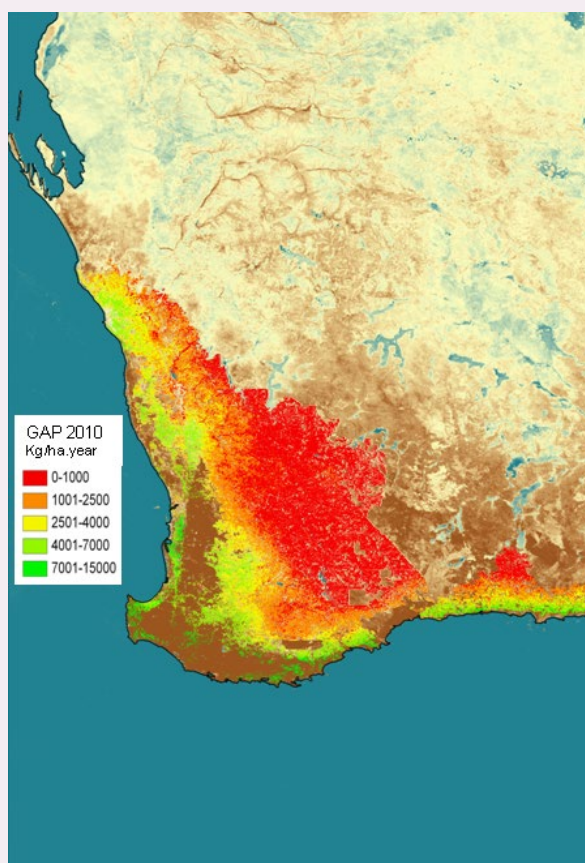




c. GAP 2009



d. GAP 2010



### 14.3.3 Hyperspectral

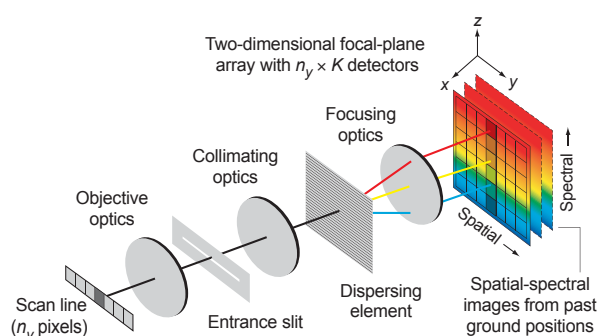
Hyperspectral scanners, or imaging spectrometers, collect image data for hundreds of spectral channels. A push-broom scanner incorporating a two-dimensional detector array records scan lines for multiple spectral bands to form a three-dimensional data cube (see Figure 14.15). This data cube can be viewed as:

- a set (size  $z$ ) of two-dimensional images ( $x$  and  $y$  in Figure 14.15), one for each spectral channel; or as
- a set (size  $x \times y$ ) of one-dimensional spectra, one for each image pixel.

The process of image collection, data dimensions and the derived spectra are illustrated in Figure 14.16. This type of imaging allows detailed spectra for individual pixels and/or target features to be compiled (see Figure 14.16d). By comparison, a simplified form of the spectral signatures for two types of Australian vegetation and two types of bare ground that would be derived from Landsat TM optical bands is illustrated in Figure 14.17.

**Figure 14.15** Compilation of hyperspectral data cube

An imaging spectrometer disperses light onto a two-dimensional array of detectors, with  $n_y$  elements in the cross-track (spatial) dimension and  $K$  elements in the spectral dimension, for a total of  $N = K \times n_y$  detectors.

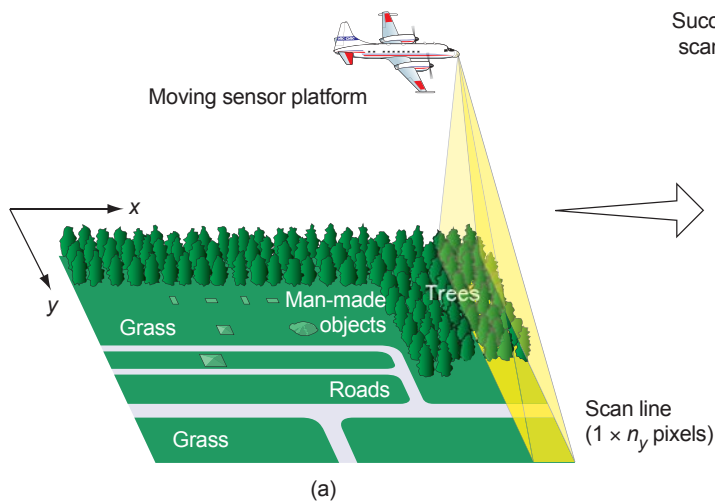


Source: Shaw and Burke (2003) Figure 3b. Reprinted with permission courtesy of MIT Lincoln Laboratory, Lexington, Massachusetts.

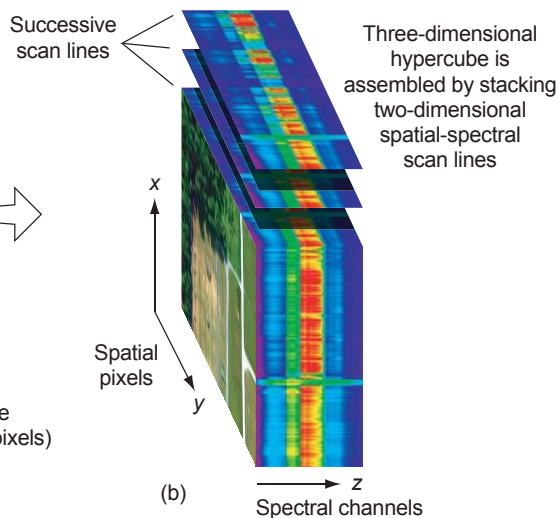


**Figure 14.16** Hyperspectral image interpretation

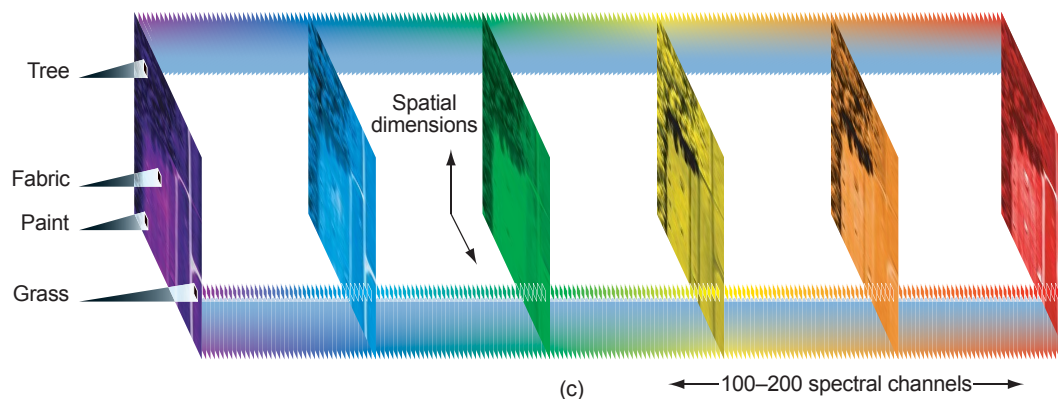
a. Target scene is imaged line by line using a hyperspectral scanner



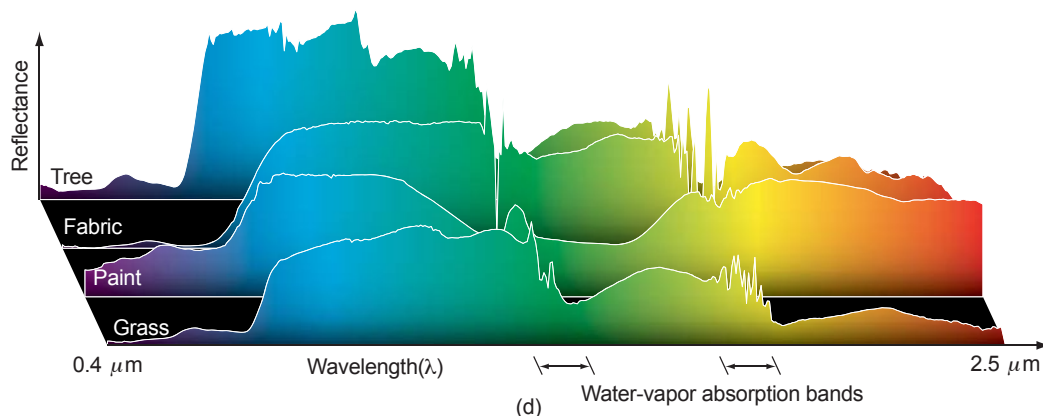
b. Multiple spectral bands for each scan line are stacked into a three-dimensional datacube



c. Each spectral channel can be viewed as a two-dimensional image



d. Detailed spectral information for individual pixels and target features can be viewed as one-dimensional spectra across all spectral bands



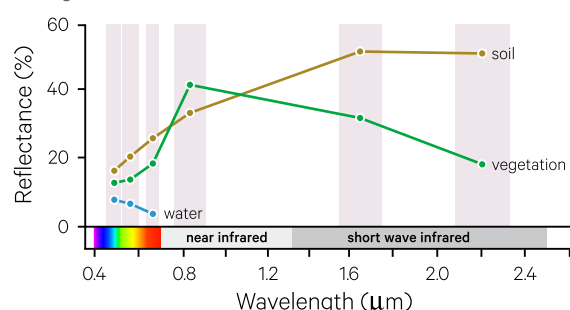
Source: Shaw and Burke (2003) Figure 4. Reprinted with permission courtesy of MIT Lincoln Laboratory, Lexington, Massachusetts.

**Table 14.7** Examples of hyperspectral imagers

Sensor	Mission (Agency)	Maximum number of channels	Spectral range ( $\mu\text{m}$ )	Ground resolution <sup>53</sup> (m)
AVIRIS (Airborne Visible Infrared Imaging Spectrometer)	Airborne (JPL)	224	0.40–2.50	2.2–20
CASI-1500 (Compact Airborne Spectrographic Imager)	Airborne (ITRES)	288	0.38–1.05	0.2–1.5
HyMap	Airborne (HyVista Corp)	128	0.45–2.5	2–10
CHRIS (Compact High Resolution Imaging Spectrometer)	Proba-1 (ESA)	150 <sup>54</sup>	0.415–1.05	17–34
HICO (Hyperspectral Imager for Coastal Ocean)	ISS (NASA)	128	0.35–1.08	90
Hyperion	EO-1 (NASA)	220	0.40–2.5	30

**Figure 14.17** Simulated Landsat TM spectral signature

Simplified spectral signatures for vegetation, soil and water, based on mid-points of Landsat TM/ETM+ optical channels (see Figure 14.11b).



Hyperspectral imaging is used for an expanding range of laboratory, industrial and airborne applications, including astronomy, surveillance, food processing and biomedical research. In EO, it is especially valuable for identifying geological features, mapping surface mineral deposits and distinguishing between plant species. In particular, the narrow spectral channels of hyperspectral imagers allow the spectral feature known as the ‘red-edge’ (transition from low

reflectance to high NIR reflectance) to be located precisely. This feature is considered as a significant indicator of plant biochemistry (see Volume 1B—Section 6 and Volume 3A), which is indicative of plant condition. Hyperspectral imagery has also been used to monitor volcanic activity and emissions from industrial plants and wildfires, as well as mapping the changing composition of coastal waters.<sup>5152</sup>

Some hyperspectral imaging instruments are listed in Table 14.7. While most hyperspectral imaging for EO has been undertaken on aerial platforms, several satellite borne sensors have acquired substantial archives of hyperspectral imagery. The Hyperion sensor, for example, operated for 11 years from November, 2000. It imaged hundreds of narrow spectral channels (10 nm) over a 7.5 km swath (see Table 14.7; Pearlman *et al.*, 2003), which can be used to derive detailed spectra for selected features. Examples of Hyperion data analyses have been reported by Apan *et al.* (2004), Griffin *et al.* (2005), and Zhu *et al.* (2013). Additional satellite borne hyperspectral instruments are being developed, including HypsIRI (NASA), EnMAP (Germany), PRISMA (Italy) and HISUI (Japan).

## 14.4 Thermal infrared

Thermal infrared emission is introduced in Sections 2.7 and 5.2.2. Thermal infrared radiometers detect energy emitted from the Earth’s surface in the wavelength range 3–15  $\mu\text{m}$ . It should be noted that EO thermal sensors record emittance from the upper layer of the Earth’s surface, possibly as thin as 50  $\mu\text{m}$ , which may or may not be characteristic of the thermal properties of the observed features (Campbell and Wynne, 2011).

A detailed account of the development of infrared detectors and their characteristics is given in Rogalski (2012). Modern thermal sensors incorporate materials that rapidly respond to thermal infrared radiation, with different detector materials responding to different thermal infrared wavelengths (see Section 14.1). For example, characteristics of the versatile and commonly used Mercury Cadmium Telluride (HgCdTe) IR detector are detailed in Rogalski (2005) and Rogalski (2010). Detectivity, which characterises the normalised signal-to-noise performance of detectors (see Table 13.2 and Volume 1B—Section 2.1), is illustrated for a range of IR detectors in Figure 14.18.

51. Ground resolution varies with flying altitude and speed.

52. The number of channels and spatial resolution vary with configuration: 17 m pixels can be imaged for 19 spectral bands or 34 m pixels can be imaged for 63 spectral bands. Spectral bands can be selected from a total of 150 available channels.

**Figure 14.18** Detectivity of IR detectors

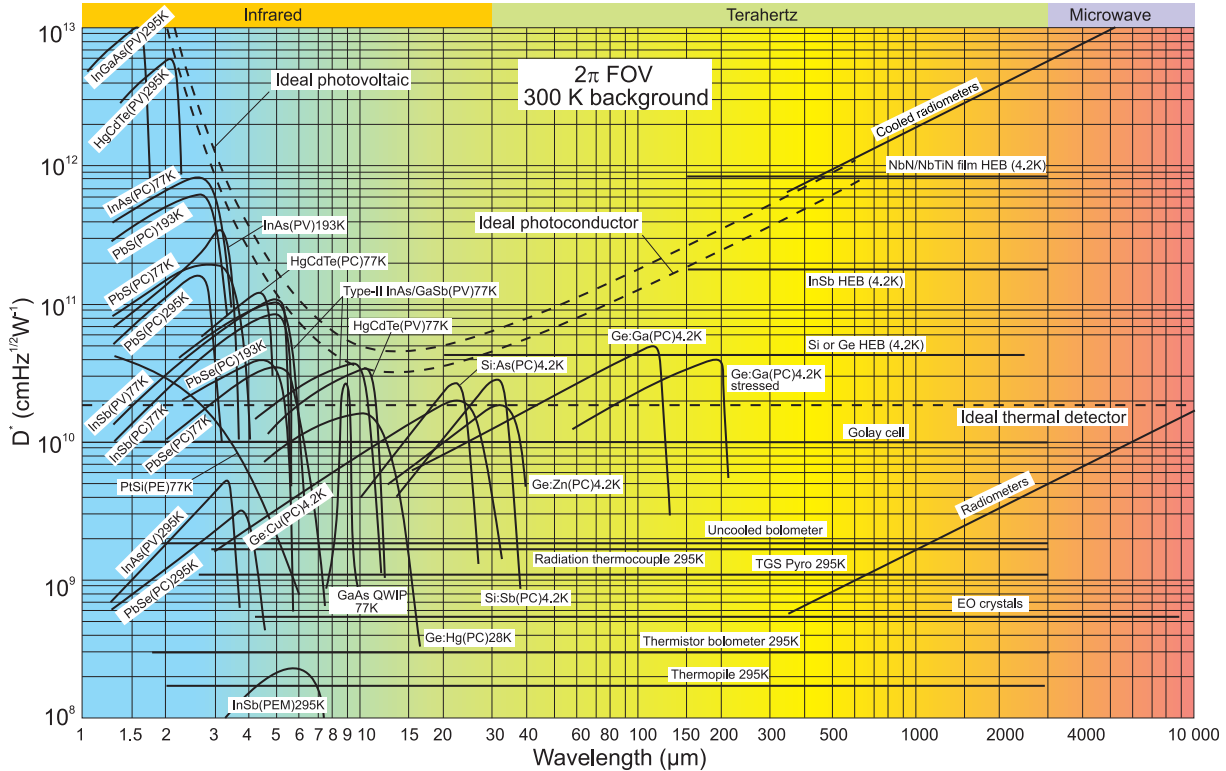
Detectivity ( $D^*$ ) for a range of IR detectors viewing hemisphere surrounding at 300K.

PC—photoconductive detector

PV—photovoltaic detector

PEM—photoelectromagnetic detector

HEB—hot electron bolometer



Source: Rogalski (2012) Figure 9. Used with permission.

Atmospheric gas absorption restricts thermal remote sensing for EO to two spectral windows in the thermal infrared region (see Section 5.4):

- 3–5  $\mu\text{m}$ , and
- 8–14  $\mu\text{m}$ .

To allow for the weaker energy levels associated with longer EM wavelengths, thermal sensors require larger IFOV and thus thermal imagery is generally only available with larger pixel sizes than optical imagery. The trade-off here is allowing sufficient integration time for a thermal observation to achieve acceptable signal fidelity without reaching saturation at the maximum design temperature (see Section 13.4). From a moving platform (aerial and spaceborne), a further consideration is ground speed, and the distance travelled during one observation. Ground speed of Landsat-8, for example, is about 7.6 km/sec<sup>53</sup>. With an integration time of 3.49 milliseconds per observation, one observation involves 25 m of satellite movement (Reuter *et al.*, 2015). The net result of these factors is that thermal sensors need to have lower spatial resolution to achieve high radiometric resolution (see

Volume 1B—Section 1). Given the inverse-square law (that is, the intensity of detected radiation is stronger when the sensor is closer to the target—see Section 2.9.1) and to ensure that the detected signal is stronger than sensor noise, these restrictions are most significant for satellite sensors.

Since thermal sensors require large IFOV, thermal imaging scanners are generally designed to scan across a large field of view (FOV) to avoid narrow image swaths. This imaging perspective introduces characteristic geometric distortions in thermal imagery, which are more pronounced with increasing proximity to the outer edges of each swath. Distortions include:

- larger ground pixel areas—pixels at the edges of the image swath are larger than those near the centre;
- one-dimensional relief displacement—tall structures near the image edges appear to lean away from the image centre; and
- tangential scale distortions—circles near the edges of the image appear elongated (see Figure 11.1).

53. For more information, visit [http://landsat.gsfc.nasa.gov/wp-content/uploads/2012/12/LDCM\\_Brochure\\_Dec20121.pdf](http://landsat.gsfc.nasa.gov/wp-content/uploads/2012/12/LDCM_Brochure_Dec20121.pdf)

Thermal scanners have typically operated using across-track (whisk broom) scanning but recent advances have allowed development of along-track (pushbroom) thermal scanners (see Section 14.2). Landsat thermal scanners, for example, have traditionally used pushbroom, rather than whiskbroom imaging (see Section 14.2.2). Landsat-8 Thermal InfraRed Sensor (TIRS) is the first satellite-borne sensor to use Quantum Well Infrared Photodetector (QWIP<sup>54</sup>) arrays, with three overlapping arrays of 640 detectors scanning across each image line (Jhabvala *et al.*, 2009; Jhabvala *et al.*, 2010). Inbuilt redundancy within the array minimises the chance of missing columns of pixels due to detector failure.

Most thermal sensors used for EO rely upon inbuilt temperature references to calibrate measured temperatures. In Landsat-8 TIRS, a two-stage cryocooler maintains the QWIP arrays between 180K and 190K. Before and after imaging each orbit, the field of view (FOV) is rotated from the ground to focus on a blackbody calibrator for one minute, then into deep space for one minute, before observing the ground again. These calibration measurements verify instrument measurements and allow

thermal background radiance to be removed from observations of ground targets. Additional calibration modes can be activated as required. By contrast, the thermal sensors on previous Landsat satellite needed to be calibrated twice for each image line (Reuter *et al.*, 2015).

The TIRS has been designed to capture two thermal channels with a spatial resolution of 100 m whereas the optical channels recorded by Landsat-8 OLI have spatial resolutions of 15 or 30 m. The relative spectral responses of the two Landsat-8 TIRS thermal bands compared with the thermal bands of previous Landsat satellites are illustrated in Figure 14.19. Two thermal channels allow a split-window algorithm to be used for atmospheric correction (Kerr *et al.*, 1992; Coll and Caselles, 1997) and offer feature discrimination advantages over the single thermal band acquired by the previous Landsat satellites. The TIRS pixel size is larger than the thermal channel of Landsat-7 and slightly smaller than that of Landsat-4 and Landsat-5, but deemed sufficient for imaging of centrally irrigated, circular agricultural fields, with diameters 400–800 m, which are commonly used for agriculture (Irons *et al.*, 2012).

**Figure 14.19** Spectral response of Landsat thermal bands

Relative spectral response for thermal channels for:

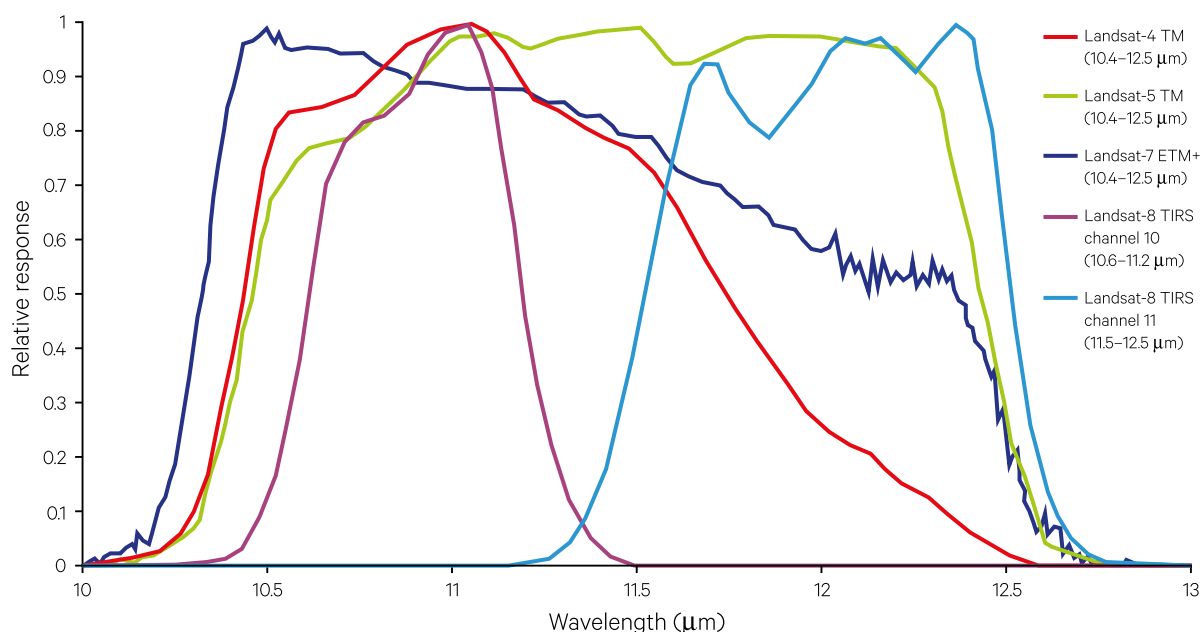
Landsat-4 TM (10.4–12.5  $\mu\text{m}$ )—red

Landsat-5 TM (10.4–12.5  $\mu\text{m}$ )—green

Landsat-7 ETM+ (10.4–12.5  $\mu\text{m}$ )—blue

Landsat-8 TIRS channel 10 (10.6–11.2  $\mu\text{m}$ )—purple

Landsat-8 TIRS channel 11 (11.5–12.5  $\mu\text{m}$ )—aqua



Adapted from: Reuter *et al.* (2015)

54. Thermal sensitivity of QWIP is based on charge-sensitive infrared phototransistors (based on Gallium arsenide (GaAs)/Aluminium Gallium Arsenide (AlGaAs) semiconductor chips)—Jhabvala *et al.* (2009); Jhabvala *et al.* (2010)



TIR imagery can be acquired at any time of the day or night. It is used for numerous EO applications, including fire mapping, military applications, and monitoring heat loss in built-up areas. Thermal remote sensing is also important for monitoring land surface and sea surface temperature, cloud temperature and other meteorological features. Handheld and laboratory-based thermal sensors are now routinely utilised in a wide range of fields, including medicine, engineering, and surveillance (see Figure 14.20). By detecting warm objects, these instruments also enable night vision.

Some commonly used thermal imaging sensors for EO are listed in Table 14.8. TIR radiometers are also used as non-imaging sensors (see Section 16.1.1.1). Interpretation of TIR imagery is considered in Volume 1B—Section 7.

**Figure 14.20** Thermography

Thermal imagery is used for a wide range of applications, such as highlighting insulation problems in buildings and detecting people and motor vehicles at night.



Source: Wikimedia Commons. Retrieved from [https://upload.wikimedia.org/wikipedia/commons/thumb/c/cf/lr\\_girl.png/1024px-lr\\_girl.png](https://upload.wikimedia.org/wikipedia/commons/thumb/c/cf/lr_girl.png/1024px-lr_girl.png)

**Table 14.8** Commonly used thermal imaging sensors

Instrument	Mission(s)	Agency	Number of thermal bands in 3–5 $\mu\text{m}$	Number of thermal bands in 8–14 $\mu\text{m}$	Ground resolution (m)
HCMR (Heat Capacity Mapping Radiometer)	HCMM (Heat Capacity Mapping Mission)	NASA	0	1 (10.5–12.5)	600
TIMS (Thermal Infrared Multispectral scanner)	Airborne	NASA/JPL/Daedalus	0	6 (8.2–12.2)	50 (at 20,000 m)
ATLAS (Advanced Thermal and Land Applications Sensor)	Airborne	NASA	1 (3.35–4.20)	6 (8.2–12.2)	10 (at 5,000 m)
Daedalus AMS (AA3607DS)	Airborne	Daedalus	1 (3.0–5.4 $\mu\text{m}$ )	1 (8.5–12.5)	Selectable
TM (Thematic Mapper)	Landsat-4/Landsat-5	NASA/USGS	0	1 (10.4–12.5)	120
ETM+ (Enhanced Thematic Mapper Plus)	Landsat-7	NASA/USGS	0	1 (10.4–12.5 $\mu\text{m}$ )	60
TIRS (Thermal Infrared Sensor)	Landsat-8	NASA/USGS	0	2 (10.6–11.2; 11.5–12.5)	100
ASTER (Advanced Spaceborne Thermal Emission and Reflection Radiometer)	Terra	NASA/USGS	0	5 (8.125–11.65)	90
MODIS (Moderate Resolution Imaging Spectroradiometer)	Terra/Aqua	NASA/USGS	7 (3.66–4.549)	8 (8.4–14.385)	1000
Imager	GOES	NOAA	1 (3.8–4.0)	2 (10.2–11.2; 11.5–12.5)	4000 8000
AVHRR/ <sup>55</sup> (Advanced Very High Resolution Radiometer)	TIROS-N to NOAA-19	NOAA	1 (3.55–3.93)	2 (10.3–11.3; 11.5–12.5)	1100 (LAC) 4000 (GAC)

Adapted from: Geoscience Australia (2011) Tables F-1 and F-2 <sup>55</sup>

55. Earlier AVHRR instruments acquired fewer thermal channels

## 14.5 Passive microwave

Passive microwave radiometers operate in microwave wavelengths from 1 to 300 mm, which are shorter than radar. They rely on detecting the emissions of thermal radiation in the microwave region. The range of wavelengths detected by microwave radiometers (shown in Figure 5.3) corresponds to the very low energy end of the Earth's energy spectrum (see Figure 5.6). The intensity of passive microwave radiation depends on an object's temperature and incident radiation plus the emittance, reflectance and transmittance properties of the object. Because these sensors are detecting low energy levels, their imagery

is relatively 'noisy', has lower spatial resolution and usually requires more complex interpretation.

Although a large volume of knowledge has already been obtained, the acquisition, processing and interpretation of microwave data are still largely experimental. Some aspects of microwave data interpretation are discussed in Volume 1B—Section 8. Of the available texts on the subject, Ulaby and Long (2014) offer an extensive reference on microwave remote sensing<sup>56</sup>. Examples of satellite-borne passive microwave sensors are listed in Table 14.9.

**Table 14.9** Examples of satellite passive microwave sensors

Instrument	Mission(s)	Agency	Ground Resolution <sup>59</sup> at nadir (km)
AMSR-2 (Advanced Microwave Scanning Radiometer-2)	GCOM-W (Global Change Observation Mission-Water)	JAXA	5–50
Aquarius L-band radiometer	SAC-D (Satellite for Scientific Applications-D) /Aquarius	CONAE/NASA	100
MIRAS (Microwave Imaging Radiometer using Aperture Synthesis)	SMOS (Soil Moisture and Ocean Salinity)	ESA	33–50
MWRI (Microwave Radiation Imager)	FY-3A, FY-3B, FY-3C (FengYun)	NSMC, CMA	7.5x12; 51x85
SSM/I (Special Sensor Microwave Imager)	DMSP F-14, DMSP F-15 (Defence Meteorological Satellite Program)	NOAA (DoD, USA)	15.7x13.9; 68.9x44.3
TMI (TRMM Microwave Imager)	TRMM (Tropical Rainfall Measuring Mission)	NASA/JAXA	18

Adapted from: CEOS (2015)<sup>57</sup>

## 14.6 Further Information

EO Handbook (CEOS, 2015)

Photodiode detectors: (including graph of spectral responsivity for Si, Ge and In detectors):

<http://course.ee.ust.hk/elec509/notes/Lect12-photodiode%20detectors.pdf>

CMOS sensors: <http://www.olympusmicro.com/primer/digitalimaging/acquisition.html>

Landsat: [http://landsat.gsfc.nasa.gov/?page\\_id=11](http://landsat.gsfc.nasa.gov/?page_id=11)

Comparison of Landsat-7 ETM+ and Landsat-8 OLI/TIRS channels superimposed on atmospheric windows<sup>58</sup>: <http://landsat.gsfc.nasa.gov/?p=3186>

MODIS: <http://modis.gsfc.nasa.gov>

Introduction to Photogrammetry (Schenk, 2005)

Thermal Sensors: <http://www.temperatures.com>

<sup>56</sup> Microwave, Radar and Radiometric Remote Sensing: <http://mrs.eecs.umich.edu>

<sup>57</sup> Depending on frequency

<sup>58</sup> Note that the ETM+ channels are not numbered sequentially with increasing wavelength as the decision to include thermal measurements (band 6) for geological and other applications was made after the initial design was underway.

## 14.7 References

- Apan, A., Held, A., Phinn, S. R., and Markley, J. (2004). Detecting sugarcane 'orange rust' disease using EO-1 Hyperion hyperspectral imagery. *International Journal of Remote Sensing*, 25(2), pp. 489-498. doi:<http://dx.doi.org/10.1080/01431160310001618031>.
- Campbell, J. B., and Wynne, R. H. (2011). *Introduction to Remote Sensing*, Fifth Edn. The Guilford Press, New York.
- CEOS (2015). *The Earth Observation Handbook*. Committee on Earth Observation Satellites, ESA Communications, The Netherlands. Retrieved from <http://www.eohandbook.com>.
- Coll, C., and Caselles, V. (1997). A split-window algorithm for land surface temperature from advanced very high resolution radiometer data: Validation and algorithm comparison. *Journal of Geophysical Research-Atmospheres*, 102(D14), pp. 16697-16713. doi:<http://dx.doi.org/10.1029/97jd00929>.
- Geoscience Australia (2011). *Continuity of Earth Observation Data for Australia: Operational Requirements to 2015 for Lands, Coasts and Oceans*. Geoscience Australia, Canberra.
- Griffin, M. K., Hsu, S. M., Burke, H. K., Orloff, S. M., and Upham, C. A. (2005). Examples of EO-1 Hyperion Data Analysis. *Lincoln Laboratory Journal*, 15(2), pp. 271-298.
- Harrison, B. A., and Jupp, D. L. B. (1989). *Introduction to Remotely Sensed Data. Part ONE of the microBRIAN Resource Manual (156 pages)*. CSIRO Australia, Melbourne.
- Irons, J. R., Dwyer, J. L., and Barsi, J. A. (2012). The next Landsat satellite: The Landsat Data Continuity Mission. *Remote Sensing of Environment*, 122, pp. 11-21. doi:<http://dx.doi.org/10.1016/j.rse.2011.08.026>.
- Jhabvala, M., Reuter, D., Choi, K., Jhabvala, C., and Sundaram, M. (2009). QWIP-based thermal infrared sensor for the Landsat Data Continuity Mission. *Infrared Physics & Technology*, 52(6), pp. 424-429. doi:<http://dx.doi.org/10.1016/j.infrared.2009.05.027>.
- Jhabvala, M., Reuter, D., Choi, K., Sundaram, M., Jhabvala, C., La, A., Waczynski, A., and Bundas, J. (2010). The QWIP focal plane assembly for NASA's Landsat Data Continuity Mission. *Proc. SPIE 7660 'Infrared Technology and Applications XXXVI*, 76603J (May 3, 2010) doi:10.1117/12.849305.
- Kerr, Y. H., Lagouarde, J. P., and Imbernon, J. (1992). Accurate Land Surface-Temperature Retrieval from AVHRR Data with Use of an Improved Split Window Algorithm. *Remote Sensing of Environment*, 41(2-3), pp. 197-209. doi:[http://dx.doi.org/10.1016/0034-4257\(92\)90078-x](http://dx.doi.org/10.1016/0034-4257(92)90078-x).
- Kim, Y., Huete, A. R., Miura, T., and Jiang, Z. (2010). Spectral compatibility of vegetation indices across sensors: band decomposition analysis with Hyperion data. *Journal of Applied Remote Sensing*, 4. doi:<http://dx.doi.org/10.1117/1.3400635>.
- Kinch, M. A. (2000). Fundamental physics of infrared detector materials. *Journal of Electronic Materials*, 29(6), pp. 809-817. doi:<http://dx.doi.org/10.1007/s11664-000-0229-7>.
- Pearlman, J. S., Barry, P. S., Segal, C. C., Shepanski, J., Beiso, D., and Carman, S. L. (2003). Hyperion, a space-based imaging spectrometer. *IEEE Transactions on Geoscience and Remote Sensing*, 41(6), pp. 1160-1173. doi:<http://dx.doi.org/10.1109/tgrs.2003.815018>.
- Reuter, D. C., Richardson, C. M., Pellerano, F. A., Irons, J. R., Allen, R. G., Anderson, M., Jhabvala, M. D., Lunsford, A. W., Montanaro, M., Smith, R. L., Tesfaye, Z., and Thome, K. J. (2015). The Thermal Infrared Sensor (TIRS) on Landsat 8: Design Overview and Pre-Launch Characterization. *Remote Sensing*, 7(1), pp. 1135-1153. doi:<http://dx.doi.org/10.3390/rs70101135>.
- Rogalski, A. (2005). HgCdTe infrared detector material: history, status and outlook. *Reports on Progress in Physics*, 68(10), pp. 2267-2336. doi:<http://dx.doi.org/10.1088/0034-4885/68/10/r01>.
- Rogalski, A. (2010). *Infrared Detectors*, Second Edn. CRC Press, Taylor & Francis Group, Boca Raton.
- Rogalski, A. (2012). History of infrared detectors. *Opto-Electronics Review*, 20(3), pp. 279-308. doi:<http://dx.doi.org/10.2478/s11772-012-0037-7>.
- Schenk, T. (2005). *Introduction to Photogrammetry*. Department of Civil and Environmental Engineering and Geodetic Science, The Ohio State University, Columbus, OH. Retrieved from <http://www.mat.uc.pt/~gil/downloads/IntroPhoto.pdf>.
- Sharma, D. (2005). *Handbook of Spectroscopy*. International Scientific, New Delhi.
- Shaw, G. A., and Burke, H. K. (2003). Spectral Imaging for Remote Sensing. *Lincoln Laboratory Journal*, 14(1), pp. 3-27.
- Ulaby, F. T., and Long, D. G. (2014). *Microwave, Radar and Radiometric Remote Sensing*. Retrieved from <http://mrs.eecs.umich.edu/>.
- Zhu, W., Tian, Y. Q., Yu, Q., and Becker, B. L. (2013). Using Hyperion imagery to monitor the spatial and temporal distribution of colored dissolved organic matter in estuarine and coastal regions. *Remote Sensing of Environment*, 134, pp. 342-354. doi:<http://dx.doi.org/10.1016/j.rse.2013.03.009>.



# 15 Active Imaging Systems

Authors: Glenn Newnham, John Armston, Bruce C. Forster, Catherine Ticehurst<sup>59</sup>

The principle underlying active remote sensing devices is that they transmit energy towards a specific target, either as pulses or as a continuous signal, then measure the energy returned from the target. Two distinct categories of active imaging sensors are radar and lidar technologies:

- lidar—irradiates with pulses of selected ‘optical’ wavelengths (see Section 5.1) then records the range and intensities of returns or ‘echoes’ (see Section 15.1); and
- radar—irradiates with pulses of microwaves then records the range and intensity of ‘echoes’ (see Section 15.2).

Being independent of solar illumination, active sensors may be used 24 hours a day. In addition, radar sensors are less sensitive to atmospheric scattering.

In many applications and geographic regions, such as the perennially cloudy tropics, these features provide a guarantee of data acquisition that is not available for passive systems operating in optical wavelengths.

While some active optical sensors (which illuminate a target with selected ‘optical’ wavelengths) are available (Holland *et al.*, 2012), they will not be considered in detail here. Examples of these systems include CropCircle™ (Lamb *et al.*, 2009) and Raptor™ (Lamb *et al.*, 2011).

## 15.1 Lidar

Light Detection and Ranging (lidar) is a technique that uses a transmitted laser pulse to detect the presence of a target and measures the distance to the target based on the time and intensity of any reflected return pulse. Lidar is an active remote sensing technology that operates in the wavelength range from ultraviolet to near infrared. The laser directs pulsed or continuous radiation through a collimating (laser) system while a second optical system collects the returned radiation and focuses it onto a detector. Both the time for any reflected return pulses and their intensity are measured.

Lidar instruments pulse very high peak intensities of light energy within a temporally narrow and highly collimated beam. An accurate clock records the time interval ( $t$ ) between transmission of the laser pulse and reception of any return to determine the range ( $r$ ) from the sensor to the target:

$$r = \frac{ct}{2}$$

where  $c$  is the speed of light in an atmospheric medium. When this distance and the beam direction to an object are known, then the location of that object, relative to the location of the sensor, can be calculated. If the absolute location of the sensor is known, then the absolute location of the target object can also be determined.

Lidar systems exist on many different sensing platforms including satellite, airborne and ground-based systems. Airborne systems generally include an Inertial Measurement Unit (IMU), which records the platform’s velocity and orientation. These are often combined with differential GPS measurements in order to determine a very accurate location and orientation of the aircraft. This location and orientation accuracy directly translates to the accuracy of derived absolute coordinates of any detected targets. Current airborne systems can deliver sub-centimetre accuracy for target positioning information.

Background image: PALSAR image, acquired on 3 January 2009 with HH polarisation, shows rivers feeding into the Gulf of Carpentaria in flood conditions.  
Source: Norman Mueller, Geoscience Australia

59. Recommended Chapter Citation: Newnham, G., Armston, J., Forster, B., and Ticehurst, C. (2016) Active Imaging Systems. Ch 15 in Volume 1A of Earth Observation: Data, Processing and Applications. CRCSI, Melbourne.



The laser light transmitted by a lidar systems can either be:

- pulsed—the system transmits short pulses of laser light, which may be intercepted by targets and scattered back towards the instrument. These return pulses are received and amplified by an optical telescope then converted to an electrical impulse by a photomultiplier; or
- continuous—the system emits a continuous stream of laser energy with modulated intensity. The phase difference between transmitted and received signals can be used to determine range. A number of different frequency modulations can be superimposed in order to overcome the possible ambiguity of receiving the same phase shift for different ranges, corresponding to different numbers of full modulation wavelengths.

Two return pulse detection systems are commonly used in Earth Observation (EO) lidar:

- discrete return—single or a small number of returns are sampled for each outgoing pulse; or
  - full waveform—a digitised profile is recorded of all return intensity as a function of time (see Figure 15.1).
- Discrete return instruments can be designed to record the first return, last return or multiple returns. Each of these may be based on either pulsed or continuous phase-shift ranging techniques. However, recording of a full-waveform can only be achieved using pulsed lidar systems. Jutzi and Stilla (2005) describe how continuous intensity returns can be converted into discrete ranges, thus linking full waveform and discrete lidar technologies.

A lidar system may also scan across track to increase coverage of measurements. Scan patterns used can vary (Gatzolis and Andersen, 2008), but are commonly the saw tooth pattern, which produces an irregular pattern of irradiated points. The accumulation of returns from these irradiated points is generally referred to as a point cloud. These can be resampled into a regular grid via nearest neighbour or surface fitting, for use in image processing and GIS software packages. Imagery derived from lidar data may belie their acquisition method, and imply a greater spatial resolution than was actually present in the original measurements. Recommendations for the acquisition and validation of airborne lidar surveys are given in Quadros and Keyzers (2015).

Different wavelengths of light can be used in lidar systems, as appropriate to particular applications. Blue-green wavelength (532 nm) lidar systems are used for bathymetric measurements in shallow coastal waters (see Volume 3B) and NIR lidar are used to provide topographic data, characterise vegetation canopies (see Volume 3A) and map urban environments (Lefsky *et al.*, 2002). Ground-based

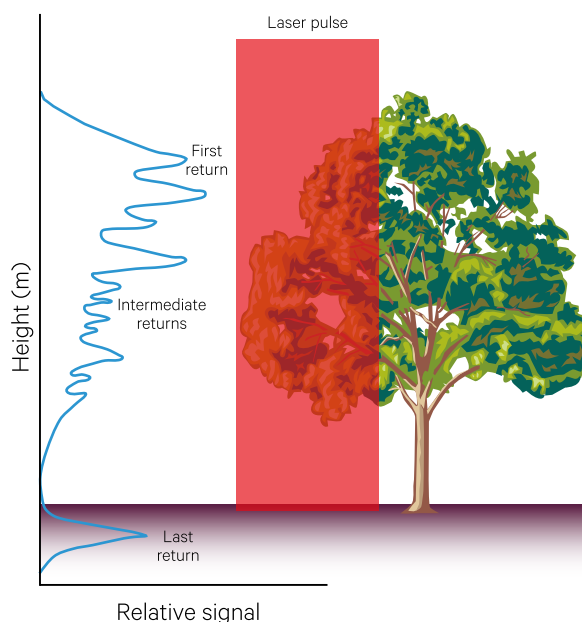
lidar (such as the many commercial Terrestrial Laser Scanning instruments and dedicated vegetation measurement system like the Echidna®) provides valuable verification of vegetation structure and density (see Section 10).

Lidar is only effective in clear atmospheric conditions and such devices are generally aircraft-borne or land-based. No satellite-based scanning lidar systems are currently in operation. However, the Geoscience Laser Altimeter, that was in operation on the ICESat satellite between 2003 and 2010, has been used in combination with other sensors for vegetation mapping (for example, Scarth *et al.*, 2015). The NASA Global Ecosystems Dynamics Investigation (GEDI) lidar is planned for deployment on the International Space Station in early 2019, to generate the first comprehensive high-resolution dataset of vertical forest structure at a global scale.

Airborne lidar is now ubiquitous within the global surveying industry with a primary focus on accurate and precise surface elevation and bathymetric mapping. Secondary applications focus on measurement and structural properties of vegetation (such as height and biomass), topography, built infrastructure and mine site environs (see Excursus 15.1). Other uses of lidar include spectroscopy (for air and water pollution studies) and altimetry (see Section 16).

**Figure 15.1** Lidar operation

A continuous waveform sensor would record the continuous height profile shown on the left of tree. Multiple discrete return sensors record the heights of discrete targets intercepted by the laser pulse. A first-return sensor would only record the height of the first target encountered, in this case the height of the first intercepted branch. A last-return sensor would only record the distance to the last object encountered by the laser beam, so is useful for terrain mapping.



## Excursus 15.1—Airborne Lidar Applications

**Source:** AAM Group

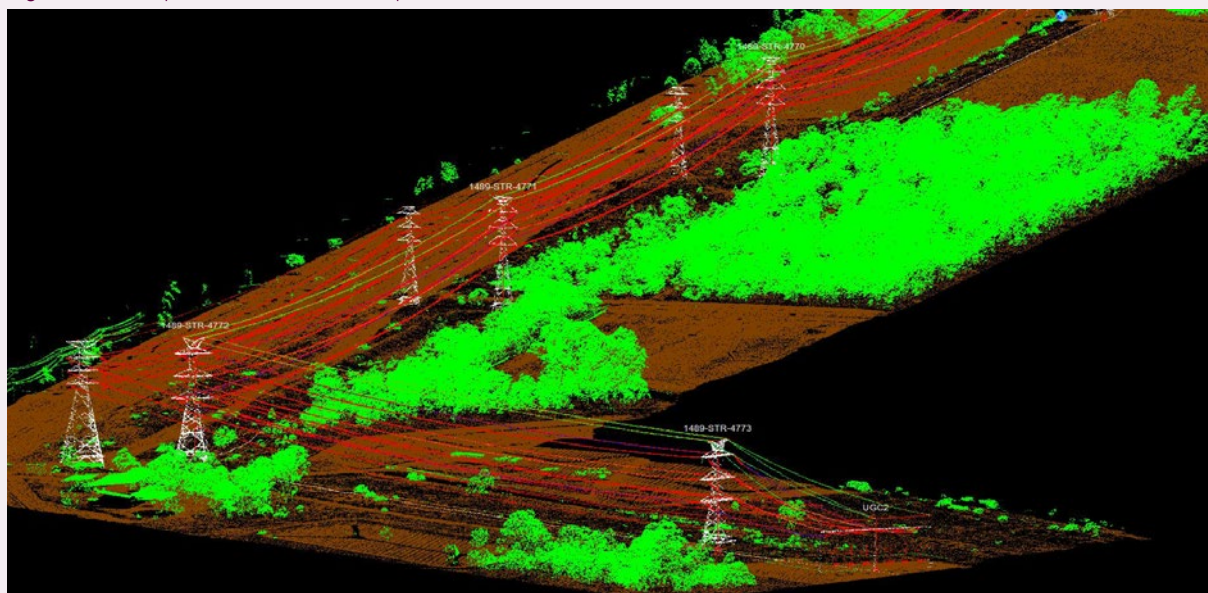
**Further information:** [www.aamgroup.com](http://www.aamgroup.com)

Airborne Lidar (Light Detection And Ranging) uses laser scanner(s) mounted in an aircraft to measure the height of discrete points below the aircraft. Lidar can penetrate gaps in dense canopy, enabling the capture of both canopy and topographic heights.

Various derived products can be generated for:

- vegetation,
- built infrastructure (such as power lines, towers, buildings), and
- bathymetry.

**Figure 15.2** Perspective view of classified point cloud



### Application 1: Power line survey

132 kV transmission lines were flown by helicopter in Brisbane at 76 kph (41 knots) in 2015. Lidar point data was acquired at 25 points/m<sup>2</sup>, with relative accuracy better than 5 cm. Natural colour imagery (6cm resolution) was acquired simultaneously. Based on field data collected independently by surveyors, the final derived tower and power line models were accurate to 5 cm, in both vertical and horizontal measurements (see Figures 15.2 and 15.3).

### Application 2: Terrain model from topographic lidar

Lidar terrain data and imagery were captured for a recent engineering study of a potential wind farm site in NSW (220 km<sup>2</sup>). As illustrated in Figure 15.4, these data sets were processed to deliver:

- .las point cloud (showing density of lidar points);
- terrain as 0.5 m contours (for road planning);
- 1 m ESRI grids (to generate terrain model); and
- 15 cm, three band (natural colour) ortho imagery (to provide locational context).

**Figure 15.3** Enlarged perspective view showing details of towers and power lines

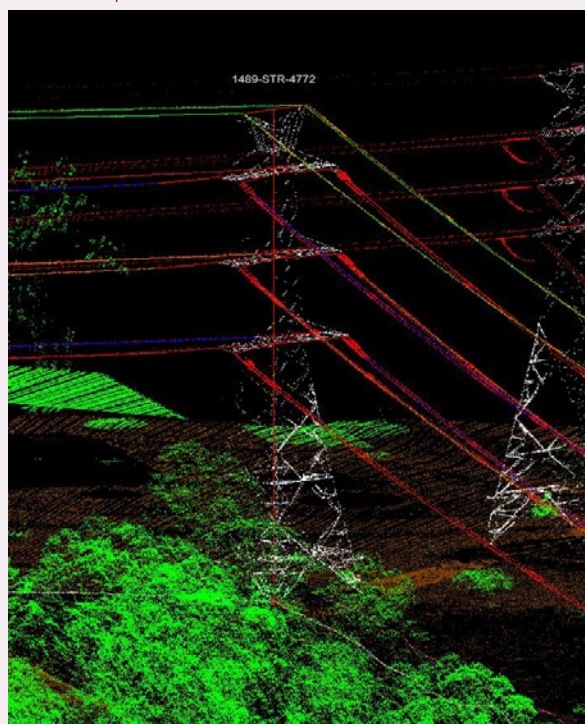
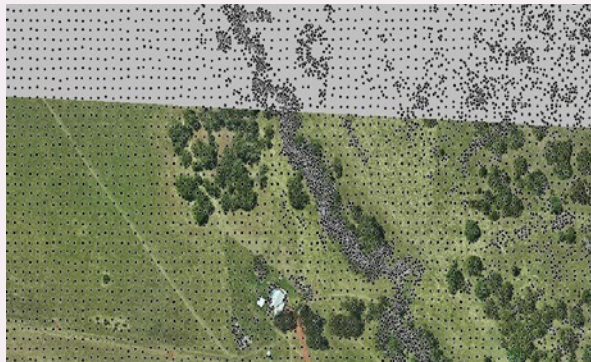


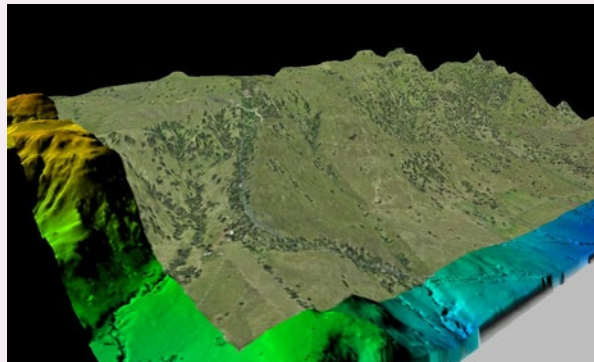


**Figure 15.4** Terrain model

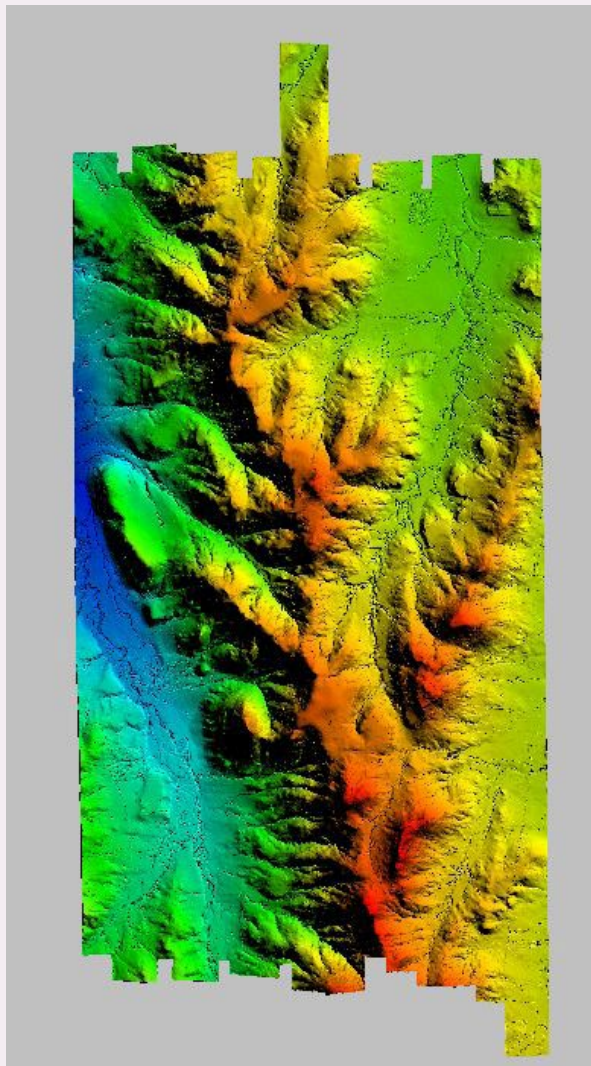
a: Laser strikes, overlaid on colour imagery to illustrate density of coverage on site



b: Mosaicked natural colour imagery draped over terrain model (mosaic spans 6 km east to west)



c: Terrain model generated from 1 m ESRI grid. Flight swaths (and overlaps) are indicated in this image. Colours range from blue for low lying areas, through green then yellow to red for higher elevations.



d: 15cm orthorectified imagery, natural colour



15.2 Radar

Radar is an acronym for RAdio Detection And Ranging, that is, using actively transmitted radio waves to detect objects and determine their position or ‘range’. The principle of operation for these devices is to direct pulses of microwave (a type of radio wave with wavelengths from approximately 1 cm to 100 cm) energy at an object then record the strength, direction and sometimes polarisation of the reflected energy. As with lidar systems, microwave pulses are transmitted for a very short time period (microseconds) and alternate with recording of returns. The distance between the transmitter and the reflecting object is then determined from the return time of the signal.

Radar signals may be transmitted at a range of wavelengths/frequencies. The standard wavelengths used and their standard radar frequency letter codes are given in Table 15.1.

These ranges are illustrated in Figure 15.5 relative to the electromagnetic spectrum. The effect of atmospheric composition on transmitted signals varies with wavelength. In general, atmospheric precipitation has minimal effect on radar signals with frequency <10 GHz, which provides a distinct advantage over passive and active optical sensors for EO when cloud cover is present. Slight attenuation occurs at wavelengths less than 30 mm under clear atmospheric conditions, with attenuation increasing as wavelength decreases. Heavy precipitation will cause a strong radar echo at wavelengths of 10 mm or less (this principle being used in both ground and aircraft mounted weather detection radar systems).

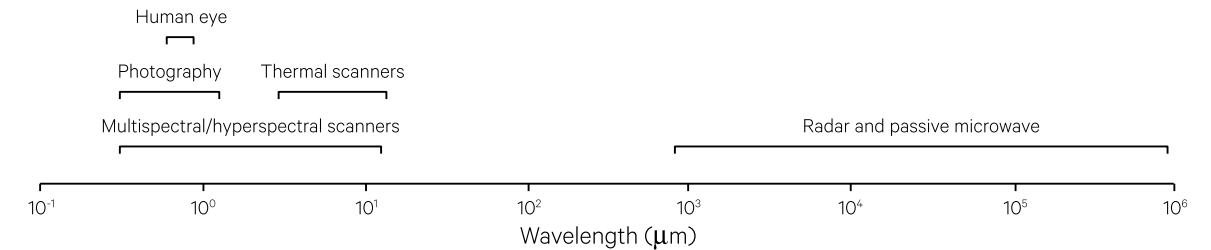
X, C and L bands are most commonly used for EO. Typical wavelengths used by airborne radars are illustrated in Figure 15.6. The interaction between these wavelengths and features on the Earth’s surface is partly a function of the scale of the surface ‘texture’ and its dielectric properties (electrical reflectivity and conductivity; see Volume 1B—Section 8 for details). Scattered signal amplitude and polarization provides information about scattering properties and structure. Phase measurements of the return pulse are used in interferometry to reconstruct 3D topography and, more recently, vegetation height and reflectivity profiles using tomographic techniques. For vegetation canopies, the interactions depend on the size, density and orientation of elements. For example, X-band radar, with wavelengths of around 3 cm, is scattered strongly by foliage, while L-band, with wavelengths of 27 cm, is scattered more strongly by tree branches and P-bands (wavelengths around 70 cm) is predominantly scattered by tree trunks (see Figure 15.7).

Table 15.1 Standard radar frequency and wavelength letter bands.

Band	Wavelength (mm = 10 <sup>3</sup> μm)	Frequency (GHz = 10 <sup>9</sup> Hz)
W	2.7-4.0	75.0-110.0
V	4.0-7.5	40.0-75.0
Q	6.0-9.0	33.0-50.0
K	7.5-25.0	12.0-40.0
X	25.0-37.5	8.0-12.0
C	37.5-75.0	4.0-8.0
S	75.0-150.0	2.0-4.0
L	150.0-300.0	1.0-2.0
P	300.0-1000.0	0.3-1.0

Figure 15.5 The microwave and radio wave spectra

Frequencies of bands commonly referenced with long wave EMR. Note: scales are logarithmic.

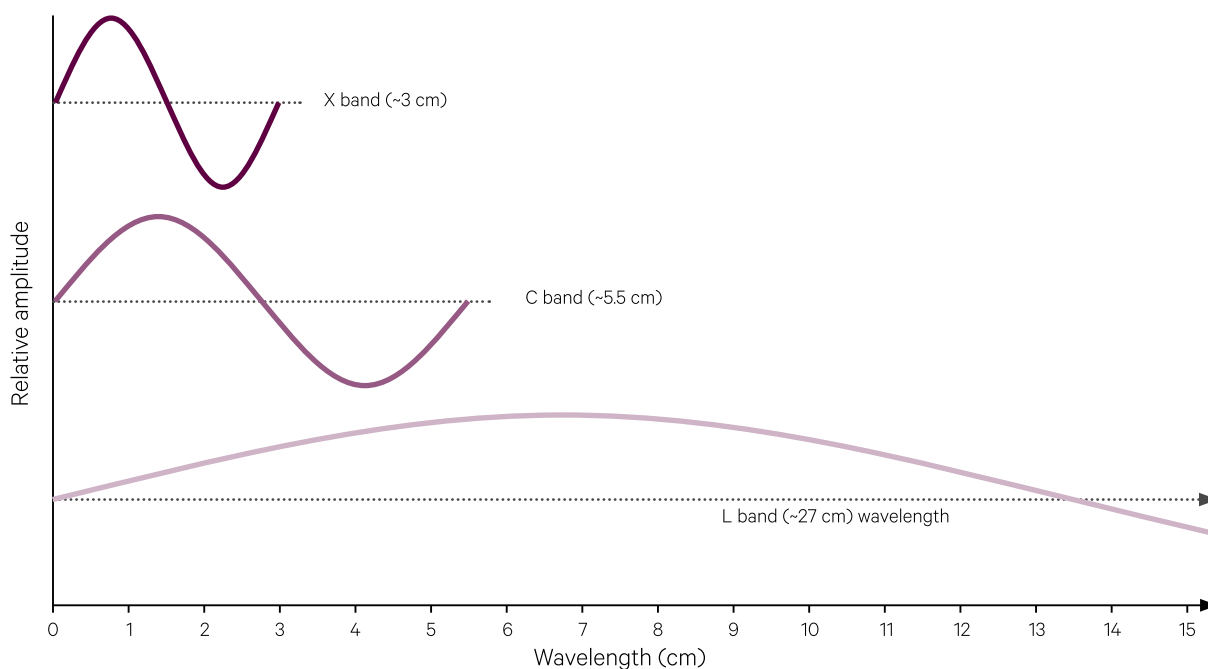


Adapted from: Harrison and Jupp (1989) Figure 22



**Figure 15.6** Radar wavelengths

Actual size of wavelengths for radar bands commonly used for EO



The transmitted radar signals can be generated so that the electrical wave vibrations are restricted to a single plane, that is, perpendicular to the direction of wave propagation (rather than vibrate in all directions perpendicular to that of propagation). This filtering process is referred to as polarisation. Two orthogonal modes of polarisation are used in imaging radar: these are referred to as horizontal (H) and vertical (V) and are typically transmitted separately. Interaction with features on the Earth's surface can change the polarisation of the scattered signal, so radar antennae are often designed to receive the H and V signals simultaneously. As a result, polarimetric radar detection systems can measure backscatter amplitude and phase in up to four specific polarisation modes (see Table 15.2). More recently, circular polarisation (the tip of the electric field vector is rotating in a circle as it propagates) is also used, where a circularly polarised wave is transmitted and H and V signals are received. This allows any configuration of transmit and receive to be derived (see Volume 1B—Section 8).

HH or VV images are referred to as 'co-polarised'; HV or VH are 'cross-polarised'. Radar system measurements are typically single-polarised (HH or VV or HV or VH), dual-polarised (HH and HV, VV and VH, or HH and VV), or quadrature polarised (HH, VV, HV, and VH). A quadrature polarized (that is, polarimetric) radar and some dual-polarised systems also measure the signal phase difference between the modes as well as the signal magnitude since it is important in polarimetric analysis. Differences in the structure (for example, orientation, shape) of

surface features modify the polarisation of reflected microwave energy in varying degrees, with the polarisation mode affecting the scattering intensity 'echo' and thus how the objects appear in the resulting imagery.

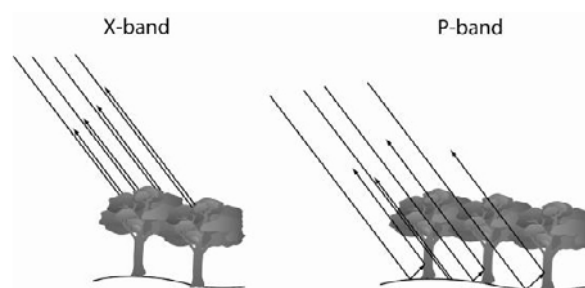
Two types of radar-based systems are commonly used for microwave imaging on aircraft and satellite platforms:

- Side-Looking Airborne Radar (SLAR) or Real Aperture Radar (RAR)—see Section 15.2.1; and
- Synthetic Aperture Radar (SAR)—see section 15.2.2.

**Figure 15.7** Interaction of radar wavelengths with vegetation

The interaction between radar wavelengths and vegetation depends on the size, density and orientation of vegetative components.

- X-band radar, with wavelengths around 3 cm, is strongly scattered by foliage.
- P-band radar, with wavelengths around 70 cm, is mostly scattered by tree trunks



Adapted from: Moreira (2001). Retrieved from [http://forsys.cfr.washington.edu/JFSP06/radar\\_overview.htm](http://forsys.cfr.washington.edu/JFSP06/radar_overview.htm)

Table 15.2 Polarisation options for radar signals

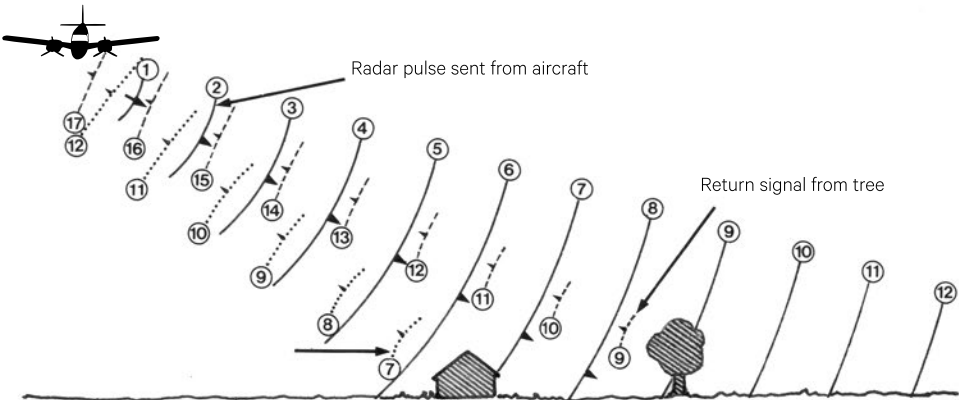
Transmitted	Received	Code	Type
H	H	HH	Co-polarised
H	V	HV	Cross-polarised
V	H	VH	Cross-polarised
V	V	VV	Co-polarised

15.2.1 Side-Looking Airborne Radar (SLAR) or Real Aperture Radar (RAR)

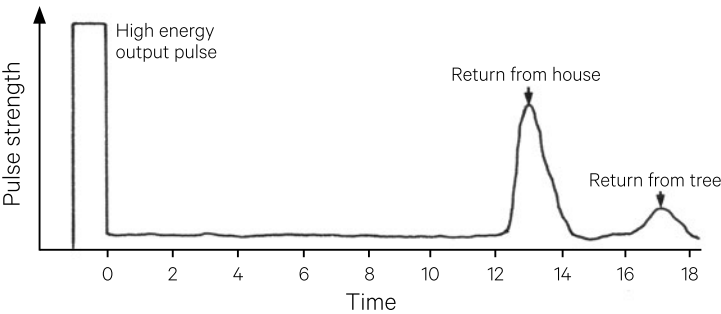
A radar pulse is transmitted off-nadir by an antenna fixed below an aircraft. This is used to image large ground areas adjacent to the flight line. The echoes are processed to produce an amplitude/time electrical signal that is then recorded as an image line, with 'brighter' pixels indicating higher scattering intensities. This procedure is illustrated in Figure 15.8.

Figure 15.8 Operation of side-looking airborne radar

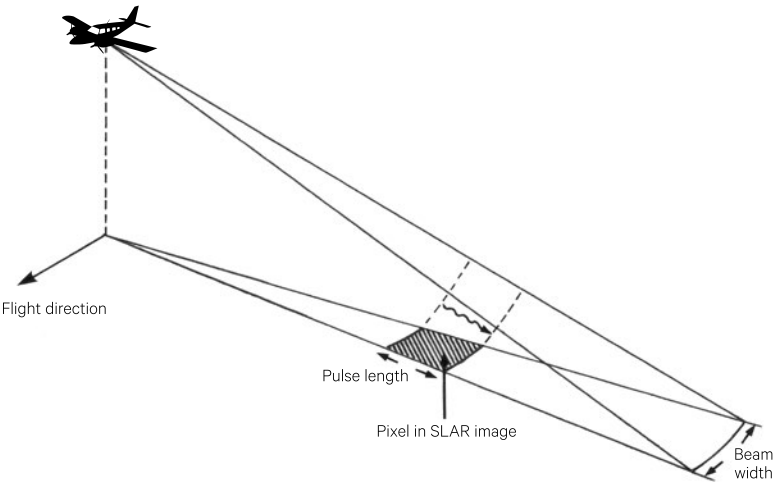
a. The propagation of one radar pulse is shown using solid lines to indicate the wavefront locations at time intervals 1 to 12. The reflected waves or echoes are shown by dashed lines beginning at time 7 for the house and time 9 for the tree. These return signals reach the antennae at times 13 and 17 respectively.



b. The antennae response graph shows a strong echo for the house at time 13 and a weaker echo for the tree at time 17. The strength of the echo depends on the way an object reflects radio waves.



c. Range resolution and azimuth resolution in SLAR imagery is determined by the time duration of the pulse and the beamwidth of the SLAR antennae.



Source: Harrison and Jupp (1989) Figure 23

The spatial resolution in such imagery is determined by the pulse time length and the beamwidth of the antenna as shown in Figure 15.8. The beamwidth of the SLAR antenna is directly proportional to the microwave signal wavelength and inversely proportional to the length of the antenna. The time duration of the pulse determines whether the signals from adjacent objects will be overlapped and hence not distinguished separately.

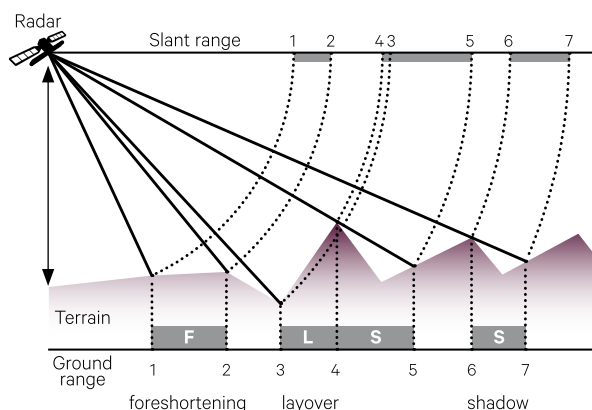
The oblique look angle used to acquire radar imagery results in characteristic geometric distortions such as radar shadows, foreshortening and layover effects (see Figure 15.9 and Volume 1B—Section 8). Foreshortening occurs when the true length of a tall feature, such as a mountain, appears compressed, while layover occurs when the radar beam reaches the top of a tall feature before it reaches the base. While these effects are more pronounced in aircraft radar images, they also occur in satellite imagery, and are more pronounced in mountainous terrain. The impact of these distortions on radar imagery is illustrated in Figure 15.10. Microwave image interpretation is discussed in greater detail in Volume 1B—Section 8.

Systems that utilise the actual antenna size, such as the SLAR systems described, are called real aperture radars (RAR). Because of the physical limitation of antenna size on aircraft, such systems are restricted to short range and low altitudes (which limit the extent of coverage) and relatively short wavelengths (which experience greater atmospheric attenuation and scattering).

**Figure 15.9** Radar image distortions

Specific distortions in radar imagery resulting from its side-looking viewing geometry include:

- Shadowing—locations shielded from the radar pulse cannot generate a return so appear as shadow.
- Foreshortening—more elevated locations on a slope generate radar returns in a shorter time interval after lower elevations on the slope than if the points were separated horizontally.
- Layover—where higher elevations on a slope are physically closer to the radar sensor, they will generate a return before lower elevations on that slope, which results in the top of the slope appearing to ‘lay over’ the base.

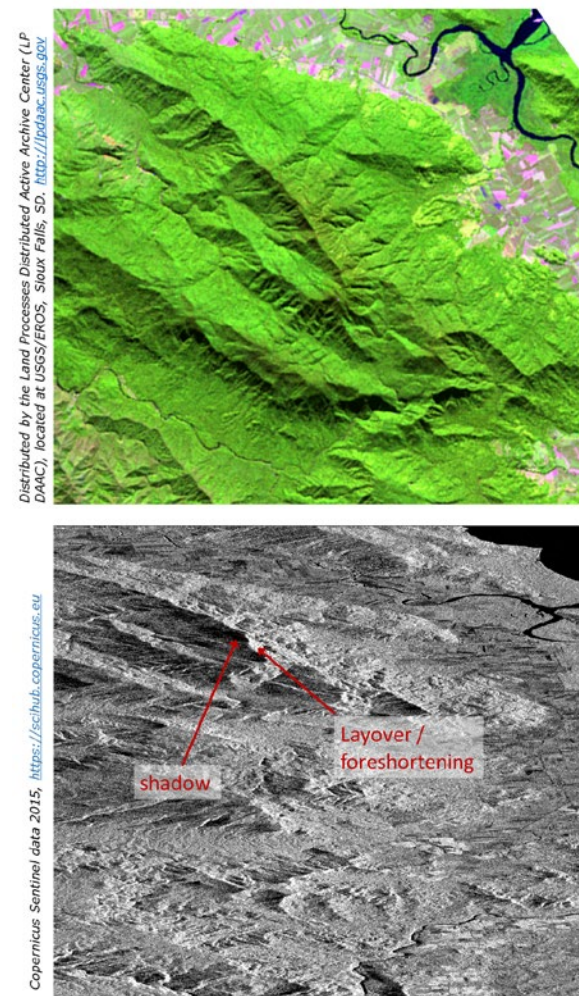


Source: Kerle *et al.* (2004). Used with permission from ITC.

**Figure 15.10** Impact of radar distortions in imagery

Wooroonooran National Park, Queensland (30 km south of Cairns).

- Landsat-8 OLI image 17 July 2015 (bands 6,5,4) showing terrain features
- Sentinel-1 image 25 February 2015 (HV polarisation) showing different spatial relocation of terrain features due to foreshortening and layover



Source: NASA/ESA, prepared by Catherine Ticehurst, CSIRO

## 15.2.2 Synthetic Aperture Radar (SAR)

The physical antenna length may be effectively lengthened using the flight path of the radar platform by processing return signals according to their Doppler shifts (that is, a change in wave frequency as a function of the relative velocities of transmitter and receiver; see Section 2.5.4). This basic principle is used in Synthetic Aperture Radar (or SAR) as shown in Figure 15.11. This processing requires that both amplitude and phase information be recorded from objects throughout the time period in which they are within the beam of the moving antenna. The theoretical increase in the antennae length (the synthetic aperture) allows the computer-processed cross-range or azimuth resolution to be equal to half the real aperture for the whole of the range (near



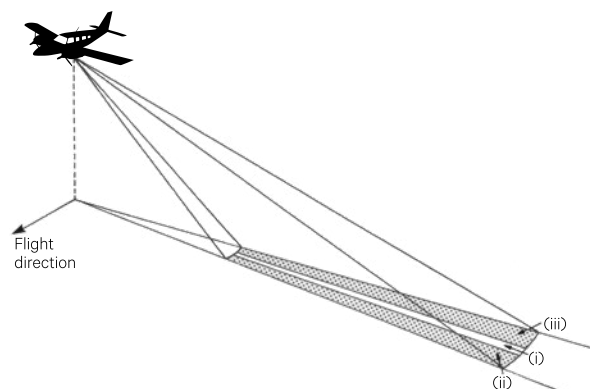
range to far range). Weighted averaging of multiple returns using the platform motion and Doppler shift effects allows the signal that would have been obtained by a longer antenna to be reconstructed. The consequently larger synthetic aperture results in higher spatial resolution imagery that is constant in the along-track (azimuth) and across-track (range) directions (see Volume 1B—Section 8 for details).

An example of a SAR image acquired by Sentinel-1a is shown in Figure 15.12 over the Menindee Lakes in western NSW. This image shows the amplitude of the VV polarization data, corrected to Sigma 0. Very dark areas occur where very little of the incident microwave energy is reflected back to the sensor, and mostly correspond to open water. Very bright areas occur where a large amount of the incident energy is reflected back to the sensor. This may correspond to vegetation or very rough surfaces (where 'rough' is relative to the incident wavelength), such as a dry lake with a 'rough' lake floor. A 'double-bounce' effect occurs along the river where incident microwaves reflect off water in the river channel and then again reflect off the woody structures in the surrounding riparian vegetation. Terrain undulations and variations in vegetative cover and soil moisture change the way the incident microwaves interact with the ground and create a mottled effect. Sand dunes in the northern portion of the image introduce horizontal striping patterns due to variations in topography and soil moisture.

**Figure 15.11** Operation of synthetic aperture radar

Recording the frequency as well as the amplitude of echoes allows the surface illuminated by the radar beam to be subdivided into three regions, where the frequency of the return signal from an object will change (due to Doppler shift), which allows the position of the ground object to be more precisely located and thus greatly improves the azimuth or cross-range resolution:

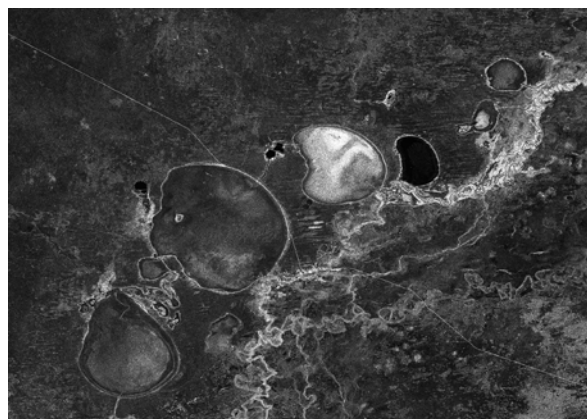
- (i) a narrow strip perpendicular to the flight line where the echo frequency matches the transmitted frequency,
- (ii) a region ahead of the aircraft where echoes are up-shifted in frequency, and
- (iii) a region behind the aircraft where echoes are down-shifted in frequency.



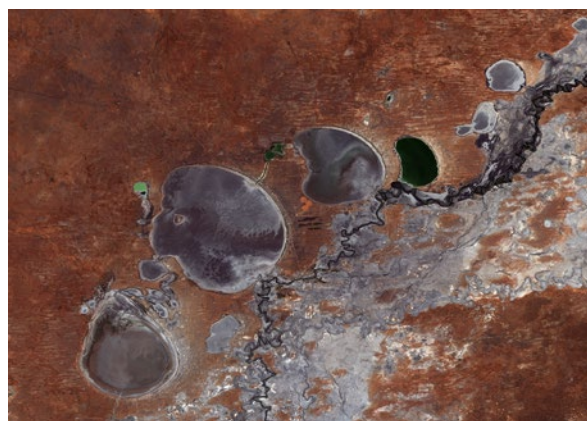
Source: Harrison and Jupp (1989) Figure 24

**Figure 15.12** Comparing SAR and Optical imagery

a. Sentinel-1a image over the Menindee Lakes (western NSW) acquired on the 29 December 2015. This is the amplitude of the VV polarization data, corrected to Sigma 0. Very dark areas occur where very little of the incident microwave energy is being reflected back to the sensor, while very bright areas occur where a large amount of the incident energy is being reflected back to the sensor. The mottling of the landscape in general is due to undulations in terrain, vegetation and variations in soil moisture changing the way the incident microwaves interact with the ground. The intermittent, but fairly regular, horizontal stripes in the northern part of the image are caused by sand dunes, creating some topographic effects and also showing variations in soil moisture between the peaks and troughs of the dunes.



b. Landsat-8 image over Menindee Lakes, acquired on 9 January 2016, displayed as a natural colour composite (using band 2 as blue, band 3 and green and band 4 as red).



Source: ESA, prepared by Norman Mueller, Geoscience Australia



Stripmap, spotlight and scan are different SAR acquisitions modes. Current SAR instruments acquire each mode to develop products that are suited to different applications. Scan mode involves moving the antenna in a scan pattern, and is used to capture larger areas (e.g. for flood mapping) but at the cost of lower spatial resolution. Spotlight is used to capture data over small target areas at high spatial resolution, and involves pointing the beam as the platform moves so that the target is in the beam for longer, thus making the synthetic aperture larger. Stripmap is the standard acquisition mode (fixed beam direction, no scanning) and corresponds with the SLAR described in Section 15.2.1.

TOPS (Terrain Observation by Progressive Scans) is a recent SAR mode for wide swath acquisition (the default mode of Sentinel-1), which aims at achieving the same coverage and resolution as the scan mode (besides creating scalloping-free images). Some recent SAR missions employ satellite constellations to enable single pass interferometry (e.g. TanDEM-X) and shorten revisit times.

A comprehensive list of airborne and satellite-borne SAR sensors is available in the Watt *et al.* (2012). Current and future spaceborne SAR imaging sensors are detailed in CEOS (2015). Satellite SAR sensors that are currently used or planned for use in Australia are listed in Table 15.3.

**Table 15.3** Examples of active and future satellite SAR sensors

Each of these sensors can have different observation models (stripmap, spotlight and scansar) with inherently different polarisations and spatial resolutions.

Frequency Band	Launch Year	Mission(s)	Agency (Country)
C-band	2007	RADARSAT-2	CSA/MDA (Canada)
C-band	2014 2016	Sentinel-1A Sentinel-1B	EC/ESA (Europe)
X-band	2007 2007 2008 2010	COSMO-SkyMED-1 COSMO-SkyMED-2 COSMO-SkyMED-3 COSMO-SkyMED-4	ASI (Italy)
X-band	2007	TerraSAR-X	DLR/Airbus DS (Germany)
X-band	2010	TanDEM-X	DLR/Airbus DS (Germany)
X-band	2009	RISAT-2	ISRO (India)
X-band	2015 2017 2022	HY-3A WSAR Hy-3B WSAR HY-3C WSAR	NSOAS/CAST (China)
L-band	2014	ALOS-2 PALSAR-2	JAXA (Japan)
L-band	2020	NISAR	NASA/ISRO (USA/India)
L-band	2017 2018	SAOCOM-1A SAOCOM-1B	CONAE (Argentina)
P-band	2021	BIOMASS SAR	EC/ESA (Europe)

Adapted from: CEOS (2015)

## 15.3 Further Information

### Lidar:

Terrestrial Laser Scanning Database, University of Calgary: <http://www.tlsdatabase.ucalgary.ca>

Spatial Scientific Technologies: <http://www.lidar.com.au/index.htm>

Lefsky *et al.* (2002)

Quadros and Keyser (2015)

### Microwave Remote Sensing:

Natural Resources Canada website: <http://www.nrcan.gc.ca/earth-sciences/geomatics/satellite-imagery-air-photos/satellite-imagery-products/educational-resources/9371>

Radar Tutorial: <http://www.radartutorial.eu>

Christian Wolff Radar Tutorial: <http://www.radartutorial.eu/index.en.html>

Kasischke *et al.* (1997)

Richards (2009)

Toutin and Gray (2000)

Ulaby and Long (2014)

Woodhouse (2004)

### Radar Animations:

Iain Woodhouse: <http://www.intro2radar.com>

### SAR:

JPL Imaging radar: <http://southport.jpl.nasa.gov>

Radarsat: <http://gs.mdacorporation.com/>

### Imaging Sensors and Applications:

Robust Imaging from Space (Watt *et al.*, 2012), including the following Adjunct Reference Documents:

Satellite and Airborne SAR Sensor Specifications: <http://www.crcsi.com.au/assets/Uploads/Files/Adjunct-Reference-1-SAR-Sensor-Specifications-FINAL.pdf>

SAR Application Case Studies: <http://www.crcsi.com.au/assets/Uploads/Files/Adjunct-Reference-2-SAR-Application-Case-Studies-FINAL.pdf>

Moreira (2014)

## 15.4 References

CEOS (2015). The Earth Observation Handbook. Committee on Earth Observation Satellites, ESA Communications, The Netherlands. Retrieved from <http://www.eohandbook.com>.

Gatzliolis, D., and Andersen, H. E. (2008). A guide to LIDAR data acquisition and processing for the forests of the Pacific Northwest. Pacific Northwest Research Station, Forest Service, US Department of Agriculture.

Harrison, B. A., and Jupp, D. L. B. (1989). Introduction to Remotely Sensed Data. Part ONE of the microBRIAN Resource Manual (156 pages). CSIRO Australia, Melbourne.

Holland, K. H., Lamb, D. W., and Schepers, J. S. (2012). Radiometry of Proximal Active Optical Sensors (AOS) for Agricultural Sensing. IEEE Journal of Selected Topics in Applied Earth Observations and Remote Sensing, 5(6), pp. 1793-1802. doi:<http://dx.doi.org/10.1109/jstars.2012.2198049>.

Jutzi, B., and Stilla, U. (2005). Measuring and processing the waveform of laser pulses. Paper presented at the 7th Conference on Optical 3-D Measurement Techniques, Vienna, Austria.

Kasischke, E. S., Melack, J. M., and Dobson, M. C. (1997). The use of imaging radars for ecological applications - A review. Remote Sensing of Environment, 59(2), pp. 141-156. doi:[http://dx.doi.org/10.1016/s0034-4257\(96\)00148-4](http://dx.doi.org/10.1016/s0034-4257(96)00148-4).

Kerle, N., Janssen, L. F., and Huurneman, G. C. (2004). Principles of Remote Sensing, an introductory handbook. , ITC Educational textbook Series 2, 3rd edition. The international Institute for Geo-Information Science and Earth Observation (ITC), Enschede, The Netherlands.

Lamb, D. W., Schneider, D. A., Trotter, M. G., Schaefer, M. T., and Yule, I. J. (2011). Extended-altitude, aerial mapping of crop NDVI using an active optical sensor: A case study using a Raptor (TM) sensor over wheat. Computers and Electronics in Agriculture, 77(1), pp. 69-73. doi:<http://dx.doi.org/10.1016/j.compag.2011.03.009>.

Lamb, D. W., Trotter, M. G., and Schneider, D. A. (2009). Ultra low-level airborne (ULLA) sensing of crop canopy reflectance: a case study using a CropCircle TM sensor. Computers and Electronics in Agriculture, 69(1), pp. 86-91. doi:<http://dx.doi.org/10.1016/j.compag.2009.07.004>.

- Lefsky, M. A., Cohen, W. B., Parker, G. G., and Harding, D. J. (2002). Lidar remote sensing for ecosystem studies. *Bioscience*, 52(1), pp. 19-30. doi:[http://dx.doi.org/10.1641/0006-3568\(2002\)052\[0019:LRSFES\]2.0.CO;2](http://dx.doi.org/10.1641/0006-3568(2002)052[0019:LRSFES]2.0.CO;2).
- Moreira, A. (2014). A Golden Age for Spaceborne SAR Systems. 20th International Conference on Microwaves, Radar, and Wireless Communication (MIKON). doi:<http://dx.doi.org/10.1109/MIKON.2014.6899903>.
- Moreira, J., Schwabisch, M., Wimmer, C., Rombach, M., Mura, J. (2001). Surface and ground topography determination in tropical rainforest areas using airborne interferometric SAR. . 'Photogrammetric Week '01' (Ed: D. Fritsch, Spiller, R.). Herbert Wichmann Verlag, Heidelberg.
- Quadros, N., and Keysers, J. (2015). Airborne LiDAR Acquisition and Validation. Chapter 15 in 'AusCover Good Practice Guidelines: A technical handbook supporting calibration and validation activities of remotely sensed data products' (Eds: A. Held, S. Phinn, M. Soto-Berelev, and S. Jones). TERN AusCover, Australia. ISBN 978-0-646-94137-0.
- Richards, J. A. (2009). Remote Sensing with Imaging Radar. Springer-Verlag, Berlin.
- Scarth, P., Phinn, S. R., Armston, J., and Lucas, R. (2015). Continental Scale Vegetation Structure Mapping Using Field Calibrated Landsat, ALOS Palsar and GLAS ICESat. Paper presented at the AGU Fall Meeting, San Francisco, USA.
- Toutin, T., and Gray, L. (2000). State-of-the-art of elevation extraction from satellite SAR data. *ISPRS Journal of Photogrammetry and Remote Sensing*, 55(1), pp. 13-33. doi:[http://dx.doi.org/10.1016/S0924-2716\(99\)00039-8](http://dx.doi.org/10.1016/S0924-2716(99)00039-8).
- Ulaby, F. T., and Long, D. G. (2014). Microwave, Radar and Radiometric Remote Sensing. Retrieved from <http://mrs.eecs.umich.edu/>.
- Watt, M., Milne, T., Williams, M., and Mitchell, A. (2012). Robust Imaging from Space: Satellite SAR (Synthetic Aperture Radar). CRCSI. Retrieved from <http://www.crcsi.com.au/library/resource/robust-imaging-from-space>.
- Woodhouse, I. H. (2004). Introduction to Microwave Remote Sensing. CRC Press.

# 16 Non-imaging and Sounding Systems

Some remote sensing devices operate in a non-imaging mode to detect information about specific locations or lines on the Earth's surface, and also to measure characteristics of either the atmosphere at selected altitudes or the oceans at nominated depths. These sensors are particularly informative for meteorological applications and have a significant impact on the accuracy of weather forecasts (see Excursus 16.1). Such systems include:

- passive non-imaging devices, which are particularly relevant to atmospheric studies—including thermal infrared sensors and passive microwave radiometers (see Section 16.1.1);
- active non-imaging altimeters or profilers—use laser or radar ranging and scattering instruments to measure detailed distances from sensor to target, which can be used to determine surface height and texture (see Section 16.1.2);
- sounding devices—measure atmospheric properties at specific altitudes or water properties at particular depths using both active and passive sensors (see Section 16.2); and
- sounding techniques, such as radio occultation, which limb sound the atmosphere by measuring the bending of EMR travelling from one satellite to another.

## Excursus 16.1—Value of EO to Numerical Weather Prediction

**Source:** John Le Marshall, Bureau of Meteorology

**Further information:** Le Marshall *et al.* (2013a), Bureau of Meteorology: <http://bom.gov.au>

Numerical Weather Prediction (NWP) models combine our understanding of the physics of weather with current observations of weather conditions to predict future weather conditions. Current observations can be based on both conventional meteorological measurements (e.g. balloon-based temperature measurements) and various forms of EOS data: imaging, non-imaging and sounding. When only conventional observations are used, the accuracy of a one-day forecast is the same as the accuracy of a four-day forecast in the northern hemisphere based on both conventional and EOS data.

### Observing System Experiments (OSE)

Various experiments have been conducted to test the value of EOS data in operational NWP. Two recent experiments used:

1. the ACCESS-G operational system at the Australian Bureau of Meteorology and analysed data from 28 October to 30 November 2011; and
2. the Global Forecast System (GFS) at the US National Centres for Environmental Prediction (NCEP) and analysed data from 15 August to 30 September 2010.

The correlation between the actual and predicted 500 hPa geopotential height anomaly surfaces was used to analyse these datasets. Marked differences in the rate of die-off in these curves were observed using both EOS and conventional meteorological observations compared with only using conventional data. The EOS analyses were based on the complete operational database and treated as the control.



## Geopotential Height Anomalies

While geometric height is the elevation above mean sea level, the Geopotential Height adjusts this measure for gravity variations with changes in latitude and elevation. In meteorology it is used to represent the actual height of a pressure surface.

Deviations from the average geopotential height surface are called anomalies. Positive anomalies correlate with hotter than average temperatures and negative anomalies are indicative of colder temperatures. The 500 hPa geopotential height anomaly correlation between actual and predicted weather is regarded as a robust measure of forecast accuracy.

## OSE Results

As can be seen in Figure 16.1, the duration of accurate numerical weather forecasts in the Southern Hemisphere is increased fourfold by the inclusion of EOS datasets. These analyses demonstrated that a 24 hour forecast without EOS data has the same accuracy as a 96 hour forecast that includes EOS data. In the Northern Hemisphere, where a higher density of conventional meteorological observations is available, the inclusion of EOS data improved forecast duration by a factor of 1.6.

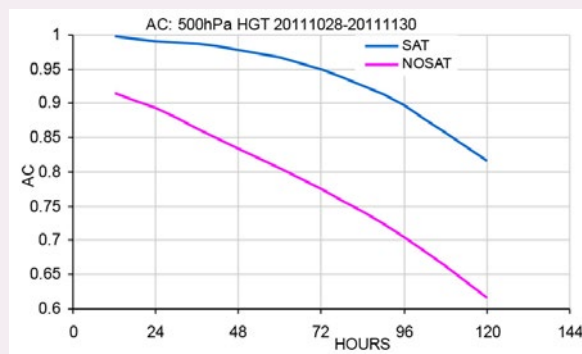
These improvements in NWP capability are also reflected in forecasting individual extreme weather events, such as cyclones. This gain in forecast skill has resulted in significant societal benefits from:

- more reliable weather forecasts;
- improved weather warnings; and
- more time to prepare for extreme weather.

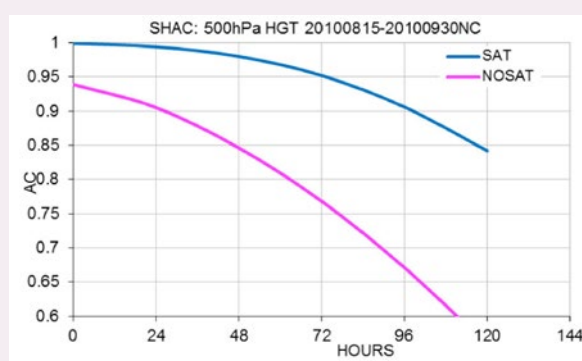
**Figure 16.1** 1500 hPa height anomaly correlations

Anomaly correlations for the operational system relying on both EOS and conventional meteorological observations (blue) compared with conventional meteorological observations used without EOS (pink).

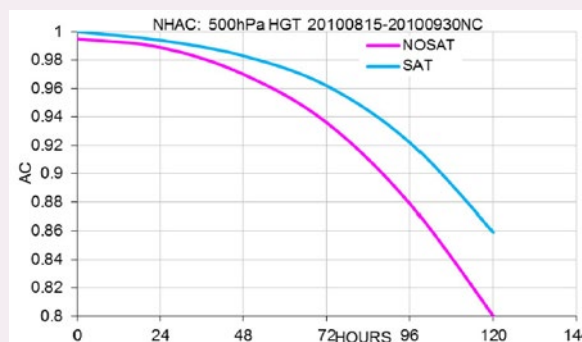
a. Southern Hemisphere ACCESS-G results 2011



b. Southern Hemisphere GFS results 2010



c. Northern Hemisphere GFS results 2010



## 16.1 Non-imaging systems

### 16.1.1 Passive

#### 16.1.1.1 Thermal infrared

Non-imaging thermal infrared radiometers are used to measure atmospheric temperature, pressure, humidity and composition at defined locations. These measurements are particularly informative for atmospheric modelling, weather forecasting and climatic studies (see also Volume 1B—Section 7 and Volume 3).

#### 16.1.1.2 Passive microwave

Passive microwave is used for atmospheric observations by detecting the thermal emission of broad atmospheric layers, with altitude being determined by observing at a number of frequencies. The atmospheric temperature and composition can be determined using the microwave spectrum data, with other data being used for calibration (such as infrared observations or meteorological forecasts). Non-imaging passive microwave radiometers are used to infer ocean surface wind speed, and atmospheric water content and temperature.

There are detectable differences in microwave emission intensity between water and sea-ice, the differentiation of which is important for climatic studies. Other applications include determination of:

- sea surface temperature (even in cloudy conditions) for global climate studies;
- precipitation rates; and
- characteristics (including age estimates) for ice and snow cover.

### 16.1.2 Active

Active non-imaging systems involve:

- ranging—recording the time interval between transmitting a signal and detecting its return; and/or
- scattering—recording the strength of the returned signal.

Some of the active non-imaging technologies used to detect radiation from Earth include:

- laser altimetry (see Section 16.1.2.1);
- radar altimetry (see Section 16.1.2.2); and
- microwave scatterometry (see Section 16.1.2.3).

#### 16.1.2.1 Laser altimetry

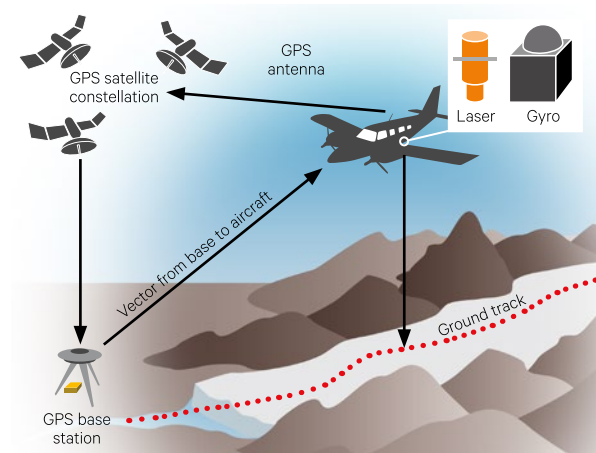
Laser imaging systems are introduced in Section 15.1. Laser altimeters or profilers transmit a light pulse towards the Earth and measure the time delay of the return to determine the distance between the target and the sensor. The pulse generally uses an infrared wavelength selected within an atmospheric window. A series of pulses allows a surface profile to be generated for the target terrain. The terrain surface is sampled by a series of point measurements along the platform direction.

Laser profilers have been carried by both aircraft and satellites. For example, the highly successful satellite laser altimetry mission, ICESat<sup>60</sup>, has been valuable for augmenting radar altimetry data, including quantifying its accuracy (Brenner *et al.*, 2007). Figure 16.2 illustrates an airborne laser altimeter that has been used to measure the surface height of glaciers in Alaska (Valentine *et al.*, 2004). The altimetry system in this example comprises:

- a GPS receiver, which records the plane position;
- a laser, which continually measures the distance from the plane to the glacier; and
- a gyroscope, which measures the direction of the laser.

Using precise positional information for both the target and sensor, the surface profile along the laser beam can subsequently be interpolated from the points. In this case, surface profiles are used to compute long-term changes in glacier thickness by comparison with older topographic records (Arendt *et al.*, 2002).

Figure 16.2 Laser altimeter



Adapted from: Chris Larsen, University of Alaska Fairbank at [http://fairweather.alaska.edu/chris/altimetry\\_text.html](http://fairweather.alaska.edu/chris/altimetry_text.html)

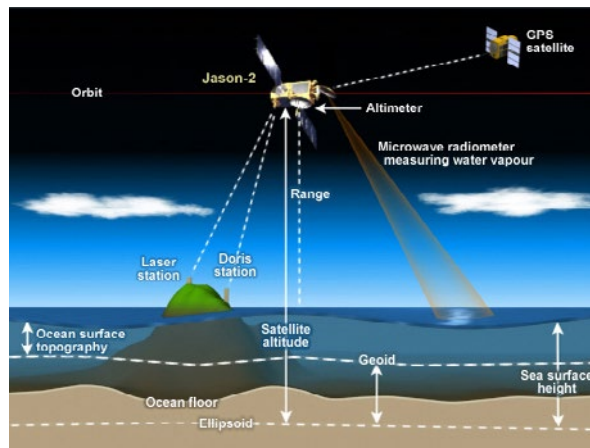
60. ICESat: <http://icesat.gsfc.nasa.gov>

A variation on this configuration is used in Satellite Laser Ranging (SLR) where a laser beam is transmitted from Earth to a reflector carried by a satellite (see Excursus 3.2). These measurements are used to track satellite orbits, monitor Earth's gravitational field, quantify movement of tectonic plates and define geodesic reference points. A growing number of satellites are now fitted with corner-cube reflectors to return the laser beams from the global network of SLR stations, allowing triangulation of both satellite and ground station positions. These activities are coordinated by the International Laser Ranging Service (ILRS)<sup>61</sup>. Laser Ranging data products are essential inputs to the International Terrestrial Reference Frame (ITRF)<sup>62</sup> (see Section 3).

### 16.1.2.2 Radar altimetry

Radar altimeters have been carried on several satellites, starting with Skylab in 1973, and more recently including the ERS, Jason and Cryosat platforms. This non-imaging radar detects the microwave backscattering of a surface using a narrow pulse with near normal incidence. As introduced in Section 15.2, the basic design of radar devices is to measure distance. By directing the pulse onto the Earth's surface from directly overhead (nadir) the distance being measured is the altitude of the platform above the surface. This relies on accurate knowledge of the platform position, with reference to positioning satellites and ground locating systems, such as the Doppler Orbitography and Radiopositioning Integrated by Satellite (DORIS; Guijarro *et al.*, 2000). Factors relevant to interpretation of satellite radar altimetry data are shown in Figure 16.3.

**Figure 16.3** Radar altimetry

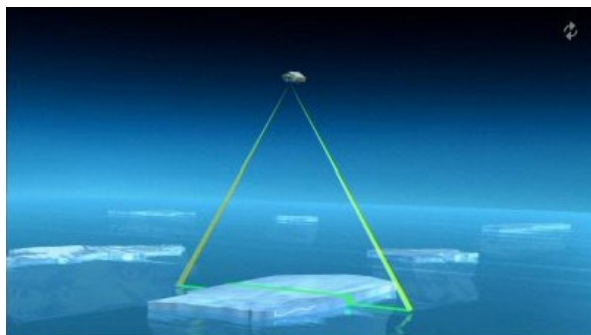


Source: © EUMETSAT. Retrieved from <https://www.eumetsat.int/jason/print.htm>

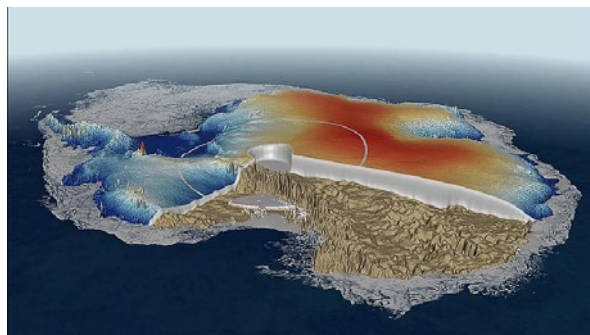
Data from these non-imaging devices can be plotted in image format, for example to map sea surface topography, if the required data volume is available. Routine observation of sea surface topography using satellite radar altimetry has been critical for monitoring sea level changes and global climatic variations (Hwang *et al.*, 2004). Over oceans, radar altimeters are also used to determine significant wave height, wind speed and mesoscale topography. The latter application has produced otherwise unattainable data describing the marine geoid, and the related sea floor topography (Vignudelli *et al.*, 2011). Other applications include mapping land surface topography, identifying types of ice masses, monitoring sea/ice boundaries and modelling ice sheet elevation (see Figure 16.4 and Helm *et al.*, 2014).

**Figure 16.4** Cryosat radar altimeter

a. Height of ice above sea level is measured by the radar altimeter carried on Cryosat-2.



b. Antarctic ice sheet: preliminary map from Cryosat-2 (ESA, UCL).



Source: © ESA, UCL. Retrieved from

a. <http://wattsupwiththat.com/2010/04/13/cryosat-passes-first-operational-tests/>

b. <https://eoportal.org/web/eoportal/satellite-missions/c-missions/cryosat-2>

61. ILRS: <http://ilrs.gsfc.nasa.gov>

62. ITRF: <http://itrfensg.ign.fr>

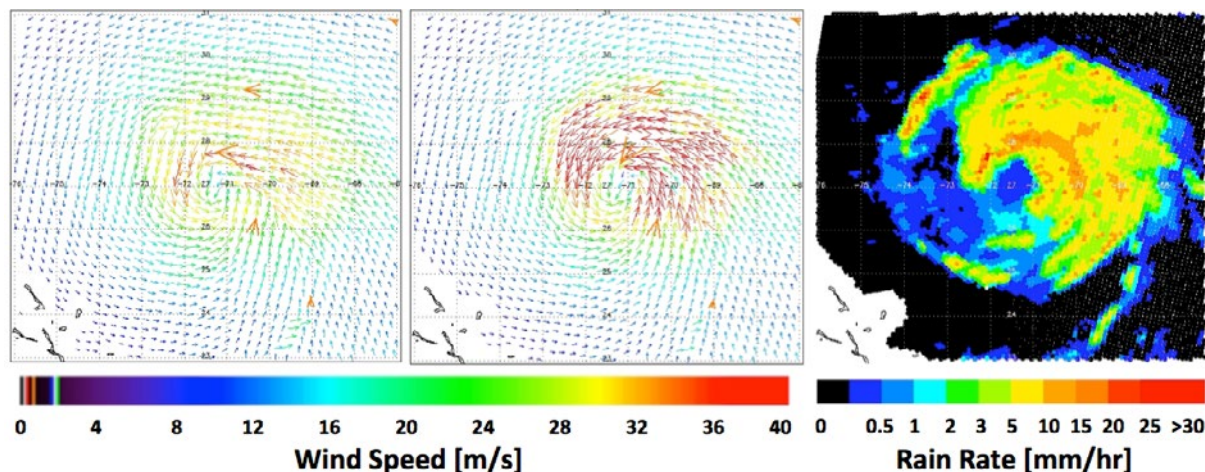
**Figure 16.5** Wind estimates derived from SeaWinds observations

SeaWinds scatterometer observations of Hurricane Isabel acquired on 16 September 2003 were used to derive estimates of near-surface horizontal wind speed and direction over the ocean. Where the ocean surface is obscured by significant rain, passive microwave radiometry, when available, can be used to correct the scatterometer wind estimates.

a. Wind estimates using SeaWinds standard algorithm

b. Corrected estimates incorporating radiometer-based estimation of precipitation attenuation

c. Precipitation measured by the AMSR radiometer, illustrating that the correction is greatest in the most active parts of the storm



Source: Svetla Hristova-Velleva, Courtesy NASA/JPL-Caltech. NASA.

### 16.1.2.3 Microwave scatterometer

This non-imaging device measures the microwave scattering or reflective properties of surfaces and is specifically designed to measure backscattering. This requires that the sensor detect more detailed spectral information than acquired by imaging radar but with reduced spatial resolution and areal coverage. The surface is scanned in two or more directions, usually by multiple sensors using either a series of radar pulses or a continuous signal. Spaceborne microwave scatterometers have been carried on several satellite missions, using varying viewing geometries.

The primary application of microwave scatterometers is to measure wind vectors (that is, speed and direction) over the ocean surface (Barale *et al.*, 2010). This is based on the principle of ocean ‘roughness’ being caused by wind and resulting in a characteristic surface pattern that may be identified by its scattering properties. A mathematical model uses the reflectivity data with other sensor characteristics to determine wind speed and direction over the surface. Although radar scatterometers are non-imaging, their data may be used to construct global wind maps when collected over a sufficiently large area (see Figure 16.5). These data are also used to map soil moisture and texture, monitor vegetation and measure the extent and condition of ice and snow.

## 16.2 Sounding Systems

Sounding systems measure specific properties of air or water at predefined heights or depths. Such systems are primarily used to determine the vertical distribution of atmospheric parameters such as temperature, pressure, water volume, chemical composition, and wind speed and direction (see Excursus 16.2). They are also used to map water profiles of colour, depth and temperature. Sounding systems can also detect ionospheric disturbances emanating from seismic waves (Lognonné *et al.*, 2006).

### 16.2.1 Passive

Passive sounders measure the thermal infrared or microwave extinction, emission or scattering for atmospheric properties at particular altitudes. Gases that are uniformly mixed through the atmosphere, such as oxygen or carbon dioxide, are used as ‘tracers’ to estimate temperature profiles, whereas water vapour concentration is used to estimate humidity profiles. The sounding instruments are then designed to measure the EM emission of these gases. Altitude is inferred from the spectral dependence of absorption, such that the less absorbed the wavelength, the deeper the sensor ‘sees’ into the atmosphere.



Atmospheric sounders routinely deliver profiles of temperature and humidity for weather prediction and climate modelling. A radiosonde is the most common *in situ* passive sounding device, carried by a weather balloon, rockets, ships or aircraft. The three broad groups of passive sounders carried by aircraft or satellites are:

- multispectral radiometers—examples of selective filter radiometers are ISAMS (Improved Stratospheric and Mesospheric Sounder) and MOPITT (Measurements of Pollution in the Troposphere); AMSU (Advanced Microwave Sounding Unit) is a 15-channel microwave radiometer used to detect atmospheric water vapour and precipitation;
- hyperspectral spectrometers—for example, AIRS (Atmospheric Infrared Sounder) is a 2,378 channel grating spectrometer measuring radiance in the range 3.7–15.4  $\mu\text{m}$  with nadir spatial resolution of approximately 13.5 km designed to determine atmospheric temperature and humidity; and
- laser sensors—laser heterodyne spectroscopy is used for atmospheric and astronomical observations to derive ultra-high spectral resolution measurements. This technology has enabled accurate altitude profiles for atmospheric constituents such as ozone and nitrous oxide.

## 16.2.2 Active

Active sounding systems use lidar or radar technologies. Pulses or continuous signals are transmitted into the atmosphere to derive information from:

- backscattering—indicating density, shape and size of scattering particles;
- absorption—indicating concentration and distribution of absorbing materials;
- polarisation—indicating shape of scattering particles, which can be used to differentiate between water droplets and snow; and
- phase change—indicating mass of particles.

### 16.2.2.1 Lidar

The operation of lidar systems is introduced in Section 15.1. Lidar sounding instruments measure aerosol backscatter, concentration, and temperature profiles as well as properties of winds and clouds, using:

- backscatter lidar—measures intensity and polarisation to determine properties of atmospheric layers, particularly aerosols and thin cloud, such as cirrus;
- differential absorption lidar (DIAL)—measures extinction of light at two wavelengths to derive atmospheric constituents, their densities, water vapour content and temperature profiles;
- Doppler lidar—measures phase shift from backscattering of atmospheric particles to determine wind velocity; or
- Fluorescence Lidar and Raman Lidar—both measure intensity using a pulse wavelength which differs from the measured wavelength.

The Australian Hydrographic Service uses a Laser Airborne Depth Sounder (LADS<sup>63</sup>) to gather hydrographic data. This system incorporates a split laser beam, comprising a green beam (which can penetrate water depths down to 70 m depending on water conditions and type of substrate) and an infrared beam (which is reflected from the water surface). The difference between the two readings is used to determine water depth. Airborne lidar measurements have also been used to locate fishing opportunities.

The LITE (Lidar In-Space Technology Experiment)<sup>64</sup> was briefly flown on the 1994 Space Shuttle for altimetry measurements. The CALIOP (Cloud-Aerosol Lidar with Orthogonal Polarisation) sensor, a dual wavelength, polarisation lidar, has been carried on the CALIPSO (Cloud-Aerosol Lidar and Infrared Pathfinder Satellite Observations) satellite since 2006, providing high-resolution profiles of clouds and aerosols. Data from both these satellites have been particularly valuable for quantifying global dust circulation and Earth's radiation budget (see Figures 16.6 and 16.7).

---

*One look is worth a thousand words.*

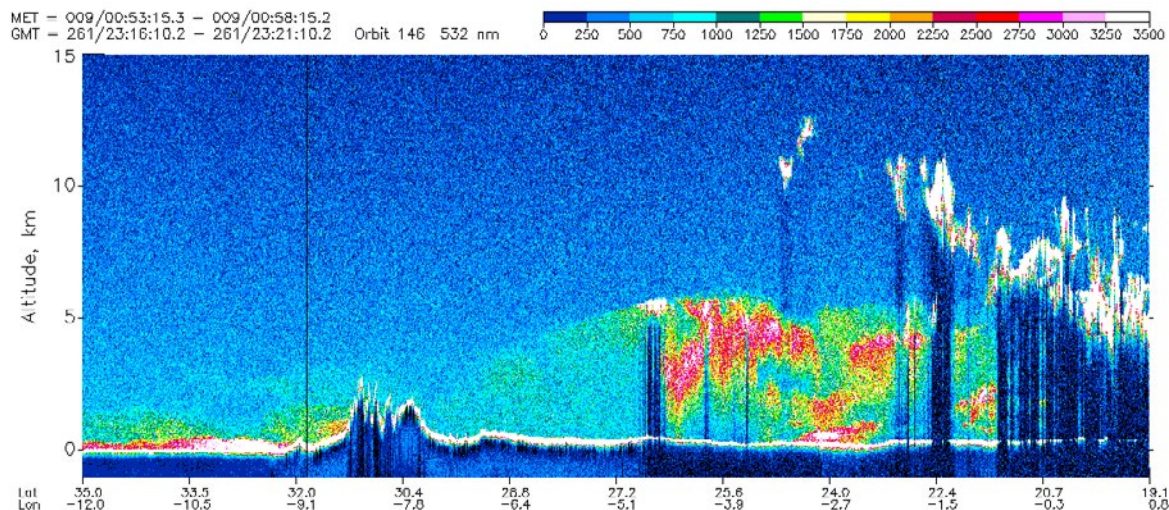
---

63. Laser Airborne Depth Sounder (LADS): <http://hydro.gov.au/aboutus/lads.htm>

64. Lidar In-space Technology Experiment (LITE): <http://lidar.jpl.nasa.gov/lite.htm>

**Figure 16.6** Profile of LITE observations over Sahara Desert

LITE thumbnail image acquired over a period of 5 minutes on 18 September 1994 showing intensity of the return pulse up to 15 km altitude. The terrain profile is visible along the lower edge, with the Atlas Mountain range showing the highest elevation in this sequence. The thickness of aerosol air masses is visible, with cleaner (blue) air to the northwest (left of mountains) and an optically thick aerosol plume (about 5 km thick and coloured yellow to red with increasing density) to the southeast (right of mountains). This plume occurs over the Sahara Desert due to dust circulation. The rightmost segment of the image shows cloud coloured as white.

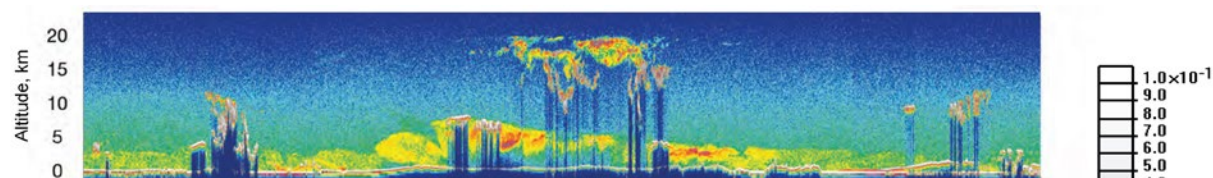


Source: NASA.

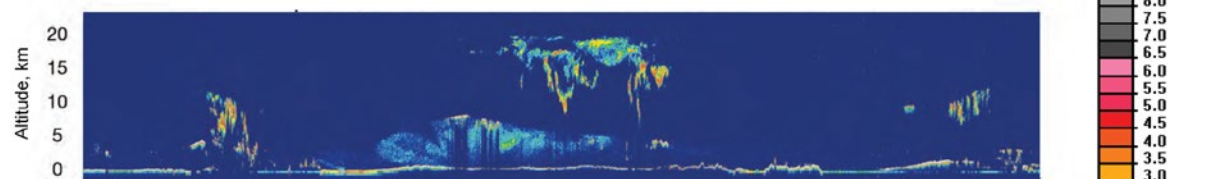
**Figure 16.7** Profiles of CALIOP observations over Sahara Desert

CALIOP profiles acquired on 9 June 2006. Grey tones indicate strong returns from clouds and terrain surface. Yellow and red tones represent weak cloud and strong aerosol scattering. Green and blue tones represent molecular scattering, plus scattering from weak aerosol and cloud layers.

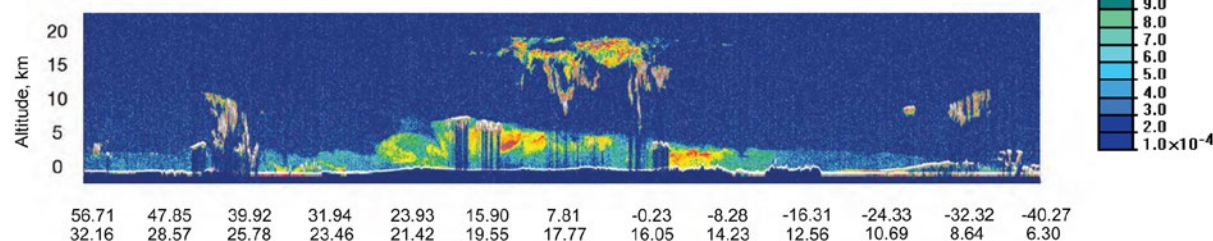
a. Total 532 nm return



b. 532 nm perpendicular return



c. Total 1064 nm return



Source: Winker *et al.* (2007) Figure 1. Provided by NASA Langley Research Centre.

### 16.2.2.2 Radar

Radar imaging sensors are introduced in Section 15.2. Radar techniques are used for sounding to determine water content:

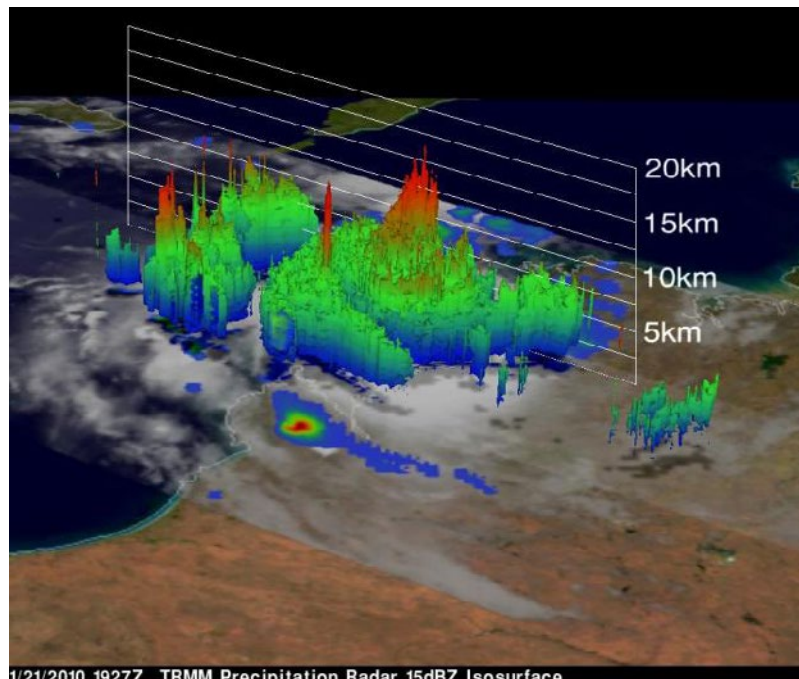
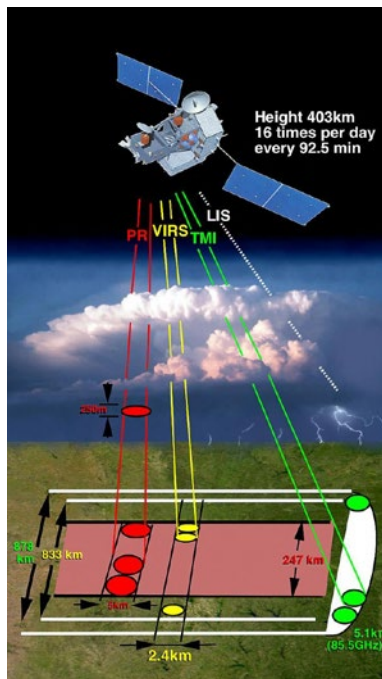
- weather radar detects precipitation in conjunction with ground-based networks; and
- Doppler radar measures wind speed and direction based on the Doppler shift between the frequencies of transmitted and returned signals (see Section 2.5.4). Doppler radars have only been carried by aircraft or used in ground-based studies.

TRMM was the first satellite-based weather radar, launched in 1997 and operated for over 17 years. Amongst other instruments, this satellite carried the first precipitation radar, which collected vertical profiles of rain and snow, extending from the Earth's surface to a height of 20 km. These data enabled modelling of three-dimensional storm structure, and delineation of the type, intensity and duration of precipitation (see Figure 16.8). Cloudsat, launched in 2006, carries a Cloud Profiling Radar (CPR). This radar sensor was designed to measure the backscatter from clouds, from which the distance from the sensor is derived. Combined with data from other sensors, this dataset allows detailed cloud and storm profiles to be created (see Figure 16.9).

**Figure 16.8** TRMM Precipitation Radar

a. TRMM satellite carried a Precipitation Radar (PR), a Microwave Imager (TMI), a Visible Infrared Scanner (VIRS), a Lightning Imaging Sensor (LIS) and the Clouds and Earth's Radiant Energy System (CERES—not shown).

b. A three-dimensional image showing the intensity of tropical cyclone Magda approaching northwest Australia on 21 January 2010 was generated from profiles acquired by the TRMM PR and TMI sensors.

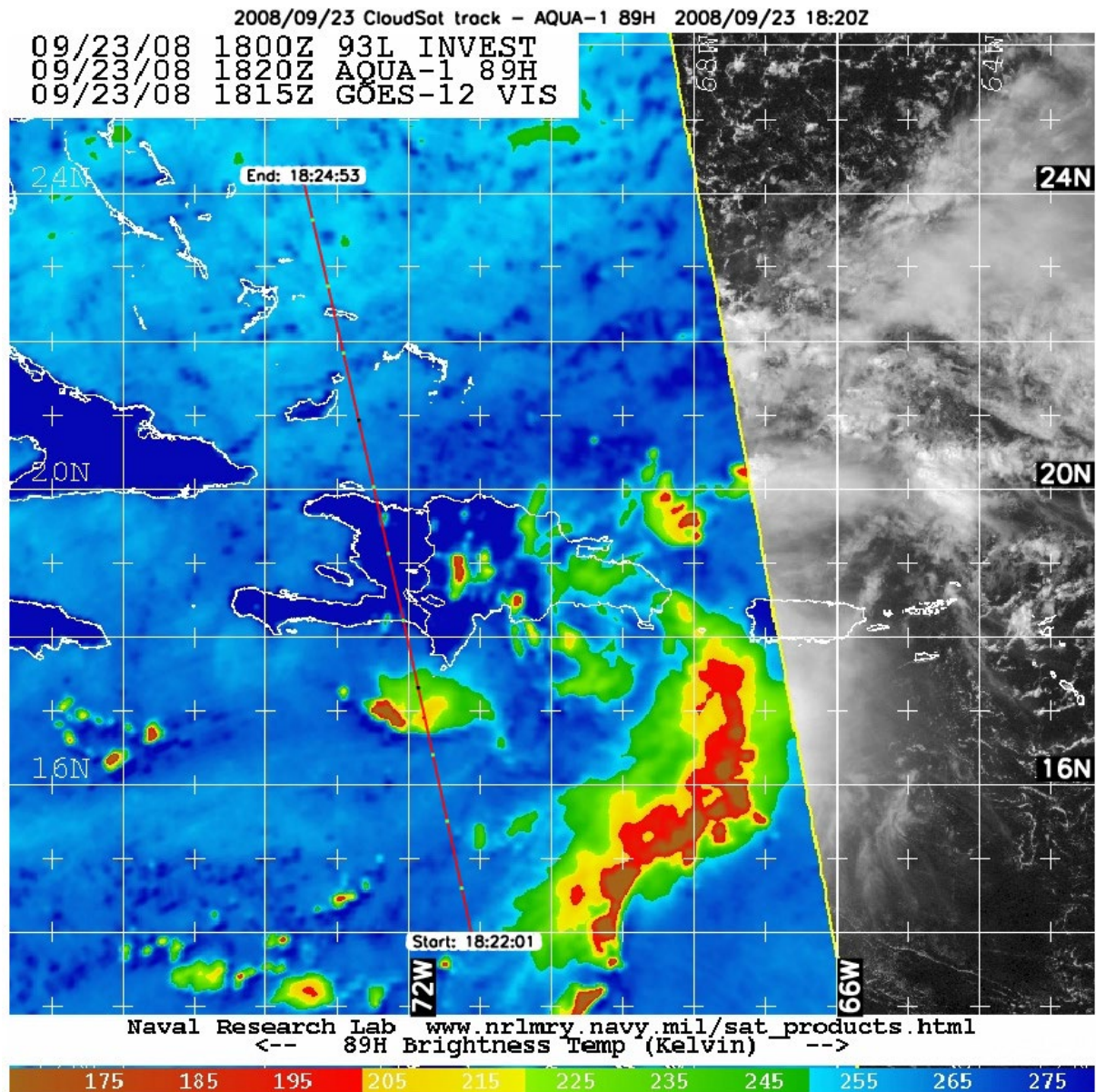


Source: NASA. Retrieved from <https://pmm.nasa.gov/image-gallery/trmm-precipitation-radar-image-magda>

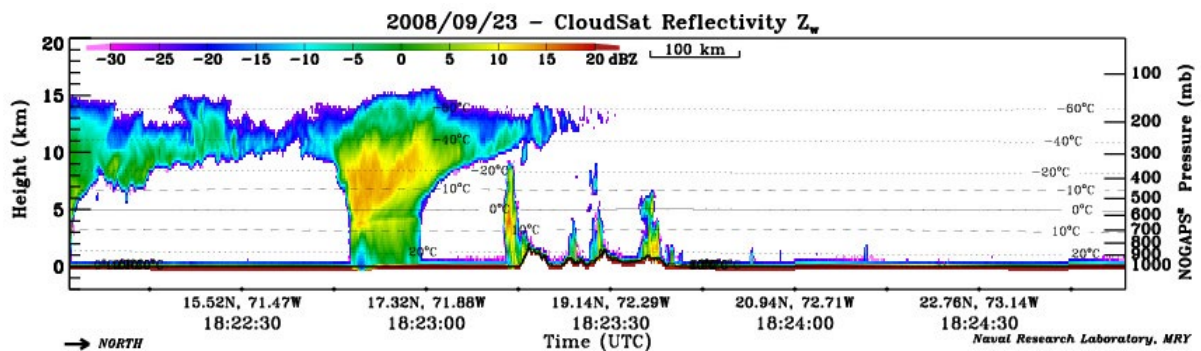


**Figure 16.9** Cloudsat Cloud Profiling Radar

a. Cloudsat orbit over Caribbean on 23 September 2008 shown on background of thermal imagery acquired by the Aqua satellite.



b. Cloud profile derived from Cloudsat Cloud Profiling Radar data showing height of clouds along orbital track.



Source: US Naval Research and NASA Cloudsat Project. CloudSat data courtesy CSU/CIRA.



## Excursus 16.2—Meteorological Sensors and Applications

**Source:** John Le Marshall, Bureau of Meteorology

**Further Information:** [j.lemarshall@bom.gov.au](mailto:j.lemarshall@bom.gov.au), [johnlemarshall@hotmail.com](mailto:johnlemarshall@hotmail.com)

### Early Applications

From the early 1960s, when imagery was first received from weather satellites, analysis and forecasting have depended heavily on these data sets. For the first time, these satellites provided information over data-sparse regions of the globe (see Excursus 12.1). Early work on satellite image interpretation was done by Vincent Oliver and others in a number of application areas, including rainfall and wind estimation (Anderson *et al.*, 1973).

The use of early images via subjective cloud picture interpretation provided the ability to position and analyse synoptic systems away from the conventional data network. Later quantitative estimates of Mean Sea Level Pressure (MSLP) and 1000–500 hPa geopotential thickness (see Excursus 16.2) were derived systematically from this imagery using methods such as those in Zillman (1968) and Guymer (1968, 1978).

### Sounding the Atmosphere

By the late 1960s, sounding of the atmosphere from space for temperature and moisture using thermal infrared observations from the Satellite IR Spectrometers SIRS-A and -B had been reported (Wark and Hilleary, 1969), followed by the first example of using the soundings to improve numerical weather prediction (Smith *et al.*, 1970).

Soundings from the subsequent operational instrument, the Vertical Temperature Profile Radiometer (VTPR; McMillin *et al.*, 1973) were received globally via the Global Telecommunications System (GTS) in the 1970s and used directly in operational analysis and prognosis systems. In the mid-1970s, after the utility of satellite vertical temperature profiles was established, clear column radiance (CLRAD) data (McMillin *et al.*, 1973) from the VTPR instrument (carried on the NOAA polar orbiting satellites) were distributed and used operationally at a number of places (including the National Meteorological Analysis Centre—NMAC, Australia). These sounders were followed by the TIROS Operational Vertical Sounder (TOVS) in 1979 and later the Advanced TOVS in 1998.

### The New Millennium

In February 2002, the Atmospheric InfraRed Sounder (AIRS), the first new generation ultraspectral

instrument able to provide operational data was launched. This instrument is able to provide radiance observations at 2378 infrared frequencies and these spectra are being used to produce temperature and moisture profiles (Chahine *et al.*, 2006). The temperature profiles have accuracies greater than 1K with moisture accuracies of the order of 15%. Temperature accuracies for the second-generation operational sounders (e.g. ATOVS) are generally 1.5K–2.0K and from 25% to 30% for moisture.

Several new hyperspectral/ultraspectral instruments are now flying, including AIRS, the Infrared Atmospheric Sounding Interferometer (IASI) and the Cross-track Infrared Scanner (CrIS), with a major impact on NWP. The increasing spectral resolution afforded by the AIRS instrument is seen in Figure 16.10 where the bandwidth of the TOVS HIRS instrument on the earlier NOAA satellites is displayed with spectra from AIRS. The improved spectral resolution shown has led to a significant increase in vertical and thermal resolution and increased accuracy in determination of concentrations of absorbers such as moisture and ozone in comparison to second generation sounders (see Table 16.1).

The first evidence of significant positive impact from higher spatial and temporal resolution ultra spectral AIRS data on global forecasts in both northern and southern hemispheres was recorded in Le Marshall *et al.* (2005). The improvement in forecast skill at six days for the US Global Forecast System (GFS) was equivalent to gaining an extension of forecast capability of several hours. This improvement is quite significant when compared to the rate of general forecast improvement over a decade. A several hour increase in forecast range at five or six days normally takes several years to achieve at operational weather centres.

**Table 16.1** Characteristics of AIRS and HIRS sounding instruments

Characteristic	HIRS	AIRS
Spectral range	3.7–15 $\mu\text{m}$	3.7–15 $\mu\text{m}$
Spatial Resolution (sub-sat)	174 km	13.5 km
Number of Channels	20	2378
Spectral Resolution (DI/I)	~1/70	~1/1000
Vertical Resolution	~3 km	~1 km
Temperature Accuracy	~1.5–2 K	<1 K in 1 km layers
Moisture Accuracy	~30%	15% in 2 km layers

**Figure 16.10** Spectral resolution of HIRS/2 compared with simulated AIRS spectra

HIRS/2 = Half power Spectral Response Function

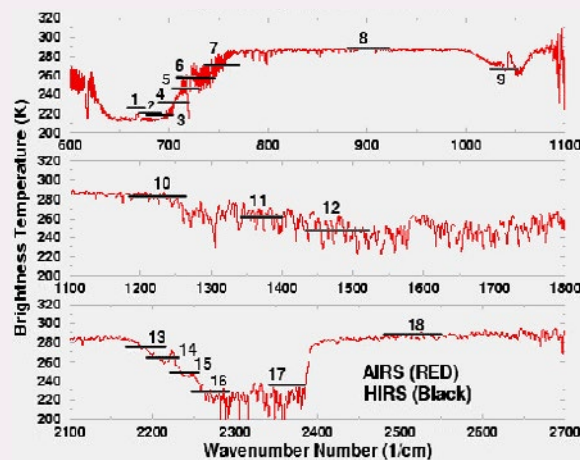


### Image-based Applications

Many improvements in Earth System science, analysis and forecasting were due to the availability of imagery in the meteorological database. In particular the work of Dvorak (1972, 1975) estimating tropical cyclone intensity using satellite imagery remains important to this day (Velden *et al.*, 2006). Forecasts are often dependent on many of the image-based applications which have demonstrably benefitted from improved spatial, spectral and temporal resolution EOS, including:

- Atmospheric Motion Vectors (AMV);
- cloud top temperature/cloud height;
- cloud type and amount determination
- detection of low cloud/fog
- timing of fog clearing
- frost detection (land surface temperature)
- detection of volcanic ash
- detection of dust clouds
- detection of inversions
- rainfall estimation
- snow cover
- forest fire detection
- sea surface temperature (SST)
- NDVI estimation
- flood monitoring
- sea ice, cloud discrimination and mapping
- solar radiation
- surface albedo
- land surface temperature
- soil moisture

These improvements will continue into the future, now that the next generation Japanese geostationary satellite, Himawari-8, has replaced MTSAT-2, again providing improved spatial, temporal and spectral resolution imagery.

### Recent EOS Impact Studies

In addition to the studies cited previously, data from a considerable number of other satellite instruments have been recently assimilated. These include data from the COSMIC Constellation, CHAMP, WindSat and AMSR(E).

Radio Occultation (RO) data from the COSMIC Constellation (a new remote sensing technology, Anthes *et al.* (2008) have shown significant positive impact on forecasts through the whole troposphere, particularly over the Southern Hemisphere (Healy and Thépaut, 2006; Cucurull and Derber, 2008; Le Marshall *et al.*, 2010; Le Marshall *et al.*, 2012). An important benefit of the COSMIC/GNSS system of satellites is that they provide near bias-free observations. In NWP, this helps to calibrate instruments such as the advanced sounders during tuning, resulting in analyses close to climate quality. Another important contribution from GPS RO is climate monitoring. Recently, RO data has been used to examine annual average of tropospheric temperature over the Southern Hemisphere. This use of GPS RO data has been shown to provide significant new information particularly over the data-sparse regions of the southern oceans (Le Marshall *et al.*, 2012).

WindSat data have also demonstrated a positive impact on forecasts (Le Marshall *et al.*, 2007). While WindSat covered much the same areas as QuikSCAT, it improved operational forecasts and provided an in-orbit backup covering the loss of QuikSCAT. In addition to these assimilation experiments, ASCAT, AMSR(E), SSMIS and AURA/OMI observations have also been successfully assimilated into the National Centre for Environmental Prediction's Global Forecast System (NCEP GFS). AMSR(E) and SSMIS have also been shown to improve forecasts in the Southern Hemisphere.

Considerable work has also been undertaken to enhance the use of AMV data (Holmlund, 1998; Holmlund *et al.*, 2001; Le Marshall *et al.*, 2004). The importance of these high spatial and temporal resolution vectors in NWP is seen in recent results (Le Marshall *et al.*, 2013b) where the advantage of high resolution, near-continuous data have been exploited by using 4D-Var. This approach is also being applied with the new Himawari-8 satellite where AMV are being generated operationally every 10 minutes over Australasia and Asia (see Excursus 12.1).

## 16.3 Further Information

### Sensors:

The CEOS Database (CEOS, 2016)

### Microwave Remote Sensing:

Ulaby and Long (2014)

Woodhouse (2004)

### Atmospheric Research:

University Corporation for Atmospheric Research (UCAR): <http://www2.ucar.edu>

### Laser Altimetry:

AAM Surveys—Local airborne laser data specialists: <http://www.aamgroup.com/services-and-technology/aerial-survey>

National Elevation Data Framework Portal: <http://nedf.ga.gov.au>

ICESAT—Ice, cloud and land elevation satellite: <http://icesat.gsfc.nasa.gov>

(also used to map vegetation height and structure across Australia: <http://www.auscover.org.au/xwiki/bin/view/Product+pages/ICESat+Vegetation+Structure>)

### Radar Altimetry:

Radar Altimetry Tutorial (Rosmorduc *et al.*, 2011)

Sea Level Rise (CMAR, CSIRO): [http://www.cmar.csiro.au/sealevel/sl\\_meas\\_sat\\_alt.html](http://www.cmar.csiro.au/sealevel/sl_meas_sat_alt.html)

Satellite Altimetry Lectures (Le Traon, 2007)

Radar Basics: <http://www.radartutorial.eu/02.basics/Altimeter.en.html>

Fu and Cazenave (2000)

### DORIS system:

Guijarro *et al.* (2000)

### Scatterometry:

NASA Winds: Measuring Ocean Winds from Space: <http://winds.jpl.nasa.gov/aboutscatterometry/history>

Centre for Ocean-Atmospheric Prediction Studies: <https://coaps.fsu.edu/scatterometry/about/overview.php>

Laing and Evans (2011)

### Sounding:

Laing and Evans (2011)

Australian Atmospheric Sounding Information: <http://slash.dotat.org/cgi-bin/atmos>

Elachi and van Zyl (2006)

## 16.4 References

Anderson, R. K., Ferguson, E. W., Ashman, J. P., Farr, G. R., Isayeva, G. N., Oliver, V. J., Parmenter, F. C., Popova, T. P., Skidmore, R. W., Smith, A. H., and Veltishchev, N. F. (1973). The use of satellite pictures in weather analysis and forecasting (WMO 333). World Meteorological Organisation.

Anthes, R. A., Bernhardt, P. A., Chen, Y., Cucurull, L., Dymond, K. F., Ector, D., Healy, S. B., Ho, S.-P., Hunt, D. C., Kuo, Y.-H., Liu, H., Manning, K., McCormick, C., Meehan, T. K., Randel, W. J., Rocken, C., Schreiner, W. S., Sokolovskiy, S. V., Syndergaard, S., Thompson, D. C., Trenberth, K. E., Wee, T.-K., Yen, N. L., and Zeng, Z. (2008). The COSMIC/FORMOSAT-3 Mission: Early Results. *Bulletin of the American Meteorological Society*, 89, pp. 313-333.

Arendt, A. A., Echelmeyer, K. A., Harrison, W. D., Lingle, C. S., and Valentine, V. B. (2002). Rapid wastage of Alaska glaciers and their contribution to rising sea level. *Science*, 297(5580), pp. 382-386. doi:<http://dx.doi.org/10.1126/science.1072497>.

Barale, V., Gower, J. F. R., and Alberotanza, L. (2010). *Oceanography from Space: Revisited* (374 pages). doi:<http://dx.doi.org/10.1007/978-90-481-8681-5>.

Brenner, A. C., DiMarzio, J. R., and Zwally, H. J. (2007). Precision and accuracy of satellite radar and laser altimeter data over the continental ice sheets. *IEEE Transactions on Geoscience and Remote Sensing*, 45(2), pp. 321-331.

CEOS (2016). The CEOS Database. Retrieved from <http://database.eohandbook.com>.

Chahine, M. T., Pagano, T. S., Aumann, H. H., Atlas, R., Barnett, C., Blaisdell, J., Chen, L., Divakarla, M., Fetzer, E. J., Goldberg, M., Gautier, C., Granger, S., Hannon, S., Irion, F. W., Kakar, R., Kalnay, E., Lambrigtsen, B. H., Lee, S.-Y., Le Marshall, J. L., McMillan, W. W., McMillin, L., Olsen, E. T., Revercomb, H., Rosenkranz, P., Smith, W. L., Staelin, D., Strow, L. L., Susskind, J., Tobin, D., Wolf, W., and Zhou, L. (2006). AIRS: Improving Weather Forecasting and Providing New Data on Greenhouse Gases. *Bulletin of the American Meteorological Society*, 87(7), pp. 911-926. doi:<http://dx.doi.org/10.1175/BAMS-87-7-911>.

- Cucurull, L., and Derber, J. C. (2008). Operational Implementation of COSMIC Observations into NCEP's Global Data Assimilation System. *Weather and Forecasting*, 23(4), pp. 702-711. doi:<http://dx.doi.org/10.1175/2008WAF2007070.1>.
- Dvorak, V. F. (1972). A technique for the analysis and forecasting of tropical cyclone intensities from satellite pictures (NESS 36). NOAA Technical Memorandum. National Environmental Satellite Service, National Oceanographic and Atmospheric Administration, U.S. Department of Commerce.
- Dvorak, V. F. (1975). Tropical Cyclone Intensity Analysis and Forecasting from Satellite Imagery. *Monthly Weather Review*, 103(5), pp. 420-430. doi:[http://dx.doi.org/10.1175/1520-0493\(1975\)103%3C0420:TCIAAF%3E2.0.CO;2](http://dx.doi.org/10.1175/1520-0493(1975)103%3C0420:TCIAAF%3E2.0.CO;2).
- Elachi, C., and van Zyl, J. (2006). *Introduction to the Physics and Techniques of Remote Sensing*, Second Edn. Wiley Interscience, New Jersey.
- Fu, L. L., and Cazenave, A. (2000). *Satellite Altimetry and Earth Sciences: A Handbook of Techniques and applications*. Academic Press, San Diego, London.
- Guijarro, J., Auriol, A., Costes, M., Jayles, C., and Vincent, P. (2000). MWR and DORIS - Supporting Envisat's radar altimetry mission. *ESA Bulletin-European Space Agency*(104), pp. 41-46.
- Guymer, L. B. (1968). Estimation of 1000 - 500 mb Thickness Patterns from Satellite Pictures of Convective Areas. Paper presented at the Inter-Regional Seminar on the Interpretation of Meteorological Satellite Data, Melbourne, Australia.
- Guymer, L. B. (1978). Operational Application of Satellite Imagery to Synoptic Analysis in the Southern Hemisphere (Technical Report No. 29). Commonwealth Bureau of Meteorology, Melbourne, Australia.
- Harrison, B. A., and Jupp, D. L. B. (1989). *Introduction to Remotely Sensed Data. Part ONE of the microBRIAN Resource Manual (156 pages)*. CSIRO Australia, Melbourne.
- Healy, S. B., and Thépaut, J. N. (2006). Assimilation experiments with CHAMP GPS radio occultation measurements. *Quarterly Journal of the Royal Meteorological Society*, 132(615), pp. 605-623. doi:<http://dx.doi.org/10.1256/qj.04.182>.
- Helm, V., Humbert, A., and Miller, H. (2014). Elevation and elevation change of Greenland and Antarctica derived from CryoSat-2. *Cryosphere*, 8(4), pp. 1539-1559. doi:<http://dx.doi.org/10.5194/tc-8-1539-2014>.
- Holmlund, K. (1998). The Utilization of Statistical Properties of Satellite-Derived Atmospheric Motion Vectors to Derive Quality Indicators. *Weather and Forecasting*, 13(4), pp. 1093-1104. doi:[http://dx.doi.org/10.1175/1520-0434\(1998\)013%3C1093:TUOSPO%3E2.0.CO;2](http://dx.doi.org/10.1175/1520-0434(1998)013%3C1093:TUOSPO%3E2.0.CO;2).
- Holmlund, K., Velden, C. S., and Rohn, M. (2001). Enhanced Automated Quality Control Applied to High-Density Satellite-Derived Winds. *Monthly Weather Review*, 129(3), pp. 517-529. doi:[http://dx.doi.org/10.1175/1520-0493\(2001\)129%3C0517:EAQCAT%3E2.0.CO;2](http://dx.doi.org/10.1175/1520-0493(2001)129%3C0517:EAQCAT%3E2.0.CO;2).
- Hwang, C., Shum, C., and Li, J. (2004). *Satellite Altimetry for Geodesy, Geophysics and Oceanography. Proceedings of: International Workshop on Satellite Altimetry. Berlin Heidelberg: Springer-Verlag.*
- Jupp, D. L. B. (1997). *Issues in Reflectance Measurement*. CSIRO Earth Observation Centre, Canberra.
- Laing, A., and Evans, J.-L. (2011). *Introduction to Tropical Meteorology, Second Edn. The COMET Program*. Retrieved from [http://www.goes-r.gov/users/comet/tropical/textbook\\_2nd\\_edition/index.htm](http://www.goes-r.gov/users/comet/tropical/textbook_2nd_edition/index.htm).
- Le Marshall, J. F., Bi, L., Jung, J., Zapotocny, T., and Morgan, M. (2007). WindSat Polarimetric Microwave Observations Improve Southern Hemisphere Numerical Weather Prediction. *Australian Meteorological Magazine*, 56, pp. 35-40.
- Le Marshall, J. F., Jung, J. D., J., Treadon, R., Lord, S., Goldberg, M., Wolf, W., Liu, H. C., Joiner, J., Woollen, J., and Todling, R. (2005). AIRS hyperspectral data improves southern hemisphere forecasts. *Australian Meteorological Magazine*, 54, pp. 57-60.
- Le Marshall, J. F., Lee, J., Jung, J. A., and Roux, B. (2013a). The Considerable Impact of Earth Observations from Space on Numerical Weather Prediction. *Australian Meteorological and Oceanographic Journal*, 63(4), pp. 497-500.
- Le Marshall, J. F., Rea, A., Leslie, L., Seecamp, R., and Dunn, M. (2004). Error characterization of atmospheric motion vectors. *Australian Meteorological Magazine*, 53, pp. 123-131.
- Le Marshall, J. F., Seecamp, R., Xiao, Y., Gregory, P., Jung, J., Stienle, P., Skinner, T., Tingwell, C., and Le, T. (2013b). The Operational Generation of Continuous Winds in the Australian Region and Their Assimilation with 4DVAR. *Weather and Forecasting*, 28(2), pp. 504-514. doi:<http://dx.doi.org/10.1175/WAF-D-12-00018.1>.



- Le Marshall, J. F., Xiao, Y., Norman, R., Zhang, K., Rea, A., Cucurull, L., Seecamp, R., Steinle, P., Puri, K., and Le, T. (2010). The Beneficial Impact of Radio Occultation Observations on Australian Region Forecasts. *Australian Meteorological and Oceanographic Journal*, 60, pp. 121-125.
- Le Marshall, J. F., Xiao, Y., Norman, R., Zhang, K., Rea, A., Cucurull, L., Seecamp, R., Steinle, P., Puri, K., and Le, T. (2012). The Application of Radio Occultation for Climate Monitoring and Numerical Weather Prediction in Australian Region. *Australian Meteorological and Oceanographic Journal*, 62, pp. 323-334.
- Le Traon, P.-Y. (2007). Satellite Altimetry. Lectures for ESA-MOST Dragon Programme. ESA. Retrieved from [http://earth.eo.esa.int/dragon/ocean\\_training/Lecture\\_Material/DAY5-19Oct2007/D5\\_L1-2\\_letraon\\_lecture1\\_2.pdf](http://earth.eo.esa.int/dragon/ocean_training/Lecture_Material/DAY5-19Oct2007/D5_L1-2_letraon_lecture1_2.pdf).
- Lognonné, P., Garcia, R., Crespon, F., Occhipinti, G., Kherani, A., and Artru-Lambin, J. (2006). Seismic waves in the ionosphere. *Europhysicsnews*, 37(4), pp. 11-14.
- McMillin, L. M., Wark, D. Q., Siomkajlo, J. M., Abel, P. G., Werbowetzki, A., Lauritson, L. A., Pritchard, J. A., Crosby, D. S., Woolf, H. M., Luebbe, R. C., Weinreb, M. P., Fleming, H. E., Bittner, F. E., and Hayden, C. M. (1973). Satellite Infrared Soundings from NOAA Spacecraft (NESS 65). NOAA Technical Memorandum. National Environmental Satellite Service, National Oceanographic and Atmospheric Administration, U.S. Department of Commerce.
- Nicodemus, F. E., Richmond, J. C., and Hsia, J. J. (1977). Geometrical considerations and nomenclature for reflectance (NBS Monograph 160). US Department of Commerce, National Bureau of Standards.
- Rosmorduc, V., Benveniste, J., Bronner, E., Dinardo, S., Lauret, O., Maheu, C., Milagro, M., and Picot, N. (2011). Radar Altimetry Tutorial. Retrieved from <http://www.altimetry.info>.
- Sardar, A. M. (1997). Chronology of the development of remote sensing technology. *Asian-Pacific Remote Sensing and GIS Journal*, 2, pp. 35-49.
- Smith, W. L., Woolf, H. M., and Jacob, W. J. (1970). A Regression Method for Obtaining Real-time Temperature and Geopotential Height Profiles from Satellite Spectrometer Measurements and its Application to Nimbus-3 SIRS Observations. *Monthly Weather Review*, 98(8), pp. 582-603. doi:[http://dx.doi.org/10.1175/1520-0493\(1970\)098%3C0582:ARMFOR%3E2.3.CO;2](http://dx.doi.org/10.1175/1520-0493(1970)098%3C0582:ARMFOR%3E2.3.CO;2).
- Ulaby, F. T., and Long, D. G. (2014). Microwave, Radar and Radiometric Remote Sensing. Retrieved from <http://mrs.eecs.umich.edu/>.
- Valentine, V., Echelmeyer, K., Campbell, S., and Zirheld, S. (2004). Harding Icefield's Clues to Climate Change. *Alaska Park Science Journal*, 3(1), pp. 13-17.
- Velden, C., Harper, B., Wells, F., II, J. L. B., Zehr, R., Olander, T., Mayfield, M., Guard, C. C., Lander, M., Edson, R., Avila, L., Burton, A., Turk, M., Kikuchi, A., Christian, A., Caroff, P., and McCrone, P. (2006). The Dvorak Tropical Cyclone Intensity Estimation Technique: A Satellite-Based Method that Has Endured for over 30 Years. *Bulletin of the American Meteorological Society*, 87(9), pp. 1195-1210. doi:<http://dx.doi.org/10.1175/BAMS-87-9-1195>.
- Vignudelli, S., Kostianoy, A. G., Cipollini, P., and Benveniste, J. (2011). *Coastal Altimetry*. Springer-Verlag, Berlin Heidelberg.
- Wark, D. Q., and Hilleary, D. T. (1969). Atmospheric Temperature: Successful Test of Remote Probing. *Science*, 165(3899), pp. 1256-1258. doi:<http://dx.doi.org/10.1126/science.165.3899.1256>.
- Winker, D. M., Hunt, W. H., and McGill, M. J. (2007). Initial performance assessment of CALIOP. *Geophysical Research Letters*, 34(19). doi:<http://dx.doi.org/10.1029/2007gl030135>.
- Woodhouse, I. H. (2004). *Introduction to Microwave Remote Sensing*. CRC Press.
- Zillman, J. W. (1968). Interpretation of satellite data over the Southern Ocean using the technique of Martin. Paper presented at the Inter-Regional Seminar on the Interpretation of Meteorological Satellite Data, Melbourne, Australia.



